



**An experimental study of the
hydrodynamic impact of turbine
layout and design considerations in
tidal range schemes.**

By

Catherine Leech

Supervised by
Professor Reza Ahmadian and Professor Roger A. Falconer

A thesis submitted to Cardiff University in candidature for the
degree of Doctor of Philosophy (PhD)

School of Engineering

Cardiff University

2022

Genesis 1:9-10 – And God said, “Let the water under the sky be gathered to one place, and let dry ground appear.” And it was so. God called the dry ground “land,” and the gathered waters he called “seas.” And God saw that it was good.

Thank you, God for giving me the ability to study these things.

Abstract

Tidal Range Energy (TRE) is a reliable and sustainable source of energy found in abundance along the UK coast. It is thus far undeveloped on our shores due to environmental and financial concerns which have hindered it from competing with offshore wind and other renewable sources to meet UK energy demand. With current challenges to find clean and secure energy sources it is worth addressing these environmental concerns in order for TRE to reach its potential in our waters and worldwide.

The present study looks specifically at the hydrodynamic impacts of the turbines in Tidal Range Schemes (TRSs) and how these are affected by different design parameters, including: the number of turbines, turbine spacing, TRS shape and TRS bed conditions. Physical experiments were conducted in the Hydro-environmental Research Centre at Cardiff University to quantify the changes in velocity induced by these design adaptations. Interruption to study reduced the number of physical experiments able to be carried out and numerical modelling was investigated to supplement results. Underlying asymmetrical flow in the laboratory impacted experimental results and presented challenges for calibrating the numerical model.

Results from the physical experiments revealed that velocity patterns are most influenced by turbine spacing and that tightly spaced turbines lead to the greatest impact on baseline conditions due to concentrated wake effects. Wider spacing promotes slower circulation which would enable other activities to take place within TRSs but may lead to issues with water quality if flows are too slow to facilitate effective flushing. Both square and rectangular TRS designs showed similar results with regards to turbine spacing and circulation inside the TRS, but the rectangular TRS led to greater blockage effects outside the TRS. This emphasises the need for site specific design to take coastal conditions into account. Neither bed material nor bed slope were found to cause a significant difference to baseline flow conditions. Overall, turbine spacing had a greater impact on flow conditions than the number of turbines, and central placement with wider spacing was found to be best for maintaining natural conditions.

Acknowledgements

This research is funded as part of the Water Informatics Science and Engineering Centre for Doctoral Training (WISE CDT) under a grant from the Engineering and Physical Sciences Research Council (EPSRC), grant number EP/L016214/1.

I would like to thank my supervisors, Dr Reza Ahmadian and Professor Roger A. Falconer, for their professional help and guidance throughout my studies. Particularly in the initial concept of the project and their unfailing knowledge on all things relating to tidal range energy.

Thanks also to the WISE CDT administrators Debbie Ford and Nia Owen who have ceaselessly supported the students of WISE, enabling our research to thrive even through a global pandemic.

Thank you to the extremely talented and hard-working technicians and engineers in the Hydro-environmental Research Centre, to Paul Leach in particular, for supporting my experiments, making my plans a reality, and always being ready to shore up the pipes whenever the ceiling threatened to fall in!

Thanks to the other WISE CDT students, especially Stephanie Muller and Nefeli Makrygianni, without whom, independent study would sometimes be unbearable. Their camaraderie and peer support have been invaluable, and I really appreciate their sympathetic and practical counsel.

To Sarah, Chloe, Katie and Tamsin for our weekly check-ins and for always being willing to listen to my ongoing research challenges.

And finally, my most heartfelt thanks go to my family for consistently upholding me whilst I battled with this work. To Mum, Dad, Jonny, Ben, Hannah, Lex and Elise (my tiny brightside) thank you for your love and unfailing support.

Table of Contents

Abstract.....	iii
Acknowledgements.....	iv
Table of Contents.....	v
List of Figures	x
List of Tables.....	xxii
Nomenclature.....	xxiv
1 Introduction.....	2
1.1 Research Background	2
1.2 Scope of Study	6
1.3 Research Aims and Objectives.....	7
1.4 Thesis Outline.....	8
2 Literature Review.....	10
2.1 Introduction	10
2.2 Tidal Range Energy Structures and Operation	12
2.3 Tidal Range Energy and Renewable Energy Targets.....	19
2.4 Other Renewable Energy Sources	21
2.4.1 Hydropower.....	21
2.4.2 Nuclear.....	21
2.4.3 Wind.....	22
2.4.4 Wave	22
2.4.5 Tidal Stream.....	23
2.4.6 Tidal Range.....	23
2.5 State of Knowledge of Tidal Range Energy	24
2.5.1 Existing Sites.....	24
2.5.2 Possible Sites Worldwide.....	26
2.5.3 Possible Sites UK.....	27

Contents

2.5.4	Advantages of Tidal Range Energy	31
2.5.5	Barriers to Tidal Range Energy	34
2.5.6	How to Overcome Barriers to Tidal Range Energy.....	37
2.6	Gaps in Tidal Range Energy Research.....	54
2.7	Research Methods for Investigating Tidal Range Structures	55
2.7.1	Physical Modelling.....	55
2.7.2	Numerical Modelling.....	59
2.8	Summary	62
3	Methodology – Physical Model	64
3.1	Introduction	64
3.2	Methodology	65
3.3	Model Design.....	67
3.3.1	Scale	68
3.3.2	Idealised Geometry	73
3.3.3	Interruption to Study	76
3.4	Experimental Setup	80
3.4.1	Test Cases and Configurations	80
3.4.2	Domain and boundary conditions	83
3.5	Data Collection	84
3.5.1	Velocity Data Collection	84
3.5.2	Water Level Data Collection	88
3.5.3	Flow Circulation Data Collection.....	89
3.6	Data Processing and Analysis	90
3.7	Summary	94
4	Test Case 1 – Impact of varying turbine layout.....	96
4.1	Introduction	96
4.2	Asymmetric Flow	98

4.3	Results.....	99
4.3.1	Comparison A – Varying the number of turbines in a square TRS.	99
4.3.2	Comparison B – Varying the position of a single turbine in a square TRS.....	123
4.3.3	Comparison C – Varying the position of two turbines in a square TRS	141
4.3.4	Comparison G – Varying the position of two turbines in a rectangular TRS.....	162
4.4	Summary	183
5	Test Case 2 – Impact of varying bed conditions	186
5.1	Introduction	186
5.2	Results.....	187
5.2.1	Comparison D – Varying bed materials.....	187
5.2.2	Comparison E – Varying bed slopes	206
5.3	Summary	223
6	Test Case 3 – Impact of varying geometry	225
6.1	Introduction	225
6.2	Results.....	227
6.2.1	Comparison F i – Square vs Rectangular TRS with 0 turbines	227
6.2.2	Comparison F ii – Square vs Rectangular TRS with 1 turbine	240
6.2.3	Comparison F iii – Square vs Rectangular TRS with 2 turbines side by side.....	256
6.2.4	Comparison F iv – Square vs Rectangular TRS with 2 turbines at opposite ends of seawall.....	272
6.2.5	Comparison O – All cases compared to pre-lagoon levels.....	289
6.3	Summary	302

Contents

7	Numerical Model.....	306
7.1	Introduction.....	306
7.2	Methodology.....	307
7.3	Model Design.....	308
7.3.1	Assumptions.....	308
7.4	Calibration.....	309
7.4.1	Boundary Conditions.....	309
7.4.2	Bed Roughness.....	322
7.4.3	Horizontal Eddy Viscosity.....	324
7.4.4	Other Calibration Considerations.....	325
7.5	Validation.....	328
7.6	Summary.....	328
8	Discussion.....	330
8.1	Introduction.....	330
8.2	Physical Limitations and Practicalities.....	330
8.2.1	Facilities.....	330
8.2.2	Equipment and Operation.....	339
8.2.3	Software and Calibration Challenges.....	341
8.3	Summary.....	341
9	Summary and Conclusions.....	343
9.1	Introduction.....	343
9.2	Summary.....	343
9.3	Discussion.....	344
9.3.1	Impact of varying turbine layout.....	344
9.3.2	Impact of varying bed conditions.....	345
9.3.3	Impact of varying TRS geometry.....	346
9.4	Applications.....	347

Contents

9.5	Overall Conclusion.....	348
9.6	Recommendations for Future Study	349
10	References.....	352
	Annex 1: Studies of TST Spacing	368
	Annex 2: Regression analysis of experiment results for flow velocity magnitude and direction compared to pre-lagoon tank conditions.....	374
	Annex 3: Comparison of points of statistically similar and different resultant velocity.....	393
	Annex 4: Advantages and disadvantages of dimensional numerical models	403
	Annex 5: Numerical Model Design Schedule	406
	A5.1 Test Cases and Configurations.....	406
	A5.1.1 Further testing of different turbine spacings	406
	A5.1.2 Investigation of different lagoon geometries	407
	A5.1.3 Modelling more realistic TRSs.....	408
	A5.2 Domain and Boundary Conditions	408

List of Figures

Figure 2.1 Plan view of tidal range structure at La Rance (Rtimi et al., 2021).	14
Figure 2.2 Side view of a bulb turbine caisson used TRSs (Yates et al., 2013)	14
Figure 2.3 Water elevation on each side of a TRS seawall during ebb only operation, solid line: basin level, dashed line: sea level (Yates et al, 2013). 15	
Figure 2.4 Water elevation on each side of a TRS seawall during flood only operation, solid line: basin level, dashed line: sea level (Yates et al, 2013). 16	
Figure 2.5 Water elevation on each side of a TRS seawall during two-way operation, solid line: basin level, dashed line: sea level (Yates et al, 2013). 16	
Figure 2.6 Water elevation on each side of a TRS seawall during two-way operation with the addition of pumping, solid black line: sea level, solid blue line: basin level.	17
Figure 2.7 Areas of greatest tidal range around the UK coast (Tidal Lagoon Swansea Bay, 2017).....	28
Figure 2.8 Common design layout for TRSs, with sluices and turbines grouped together in a single block in a seawall (based on multiple sources).	44
Figure 2.9 Existing layout of La Rance tidal barrage (Rtimi et al., 2021).	45
Figure 2.10 Existing layout of Lake Sihwa tidal lagoon (Bae et al., 2010)....	45
Figure 2.11 Proposed layout for Mersey tidal barrage (Petley et al., 2019). 46	
Figure 2.12 Proposed layout for tidal lagoon on North Wales Coast (Angeloudis et al., 2016).	46
Figure 2.13 Proposed layout for Swansea Bay tidal lagoon (Angeloudis et al., 2016).....	47
Figure 2.14 Conceptual design for a tidal barrage in the Bay of Fundy (Cornett et al., 2013).	47
Figure 2.15 Proposed layout for West Somerset tidal lagoon (Guo et al., 2021).....	49
Figure 3.1 Tidal basin dimensions in HRC laboratory.	65
Figure 3.2 Photograph of tidal basin in HRC laboratory highlighting key apparatus.	66

Contents

Figure 3.3 Photograph of tidal basin weir gate.....	66
Figure 3.4 Scale analysis of potential schemes for testing in the tidal basin	70
Figure 3.5 a) Idealised square and b) rectangular coastally attached TRSs as built in HRC tidal basin.....	76
Figure 3.6 a) blank box section and b) turbine opening box section as used to create the front seawall of the TRS structures. (Not drawn to scale).	78
Figure 3.7 Example of box section arrangement with two turbine opening box sections and eight blank box sections.....	78
Figure 3.8 Working principle of an ADVP (Zhai, et al., 2014).....	84
Figure 3.9 Photograph of laboratory illustrating ADVP system movement in three dimensions.....	86
Figure 3.10 Data collection sample grid for a) square and b) rectangular lagoon.	86
Figure 4.1 X-velocity magnitude at opposite ends of the inflow boundary. ...	98
Figure 4.2 Experient layouts for Comparison A: S0, S1A, S2A.....	99
Figure 4.3 Map of depth averaged velocity plots for Comparison A: S0, S1A and S2A.	100
Figure 4.4 Closer detail of velocity at (250,50).....	102
Figure 4.5 Closer detail of velocity at (200,100).....	102
Figure 4.6 Closer detail of velocity at (350,250).....	102
Figure 4.7 Closer detail of velocity at (200,400).....	102
Figure 4.8 Closer detail of velocity at (200,300).....	102
Figure 4.9 Closer detail of velocity at (225,440).....	102
Figure 4.10 Closer detail of velocity at (225,500).....	104
Figure 4.11 Closer detail of velocity at (225,525).....	104
Figure 4.12 Closer detail of velocity at (225,550).....	104
Figure 4.13 Comparison A - Velocity contour maps at elevations of 50, 100, 150, 200 and 250 mm above the bed during the ebb tide.	108
Figure 4.14 Comparison A - Velocity contour maps at elevations of 50, 100, 150, 200 and 250 mm above the bed during low tide.	109
Figure 4.15 Comparison A - Velocity contour maps at elevations of 50, 100, 150, 200 and 250 mm above the bed during the flood tide.	110
Figure 4.16 Comparison A - Velocity contour maps at elevations of 50, 100, 150, 200 and 250 mm above the bed during high tide.	111

Figure 4.17 Comparison A – Contour maps of residual velocity magnitude and direction at elevations of 50, 100, 150, 200 and 200 mm from the bed.	114
Figure 4.18 Flow visualisation for experiment S1A.	116
Figure 4.19 Flow visualisation for experiment S2A.	118
Figure 4.20 Comparison A - Regression analysis of residual flow velocity.	120
Figure 4.21 Comparison A – Distribution analysis of residual flow velocity.	120
Figure 4.22 Comparison A - Regression analysis of residual flow direction.	121
Figure 4.23 Comparison A – Distribution analysis of residual flow direction.	121
Figure 4.24 Experiment layouts for Comparison B: S1A and S1B.	123
Figure 4.25 Closer detail of velocity at (300,200).....	124
Figure 4.26 Closer detail of velocity at (200,400).....	124
Figure 4.27 Closer detail of velocity at (225,440).....	124
Figure 4.28 Closer detail of velocity at (200,440).....	124
Figure 4.29 Map of depth averaged velocity plots for Comparison B: S1A and S1B.	125
Figure 4.30 Closer detail of velocity at (225,525).....	126
Figure 4.31 Closer detail of velocity at (225,550).....	126
Figure 4.32 Closer detail of velocity at (200,500).....	126
Figure 4.33 Closer detail of velocity at (200,550).....	126
Figure 4.34 Comparison B - Velocity contour maps at elevations of 50, 100, 150, 200 and 250 mm above the bed during the ebb tide.	129
Figure 4.35 Comparison B - Velocity contour maps at elevations of 50, 100, 150, 200 and 250 mm above the bed during low tide.	130
Figure 4.36 Comparison B - Velocity contour maps at elevations of 50, 100, 150, 200 and 250 mm above the bed during the flood tide.	131
Figure 4.37 Comparison B - Velocity contour maps at elevations of 50, 100, 150, 200 and 250 mm above the bed during high tide.	132
Figure 4.38 Comparison B – Contour maps of residual velocity magnitude and direction at elevations of 50, 100, 150, 200 and 200 mm from the bed.	134

Contents

Figure 4.39 Flow visualisation for experiment S1A.	136
Figure 4.40 Flow visualisation for experiment S1B.	137
Figure 4.41 Comparison B - Regression analysis of residual flow velocity.	139
Figure 4.42 Comparison B – Distribution analysis of residual flow velocity.	139
Figure 4.43 Comparison B - Regression analysis of residual flow direction.	140
Figure 4.44 Comparison B – Distribution analysis of residual flow direction.	140
Figure 4.45 Experiment layouts for Comparison C: S2A, S2B, S2C and S2D.	141
Figure 4.46 Map of depth averaged velocity plots for Comparison C: S2A, S2B, S2C and S2D.	143
Figure 4.47 Closer detail of velocity at (150,350).....	144
Figure 4.48 Closer detail of velocity at (200,100).....	144
Figure 4.49 Closer detail of velocity at (175,440).....	144
Figure 4.50 Closer detail of velocity at (225,440).....	144
Figure 4.51 Closer detail of velocity at (200,440).....	144
Figure 4.52 Closer detail of velocity at (200,400).....	144
Figure 4.53 Closer detail of velocity at (200,550).....	146
Figure 4.54 Closer detail of velocity at (225,550).....	146
Figure 4.55 Closer detail of velocity at (200,525).....	146
Figure 4.56 Closer detail of velocity at (225,525).....	146
Figure 4.57 Closer detail of velocity at (200,500).....	146
Figure 4.58 Closer detail of velocity at (225,500).....	146
Figure 4.59 Comparison C - Velocity contour maps at elevations of 50, 100, 150, 200 and 250 mm above the bed during the ebb tide.....	149
Figure 4.60 Comparison C - Velocity contour maps at elevations of 50, 100, 150, 200 and 250 mm above the bed during low tide.	150
Figure 4.61 Comparison C - Velocity contour maps at elevations of 50, 100, 150, 200 and 250 mm above the bed during the flood tide.	151
Figure 4.62 Comparison C - Velocity contour maps at elevations of 50, 100, 150, 200 and 250 mm above the bed during high tide.	152

Figure 4.63 Comparison C – Contour maps of residual velocity magnitude and direction at elevations of 50, 100, 150, 200 and 200 mm from the bed.	154
Figure 4.64 Flow visualisation for experiment S2A.	155
Figure 4.65 Flow visualisation for experiment S2B.	156
Figure 4.66 Flow visualisation for experiment S2C.	157
Figure 4.67 Flow visualisation for experiment S2D.	158
Figure 4.68 Comparison C - Regression analysis of residual flow velocity.	160
Figure 4.69 Comparison C – Distribution analysis of residual flow velocity.	160
Figure 4.70 Comparison C - Regression analysis of residual flow direction.	161
Figure 4.71 Comparison C – Distribution analysis of residual flow direction.	161
Figure 4.72 Experient layouts for Comparison G: R2A, R2B, R2C, R2D. ...	162
Figure 4.73 Closer detail of velocity at (200,400).	163
Figure 4.74 Closer detail of velocity at (250,450).	163
Figure 4.75 Closer detail of velocity at (225,475).	163
Figure 4.76 Closer detail of velocity at (250,475).	163
Figure 4.77 Map of depth averaged velocity plots for Comparison G: R2A, R2B, R2C, R2D.	164
Figure 4.78 Closer detail of velocity at (250,525).	166
Figure 4.79 Closer detail of velocity at (250,550).	166
Figure 4.80 Closer detail of velocity at (225,525).	166
Figure 4.81 Closer detail of velocity at (225,550).	166
Figure 4.82 Comparison G - Velocity contour maps at elevations of 50, 100, 150, 200 and 250 mm above the bed during the ebb tide.	169
Figure 4.83 Comparison G - Velocity contour maps at elevations of 50, 100, 150, 200 and 250 mm above the bed during low tide.	170
Figure 4.84 Comparison G - Velocity contour maps at elevations of 50, 100, 150, 200 and 250 mm above the bed during the flood tide.	171
Figure 4.85 Comparison G - Velocity contour maps at elevations of 50, 100, 150, 200 and 250 mm above the bed during high tide.	172

Contents

Figure 4.86 Comparison G – Contour maps of residual velocity magnitude and direction at elevations of 50, 100, 150, 200 and 200 mm from the bed.	174
Figure 4.87 Whirlpool to left of TRS during tank filling.	175
Figure 4.88 Evidence of whirlpool left in dust once tank is emptied.	175
Figure 4.89 Flow visualisation for experiment R2A.	176
Figure 4.90 Flow visualisation for experiment R2B.	177
Figure 4.91 Flow visualisation for experiment R2C.	178
Figure 4.92 Flow visualisation for experiment R2D.	179
Figure 4.93 Comparison G - Regression analysis of residual flow velocity.	181
Figure 4.94 Comparison G – Distribution analysis of residual flow velocity.	181
Figure 4.95 Comparison G - Regression analysis of residual flow direction.	182
Figure 4.96 Comparison G – Distribution analysis of residual flow direction.	182
Figure 5.1 Experiment layout and bed materials for Comparison D: B1, B2, B3 and B4.	188
Figure 5.2 Map of depth averaged velocity plots for Comparison D: B1, B2, B3 and B4.	190
Figure 5.3 Closer detail of velocity at (100,100).	191
Figure 5.4 Closer detail of velocity at (200,100).	191
Figure 5.5 Closer detail of velocity at (300,100).	191
Figure 5.6 Closer detail of velocity at (200,400).	191
Figure 5.7 Closer detail of velocity at (150,350).	192
Figure 5.8 Closer detail of velocity at (350,350).	192
Figure 5.9 Closer detail of velocity at (350,450).	192
Figure 5.10 Closer detail of velocity at (175,440).	192
Figure 5.11 Closer detail of velocity at (175,525).	194
Figure 5.12 Closer detail of velocity at (225,525).	194
Figure 5.13 Comparison D - Velocity contour maps at elevations of 50, 100, 150, 200 and 250 mm above the bed during the ebb tide.	197
Figure 5.14 Comparison D - Velocity contour maps at elevations of 50, 100, 150, 200 and 250 mm above the bed during low tide.	198

Figure 5.15 Comparison D - Velocity contour maps at elevations of 50, 100, 150, 200 and 250 mm above the bed during the flood tide.	199
Figure 5.16 Comparison D - Velocity contour maps at elevations of 50, 100, 150, 200 and 250 mm above the bed during high tide.	200
Figure 5.17 Comparison D – Contour maps of residual velocity magnitude and direction at elevations of 50, 100, 150, 200 and 200 mm from the bed.	202
Figure 5.18 Comparison D - Regression analysis of residual flow velocity.	204
Figure 5.19 Comparison D – Distribution analysis of residual flow velocity.	204
Figure 5.20 Comparison D - Regression analysis of residual flow direction.	205
Figure 5.21 Comparison D – Distribution analysis of residual flow direction.	205
Figure 5.22 Experient layout for Comparison E: B1, B5 and B6.	206
Figure 5.23 Bed configuration of experiments a) B5 and b) B6.	206
Figure 5.24 Map of depth averaged velocity plots for Comparison E: B1, B5 and B6.	207
Figure 5.25 Closer detail of velocity at (150,350).	208
Figure 5.26 Closer detail of velocity at (200,400).	208
Figure 5.27 Closer detail of velocity at (175,440).	208
Figure 5.28 Closer detail of velocity at (225,500).	210
Figure 5.29 Closer detail of velocity at (225,550).	210
Figure 5.30 Closer detail of velocity at (200,500).	210
Figure 5.31 Closer detail of velocity at (200,550).	210
Figure 5.32 Closer detail of velocity at (175,500).	210
Figure 5.33 Closer detail of velocity at (175,550).	210
Figure 5.34 Comparison E – Velocity contour maps at elevations of 50, 100, 150, 200 and 250 mm above the bed during the ebb tide.	213
Figure 5.35 Comparison E – Velocity contour maps at elevations of 50, 100, 150, 200 and 250 mm above the bed during low tide.	214
Figure 5.36 Comparison E – Velocity contour maps at elevations of 50, 100, 150, 200 and 250 mm above the bed during the flood tide.	215

Figure 5.37 Comparison E – Velocity contour maps at elevations of 50, 100, 150, 200 and 250 mm above the bed during high tide.	216
Figure 5.38 Comparison E – Contour maps of residual velocity magnitude and direction at elevations of 50, 100, 150, 200 and 200 mm from the bed.	218
Figure 5.39 Flow visualisation for experiment B1.....	219
Figure 5.40 Comparison E - Regression analysis of residual flow velocity.	221
Figure 5.41 Comparison E – Distribution analysis of residual flow velocity.	221
Figure 5.42 Comparison E - Regression analysis of residual flow direction.	222
Figure 5.43 Comparison E – Distribution analysis of residual flow direction.	222
Figure 6.1 Experient layouts for Comparison F i: S0 and R0.	227
Figure 6.2 Closer detail of flow velocity at (100,400).	228
Figure 6.3 Closer detail of flow velocity at (200,400).	228
Figure 6.4 Closer detail of flow velocity at (350,250).	228
Figure 6.5 Map of depth averaged velocity plots for Comparison F i: S0 and R0.	229
Figure 6.6 Comparison F i - Velocity contour maps at elevations of 50, 100, 150, 200 and 250 mm above the bed during the ebb tide.	231
Figure 6.7 Comparison F i - Velocity contour maps at elevations of 50, 100, 150, 200 and 250 mm above the bed during low tide.	232
Figure 6.8 Comparison F i - Velocity contour maps at elevations of 50, 100, 150, 200 and 250 mm above the bed during the flood tide.	233
Figure 6.9 Comparison F i - Velocity contour maps at elevations of 50, 100, 150, 200 and 250 mm above the bed during high tide.	234
Figure 6.10 Comparison F i – Contour maps of residual velocity magnitude and direction at elevations of 50, 100, 150, 200 and 200 mm from the bed.	236
Figure 6.11 Comparison F i - Regression analysis of residual flow velocity.	238
Figure 6.12 Comparison F i – Distribution analysis of residual flow velocity.	238

Figure 6.13 Comparison F i - Regression analysis of residual flow direction.	239
Figure 6.14 Comparison F i – Distribution analysis of residual flow direction.	239
Figure 6.15 Experient layouts for Comparison F ii: S1A and R1.....	240
Figure 6.16 Map of depth averaged velocity plots for Comparison F ii: S1A and R1.	241
Figure 6.17 Closer detail of velocity at (200,550).....	242
Figure 6.18 Closer detail of velocity at (200,525).....	242
Figure 6.19 Comparison F ii – Velocity contour maps at elevations of 50, 100, 150, 200 and 250 mm above the bed during the ebb tide.	245
Figure 6.20 Comparison F ii – Velocity contour maps at elevations of 50, 100, 150, 200 and 250 mm above the bed during low tide.	246
Figure 6.21 Comparison F ii – Velocity contour maps at elevations of 50, 100, 150, 200 and 250 mm above the bed during the flood tide.	247
Figure 6.22 Comparison F ii – Velocity contour maps at elevations of 50, 100, 150, 200 and 250 mm above the bed during high tide.	248
Figure 6.23 Comparison F ii – Contour maps of residual velocity magnitude and direction at elevations of 50, 100, 150, 200 and 200 mm from the bed.	250
Figure 6.24 Flow visualisation for experiment S1A.	252
Figure 6.25 Flow visualisation for experiment R1.	252
Figure 6.26 Comparison F ii - Regression analysis of residual flow velocity.	254
Figure 6.27 Comparison F ii – Distribution analysis of residual flow velocity.	254
Figure 6.28 Comparison F ii - Regression analysis of residual flow direction.	255
Figure 6.29 Comparison F ii – Distribution analysis of residual flow direction.	255
Figure 6.30 Experient layouts for Comparison F iii: S2A and R2A.....	256
Figure 6.31 Closer detail of velocity at (200,100).....	257
Figure 6.32 Closer detail of velocity at (200,300).....	257

Figure 6.33 Map of depth averaged velocity plots for Comparison F iii: S2A and R2A.....	258
Figure 6.34 Comparison F iii - Velocity contour maps at elevations of 50, 100, 150, 200 and 250 mm above the bed during the ebb tide.	261
Figure 6.35 Comparison F iii - Velocity contour maps at elevations of 50, 100, 150, 200 and 250 mm above the bed during low tide.	262
Figure 6.36 Comparison F iii - Velocity contour maps at elevations of 50, 100, 150, 200 and 250 mm above the bed during the flood tide.	263
Figure 6.37 Comparison F iii - Velocity contour maps at elevations of 50, 100, 150, 200 and 250 mm above the bed during high tide.	264
Figure 6.38 Comparison F iii – Contour maps of residual velocity magnitude and direction at elevations of 50, 100, 150, 200 and 200 mm from the bed.	266
Figure 6.39 Flow visualisation for experiment S2A.	268
Figure 6.40 Flow visualisation for experiment R2A.	268
Figure 6.41 Comparison F iii - Regression analysis of residual flow velocity.	270
Figure 6.42 Comparison F iii – Distribution analysis of residual flow velocity.	270
Figure 6.43 Comparison F iii - Regression analysis of residual flow direction.	271
Figure 6.44 Comparison F iii – Distribution analysis of residual flow direction.	271
Figure 6.45 Experient layouts for Comparison F iv: S2B and R2D.	272
Figure 6.46 Closer detail of flow velocity at (150,350).	272
Figure 6.47 Map of depth averaged velocity plots for Comparison F iv: S2B and R2D.....	273
Figure 6.48 Closer detail of velocity at (150,550).....	275
Figure 6.49 Closer detail of velocity at (175,550).....	275
Figure 6.50 Closer detail of velocity at (250,550).....	275
Figure 6.51 Closer detail of velocity at (225,550).....	275
Figure 6.52 Closer detail of velocity at (200,550).....	275
Figure 6.53 Comparison F iv - Velocity contour maps at elevations of 50, 100, 150, 200 and 250 mm above the bed during the ebb tide.	278

Figure 6.54 Comparison F iv - Velocity contour maps at elevations of 50, 100, 150, 200 and 250 mm above the bed during low tide.	279
Figure 6.55 Comparison F iv - Velocity contour maps at elevations of 50, 100, 150, 200 and 250 mm above the bed during the flood tide.	280
Figure 6.56 Comparison F iv - Velocity contour maps at elevations of 50, 100, 150, 200 and 250 mm above the bed during high tide.	281
Figure 6.57 Comparison F iv – Contour maps of residual velocity magnitude and direction at elevations of 50, 100, 150, 200 and 200 mm from the bed.	283
Figure 6.58 Flow visualisation for experiment S2B.	285
Figure 6.59 Flow visualisation for experiment R2D.	285
Figure 6.60 Comparison F iv - Regression analysis of residual flow velocity.	287
Figure 6.61 Comparison F iv – Distribution analysis of residual flow velocity.	287
Figure 6.62 Comparison F iv - Regression analysis of residual flow direction.	288
Figure 6.63 Comparison F iv – Distribution analysis of residual flow direction.	288
Figure 7.1 Model domain of idealised a) square and b) rectangular TRSs.	308
Figure 7.2 Water level inflow boundary conditions for Delft3D model.	310
Figure 7.3 Velocity inflow boundary conditions for Delft3D model.	311
Figure 7.4 Discharge inflow boundary conditions for Delft3D model.	312
Figure 7.5 Experiment S0 depth averaged velocity results for different inflow boundaries in Delft3D, black: ADVP measurements, red: water level inflow boundary, blue: velocity inflow boundary, yellow: discharge inflow boundary results.	314
Figure 7.6 Regression analysis of experiment S0 depth averaged velocity results for different inflow boundaries in Delft3D, red: water level inflow boundary, blue: velocity inflow boundary, yellow: discharge inflow boundary results.	315
Figure 7.7 Root mean square error of Delft3D models calibrated with water, velocity and discharge inflow boundaries.	316

Figure 7.8 Water level results from water level inflow boundary model at (15,15).	316
Figure 7.9 Water level results from velocity inflow boundary model at (15,15).	317
Figure 7.10 Water level results from discharge inflow boundary model at (15,15).	317
Figure 7.11 a) Single inflow boundary and b) inflow boundary in four sections in Delft3D model.	319
Figure 7.12 Velocity values for Delf3D inflow boundary in four sections....	320
Figure 7.13 Discharge values for Delft3D inflow boundary in four sections.	320
Figure 7.14 Depth averaged velocity results from Delf3D model with discharge and velocity boundaries split into four sections.	321
Figure 7.15 Water level results from Delft3D model with discharge inflow boundary split into four sections at (50,50).	321
Figure 7.16 Depth averaged velocity results varying Manning's n.	323
Figure 7.17 Depth averaged velocity results varying horizontal eddy viscosity.	323
Figure 7.18 S2B 3D trial, velocity time series for different layers at (50,50).	327
Figure 7.19 S2B velocity time series of 2D vs 3D trials at (50,50) (2D results not visible after 80 seconds as they align with 3D results).	327
Figure 8.1 Evidence of asymmetric flow in tidal basin.....	335
Figure 8.2 Holding basin components adapted to address asymmetric flow.	338

List of Tables

Table 2.1 Advantages and disadvantages of different forms of TRS.	13
Table 2.2 Details of existing tidal range power plants worldwide.	25
Table 2.3 Most recent UK TRS proposals.....	29
Table 2.4 Advantages of TRE schemes, listed alphabetically by source.	31
Table 2.5 Perceived negative impacts of TRSs and their sources.	34
Table 3.1 Potential tidal range schemes in the UK (Hendry, 2016).....	67
Table 3.2 Proposed scales for testing TRSs in tidal basin.	71
Table 3.3 Scale parameters applied to design aspects of proposed TRSs in the Severn Estuary for testing in the laboratory.	73
Table 3.4 Proposed TRS schemes from the Hendry Review (2016) scaled to fit the size of the physical model.	75
Table 3.5 Dimensions of square and rectangular TRSs tested in the HRC.	77
Table 3.6 Experiment variables for each test, including geometry, number and position of turbines and bed conditions as denoted by the test code. ...	80
Table 3.7 Turbine layout for test configurations of square cases. Numbers 1 to 10 represent box section number.....	82
Table 3.8 Turbine layout for test configuration of rectangular case. Numbers 1 to 14 represent box section number.....	82
Table 4.1 Turbine layout for test configurations of square cases. Numbers 1 to 10 represent box section number.....	96
Table 4.2 Comparison A - Statistical analysis of residual velocity magnitude of S1A and S2A compared to S0.	122
Table 4.3 Comparison B - Statistical analysis of residual velocity magnitude of S1A and S1B compared to S0.	138
Table 4.4 Comparison C - Statistical analysis of residual velocity magnitude of S2A, S2B, S2C and S2D compared to S0.	159
Table 4.5 Comparison G - Statistical analysis of residual velocity magnitude of R2A, R2B, R2C and R2D compared to R0.	180
Table 5.1 Test cases for bed materials in a square TRS.	186
Table 5.2 Comparison D - Statistical analysis of residual velocity magnitude of B2, B3 and B4 compared to B1.....	203

Table 5.3 Comparison E - Statistical analysis of residual velocity magnitude of B5 and B6 compared to B1.	220
Table 6.1 Turbine layout for test configuration of square and rectangular case. Numbers 1 to 14 represent box section number.	225
Table 6.2 Comparison F – Statistical analysis of residual velocity magnitude.	237
Table 6.3 Discussion of regression analysis between experiments and pre-lagoon conditions (Graphs in Annex 2).	289
Table 6.4 Discussion of regression analysis between experiments and pre-lagoon conditions (Graphs in Annex 3).	294
Table 8.1 Laboratory challenges, tested solutions and their impacts.	332
Table 8.2 Evaluation of solutions to challenge of asymmetric flow.	336
Table 8.3 Potential issues with ADVPs and how they were overcome.	340
Table A1.0.1 Timeline and outcomes of studies on TST spacing.	369
Table A5.0.1 Test schedule for turbine spacing in idealised square lagoon.	406
Table A5.0.2 Dimensions for varying lagoon length-to-width ratio with constant area.	407
Table A5.0.3 Scaled dimensions of proposed TRSs.	408

Nomenclature

Abbreviations

0D	Zero-dimensional
1D	One-dimensional
2D	Two-dimensional
3D	Three-dimensional
ADV	Acoustic Doppler Velocimeter
ADVP	Acoustic Doppler Velocity Profiler
BEIS	Department for Business, Energy and Industrial Strategy
BODC	British Oceanographic Data Centre
CFD	Computational Fluid Dynamics
D3D	Delft3D
DECC	Department for Energy and Climate Change
HEV	Horizontal Eddy Viscosity
HRC	Hydro-environmental Research Centre
MRE	Marine Renewable Energy
PIV	Particle Image Velocimetry
RMSE	Root Mean Square Error
SNR	Signal to Noise Ratio
TRE	Tidal Range Energy
TRS	Tidal Range Structure
TST	Tidal Stream Turbine

Physical Experiment Codes

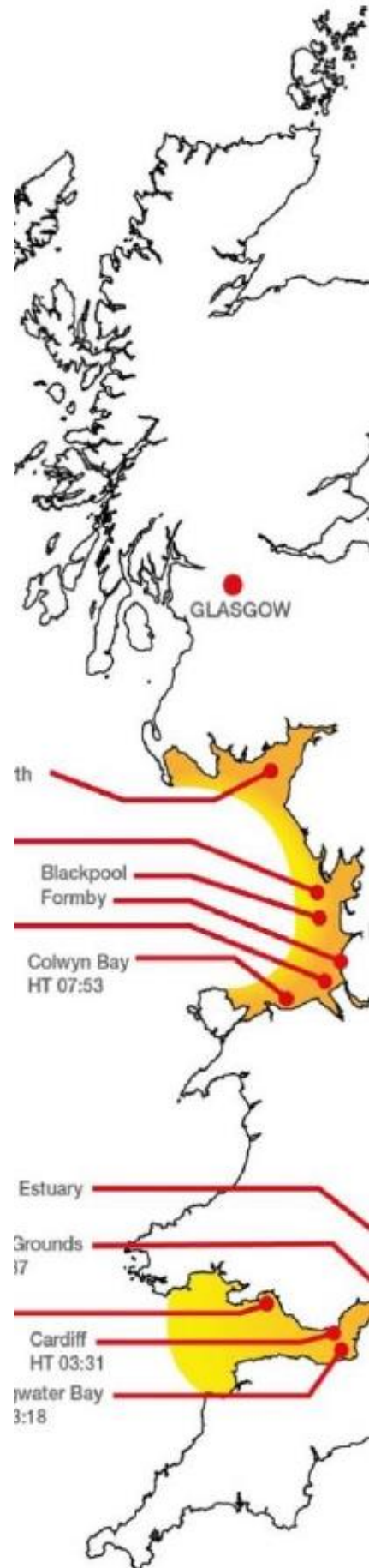
Test Code	Geometry	Number of Turbines	Slope	Bed material
00	N/A	0	0°	Smooth plastic
S0	Square	0	0°	Smooth plastic
S1A	Square	1	0°	Smooth plastic
S1B	Square	1	0°	Smooth plastic
S2A	Square	2	0°	Smooth plastic
S2B	Square	2	0°	Smooth plastic
S2C	Square	2	0°	Smooth plastic
S2D/ B1	Square	2	0°	Smooth plastic
B2	Square	2	0°	20 mm grass
B3	Square	2	0°	20 mm gravel
B4	Square	2	0°	10 mm gravel
B5	Square	2	10°	Smooth plastic
B6	Square	2	5°	Smooth plastic
R0	Rectangle	0	0°	Smooth plastic
R1	Rectangle	1	0°	Smooth plastic
R2A	Rectangle	2	0°	Smooth plastic
R2B	Rectangle	2	0°	Smooth plastic
R2C	Rectangle	2	0°	Smooth plastic
R2D	Rectangle	2	0°	Smooth plastic

List of symbols

Symbol	Units	Definition
A	m ²	Area
d	m	Water depth
Fr	-	Froude number
G	-	Distortion ratio
<i>h</i>	m	Water level
<i>l</i>	m	Length
λ	s	Tidal Period
n	m	Manning's n
m	-	Model
p	-	Prototype
Q	m ³ /s	Discharge
<i>r</i>	-	Pearson's Correlation Coefficient
Re	-	Reynold's number
s	-	Variance (standard deviation)
T	s	Time
<i>u</i>	m/s	Velocity in x-direction
U	m/s	Maximum velocity
<i>v</i>	m/s	Velocity in y-direction
V	m/s	Velocity
<i>w</i>	m/s	Resultant velocity magnitude
ω	degrees	Resultant velocity direction
Wi	m	Width opening
<i>x</i>	-	x-variable
X	-	Horizontal length scale
<i>y</i>	-	y-variable
Y	-	Vertical length scale

Chapter 1

Introduction



1 Introduction

1.1 Research Background

Staring out to sea it is not hard to imagine the immense power held within its watery depths. The sea brings us food and refreshment, affects our mood and our climate, we rely on it for trade and transport and on a calm sunny day for fun and recreation, but so far, we do not look to the sea for our energy.

Tidal range energy (TRE) exploits the potential energy from the head difference between high and low tides, using turbines traditionally housed in the seawall of a barrage or lagoon (this technology is discussed in greater detail in Chapter 2). Calculations of the theoretical TRE potential of UK waters range from 40 to 638 TWh per year (Neill et al., 2018), with the larger figure representing more than double the current annual electricity demand of the UK of 300 TWh (Department for Business, Energy and Industrial Strategy, 2021). More conservative models estimate an extractable resource of 50 TWh per year from tidal range energy, roughly 12% of the UK electricity market (Angeloudis, 2019), but all of these figures remain purely theoretical until tidal range structures (TRSs) are built to harness its potential.

This vast resource is not only available for the UK but also along the shores of many other countries worldwide, and the tidal range of Europe alone has the potential to produce 2190 TWh if exploited (Neill et al., 2018). With proposals for TRSs in Australia, Brazil, Mexico, India and China too, developing TRE in the UK to prove its potential could cause ripples around the world.

The urgent need for sustainable sources of energy in order to combat climate change and promote energy security is well known and has led to innovation in the energy sector but so far without the use of TRE. Unlike wind and solar power, TRE output does not vary with the weather, its structures do not require replacing every 20 to 40 years and unlike biomass, it does not require any fuel. It is clean and reliable, robust and predictable, and capable of fulfilling the energy demand of 2 million homes according to figures

1. Introduction

calculated by Hinson (2018). The potential along the coast of Wales alone is as rich as a seam of coal, as yet untouched, but why?

Just as the tide itself washes in and out with undeniable reliability, so too the idea of utilising the power of the tide washes in and out of the news with indefatigable regularity. The demand for clean and sustainable energy in the fight against climate change races like waves up the beach, whilst fears of the expense and environmental risk of such projects ebb the ideas out to sea once more.

The inarguable benefits of tidal range energy are:

- Its predictability and reliability as an alternative to coal and other fossil fuels for providing base load power (Hendry, 2016).
- Its cleanliness, with no chemical or noise pollution and lesser visual impact than other traditional power plants (Neill et al., 2018).
- Its proximity to demand in densely populated coastal areas, paving the way for changes to a decentralised grid for the future (Yates et al., 2013).
- The addition of new infrastructure to regenerate coastal areas, providing both industry and flood prevention in the face of rising sea levels (Waters and Aggidis, 2016b).
- Answering the demand for sustainable energy to meet the needs of a growing population whilst fulfilling national and international energy targets (Waters and Aggidis, 2016b).
- The development of a new industry at home in the UK, where the potential for utilising TRE is extensive (Hendry, 2016).

It has also been voiced that if properly managed, Marine Renewable Energy (MRE) projects can benefit ecology (Inger et al., 2009), the economy, and wider society (Petley et al., 2019).

Whilst the positive aspects of TRE are clearly visible, the negative impacts are somewhat more difficult to fathom and it is this dive into uncharted waters that have caused repeated hesitation for the development of TRE not just in the UK, but worldwide (Acadia Tidal Energy Institute, 2013). TRSs

1. Introduction

represent a large investment in infrastructure, designed to last for over a century, and it is the scale and longevity of these projects that drives the cautious approach to their development whilst many factors are still considered unknown.

Barriers to the development of tidal range energy include:

- Unknown environmental impacts, such as changes to maximum and minimum water levels, potentially leading to loss of intertidal habitats (Elliott et al., 2019).
- Changes to water current patterns and flow velocities, affecting sediment transportation and water quality (Kadiri et al., 2012).
- Irreversible alteration of delicate and significant ecosystems (Mackinnon et al., 2018).
- Interruption of fish migration and commercial fishing activities, through the introduction of physical barriers (Hooper and Austen, 2013).
- The large initial investment required to make the technology financially viable, and the implications of this on the cost of energy production (Zainol et al., 2017).
- Limited knowledge of the operation and maintenance of such a facility due to lack of existing schemes from which to learn (Angeloudis and Falconer, 2017).

Although these impacts may appear insurmountable, numerous studies have already been undertaken to reduce uncertainty surrounding tidal range technology, and with the pressing need for sustainable energy only ever growing, it is a worthwhile endeavour to address these concerns and answer once and for all whether TRE can be a sustainable solution to global energy demand.

It is often agreed that TRE is a proven technology and that as there are no major technical issues to resolve. It is only unknown environmental issues and high construction costs that remain as barriers to deployment (Mackinnon et al., 2018; Petley et al., 2019; Wang and Wang, 2019).

Therefore, research is needed to bridge the gap in understanding of

1. Introduction

interactions between TRSs and the environment to overcome obstacles to development (Copping et al., 2014).

The 2011 DECC feasibility study of tidal power in the Severn Estuary concluded that “many years of further detailed work would be needed to plan, finance and assess the impacts” of proposed TRSs (DECC, 2011, p.6). Following this report many studies have been undertaken, covering topics from potential power (Petley and Aggidis, 2016) to potential location (Yates et al., 2013), operational regime (Xia et al., 2010b) to tidal regime (Pappas et al., 2022), but very little is still known about the particular effects of the layout of TRSs.

Conventional designs restrict hydraulic structures, such as turbines and sluices, to a single area to save on construction and maintenance costs but the design as well as the operation of TRSs is important as this will affect the extent to which normal hydrodynamic conditions are altered. Existing tidal range schemes in France, South Korea, Russia and Canada provide important lessons for the deployment of TRSs (discussed in greater detail in Section 2.5.1) but gaps remain around TRS design. Whilst the performance of single turbines has been modelled extensively, and the layout of tidal stream turbines (TSTs) often comes under scrutiny, the impacts of the spacing of multiple turbines in a TRS are less well known. This oversight in the design of TRSs is worth investigating in order to learn how their configuration impacts both the environment and each other to understand how or if this can be controlled by their arrangement (Shields et al., 2011).

The aim of this study is therefore to answer the question of what effect the spacing of hydraulic structures (turbines and sluice gates) in TRSs has on the hydrodynamic environment, particularly for resultant velocity profiles and circulation patterns, both of which have a significant impact on marine life and water quality as well as impacting the kind of activities that can take place in the area. Studying these factors will thereby help determine the best layout for generating the optimum power output whilst minimising the effects on the environment, a goal shared by many other studies (Ahmadian et al., 2014; Angeloudis et al., 2018; Bijlsma, 2015).

1.2 Scope of Study

The current study deploys physical modelling to investigate the effects of TRS design on environmental conditions. This work tests TRE systems rather than tidal stream energy devices, focussing specifically on tidal range lagoon schemes rather than barrages (see Section 2.2 for technical details) as this has been identified as a knowledge gap (Mackinnon et al., 2018). Lessons can be learnt from other studies of tidal range and tidal stream technologies, and it is hoped that findings from the present study will have applications for the development of all marine renewables in general.

A literature review of current knowledge pertaining to TRSs showed that although location and operation are commonly modelled to determine power output and environmental impact, fewer studies examine other design parameters, such as the spacing of hydraulic structures or the dimensions of a TRS. This research will therefore focus on the design variables of turbine positioning as well as bed conditions and a brief comparison of lagoon geometry whilst maintaining constant tidal conditions and lagoon area. The majority of existing research also focuses on numerical modelling whilst the current study seeks to fill the research gap in terms of physical modelling to investigate the hydrodynamic impacts of TRS design.

During the study period disruptions came from a number of sources, including equipment failure, laboratory maintenance and an international pandemic, all of which had consequences on the number of variables that were able to be tested in the available time. As a result, two simplified tidal range lagoons were tested rather than the intended six specific designs. The obtained results still produce a reliable picture of the expected conditions given the development of TRSs with various designs. Numerical modelling was considered to supplement the reduced physical experiments, the results of which are discussed in Chapter 7.

1.3 Research Aims and Objectives

This research aims to answer the following questions, based on gaps identified in literature and concerns raised by political and societal voices:

1. To what extent does the presence of hydraulic structures alter the hydrodynamic environment?
2. How are baseline conditions affected by changes to hydrodynamics in the presence of hydraulic structures?
3. What difference, if any, does the spacing of turbines in tidal range schemes make to hydrodynamics?

To answer these questions, physical experiments have been designed to:

- Determine baseline conditions in an uninterrupted system with which to compare conditions once a TRS has been built in that area.
- Test the effect of different turbine spacing on water levels and flow patterns to determine the effect of TRS design on the natural environment.
- Investigate the hydrodynamic impacts of varying TRS conditions, such as bed slope and bed material.
- Collate data with which to calibrate a numerical model for the testing of more complex schemes in future.

These objectives have been designed to try to ascertain what conditions could be realistically expected if a TRS were finally to be built. It is also hoped that the answers to these questions will have applications for natural lagoons with narrow inlets, as well as being useful for the implementation of other hydraulic structures, such as coastal reservoirs, and therefore will be of interest to conservation groups and water companies. Further details of the research plan can be found in Chapter 3. Although disruption due to the pandemic altered the test schedule and some elements of the experiment design, this did not affect the aims and objectives of this research.

1.4 Thesis Outline

The thesis is organised into nine chapters:

Chapter 1: Introduction, outlining the context of the research and the motivation for the current study.

Chapter 2: Literature Review, an overview of published literature relating to the history and current state of knowledge of the research topic, setting the context of the current research and enabling the identification of knowledge gaps which this study aims to fill.

Chapter 3: Methodology – Physical Model, describing the design and execution of a physical experimental model built in Cardiff Universities' Hydro-environmental Research Centre (HRC) and used to collate data for the calibration and validation of a numerical model counterpart.

Chapter 4 to 6: Physical Model Results, presentation and discussion of the results obtained from the physical model, divided into four areas of analysis:

- i) An idealised square TRS with a smooth, flat bed.
- ii) Idealised square TRS with a smooth, sloped bed.
- iii) Idealised square TRS with a textured, flat bed.
- iv) An idealised rectangular TRS with a smooth, flat bed.

All cases have tested a number of turbine spacings to compare velocity flow fields around TRSs, discussed in greater detail in these chapters.

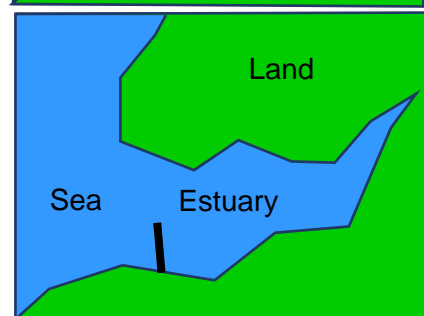
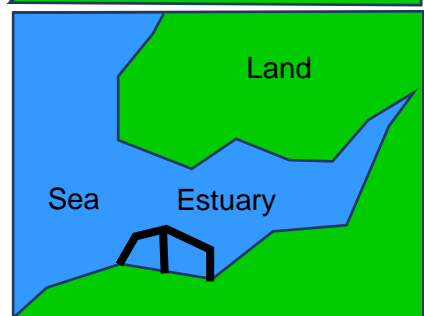
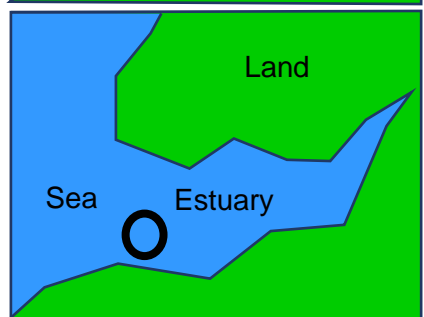
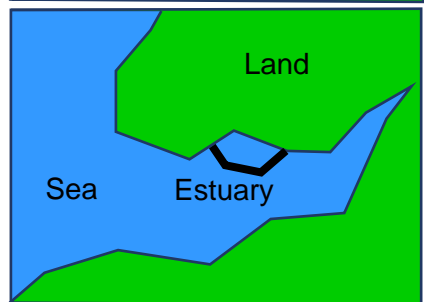
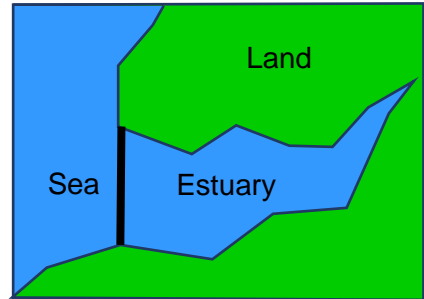
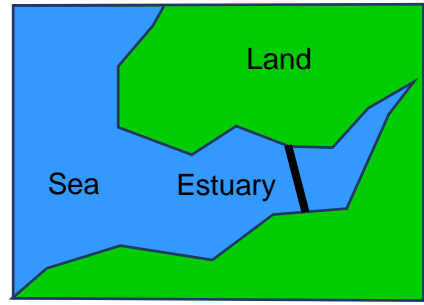
Chapter 7: Numerical Model, an exposition of the hydrodynamic computational model, Delft3D, used in this study, with detailed analysis of the calibration methods used in order to test more complex TRS designs in future.

Chapter 8: Discussion, an evaluation of the outcomes and limitations of the current study.

Chapter 9: Summary and Conclusion, an overall discussion and final remarks on the presented research alongside recommendations for potential further study and other possible applications of these findings.

Chapter 2

Literature Review



2 Literature Review

2.1 Introduction

This chapter presents the current state of knowledge found in literature relating to Tidal Range Energy (TRE). Existing studies look into: renewable energy targets and the ability of TRE to fulfil them; the comparison of TRE against other existing renewable technologies; existing TRSs and potential sites for future projects; the advantages and disadvantages of TRSs; and their design and operation. These findings have been summarised and synthesised to identify gaps in current knowledge as a basis for the present study and are reported here in order to answer the following questions:

- What is Tidal Range Energy and why is it important?
- How does it compare to other sources of renewable energy?
- What is known about it and what is there still to know?
- How can TRE be investigated further?

Key Words and Terms in Chapter 2

Marine Renewable Energy (MRE): All sources of power generated from the sea, e.g., tidal range, tidal stream, wave energy, etc.

Tidal Range Energy (TRE): Power generated from the head difference between high and low tide.

Tidal Stream Energy: Power generated from tidal currents below the water surface.

Ebb tide: The period between high and low tide when water flows away from the shore.

Flood tide: The period between high and low tide when water flow towards the shore.

Hydraulic Structures: Manmade structures that intentionally alter hydro-environmental conditions for a purpose, e.g., to divert or store water, can be fully or partially submerged, e.g., turbines, sluices, weir gates, etc.

Turbine: A device for harnessing kinetic energy from water, steam or air.

Sluice: A gate for controlling water flow.

Barrage: A barrier built to block a channel either for transport, coastal defence or power generating purposes.

Lagoon: An impounded body of water protected from a larger water body, either naturally by sandbars or barrier islands, or artificially by a seawall.

The Hendry Review: An independent commission by the UK Government in 2016 to investigate the case for tidal lagoons as a cost-effective part of the UK energy mix.

Tidal Range Structures (TRSs): Any form of barrier built to create an artificial head difference in tidal flows to generate power.

Tidal Stream Turbines (TSTs): Power generating turbines deployed underwater to harness the kinetic energy of tidal stream currents.

2.2 Tidal Range Energy Structures and Operation

The power of the tide has long captured mankind's imagination along with the desire to control its energy potential. Tidal power was first exploited by the Romans and tidal mills were used in Spain, France and Britain as long ago as the 11th century (Frau, 1993). Modern proposals for a significant tidal power plant in Britain date back to Victorian times (Neill et al., 2018) but the first large scale tidal power plant was built in France, at La Rance, in 1967 (Charlier, 2007). Since the construction at La Rance other projects have been built in Russia, China and Canada and most recently in South Korea, further details of which are discussed in Table 2.2.

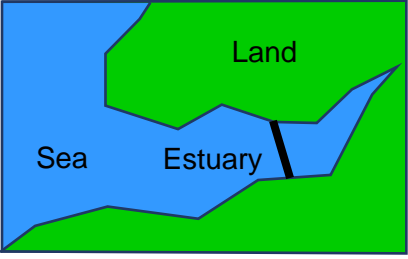
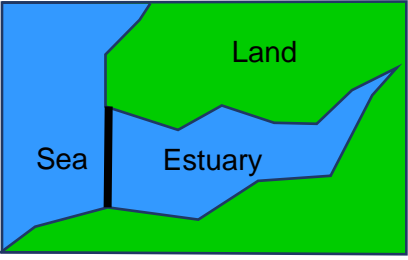
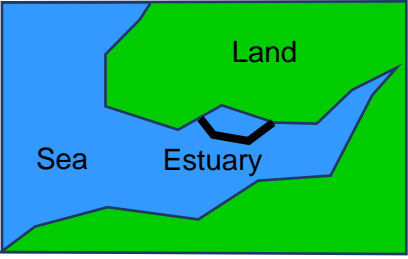
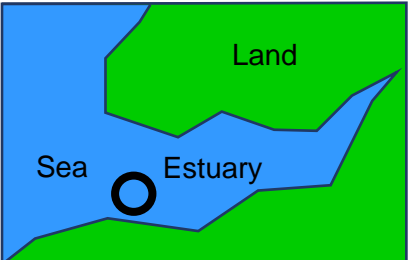
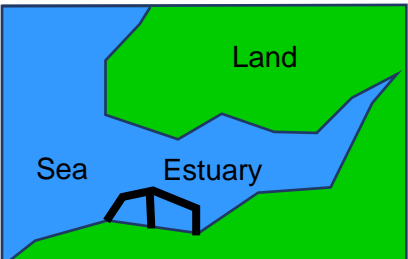
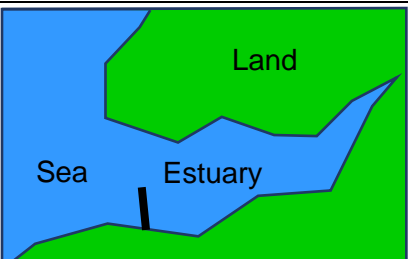
New proposals for utilising tidal range energy include lagoons, tidal reefs and tidal fences as a means for exploiting the same natural phenomenon at less environmental expense than a full barrage (Angeloudis and Falconer, 2017; Waters and Aggidis, 2016b). Although tidal lagoon schemes have been recommended since 1981, they are yet to be actualised (Petley and Aggidis, 2016).

Tidal range technology operates using the height difference between high and low tide and differs from tidal stream energy in that it uses this potential energy from water level difference rather than the kinetic energy of tidal currents below the surface. This energy is traditionally captured by building a dam or barrier across an estuary where extreme tidal ranges occur. Table 2.1 describes the different types of schemes available for extracting TRE.

The present study focuses on experiments with coastally attached tidal lagoons but as the investigation looks into the positioning of hydraulic structures it is hoped that the findings will be applicable to other TRSs too. The advantages and disadvantages of each form of TRS are also discussed.

2. Literature Review

Table 2.1 Advantages and disadvantages of different forms of TRS.

	Image	TRS Type and definition	Advantages	Disadvantages
Barrage		A seawall spanning the entire length of a river or estuary. Can operate on ebb, flood or both tides by holding water to gain the maximum head difference. Most common type of TRS, already built at multiple locations worldwide.	<ul style="list-style-type: none"> Reduced velocities lead to a decrease in sediment transport and steadier state bed conditions (Roberts et al., 2016). Barriers across a whole estuary can control water levels and offer flood protection (Ma and Adcock, 2020). Could provide additional benefits such as transport links (Burrows et al., 2009b). 	<ul style="list-style-type: none"> Reduced tidal range means a loss of intertidal zones and their associated habitats (Roberts et al., 2016). Reduction of dissolved nutrients and oxygen concentration (Roberts et al, 2016). Increased wave heights of up to 20% downstream, could lead to increased coastal erosion (Roberts et al., 2016).
Coastal Reservoir		A seawall spanning the mouth of an estuary to provide fresh water supply. Can also incorporate turbines to generate electricity during ebb tide if riverine water is released. None yet developed.	<ul style="list-style-type: none"> Provides urban regeneration and fresh water supply (Falconer et al., 2020). 	<ul style="list-style-type: none"> Not yet proven for generating tidal power (Falconer et al., 2020). Concerns over water quality during retention time (Falconer et al., 2020).
Coastally Attached Lagoon		A seawall connected to the coast without cutting off the whole estuary. Can operate on any tide. Currently only in design phase.	<ul style="list-style-type: none"> Less change to hydrodynamics and lesser loss of habitats than caused by a full barrage (Roberts et al., 2016). Less impact on tidal resonance than a barrage (Ma and Adcock, 2020). 	<ul style="list-style-type: none"> Larger cost than barrages because a longer seawall is needed to achieve the same size basin (Roberts et al., 2016). Greater change to sediment transport, requires dredging and beach nourishment to compensate (Roberts et al., 2016). Less effective at reducing flood risk than a complete barrage (Roberts et al., 2016).
Offshore Lagoon		An impoundment built away from the coast. Can operate on any tide. Currently only in design phase.	<ul style="list-style-type: none"> Greater freedom of choice of location so can ensure no competition with other marine users. Reduced impact on local community. Reduced impact on hydrodynamics (Cornett et al., 2013). 	<ul style="list-style-type: none"> Greater costs for building a longer seawall and associated infrastructure to transmit energy to shore. Loss of additional benefits such as transport and recreation as further away from society.
Linked Lagoon		An on or offshore lagoon divided into sub-basins to maximise operation time through holding water and releasing in different phases. Currently only in design phase.	<ul style="list-style-type: none"> Continuous power generation for little extra construction cost (Angeloudis et al., 2020). Less dependent on timing of tidal cycle, more control over the timing of power generation (Todeschini, 2017). 	<ul style="list-style-type: none"> Issues with bottlenecks in the grid during times of generation (Mackie et al., 2020). Only 30% of energy extracted compared to an equivalent sized single basin due to reduced head (Angeloudis et al., 2020).
Dynamic Tidal Power Scheme		A seawall perpendicular to the coast and connected at one end only. Can operate in both directions. Currently only in design phase.	<ul style="list-style-type: none"> Cheaper construction as seawall only needs to connect to coast at one end (Dai et al., 2017). 	<ul style="list-style-type: none"> Still significantly affects regional hydrodynamics, blocking tidal propagation and creating rogue waves (Dai et al., 2018).

2. Literature Review

The seawall of a tidal range scheme (TRS) houses sluices to allow water to flow in and out of the impoundment and turbines to generate electricity.

Figure 2.1 gives a plan view of La Rance barrage to give an example of the layout of a TRS whilst Figure 2.2 offers a side view of a turbine in situ. Other structures such as shipping locks or fish passages may also be included in the seawall and proposed schemes around the UK could also incorporate roads, light-railway lines or secondary sustainable energy functions such as wind turbines or floating solar panels (Pennock et al., 2022).

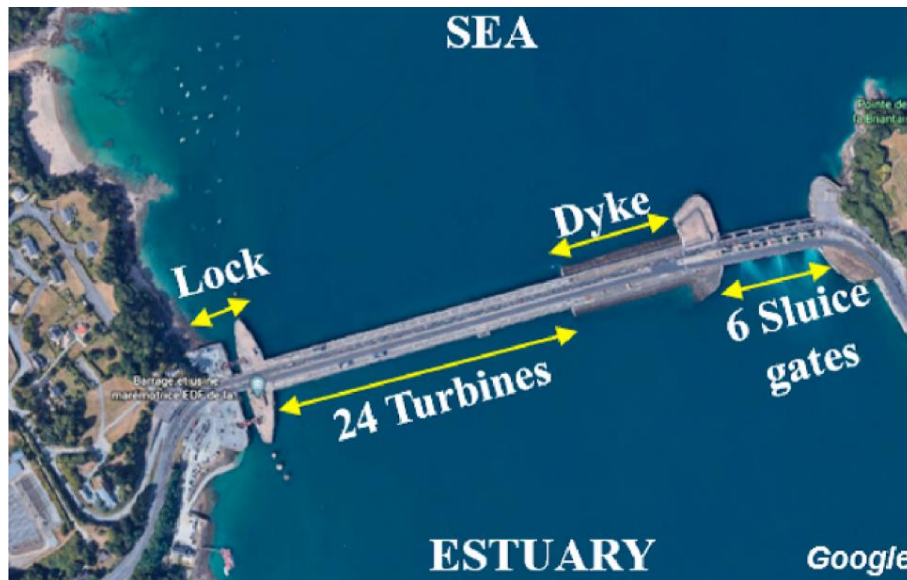


Figure 2.1 Plan view of tidal range structure at La Rance (Rtimi et al., 2021).

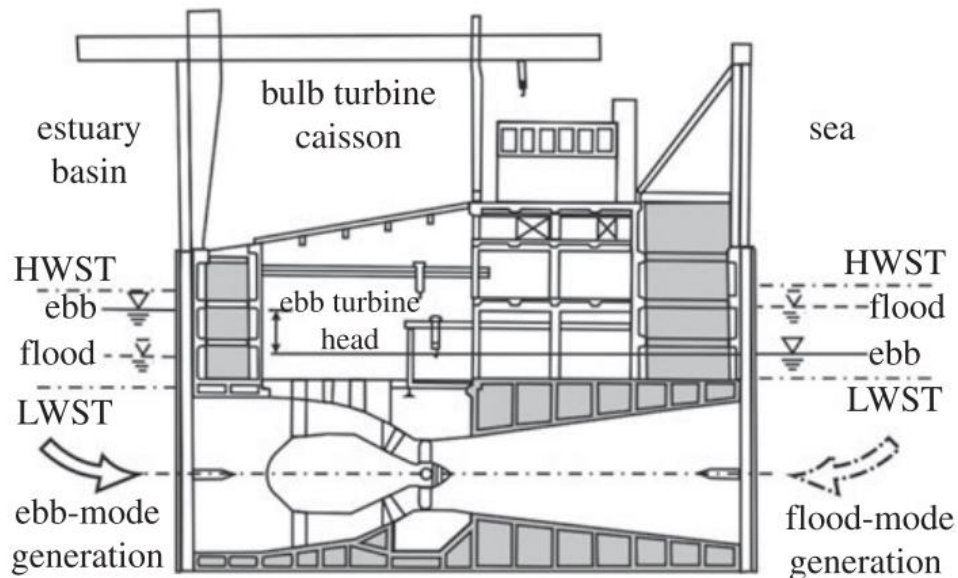


Figure 2.2 Side view of a bulb turbine caisson used TRSs (Yates et al., 2013)

2. Literature Review

Timing the closing and opening of the sluices allows water to be held behind the seawall to create an artificial tidal phase. Once water levels reach a sufficient head difference, the water is released to generate electricity through the turbines. Power can be generated on a single tide (either as the tide floods or ebbs) or on both tides, in what is known as two-way or dual mode operation. Figure 2.3 shows the water elevation on each side of the seawall during ebb only operation whilst Figure 2.4 and 2.5 show this process during flood only and two-way operation respectively.

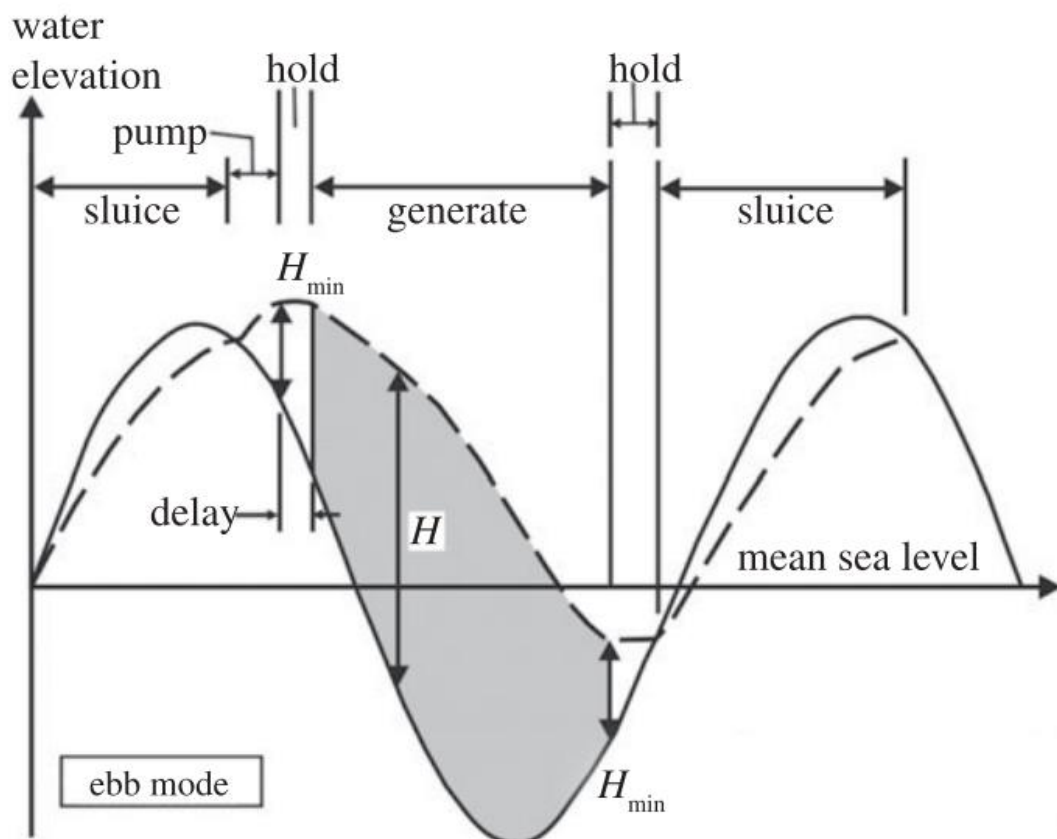


Figure 2.3 Water elevation on each side of a TRS seawall during ebb only operation, solid line: basin level, dashed line: sea level (Yates et al, 2013).

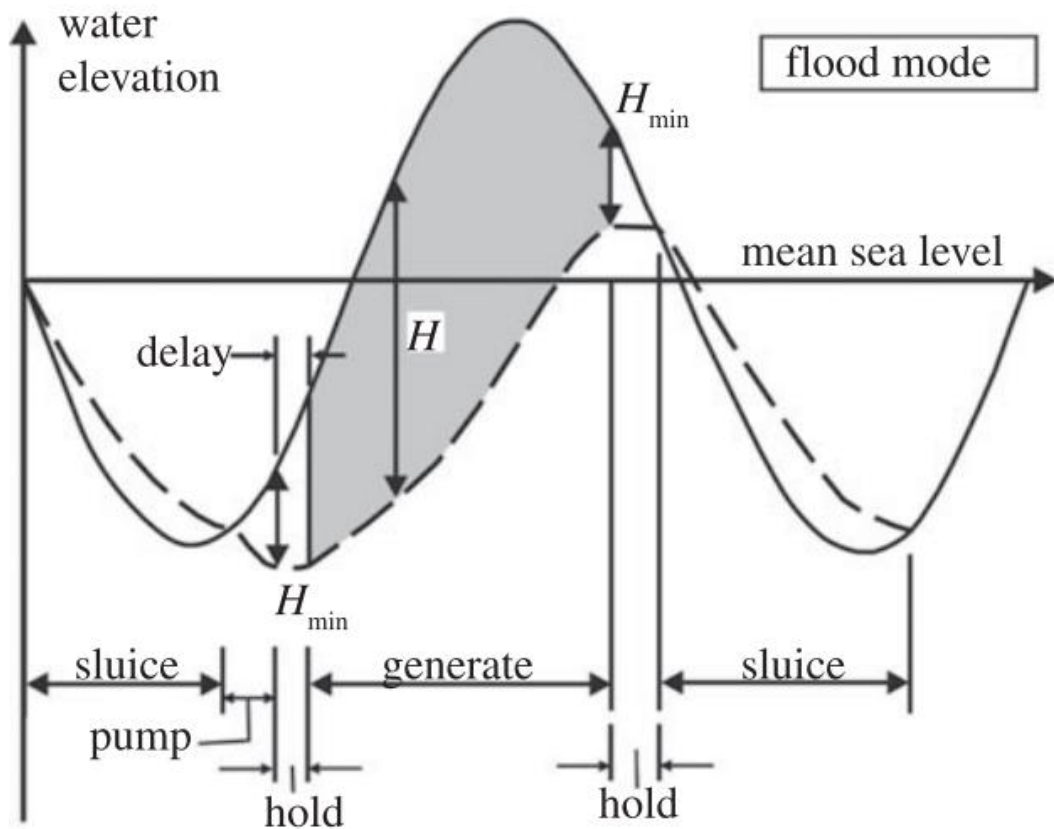


Figure 2.4 Water elevation on each side of a TRS seawall during flood only operation, solid line: basin level, dashed line: sea level (Yates et al, 2013).

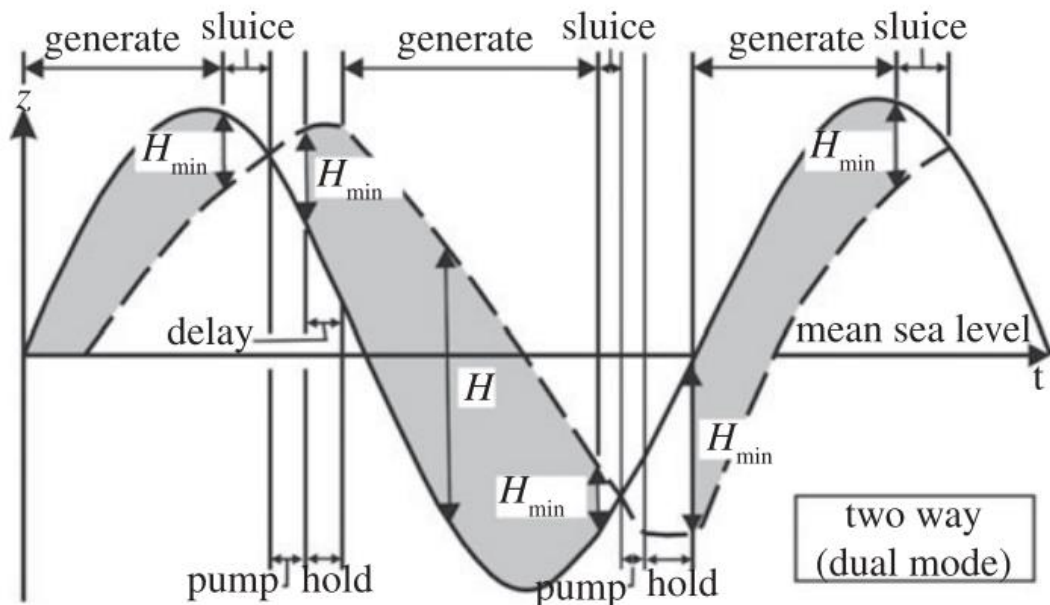


Figure 2.5 Water elevation on each side of a TRS seawall during two-way operation, solid line: basin level, dashed line: sea level (Yates et al, 2013).

2. Literature Review

Whilst generating power via two-way operation provides electricity over a longer period of time it does increase the cost of the TRS due to the need for specialised turbines that can work in both directions as well as increased operating costs (Neill et al., 2018). It also leads to a lower operating head since it is operating for longer so there is less time for filling. Operating head is key to the amount of power generated by a TRS, as shown by Equation 2.1, which shows how instantaneous potential power (P) is proportional to the surface area of the impounded water (A) multiplied by the square of the water level difference upstream and downstream of the seawall (H).

$$P \propto AH^2 \quad \text{Equation 2.1}$$

To counteract this loss in head difference, pumping can be added to the operating scheme to increase the operating head, as demonstrated in Figure 2.6.

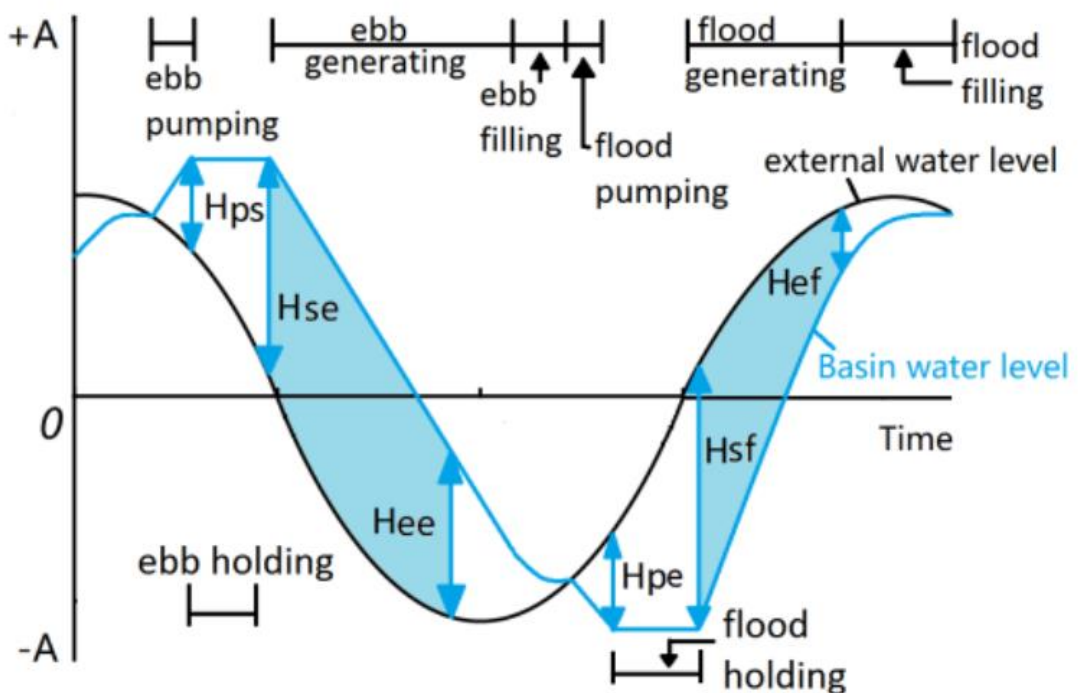


Figure 2.6 Water elevation on each side of a TRS seawall during two-way operation with the addition of pumping, solid black line: sea level, solid blue line: basin level. H_{ps} : Pumping to raise the water level and increase head difference, H_{se} : Starting head for ebb tide, H_{ee} : Ending head for ebb tide, H_{pe} : Pumping to lower the water level and increase head difference, H_{sf} : Starting head for flood tide, H_{ef} : Ending head for flood tide. (Xue et al 2019).

2. Literature Review

Further gains can be made by operating using flexible generation rather than fixed head generation, calculating the optimum head difference based on monthly variation in the tidal cycle (Guo et al., 2021). All of these options for operation mode have an impact not only on power output but also on operating costs and environmental impacts. Pumping can help generate more electricity but costs more as it requires energy to pump the water to a greater head difference. Optimising operating mode using flexible head levels requires greater computational time to tune to the right levels (Xue et al., 2020). Careful timing of electricity generation could also be the key to cost-effective operation for TRSs by balancing the time of generation with that of greatest demand and highest wholesale energy cost (Mackie et al., 2020). Operation mode can also be considered to reduce environmental impact due to the effects of each scheme on water level and tidal phase. For example, Ahmadian, et al. (2014) found that although two-way and ebb-only generation both reduce suspended sediment concentration upstream and downstream of a tidal barrage, ebb-only generation would cause a larger reduction, which would impact upon sedimentation as well as nutrient availability in the water column.

2.3 Tidal Range Energy and Renewable Energy Targets

The Paris Agreement for action on Climate Change saw 145 countries make legal commitments to reduce emissions and dependency on fossil fuels by committing to strict renewable energy targets to address growing concerns over the irreversible effects of climate change (Elliott et al., 2019). In working towards the targets of the Paris Agreement, the UK has reduced its carbon emissions by 40% since 1990 with updated targets to reduce emissions by 63% by 2035, on the way to Net Zero by 2050 (Climate Change Committee, 2021a).

The Climate Change Committee Net Zero Pathway (2021b) predicts an increase in electricity demand of 50% by 2035, whilst promoting the decarbonisation of electricity production in this time. Although targets have been met so far without TRE the final push to irradicate fossil fuels from our energy supply requires the production of baseload energy from a reliable and powerful source. Whilst on and offshore wind power has bolstered our supply thus far, the variability of this technology has been felt in recent years with high wind speeds in 2020 and low in 2021 both affecting production (Climate Change Committee, 2021b; Department for Business Energy and Industrial Strategy, 2021).

Although it is not possible to predict the exact composition of the UK's future energy supply, it is agreed that energy security will be achieved by using a variety of sources (Hendry, 2016; HM Government, 2009; Ramos et al., 2021). In 2003, DTI's vision for the future energy system of the UK, saw marine energy, including tidal power, as the basis of large power stations whilst windfarms would make a smaller contribution, that local distributed networks would dominate the system and that the national grid should be adapted accordingly (Department for Trade and Industry, 2003). Many studies have anticipated that marine energy will be vital in meeting UK renewable energy targets (Langston et al., 2010; Mackinnon et al., 2018) with Yates et al., (2013) going as far as to say that our renewable energy targets are unattainable without exploiting tidal resources. However, this is not what is seen in the current energy market or in the majority of future

2. Literature Review

planning scenarios, where offshore wind bears the brunt of the renewable energy burden (Centre for Economics and Business Research, 2014; Department of Energy and Climate Change, 2011; Langston et al., 2010; Mackinnon et al., 2018). Indeed, latest figures reveal that 15% of electricity in the UK came from wind power, a 42% share of all power generated from renewable sources, whilst MRE was not used at all (Department for Business Energy and Industrial Strategy, 2021).

Despite the proven technology and ability of tidal range power to meet each of these aims, it is still not counted within the energy mix for meeting the UK's renewable energy goals. Although the Welsh Government are committed to generating 50% of their electricity from marine energy (Department of Energy and Climate Change, 2011; Willis et al., 2010), this barely scratches the surface of the available resource and is not a major contributor to the UK's supply as a whole. From their numerical modelling, Angeloudis (2019) estimates potential energy from tidal stream sources to be capable of meeting 15% of UK demand, whilst TRE could produce 12% and the Centre for Economics and Business Research (2014) calculated that tidal lagoons would provide 24 TWh of electricity by 2030 if adopted by 2020 but this has still not been actualised.

2.4 Other Renewable Energy Sources

With a view to future energy security, the diverse range of renewable energy sources in the UK includes marine energy, biomass, wind, hydro and solar power, with nuclear power and carbon, capture, usage and storage (CCUS) seen as low carbon technologies that could also help meet emission targets. The most abundant natural resources in the UK are offshore wind and marine energy (Hendry, 2016; Renewable UK, 2016).

Marine Renewable Energy (MRE) refers to all sources of energy harvested from the sea, including tidal range, tidal stream, wave energy and saline and thermal gradients. It is estimated that the worldwide potential for MRE is 337 GW (Waters and Aggidis, 2016b) with 118 GW to be sourced in the UK alone (Hinson, 2018; Roche et al., 2016), but more modest models predict that once technological and financial hurdles are overcome, the maximum capacity of MRE would be around 4 GW by 2050, only 3% of UK demand (Parliamentary Office of Science and Technology, 2020). However, the government view is that MRE has the potential to make a significant contribution to the UK's decarbonisation targets and support hundreds of green jobs (Department for Business Energy and Industrial Strategy, 2022).

2.4.1 Hydropower

Hydropower is a highly efficient and proven technology with a large global resource. Operating on the same principle as tidal range technology, it is an attractive option in areas with a decentralised power supply and can provide opportunities for rural societies with no grid connection to gain a reliable source of electricity (Andritz, 2018). The use of hydropower is limited to locations with suitable topography and whilst tidal range schemes use the same methods as hydropower, the benefit of tidal range technology is that it can operate in both directions if needed (Zainol et al., 2017).

2.4.2 Nuclear

Nuclear power is the most advanced low carbon technology, with CCUS technology still at the experimental stage (Energy and Climate Change Committee, 2012). In 1966, McMillan saw nuclear power as "the final blow against these brave dreams of stupendous tidal projects so long beloved by

2. Literature Review

seamen and engineers” (p.179) as developers looked to embrace nuclear power over long discussed tidal range ideas.

2.4.3 Wind

Offshore wind energy is widely accepted by the public based on the removal of visual and sound pollution which had previously been of concern to onshore windfarm sites (Acadia Tidal Energy Institute, 2013). The successful and widespread deployment of wind turbines has made everyone keen to rely on this source of renewable energy to help meet our emissions targets but there will be an upper limit for what can be achieved by wind and solar power (Clarke, 2006; Hendry, 2016; O'Rourke et al., 2010). The appeal of this safe and proven technology has put people off investing in other sources, with technologies such as tidal stream and wave energy devices seen as “hobbiest” (Acadia Tidal Energy Institute, 2013).

In their latest path to Net Zero, the UK Government plans to grow the offshore wind industry capacity from 10.5 GW to 40 GW by 2030 as they aim to decarbonise electricity generation (Climate Change Committee, 2021b) but for the future of our energy supply to be secure there needs to be a diversity of sources. Wind power may be the most advanced technology, but it is also unpredictable, and variable compared to tidal range energy which is easily forecastable and does not rely on the weather. Therefore, tidal range energy could provide reserve capacity for the intermittency of wind and solar energy to reduce challenges to the grid (Denny, 2009).

2.4.4 Wave

The UK is currently the world leader in the development of wave energy devices, with two full-scale prototypes currently deployed in UK waters (Climate Change Committee, 2021b). Whilst wave power is driven by the wind, it is less variable than wind power, with currents travelling much more slowly in water than in air and are therefore somewhat forecastable (Zainol et al., 2017). Potential sites for harnessing wave energy are restricted between 40° and 60° latitude, coinciding with the strongest air streams (Harries et al., 2006) and are hampered by variability of electricity production and grid connection challenges (Uihlein and Magagna, 2016). The UK originally had a

2. Literature Review

target of producing 200-300 MW of energy from tidal and wave energy by 2020 but this has not yet been met, with the government deciding to exploit offshore wind energy based on economic considerations instead (Ramos et al., 2021).

2.4.5 Tidal Stream

Unlike TRE schemes which convert the potential energy of the height difference of tides, tidal stream projects such as turbine fences and arrays convert the kinetic energy of tidal currents (International Renewable Energy Agency, 2014; Zainol et al., 2017). Tidal stream energy devices are a proven technology with successful full-scale demonstrations in many locations (Garcia-Oliva et al., 2017) and improvements in power output efficiency that match that of wind turbines (Simmons et al., 2018). The next stage in the development of its widescale deployment is to test the logistics and impacts of turbine arrays as well as solving issues around maintenance, transmission and environmental impacts (DTOceanPlus, 2018; Myers et al., 2011). The low variability of tidal stream turbines makes them attractive as a reliable energy source (Lewis et al., 2019) and 73% of all MRE projects are based on exploiting tidal streams (Soudan, 2019). Although tidal range technology is mature, attention has turned to tidal stream turbines due to perceived lesser environmental impacts and financial cost (Suárez-López et al., 2019). The UK electricity grid has an in-built tidal stream capacity of 10 MW (equivalent to a single large offshore wind turbine) and the global capacity for tidal stream energy is currently at 45 GWh, an increase of 40 GWh in the last decade (Parliamentary Office of Science and Technology, 2020).

2.4.6 Tidal Range

Tidal range technology is at a further stage of development than other marine renewables and can be regarded as a mature technology (Neill et al., 2018; O'Rourke et al., 2010). The advantage of TRE over other renewable energy sources is that it is predictable, which makes it an attractive option for being able to balance demand. However, no TRSs have ever been built in the UK due to concerns over financial and environmental costs.

2.5 State of Knowledge of Tidal Range Energy

2.5.1 Existing Sites

Although no tidal range lagoons exist for direct study, operational tidal range barrages are available for comparison in other global locations as presented in Table 2.2. (Data presented in this table has been compiled from Charlier, 2003; Neill et al., 2018; Waters and Aggidis, 2016a; Zainol et al., 2017).

Whilst the plants at La Rance in France and Kislaya Guba in Russia were constructed before the convention of environmental impact assessments and monitoring (Hooper and Austen, 2013), Lake Sihwa in South Korea, the largest existing tidal power plant in the world, has the advantage of being monitored before and during its construction providing a knowledge base from which lessons can be learnt regarding the construction of TRSs.

2. Literature Review

Table 2.2 Details of existing tidal range power plants worldwide.

Power Plant	La Rance	Lake Sihwa	Annapolis Royal	Jiangxia	Kislaya Guba
Country	France	South Korea	Canada	China	Russia
Commissioned	1967	2011	1984	1985	1968
Tidal Range	14 m	6 m	7 m	8.4 m	9-13 m
Build Cost (M)	\$100 US	\$355 US	\$36 US	\$9.8 US	unreported
Area	22 km ²	30 km ²	6 km ²	2 km ²	2 km ²
Turbines	24	10	1	6	1
Turbine Type	Bulb	Bulb	Straflo	Bulb	Bulb
Operation	Two way	Flood	Ebb	Two way	Two way
Installed Cap.	240 MW	254 MW	20 MW	3.9 MW	1.5 MW
Annual Output	540 GWh	550 GWh	50 GWh	7 MWh	3 GWh
Details	La Rance was built as an industrial prototype during a time when there was much interest in tidal power. During its 55 years of operation, it has proved to be reliable and sustainable, with no structural issues and very little downtime as well as having a favourable impact on the regional economy (Charlier, 2007; Neill et al., 2018).	First built as a closed lake for agricultural irrigation, it became contaminated from industrial effluent and was re-opened to manage pollution (Bae et al., 2010). Tidal turbines were added to the barrage to generate electricity whilst improving flow conditions and water quality in the lake (Binnie, 2016; Neill et al., 2018).	Originally built as a transport link and flood defence, a single turbine was added to the structure to test the potential of tidal power in North America (Waters and Aggidis, 2016b). The plant was recently decommissioned following generator failure and serious concerns over fish mortality (Gibson et al., 2019; Withers, 2021).	Jiangxia is the largest tidal power plant currently operating in China. Several short-lived TRSs operated in China between 1978 and 1992 but were swiftly closed due to poor choice of location and flawed turbine designs, making projects unproductive (Waters and Aggidis, 2016a).	Harsh arctic conditions required adaptation of the technology and was the first to use the floating caisson construction method (Federov, 2010). Viewed as a success, there were plans to build larger stations but these have not yet been fulfilled (Neill et al., 2018).

2. Literature Review

2.5.2 Possible Sites Worldwide

Tidal range technology requires a large tidal range with strong predictability and therefore is best suited to areas with semi-diurnal tides. Other factors influencing suitable locations for exploiting TRE include tidal conditions, natural environment, proximity to demand, existing facilities, and above all, cost (Hendry, 2016; Mackay, 2009). Potential sites can be identified through field surveys (Willis et al., 2010), GIS searches and aerial imagery (Alifidini et al., 2018; Baig et al., 2021; Schmitt and Lieber, 2021), and numerical modelling (Prandle, 1984).

According to the World Energy Council, potential sites with large tidal range and suitable landforms are rare with only twenty-six viable sites listed worldwide (Harries et al., 2006). However, Etemadi, et al., (2011) mapped forty suitable sites whilst a study conducted by the European Commission (1996) identified 106 sites in Europe alone. Modelling of the global tidal range resource has led to estimates of a theoretical annual output of 25,880 TWh, distributed across eleven countries based on tidal range and water depths (Neill et al., 2018). Practical locations are concentrated in the Northwest European Shelf Seas in the UK and France, with other sites in Canada, Australia and the USA presenting additional possibilities. Charlier (2003) estimates a global theoretical tidal resource of 3000 GW. However, he admits that only 20% is thought to be extractable due to the head required by current technology to make the resource viable. Future development of low head turbines will increase the number of viable sites.

Although many plans have been made worldwide throughout the 20th Century, very few have come to fruition. Charlier (2003) lists the many reasons for this including financial issues (as in Argentina and the UK), political issues (South Korea and France), and geographical issues (Japan and Australia). There are thought to be brief instances of functioning plants in Iceland, Suriname and the USA with several sites developed in China by opening existing dams only to be brought to a standstill by sedimentation. In the year 2000, a proposed 48 MW tidal range project at Doctor's Creek, Australia, would have become the second largest tidal power plant in the

2. Literature Review

world but the \$75 million required in Government support, alongside environmental concerns, meant that the plan was dropped in favour of developing natural gas extraction in the area instead (Harries et al., 2006).

The most recent research in TRE from around the world looks at: resource assessment in Mexico (Mejia-Olivares et al., 2020) and Brazil (Shadman et al., 2019), new methods for site characterisation in Pakistan (Baig et al., 2021), and cost benefit analysis of energy from coastal lagoons in Portugal (Rodrigues et al., 2021).

2.5.3 Possible Sites UK

It is estimated that the UK holds 10% of the world's tidal resource and half of the potential tidal resource of Europe (Hinson, 2018; Yates et al., 2013). At present consumption rates, various models calculate that a fleet of tidal range schemes could generate between 8% and 20% of the UK's demand (Elliott et al., 2019; Waters and Aggidis, 2016b). Much of this resource lies on the west coast of the UK which experiences the extreme tidal range necessary for exploiting the resource commercially. Figure 2.7 displays the areas of greatest tidal range and potentially most viable for TRS development whilst Table 2.3 discusses the current state of TRS proposals in the UK.

Global expectation is for the UK to be the first to implement a tidal range lagoon, from which knowledge base other schemes will take shape (Elliott, et al., 2019). With designers, developers, regulators, and consultants all involved in UK projects, there is potential for exporting this expertise worldwide with interest already from countries such as Canada, New Zealand and the USA (Centre for Economics and Business Research, 2014; Department for Business Energy and Industrial Strategy, 2018; Energy and Climate Change Committee, 2012; Hendry, 2016). Therefore, it is important to develop this interest and make sure that the UK remains the market leader in this technology (Marine Energy Group, 2012; Renewable UK, 2016).

2. Literature Review

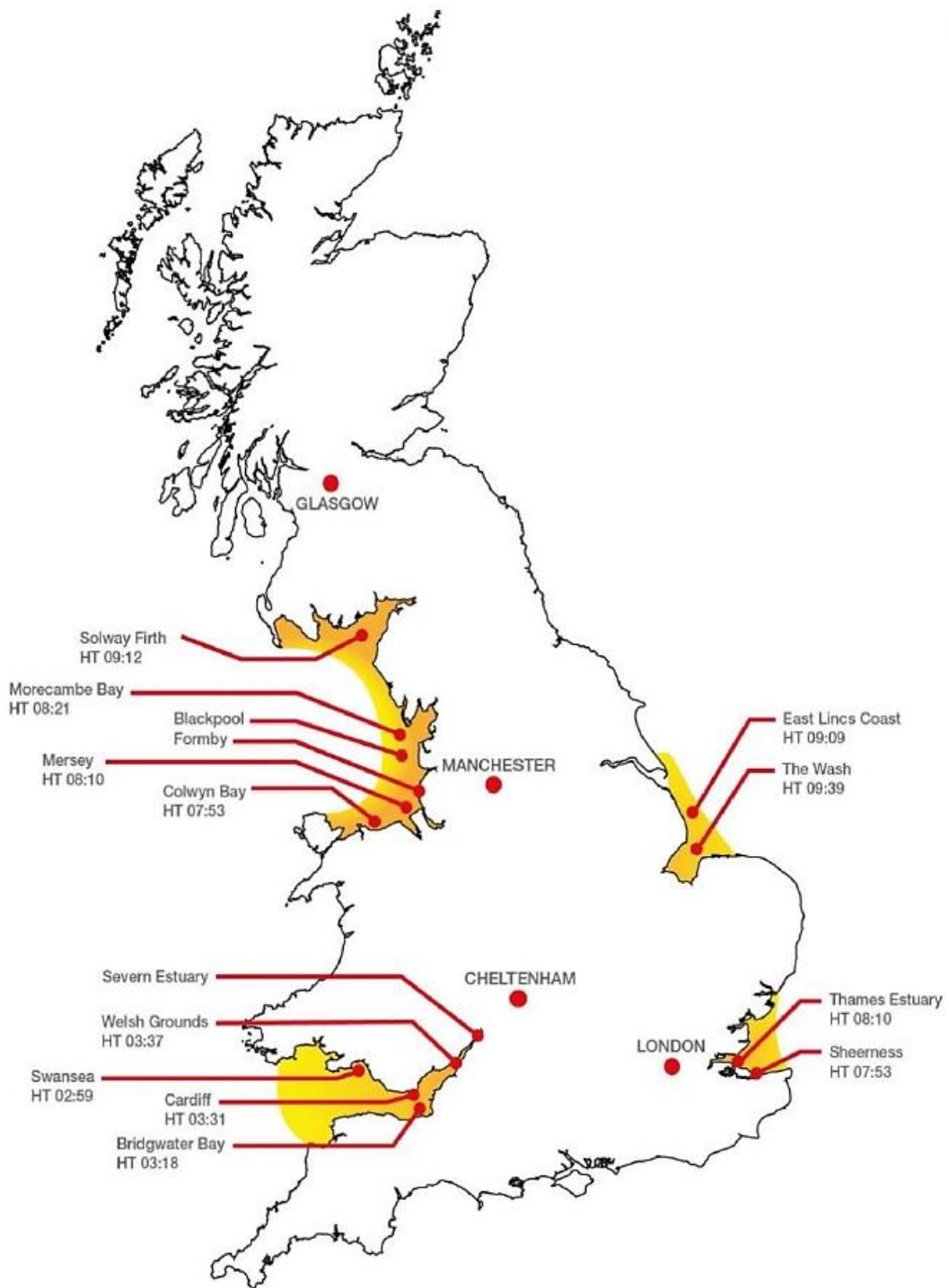


Figure 2.7 Areas of greatest tidal range around the UK coast (Tidal Lagoon Swansea Bay, 2017).

2. Literature Review

Table 2.3 Most recent UK TRS proposals.

Location	Potential Output (TWh/yr)*	Latest report
Severn Estuary		
Severn Estuary	16.8	The first detailed proposals for a barrage were discussed in the Bondi Committee Report of 1981 and although extensively modelled, no new plans are currently being discussed (Melikoglu, 2018).
Swansea	0.53	Proposed as a pathfinder project from which other schemes could learn, Swansea Bay Lagoon was granted a Development Consent Order in 2015 and TLP Ltd are seeking private financial investment whilst awaiting a Marine Planning Licence (Tidal Lagoon Swansea Bay, 2020).
Cardiff	5.5	Proposals for a tidal lagoon at Cardiff continue to be modelled alongside other sites in the Severn Estuary to investigate the cumulative impacts of developing multiple schemes in the area (Angeloudis, 2019).
Bridge-water Bay/ Minehead	2.5	Potential locations on the south shore of the Severn Estuary have provided case studies for recent numerical models of tidal range lagoon operation (Guo et al., 2021; Xue et al., 2021).
North Wales and Liverpool		
Conwy and Colwyn Bay	4.5	Research into the TRE potential of the North Wales coast have focused on synchronising the operation of a fleet of lagoons (Angeloudis et al., 2016a; Angeloudis et al., 2016b).
Mersey	0.92	Investigations into the potential development of TRE in the Mersey Estuary began in 1988. The latest research investigates the potential extended benefits of a TRS here (Petley et al., 2019) and the Mersey Tidal Power Plan has most recently been awarded £2.5m government funding (BBC News, 2020).
Northwest		
Morecambe Bay	4.63	This large hybrid, transport link/tidal barrage is currently in the review stage, engaging with research institutes, the Environment Agency and the Government's Marine Management Organisation (Northern Tidal Power Gateway, 2019).
Wyre	0.3	The Wyre tidal barrage scheme continues to make steady progress, taking steps to achieve private investment (Natural Energy Wyre, 2016), long term lease of the riverbed (SIMEC Atlantis Energy, 2017) and most recently, lobbying the Commons Environmental Audit Committee (Hunt, 2021).
Other sites listed in the Hendry Review include Barrow-in-Furness and Solway Firth in N.W. England and The Wash, Sheerness and Thames Estuary on the East coast, but no further details exist for development of these sites beyond the consideration of the Hendry Review.		

*potential output values taken from (Hendry, 2016; Petley et al., 2019).

2. Literature Review

At 14 m, the tidal range of the Severn estuary is one of the largest in the world, second only to that of the Bay of Fundy in Canada (Xia et al., 2010a), making it attractive for developing a TRE project. Plans to develop what was then known as the Severn Barrage, have been under serious consideration since 1925 (Langston et al., 2010) with more recent plans evaluating multiple sites as well as options for a tidal fence or lagoon (Binnie, 2016). All plans thus far have been abandoned due to the high financial and environmental cost of proposed designs, solutions for which are earnestly being sought. The Swansea Bay tidal lagoon is the closest scheme to commercial viability so far (Neill et al., 2018).

Swansea Bay tidal lagoon was proposed as a cheaper and more environmentally friendly alternative to a complete barrage (Adcock et al., 2015; Angeloudis and Falconer, 2017; O'Rourke et al., 2010; Zhao et al., 2018). Proposals for the lagoon were designed to generate electricity for 155,000 homes, enough to meet the demand of Swansea and nearby Port Talbot (Hinson, 2018; Tidal Lagoon Swansea Bay, 2014a). It was hoped that lagoon construction at Swansea Bay would commence in 2015 and be online by 2019 (Waters and Aggidis, 2016b). Hendry's 2016 report stressed the importance of building a small tidal lagoon as a "pathfinder" project from which other schemes could develop based on the lessons learned, without which all future projects are hindered (Binnie, 2016; Elliott et al., 2019; Hough and Delebarre, 2016; Waters and Aggidis, 2016b). Although Swansea Bay received the necessary development consent, the Marine Licence is still pending (Hinson, 2018; Todeschini, 2017).

2. Literature Review

2.5.4 Advantages of Tidal Range Energy

As with any major engineering work there are both positives and negatives to be considered and studies of trade-off analysis stress the importance of balancing the two to meet the objectives of the project whilst protecting the interests of the local environment and society (Inger et al., 2009; Tidal Lagoon Swansea Bay, 2014b). Many benefits have been identified during studies of tidal lagoon proposals, summarised in Table 2.4.

Table 2.4 Advantages of TRE schemes, listed alphabetically by source.

Positive Impact/Source	Sustainable/ replaces fossil fuels	Reliable and predictable	Lesser visual impact	Provide baseload capacity	Improve environmental conditions	Close to demand	Employment/business opportunities	Increased tourism and local amenities	Additional infrastructure	Flood Defences
(Acadia Tidal Energy Institute, 2013)	✓	✓	✓	✓		✓	✓			
(Copping et al., 2016)	✓				✓				✓	
(Elliott et al., 2019)		✓		✓						
(Federov, 2010)	✓		✓		✓			✓	✓	✓
(Harcourt et al., 2019)		✓		✓						
(Hinson, 2018)						✓	✓	✓	✓	✓
(International Renewable Energy Agency, 2014)		✓	✓		✓			✓	✓	✓
(Mackay, 2009)	✓	✓	✓	✓						
(Mackie et al., 2019)		✓		✓						
(Mackinnon et al., 2018)				✓	✓		✓	✓		
(Neill et al., 2018)	✓	✓	✓	✓				✓		
(Todeschini et al., 2022)	✓	✓		✓						
(Waters and Aggidis, 2016a)		✓		✓			✓			✓
(Wolf, 2009)	✓				✓		✓	✓		

2. Literature Review

The main advantages of TRE over other renewable sources are its predictability and reliability, whilst the longevity of tidal power plants mean that the benefits will be felt for years to come without the need for costly replacements (AECOM Canada Ltd., 2014). Many plans for tidal range schemes are located in previously industrialised areas in need of regeneration and would benefit from new investment. Benefits for the local community would include, job creation, industry development, localised energy production and increased tourism (Hinson, 2018). The redevelopment of Cardiff Bay through the introduction of a barrage is a positive example of what can be achieved from large scale coastal engineering (Falconer et al., 2020; Hendry, 2016).

Besides the benefits of regional enhancement and reduction of carbon emissions, the development of TRE in the UK would improve national energy security and long-term price stability reducing our dependence on other countries for energy (Climate Change Committee, 2021a). The best outcomes for TRS development would be good environmental status, cost competitiveness, area regeneration and reliability of electricity supply and it is essential to the success of TRSs that these benefits are actualised (Mackinnon et al., 2018).

One reason that makes tidal range proposals difficult to evaluate is that unlike other power stations they can be multi-functional and therefore have many extended benefits. Some studies argue that when evaluating the impacts of TRSs you should focus only on the energy potential and impact of the structure, ignoring any additional benefits of a scheme (Hendry, 2016). Whilst others advocate that if a project can be critiqued on all possible negative outcomes, then it is only fair to consider all possible benefits too and complimentary investigations should look into these secondary functions, especially in terms of cost effectiveness (Petley et al., 2019). However, the efficiency of tidal range schemes can be compromised by multi-purpose design and must be planned carefully, as seen at Jiangxia power station in China where the site was poorly chosen due to secondary

2. Literature Review

demands such as land reclamation and aquaculture which has led to low energy efficiency and poor environmental performance (Zhang et al., 2018).

Tidal range structures can serve society in many ways as demonstrated by the tidal power plant at Annapolis Royal, which combined energy production with transport links and coastal defence (Burrows et al., 2009b; International Renewable Energy Agency, 2014). It has also been suggested that a barrage located in the Solway Firth would create a valuable communication network connecting remote locations in Scotland and Cumbria, with potential for a railway line and additional infrastructure (Howard et al., 2007). The freshwater lake created behind it could also act as a reservoir for drinking water.

Numerous studies have demonstrated how TRSs can provide flood protection by limiting the maximum water level within the estuary (Neill et al., 2018; Rtimi et al., 2021; Xia et al., 2010b). The seawalls proposed for the Swansea Bay tidal lagoon were designed to withstand a 500-year storm with a view to sea level rise from climate change thus acting as a flood defence during its lifetime, saving the cost of building separate flood defence structures (Ma et al., 2019; Waters and Aggidis, 2016b; Xia et al., 2011). Integral to the idea of a manmade lagoon at Swansea were embedded art, education and recreational facilities which would attract many visitors (Tidal Lagoon Swansea Bay, 2022) whilst aspirational proposals for a Mersey barrage include a world leading centre for hydropower research, monorail, and compensatory habitats to support ecosystem services and regenerate the area (Petley et al., 2019).

2. Literature Review

2.5.5 Barriers to Tidal Range Energy

Throughout the history of all proposals for tidal range schemes the repeated reason for their refusal is that they are too expensive and too much is unknown about their effect on the environment (Borthwick, 2016; Etemadi et al., 2011; Mackinnon et al., 2018). These concerns need to be addressed to gain public support and governmental investment, to bring the cost down and determine what the expected environmental impact will be (Energy and Climate Change Committee, 2012). The main limitations and expected negative impacts of tidal range projects are listed in Table 2.5.

Table 2.5 Perceived negative impacts of TRSs and their sources.

Negative Impact/Source	Negative environmental impacts	Impacts on hydrological conditions	Loss of habitats	Impacts on marine life	High initial cost	Large production cost	Insufficient grid infrastructure	Competition with other marine users	Noisy and unsightly	Unknown impacts
(Acadia Tidal Energy Institute, 2013)		✓	✓	✓						
(Charlier, 2007)		✓	✓							
(Copping et al., 2016)		✓		✓						✓
(Elliott et al., 2019)	✓				✓					✓
(Energy and Climate Change Committee, 2012)							✓	✓		✓
(Henderson and Bird, 2010)	✓			✓					✓	✓
(Inger et al., 2009)			✓	✓					✓	
(International Renewable Energy Agency, 2014)	✓				✓	✓	✓	✓		
(Mackinnon et al., 2018)	✓	✓	✓	✓						
(Ramos et al., 2021)	✓	✓						✓		✓
(Waters and Aggidis, 2016a)					✓	✓				
(Wolf, 2009)	✓	✓	✓	✓					✓	
(Zainol et al., 2017)	✓	✓	✓		✓					

2. Literature Review

These impacts have been identified through desktop studies and observations of operation TRSs such as La Rance and Lake Sihwa, but other unidentified and unpredictable impacts are of concern for many groups (Elliott et al., 2019). As so much remains unknown about TRSs, the government review recommended a pilot scheme lagoon that could be carefully monitored to remove uncertainty and inform future plans (Hendry, 2016). However, the government has rejected all recent plans for lagoon schemes on economic grounds (Hinson, 2018).

Environmental impact assessments of potential TRSs highlight the following potential areas of impact:

- Physical impacts – The physical impacts of building a TRS include reducing the tidal range and altering circulation patterns and flow velocities in the near and far field by creating a barrier to natural flows, restricting the tide and accelerating flow around turbines and sluices (Roche et al., 2016). Changes in flow velocity magnitude and direction will have a knock-on effect on sediment dynamics which may affect the cost of the project by having to dredge areas of accretion or replenish depleted areas. Sediment dynamics also affect water quality, by recirculating or depositing contaminants, and marine life by altering breeding and feeding grounds (Boehler and Gill, 2010). The noise from construction and operation of such a large project will also effect inhabitants above and below water (AECOM Canada Ltd., 2014).
- Chemical impacts – Although TRSs are much cleaner than non-sustainable energy alternatives such as nuclear and fossil fuels, the structure can release contaminants if materials are not chosen correctly e.g., gearbox lubricants, anti-corrosion coatings, and anti-fouling paints (Roche et al., 2016). Aspects of water quality, such as salinity, temperature and pollution, will also be effected by TRS construction and operation by creating a barrier to natural circulation and developing new circulation patterns or areas of stagnation (Burrows et al., 2009a; Hooper and Austen, 2013). This can be

2. Literature Review

managed by careful design and operation to ensure a healthy environment as demonstrated at Cardiff Bay (Falconer et al., 2020).

- Biological impacts – The impacts of TRSs on marine life are the largest concern to interest groups (Elliott et al., 2019). Many news articles report concerns over the disorientation, injury or death of aquatic animals caused by underwater turbines specifically. However, academic research has shown that this risk is less than supposed (Copping et al., 2017). A more pressing concern is the loss of habitats changed by decreasing the tidal range, permanently submerging intertidal areas (AECOM Canada Ltd., 2014; Burrows et al., 2009a; Copping et al., 2014; Frau, 1993) . Building the physical structure of the TRS can also inhibit migration, feeding and breeding of aquatic life (Acadia Tidal Energy Institute, 2013).
- Human impacts – The socio-economic impacts of TRSs have both positive and negative aspects. Such a large-scale and long-lived project will impact upon the landscape, changing the look and use of natural coastline. These will be welcome changes to some where the area was previously industrialised but has now fallen into disuse as it will bring employment opportunities and increase tourism and recreation as demonstrated at La Rance (Charlier, 2007). However, others may see this as a strain on the existing resources of the community and not wish for such a large development in their area as it will compete with other activities and industry, e.g. commercial fishing, mining marine aggregates, recreational activities, etc. (Acadia Tidal Energy Institute, 2013; Burrows et al., 2009a)

All of these factors will depend on the extent to which a tidal range scheme alters the natural environment. The current research focusses on physical impacts, looking at alteration to circulation patterns and flow velocities but will also consider human impacts, looking at the possibility for competing activities to continue in the area. This supports Borthwick's (2016) review of the current state of marine renewable technologies, that research is needed specifically to investigate local flow hydrodynamics, currents, turbulence, wake mixing and sediment transport.

2.5.6 How to Overcome Barriers to Tidal Range Energy

Support for tidal lagoons as an attractive renewable energy option has come from successive reports (Etemadi et al., 2011; Hendry, 2016; Hooper and Austen, 2013; Mackinnon et al., 2018) but environmental concerns are still the main barrier to their development. There is some dispute over the most environmentally friendly way of extracting energy from the tides, with some favouring tidal lagoons (Elliott et al., 2019; Petley and Aggidis, 2016; Zhao et al., 2018) whilst others champion tidal fences (Qian and Jin, 2018), dynamic tidal power schemes (Dai et al., 2018) or tidal stream turbines (Garcia-Oliva et al., 2017), but Qian and Jin (2018) are pragmatic in noting that whichever way you capture tidal energy, there will be disruption to the natural system. Previous proposals for the Severn barrage failed to adequately address environmental concerns (Angeloudis and Falconer, 2017) and recent engagement with stakeholders found the most significant environmental concerns to be changes to hydrodynamics, marine life and sediment regime (Elliott et al., 2019).

Mitigation methods applied successfully to hydroelectric power stations and coastal defences could also be used for tidal range schemes (Elliott et al., 2019; Mackinnon et al., 2018). Solutions to environmental concerns can be grouped into three themes:

- 1) Engineering, site or technology design
 - a. Phased development – building the structure in stages to allow the environment to adapt to new conditions gradually (Tidal Lagoon Swansea Bay, 2014b).
 - b. Sensitive construction techniques – floating caissons into place is considered more environmentally friendly than the use of coffer dams during construction (Jacob et al., 2016).
 - c. Modified equipment and material designs – turbines with different number of blades may be deployed to prevent injury to aquatic life (Hooper and Austen, 2013).
- 2) Operation and maintenance

2. Literature Review

- a. Modified operation to maintain natural conditions – generating electricity on both tides and adding pumping to the operating mode can help maintain the natural tidal regime and reduce loss of intertidal habitats (Bulleri and Chapman, 2010).
 - b. Improved turbine design to reduce need for maintenance – (Waters and Aggidis, 2016a).
 - c. Acoustic fish deterrents near turbines – (Tidal Lagoon Swansea Bay, 2014b).
- 3) Compensation and catchment-based measures
- a. Compensatory habitats – compensatory habitats such as wetlands and wildlife sanctuaries can be created close to the new structure as with demonstrated at other coastal developments such as Cardiff Bay (Elliott et al., 2019).
 - b. Buffer zones and screens – (Jacob et al., 2016).
 - c. Artificial habitats – new developments have introduced artificial rockpools into seawalls to provide new habitats for marine organisms (Tidal Lagoon Swansea Bay, 2014b).

Developers favour solutions that work at stage one, addressing impacts through engineering design and technology, which the present study seeks to do by investigating the impacts of turbine spacing in TRSs. The following section investigates current proposals for solutions to TRS issues according to the three themes above.

2. Literature Review

2.5.6.1 Engineering, site or technology design

The deployment of TRSs will have environmental impacts at every stage of the project, from installation to operation, maintenance to transmission and finally decommissioning (Bas et al., 2016; Gill, 2005; Hooper and Austen, 2013; Shields et al., 2009; Zainol et al., 2017). To this end studies have been conducted to design turbines as simply as possible to allow easy installation and low maintenance (Waters and Aggidis, 2015). As well as the conditions of their locations, TRSs can vary in their shape, size, and the layout of their hydraulic structures. Each of these attributes will have an impact on the environment and TRS performance.

2.5.6.1.1 Location

A key theme drawn from many studies is that the design of a TRS needs to be site specific, paying attention to the characteristics of each area before settling on the best option (AECOM Canada Ltd., 2014; Mackie et al., 2021; Neill et al., 2021). This not only has the benefit of making the most of each site, extracting the optimum amount of energy and taking the natural environment into account but also has been deemed to be the most cost-effective method for TRS design (Acadia Tidal Energy Institute, 2016). Aggidis and Židonis (2014) capitalised on this idea by developing a system whereby the user inputs all that is known about the conditions of a site and the performance of various turbines are tested automatically to determine the best option for the location. They found their system performed well for hydro-electric power stations and it is to be wondered whether a similar system could be adapted for TRSs (Aggidis and Židonis, 2014).

Although site specific TRS design is preferred in order to extract maximum energy and maintain environment conditions, Mackie et al. (2021) point out that the specificity of projects may mask factors that would only be due to distinctive localised features. To investigate this further they tested a consistent design scheme at seven sites in the Bristol Channel and Irish Sea to determine generic issues raised by tidal range lagoons. Their TRS maintained a constant shape, size and operation, and constant ratio of turbines and sluices proportional to the intertidal area to gain the same

2. Literature Review

energy output at each site. By keeping these aspects constant, they aimed to assess the impacts that are due purely to the physical marine environment, e.g., coastline morphology, bathymetry and tidal regime, rather than design. They also looked at the cumulative effects of building at all locations.

Using a zero-dimensional model to look at tidal elevation and energy output and a 2D hydrodynamic model to evaluate fluxes, they found that the large tidal resonance and constrained geometry of the Bristol Channel made it more susceptible to blockage effects with higher individual and cumulative impacts of TRSs compared to the Irish Sea. They reported that development in the Irish Sea alone would have a negligible effect on tidal constituents, whereas developing only the Bristol Channel could reduce the M2 tidal constituent by 0.1 to 0.2 m with smaller reductions reaching around the coast. However, their results for far field impacts were less pronounced than predictions from other TRS modelling studies. Overall, it was found that conditions outside of a lagoon are most influenced by coastal geometry, which is why the Bristol Channel was most susceptible to change, whilst conditions inside tidal lagoons depend on bathymetry, operating regime and the placement of hydraulic structures. They conclude that consistent design is less efficient at extracting energy and designs do indeed need to be site specific in reality with special attention paid to adaptive operating regimes to mitigate the cumulative effects of energy extraction.

Rtimi et al. (2021) demonstrate the importance of robust understanding of a location, using detailed historic site characterisation to identify changes to the La Rance estuary before and after the construction of the barrage. Using 2D depth averaged modelling to investigate tidal propagation and asymmetry and their effects on bathymetry they found that without the barrage the bathymetry did not evolve sufficiently to influence hydrodynamics in the estuary but with the structure the tidal range decreased, water levels were lowered and flood and ebb currents both decreased on the estuary side of the dam. However, closer to the structure the flood current increased upstream of the sluice gates and ebb currents increased downstream of the turbines. This led to erosion zones and localised scouring upstream of the

2. Literature Review

sluice gates and sediment accretion lower in the estuary but no significant difference to bathymetry was identified in the middle estuary zone either by LIDAR data or historic maps. They call for further investigation into sediment transportation around TRSs which they note will be affected by sediment type and local morphology. Overall, they found that the presence of the TRS did not change the characteristics of the tidal regime, which is flood dominant with and without the barrage, however, the La Rance barrage does use bi-directional operation, which maintains natural conditions more closely than a single ebb or flow operated system would. It is also important to note that a natural sea level rise of 10 cm occurred in the region between 1957 and 2019, demonstrating the importance of long-term forecasting and climate change considerations when designing TRSs which are intended to last for generations.

2.5.6.1.2 Shape

Vouriot et al. (2018) looked at the effects of TRS design on tidally induced vortices and their impact on regional water quality and sediment processes. They modelled an idealised tidal lagoon, varying the inlet width, bathymetry and lagoon length-to-width ratio to test the effects of lagoon design. Tests of three different inlet widths showed that vortices do not dissipate or flush in a single tide but that subsequent flood tides create new recirculation zones, and that vorticity intensity is indirectly proportion to inlet width as it accelerates faster through narrower inlets. In adapting the sloped area of their lagoon, they found that bathymetry affected vortex lifetime, in that vortices advected closer to shallower, near-coast waters and the increased effects of friction in these areas led vortices to dissipate more quickly.

Their experiments maintained a constant area of 25 km² to model schemes that would have the same power output but varied the length-to-width ratio of the TRS seawalls. They found that lagoon shape influenced vortex lifespan with vortices dissipating in a single tidal period for the longest domain (length-to-width ratio 25:4) and that wider inlets also led to the rapid vortex dissipation. Overall, they discovered that lagoon geometry had a great influence on vortices, with flushing behaviour dictated by the ratio of the inlet width to the maximum velocity multiplied by tidal period, and that bathymetry and side wall proximity also affect vortex dissipation.

The current research builds on this work by adapting bathymetry and TRS seawall length-to-width ratio whilst maintaining constant area and follows their recommendation to investigate inlet spacing across the length of the seawall to test the effects of this aspect of TRS design on flow patterns.

2. Literature Review

2.5.6.1.3 Size

Tidal range lagoons are also under consideration in Canada. In 2013, Cornett et al, investigated the effects of various TRS scenarios in the Bay of Fundy. They used Telemac, a 2D depth averaging modelling system calibrated using BODC data, to test 19 scenarios, varying the size, location, number of turbines and operating mode for a range of hypothetical, coastally attached and offshore lagoons in the region.

In comparing their results with existing conditions at five tidal stations they found that the larger the scheme the greater the power output but also the greater the impact on hydrodynamics. The largest schemes were predicted to increase the tidal range along the whole coast by up to 2.4% whilst smaller schemes could cause less than a 1% change outside of the lagoon. Larger schemes also caused the greatest change to current velocities, decreasing current velocity by up to 45% in the immediate area outside of the lagoon. Smaller schemes would however, cause less than a 10% reduction in current velocities outside of the lagoon. None of the projects led to an increase in current velocity of more than 1%, either within or outside of the lagoon due to the energy extraction in the area. All TRS developments were found to have an impact on local hydrodynamics, but offshore lagoons had a slightly lesser impact than coastally attached projects. The sensitivity of certain areas was closely linked to proximity to the development, leading to careful consideration of the placement of future projects and the areas they will impact. Overall, the greatest changes to current velocities occurred in the near field area, close to the hydraulic structures and seawall, with the greatest reductions in speed inside the lagoon. Conditions in the far field of the estuary, however, remained relatively unchanged. Areas closest to the lagoon were most sensitive to operating mode, and impacts are reduced by keeping the sluice gates open but tidal flows further afield were found to be insensitive to operating mode. The current study builds on this work by testing the impacts of varying lagoon design on near and far field hydrodynamics, including water level, velocity and circulation patterns but varies in that it investigates turbine spacing as the design variable rather than size and location.

2. Literature Review

2.5.6.1.4 Turbine number and spacing

Despite these arguments for optimising TRS design, schemes tend to follow a very basic pattern of a coastally attached seawall with turbines and sluices housed together in a single block, as shown in Figure 2.8. This is based on geomorphology and competing activities in the area, whilst also keeping construction and maintenance costs down by building the hydraulic structures in a single area and allowing easier passage for fish and ships (Angeloudis and Falconer, 2017).

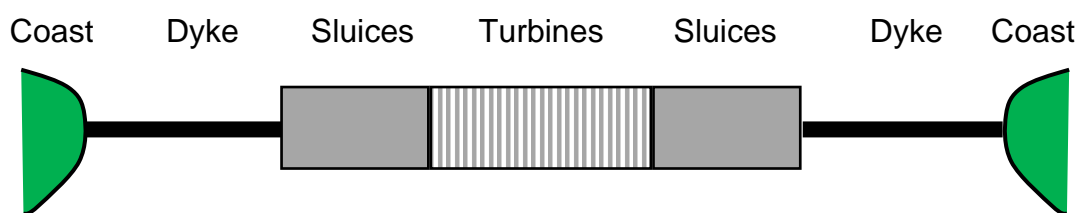


Figure 2.8 Common design layout for TRSs, with sluices and turbines grouped together in a single block in a seawall (based on multiple sources).

This design may vary in the length of the dykes/embankments or the addition of a shipping lock or substation, but hydraulic structures are generally grouped together rather than spaced apart. Analysis of existing literature relating to TRS structures revealed how this layout is commonly used in existing and proposed TRSs. These findings are highlighted in Figure 2.9 to Figure 2.14 which all show the repetition of the original pattern in Figure 2.8.

2. Literature Review

Figure 2.9 and Figure 2.10 show the existing schemes at La Rance and Lake Sihwa tidal power plants respectively. In both cases, the turbines are confined to a single area and the sluices to another block. This allows ease of access for ships and reduces the risk for fish which can pass in a single designated area away from the turbines.

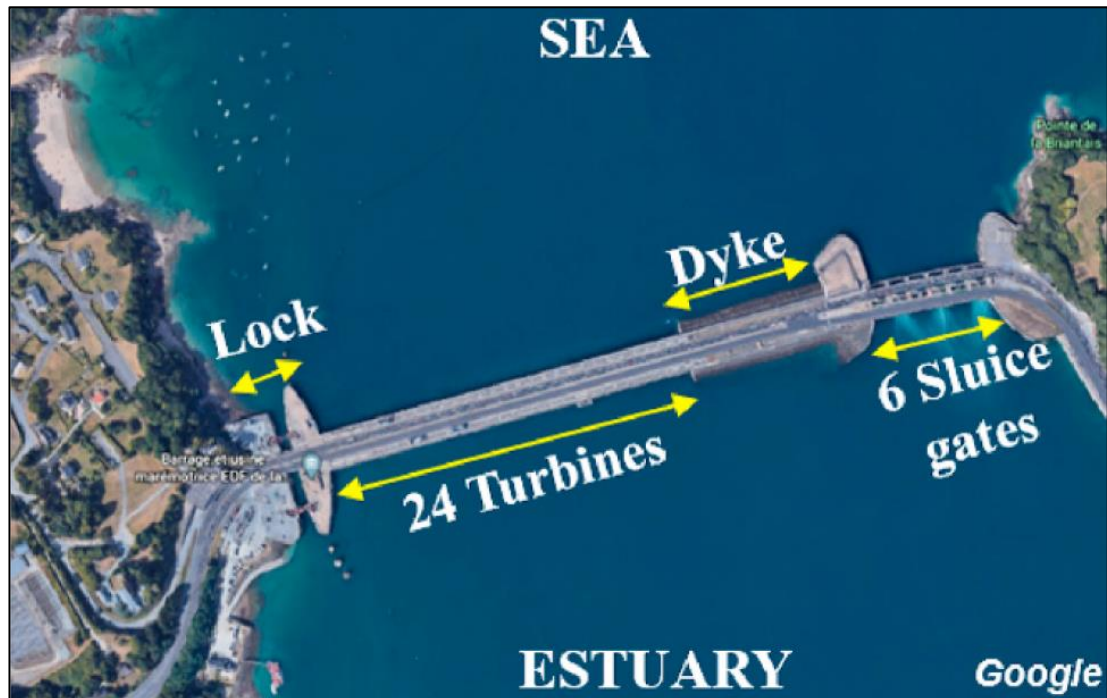


Figure 2.9 Existing layout of La Rance tidal barrage (Rtimi et al., 2021).

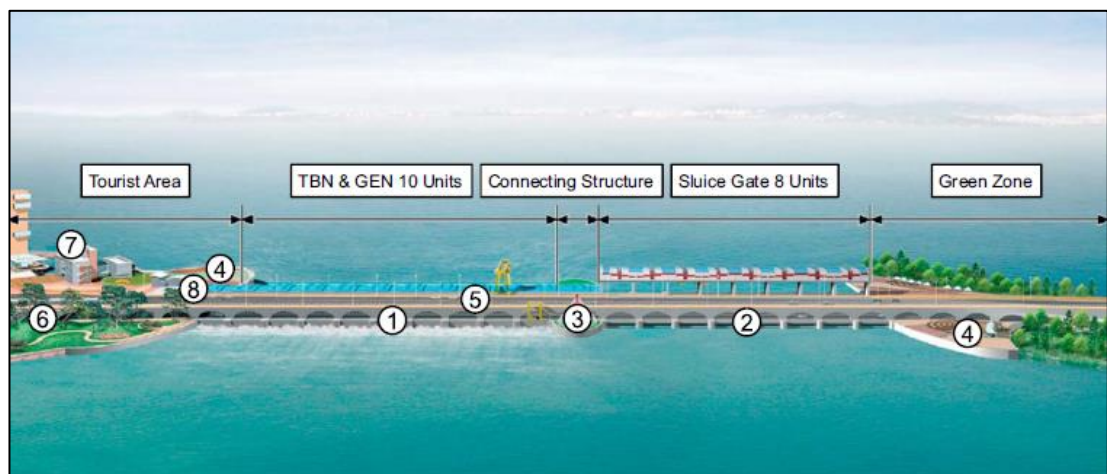


Figure 2.10 Existing layout of Lake Sihwa tidal lagoon (Bae et al., 2010).

2. Literature Review

This simple layout, with turbines and sluices located in a single block within a coastally attached sea wall, is closely followed by designs for proposed tidal range schemes around the UK coast too. Figure 2.11 shows this repeated pattern of turbines and sluices in a single block in the proposals for a tidal barrage in the Mersey Estuary and Figure 2.12 and Figure 2.13 have the same pattern in designs for tidal lagoons on the North and South coasts of Wales. This same pattern was even used internationally in the proposals for a tidal barrage in the Bay of Fundy as shown in the Figure 2.14.

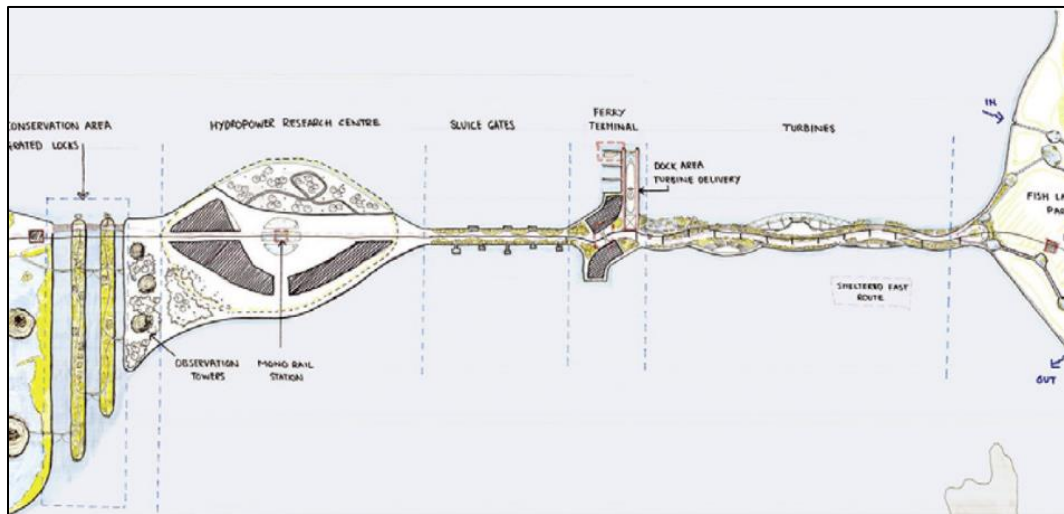


Figure 2.11 Proposed layout for Mersey tidal barrage (Petley et al., 2019).

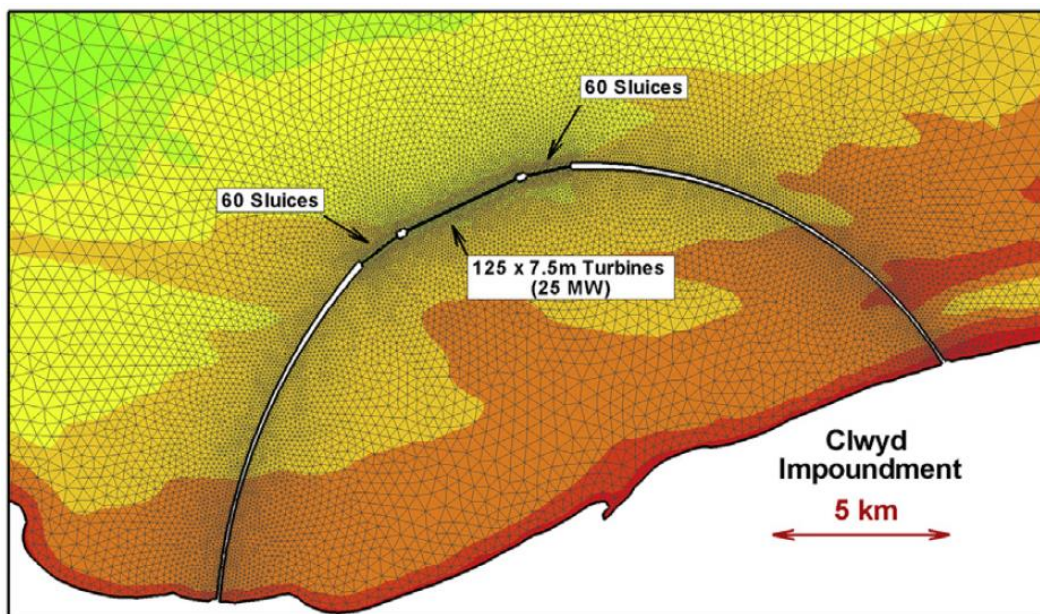


Figure 2.12 Proposed layout for tidal lagoon on North Wales Coast (Angeloudis et al., 2016).

2. Literature Review

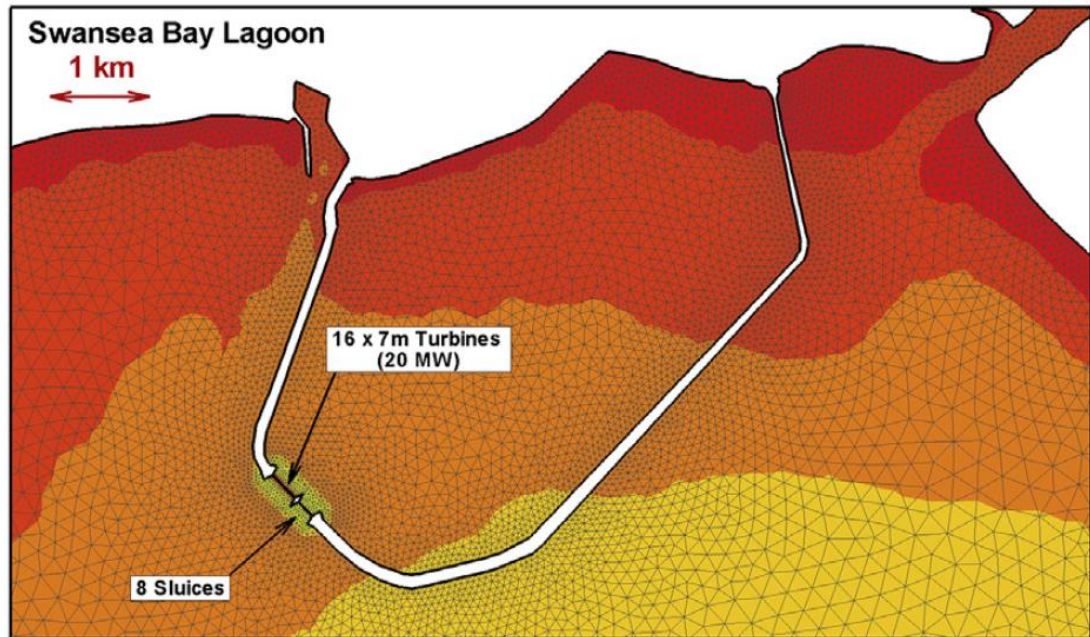


Figure 2.13 Proposed layout for Swansea Bay tidal lagoon (Angeloudis et al., 2016).

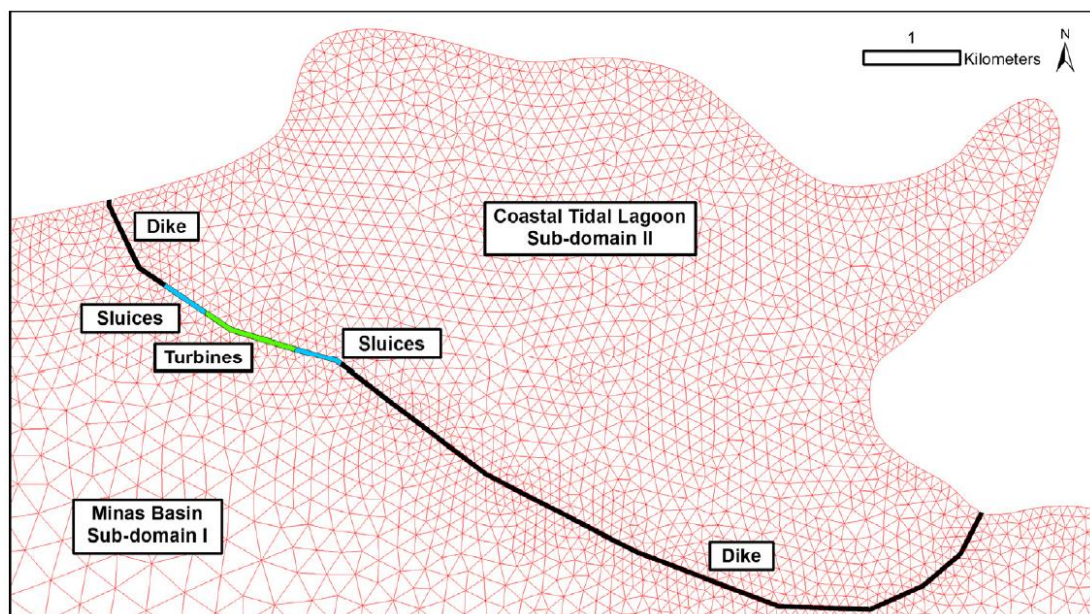


Figure 2.14 Conceptual design for a tidal barrage in the Bay of Fundy (Cornett et al., 2013).

2. Literature Review

Turbine spacing has been studied extensively in tidal stream turbine (TST) arrays, examining the impact of turbine wakes on marine life, hydrodynamics, and each other (Myers et al., 2011) (see Annex 1 for a detailed summary of studies on TST spacing), but the positioning of turbines in TRSs is less commonly investigated. An element of this is down to the ability to choose TST placement in three dimensions: width, length and depth, rather than TRS turbines which are limited to just two: width and depth, with depth usually dictated by geomorphology. However, investigations into the spacing of tidal stream turbines could also prove relevant to tidal range schemes.

In the case of both technologies, the greater the number of turbines, the higher the power output, which is important for economic viability (Funke et al., 2014; Vennell, 2010). However, increasing the number of obstructions in the water column decreases the amount of available energy and the knock-on effects of turbine wake interactions impacts the performance of individual devices as well as affecting the environment, so layout is important (Myers et al., 2011). Vogel, et al (2016) are certain that the key to maximising power extraction is to determine optimum inter-turbine spacing, a view shared by Tralli et al. (2015) when looking at TRSs.

In TST arrangements, lateral spacing of the devices was found to have important implications for wake recovery length (Stallard et al., 2013) and this is no less the case in TRSs, where the vortex size and recirculation zone of wakes is affected by the number, size and distribution of turbines (Angeloudis et al., 2016a). However, in TRSs there are options to vary turbine operation, and this can also have an effect. Fallon et al. (2014) found that the effects of TSTs on hydrodynamics are highly sensitive to turbine spacing. Studies into the spacing of turbines and sluices in TRSs demonstrate that, ideally, turbines should be spaced evenly across the length of the structure to enable balanced water transfer and best maintain conditions inside and outside of a lagoon (Angeloudis et al., 2016a).

In studying the performance of a proposed TRS design in North Wales, Angeloudis et al. (2016b) found much lower velocity magnitudes, both inside

2. Literature Review

and outside of the lagoon, due to the large distribution of the 125 turbines across the deepest part of the seawall, which lead to smaller recirculation zones and mitigated wake effects within the lagoon. Placing sluice gates adjacent to areas prone to recirculation also helps reduce these effects. Although they improve the hydrodynamic impact of the TRS, these design options are more expensive due to having to construct the turbines in separate structures as well as preparing the ground in more areas.

More research is needed into TRS design to find the best configuration for minimising negative impacts both upstream and downstream of the structure and Tralli et al. (2015) propose future studies into the optimum placement of turbines to increase energy yields and to better understand the effects of turbines placement on sediment transport and water quality.

2.5.6.2 Operation and maintenance

In looking at proposals for the West Somerset Lagoon, Guo et al., (2021) found that although lagoon operation improved water quality in the area it reduced the high-water level and intertidal area of the Bristol Channel and Severn Estuary. They tested a design with 125 bulbs split between five housing blocks and spread out evenly across the sea wall interspaced with eight blocks of sluice gates, as shown in Figure 2.15.

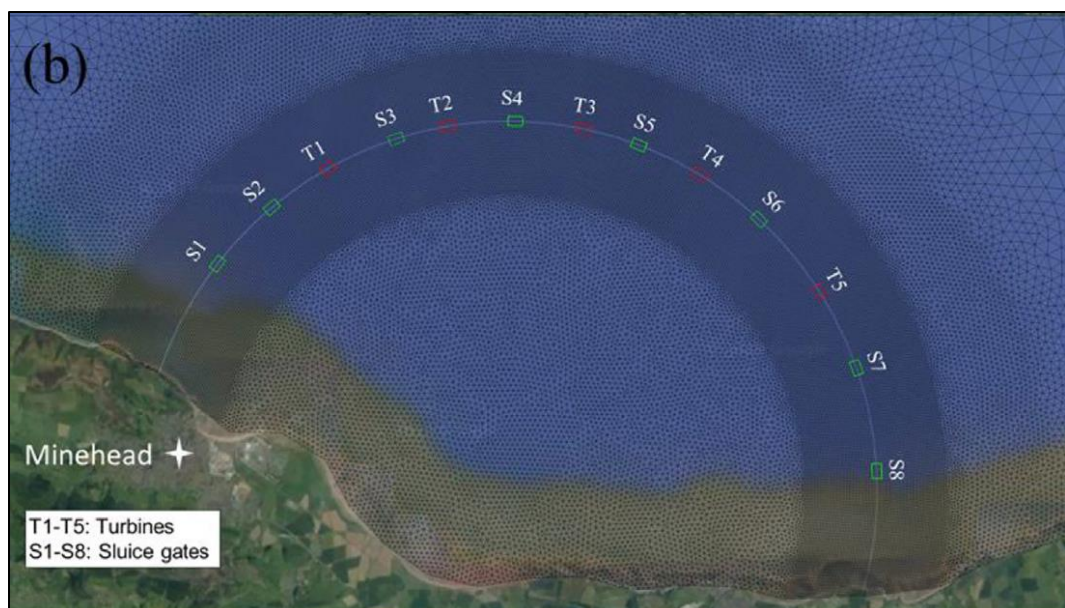


Figure 2.15 Proposed layout for West Somerset tidal lagoon (Guo et al., 2021).

2. Literature Review

Their model showed that the turbines and sluices changed the tidal currents and that jets from the hydraulic structures increased the velocity by up to 1.5 m/s in the near field and 0.25 – 0.75 m/s in the far field outside of the lagoon. Inside the lagoon, velocity was reduced with the exception of the jets directly around the hydraulic structures. These higher velocities would have benefits for water quality by increasing flushing and pollution transport.

Water quality surveys were carried out at Swansea Bay within the proposed development area to evaluate the risk of eutrophication. No evidence of stratification was found in the area under current conditions and the water column was uniformly nutrient rich with low turbidity and no signs of eutrophication. Using models to examine water quality if a TRS were to be built showed that existing management strategies in Swansea Bay are sufficient to manage the risk of eutrophication under a two-way generation operating scheme. However, an ebb-only generation scheme would pose a slightly higher risk to eutrophication and therefore nutrient levels would have to be controlled as a precaution if this mode of operation were selected (Kadiri et al., 2021).

A limitation of previous models assessing the performance of TRSs is that they generalise operation mode giving universal predictions when actual schemes will be sensitive to site specific conditions and varying operation. Elliot, et al. (2019) found that the majority of studies on the tidal lagoon industry focus on design and compensation measures and that there was room for improvement to be made in the operation and maintenance of tidal range projects.

Several recent studies address this by adapting models with plant specific operation algorithms (Angeloudis, 2019; Xue et al., 2020). With these adaptive models it is possible to tailor the layout and operation of turbines and sluices to test specific proposed cases and reach more accurate conclusions about expected hydrodynamic conditions. Observation of the impacts of various modes of operation at La Rance proved that adapting operation not only limited wear on parts but also improved the quality of the environment. Research into adaptive operation methods found that smaller

2. Literature Review

scale TRSs gain more from operational optimisation than larger ones (Angeloudis et al., 2018).

Investigations into different modes of operation show that whilst ebb generation is the most cost effective (Xia et al., 2010b), two-way operation is better for maintaining natural conditions with less intertidal area lost (Falconer et al., 2017) and adaptive operation is optimal for converting the maximum potential energy (Angeloudis, 2019). It is also hoped that adaptive operation could support the environment, “indeed it has long been noted that the success of a tidal barrage scheme depends upon striking the right balance between the mode of operation and biological harmony” (Retiere, 1994).

The non-linear predictive control strategy, advocated by Shen and Nyman (2021) aims not only to increase energy output but also to reduce environmental impacts by dynamically balancing the tides with turbine performance and hydraulic structure discharge to ensure reliable electrical output and minimal disruption to natural conditions. Mackinnon et al. (2018) recommend sympathetic operation for reducing and restoring environmental changes, altering or pausing operation during significant ecological seasons. Mackie et al (2021) also argue that adaptive operation is needed to mitigate the cumulative impacts of energy extraction on the environment and Guo et al, (2021) demonstrated that optimised operation can support better water quality by enabling circulation, sediment transport and contaminant flushing.

As well as increasing power output and decreasing environmental impact, optimising operation can also manage electricity production to maximise income by balancing the timing of generation to coincide with the maximum price of energy (Mackie et al., 2019). Investigation of income based optimisation controls at Swansea Bay Lagoon showed an increase in income of 23% compared to non-adaptive operation and a 10% gain over energy maximisation approaches (Harcourt et al., 2019). Being able to use flexible operation is a definite benefit of TRE over wind or solar power and has repeatedly been proven to increase power output (Mackie et al., 2019; Xue et al., 2020). However, it is acknowledged that flexible operation methods are

2. Literature Review

computationally expensive and do not perform real time control, relying on accurate tidal prediction (Moreira et al., 2022).

These optimisation techniques have so far looked at individual schemes, but further gains can be made from optimising the operation of multiple TRSs (Neill et al., 2018). By strategically developing a series of TRSs around the UK coast and modulating their operation to complement tidal phases, TRE could provide near continuous energy (Todeschini et al., 2022) and significant gains can be made in income from optimising a fleet of TRSs (Mackie et al., 2019). These systems could also include TSTs to extract maximum power from areas with strong tidal currents and to bridge the gap in continuity during synchronised tidal phases and neap tides (Mackie et al., 2020; Todeschini et al., 2022). However, developing multiple projects will have knock on effects on energy, income, the environment and on each other's performance, therefore further investigation is needed into proposals for a fleet of TRSs (Angeloudis et al., 2020; Mackie et al., 2019). As the deployment of multiple TRSs and TST arrays will change channel dynamics and near and far flow fields, their placement must be strongly regulated and regional planning is needed (Waldman et al., 2019).

2.5.6.3 Compensation and catchment-based measures

Given the sensitive nature of many sites identified for TRSs it is important to consider all users of the marine environment, including fishing, aquaculture and recreation (Ramos et al., 2021; Uihlein and Magagna, 2016), this requires an interdisciplinary approach to evaluate effects on aquatic life and society (Ross et al., 2021). The AECOM (2014) Strategic Environmental Assessment requires an integrated coastal management plan to identify overlapping areas of interest and design processes for resolving conflicts. In particular they wish to identify how tidal energy structures would disrupt regular activities and whether the effects could be mitigated so that different industries and activities could co-exist. This holistic view of TRSs as benefiting multiple users has always been the aim of the tidal lagoon industry in the UK with promises of aquaculture and leisure opportunities being foremost in the planning of schemes such as the Swansea Bay Lagoon

2. Literature Review

(Tidal Lagoon Power, 2022, Hendry, 2016). This research will therefore undertake to investigate whether conditions in a tidal range lagoon will be such that it will be possible for each of these activities to take place.

Current studies of the Swansea Bay Lagoon site discuss that although the navigation of commercial and recreation vessels will be restricted due to the obvious obstruction of a seawall. Conditions for small craft within a lagoon would be improved due to longer high water stand and reduction in current speeds (Burrows et al., 2009a; Hooper and Austen, 2013; Wolf, 2009). However, Angeloudis et al. (2016b) report that turbine wakes could cause artificial rip currents which would prohibit sailing and swimming. Overall, their model of a TRS in Swansea Bay predicted that a third of the impounded area would have currents greater than 0.9 m/s (the average human swimming speed) and would thus prohibit promised sporting activities. The potential effects on fisheries are also uncertain, with contradictory reports suggesting that they may suffer or thrive due to the change in current speeds and sediment regime (Hooper and Austen, 2013). Hydropower plants in the USA are legally required to maintain flow conditions that enable boating, fishing and other lake-based recreation (Schramm et al., 2016) a practice which could be borrowed and adapted to TRS development in the UK.

2.6 Gaps in Tidal Range Energy Research

Multiple literature reviews and summaries of current research in MRE have identified the following as research priorities for the future of TRSs:

1. Gathering accurate, long-term data at proposed sites to improve resource assessment and validate reliable numerical models.
2. Detailed site characterisation and hydrodynamic modelling to define conditions before and after lagoon construction, including scenarios with and without climate change (Neill et al., 2021).
3. Better understanding of interactions between the proposed lagoon and the tidal environment (Guo et al., 2021).
4. Refinement of existing models to test a variety of lagoon designs and turbine parameters (Mackie et al., 2021).
5. Improved simulation of turbulence and wake characterisation, especially in real sea conditions (Čoř et al., 2019).
6. Hydrodynamic and sediment transport modelling to better understand the fate of contaminants (Roche et al., 2016).
7. Understanding the cumulative impacts of developing multiple schemes and exploiting phasing to enable continuous output and minimise variability (Mackie et al., 2020; Xue et al., 2019).
8. Detailed lifespan assessment of TRSs including lifetime cost benefit analysis, grid integration and energy security (Uihlein and Magagna, 2016).

This study speaks directly to the third and fourth of these suggestions, by testing a variety of lagoon designs and turbine layouts to better understand interactions between tidal range lagoons and hydrodynamics. A particular design parameter missing from previous research is the spacing of hydraulic structures in TRS seawalls, as highlighted by several studies (Myers et al., 2011; Tralli, 2015; Vouriot et al., 2018). Investigations into TST arrays expose how sensitive they are to turbine spacing in terms of the impacts on power extraction (Vogel et al., 2016), the environment (Fallon et al., 2014) and wake recovery (Stallard et al., 2013) and it would be worth investigating whether this is also the case for TRSs.

2.7 Research Methods for Investigating Tidal Range Structures

2.7.1 Physical Modelling

Physical models are commonly used to test turbine performance at a range of scales and to provide experimental data with which to calibrate and validate numerical models to improve their performance. Primary examples of physical models used in the study of TRSs include, Jeffcoate et al. (2013) who looked at the distance at which flows through TRS hydraulic structures change from 3D to 2D, and Brammer et al. (2014) who investigated varying operation modes in the proposed Severn Barrage.

From 2013 to 2017, Jeffcoate et al. devised a series of experiments to investigate flows around tidal turbines. In 2013, Jeffcoate et al. analysed the three-dimensional nature of jets downstream of turbines in a tidal barrage which had previously been predicted, inaccurately, by depth averaged modelling. In 2017 they took this investigation a step further by adding stators and rotating turbines to the draft tubes. They showed that at distances closer than twenty tube diameters from the turbines, 3D modelling was required to accurately predict water level, velocity and bed shear stress. The influence of these experiments has led to the current study taking measurements for the full depth of the tidal tank ensuring the consideration of the flow field in all dimensions rather than assuming depth averaging to be sufficient to understand conditions around a TRS. Similarly to their original experiments, the present study will use open draft tubes to represent a simplified case for flow through a TRS, but unlike Jeffcoate et al. (2013) this study will also look at varying the spacing of turbines to examine this influence on 2D and 3D flows.

Brammer et al. (2014) used the facilities of the HRC at Cardiff University to build a scale model of the Severn Barrage to investigate the hydrodynamic impacts of different operating modes. Their results showed that ebb only generation would increase minimum water levels upstream and reduce mean water levels downstream, with a general reduction in tidal velocity in the area, whilst two-way generation would cause alterations to the tidal regime but could moderate these changes through sympathetic operation. These

2. Literature Review

results were then used to calibrate a depth averaged numerical model to simulate the effects of modifying the barrage structure. The current study seeks to further this investigation by looking into the effects of design modification as well as operation and will follow a similar method but at a larger scale. The main difference between these two studies is that the current research uses an idealised rather than specific TRS design.

Tidal environments are extremely complex with interconnecting influences from hydrodynamics, geomorphology, human activity and the effects of climate change, all of which require greater understanding before change is wrought on an area. Rampazzo et al. (2019) suggest that more research is needed to understand tidal systems in general, to which end they designed an artificial tide generation system that could be used to analyse the morphometrics of tidal networks.

Their laboratory scale experiment looked at tidal forcing in a lagoon environment, controlling tidal flows to compare different types of intelligent controllers for tide generating systems. They described the electric-mechanical components (stepper motor and weir) and the hydraulic components (water pump, water and lagoon basin) of their experiment as two separate subsystems so that they could control conditions and observe the results of altering each. The walls of their lagoon basin were made of wooden panels which could be moved to alter the shape and position of the inlet, although this was not a variable of their experiment. They used the results of their extensive experiments to calibrate and validate a dynamic model to develop a real time control tidal generating system for future studies.

The similarities of this experiment to the current study will help inform design elements such as the control of artificial tide behaviour to ensure the quality of the experiments, the positioning of lagoon inlets and the management of equipment.

However, unlike the current study, Rampazzo et al.'s (2019) research created a wave directly in front of the lagoon so that the desired characteristic wave reached the lagoon uninterrupted. This distinction

2. Literature Review

between their study and the current research, which looks at the propagation of tidal waves flowing across a larger area before reaching a TRS lagoon, will enable the observation of how lagoon walls influence regional water levels and velocities, as well as the condition of waves as they reach a TRS after travelling across a larger area, which is a more realistic representation of the conditions in which a TRS would operate.

Physical models have also been used to test vorticity, water quality and flushing in harbours. Falconer (1974) devised an experiment where harbour area was maintained whilst the harbour entrance and seawall length-to-width ratio were varied to investigate the effects on flushing. Square geometry was found to enable the best mixing, with the second-best design being a rectangle with a length-to-width ratio of 1:2. Smaller entrance widths were shown to keep water well mixed inside harbour walls but restricted flushing which is also needed to maintain high water quality. The present study intends to test an idealised lagoon with square and rectangular geometry and vary the position of the inlet whilst keeping the width the same to investigate the effects of this design parameter on mixing and flushing.

Another area of research that could be applied to tidal range lagoons is flow through natural channel inlets, such as those around barrier islands or in estuaries that are narrower than they are long. Bryant et al. (2012) devised a laboratory experiment to test vortex formation through narrow coastal inlets, with an artificial barrier island with a constant width that they then adapted by varying the length of the inlet to investigate dipole behaviour and to compare scenarios with and without developed lateral boundary layers. Circulation patterns were observed using particle image velocimetry (PIV) and dye videos to capture images over four tidal cycles, this data was then able to be used to compile velocity vectors for flow in the tank using Matlab processing tools. Looking at their initial case, they found that starting jet vortices were the same over every tide, but that bottom friction caused vortex stretching during flood tides which led the vortices to decay over distance as energy dissipated. Using this as the control case, the results of other scenarios were compared and showed that the larger the inlet length, the smaller the starting

2. Literature Review

jet vortex and the further it deviates in the y-direction. Overall, they found that vortices expelled at the lateral boundary layer quickly travelled away from the inlet before the reverse tide and once away from the inlet the size and circulation of these vortices decreased.

Although looking at natural inlets rather than manmade structures this research demonstrates the behaviour of jets through different size openings and can be used as comparison for vortex analysis for TRS hydraulic structures. The current study will vary in that it uses dye videos to analyse flow circulation patterns rather than PIV due to the limitation of facilities.

Bijankhan et al. (2017) noted a lack of understanding of the velocity distribution of flows through sluice gates. They decided to address this issue with a series of laboratory experiments to analyse the velocity of sluice gate jets by varying the ratio of the gate opening to upstream flow depth, using an ADV and electromagnetic flow meters to examine submerged flow through the gates. Their results explain that traditional methods for modelling sluice gate flow rates were inaccurate and required the addition of an energy correction factor and head loss value to improve their performance, which they achieved by calibration using their experiment observations (Bijankhan et al., 2017).

2.7.2 Numerical Modelling

The benefit of physical experiments is that they enable the demonstration and analysis of tangible prototypes and ensuing conditions, however they are limited by the size of test facilities and scale effects will impact on the interpretation of results (Adcock et al., 2015). The benefit of numerical modelling is the ability to test complex scenarios in a relatively quick and cheap manner and computational models can help quantify the performance and impact of TRSs (Adcock et al., 2015). However, as with physical models, the limitations of numerical models are how difficult it is to accurately represent the complexity of real-life conditions to gain useful results (Rampazzo et al., 2019; Wu et al., 2017) and that data must be interpreted carefully, acknowledging the assumptions and uncertainty of calculations (Angeloudis et al., 2016a; Nash and Phoenix, 2017; Yates et al., 2013). In particular for modelling TRSs, the representation of turbines and sluices in a model is of utmost importance (Angeloudis, 2019) and inaccuracies in the original model configuration can lead to errors and inconsistencies in the final results (Burrows et al., 2009a).

Numerical models are frequently used to test the ecological, environmental and financial implications of TRSs as well as their technological performance and efficiency (Mackie et al., 2020; Mackie et al., 2019; Neill et al., 2021). Many powerful numerical models exist that can be used effectively for investigating TRE (Suárez-López et al., 2019).

Numerical modelling has been used effectively for:

- Predicting turbine performance (Aggidis and Feather, 2012).
- Estimating energy output (Burrows et al., 2009b).
- Testing operation modes (Angeloudis et al., 2018).
- Hydrodynamic site assessment (Acadia Tidal Energy Institute, 2016).
- Investigating hydrodynamic changes (Angeloudis and Falconer, 2017).
- Reducing costs (Acadia Tidal Energy Institute, 2016).
- Optimising operation to maximise money output (Harcourt et al., 2019; Mackie et al., 2020).

2. Literature Review

Variables that have been investigated to test hydrodynamic impacts of TRSs include size (Mackie et al., 2021), shape (Vouriot et al., 2018), location (Cornett et al., 2013), operation mode (Angeloudis et al., 2018), sluice area (Xue et al., 2020), power output (Petley and Aggidis, 2016) and number of turbines (Angeloudis et al., 2016b). The current study will look specifically at turbine spacing.

Zero-dimensional or 1D models are often used during the design process to predict power generation based on the simplest operation methods to reduce computational cost, they can then be developed into 2D or 3D models when more details are required after the initial design has been chosen (Xue et al., 2021). Two-dimensional models solve the full Saint-Venant equations to calculate water depth and depth averaged velocities, whereas 3D models use Reynolds Averaged Navier Stokes Equations (RANS) to account for Reynolds stresses and eddy viscosity at different depths (Nash and Phoenix, 2017; Suárez-López et al., 2019).

Tidal range structures are commonly modelled using 2D depth averaging which is generally considered suitable due to the well mixed nature of ocean waters (Angeloudis et al., 2016a; Ma and Adcock, 2020; Neill et al., 2018). Depth averaged models have been used effectively in estimating energy potential (Burrows et al., 2009b), optimising operation (Angeloudis et al., 2018), analysing effects of cumulative TRS schemes (Mackie et al., 2020), and investigating hydrodynamic impacts (Angeloudis and Falconer, 2017). However, they can miss vertical variations in hydrodynamics which require more complex modelling of the entire water column (Adcock et al., 2015). Two-dimensional modelling is most widely used as it strikes a balance between accuracy and computational complexity in both the near and far field (Vouriot et al., 2018), and Sandbach et al. (2018) found very little difference in results when comparing 2D and 3D models of tidal amplitude and average velocity, giving no apparent advantage to the more computationally expensive 3D model.

However, Čož et al. (2019) note the importance of modelling hydrodynamics around TRSs in three dimensions in order to accurately capture complex 3D

2. Literature Review

flows which can be missed in 2D. This was exemplified by Jeffcoate, et al. (2013) who found that flow through hydraulic structures had a 3D component up to twenty diameters downstream of a TRS, which would have been missed by 2D depth averaging alone. Therefore, 3D models are recommended for investigating hydrodynamic structures close to turbines giving more detailed results (Angeloudis et al., 2017; Jeffcoate et al., 2017). Computational Fluid Dynamic modelling (CFD) is acknowledged as the most accurate method for studying 3D flow structures but is also computationally expensive and therefore unsuitable for regional scale investigations (Čož et al., 2019).

An alternative to CFD is to split the domain into separate upstream and downstream constituents that are physically separated but dynamically linked source-sink pairs to simulate the exchange of seawater through sluices and turbines using the orifice equation or turbine performance hill charts (Cornett et al., 2013). This requires very careful treatment of the boundary to ensure accurate interactions between the two zones. Čož et al. (2019) tried a novel approach to the treatment of this boundary by adding a momentum equation as an extra term to represent the external force acting on the body of water due to the high velocity jet passing between the domains, a method commonly used in TSTs studies but not yet employed for TRSs. Through iterative revisions of their layered model of Swansea Bay Lagoon they were able to find the most accurate term for momentum treatment to capture flow complexity of turbine jets and improve accuracy in local results compared to the 2D baseline model.

Another proposal to address the complex nature of modelling coastal processes, is to use coupled models that consider multi-scale and multi-physics issues concurrently rather than modelling factors separately and trying to piece them together later (Tang et al., 2021). The present research answers a call for refined 2D numerical modelling looking at the near and far field hydrodynamic impacts of TRSs (Falconer et al., 2017). Annex 4 provides further consideration of the advantages and disadvantages of using numerical models in different dimensions.

2.8 Summary

Tidal range energy is a valuable and abundant resource that could be used effectively to help meet UK energy needs and carbon emissions targets.

Discussion of the advantages and disadvantages of this type of energy compared to other renewables highlight its predictability and reliability but concerns over environmental impacts and high investment costs have been barriers to development thus far.

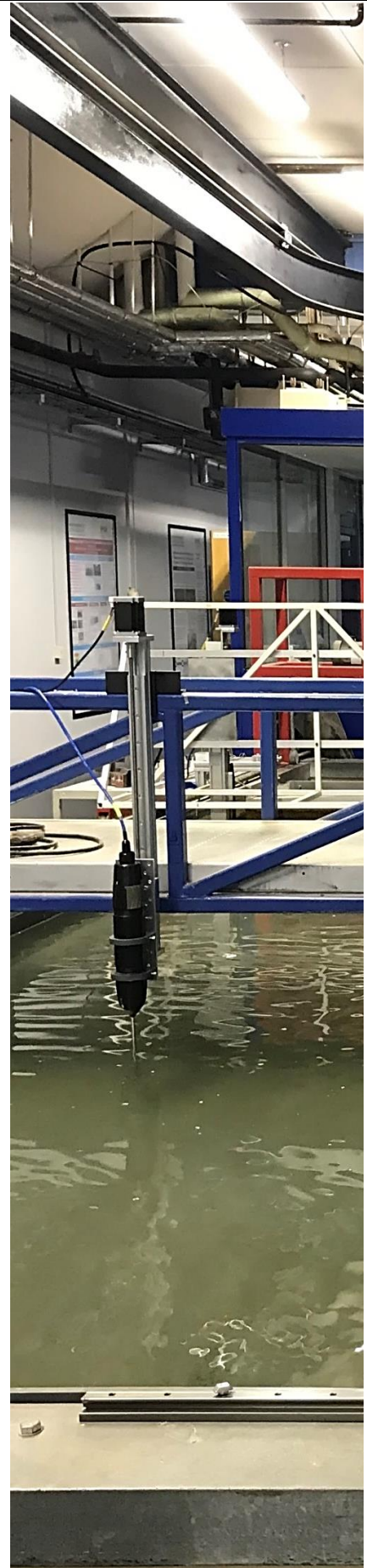
From reviewing existing literature, the following have been identified as gaps in knowledge that can be addressed by the current study:

1. To what extent does the presence of hydraulic structures alter the hydrodynamic environment?
2. How are baseline conditions affected by changes to hydrodynamics in the presence of hydraulic structures?
3. What difference, if any, does the spacing of turbines and sluices in tidal range schemes make to hydrodynamics?

These will be addressed using methods similar to those of Jeffcoate et al. (2013) and Brammer et al. (2014), deploying physical models to examine the effects of TRSs. It will also build on the work of Vouriot et al. (2018) and Angeloudis et al. (2016) who specify turbine spacing as an important aspect for further investigation in the advancement of the TRS industry.

Chapter 3

Methodology



3 Methodology – Physical Model

3.1 Introduction

This chapter presents the methodology of the physical experiments used to test hydrodynamic conditions under differing arrangements of turbines in idealised tidal range schemes (TRSs).

Physical models allow for controlled conditions to be investigated in a managed environment which can then be used to calibrate numerical models to test more complex scenarios once baseline behaviour has been determined. This can save time in the development of numerical models and reduce computational cost (Nash and Phoenix, 2017). It is therefore important to design the physical test accurately to capture the best results whilst balancing the economic and physical constraints of the testing facilities.

This chapter lays out the design process that led to the final suite of tests, details of the tidal basin and equipment, issues of scale and the rationale behind the chosen idealised TRSs.

Key Words and Terms in Chapter 3

Acoustic Doppler Velocity Profiler (ADVP): An electrical probe used for measuring water velocity by calculating the Doppler phase shift between pairs of emitted sound pulses.

Distortion Ratio: The ratio between model scales in the x and y direction, if different.

Scale Effects: Discrepancies between model and prototype behaviour caused by the reduced scale of the model.

3. Methodology

3.2 Methodology

The physical experiments used to investigate flows around hydraulic structures were carried out using a simplified scale model of a TRS in the tidal basin of Cardiff University's Hydro-environmental Research Centre (HRC). The tidal basin measures 4 m x 5.75 m x 0.7 m, dimensions shown in Figure 3.1, with key apparatus highlighted in the photograph of Figure 3.2. A motorised weir gate along the length of the inflow boundary controls water level within the tank to simulate tidal flow, displayed in Figure 3.3. The tidal basin has previously been used to test the hydrodynamic effects of the proposed Severn Barrage TRS (Brammer et al., 2014) and other more recent studies carried out by members of the HRC have looked at water quality in coastal lagoons (Falconer et al., 2020) and wake recovery of TST arrays (Müller et al., 2021).

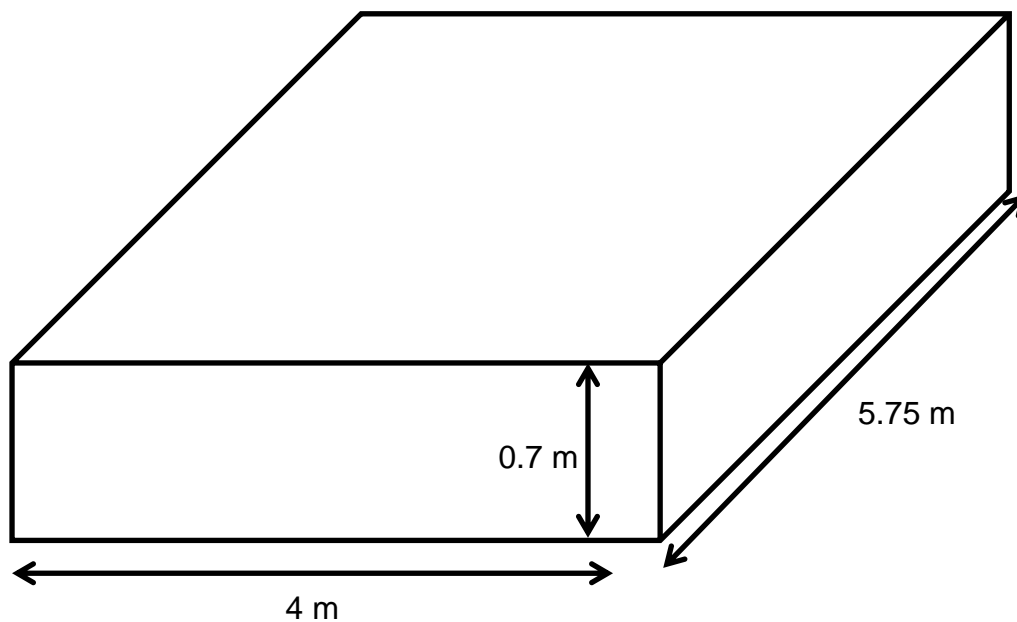


Figure 3.1 Tidal basin dimensions in HRC laboratory.

3. Methodology

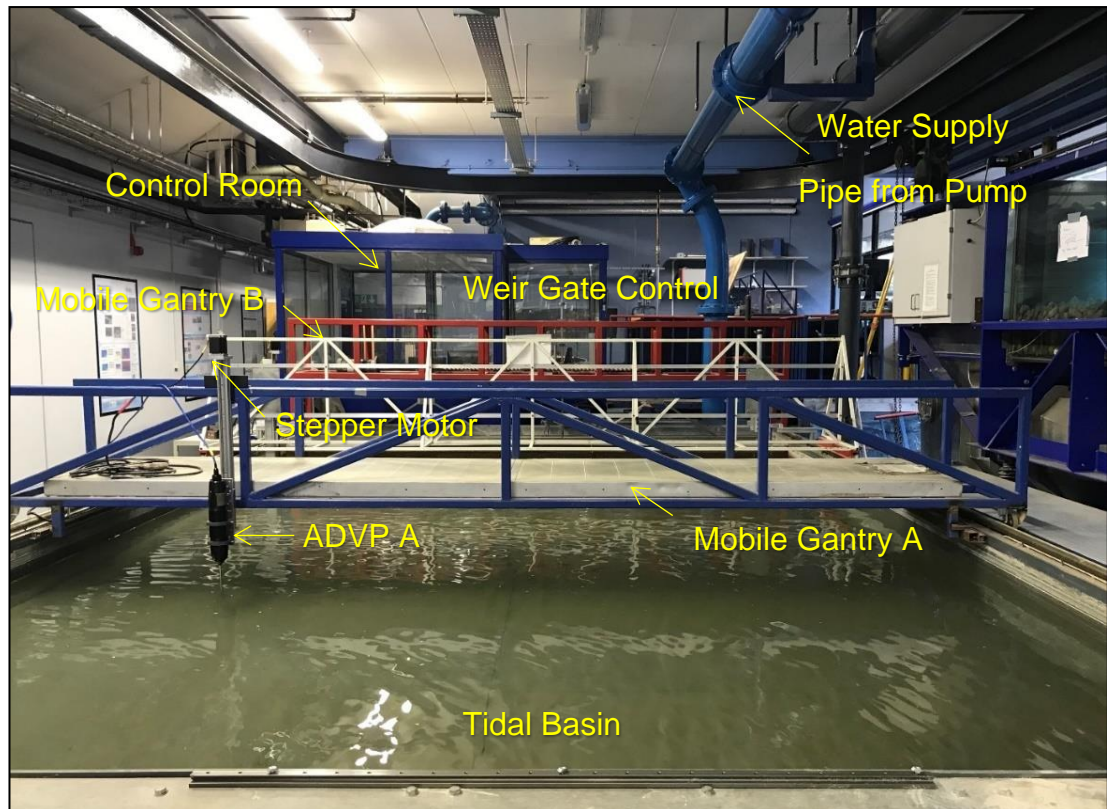


Figure 3.2 Photograph of tidal basin in HRC laboratory highlighting key apparatus.



Figure 3.3 Photograph of tidal basin weir gate.

3. Methodology

3.3 Model Design

Although no TRSs have yet been built in the UK, many proposals exist for the development of this technology along our shores. Table 3.1 summarises details of recently proposed schemes. (Further details of the progress of each proposal are discussed in Table 2.3).

Table 3.1 Potential tidal range schemes in the UK (Hendry, 2016).

Site	Tidal Range (m)	Installed Capacity (MW)	Enclosed Area (km ²)	Seawall Length (km)	Ratio of area to wall length (km ² /km)
Severn Estuary					
Swansea Bay	6.2	320	11.5	9.5	1.2
Stepping Stones	7.7	790	18.0	10.6	1.7
Cardiff	8.6	3,240	71.8	21.0	3.4
Newport	8.6	1,440	40.2	17.5	2.3
Bridgwater Bay	8.1	6,480	243.2	34.1	7.1
North Wales and Liverpool Bay					
Conwy	5.2	740	40.0	16.5	2.4
Colwyn Bay	5.5	3,200	119.8	22.8	5.3
Sefton	6.1	2,600	101.9	27.7	3.7
Wirral/Liverpool	6.3	1,600	67.1	21.9	3.1
Northwest					
West Cumbria	5.6	2,200	92.1	22.4	4.1
Blackpool	6.1	2,600	96.3	24.5	3.9
Wyre	6.5	3,045	120.0	19.9	6.0
Barrow in Furness	6.5	1,600	56.8	23.2	2.5
East Coast					
The Wash	4.5	695	50.0	18.8	2.7
East Lincs Coast	4.7	1,940	120.0	29.9	4.0
Southeast					
Sheerness	4.2	1,310	100.0	28.6	3.5
Thames Estuary	4.3	515	50.0	19.0	2.6
Sussex Coast	4.6	2,415	160.0	34.8	4.6

These details, published in the Hendry Review of Tidal Lagoons (2016), give a clear indication of the dimensions and scale that could reasonably be expected of TRSs around the UK coast, providing a baseline from which to design a research test scheme. Whilst it is not possible to test all of the proposed projects within the scope of this research, these details can be used to inform an idealised representation of a TRS within the limitations of the HRC tidal basin.

3. Methodology

3.3.1 Scale

The ability of a physical model to accurately predict the performance of a full-scale prototype relies on the hydraulic similarity between the two. Hydraulic similarity is achieved by designing a model with:

- Geometric similitude – constant ratio between length dimensions and shape.
- Kinematic similitude – constant ratio between velocity and acceleration.
- Dynamic similitude – constant ratio of forces, maintaining kinematic similitude at equivalent geometrical points.

By satisfying these criteria and maintaining scaling laws (Equations 3.2 to 3.8) similarity will exist between the model and the prototype, and data obtained from the model can be extrapolated accurately to help design full-scale prototypes (American Society of Civil Engineers, 2000). However, physical constraints and limitations of facilities mean that it is unrealistic to be able to fulfil all of these conditions and issues arise from trying to do so. Therefore, it is important to ascertain which forces are most critical in the current case and concentrate on achieving balance for these, acknowledging that a scaled model will never perfectly reflect the performance of a real-life prototype and interpreting all results accordingly (Hamill, 2011).

Hydraulic models of coastal regions are most strongly influenced by gravity and therefore are generally designed to maintain similarity of Froude number between the model and the prototype (Equation 3.9) (Hamill, 2011; Sang-Ho et al., 2016). However, limitations of test facilities can make this impractical, in which case Reynolds number is chosen as the constant parameter on which other dimension ratios are based (Equation 3.10) (American Society of Civil Engineers, 2000; Brammer et al., 2014). This is particularly the case in tests with low flow velocity as in the present study.

3. Methodology

The following equations show the effects of a distorted model on aspects of scale: (American Society of Civil Engineers, 2000; Hamill, 2011; Torres et al., 2018):

Distortion Ratio $G = \frac{X}{Y}$ *Equation 3.1*

Horizontal length ratio $\frac{l_m}{l_p} = \frac{1}{X}$ *Equation 3.2*

Vertical length ratio $\frac{l_m}{l_p} = \frac{1}{Y}$ *Equation 3.3*

Area ratio $\frac{A_m}{A_p} = \frac{1}{XY}$ *Equation 3.4*

Time ratio $\frac{T_m}{T_p} = \frac{\sqrt{Y}}{X}$ *Equation 3.5*

Velocity ratio $\frac{V_m}{V_p} = \frac{1}{\sqrt{Y}}$ *Equation 3.6*

Discharge ratio $\frac{Q_m}{Q_p} = \frac{1}{XY^{\frac{3}{2}}}$ *Equation 3.7*

Manning's n ratio $\frac{n_m}{n_p} = \frac{\sqrt{X}}{Y^{\frac{2}{3}}}$ *Equation 3.8*

Froude ratio $Fr = \frac{1}{\sqrt{Y^2 g}}$ *Equation 3.9*

Reynolds number ratio $Re = Y^{\frac{3}{2}}$ *Equation 3.10*

Where:

- A = Area
- G = Distortion ratio
- T = Time
- Q = Discharge
- V = Velocity
- X = Horizontal length scale
- Y = Vertical length scale
- Re = Reynold's Number
- Fr = Froude Number
- l = Length
- n = Manning's n
- m = Model
- p = Prototype

3. Methodology

Using figures from the Hendry Review alongside the dimensions of the HRC tank, dimensional analysis calculations led to the choice of the distorted scale: $X = 1:5000$ and $Y = 1:100$. This decision was reached based on a number of limiting factors as demonstrated in Figure 3.4 which shows the decision envelopes for the following criteria:

- X (horizontal length scale): $1:4000 < X < 1:10000$, limited by tank dimensions.
- Y (vertical length scale): $1:50 < Y < 1:150$, limited by tank dimensions.
- λ (tidal period): $60 \text{ s} < T < 120 \text{ s}$, limited by mechanical weir gate performance.
- G (distortion ratio): $10 < G < 100$, ratio of length-to-depth scales, limits recommended by American Society of Civil Engineers (2000).

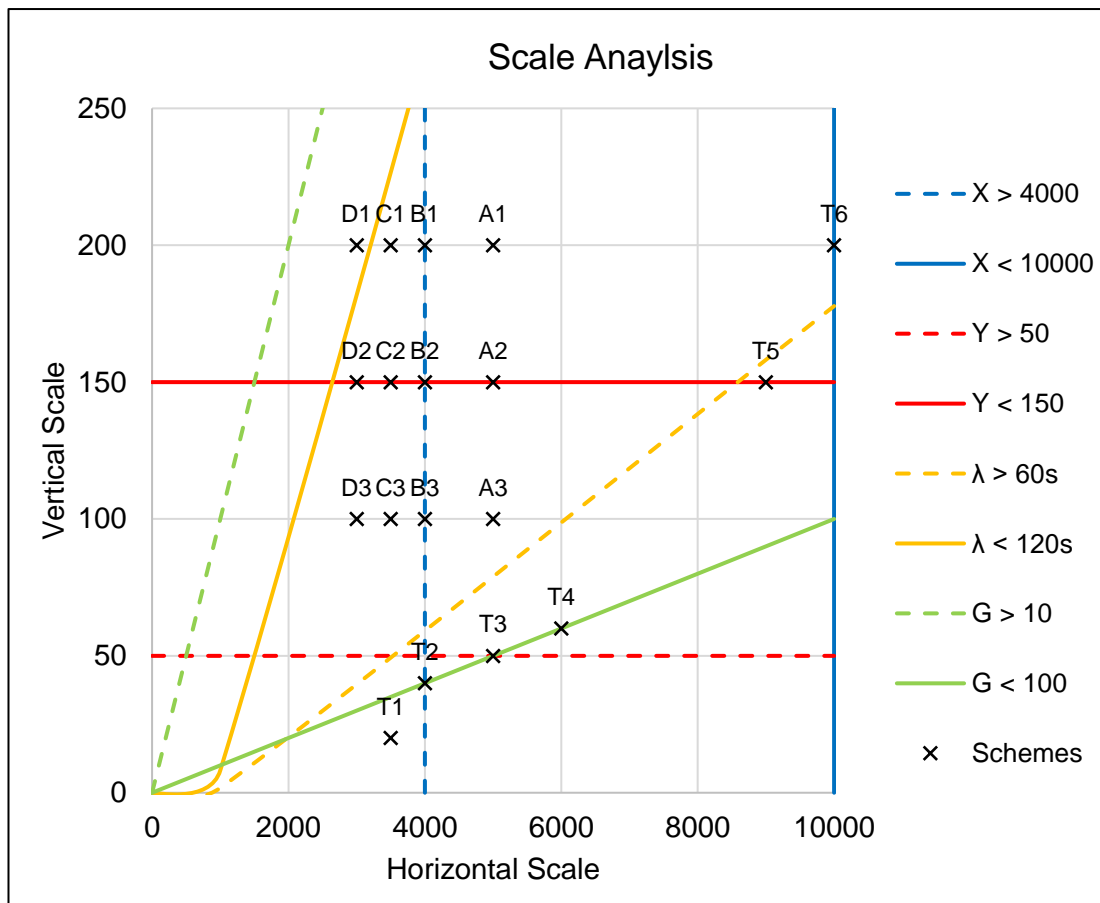


Figure 3.4 Scale analysis of potential schemes for testing in the tidal basin based on limitations for X , Y and T scales as well as considering distortion ratio, G . Proposed scale schemes, A1 – T6, as outlined in Table 3.2, are plotted within the decision envelopes.

3. Methodology

The proposed schemes listed in Table 3.2 consider various combinations of scale in the X and Y directions. For example, proposed scales A1 to A3 consider an X scale of 1:5000 whilst varying the Y scale from 1:100 to 1:200 and then comparing the resultant impact of these choices on the scale for time (T) and the distortion ratio (G). These schemes are plotted in Figure 3.4 to help decide upon the best combination of scales based on the limits described above to enable realistic modelling within the confines of the tidal basin.

Table 3.2 Proposed scales for testing TRSs in tidal basin.

Proposed Scales	X Scale (m)	Y Scale (m)	T Scale (hrs)	Tidal Period λ (s)	Distortion Ratio G (-)
A1	1:5000	1:200	1:0.0028	127.28	25.0
A2	1:5000	1:150	1:0.0024	110.23	33.3
A3	1:5000	1:100	1:0.0020	90.00	50.0
B1	1:4000	1:200	1:0.0354	159.10	20.0
B2	1:4000	1:150	1:0.0031	137.78	26.7
B3	1:4000	1:100	1:0.0025	112.50	40.0
C1	1:3500	1:200	1:0.0040	181.83	17.5
C2	1:3500	1:150	1:0.0035	157.47	23.3
C3	1:3500	1:100	1:0.0028	128.57	35.0
D1	1:3000	1:200	1:0.00471	212.13	15.0
D2	1:3000	1:150	1:0.0041	183.71	20.0
D3	1:3000	1:100	1:0.0033	150.00	30.0
T1	1:3500	1:20	1:0.0013	57.50	175.0
T2	1:4000	1:40	1:0.0016	71.15	100.0
T3	1:5000	1:50	1:0.0014	63.64	100.0
T4	1:6000	1:60	1:0.0013	58.09	100.0
T5	1:9000	1:150	1:0.0014	61.24	60.0
T6	1:10000	1:200	1:0.0014	63.64	50.0

Whilst proposed scales, A2, A3, B2 and B3 all fell within the boundaries of the decision criteria, scale A3 was chosen as it resulted in a time scale (T) that provides a tidal period (λ) of 90 seconds. This was found to be critical for generating flow rates within the tank that could be maintained consistently by the mechanical weir gate whilst falling within a detectable range for the velocity measuring equipment. The depth scale (Y) of proposed scheme A3 will also enable modelling of realistic values for the tidal range of the Severn

3. Methodology

Estuary (7 – 14 m) as well as fitting scaled TRSs with an area of up to 100 km² without encroaching on the boundaries of the tank which could cause interference with the velocity readings around the TRS. However, the limitations of the tank dimensions have led to a distortion ratio of 50, this is a common problem when modelling estuaries that are typically much wider than they are deep.

Vertically distorted models have the advantage of reducing cost by making use of available space rather than building new, bespoke facilities and also increase the accuracy of depth and flow velocity measurements rather than attempting to take readings in extremely shallow water. However, the disadvantage of significantly distorted models is that the flow patterns across depths can be distorted due to the altered width-to-depth ratio of the flow. This will have the greatest impact in situations where flow has a strong three-dimensional aspect and should be addressed by considering resistance and velocity similitude to ensure currents are not exaggerated or distorted (American Society of Civil Engineers, 2000).

Scale effects, i.e., discrepancies between forces in the model and the prototype, are caused by limitations of hydraulic similarity but can be mitigated by maintaining kinematic similitude and by quantifying the effects and compensating for them by adapting geometric scale, slopes or roughness (American Society of Civil Engineers, 2000). The scale effects of the distortion ratio in this study are addressed by adapting the scale equations and will be considered throughout the analysis of the resulting data. Other studies using distorted length ratios, accounted for scale effects by matching Reynolds number over Froude number and adapting the geometric scale of certain components (Ahmadian et al., 2010; Brammer et al., 2014).

The selected scale was applied to TRS proposals and conditions from the Severn estuary (see Table 3.3) which were then used for the laboratory test cases. Although distorted, this scale is an improvement on previous studies of the Severn Estuary which had a distortion ratio of 200 (Brammer et al., 2014).

3. Methodology

Table 3.3 Scale parameters applied to design aspects of proposed TRSs in the Severn Estuary for testing in the laboratory.

Parameter	Real Life	Scale	Model
Horizontal Scale		1:5000	
Length of seawall	9.5 km	1:5000	1.9 m
Vertical Scale		1:100	
Tidal range	8 m	1:100	8 cm
Turbine Diameter	7 m	1:100	7 cm
Velocity		1:10	
Discharge		1:5000000	
Manning's n		1:3.28	
Froude Number		1:0.003	
Reynolds Number		1:1000	
Time for Tidal Cycle	12.5 hours	1:500	90 secs

3.3.2 Idealised Geometry

Once the scale of the experiments was determined, a broad range of representative TRS schemes were selected from the list of proposals in the Hendry Review (2016), to model a variety of future scenarios and test the difference that the size of the enclosed area has on flow velocities and circulation around TRSs. The areas of the idealised TRSs have been calculated based on the A3 scale (outlined in Section 3.3.1). The area of each scheme was approximated to a representative area so that two schemes could be tried using the same model, e.g. The Wash and Barrow schemes would both be modelled with an area of 50 km² despite the Barrow scheme having a proposed area of 57 km². To account for the distortion ratio between the X and Y scales, the number of turbines used for each experiment was calculated based on the total turbine area of the proposed schemes. For example, proposals for the Stepping Stones scheme from the Hendry Review (2016) give an installed capacity of 790 MW, this would equate to approximately forty 20 MW turbines. With a diameter of 7 m (the standard size of existing TRE bulb turbines), this would give a total turbine area of 1600 m², which at the scale of the present experiments would equate to an area of 32 cm². It would be unrealistic to create a turbine opening that matched the dimensions of existing bulbs using the current scale for width (1:5000) and depth (1:100), leading to an orifice of width 0.14 cm and a

3. Methodology

height of 7 cm, therefore it was decided to scale both dimensions according to the Y scale, leading to a circular orifice with diameter 7 cm. Unfortunately, another constant limitation of physical experiments is the availability of parts and materials and so based on available pipe diameters the final turbine area of the physical model is 6 cm and the number of turbines for each experiment was then calculated based on this area. These figures for representative tidal lagoon area and number of turbines are presented in Table 3.4.

The area of each TRS will be kept constant to maintain the same energy output, whilst the ratio of the seawall's width-to-length will be varied to test the impact of geometry and turbine spacing on regional flow regime. Four idealised geometries have been designed to test the effects of varying the seawall width-to-length ratio:

- a) Square, seawall width-to-length ratio: 1:1
- b) Rectangle 1, seawall width-to-length ratio: 1:2
- c) Rectangle 2, seawall width-to-length ratio: 4:5
- d) Rectangle 3, seawall width-to-length ratio: 5:8

This will build on the work of Falconer (1974) and Vouriot et al. (2018) who investigated the effects of varying the width-to-length ratio of seawalls in rectangular harbours and TRSs respectively. Going beyond the work of Vouriot et al. (2018), the number, position and spacing of turbines will be varied to investigate the effect of turbine configuration on flow regimes to see if it is possible to minimise the environmental impact of the structures whilst maintaining financially competitive energy production. Charlier (2003) highlights the importance of the geometry of a tidal energy project on its performance and impact, rating its depth and the cross-sectional area of apertures as important as its surface area, making this investigation of the seawall ratio and turbine spacing of particular interest for TRS proposals.

3. Methodology

Table 3.4 Proposed TRS schemes from the Hendry Review (2016) scaled to fit the size of the physical model.

Scheme	Proposed Installed Capacity (MW)	Representative Number of Turbines*	Proposed TRS Area (km ²)	Representative TRS Area** (km ²)	Seawall Dimensions***						
					Sq.	Rec. 1 Ratio 1:2		Rec. 2 Ratio 4:5		Rec. 3 Ratio 5:8	
					L (m)	L (m)	W (m)	L (m)	W (m)	L (m)	W (m)
Stepping Stones	790	1	18	20	0.9	1.2	0.6	1.0	0.8	0.7	1.1
The Wash	695	1	50	50	1.4	2.0	1.0	1.6	1.4	1.1	1.8
Barrow	1600	2	57	50	1.4	2.0	1.0	1.6	1.4	1.1	1.8
Cardiff	3240	4	72	70	1.7	1.2	2.4	1.9	1.5	1.4	2.0
Liverpool	1600	2	67	70	1.	1.2	2.4	1.9	1.5	1.4	2.0
Minehead	3200	4	90	90	1.9	1.3	2.6	2.1	1.7	1.5	2.4
Sheerness	1310	2	100	90	1.9	1.3	2.6	2.1	1.7	1.5	2.4

* Number of turbines scaled to represent the total turbine area of the proposed scheme.

** Pairs of TRS proposals have been grouped with a single representative area so that two schemes can be tested using the same model.

*** Dimensions for a square TRS and three rectangular TRSs with varying seawall width-to-length ratio but constant area to test effect of varying TRS geometry on hydrodynamics.

3. Methodology

3.3.3 Interruption to Study

These initial proposals were designed to test the maximum variety of proposed TRSs within the facilities and time available. However, following the considerable disruption to all work worldwide caused by the global pandemic, investigations had to be reduced to a more modest scheme to fit around a new timescale and restricted working conditions.

This new experiment design considers only two geometries: a square with an internal area of 1 m² and a rectangle with a similar area but with a seawall width-to-length ratio of 1:2. Using these two layouts, multiple turbine configurations and seabed conditions were tested.

The simple square TRS measures 1.1 m x 1 m x 0.5 m, attached to the rear wall of the tank to represent a coastally attached TRS (shown in Figure 3.5a) as proposed along the north and south coasts of Wales. The rectangular TRS was designed and made in the same fashion but with a new seawall width-to-length ratio of 1:2 (see Figure 3.5b). The physical dimensions of both experiments are presented in Table 3.5

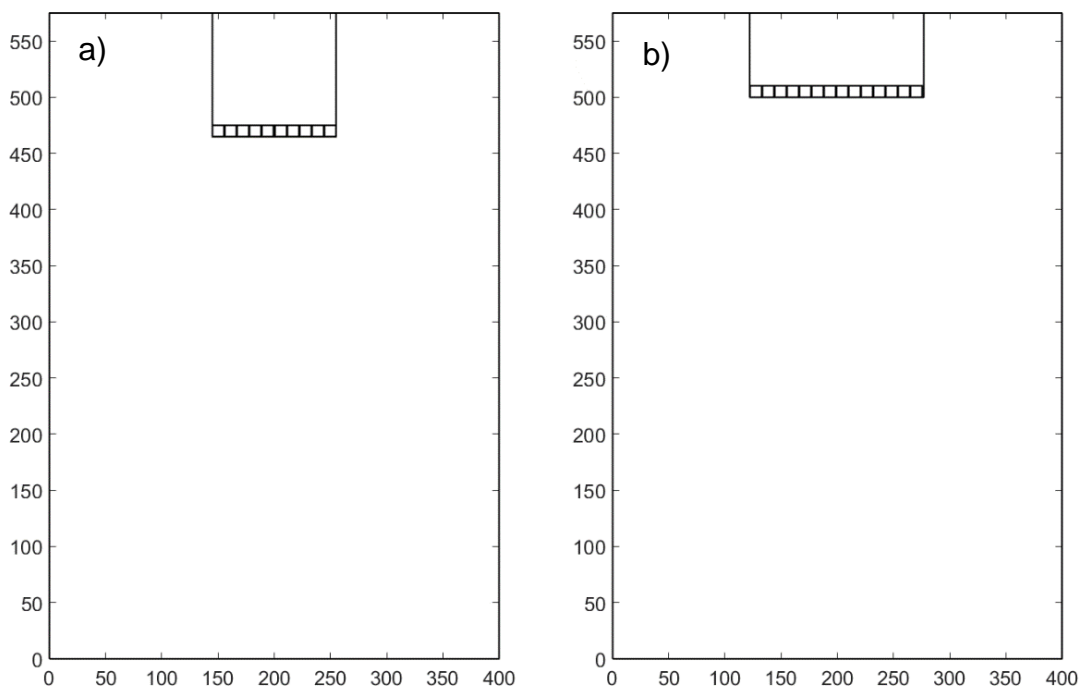


Figure 3.5 a) Idealised square and b) rectangular coastally attached TRSs as built in HRC tidal basin.

3. Methodology

Table 3.5 Dimensions of square and rectangular TRSs tested in the HRC.

Layout	Front wall	Side walls	External dimensions	Internal Dimensions
Square	1.10 m (10 turbines)	1.00 m	1.11 m ²	0.99 m ²
Rectangle	1.55 m (14 turbines)	0.75 m	1.16 m ²	1.01 m ²

The side walls are made from 12 mm thick PVC, chosen for its durability and impermeability. The front wall is made from a series of aluminium box sections (0.11 m x 0.11 m) cut to a height of 0.5 m (see Figure 3.6a) and aligned side by side, held in position by an 18 mm thick PVC support bar and sealed with clear silicone sealant to prevent water forcing through between the sections (as presented in Figure 3.7). Eight of these box sections were cut with a circular opening of diameter 0.06 m, to hold an aluminium pipe representing TRS turbine casings (shown in Figure 3.6b). The area of these openings was calculated using dimensional analysis and comparison of the turbines used in proposed schemes to accurately represent their scale in the physical model used here. By creating this wall as individual sections, they can easily be rearranged in any order to test turbines in different layouts and resealed to create a new impermeable wall at minimal cost (see Figure 3.7).

3. Methodology

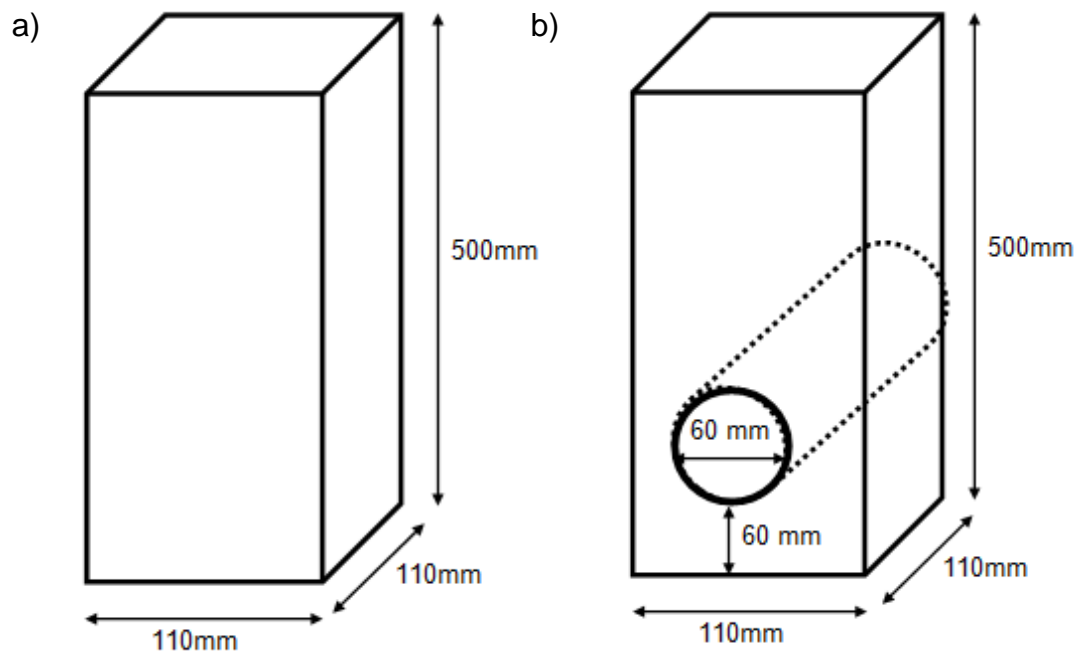


Figure 3.6 a) blank box section and b) turbine opening box section as used to create the front seawall of the TRS structures. (Not drawn to scale).



Figure 3.7 Example of box section arrangement with two turbine opening box sections and eight blank box sections.

3. Methodology

The depth of turbines in TRSs is limited by geomorphology and construction cost, and studies recommend a minimum depth of 10 m to ensure turbines are fully submerged whilst minimising dredging costs (Angeloudis et al., 2016a; Falconer et al., 2017). A height of 0.06 m from the seabed was chosen, representing a real-world height of 6 m, one turbine diameter, as depicted in proposed designs for the Swansea Bay Tidal Lagoon (Tidal Lagoon Swansea Bay, 2014b).

It was initially hoped that miniature turbines of the type used by Jeffcoate et al. (2017) would be used to test the most realistic turbine conditions in the tank, however time did not allow for testing this variation and the simplified set up used here represents the draught tubes of the turbines as tested in similar experiments by Jeffcoate et al. (2013) and Vouriot et al. (2018). At this scale it is hoped that the openings represent sufficient resistance to accurately model the behaviour of water forced through turbine openings. Water will flow freely through these openings and will not be subject to a particular operation mode.

Another option for representing the resistance caused by turbines is the use of porous discs, this method is cost effective and has the benefit of being able to tailor your choice of material to best represent thrust. Porous discs are commonly used with great success in wind turbines studies, however, they do not extract energy or create swirl as turbines would (Nash and Phoenix, 2017). In this instance draught tubes were left open to avoid any issues caused by turbine scaling.

3. Methodology

3.4 Experimental Setup

3.4.1 Test Cases and Configurations

The three main parameters under consideration in the physical model are: TRS geometry, the layout of turbines in TRSs and TRS bed conditions.

Experiments have been designed in order to test these parameters as listed in Table 3.6. Experiments with the prefix “S” represent square layouts whilst “R” denotes rectangular cases. The number following this shows the number of turbines, whilst the final letter shows subsequent tests with the same geometry and number of turbines but with a variation in turbine layout, e.g. test case S2C, is the third experiment to use a square layout with two turbines. Experiments with the prefix “B” denote cases where the bed conditions were changed, either the material or the slope, but all were conducted in a square TRS with two turbines in the same locations. Preliminary measurements were taken in the tank before a TRS was built (case “00”) and represent “baseline conditions” with which to compare all other cases to determine the impact of each design on natural conditions.

Table 3.6 Experiment variables for each test, including geometry, number and position of turbines and bed conditions as denoted by the test code.

Physical Test Code	Geometry	Number of Turbines	Slope	Bed material
00	N/A	0	0°	Smooth plastic
S0	Square	0	0°	Smooth plastic
S1A	Square	1	0°	Smooth plastic
S1B	Square	1	0°	Smooth plastic
S2A	Square	2	0°	Smooth plastic
S2B	Square	2	0°	Smooth plastic
S2C	Square	2	0°	Smooth plastic
S2D/ B1	Square	2	0°	Smooth plastic
B2	Square	2	0°	20 mm grass
B3	Square	2	0°	20 mm gravel
B4	Square	2	0°	10 mm gravel
B5	Square	2	10°	Smooth plastic
B6	Square	2	5°	Smooth plastic
R0	Rectangle	0	0°	Smooth plastic
R1	Rectangle	1	0°	Smooth plastic
R2A	Rectangle	2	0°	Smooth plastic
R2B	Rectangle	2	0°	Smooth plastic
R2C	Rectangle	2	0°	Smooth plastic
R2D	Rectangle	2	0°	Smooth plastic

3. Methodology

3.4.1.1 TRS geometry

The initial tests were carried out using a square geometry of 1.1 m x 1.0 m x 0.5 m (as shown in Figure 3.5a), which was then adapted to a rectangle of 1.55 m x 0.75 m x 0.5 m (see Figure 3.5b). This maintained the area as closely as possible whilst changing the walls from a ratio of 1:1 to 2:1 to test whether the length and width of the TRS make a significant difference to the hydrodynamics as suggested by Falconer (1984) and Vouriot et al (2018). It is hoped that testing this simplified geometry will determine accurate conditions that can be applied to more complex cases proposed across the UK and beyond (Rampazzo et al., 2019).

3.4.1.2 The layout of hydraulic structures in TRSs

In the majority of existing schemes and designs, turbines and sluices are located in the same section of the TRS sea wall to minimise costs and simplify the construction process (as discussed in Section 2.5.6.1.4).

However, it has been shown that the layout of these hydraulic structures has a significant impact on hydrodynamics (Fallon et al., 2014) and that the “design of turbine distribution is critical for optimum efficiency and minimal environmental change” (Falconer et al., 2017 p.1553). It is therefore important to test whether conventional clustered configurations or a more separated scheme would be best to maintain current environmental conditions, thus making projects more sustainable in the holistic sense.

By using individual box sections that can be moved easily, the current physical model will be able to test several configurations for both the square and rectangular cases, comprising 10 and 14 box sections respectively. The position of the turbine openings will then be altered in each case to examine the effects, the different layouts for each TRS shape are shown in Table 3.7 and Table 3.8. This selection of turbine positioning is intended to sample representative cases of certain spacings which could then be used to calibrate a numerical model to investigate other combinations. In both the square and rectangular cases, the first turbine was fixed one space in from the right-hand wall whilst the second turbine was moved to consider different spacing. This method of fixing the position of one turbine whilst varying the relative position of additional turbines was also adopted in testing the impact

3. Methodology

of the spacing of adjacent and perpendicular TSTs (Mycek et al., 2013) in order to systematically compare the effects of turbine layout. Test case S2D, centralised positioning of two turbines, was investigated to examine the effects of placing turbines away from seawalls and was also used for each of the bed condition experiments so that conditions would be symmetrical and bed slope or bed material would be the only variable under examination.

Table 3.7 Turbine layout for test configurations of square cases. Numbers 1 to 10 represent box section number.

Test Case \ Turbine Position	1	2	3	4	5	6	7	8	9	10
S0										
S1A									x	
S1B							x			
S2A								x	x	
S2B		x							x	
S2C					x				x	
S2D				x			x			

Table 3.8 Turbine layout for test configuration of rectangular case. Numbers 1 to 14 represent box section number.

Test Case \ Turbine Position	1	2	3	4	5	6	7	8	9	10	11	12	13	14
R0														
R1													x	
R2A												x	x	
R2B											x		x	
R2C										x			x	
R2D		x											x	

The initial experiment design intended to represent existing proposals as closely as possible matching the number and the area of turbines to those which had been proposed in TRS designs. The adapted test schedule means that configurations will now only comprise one or two turbines but with more spacings able to be compared. Further configurations could be tested numerically or experimentally in future.

3. Methodology

3.4.1.3 TRS bed conditions

As well as varying the position of the turbines in the TRS it is also worth testing the sensitivity of TRSs to varying bed conditions, including bed material (Hajikandi et al., 2017) and slope (Sang-Ho et al., 2016). This will help to understand flow behaviour under more realistic conditions as natural geomorphology and sediment will have an impact on TRS hydrodynamics.

3.4.2 Domain and boundary conditions

The inflow boundary of the tidal basin is controlled by a mechanically operated weir gate, which allows for the control of the water level and flow rate, whilst the other three walls of the basin are closed boundaries and reflective surfaces.

The weir gate, operated by a gear box, was programmed to maintain a tidal flow wave with a range of 0.36 m to 0.44 m, and period of 90 seconds to imitate the tidal condition of the Severn Estuary based on the previously determined scale. This simplified tide can be represented by the sine wave:

$$h = 4 \cos 4x + 40 \quad \text{Equation 3.11}$$

where h is water depth in centimetres and x is the time in seconds. Although this is a highly simplified case it enables accurate and cost-effective modelling at a laboratory scale and future numerical studies can extend to more accurate representations of the tide. Artificial tide systems of this kind, using water pumps and mechanically controlled, vertical sharp-edged weirs, are commonly used in tidal simulation studies and investigations stress the importance of accurately scaling the model tides for results to be meaningful (Rampazzo et al., 2019; Tognin et al., 2018).

3.5 Data Collection

3.5.1 Velocity Data Collection

Velocity data was collected using a Nortek Vectrino, Acoustic Doppler Velocity Profiler (ADVP). ADVPs work by transmitting a pair of short sound pulses at a specific frequency into the water column and measuring the Doppler phase shift of the pulses as they are reflected back to the probe to calculate the water velocity (probe and transmission method illustrated in Figure 3.8). This is known as the coherent Doppler method and is highly accurate, being able to differentiate very small differences in phase (Nortek, 2018).

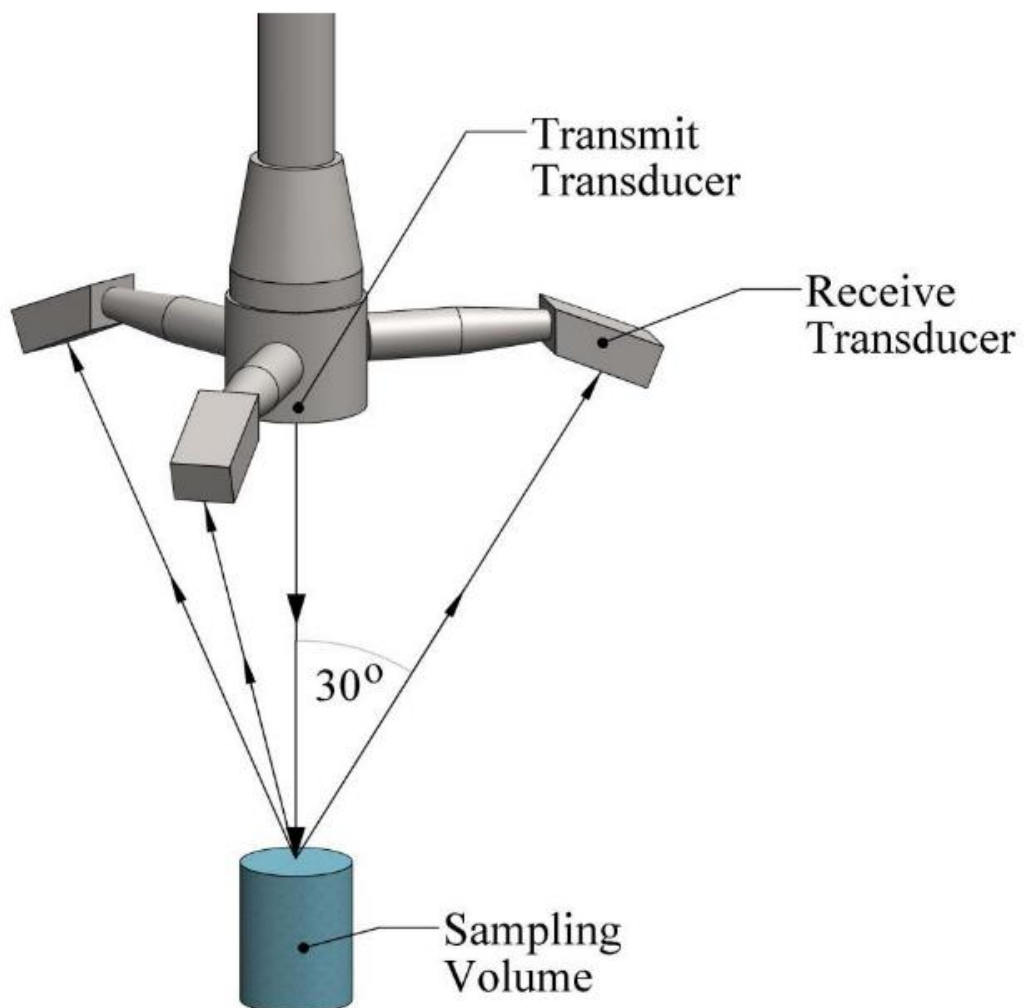


Figure 3.8 Working principle of an ADVP (Zhai, et al., 2014).

3. Methodology

The sound pulses are not reflected off the water itself but off particles suspended in the water column. Therefore, it is important to ensure that sufficient particles of an appropriate size and density are maintained in suspension to gain a strong signal from which to calculate the velocity (Müller et al., 2021). The particles must be of similar density to water so that they move at the same average speed and the measured velocity will then represent that of the water. If the water is too oily or too clear, there will not be a strong enough signal and the resultant velocity measurements will be less reliable. Hollow microspheres of density $12 \mu\text{m}$, (as recommended by the ADVP user manual, 2018) were added to the water in the tidal basin to create the right conditions and were kept in suspension through regular stirring between measurements.

The difference between an acoustic doppler velocimeter (ADV) and an acoustic doppler velocity profiler (ADVP) are that a profiler enables multiple depths to be sampled at once, meaning that it is possible to capture the velocity at all depths in the tank in the same time it would take an ADV to gather only 3% of the data. They work well in laboratory and open water settings with both high and low energy flows. ADVPs can experience greater problems with “weak spots” and boundary interference than ADVs due to the length of time that the measurement pulse is exposed but this can be countered by careful positioning and operation of the probe (Nortek, 2018).

Two ADVPs were mounted on mechanised braces controlled by stepper motors for movement in the vertical axis and fixed to mobile gantries to enable them to be moved easily in the horizontal axis. Figure 3.9 shows this set up in the laboratory. Using two ADVPs in tandem allowed quicker coverage of the whole tank. To ensure there was no interference between the readings for each device, the probes were operated separately rather than being mechanically linked which can cause cross-signal interference and were kept at a minimum distance of 1.5 m from each other to further avoid interference.

3. Methodology

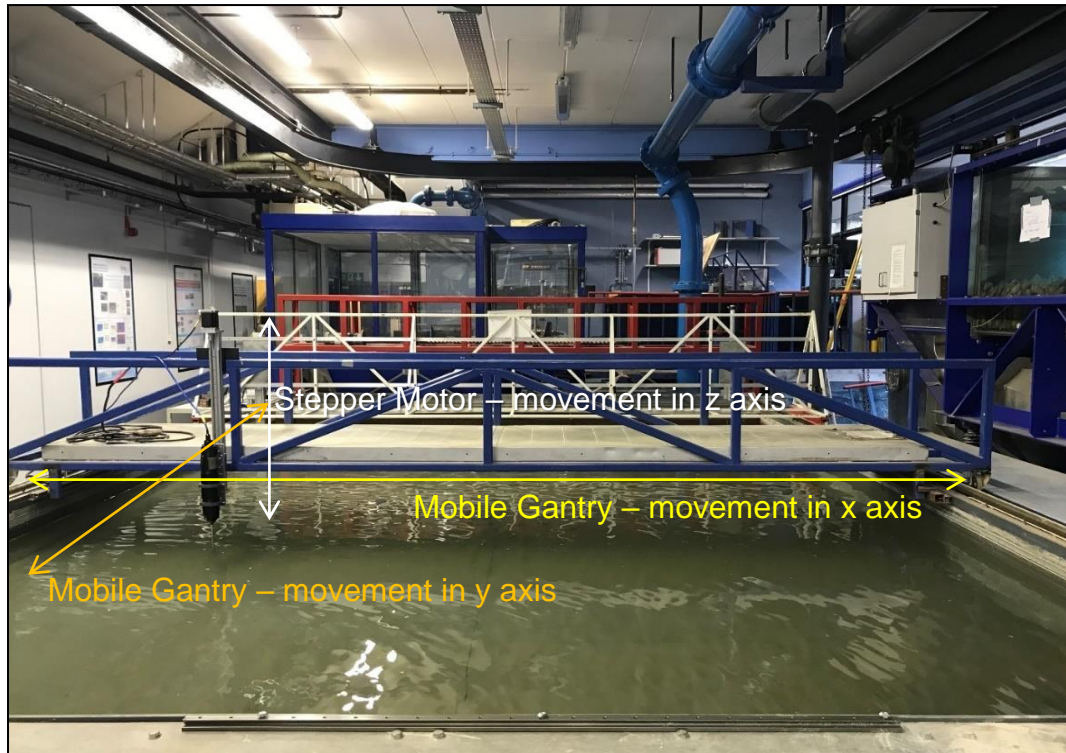


Figure 3.9 Photograph of laboratory illustrating ADVP system movement in three dimensions.

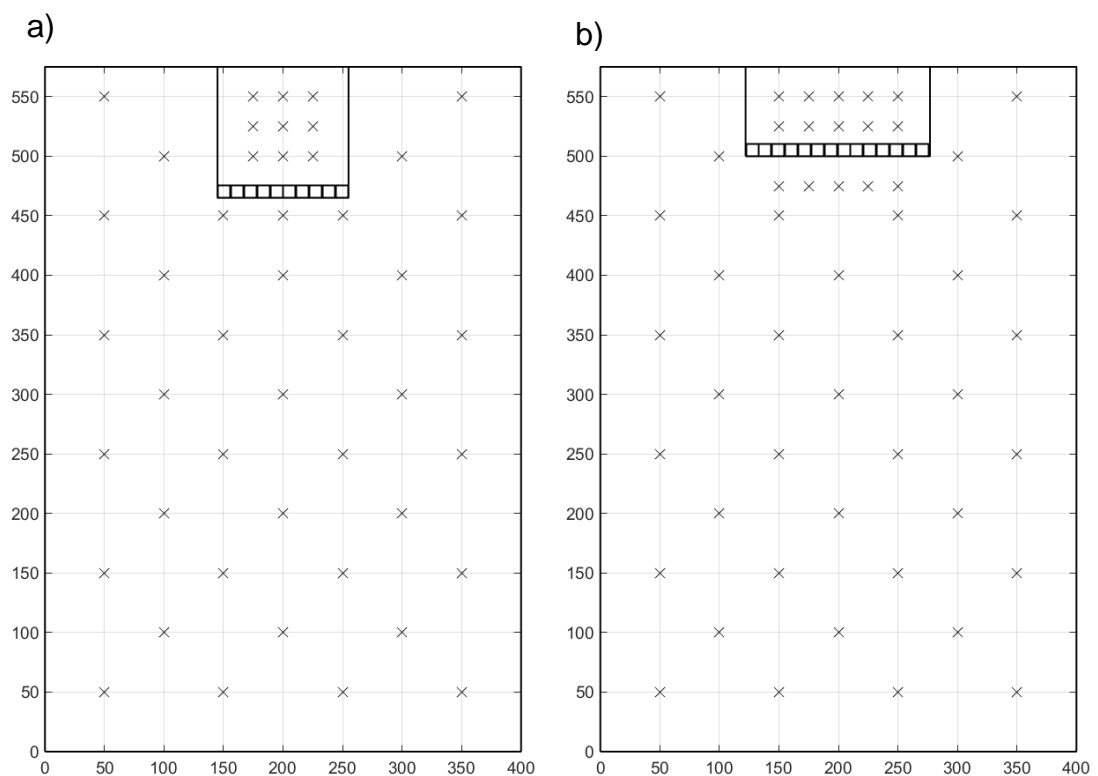


Figure 3.10 Data collection sample grid for a) square and b) rectangular lagoon.

3. Methodology

3.5.1.1 Velocity Data Sampling Method

Velocity data was collected at 1 m intervals in a staggered grid across the tank, with a more refined grid of 25 cm within the lagoon walls. Figure 3.10 shows the sampling grids for both the square and rectangular lagoons. A coarse staggered grid of 36 points in the outer lagoon area and a regular refined grid of 9/10 points in the inner lagoon area were chosen for maximum coverage of the tank in the limited time, to provide clear information from which to calibrate a numerical model (as favoured by Parsapour-Moghaddam et al, 2018).

Samples were taken every millimetre from depths of 10 mm from the tank bed to 300 mm to get a full picture of the velocity throughout the entire water column. A stepper motor enabled the probe to be raised automatically by intervals of 20 mm to save time. Samples were taken over a range of 30 mm, with overlapping data trimmed from the top and bottom 5 mm as preliminary experiments showed the results to be least reliable at these points.

Measurements were taken at the maximum sampling rate of 100 Hz for the duration of four tides, giving sufficient data to observe variations in the flow conditions across whole tides as demonstrated by Vouriot et al., (2018) and Xia et al (2010).

3. Methodology

3.5.2 Water Level Data Collection

Water level in the tank is controlled by a weir gate and measured using water level probes in the corners of the basin. These fixed probes are part of a wave gauge system that measures water level by recording the current flowing between a pair of parallel stainless-steel wires that make up the immersed probe. The current flowing between these wires is proportional to the instantaneous depth of immersion (H.R. Wallingford, 2015). The probes were calibrated relative to the mean water level of the experiments and fixed in position around the tank using rigid mounting brackets to maintain stability at the given levels and ensure accurate readings, free from interference from other equipment. Although the water level probes have a range of 300-600 mm, they became less accurate over time, losing their range and sensitivity due to temperature and chemical changes in the water, which affect conductivity. To compensate for this lack of accuracy, portable pressure transducers were also used from experiment S2B onwards to capture the water level at the same sample points as the ADVP.

Pressure transducers calculate water level by converting strain deformation into an electrical signal proportional to the pressure acting on it. Water depth can be calculated from this voltage signal by analysing the proportional pressure changes relative to atmospheric pressure (Omega Engineering, 2019). These particular transducers were based on gauge pressure rather than absolute pressure, meaning they were able to be calibrated in the lab rather than at predefined factory settings which should improve their accuracy. Unlike the water level probes, the pressure transducers were not limited to a single fixed position and were moved in sync with the ADVPs, taking readings 25 cm to the right of the velocimeters. Being able to measure water level at all points across the tank allows for more accurate calibration of the numerical model rather than relying on the measurements at the four corners alone. This method of combining velocity measured by ADVPs alongside water level gauges is often used for site characterisation of tidal energy schemes (Draycott et al., 2019; Schmitt and Lieber, 2021; Sentchev et al., 2020), and Stallard et al. (2013) used this system when investigating turbine spacing in TST arrays.

3. Methodology

3.5.3 Flow Circulation Data Collection

Another way of visually examining flow patterns caused by the presence of a TRS is to take videos of water circulation behind the hydraulic structures (Bryant et al., 2012; Wells and van Heijst, 2003). Yellow-green, fluorescent dye (fluorescein) was injected into the tank and filmed using a GoPro recording device over a series of six tides to capture flow patterns. This method of flow visualisation was chosen rather than Particle Image Velocimetry (PIV) due to the size of the tidal basin and the difficulties with controlling the levels of light and particle suspension over such a large area. Frames from the video footage alongside ADV measurements provide similar data regarding flow characterisation in a more time- and cost-effective manner. Characterising flow patterns in this way helps to understand how well mixed the water is and how effective TRS hydraulic structures are at flushing, both of which have important implications for the environment (Maganga et al., 2010).

3. Methodology

3.6 Data Processing and Analysis

Matlab was used for postprocessing all data gathered from the ADV, water level probes, pressure transducers and GoPro, employing user defined filters to screen the data. Matlab is a powerful tool for data analysis as exemplified by previous tidal studies (Aggidis and Feather, 2012; Burrows et al., 2009b; Rampazzo et al., 2019; Tognin et al., 2018; Yates et al., 2013).

Indicators of data quality for ADV measurements are signal-to-noise ratio (SNR) and correlation. SNR is the ratio of the instrument's transmitted signal to the background noise level in the tank, maintained by the suspended particles required for the signal to be reflected effectively. Correlation measures the similarity between the two pulse echoes, with 0% indicating that there is no similarity between the two echoes, and 100% meaning that the two echoes are identical. Nortek (2018) recommends an SNR of no less than 15 dB for instantaneous velocity measurements or 5 dB when calculating mean velocity, whilst correlation should be kept above 70% to ensure high quality data. However, studies of ADV data alongside sensitivity analysis from preliminary tank trials show that a correlation coefficient of 60% is still able to provide valid results without removing as much data (Mardani et al., 2020; McLelland and Nicholas, 2000). Therefore, filtering thresholds of SNR < 5 dB and correlation < 60% were chosen to screen the ADV measurements before analysis.

After filtering, velocity data underwent a number of transformations before being finally presented and analysed. ADVs measure velocity in four directions, x, y, z₁ and z₂. In order compare the resultant velocity acting in both the x and y directions, data from these two components were combined using Equation 3.12 to calculate resultant magnitude and Equation 3.13 for resultant direction.

$$w = \sqrt{u^2 + v^2} \quad \text{Equation 3.12}$$

$$\omega = \tan^{-1} \frac{v}{u} \quad \text{Equation 3.13}$$

3. Methodology

Where:

w = resultant velocity magnitude (m/s)

u = velocity in x-direction (m/s)

v = velocity in y-direction (m/s)

ω = resultant velocity direction (degrees)

This resultant velocity data was then presented in a number of ways:

- Depth averaged velocity-time maps – these maps of the whole tank present individual graphs of depth averaged resultant velocity against time, comparing experiments against each other at every location to enable a full picture of the tank for the whole time series. As results from each sample location were consistent across the three measured tides, data was averaged to present a single tide for comparison at each point. Data was also averaged over 300 samples (3 seconds of data) to smooth noise in the data series for easier analysis.
- Resultant velocity contour plots – contour plots were made using Matlab, interpolating values in between the observed velocity results. Resultant velocity magnitude is plotted as coloured contours whilst the resultant velocity direction is overlaid on the map as arrows, scaled to represent the strength of the force acting in that direction. Rather than depth averaging the data here, these contour plots were divided to look at individual layers throughout the tank to try to ascertain any three-dimensional impacts of the experiment configurations, drawing plots from data at elevations of 50, 100, 150, 200 and 250 mm from the bed. The data was then further divided to compare the effects at different times of the tide, comparing data during the ebb, low, flood and high tidal phases. This method highlights clearly where similarities exist between experiments as well as where depth or tidal phase make a difference between results for each configuration.
- Residual velocity contour plots – Simplifying the contour plots to look at all data in a single image, these plots still looked at layers throughout the tank, using the same elevations as before but instead of looking at the different phases of the tide measurements of

3. Methodology

resultant magnitude were averaged over time to show the residual flow velocity magnitude and direction throughout the tank for the whole time period.

- Regression analysis – simple linear fit models were applied to the resultant velocity magnitude and direction for each experiment, comparing them to baseline results to identify the extent to which they varied from natural conditions. Confidence intervals of 95% were applied above and below the line of best fit to show the spread of data and further quantify the relationship between the observed data and the baseline (pre-lagoon) results.
- Histograms – histograms of both the resultant velocity magnitude and direction showed the frequency distribution of the different values between experiments. This showed the variation in the range of values between experiments and highlighted relationships that were more difficult to identify in other graphical representations.
- Statistical analysis – further to the visual representations of the results, data can be analysed using statistical metrics to quantify the strength and type of relationship between data sets. Z-tests were used to compare the difference in population variance between observed and measured values of resultant velocity at each location, to test a null hypothesis for determining whether the two data sets were statistically similar or not (Equation 3.14). Z-tests were used rather than a t-test or a chi-squared test since we are comparing two groups with a sample size of over thirty points. Data was tested at the 5% significance level, with a z value threshold of 1.96, above which the null hypothesis was rejected. Further to the z-test, data was also compared using root mean square error (Equation 3.15), standard deviation (Equation 3.16) and Pearson's correlation coefficient (Equation 3.17) to identify other underlying patterns between experiments.

3. Methodology

$$z = \frac{(\bar{x} - \bar{y})}{\sqrt{\frac{s_x^2}{n_x} + \frac{s_y^2}{n_y}}} \quad \text{Equation 3.14}$$

$$RMSE = \sqrt{\frac{\Sigma(x - y)^2}{n}} \quad \text{Equation 3.15}$$

$$s = \frac{\Sigma(x - \bar{x})^s}{n - 1} \quad \text{Equation 3.16}$$

$$r = \frac{\Sigma(x - \bar{x})(y - \bar{y})}{\sqrt{\Sigma(x - \bar{x})^2 \Sigma(y - \bar{y})^2}} \quad \text{Equation 3.17}$$

Where:

x = value of the x-variable

y = value of the y-variable

s = variance (standard deviation)

n = number of sample values

r = Pearson's correlation coefficient

$RMSE$ = root mean square error

Water level data was analysed using Matlab to plot time series graphs to compare measured results from each experiment and identify points in the tide for comparison in the contour plots. Time series visualisation allows quick analysis of anomalies in the tidal data to ensure that the weir gate maintained a tidal range of 80 mm and period of 90 seconds for the duration of the experiments.

Video footage of fluorescent dye tracks within the TRS were analysed in Matlab using manual motion tracking, following the progression of dye plumes frame by frame to identify flow patterns.

3.7 Summary

Physical models enable the scaled testing of prototype TRS configurations in order to predict behaviour and hydrodynamic interactions. The present experiments, conducted in the HRC laboratory at Cardiff University, deploy a scale of $X = 5000$ and $Y = 100$ to test two different TRS geometries in the available space. Issues arising from the distortion ratio of this scale will be accounted for by maintaining similarity of Reynolds number between conditions in the laboratory and those measured in the Severn Estuary. Experiments will compare the performance of TRS layouts with zero, one and two turbines of different spacing to determine the effects of this design aspect on hydrodynamics. Further tests will look into the effects of TRS bed slope and material as well as comparing flow behaviour around TRSs with differing geometry.

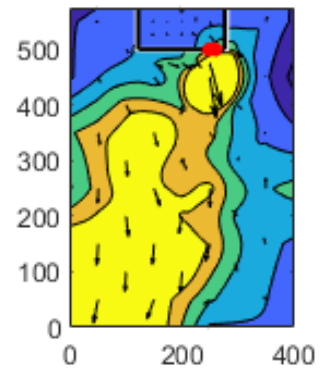
Flow velocity will be measured using an ADVP, whilst water level is measured using water level probes and pressure transducers, and flow is visualised using videos of fluorescent dye injected into the TRS and tracked using Matlab software to quantify flow behaviour.

Conclusions will be drawn from the evidence of depth averaged velocity, velocity contour plots at various depths and tidal phase, residual velocity magnitude and direction, flow visualisation and statistical analysis of the significance of these results.

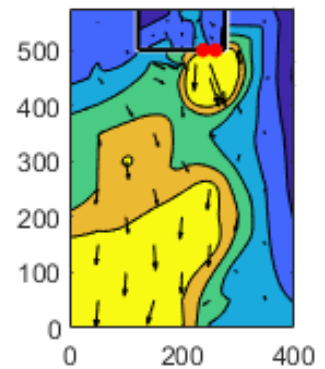
Chapter 4

Test Cast 1 – Impact of Varying Turbine Layout

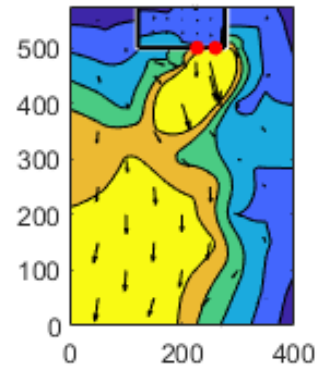
R2A 50mm Elevation



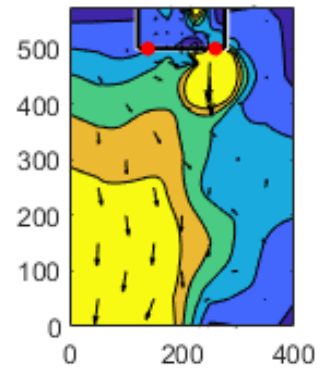
R2B 50mm Elevation



R2C 50mm Elevation



R2D 50mm Elevation



4 Test Case 1 – Impact of varying turbine layout

4.1 Introduction

Turbine spacing is considered to be a key parameter for reducing environmental impacts of TRSs but as yet has not been studied in much detail. Hydraulic structures are usually clustered together due to the cost benefits of having them in a single structure, as well as constraints of the physical environment and ease of access for maintenance purposes. Distributing turbines across the length of a seawall will have impacts on turbine performance as well as on environmental conditions by reducing the combined effects of turbines clustered in one place (Angeloudis et al., 2016b). Spacing is just one design parameter that can be considered for reducing the environmental impact of TRSs.

This first test case investigates the effects of spacing on a single turbine or pair of turbines in a TRS, varying the proximity of the turbines to adjacent seawalls and to each other. The present study looks only at the spacing of turbines in the seaward facing wall, parallel to the direction of flow, as this is conventionally where hydraulic structures are positioned. However, future tests could look at the effects of placing turbines in seawalls perpendicular to the predominant flow direction or even varying the angle of turbines in relation to the dominant direction of flow. Six scenarios are investigated for the square lagoon case as outlined in Table 4.1, two for single turbines and four for pairs of turbines, plus a baseline case with no turbines, with which to compare the effects of the other experiments.

Table 4.1 Turbine layout for test configurations of square cases. Numbers 1 to 10 represent box section number.

Test Case \ Turbine Position	1	2	3	4	5	6	7	8	9	10
S0										
S1A									X	
S1B							X			
S2A								X	X	
S2B		X							X	
S2C					X				X	
S2D				X			X			

4. Test Case 1 – Impact of Varying Turbine Layout

These experiments have been split into four comparison cases to simplify analysis by separating specific aspects of spacing and TRS geometry and comparing one at a time.

- Comparison A: Varying the number of turbines in a square TRS.
- Comparison B: Varying the position of a single turbine in a square TRS.
- Comparison C: Varying the position of a pair of turbines in a square TRS.
- Comparison G: Varying the position of a pair of turbines in a rectangular TRS.

Analysis of results from these experiments will help to answer the question: “to what extent does turbine spacing affect hydrodynamics?” and test the following hypotheses:

h_0 : There is no significant difference experienced in velocity by changing turbine layout.

h_1 : Changing turbine layout causes significant difference to velocity profiles.

Key Words and Terms in Chapters 4, 5 and 6

Depth Averaged Velocity: The average velocity across all depths of water at a single location. Assumes uniform velocity distribution across all depths and ignores variation in velocity in three dimensions. Useful for comparing the time series of velocity at a single point.

Dipole: A pair of equal currents, circulating in opposite directions, akin to magnetic fields around a pole.

Vortex: A rotating mass of fluid or air, e.g., a whirlpool.

Slack Water: The period of time between the turning of the tide where water is least effected by stress in any direction.

4. Test Case 1 – Impact of Varying Turbine Layout

4.2 Asymmetric Flow

Before beginning analysis of results, it is important to note the underlying asymmetrical flow observed in the tidal basin throughout the experiments. Evidence showed anti-clockwise circulation in the tank, with the strongest incoming flows along the right-hand side, and strongest outflow on the left. This was especially evident at the inflow boundary where the x-velocity component ranged from -0.02 to 0.06 m/s at (350,50), but only -0.05 to 0 m/s at (50,50) as shown in Figure 4.1. This represents a difference of 37% in flow rate and almost opposite polarity from one end of the boundary to the other.

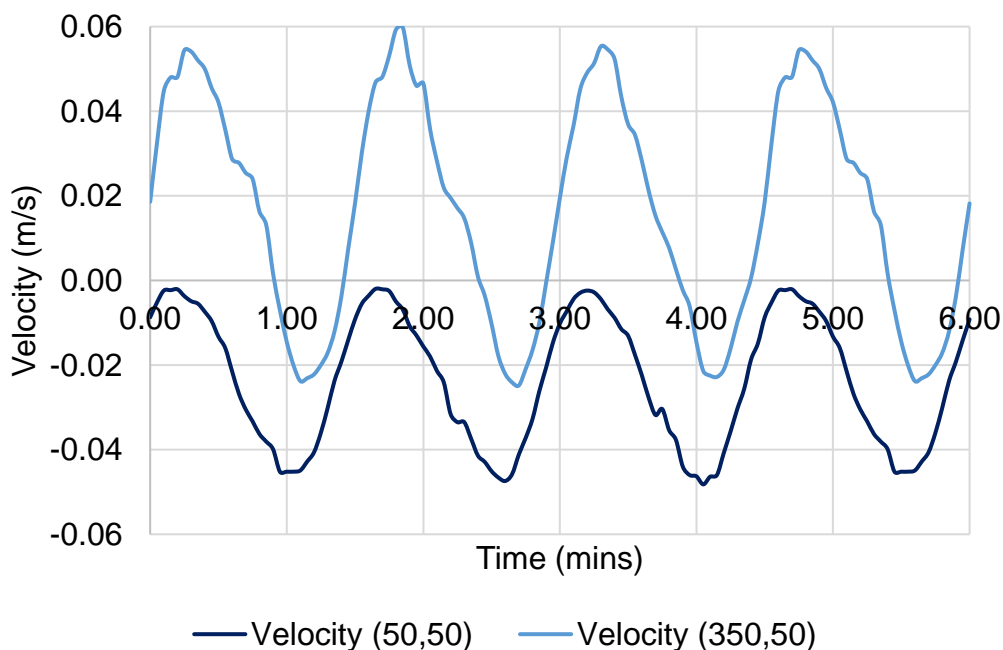


Figure 4.1 X-velocity magnitude at opposite ends of the inflow boundary.

This phenomenon is most likely due to uneven pressure along the inflow boundary caused by a 90° junction in the inflow pipe directly before the basin. Previous experiments in the tidal basin had not detected this problem as they only used a portion of the area and operated at much slower flows. Numerous attempts were made to address this issue but were unable to solve the problem (see Section 8.2 for full discussion). This ongoing issue has affected all results but has proved to be consistent for all experiments and so although results will be different from those that would be obtained with symmetrical flow conditions, the effects of individual TRS designs can still be analysed.

4. Test Case 1 – Impact of Varying Turbine Layout

4.3 Results

4.3.1 Comparison A – Varying the number of turbines in a square TRS.

Comparison A investigates the hydrodynamic impacts of varying the number of turbines in a square TRS, comparing results from experiments S0, S1A and S2A (layouts shown in Figure 4.2) against pre-lagoon conditions in order to determine which configuration has the greatest effect.

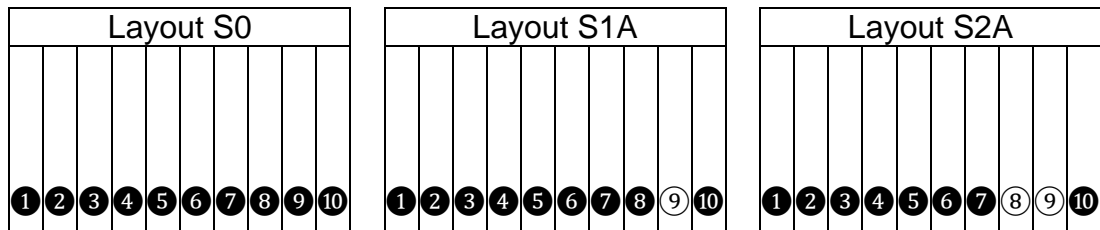


Figure 4.2 Experient layouts for Comparison A: S0, S1A, S2A.

4.3.1.1 Velocity - Depth Averaged

Figure 4.3 provides a map of depth averaged velocity at every location for each of the experiments to give a picture of the whole tank area. N.B.

Results were not taken inside the TRS for experiment S0 as the sealed box had no flow within the walls, this was confirmed by ADVP measurements and visual checks.

Examining the depth averaged velocity of experiments S0, S1A and S2A against the pre-lagoon conditions (00) we can see that the velocity profiles for S0 and S1A match very closely throughout the tank (Figure 4.3), especially along the inflow boundary and in the centre of the tank. These two cases also closely match the empty tank conditions.

Experiment S2A also shares many similarities with the results of S0 and S1A throughout the tank, but where variation occurs, it is generally S2A that shows the greatest difference. For example, at (250,50) (closer detail provided in Figure 4.4) where experiment S2A follows the line of pre-lagoon velocity but varies greatly from the results of S0 and S1A. S2A also has significantly greater velocity at (200,100) (Figure 4.5), this suggests that when two turbine openings are placed close together, they are able to cause a difference even as far away as the inflow boundary and so far field effects of turbines cannot be ignored in the design of TRS.

4. Test Case 1 – Impact of Varying Turbine Layout

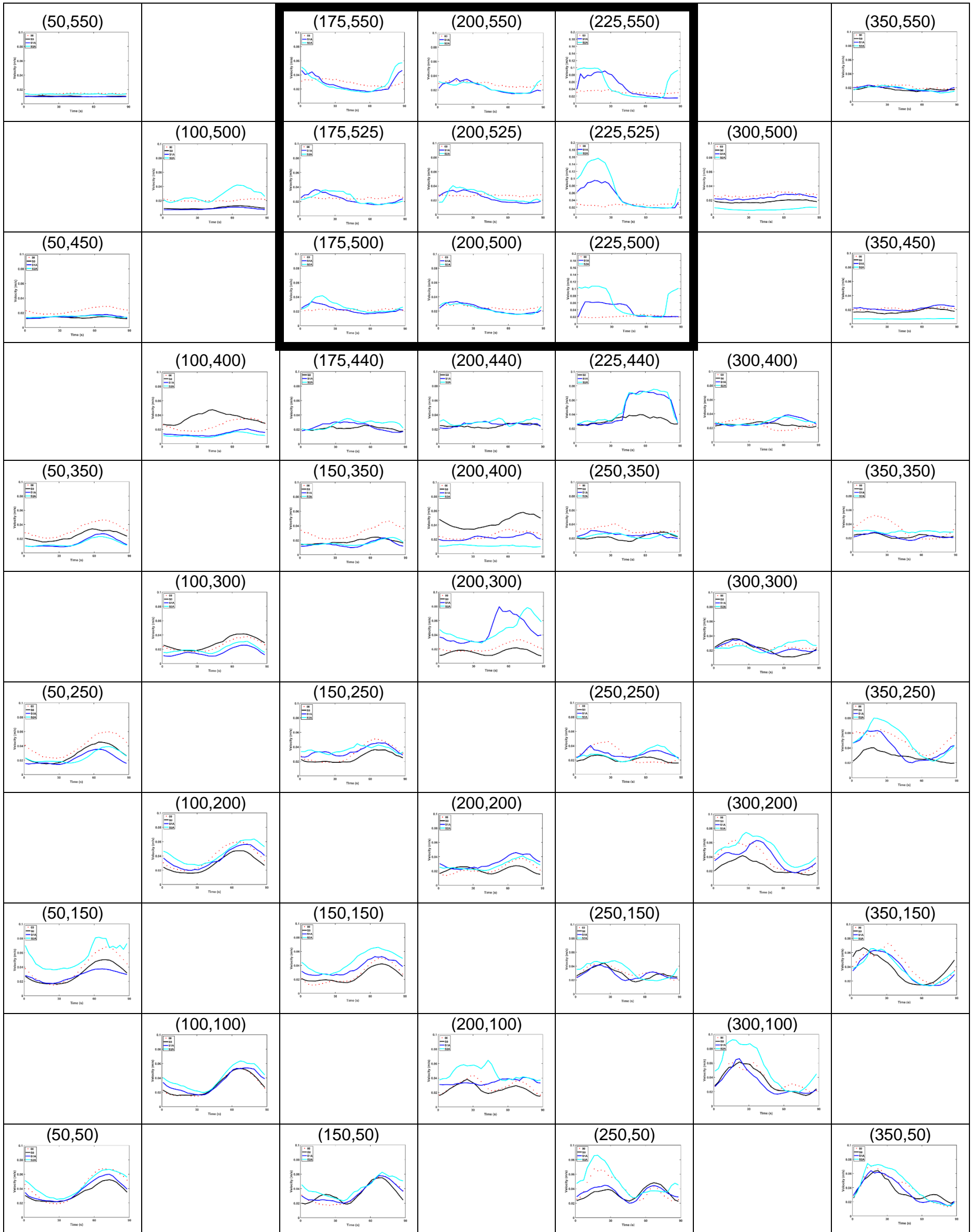


Figure 4.3 Map of depth averaged velocity plots for Comparison A: S0, S1A and S2A.

4. Test Case 1 – Impact of Varying Turbine Layout

Experiment S2A has also led to increased flow velocity along the right-hand side of the tank at (350,250) (Figure 4.6) but here experiment S1A also experiences an increase. Their pattern still closely follows that of the pre-lagoon case whereas S0 experiences a dip in flow velocity. This is perhaps due to the reflection of water off the closed TRS wall slowing flow in this area whereas water is able to flow freely through the single and two-turbine cases, maintaining the natural flow conditions of the area. This reflection off the seawall can also be seen to affect the results of S0 at (200,400) (Figure 4.7).

The greatest increase in velocity outside of the lagoon can be found in the centre of the seawall in the vicinity of the turbines, e.g. (200,300) (Figure 4.8), as is to be expected from the proximity to the TRS. Along the seawall ($y = 440$ cm), results from S0 closely match those of S1A and S2A until point (225,440) (Figure 4.9) directly in front of the turbine openings, highlighting the impact that the turbine openings cause. This similarity between all cases proves that the presence of the TRS near the rear of the tank has changed conditions from the pre-lagoon state in this area and that the velocity profiles behave very similarly whether there are zero, one or two turbines, maintaining similar amplitudes and smooth shaped velocity patterns. This is also the case near the rear of the tank ($y = 450$ cm to $y = 550$ cm) where the velocity profile is consistently low for all experiments, including the pre-lagoon case.

At point (225,440), directly in front of the turbine openings, experiments S1A and S2A have almost identical results. This is surprising as we would expect that S2A would have greater flow velocities due to having a turbine area twice that of S1A. However, their identical results on the outside of the seawall show that flows out of the TRS have the same effect on the area immediately outside of the lagoon.

4. Test Case 1 – Impact of Varying Turbine Layout

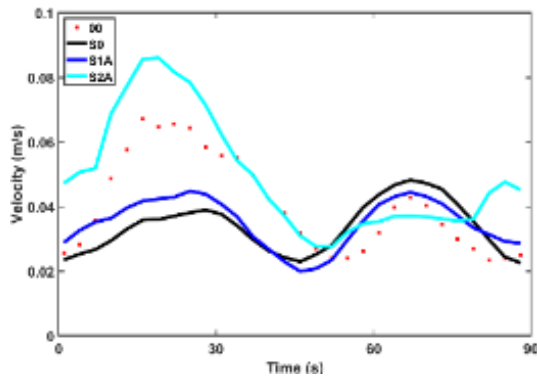


Figure 4.4 Closer detail of velocity at (250,50).

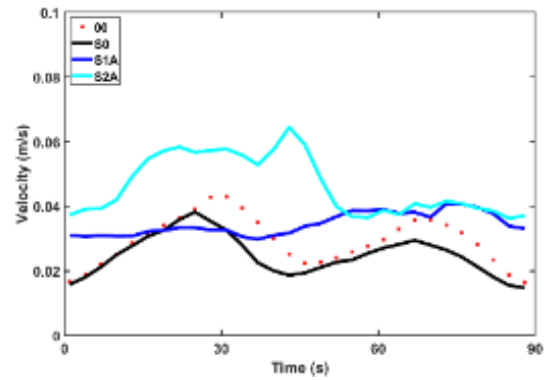


Figure 4.5 Closer detail of velocity at (200,100).

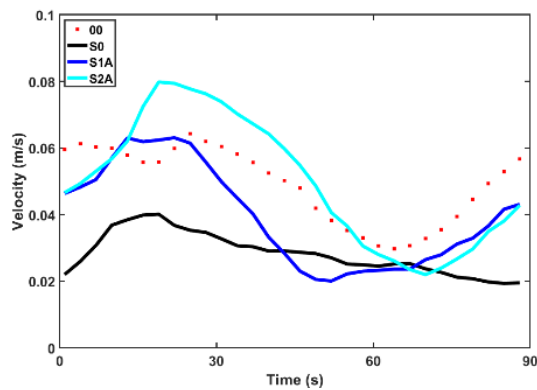


Figure 4.6 Closer detail of velocity at (350,250).

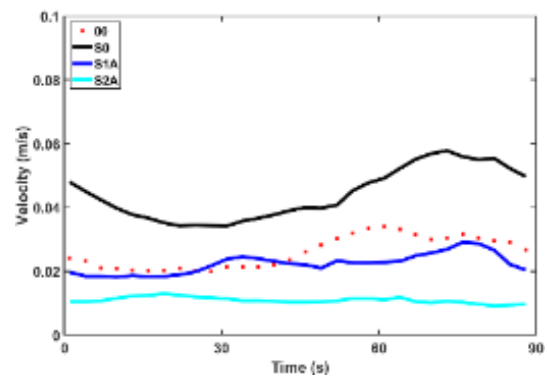


Figure 4.7 Closer detail of velocity at (200,400).

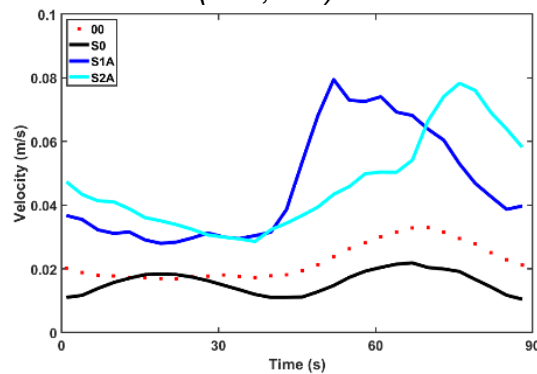


Figure 4.8 Closer detail of velocity at (200,300).

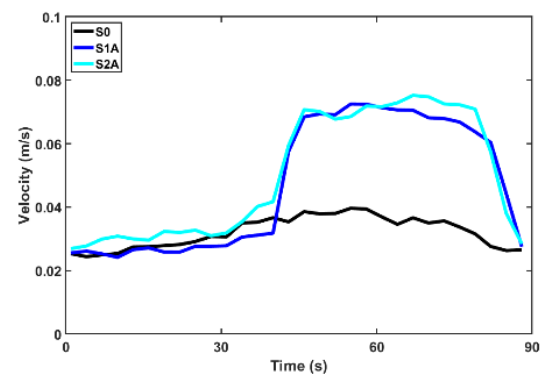


Figure 4.9 Closer detail of velocity at (225,440).

4. Test Case 1 – Impact of Varying Turbine Layout

Inside the TRS itself results for S1A and S2A are extremely similar along the left-hand wall, away from the turbines and even closely follow those of the pre-lagoon experiment, showing that further away from the turbine openings flow does not vary greatly from natural conditions. The flow is almost negligible which means that although water can be seen flowing in and out of the TRS it does not cause strong currents beyond 50 cm from the openings (less than 10 turbine diameters) which is also the reported threshold from other turbine studies (Nash and Phoenix, 2017; Neary et al., 2013; Verbeek et al., 2021). Directly behind the turbine openings however, although the two cases follow similar velocity patterns, the amplitude of the results is much greater for S2A than for S1A (closer details shown in Figure 4.10, Figure 4.11 and Figure 4.12). This shows how the presence of two turbines greatly increases the flow rate within the impounded water and that side-by-side placement also increases turbulence in the vicinity of the turbines.

Overall, there is little difference between the sealed TRS (S0) and the one turbine case (S1A) in the front of the tank, revealing that a single opening does not have far reaching effects. However, S2A presents some differences to S0, indicating that two turbines have an increased effect on flow conditions, especially when they are positioned side by side. Within the TRS, two turbines caused more disruption than one, but these differences became less pronounced further than 50 cm (10D) away from the turbine openings. These results are the opposite of those reported by Dai et al. (2017) who when investigating dynamic tidal power structures (DTPSs) found that the more openings there were in the seawall the less the impact on the regional velocity. This could be due to the type of TRS being used. Water is not restricted behind the seawall of a DTPS as it is in a TRS lagoon and so by decreasing the area of the seawall barrier by increasing the number of turbines, flow is returned to more natural conditions behind the DTPS rather than merely increasing circulation within a lagoon. The addition of sluice gates in a lagoon wall can also help reduce the effects of recirculation and mitigate the hydro-environmental impact (Angeloudis et al., 2016b). All of these effects will also be different at full scale which will conceal or reveal different velocity behaviour around the TRS.

4. Test Case 1 – Impact of Varying Turbine Layout

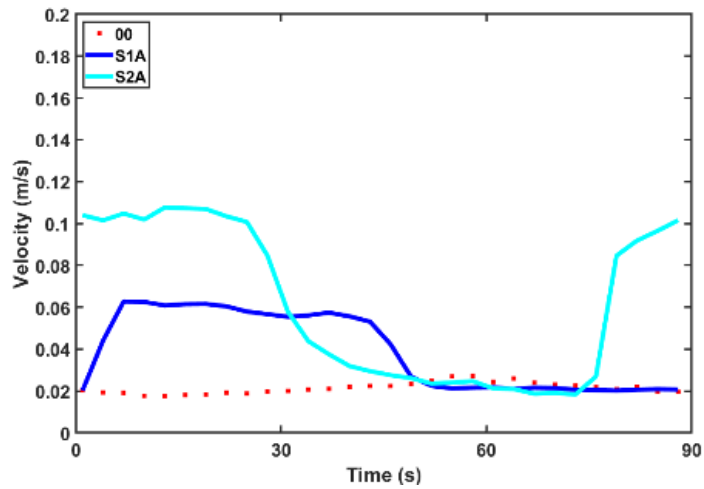


Figure 4.10 Closer detail of velocity at (225,500)

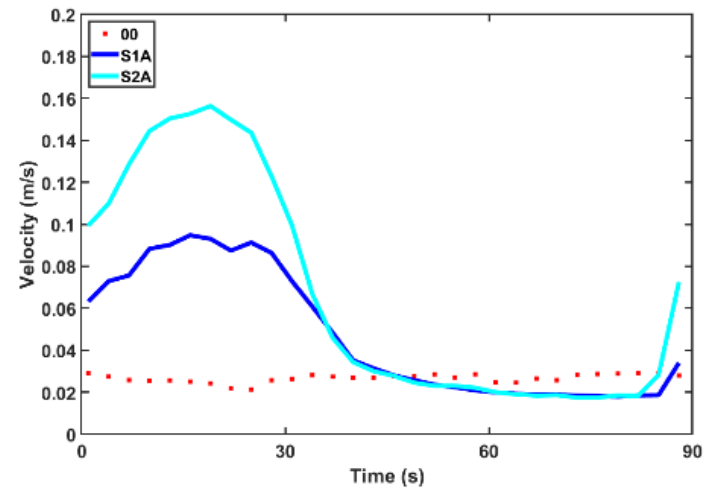


Figure 4.11 Closer detail of velocity at (225,525)

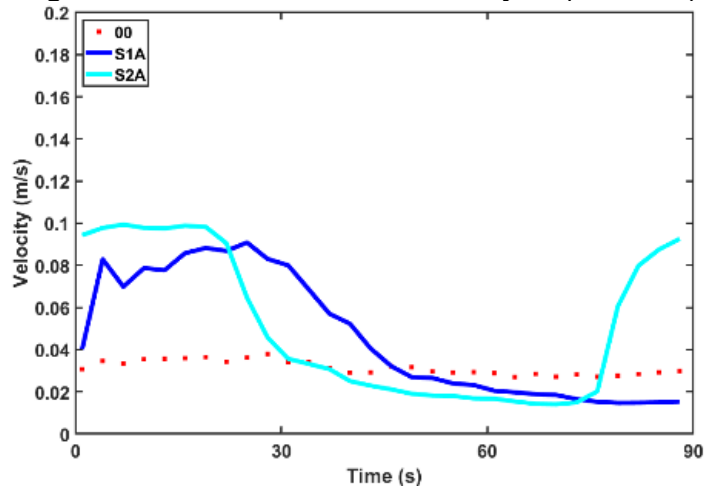


Figure 4.12 Closer detail of velocity at (225,550)

4. Test Case 1 – Impact of Varying Turbine Layout

4.3.1.2 Velocity – Analysed by tide and depth

The velocity map of the tank shown in Figure 4.3 compares depth averaged velocity of different experiments at all locations. Contour plots were also used to demonstrate the distributions of the resultant velocity across the tank (Figure 4.13 to Figure 4.16), interpolating between measurements taken at sample points to give an overview of the whole tank area. This technique has been used to analyse different layers in the water column, as well as different times of the tide to see how flow is affected by tidal phase at different depths. Flow direction is denoted by arrows overlaid on the contour plots, scaled by the flow velocity acting at that point. Results from experiments S0, S1A and S2A have been plotted side by side to allow direct comparison during ebb (Figure 4.13), low (Figure 4.14), flood (Figure 4.15) and high tides (Figure 4.16).

During the ebb tide the velocity pattern is very similar at all depths of experiment S0 (see Figure 4.13), with the strong flow directly in front of the TRS and along the left-hand wall towards the inflow boundary. This pattern is still evident in S1A and S2A but with variation in the size and location of the areas of strongest flow. In both S1A and S2A the strongest flow originates from the location of the turbine openings, as is to be expected from the forces acting through these narrow outlets. In experiment S1A, the strongest flows near the bed (elevation 50 mm) are found in the centre of the tank and then deflect to the left throughout the other layers, with flow slowing towards the surface. This pattern is also followed in S2A but with some areas of slower flow encroaching from the right-hand side of the tank which restrict stronger flows to the left. The slowest flows are found near the rear wall of the tidal basin, furthest from the inflow boundary where circulation is somewhat impeded by the presence of the TRS walls. In all cases the speed of the flow decreases towards the surface which shows how the strength of the ebb tide current diminishes further up the water column.

Although the present research is acting under much simplified conditions and at a small scale, these observations agree with Lian and Liu (2015) who, when investigating turbulence and mixing in tidal bays, found that the strongest turbulence during the ebb tide was confined to the bottom

4. Test Case 1 – Impact of Varying Turbine Layout

boundary layer and that its strength decreased with distance from the sea floor. This stratification during the ebb tide was due to increased velocity shear on the outflowing tide, whereas they found greater mixing during the flood tide. These observations will be even more obvious in the current experiments where hydraulic structures are present near the bed, exaggerating the differences between layers and affecting mixing throughout the water column.

Within the TRS there seems little flow during this phase of the tide, but flow is slightly faster directly behind the turbine openings for both S1A and S2A, as water ebbs out of the orifices, with slower flows in the rear left-hand corner further from the openings.

The low tide graphs appear to have much less variation between the layers with similar patterns outside the TRS for each experiment at all depths (see Figure 4.14). This is most likely due to slack water at this point of the tide where forces are less strong. The flow pattern in S0 most clearly demonstrates how water is reflected off the rear wall and back around to the front of the TRS causing the strongest flows to be found directly in front of the TRS seawall. This area of strong positive flow is absent from S1A and S2A results where instead the strongest flow is deflected to the left-hand wall of the basin. This seems to indicate that the turbine openings have an effect on the direction and strength of currents, deflecting flow to the opposite side of the tank to where the turbines are located, similar to the findings of Guo et al. (2021).

The turbine openings also lead to some interesting patterns inside the TRS. Previous studies have shown how the effects of slack water are more exaggerated in TRSs due to operation mode and because of the physical barrier restraining flow (Rtimi et al., 2021). This is confirmed in the present case where flow inside the TRS undergoes great change at each depth, indicating that there is a 3D component to the turbine wakes, although there is no operation mode acting here to be called into question. This is also visible by eye when dye is injected through the turbine opening. Figure 4.18, presenting flow visualisation of experiment S1A, shows the wake shooting to

4. Test Case 1 – Impact of Varying Turbine Layout

the back of the tank in a straight plume which moves up the back wall and then billows out to the left and the front. This 3D element of rotational flow can affect mixing and circulation up to twenty turbine diameters away and is dependent on the number of turbines and their representation (Jeffcoate et al., 2017).

Once again there is little variation between depths for the experiments during the flood tide (Figure 4.15). Flow is stronger on the right-hand side for all cases during the flood tide, demonstrating the impact of the asymmetric flow in the tank which has stronger inflowing water on the right and stronger ebbing water on the left. The contour patterns appear more similar between S0 and S1A than S2A, with stronger flow directly in front of the TRS wall in S2A further supporting the argument that a single turbine causes minimal change whilst changes caused by two turbines are more noticeable. Inside the TRS the patterns are similar for both S1A and S2A with the strongest flow velocity directly behind the turbine openings as water floods in, reaching more than halfway into the TRS. The strength of this flow decreases with depth as before but appears to reach further for S2A indicating a stronger wake for two turbines than one, most likely due to the larger discharge from two turbine openings.

The high tide plots have a similar pattern to that of low tide but with more contours (Figure 4.16), signifying that there is slightly more variation in flow during high tide. Inside the TRS flow becomes much weaker in both cases but especially in S2A. This suggests that flow is weaker during high tide and does not permeate the whole area of the TRS which could cause problems for water quality.

4. Test Case 1 – Impact of Varying Turbine Layout

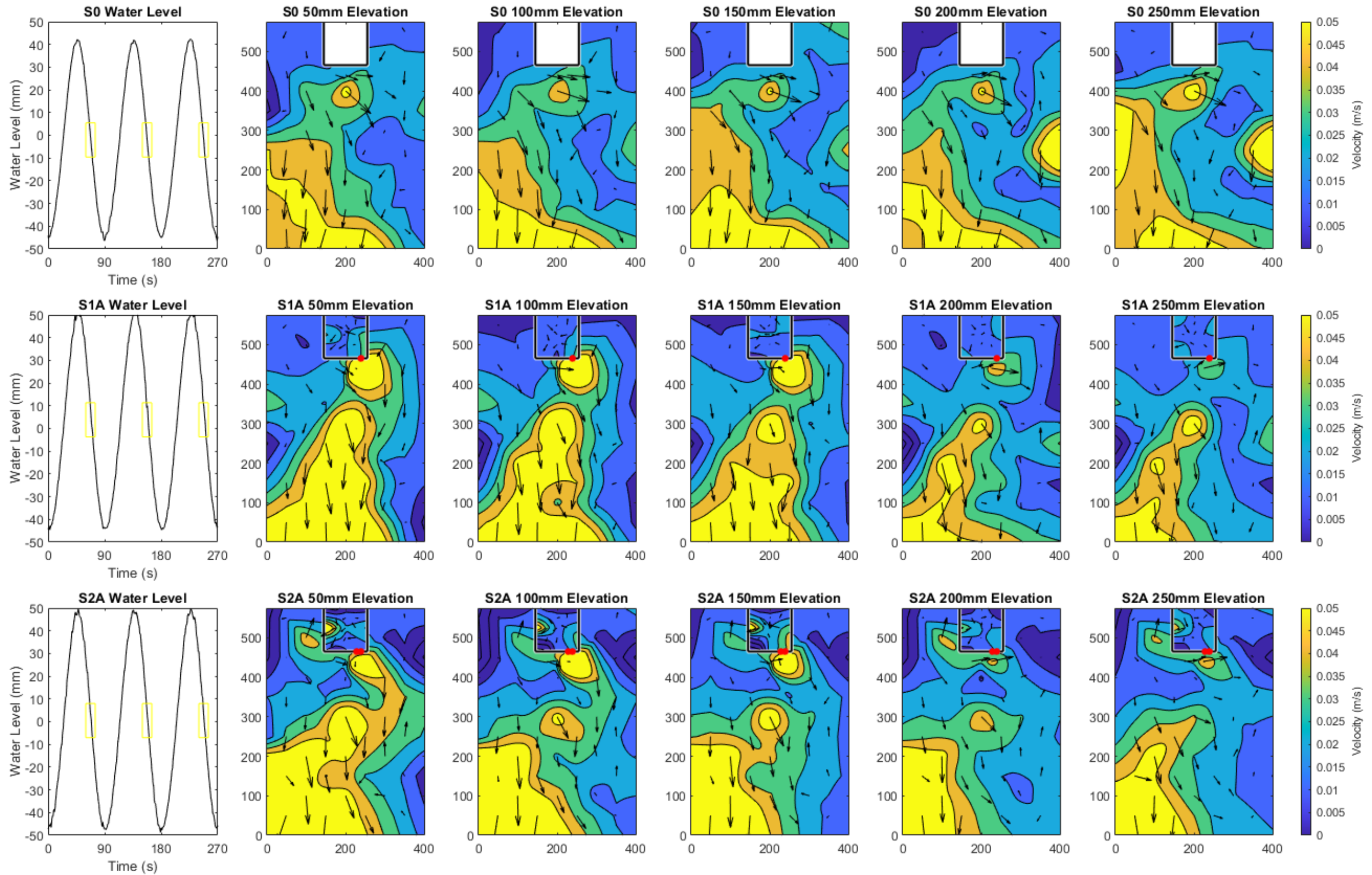


Figure 4.13 Comparison A - Velocity contour maps at elevations of 50, 100, 150, 200 and 250 mm above the bed during the ebb tide.

4. Test Case 1 – Impact of Varying Turbine Layout

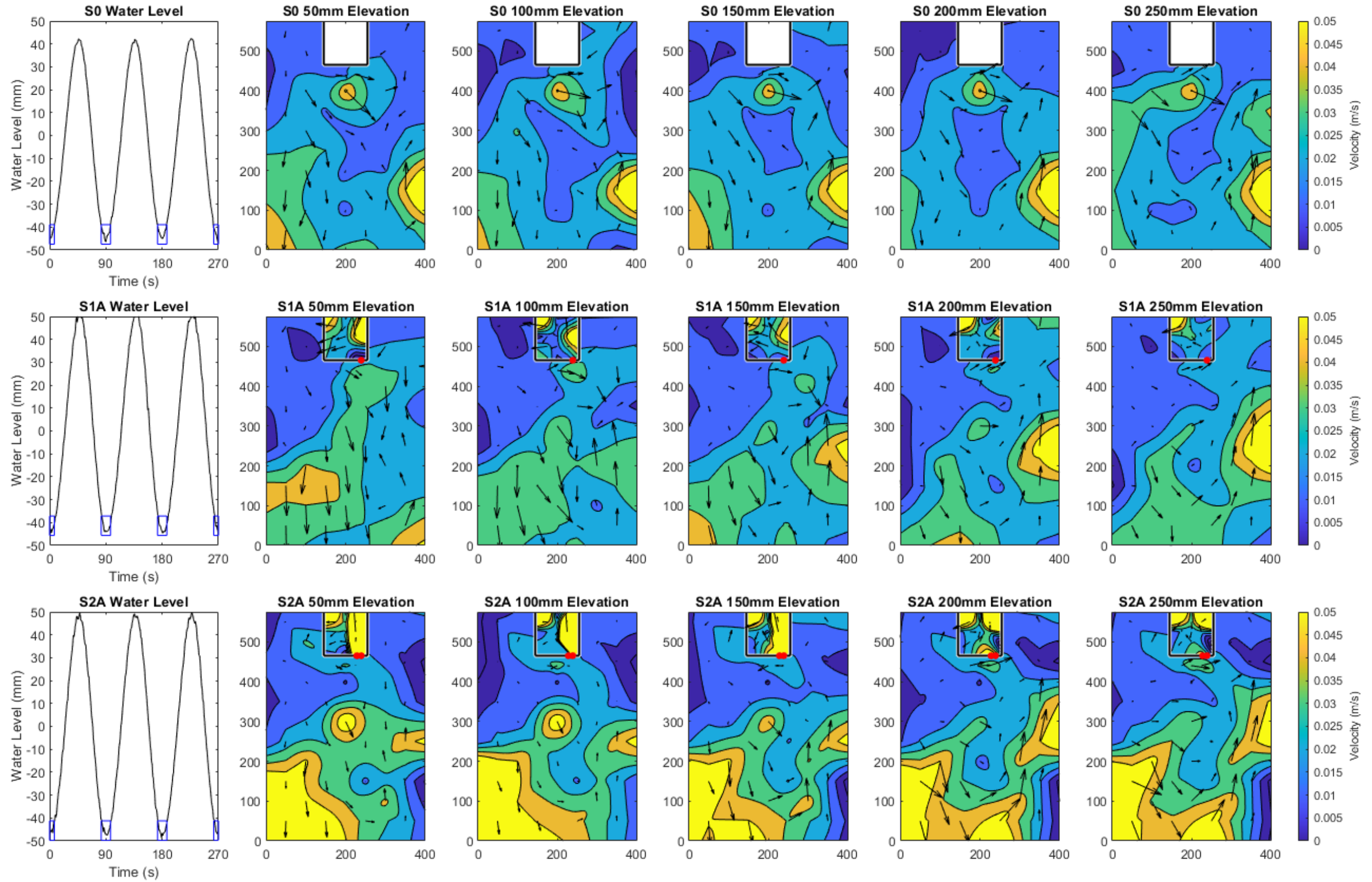


Figure 4.14 Comparison A - Velocity contour maps at elevations of 50, 100, 150, 200 and 250 mm above the bed during low tide.

4. Test Case 1 – Impact of Varying Turbine Layout

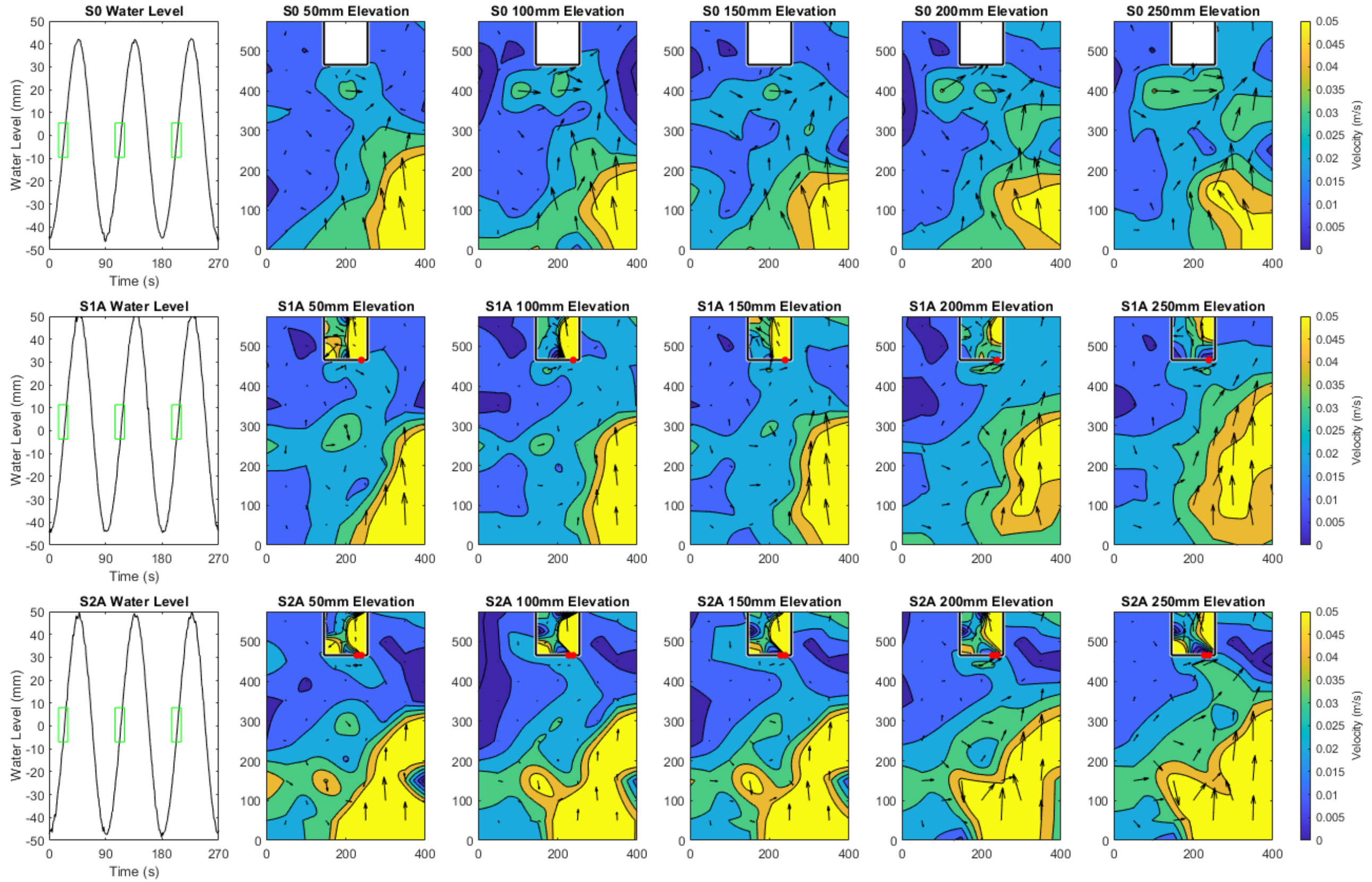


Figure 4.15 Comparison A - Velocity contour maps at elevations of 50, 100, 150, 200 and 250 mm above the bed during the flood tide.

4. Test Case 1 – Impact of Varying Turbine Layout

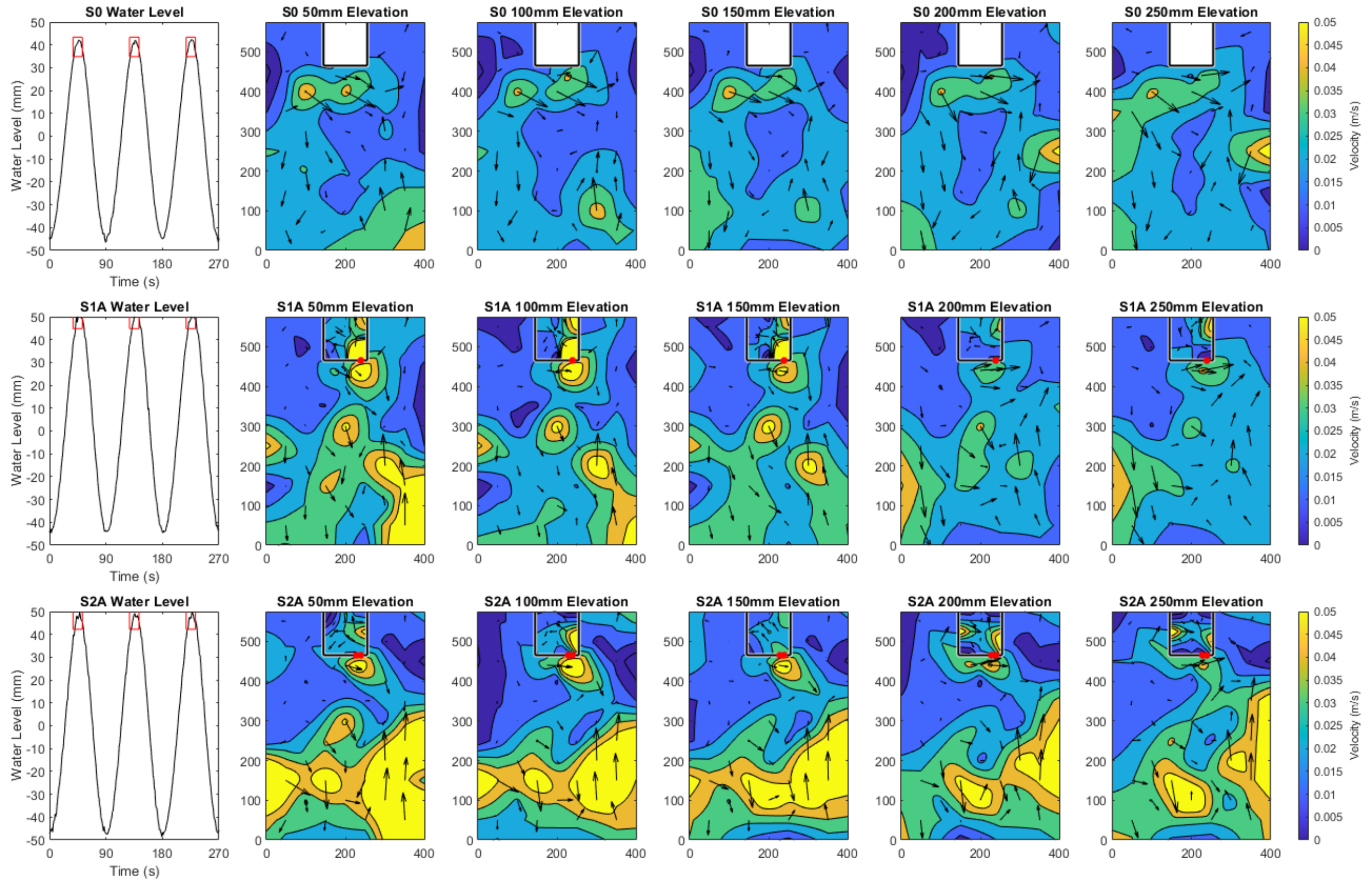


Figure 4.16 Comparison A - Velocity contour maps at elevations of 50, 100, 150, 200 and 250 mm above the bed during high tide.

4. Test Case 1 – Impact of Varying Turbine Layout

4.3.1.3 Velocity – Residual Velocity Magnitude and Direction

The velocity within the tank can also be analysed by looking at the residual magnitude and direction across all tides by averaging data across the whole time frame, to get a clearer picture of residual forces. Figure 4.17 compares these residual forces between the experiments. S0 has the least variation between the layers whilst S2A experiences the most, suggesting that the closed box causes the least variation between all layers of the tank and that the presence of two turbines in S2A causes greater change to be felt at each depth. All of these cases display the strongest flows at the inflow boundary and the weakest at the rear of the tank which is to be expected as the water is forced into the tank from the inflow boundary and is reflected from the closed boundary at the rear wall. It is particularly restricted in the rear-left hand corner where the presence of the TRS has prevented water from circulating in this area. The obstructive effects of the structure would have to be considered when designing TRSs considering the dominant direction of flow in the area which could create issues of stagnation on the leeward side of the seawall. Other areas of strong force are observed around the turbines with clear areas of strong flow found directly in front of the turbine openings.

In all cases the resultant flow direction (denoted by arrows scaled by velocity magnitude) illustrates how the water is subject to secondary circulation around the tank where the strongest inflowing water appears to originate from the front right-hand corner, before heading straight to the rear right-hand corner where it is deflected to the left and returns to the front left corner. This underlying asymmetrical flow is attributed to physical and mechanical constrictions in the tank, discussed in greater detail in Section 8.2.

Inside the TRS, S1A reveals an even pattern of fast flow behind the turbine spreading to the other side of the TRS from depths of 50 mm to 150 mm, however this changes upwards of 200 mm where the flow rates diminish. This could be due to the wake of a single turbine having less of an effect higher up the water column, further adding to the argument of turbine wakes having a 3D element, and that strong turbulence is often confined to the

4. Test Case 1 – Impact of Varying Turbine Layout

bottom boundary layer, decreasing in strength with distance from the sea floor (Lian and Liu, 2015). This pattern is very similar in S2A, with the strongest flow extending from behind the turbines but reaching further into the lagoon. This again diminishes from elevation 200 mm but does not shrink to the same extent as S1A showing once again that the strength of flow through two turbines has a greater impact in all three dimensions.

Overall, the single turbine case (S1A) yet again causes less change to the baseline conditions (S0) than the two-turbine case (S2A) due to the restricted opening of the orifice.

4. Test Case 1 – Impact of Varying Turbine Layout

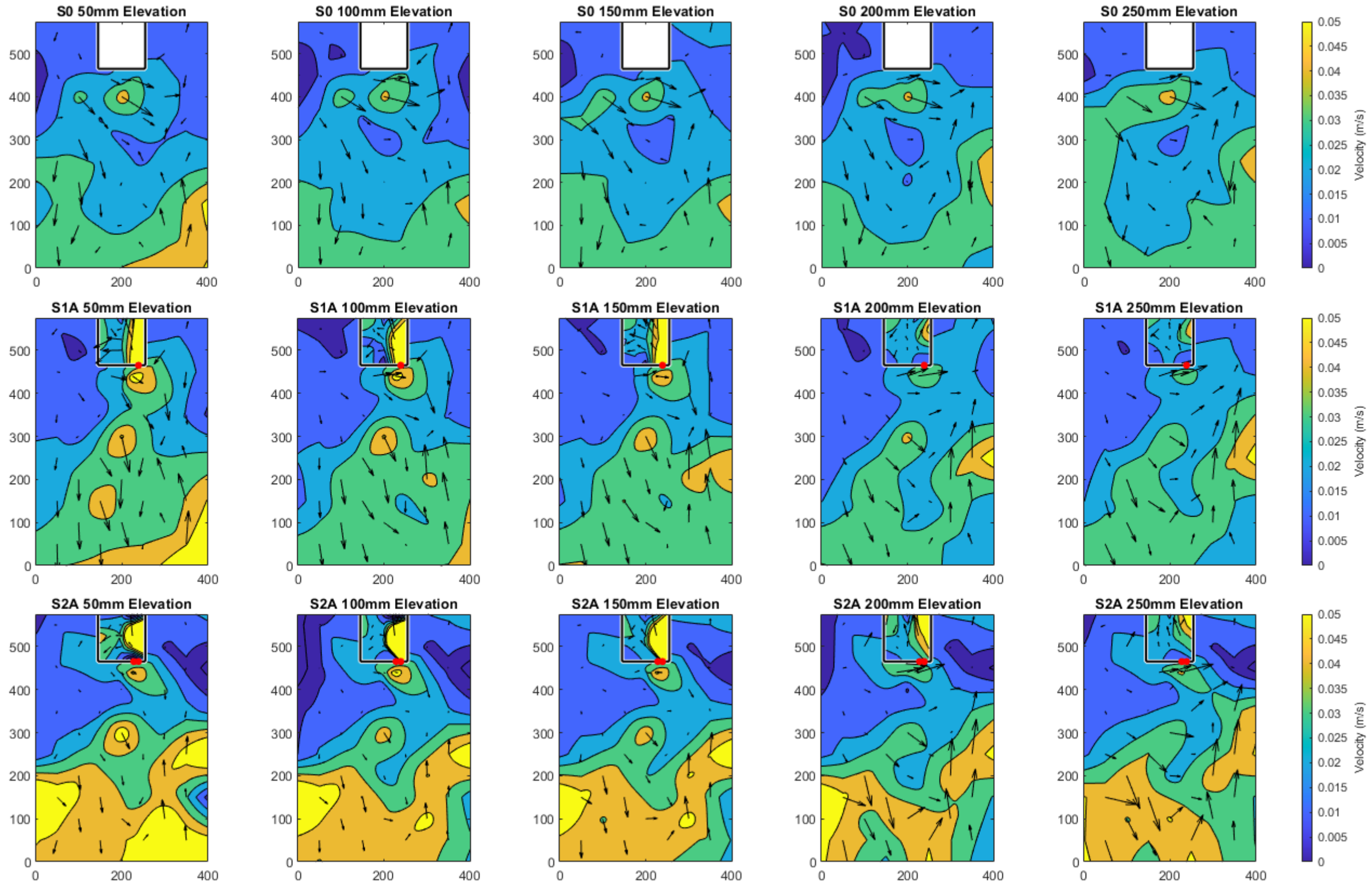


Figure 4.17 Comparison A – Contour maps of residual velocity magnitude and direction at elevations of 50, 100, 150, 200 and 200 mm from the bed.

4. Test Case 1 – Impact of Varying Turbine Layout

4.3.1.4 Flow Visualisation

Another way to analyse flow within the TRS is to add dye to the water to identify circulation patterns. Fluorescent dye was injected on the incoming tide and then observed for ten minutes (six and a half tides). Still frames from the videos were then separated and the dye tracked to see where the water flowed and how long it took to be fully mixed and then dispersed. Figure 4.18 and Figure 4.19 demonstrate the results of this process for experiments S1A and S2A as used throughout all of the experiments. Dye videos were chosen instead of PIV measurement due to cost restrictions and difficulty controlling light levels in the laboratory. Although this means that flow was only able to be analysed in two dimensions it is a cost-effective way of demonstrating flow patterns. See Section 3.5.3 for further discussions of this method.

Studies of vortices through narrow channel openings between a basin and the sea, show how two counter-rotating eddies are formed during the flood tide. These then remain constant rather than being drawn back through the opening on the ebb tide, which impacts upon sediment and nutrient transportation processes. Wells and van Heijst (2003) report a threshold value of $Wi/UT = 0.13$, where Wi is the width of the opening, U is the maximum velocity and T is the tidal period, which dictates the fate of the vortices. Below this threshold dipoles can propagate away from the source region without being drawn back into the sink, greater than this and they will dissipate. Further to their conclusion, Vouriot et al. (2018), found that vortex behaviour was ruled more by this Wi/UT factor than by proximity of the openings to the side walls. In the present study the Wi/UT ratio is constantly below this threshold value and so we would expect to see dipoles emerge from the turbine orifices and circulate within the TRS area, as we do in this and later cases. Effects of the proximity of side walls will be analysed further.

Figure 4.18 shows the results of this method for experiment S1A and illustrate how the turbine wakes do indeed form two eddies but in this case they rotate in the same direction. The wake plume moves directly to the back of the tank, staying near to the wall closest to the turbine. It then reflects up and left, off the boundary wall, and continues to spread along the rear wall. This cloud moves upwards and forwards forming dipoles, one reaching to the

4. Test Case 1 – Impact of Varying Turbine Layout

left-hand wall whilst the other lingers in the centre of the lagoon. Both move to fill the lagoon and continue to circulate clockwise until the water is fully mixed 45 seconds after the dye was injected, half of a full tidal cycle. The dye then took nine minutes to dissipate entirely, which means it was almost completely flushed from the tank within six tides. This is faster than the flushing times observed by Guo et al. (2021) whose models predicted passive tracers to take between 12 and 18 tides to be fully renewed within a TRS. This could be due to less sensitive methods for analysing the concentrations of dye remaining in the water in the present study and also to scaling since there is only one turbine opening in the present scenario so flushing time will alter.

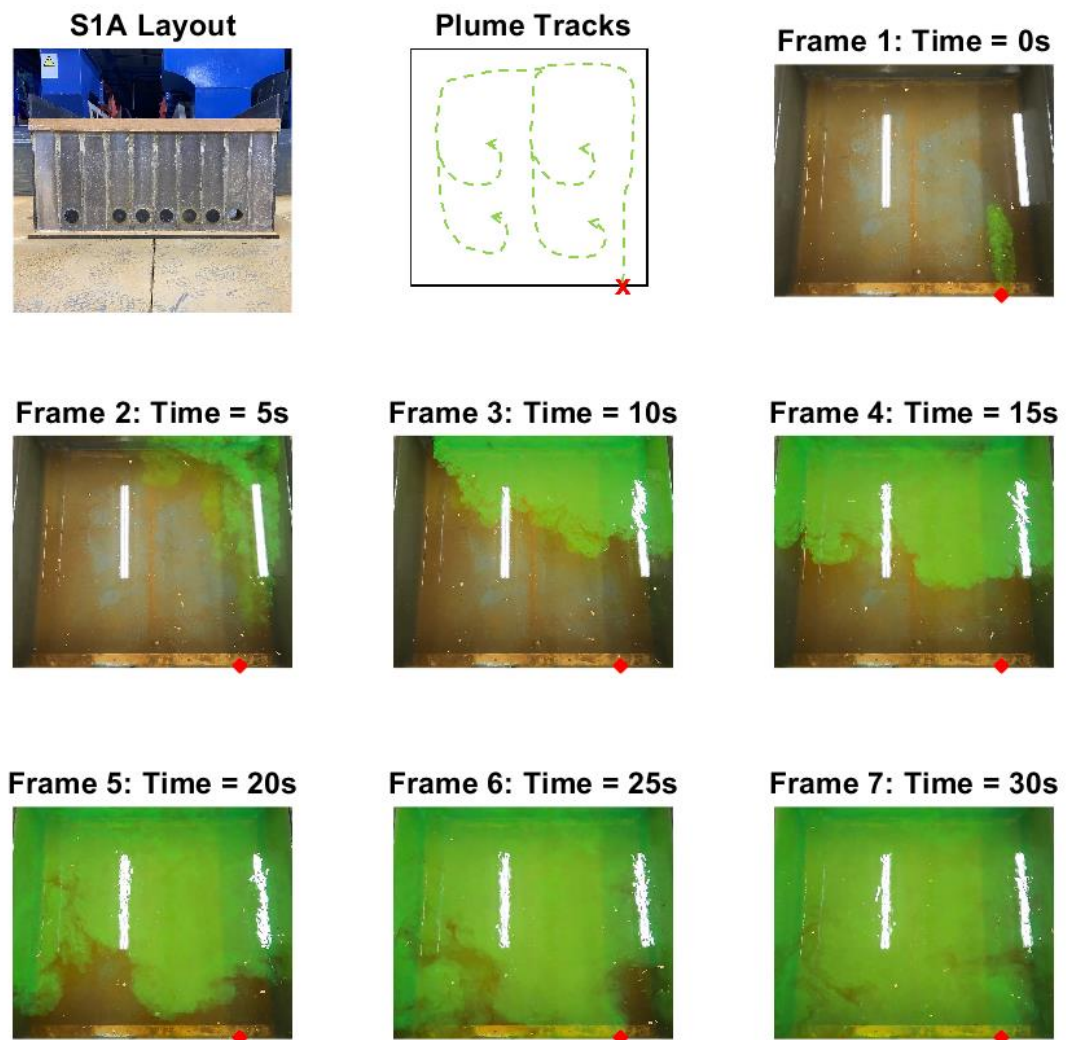


Figure 4.18 Flow visualisation for experiment S1A.

4. Test Case 1 – Impact of Varying Turbine Layout

S2A owns a very similar pattern to that of S1A just with a wider starting plume due to the turbine openings having twice the area (Figure 4.19). Once again, the wake travels straight to the rear of the tank where it is deflected to the left and upwards so that it fills the whole tank, culminating in two circulating cells. The wider cell being that on the left-hand side which has more room, being further from the starting orifice, whilst the right-hand cell is narrow, limited by the proximity of the starting orifice to the wall. This demonstrates how the circulation pattern of two closely spaced turbines matches that of a single turbine but is strengthened due to the increased discharge area. This further supports the reasons why experiment S2A varied more from S0 than S1A did. The single opening did not change conditions as much from the sealed box, but two openings exaggerated all changes that were caused by a single orifice. It also proves that proximity of the side walls has as much impact on vortex circulation as the Wi/UT ratio propounded by Wells and van Heijst (2003) and Vouriot et al. (2018). As, although S2A has double the orifice area and therefore a Wi/UT value twice that of S1A, the vortices share the same trajectory and fate due to the location of the turbine openings in relation to the boundary walls. Angeloudis et al. (2016b) found that the recirculation zone in TRSs depends on the distribution of turbines in the seawall, whilst the vortex size depends on the location, number and operation of the turbines and sluices. The present results highlight how the number of turbines affects the strength of the vortex. Further investigation of the effects of turbine distribution will be seen in Comparisons C and G (Sections 4.3.3 and 4.3.4).

4. Test Case 1 – Impact of Varying Turbine Layout

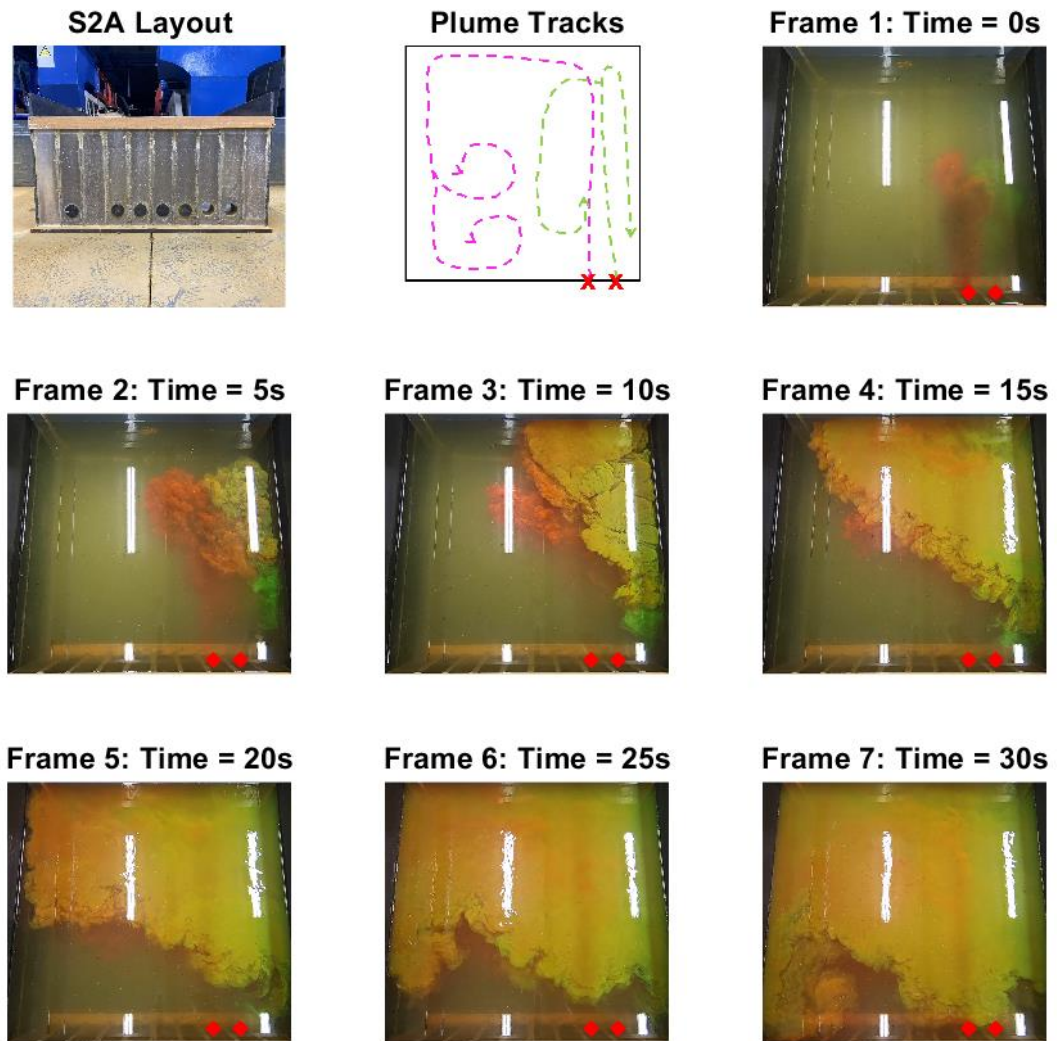


Figure 4.19 Flow visualisation for experiment S2A.

4. Test Case 1 – Impact of Varying Turbine Layout

4.3.1.5 Statistical Analysis

To quantify these observations, results of the residual velocity magnitude and direction were compared between S1A, S2A and S0, the closed box case. Figure 4.20 plots data of the residual flow velocity at each location for both experiments against the baseline case and demonstrates how although both cases cause a consistent increase in residual flow velocity compared to the baseline results, experiment S2A leads to faster flows overall, as seen in previous analysis. This relationship is further exemplified in Figure 4.21, a histogram of the frequency distribution of residual velocity magnitude which shows that although the results of S1A somewhat follow the normal distribution of S0, S2A has a much wider spread with more flow velocities at the upper end of the scale, demonstrating the impact that the introduction of turbines has had on flow variation.

Figure 4.22 shows regression analysis of the residual velocity direction for experiments S1A and S2A. The results of both when plotted against S0 are highly scattered which shows how the different conditions of each experiment altered flow direction from the baseline case, however, S1A is much more closely aligned with the results of S0 than S2A is. This shows once again how the introduction of a second turbine exaggerated the results of a single turbine and significantly altered baseline flow conditions. Figure 4.23, a histogram of frequency distribution of flow direction shows how similar flow patterns are between S1A and S2A, with a near identical distribution. This suggests that although the second turbine opening in S2A increased flow velocity magnitude from the single turbine case, it did not significantly alter the direction of flow from S1A which suggests that when turbines are located in the same part of the seawall the number of turbines does not cause a great difference to flow direction.

4. Test Case 1 – Impact of Varying Turbine Layout

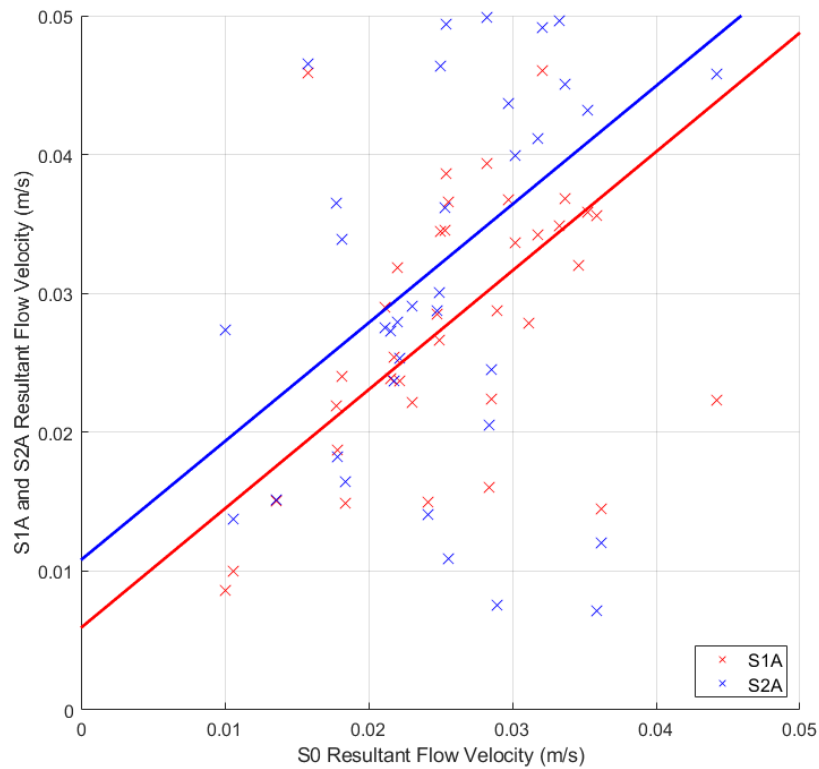


Figure 4.20 Comparison A - Regression analysis of residual flow velocity.

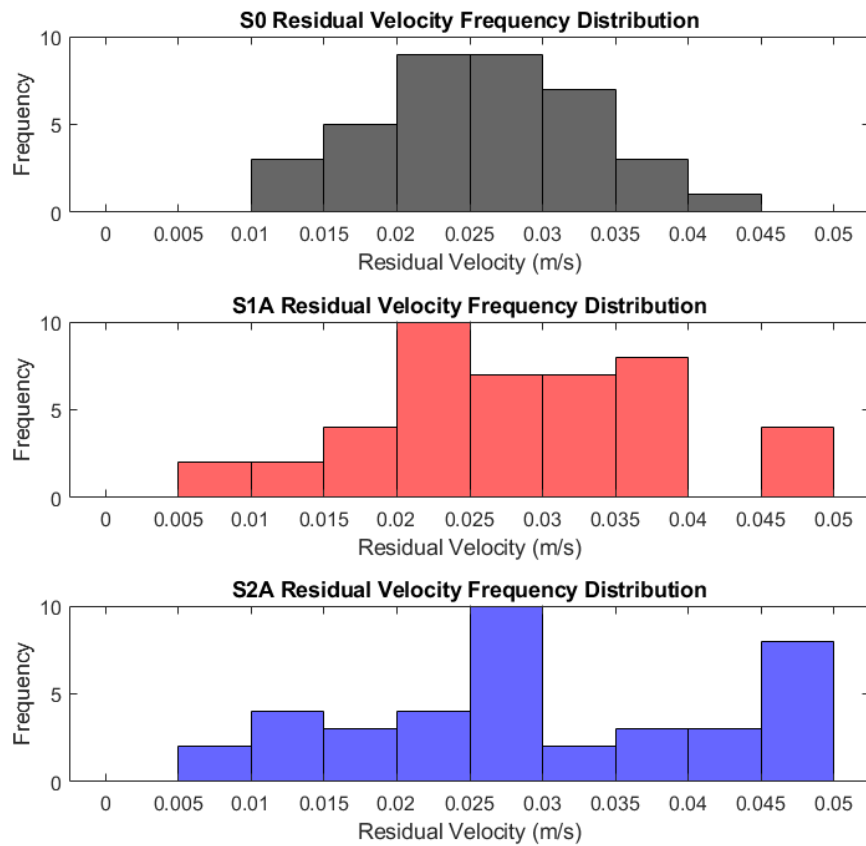


Figure 4.21 Comparison A – Distribution analysis of residual flow velocity.

4. Test Case 1 – Impact of Varying Turbine Layout

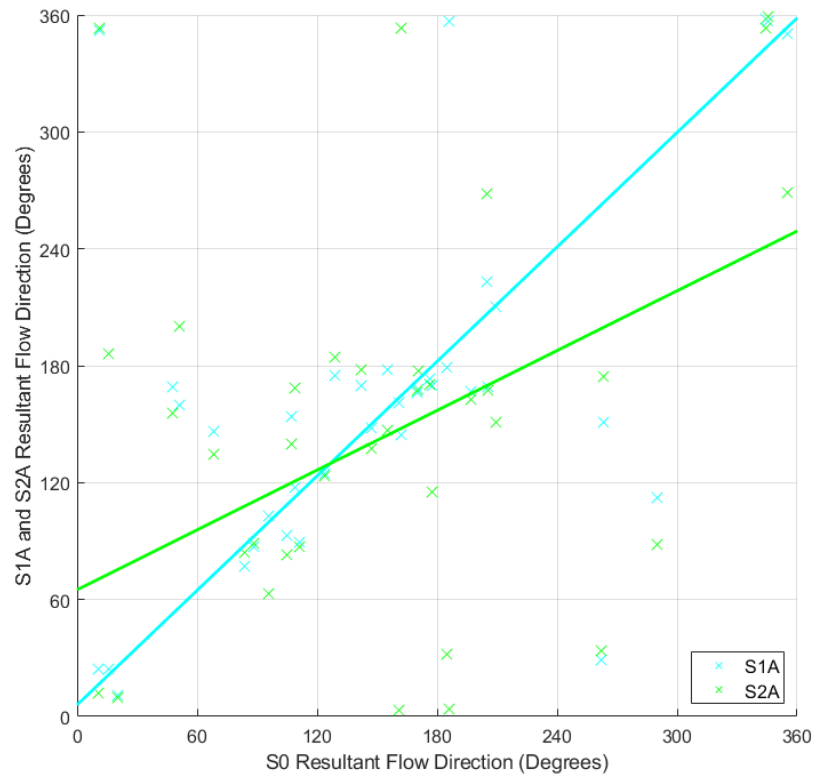


Figure 4.22 Comparison A - Regression analysis of residual flow direction.

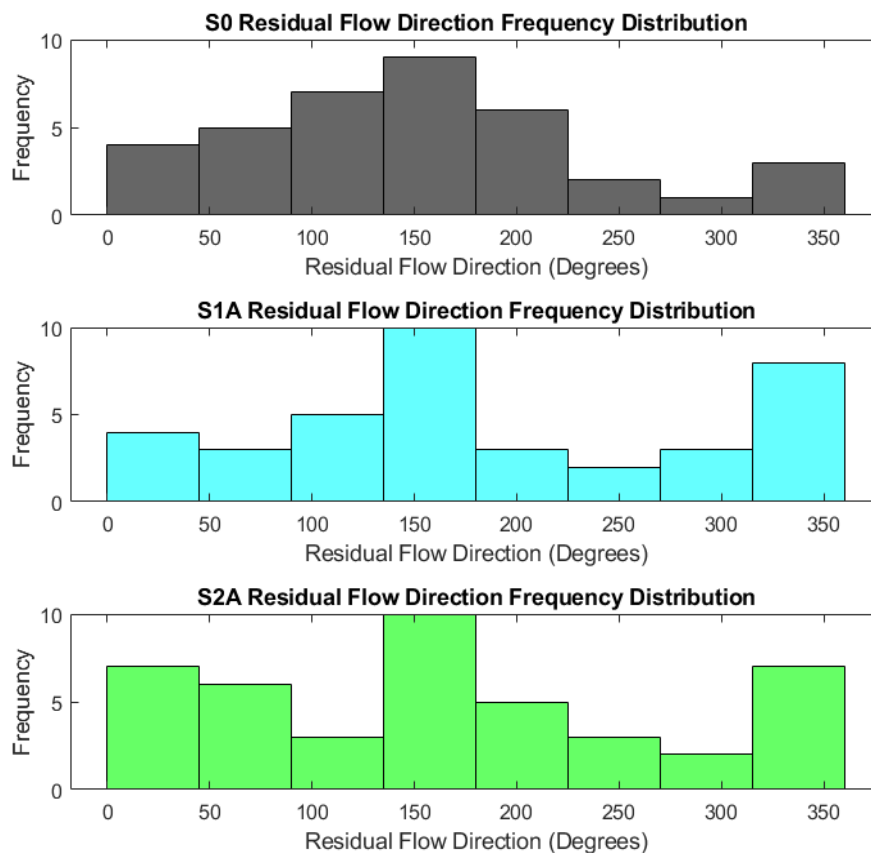


Figure 4.23 Comparison A – Distribution analysis of residual flow direction.

4. Test Case 1 – Impact of Varying Turbine Layout

Statistical analysis compares the residual velocity magnitude at each location against the baseline measurement (S0) using a number of metrics as explained in Section 3.6. These figures, presented in Table 4.2, show that experiments S1A and S2A caused an average increase in velocity magnitude from S0 of 10% and 30% respectively, once again confirming the exaggerated effects of the two turbine case over the single turbine case. The standard deviation is also greatly increased for S2A than S1A. The graphs for both S1A and S2A plotted against S0 display widely scattered results (see Figure 4.20) suggesting that there is little statistical significance between the results of these experiments and the S0 case. This is confirmed by the *r* values (Pearson's correlation coefficient) which are very low for both cases showing little correlation between either S1A or S2A with S0. However, the result of the z-test confirms that h_0 should be accepted for S1A and rejected for S2A. This proves that despite similarities between S1A and S2A, a single turbine does not cause as great a difference to baseline velocities as two turbines do. Further investigation of the effects of turbine distribution will be seen in Comparisons C and G (Sections 4.3.3 and 4.3.4).

Table 4.2 Comparison A - Statistical analysis of residual velocity magnitude of S1A and S2A compared to S0.

Comparison	\bar{x} (m/s)	SD	RMSE	r	Z	Accept/ reject h_0
S0	0.02570	0.007477				
S1A	0.02832	0.009563	0.00941	0.37727	1.38451	Accept
S2A	0.03333	0.016054	0.00941	0.27034	2.82702	Reject

4. Test Case 1 – Impact of Varying Turbine Layout

4.3.2 Comparison B – Varying the position of a single turbine in a square TRS

Comparison B investigates the hydrodynamic impacts of varying the position of a single turbine in a square TRS, comparing results from experiments S1A and S1B against pre-lagoon conditions (00) in order to determine which configuration has the greatest effect. Figure 4.24 shows the spacing of turbines in experiments S1A and S1B.

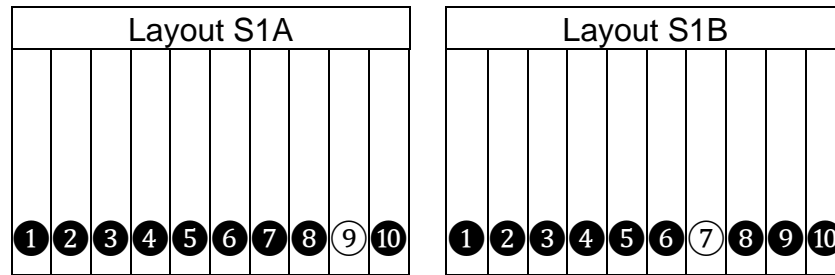


Figure 4.24 Experimental layouts for Comparison B: S1A and S1B.

4.3.2.1 Velocity - Depth Averaged

Figure 4.29 shows a map of the whole tank, with plots of depth averaged velocity for experiments S1A and S1B compared against pre-lagoon conditions (00) at each location. Looking at the depth averaged velocity it is clear that flow conditions for both cases are extremely similar, especially close to the inflow boundary and that both cases closely match the pre-lagoon case. Where variations do occur between the two cases it is usually in amplitude rather than the pattern of their results, e.g. (300,200) (close up in Figure 4.25) and (100,300) where the experiments both follow the same shape but vary slightly in their minimum and maximum values. Variation begins to occur closer to the TRS and is greatest at (200,400) (Figure 4.26). This point, directly in front of the TRS seawall is closer to the turbine opening in experiment S1B than S1A and shows the extent to which this slight offset of the turbine affects flow conditions, more than tripling the velocity at this point, whilst S1A still closely matches pre-lagoon conditions. Experiment S1A copies this pattern at (225,440) (Figure 4.27) directly in front of the turbine in this case and yet at (200,440) (Figure 4.28), closer to the turbine in S1B, both experiments show much slower flows again. This is unusual as we would expect to see a peak in S1B at (200,440) and yet this small offset has meant that the impact is not felt at this point

4. Test Case 1 – Impact of Varying Turbine Layout

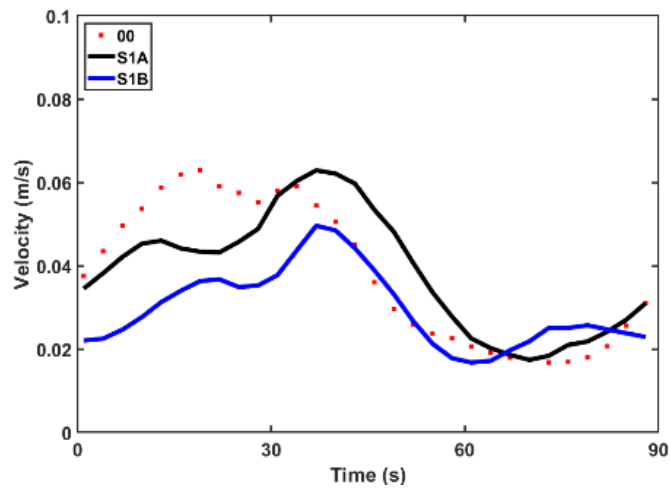


Figure 4.25 Closer detail of velocity at (300,200).

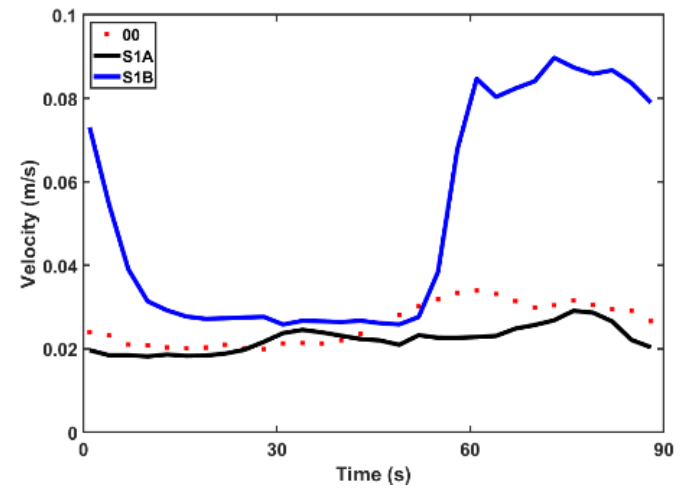


Figure 4.26 Closer detail of velocity at (200,400).

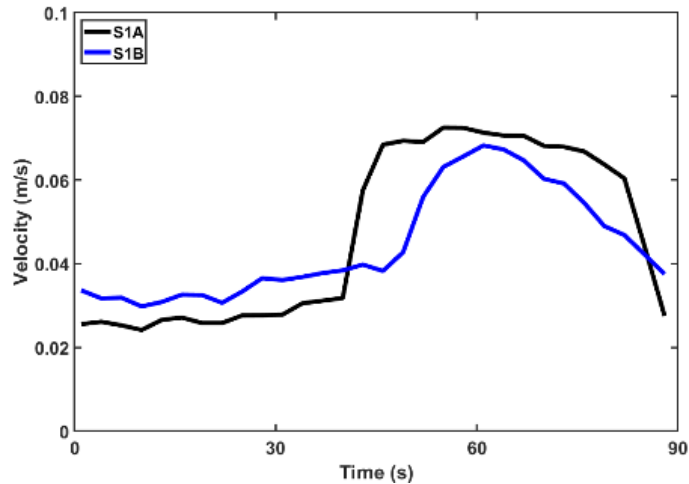


Figure 4.27 Closer detail of velocity at (225,440).

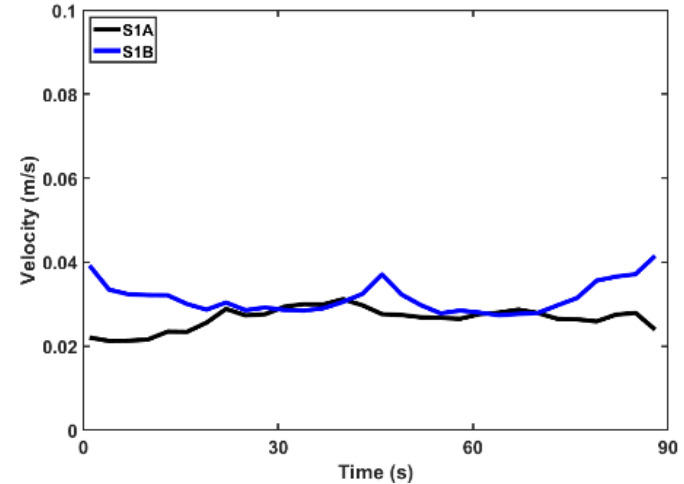


Figure 4.28 Closer detail of velocity at (200,440).

4. Test Case 1 – Impact of Varying Turbine Layout

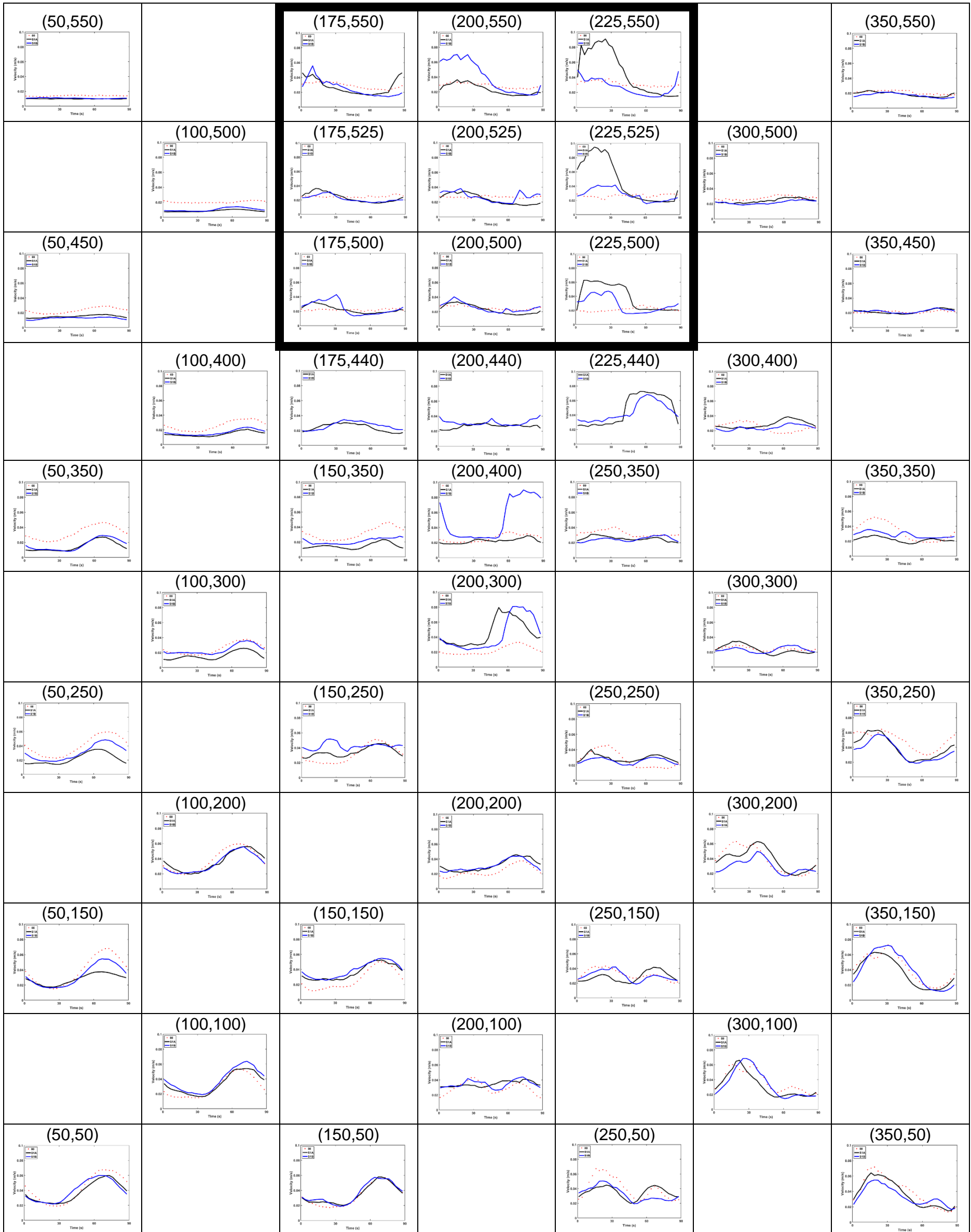


Figure 4.29 Map of depth averaged velocity plots for Comparison B: S1A and S1B.

4. Test Case 1 – Impact of Varying Turbine Layout

Inside the TRS, S1A and S1B velocity levels are very similar in pattern but vary in amplitude, with S1A having greater peaks along the line $x = 225$ cm (closer detail shown in Figure 4.30 and Figure 4.31). This seems to indicate that flow velocity is exaggerated by placing a turbine closer to a sidewall, whereas the same size turbine opening placed further away from sidewalls leads to slightly slower flows. Flows in the centre of the lagoon are nearly identical for both cases e.g. (200,500) (Figure 4.32), but S1B peaks slightly at the rear of the lagoon (200,550) (Figure 4.33), which agrees with images of flow visualisation (Figure 4.40), that wake jets through the turbine openings shoot to the back of the lagoon and are then deflected along the rear wall to the left-hand side.

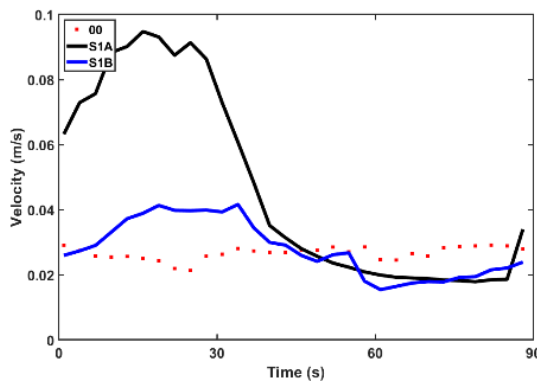


Figure 4.30 Closer detail of velocity at (225,525).

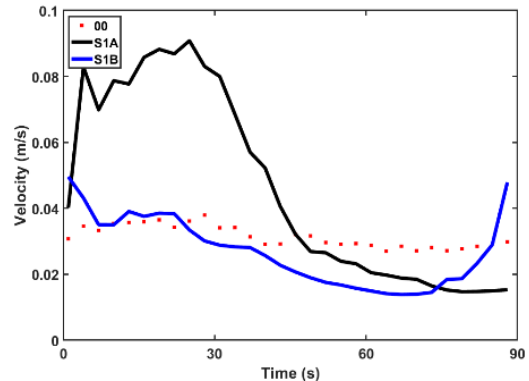


Figure 4.31 Closer detail of velocity at (225,550).

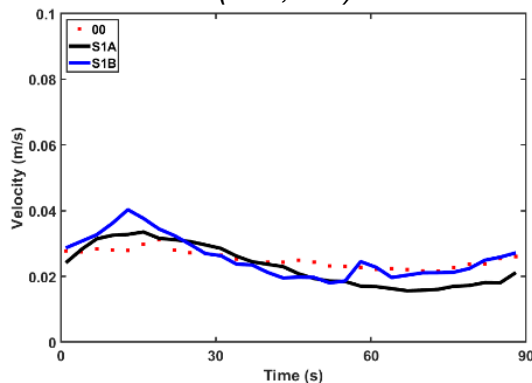


Figure 4.32 Closer detail of velocity at (200,500).

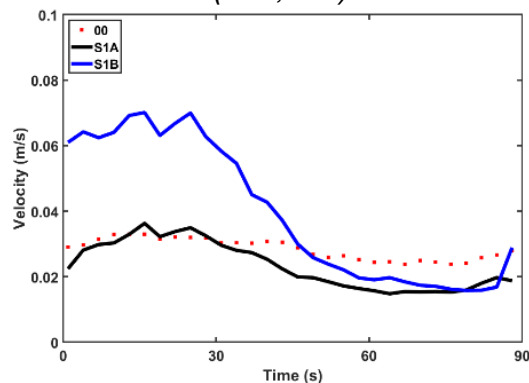


Figure 4.33 Closer detail of velocity at (200,550).

4. Test Case 1 – Impact of Varying Turbine Layout

4.3.2.2 Velocity – Analysed by tide and depth

Contour plots of resultant velocity within the tank at different depths and tidal phase show little variation outside the TRS between the depths for each experiment during the ebb tide (see Figure 4.34). Strength of flow decreases with depth as in Comparison A. The patterns between the two cases also show similarity, with areas of the strongest flow directly around the TRS seawall, stretching to the front left-hand corner of basin. This area of strong flow is, however, closer to the centre in S1B than S1A which is to be attributed to the more central location of the turbine opening in this configuration. Inside the TRS, the velocity contours are very different. S1A has very weak flow whereas S1B has stronger flow directly behind the turbine opening and also along the left-hand wall. This shows that the proximity to the sidewall effects the ability of water to circulate during this particular tide.

At low tide (Figure 4.35), flow speed has reduced significantly throughout the tank in both cases. S1B shows clearly how the strongest flows are found near the bed, where the turbine opening is located, and reduce with depth and distance from the orifice. There is stronger flow inside the TRS than there was during the ebb tide, but flow has reversed in experiment S1A with strong positive flow at the back of the TRS and slower flow near the front as water reflects off the rear wall. S1B shows some interesting patterns with the strongest flow being deflected to right and rear walls of the TRS. This is unusual as we wouldn't expect much variation in flow during times of slack water, but a current is clearly still circulating inside the TRS. This pattern seems to fade upwards of 200 mm confirming that there is a 3D element to the orifice wakes which appears to dissipate after a distance of 1.5 turbine diameters.

During the flood tide (Figure 4.36) conditions appear similar between the two experiments outside of the TRS, with areas of strong flow growing along the right-hand wall from the bed up towards the surface. Inside the TRS, however, different patterns emerge between the two layouts. S1A shows strong positive flow filling over half of the impounded area as the water rushes in through the turbine opening on the right and reaches towards the

4. Test Case 1 – Impact of Varying Turbine Layout

left-hand wall. S1B shows a similar pattern inside the TRS as it did during low tide, which is surprising given the increased force of flow that should be present during the flood tide. The strongest flow is once again deflected to the right-hand wall and circulates around to the left, which could be due to the Coanda effect where jets adhere to adjacent surfaces. These results show that even a slight variation in the position of the turbine openings can cause a large difference in flow behaviour. These extreme patterns do once again dissipate from depth 200 mm upwards, proving this to be a critical depth in the 3D nature of the flow.

The high tide graphs (Figure 4.37) maintain similar patterns at all depths for each experiment outside the TRS due to weaker flows during this phase of the tide. Inside the TRS, S1A has a weaker pattern than on the flood tide but with the strongest flows still concentrated near the turbine opening. S1B, however, shows the weakest pattern yet, with very slow flow directly behind the TRS and slightly stronger flow at the rear of the tank. This is most likely due to there being less energy at this phase of the tide, so water nears stagnation, and it is only the residual current from the flood tide that means that water continues to circulate anticlockwise inside the TRS.

4. Test Case 1 – Impact of Varying Turbine Layout

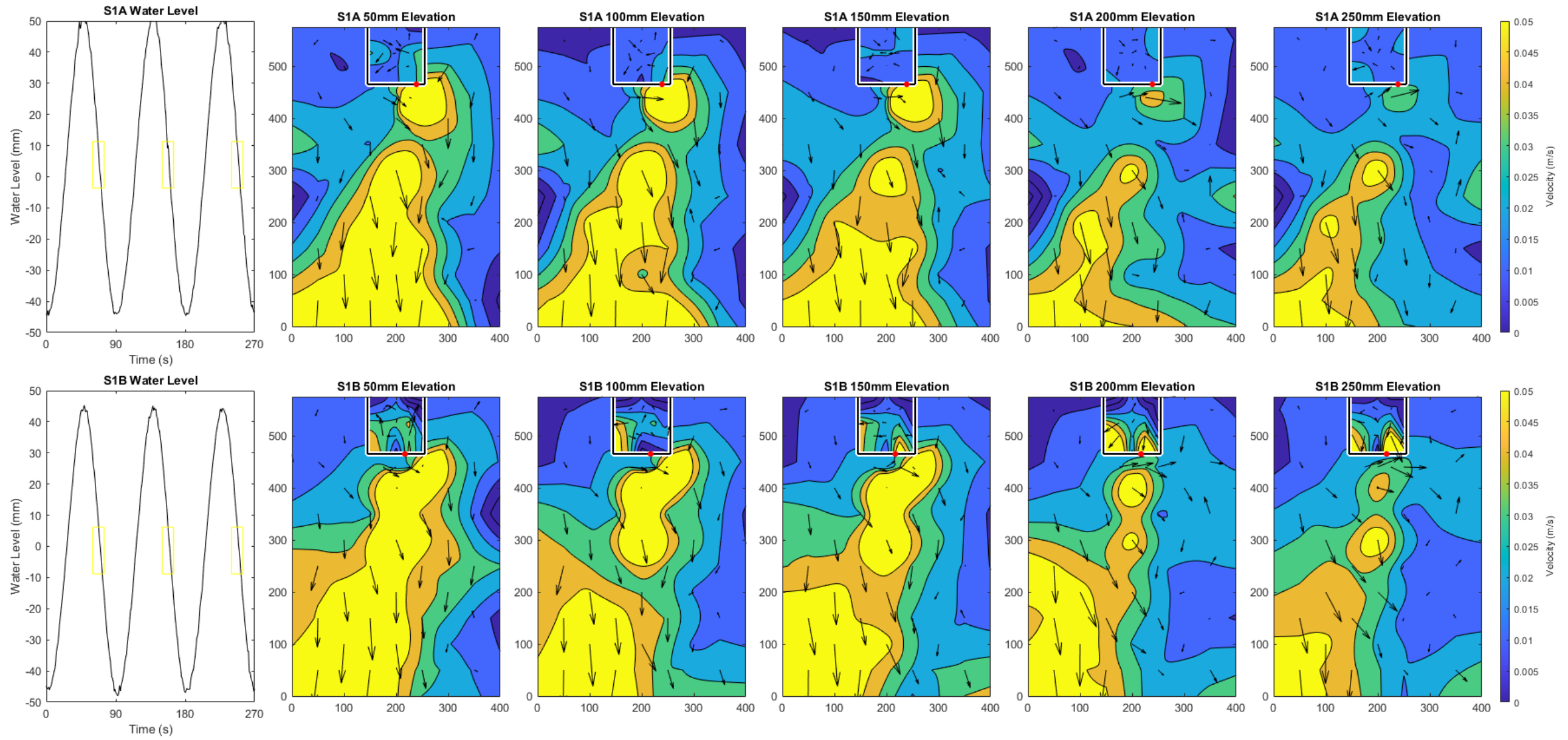


Figure 4.34 Comparison B - Velocity contour maps at elevations of 50, 100, 150, 200 and 250 mm above the bed during the ebb tide.

4. Test Case 1 – Impact of Varying Turbine Layout

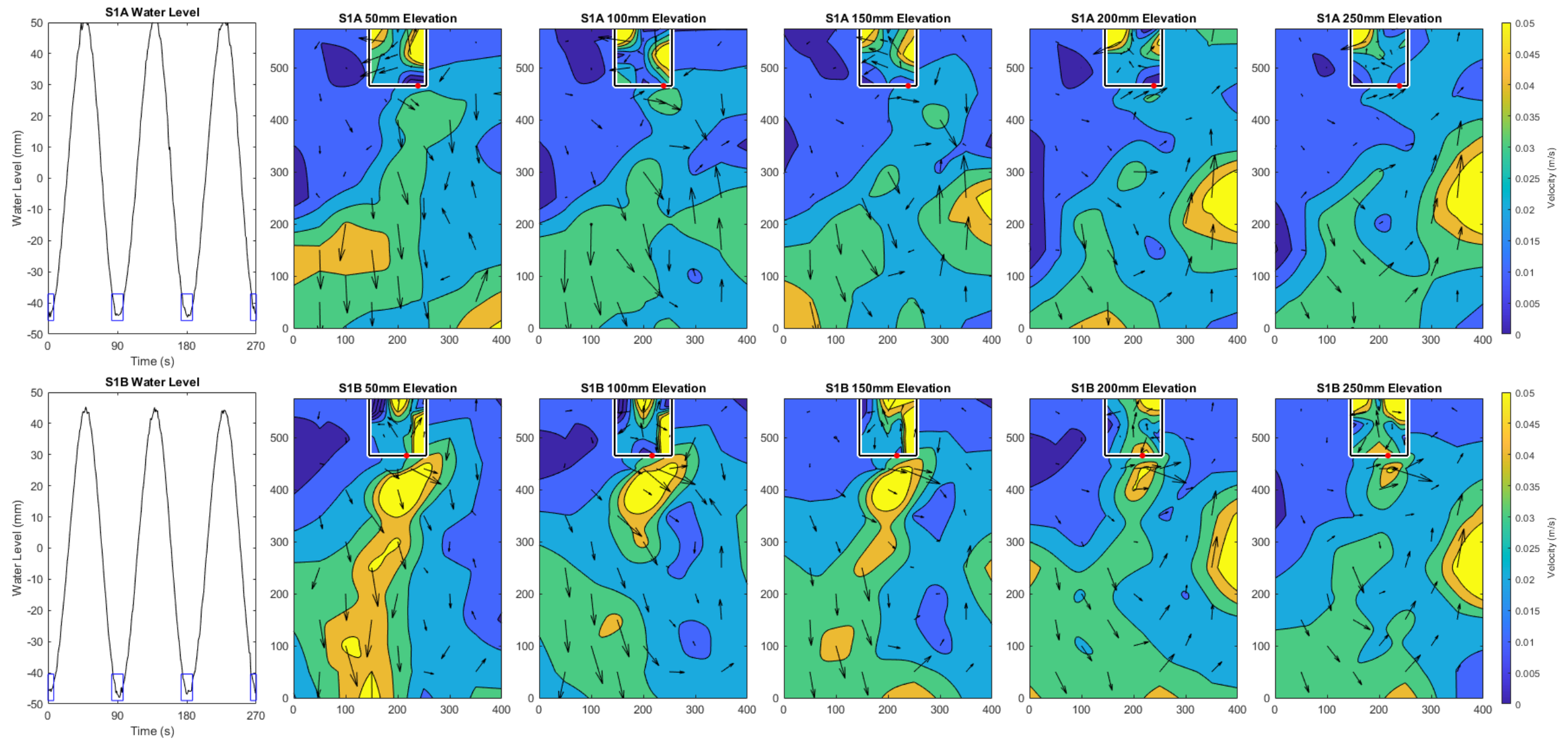


Figure 4.35 Comparison B - Velocity contour maps at elevations of 50, 100, 150, 200 and 250 mm above the bed during low tide.

4. Test Case 1 – Impact of Varying Turbine Layout

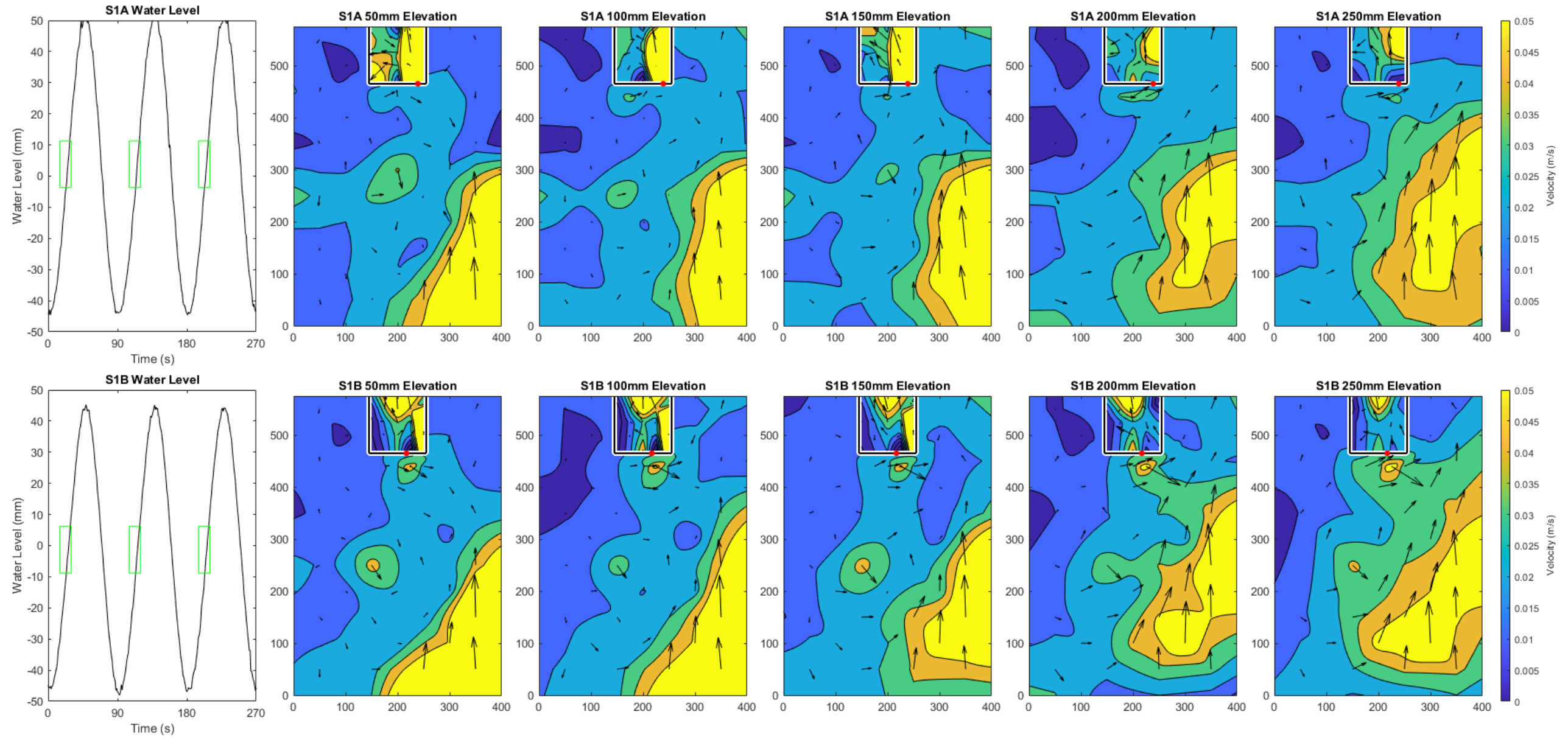


Figure 4.36 Comparison B - Velocity contour maps at elevations of 50, 100, 150, 200 and 250 mm above the bed during the flood tide.

4. Test Case 1 – Impact of Varying Turbine Layout

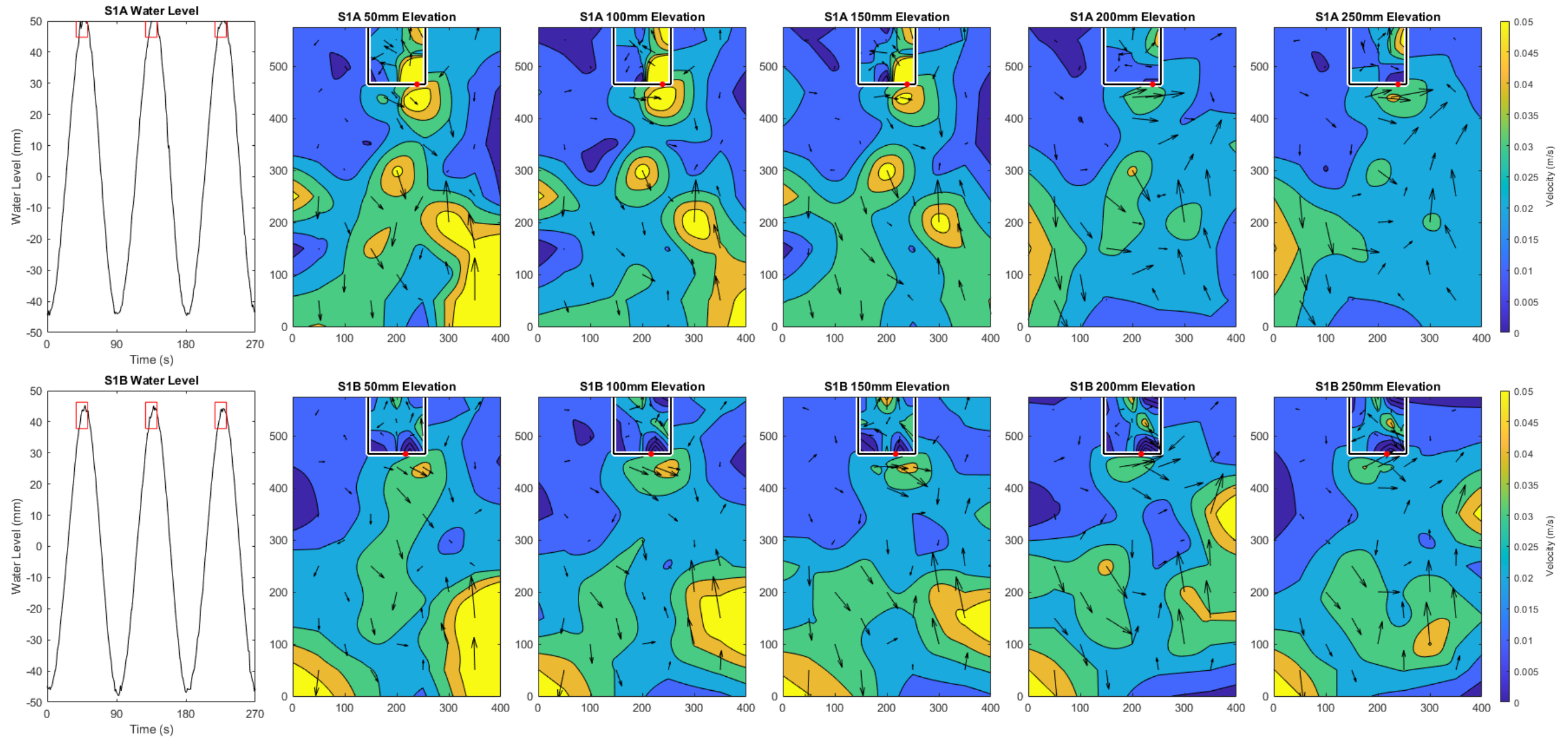


Figure 4.37 Comparison B - Velocity contour maps at elevations of 50, 100, 150, 200 and 250 mm above the bed during high tide.

4. Test Case 1 – Impact of Varying Turbine Layout

4.3.2.3 Velocity – Residual Velocity Magnitude and Direction

As with comparison A, the contour maps of residual velocity magnitude and direction in Figure 4.38 illustrate how flow within the tank is asymmetrical overall, circulating anticlockwise around the tank from the front right-hand corner to the front left. The strongest flow is visible in front of the TRS, concentrated close to the TRS wall and turbine openings for both cases. This demonstrates the effect that turbines have on the surrounding area which can result in acceleration and high velocities and must be balanced by careful operation to reduce environmental impacts (Angeloudis et al., 2016a). These patches seem to shrink and move slightly away from the TRS wall closer to the surface which proves that the flow is strongest close to the turbines (50 mm from the bed) and reduces further up the water column. Inside the TRS the flow velocity pattern is fairly linear for S1A, rippling from right to left, whilst it is slightly symmetrical for S1B reaching the rear wall before being deflected to both the right and left but is less strong than the S1A case. This shows that the position of the turbine not only affects the direction of the flow within the TRS but also its strength. I.e., when a turbine is located near a side wall, flow is forced to circulate around the boundaries of the TRS area, whereas a more centrally located turbine balances forces more equally in the whole of the TRS. In both cases, proximity to the boundary walls seem to have the greatest impact on flow direction which affects circulation and mixing in the TRS.

4. Test Case 1 – Impact of Varying Turbine Layout

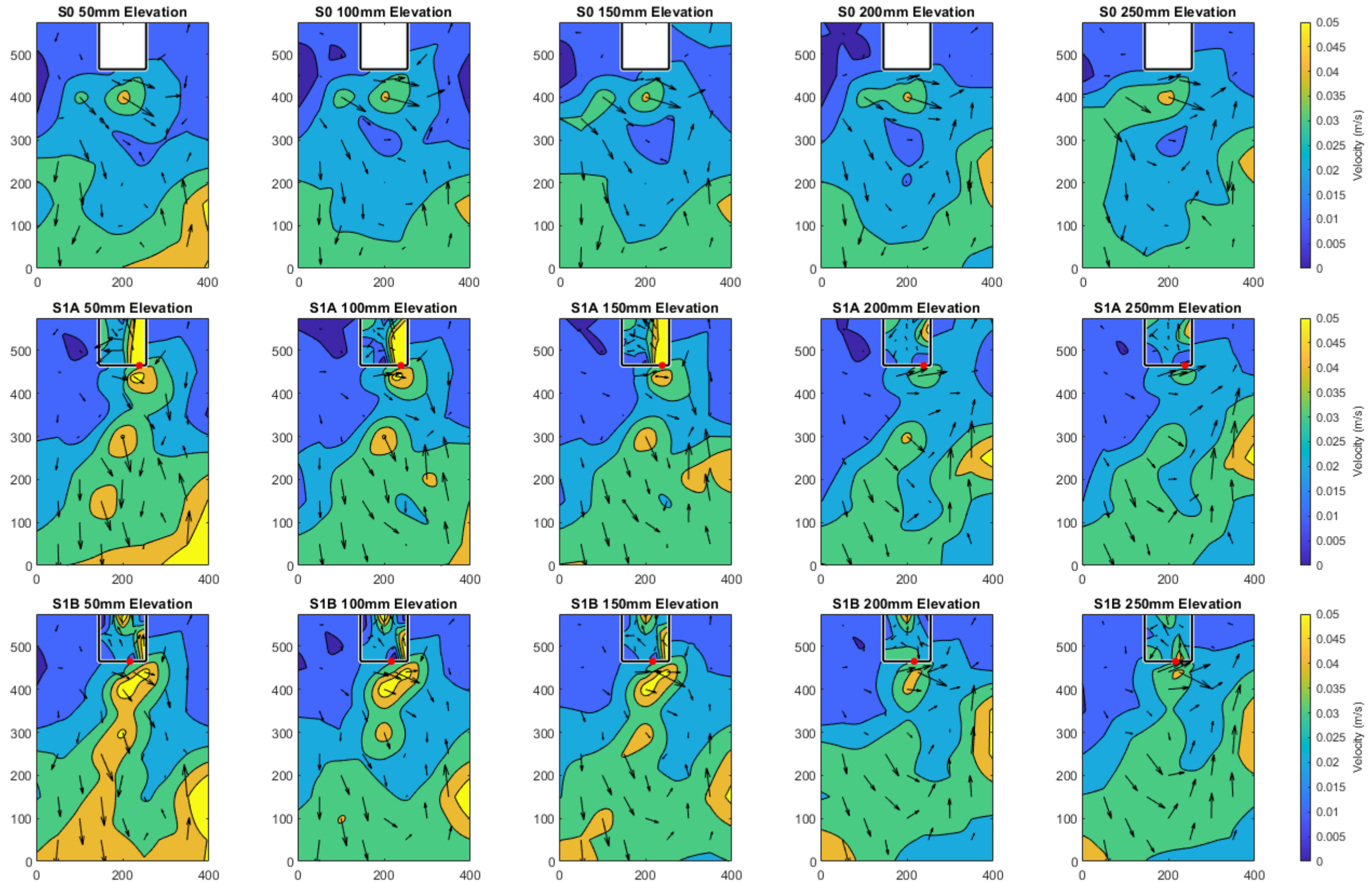


Figure 4.38 Comparison B – Contour maps of residual velocity magnitude and direction at elevations of 50, 100, 150, 200 and 200 mm from the bed.

4. Test Case 1 – Impact of Varying Turbine Layout

4.3.2.4 Flow Visualisation

Flow circulation in S1B, shown in Figure 4.40, reveals two wide counter-rotating cells emanating from the turbine opening. The left-hand cell is slightly larger and weaker owing to being further away from the opening compared to the right-hand cell which is slightly narrower and stronger as it is closer to the opening and to the side wall. Experiment S1A, displayed in Figure 4.39, also has two circulating cells but these rotate in the same direction and fill the centre of the lagoon rather than the right-hand cell adhering to the right-hand wall as in S1B. In both cases, the dye is fully mixed after 45 seconds, as in Comparison A, and fully dispersed within nine minutes of starting the experiment. Horizontal, counter-rotating cells were found to occur naturally in estuaries due to the meeting of landward and seaward water (Nguyen et al., 2018) but in the present case it is most likely due to water reflecting off the boundary walls of the TRS which can perpetuate the recirculation of dipoles (Vouriot et al., 2018).

4. Test Case 1 – Impact of Varying Turbine Layout

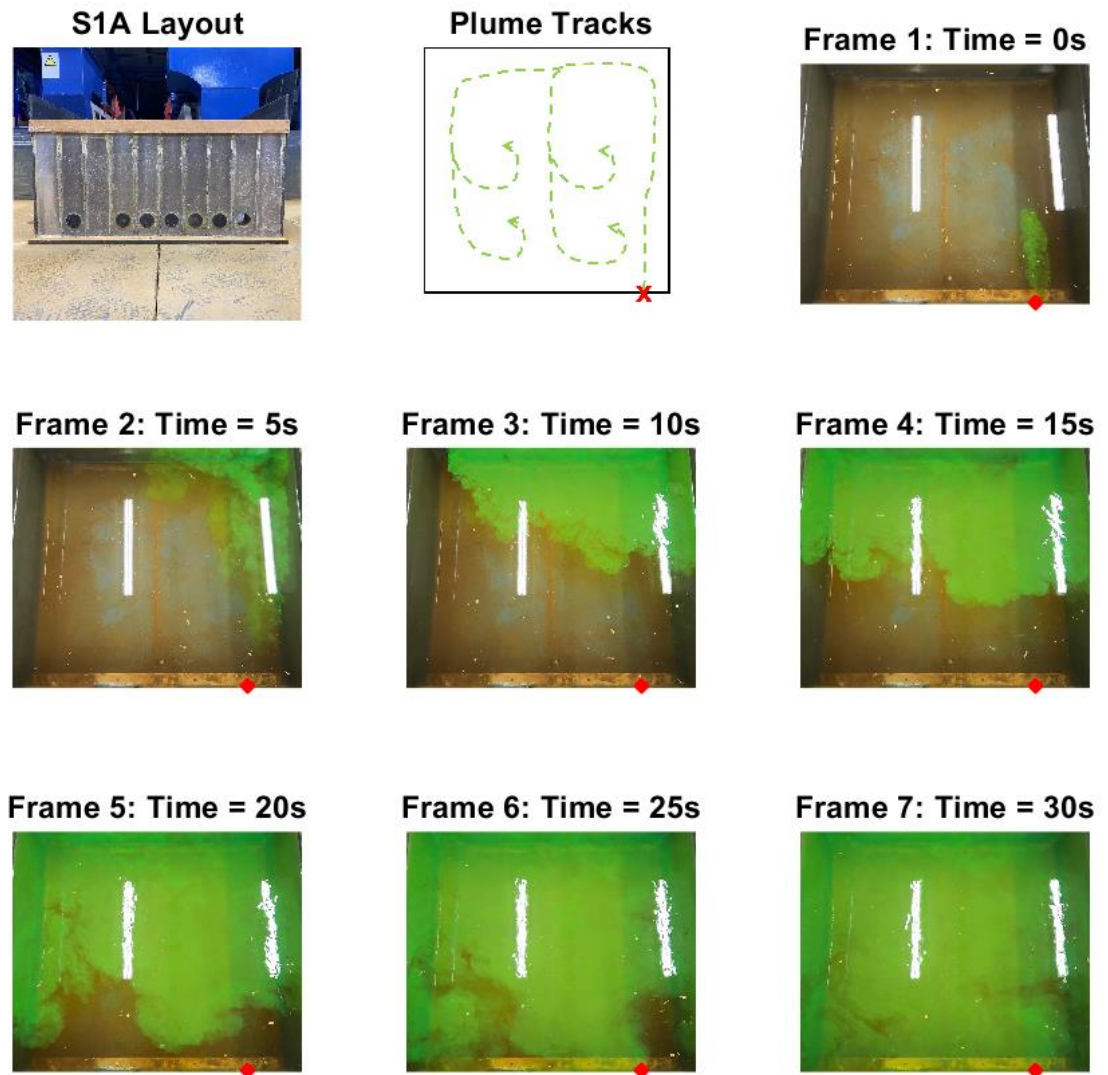


Figure 4.39 Flow visualisation for experiment S1A.

4. Test Case 1 – Impact of Varying Turbine Layout

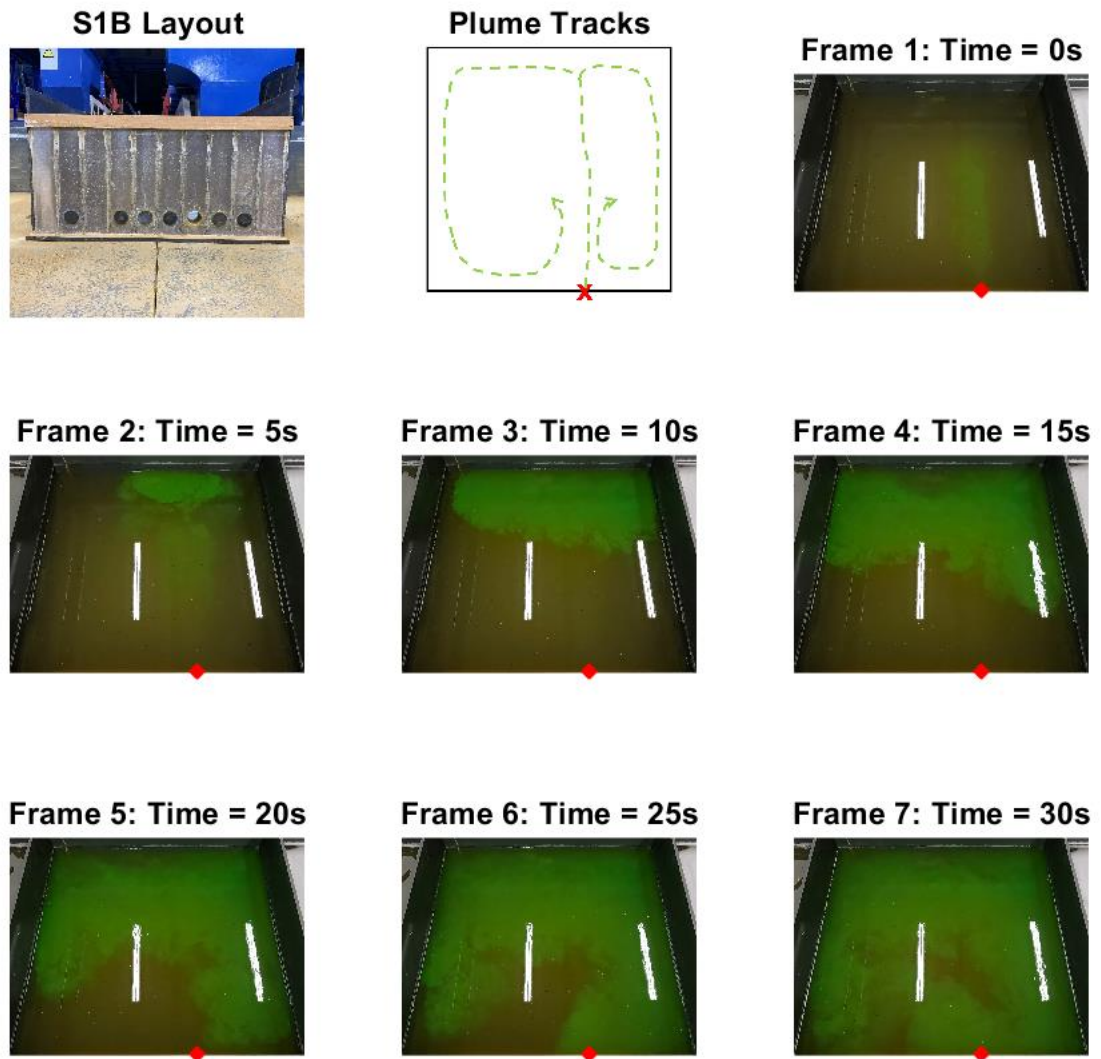


Figure 4.40 Flow visualisation for experiment S1B.

4. Test Case 1 – Impact of Varying Turbine Layout

4.3.2.5 Statistical Analysis

Figure 4.41 presents regression analysis of the residual velocity of S1A and S1B compared to the closed box case S0. This graph reveals that although both cases are quite scattered, the results from the configuration of S1B more closely match those of the closed box, with a fairly strong positive gradient. This is also confirmed by the stronger Pearson's correlation coefficient (r value) of S1B than S1A seen in Table 4.3. This slight improved in correlation suggests that when a turbine is centrally located in the seawall rather than close to the adjacent walls then conditions are less altered.

Regression analysis of the residual velocity direction reveals extremely similar results between both experiments and the baseline case (see Figure 4.43). This shows that despite the introduction of turbine openings changing the speed of flow, the direction has not been much altered by either configuration.

Further similarities between these two cases can be found by looking at statistical metrics of residual flow magnitude presented in Table 4.3. Both experiments increased average flow velocity by around 11% and have similar standard deviations to one another.

Frequency distribution analysis of the residual velocity in Figure 4.42 shows how both experiments S1A and S1B are very similar to those of S0 which supports the conclusion of the z-test results to accept h_0 for both experiments, that there is no statistical difference caused to the residual velocity by the addition of a turbine in either position.

Table 4.3 Comparison B - Statistical analysis of residual velocity magnitude of S1A and S1B compared to S0.

Comparison	\bar{x} (m/s)	SD	RMSE	r	z	Accept/ reject h_0
S0	0.02570	0.00748				
S1A	0.02832	0.00956	0.00941	0.37727	1.3845	Accept
S1B	0.02910	0.00884	0.00811	0.64275	1.8735	Accept

4. Test Case 1 – Impact of Varying Turbine Layout

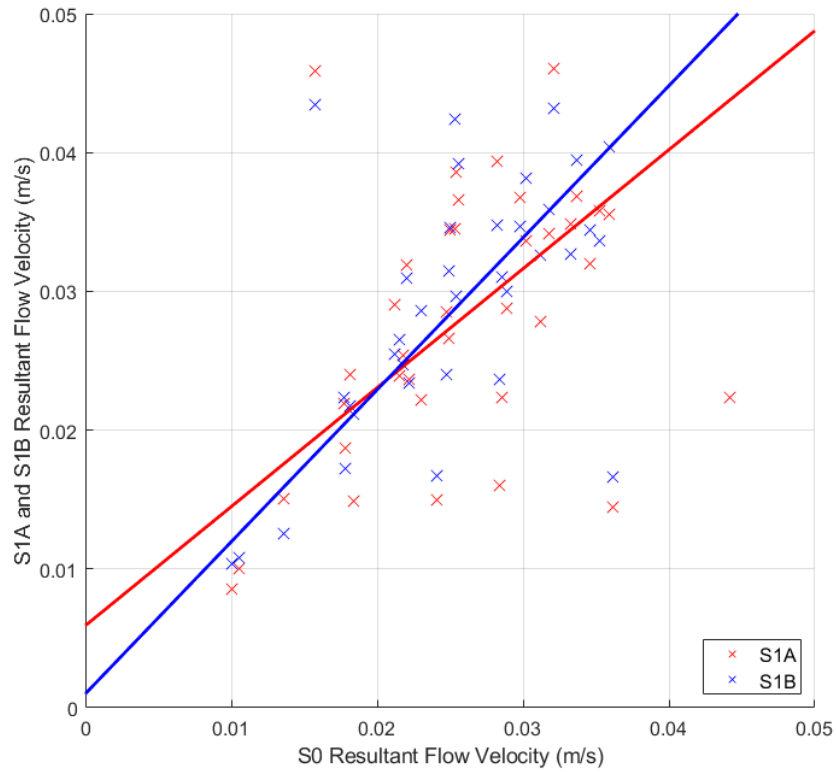


Figure 4.41 Comparison B - Regression analysis of residual flow velocity.

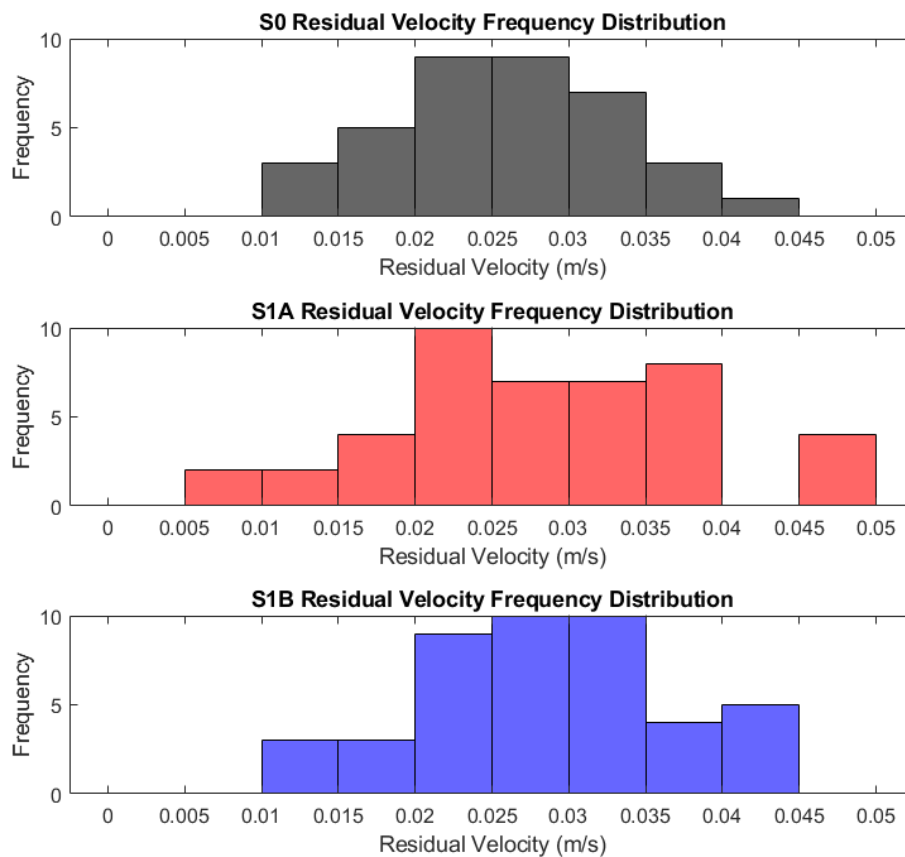


Figure 4.42 Comparison B – Distribution analysis of residual flow velocity.

4. Test Case 1 – Impact of Varying Turbine Layout

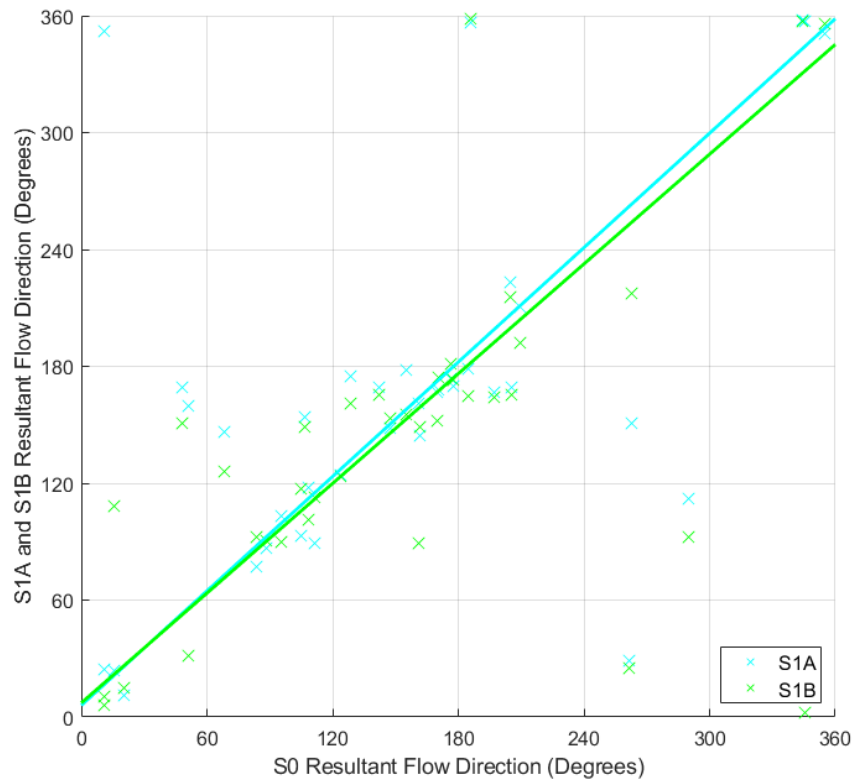


Figure 4.43 Comparison B - Regression analysis of residual flow direction.

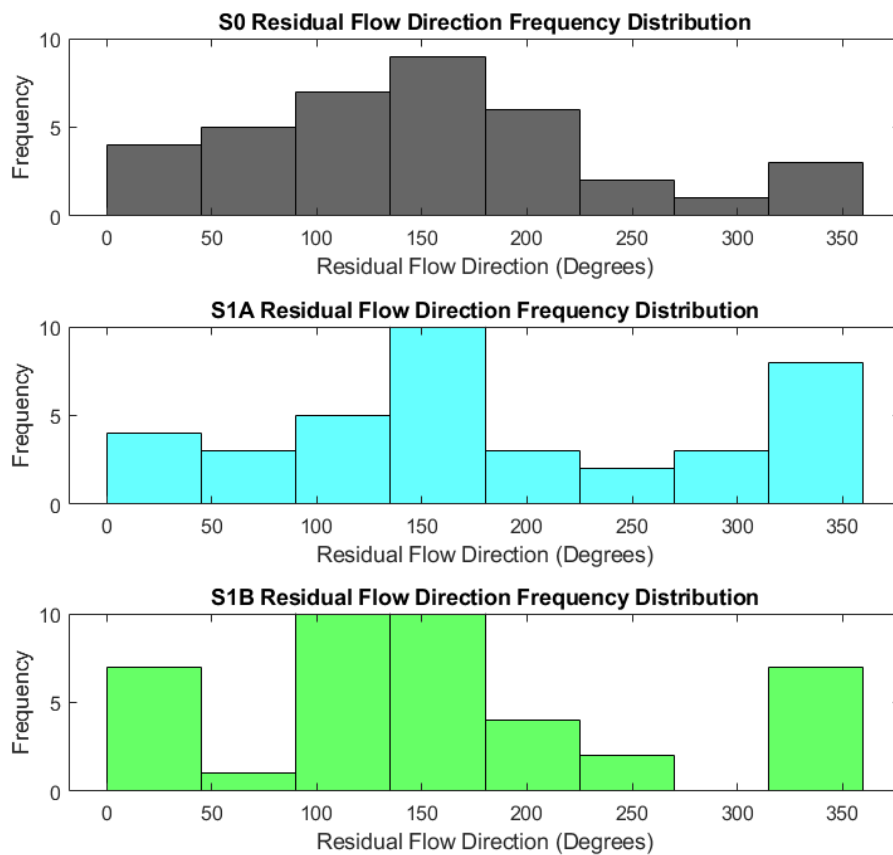


Figure 4.44 Comparison B – Distribution analysis of residual flow direction.

4. Test Case 1 – Impact of Varying Turbine Layout

4.3.3 Comparison C – Varying the position of two turbines in a square TRS
Comparison C investigates the hydrodynamic impacts of varying the spacing of a pair of turbines in a square TRS, comparing results from experiments S2A, S2B, S2C and S2D against pre-lagoon conditions in order to determine which configuration has the greatest effect. Figure 4.45 shows the layout of the turbines in each of the experiments in Comparison C.

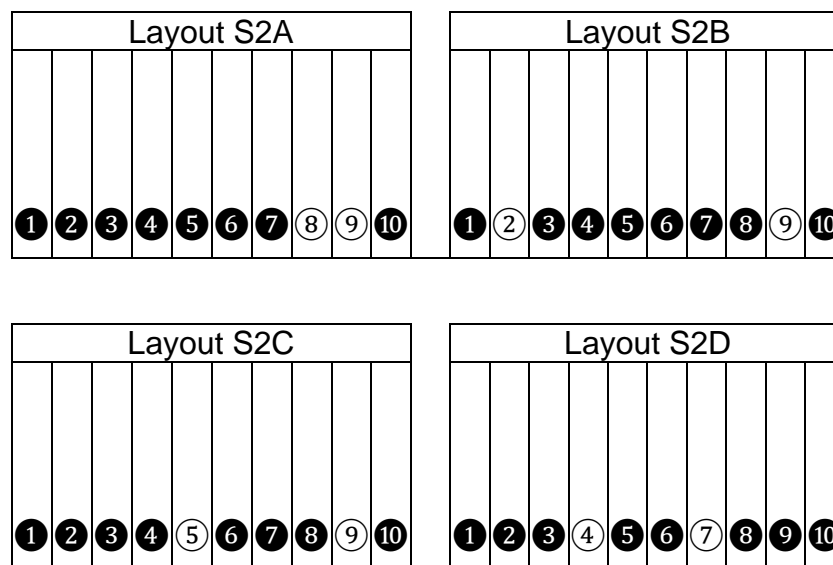


Figure 4.45 Experimental layouts for Comparison C: S2A, S2B, S2C and S2D.

4.3.3.1 Velocity - Depth Averaged

Figure 4.46 presents a map of depth averaged velocity at each location, comparing experiments S2A, S2B, S2C and S2D throughout the tank against each other as well as against pre-lagoon (00) conditions. These results display similar patterns for each experiment at most locations especially in the front of the tank at distances further than 150 cm from the TRS. Each of the cases also quite closely match pre-lagoon results indicating that the presence of the TRS does not cause a significant difference in the far field. Where differences do occur it tends to be experiment S2A that deviates from the other cases, either producing significantly lower flow velocities as at e.g., (150,350) (Figure 4.47) or significantly higher, e.g. 200,100) (Figure 4.48). This could be attributed to the close positioning of the turbines in this case compared to each of the other experiments leading to the greatest and

4. Test Case 1 – Impact of Varying Turbine Layout

furthest reaching impact on flow velocity. This aligns with the report of Falconer et al. (2017) who state that where turbine positioning is restricted, and structures are packed closely together, they cause issues with circulation which affect hydro-ecology and morphology.

Since experiment S2B is the only case to have a turbine positioned on the left-hand side of the seawall we would expect to see higher velocities on this side of the tank, which is somewhat the case at (150,350) (Figure 4.47) where S2B follows the same pattern as the other cases but with a higher peak. However, at (175,440) (Figure 4.49) close to the left-hand turbine in S2B, the velocity is of the same range as the other experiments. This could be due to a single turbine not causing strong enough flows to be noticeable different from the other cases. However, at the right-hand side of the seawall (225,440) (Figure 4.50) all of the experiments show a similar peak even those which only have a single turbine opening at this location. This could be due to underlying asymmetric flow in the tank which is generally faster on the right-hand side of the tank than the left. In the centre of the seawall, (200,440) (Figure 4.51) the flow velocities are much lower for all cases which is to be attributed to being between the turbines for cases S2B and S2D and offset from the turbines in cases S2A and C. Further away from the seawall though, at (200,400) (Figure 4.52) there are peaks again from S2C and D. This shows how reflections from the TRS seawall and deflected wakes from the turbine openings can affect flow velocity up to 60 cm (10 turbine diameters) away from the seawall, in agreement with other studies (Verbeek et al 2021). Results from S2B are much lower than the other cases at this point though which suggests that placing the two turbine openings at opposite sides of the seawall, flow returns to normal levels much sooner than for the other cases where the turbines are closer together. Flow is almost negligible for S2A at (200,400) and along the line $y = 350$ cm, which suggests that the concentration of turbines on one side of the seawall not causing disruption in this part of the tank despite having an impact further afield.

4. Test Case 1 – Impact of Varying Turbine Layout

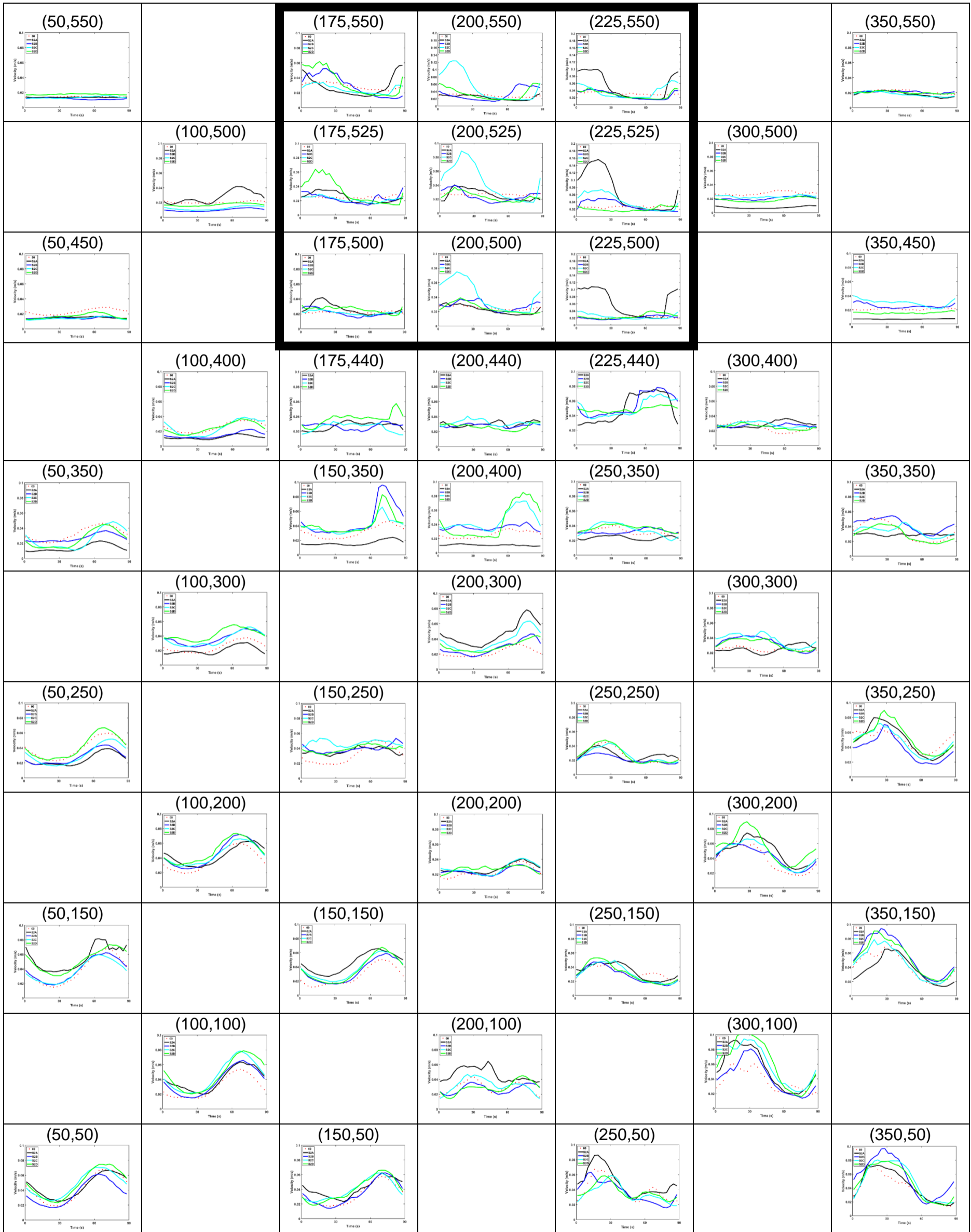


Figure 4.46 Map of depth averaged velocity plots for Comparison C: S2A, S2B, S2C and S2D.

4. Test Case 1 – Impact of Varying Turbine Layout

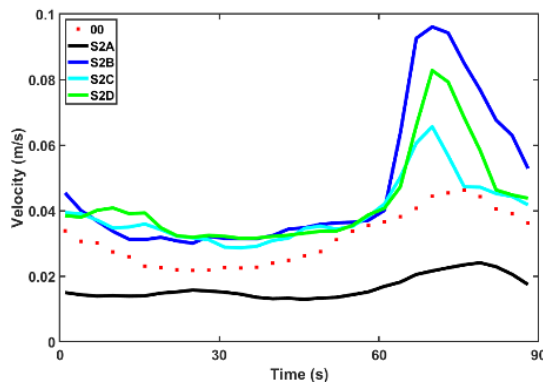


Figure 4.47 Closer detail of velocity at (150,350).

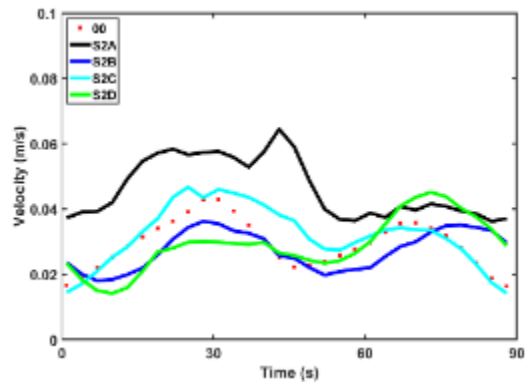


Figure 4.48 Closer detail of velocity at (200,100).

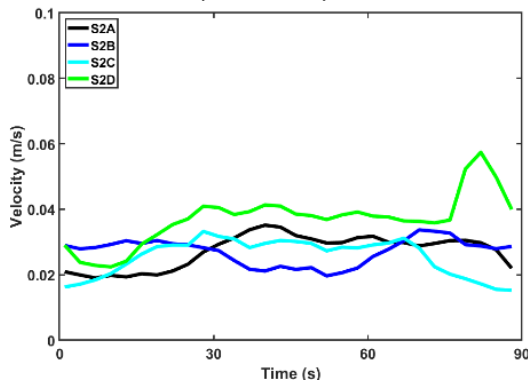


Figure 4.49 Closer detail of velocity at (175,440).

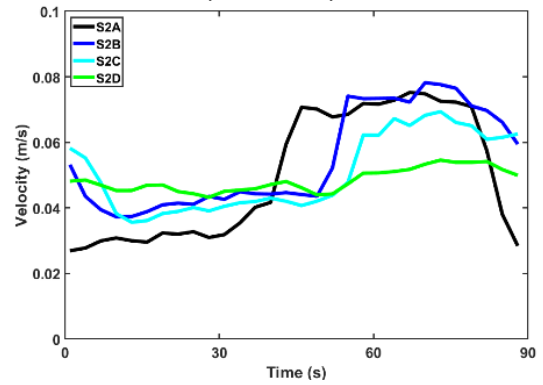


Figure 4.50 Closer detail of velocity at (225,440).

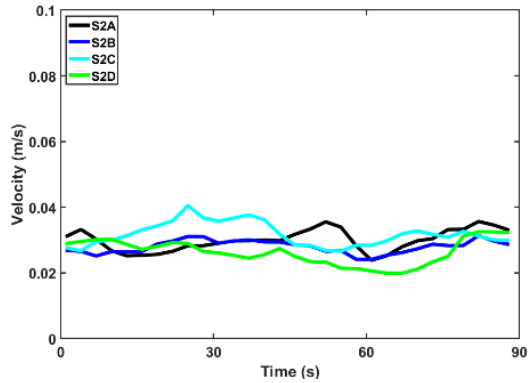


Figure 4.51 Closer detail of velocity at (200,440).

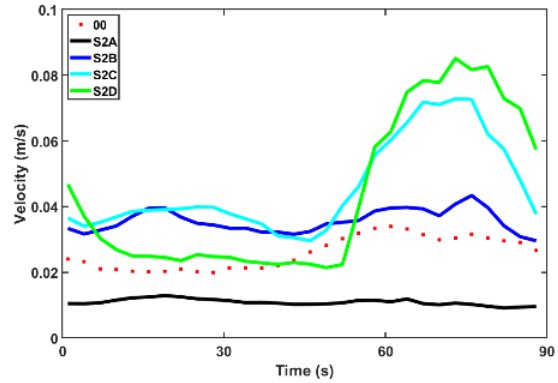


Figure 4.52 Closer detail of velocity at (200,400).

4. Test Case 1 – Impact of Varying Turbine Layout

In studying idealised TRSs, Mackie et al. (2021) observed that conditions inside tidal lagoons are impacted by the placement of hydraulic structures and also by operation regime. In this study, where there is no operational regime in action, results inside the TRS are extremely similar for all experiments at (175,500), the front left-hand corner. This is unusual as we would expect to see stronger flows in S2B as this is the only experiment with a turbine located on the left-hand side of the TRS wall, but this is not the case, and the results blend in with the others. This suggests that a single turbine does not cause a great increase in the strength of the flows and confirms the observations from Comparison A that single turbines do not cause a noticeable difference. Along the right-hand wall of the lagoon ($x = 225$ cm), S2A has significantly higher peaks than the other cases (closer detail shown in Figure 4.54, Figure 4.56 and Figure 4.58) as observed previously that two turbines located in the same part of the seawall, and close to a sidewall, lead to exaggerated wakes. S2C also experiences some peaks along the right-hand wall as well as along the centre line of the lagoon ($x = 200$ cm) (closer detail shown in Figure 4.53, Figure 4.55 and Figure 4.57). This shows that two turbines with a slight spacing can have far reaching impacts throughout the TRS since this configuration has caused the greatest impact on flow velocity and turbulence overall. Experiment S2B has a slight peak at (175,500) and (225, 525) but has the slowest flows in the TRS overall, proving that wider spacing more closely maintains natural flow conditions. The central spacing of S2D is also better at maintain natural flow conditions than S2A and C, with peaks only at the rear left corner of the tank at (175,550) and (175,525).

4. Test Case 1 – Impact of Varying Turbine Layout

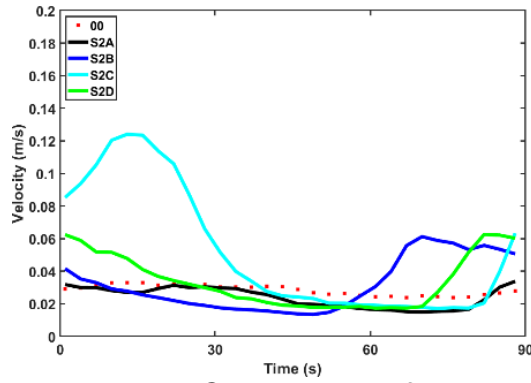


Figure 4.53 Closer detail of velocity at (200,550).

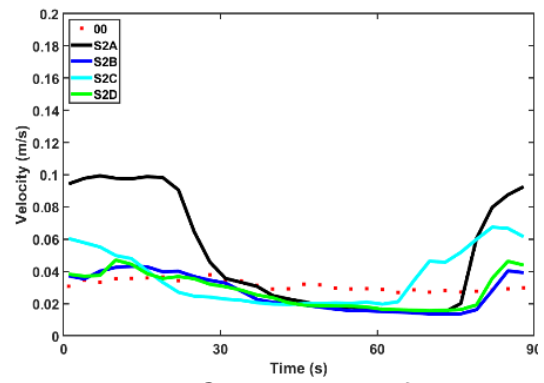


Figure 4.54 Closer detail of velocity at (225,550).

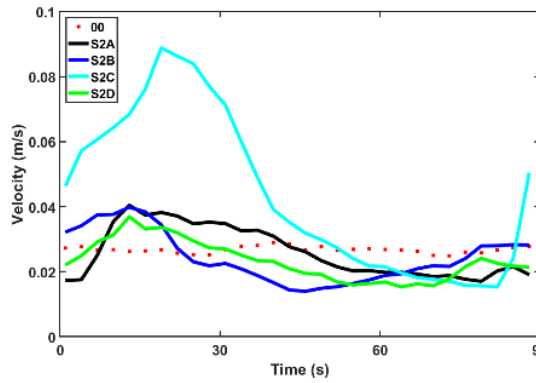


Figure 4.55 Closer detail of velocity at (200,525).

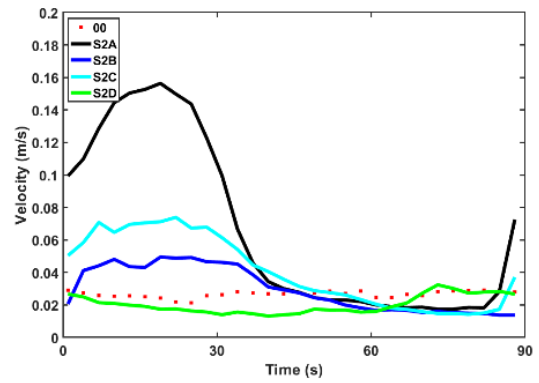


Figure 4.56 Closer detail of velocity at (225,525).

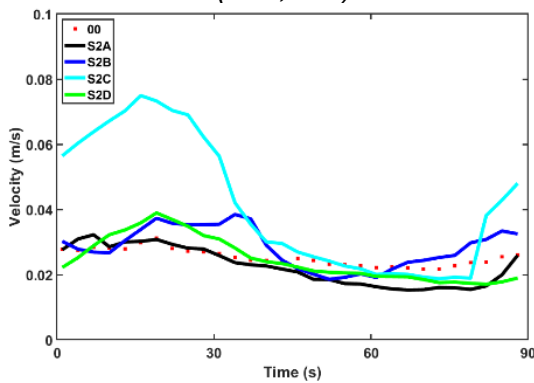


Figure 4.57 Closer detail of velocity at (200,500).

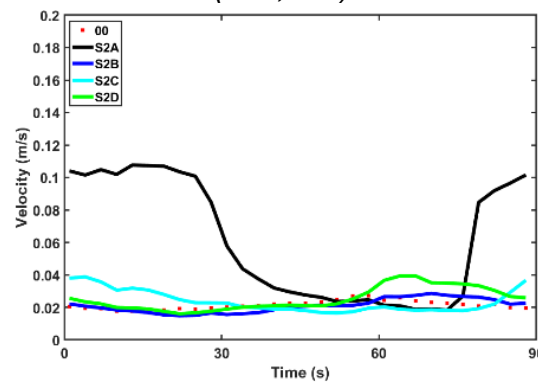


Figure 4.58 Closer detail of velocity at (225,500).

4. Test Case 1 – Impact of Varying Turbine Layout

4.3.3.2 Velocity – Analysed by tide and depth

Contour plots of residual velocity during the ebb tide reveal very little variation between depths, and flow patterns are extremely similar between experiments S2B, S2C and S2D indicating that for these layouts their effect outside the TRS is very similar (see Figure 4.59). S2A deviates slightly from the other experiments in that it has weaker flows around the TRS, particularly on the left-hand side away from the two turbine openings. This suggests that the close spacing of the two turbine openings in S2A has caused a greater difference in flow in the outer tank from the other experiments where the openings are more widely spaced. Inside the TRS, however, there is more of a difference between the experiments.

There is very little flow inside the TRS in S2A, with water nearing stagnation across most of the TRS. S2B shows the greatest movement, with flow appearing symmetrical between the two widely spaced turbine openings. This is the same pattern we would expect for S2D, where the openings are equally spaced but located closer to the centre of the seawall. But instead of a symmetrical pattern we can see a cluster of contours of strong flow in the front right-hand corner with slower flows elsewhere but no defined pattern. This could be due to the underlying asymmetrical flow in the tank which is stronger on the right-hand side overall which may cause water to circulate faster on the right-hand side than the left when the turbines are equally spaced. There is also no defined pattern in the case of S2C, where the turbine openings are offset to the right.

At low tide flow still does not vary greatly between depths and there is even less variation between the experiments, especially S2B and S2C (Figure 4.60). There are greater differences however, inside the TRS. S2A has some of the strongest flows, with strong positive currents permeating almost the whole TRS despite this period of slack water. This could be due to effects of a concentrated wake from the closely spaced turbine openings, acting almost as a single area and allowing water to continue to circulate even at low tide. Flow within the TRS seems more symmetrical for experiments S2C and S2D than before, which suggests that turbine wakes can flow unimpeded at low water and circulate throughout the

4. Test Case 1 – Impact of Varying Turbine Layout

lagoon. However, the symmetrical pattern seems less prominent near the bed in S2B (elevation 50 mm), meaning that this wider spacing has less impact close to the bed at the turn of the tide.

During the flood tide (Figure 4.61), flow patterns stay very similar throughout all layers, but the strongest flows have switched from the left-hand side of the tank during the ebb tide to the right-hand side. This highlights once again the underlying asymmetry of the tidal basin with the strongest inflowing water occurring on the right-hand side of the inflow boundary and the strongest ebbing water occurring on the left. Although there is a slight difference between S2B and the other experiments this time, yet again, it is the side-by-side location of the turbine openings in S2A that lead to the greatest differences in flow pattern in the outer basin. Inside the TRS, both S2B and S2C exemplify the symmetrical pattern we would associate with evenly spaced turbines despite the offset location of the openings in S2C. The symmetrical pattern becomes more apparent in S2D from elevation 150 mm upward, suggesting that the strong forces of the flood tide cause more turbulence close to the bed but that they even out further up the water column to allow the circulation of two equal vortices, providing more evidence for the 3D nature of turbine wakes. S2A shows the asymmetric pattern we would expect from two tightly packed turbine openings, with the strongest flow along the right-hand wall of the TRS, directly behind the openings.

The high tide graphs in Figure 4.62 once again display similarities between all layers, outside the TRS. Inside the TRS we can still see some evidence of symmetry in S2B and S2C, but the forces are much weaker than at other tides, which is too be expected during the period of slack water at high tide.

4. Test Case 1 – Impact of Varying Turbine Layout

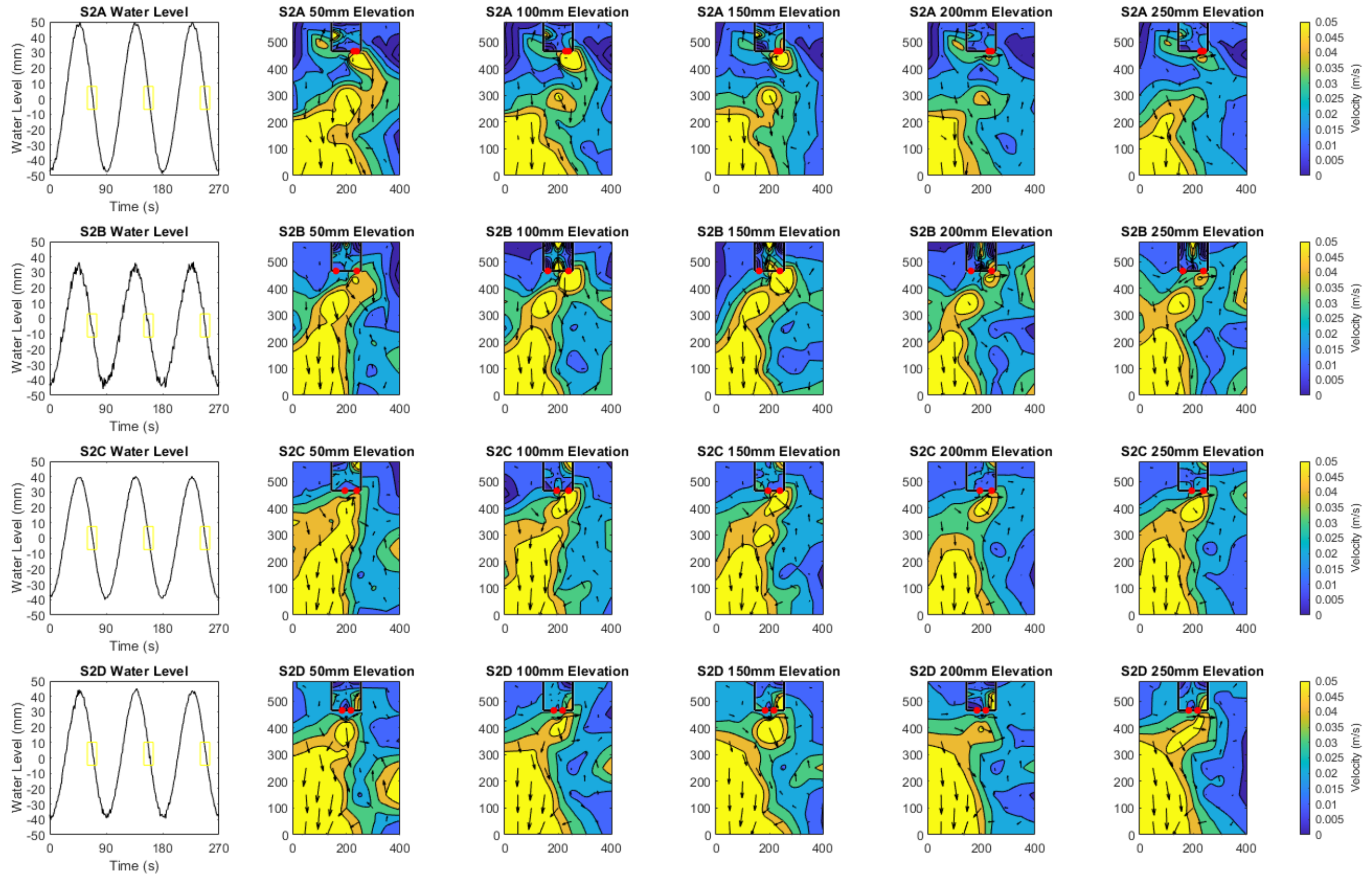


Figure 4.59 Comparison C - Velocity contour maps at elevations of 50, 100, 150, 200 and 250 mm above the bed during the ebb tide.

4. Test Case 1 – Impact of Varying Turbine Layout

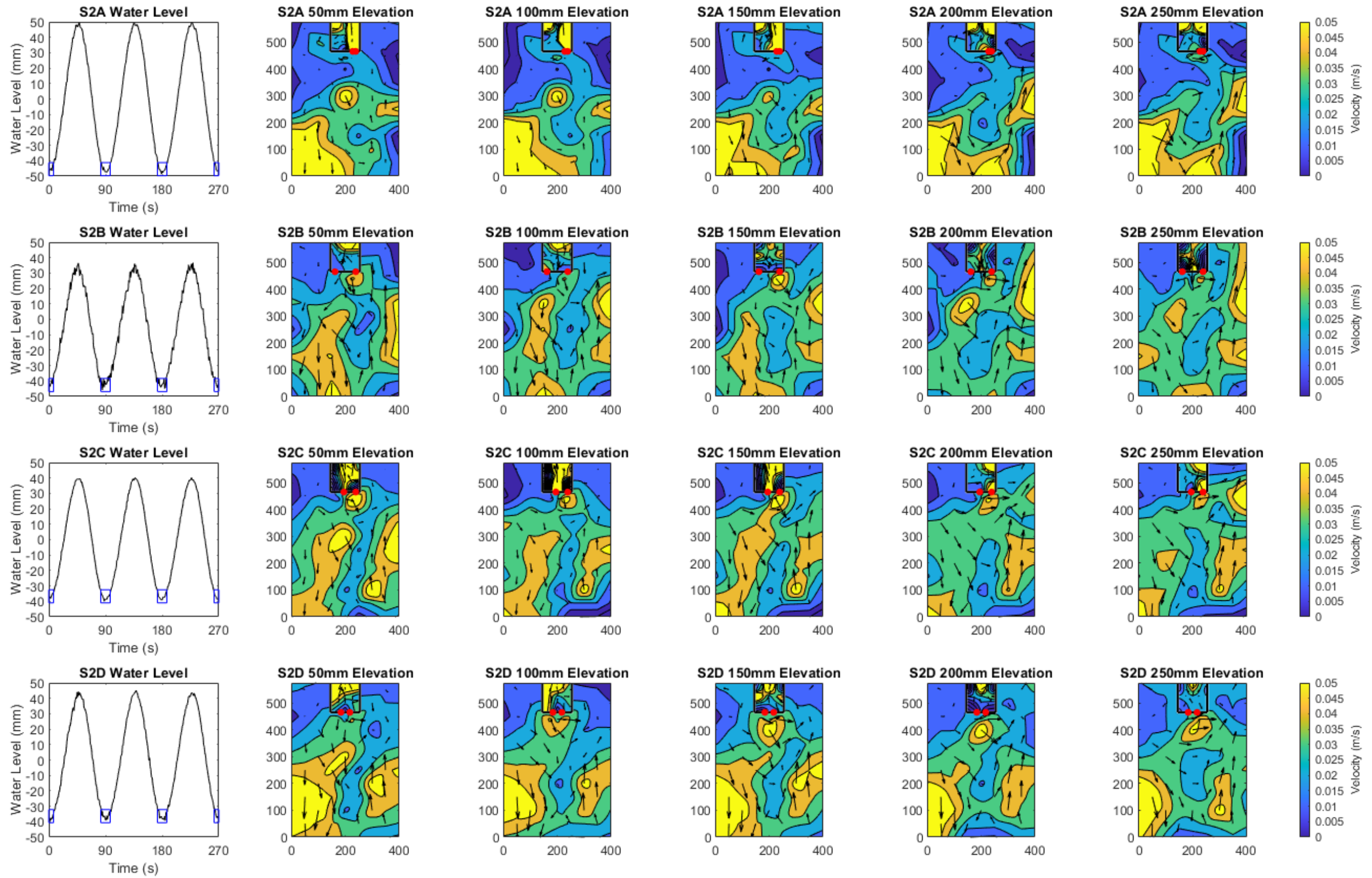


Figure 4.60 Comparison C - Velocity contour maps at elevations of 50, 100, 150, 200 and 250 mm above the bed during low tide.

4. Test Case 1 – Impact of Varying Turbine Layout

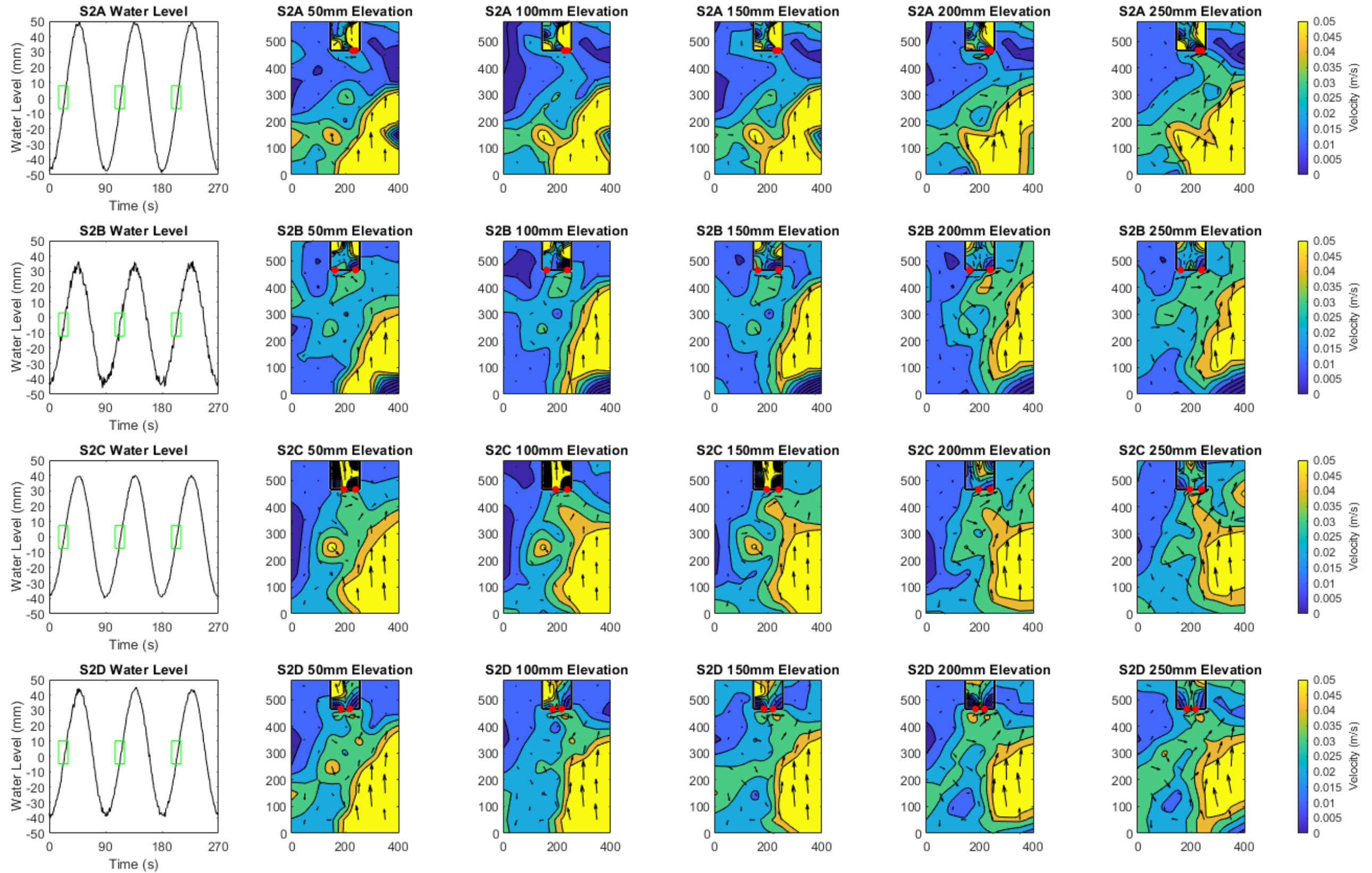


Figure 4.61 Comparison C - Velocity contour maps at elevations of 50, 100, 150, 200 and 250 mm above the bed during the flood tide.

4. Test Case 1 – Impact of Varying Turbine Layout

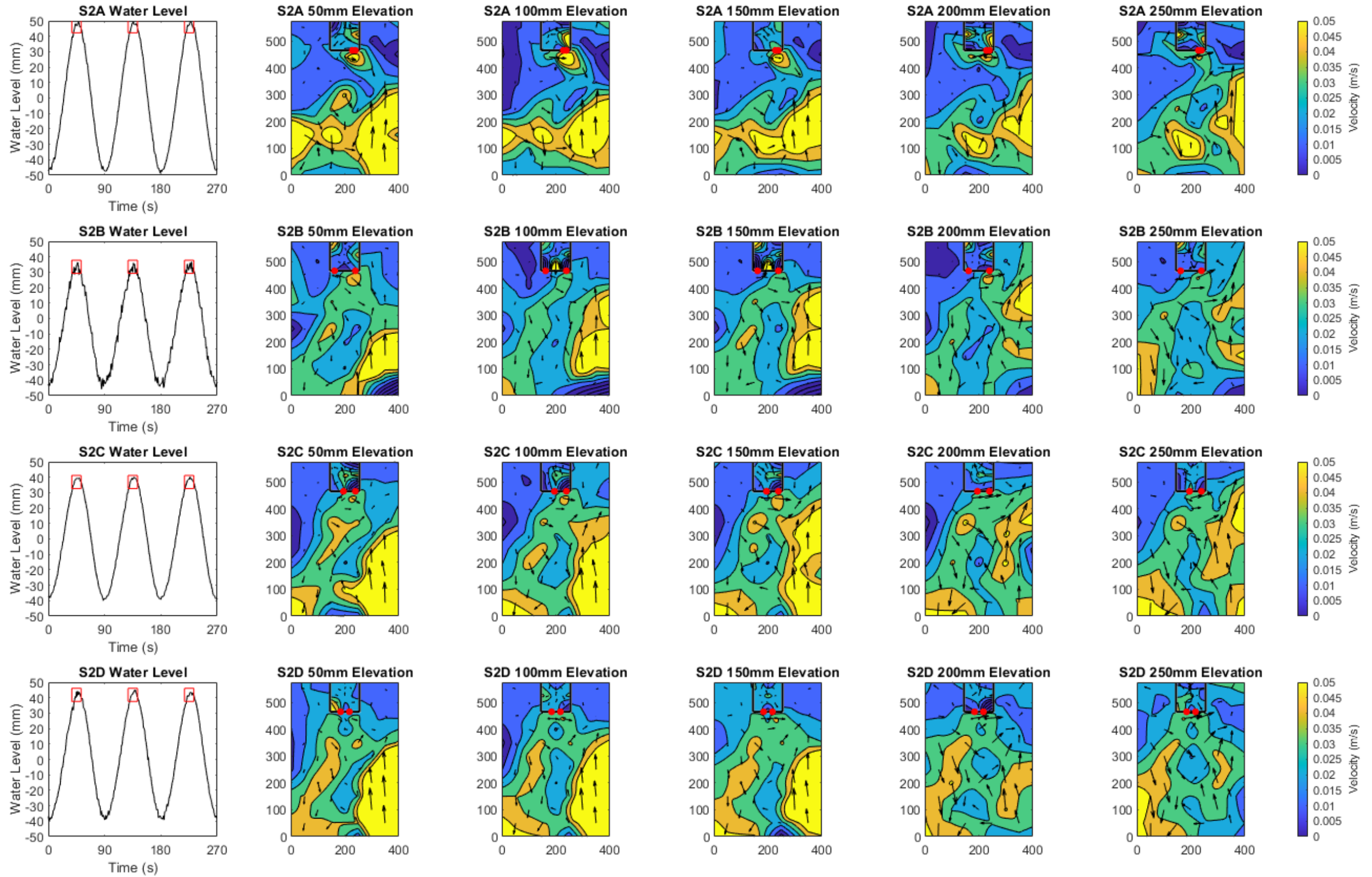


Figure 4.62 Comparison C - Velocity contour maps at elevations of 50, 100, 150, 200 and 250 mm above the bed during high tide.

4. Test Case 1 – Impact of Varying Turbine Layout

4.3.3.3 Velocity – Residual Velocity Magnitude and Direction

Examining the contour plots of residual velocity magnitude and direction, shown in Figure 4.63, reveals very similar patterns at all elevations and it is only the size of areas of strongest flow that change whilst their location stays the same. Once again, S2B, S2C and S2D are very similar but interestingly contours denoting the strongest positive flow are concentrated around the right-hand turbine of S2A, S2B and S2C but are located centrally between the two turbines for S2D. Whilst this is to be expected for S2A where both turbines are located in this area and somewhat for S2C where they are offset to the right, but it is surprising for S2B where the turbines are located at opposite sides of the seawall. This demonstrates the influence of the underlying asymmetrical flow in the tank which strengthens flows on the right-hand side. For S2D, the equal, centralised spacing of the turbines has created a more symmetrical flow pattern throughout the rest of the tank. S2B displays this to a lesser extent and certainly has a more symmetrical pattern in the tank overall compared to S2B and S2C but S2A shows some symmetry outside of the TRS too. Inside the TRS S2A maintains a linear pattern as before, whilst a slight symmetrical pattern is demonstrated in S2C up to the 200 mm elevation where flow diminishes, and the pattern is lost. S2B and S2D fail to show any strong pattern inside the TRS except at an elevation of 200 mm where symmetry appears in S2D. As with the previous results, the arrows denoting the resultant direction highlight an underlying anti-clockwise current in the tank originating from the right-hand side of the inflow boundary.

Previous studies have found that wider spacing of turbines across a TRS wall can reduce velocity magnitude to less than 1 m/s, which mitigates wake effects and hydrodynamic impacts (Angeloudis et al., 2016b). The results of the current experiment give velocities of less than 1 m/s in all cases and that wider spacing does lead to weaker flows across the tank which would have lesser impacts on the natural environment. This design is more expensive overall due to the cost of separate turbine housings and increased installation and maintenance costs from spreading turbines out rather than keeping them in a single location.

4. Test Case 1 – Impact of Varying Turbine Layout

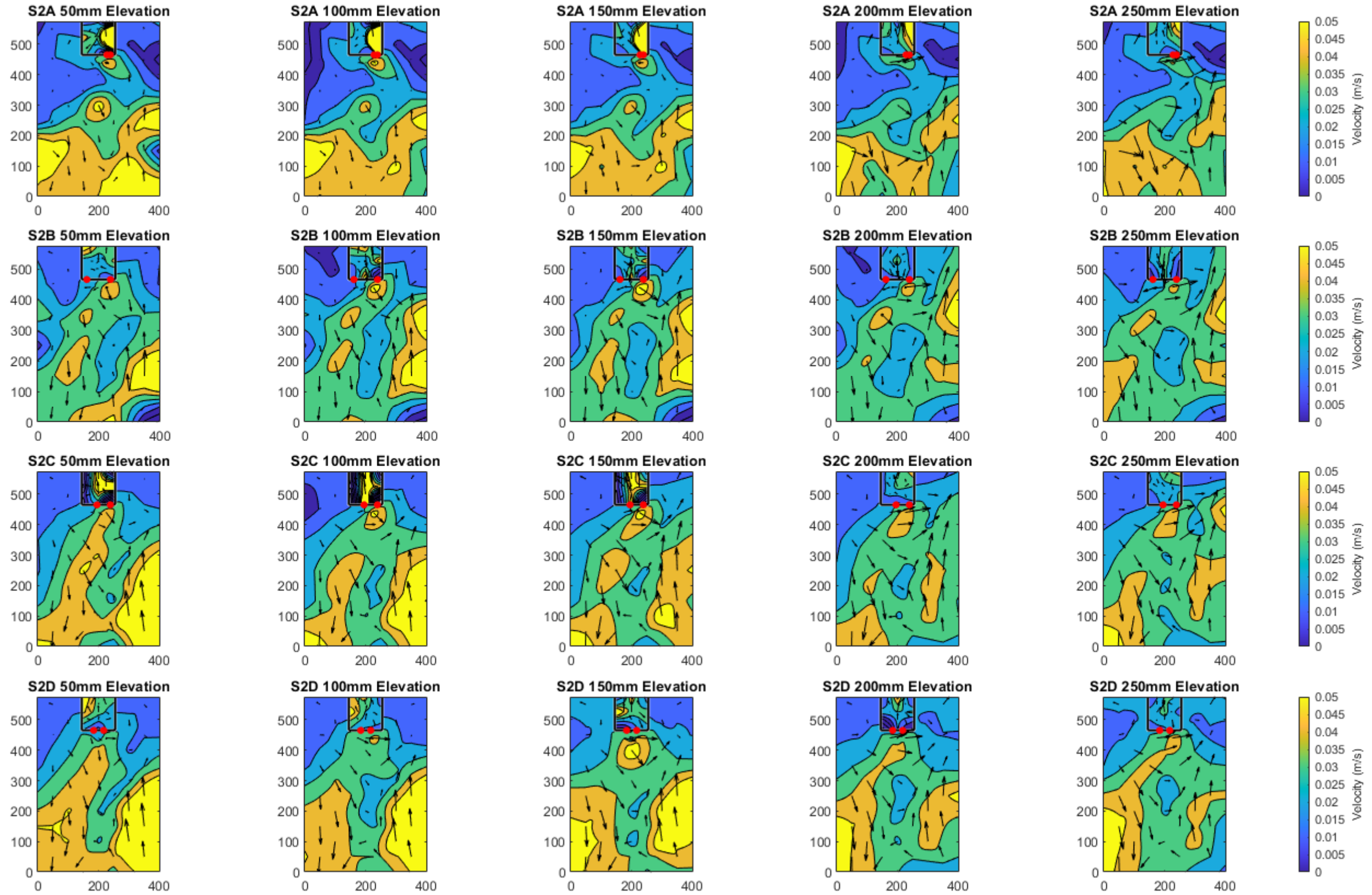


Figure 4.63 Comparison C – Contour maps of residual velocity magnitude and direction at elevations of 50, 100, 150, 200 and 200 mm from the bed.

4. Test Case 1 – Impact of Varying Turbine Layout

4.3.3.4 Flow Visualisation

Dye videos for all of these cases show two strong circulating cells with some smaller cells branching from them. These all begin in the same way with the wake jets reaching the rear wall of the lagoon before following the rear wall and then being deflected either to the left or right depending on the proximity of the side walls. In the case of S2A (Figure 4.64) the left-hand cell stretches along the rear wall to reach the left-hand wall where it follows the left wall all the way back round to the front seawall, spiralling as it does so. The right-hand cell mirrors this trajectory but is much smaller as it is restricted by its proximity to the right-hand wall. By using the two colours of dye it is interesting to see how quickly the dyes mix and that the right-hand plume actually mixes with and follows the left-hand cell quite early on. This emphasises the earlier point made that two closely spaced turbine openings exaggerate wake jets by acting almost as a single opening.

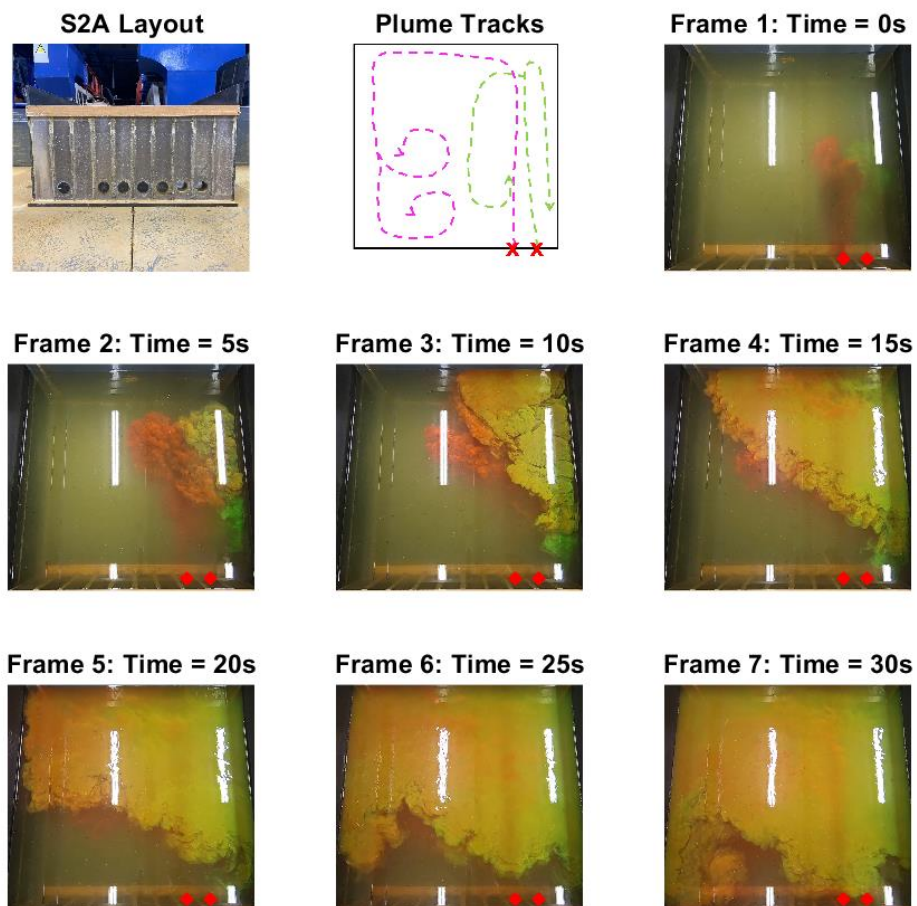


Figure 4.64 Flow visualisation for experiment S2A.

4. Test Case 1 – Impact of Varying Turbine Layout

In the case of experiment S2B (Figure 4.65), the two counter-rotating cells formed from the wide spaced turbine openings stay distinct from one another for much longer. Both jet plumes follow an identical trajectory, following the side wall closest to them before being reflected up the rear wall and back to the front seawall along the side walls and down the centre of the lagoon, staying almost entirely separate from one another and mixing only slightly where they meet along the centre line. These two equal plumes show that although the asymmetric flow in the tank has had some influence of flow patterns elsewhere in the basin, within the TRS walls, during the flooding tide, flow was equal enough to sustain identical wakes on each side of the lagoon, with neither wake dominating the other or drifting from right to left as might have been expected from the right-hand dominant flow at the tank's inflow boundary. It also shows how this wider spacing of the turbine openings allows for full circulation throughout the TRS area which would maintain good water quality.

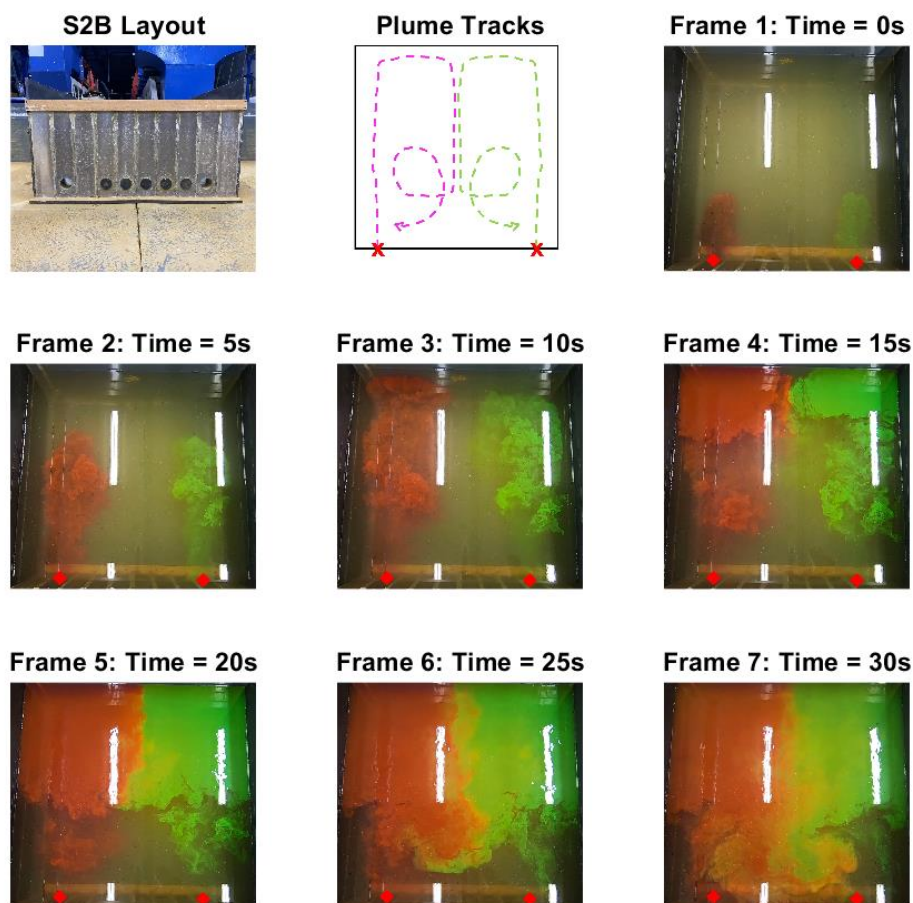


Figure 4.65 Flow visualisation for experiment S2B.

4. Test Case 1 – Impact of Varying Turbine Layout

Flow visualisation for experiment S2C (Figure 4.66) is similar to that of S2A, with two jets reaching the rear wall before rotating along the side walls to reach the front seawall. However, in this case, the right-hand cell has enough room to circulate into the centre of the TRS, rotating in the same direction as the left-hand cell. There is some mixing, as in S2A but the plumes stay distinct for slightly longer since both wakes have enough room to circulate separately at first. The right-hand (green) plume does eventually engulf the left-hand (pink) plume showing that even if one turbine is centrally located, if the other is offset towards one of the side walls it will reflect more strongly off this side wall to fill the rest of the lagoon.

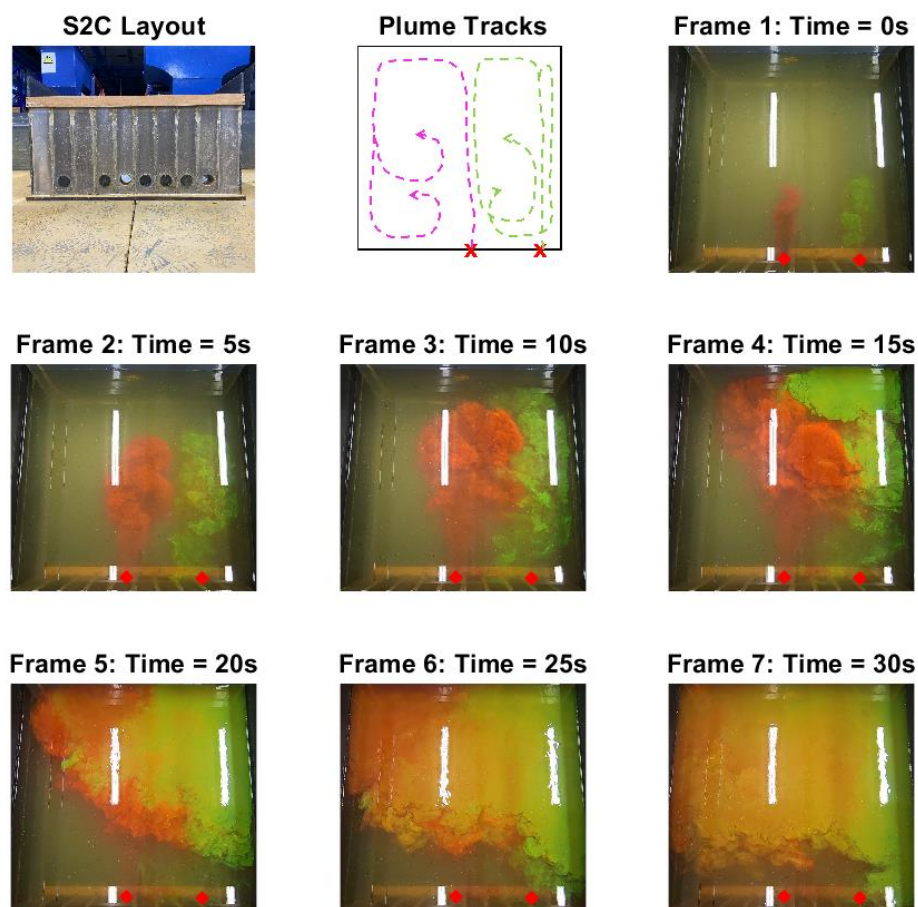


Figure 4.66 Flow visualisation for experiment S2C.

4. Test Case 1 – Impact of Varying Turbine Layout

Experiment S2D, with two centrally located turbines, shows two separate counter-rotating cells, as in S2B, but with slightly more mixing since the turbine openings are positioned more closely to each other (Figure 4.67). Interestingly these cells rotate in the opposite direction to S2B, with the initial jets reflecting off the rear-wall and along the side walls rather than towards the centre as in S2B. This shows the influence that the side walls have in directing the wake jets since they appear to dictate the direction of recirculation no matter the position of the turbine openings and needs to be considered carefully when positioning turbines in TRS designs. The plumes in this experiment are also equal sizes as in S2B which shows how equal turbine spacing and equal proximity to sidewalls impacts flow patterns, ensuring even circulation of water, nutrients and contaminants inside a TRS. Although these impacts will be exaggerated by the size of this experiment where the lagoon area is quite small, these are important aspects to be considered when predicting environmental conditions of a TRS at any scale.

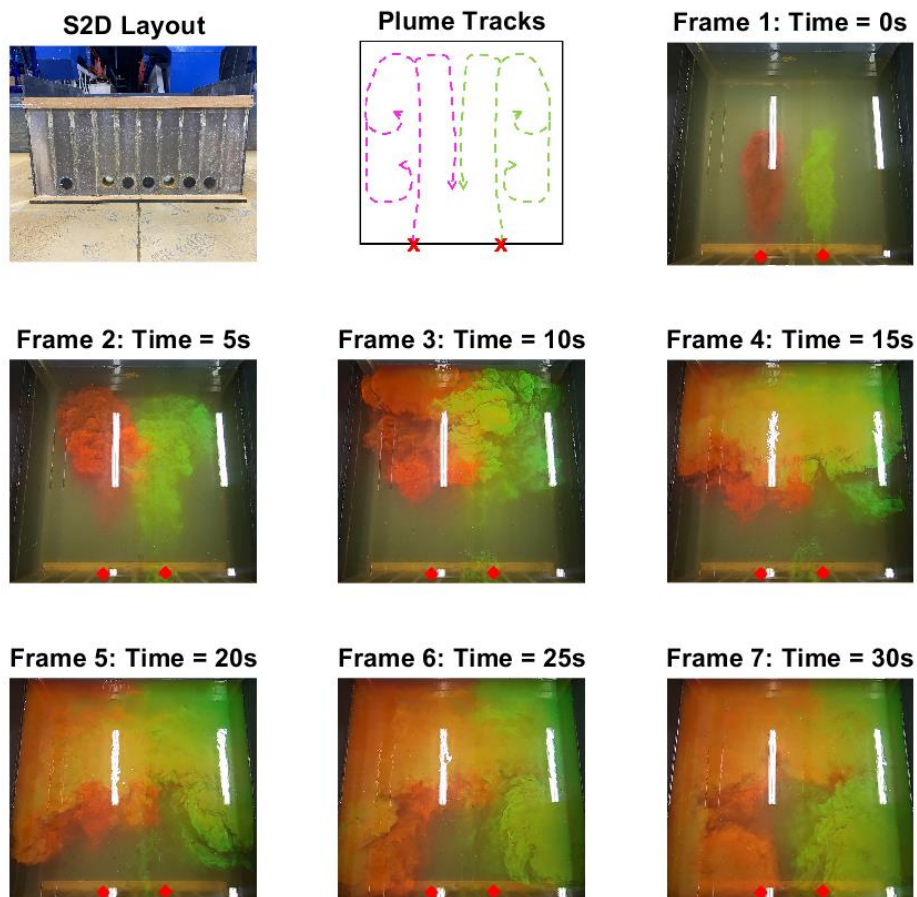


Figure 4.67 Flow visualisation for experiment S2D.

4. Test Case 1 – Impact of Varying Turbine Layout

4.3.3.5 Statistical Analysis

As with previous experiments, the results of residual velocity for experiments S2A-D are highly scattered when compared to baseline results, highlighting the variable distribution of flow velocity throughout the tank (see Figure 4.68). Each of the experiments has led to altered conditions from baseline flow with cases S2A, C and D increasing the average velocity magnitude by between 29 and 37% (results from Table 4.4). However, when comparing residual velocity results against S0, experiment S2B shows the least variation, increasing the average velocity magnitude by only 19%. This suggests that the wider spacing is better for maintaining natural velocities than placing turbines closer together but is still much higher than velocity results from the single turbine experiments. When examining the histograms of the distribution of the velocity magnitude it is experiment S2A that stands out from the others (Figure 4.69). This is to be expected since in this experiment the turbines were placed directly next to each other which has been shown in previous analysis to cause the greatest change to flow velocities.

In analysing the spread of residual flow direction, it is again S2A that stands out from the rest (Figure 4.70), and whilst the other experiments more closely match those of the baseline case, S2A has more significantly altered the direction of flow throughout the tank. Despite the slight improvement observed by S2B than the other results, z-test results confirm that the null hypothesis should be rejected in all cases (as presented in Table 4.4), which means that every one of the configurations cause significant alteration to the velocity from baseline conditions.

Table 4.4 Comparison C - Statistical analysis of residual velocity magnitude of S2A, S2B, S2C and S2D compared to S0.

Comparison	\bar{x} (m/s)	SD	RMSE	r	z	Accept/ reject h_0
S0	0.02570	0.00748				
S2A	0.03333	0.01605	0.00941	0.27034	2.8270	Reject
S2B	0.03074	0.00996	0.01106	0.50848	2.5997	Reject
S2C	0.03531	0.01138	0.01208	0.61325	4.5645	Reject
S2D	0.03506	0.01142	0.01353	0.69454	4.4337	Reject

4. Test Case 1 – Impact of Varying Turbine Layout

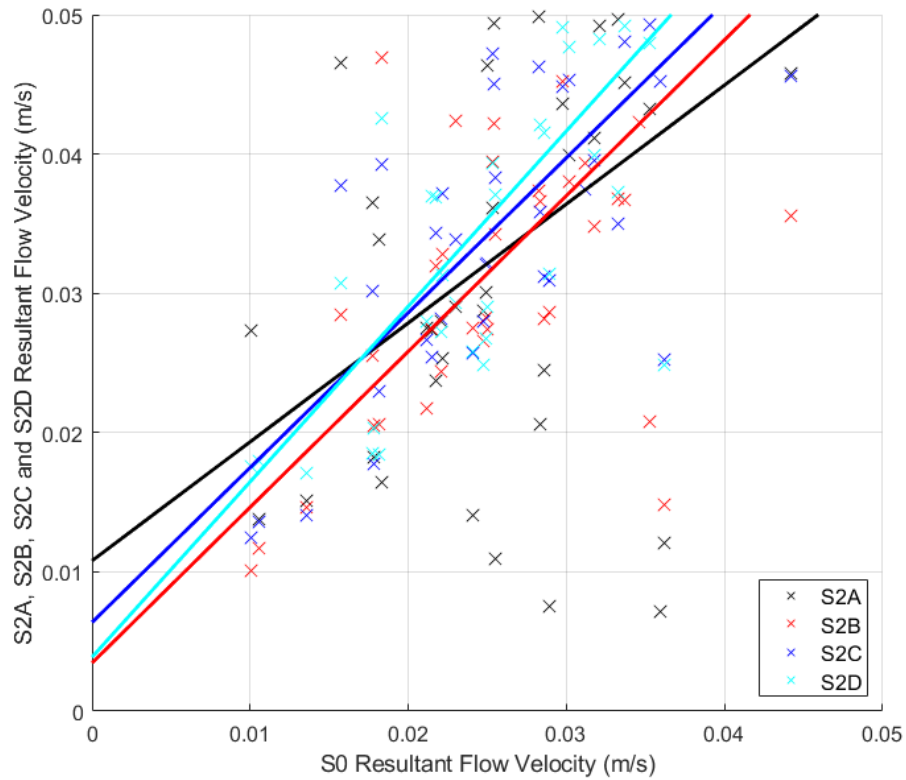


Figure 4.68 Comparison C - Regression analysis of residual flow velocity.

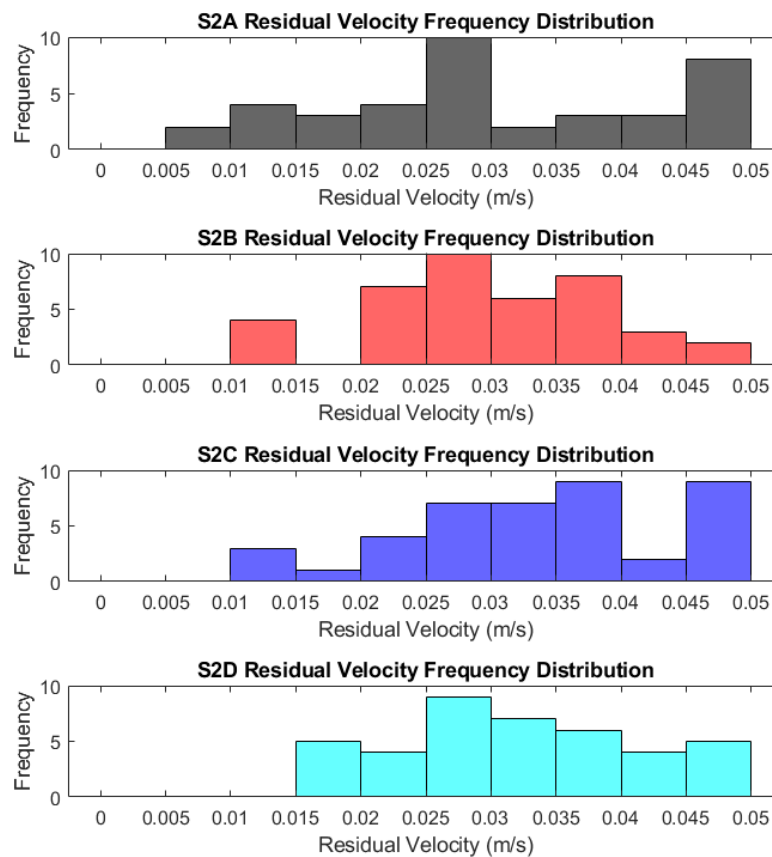


Figure 4.69 Comparison C – Distribution analysis of residual flow velocity.

4. Test Case 1 – Impact of Varying Turbine Layout

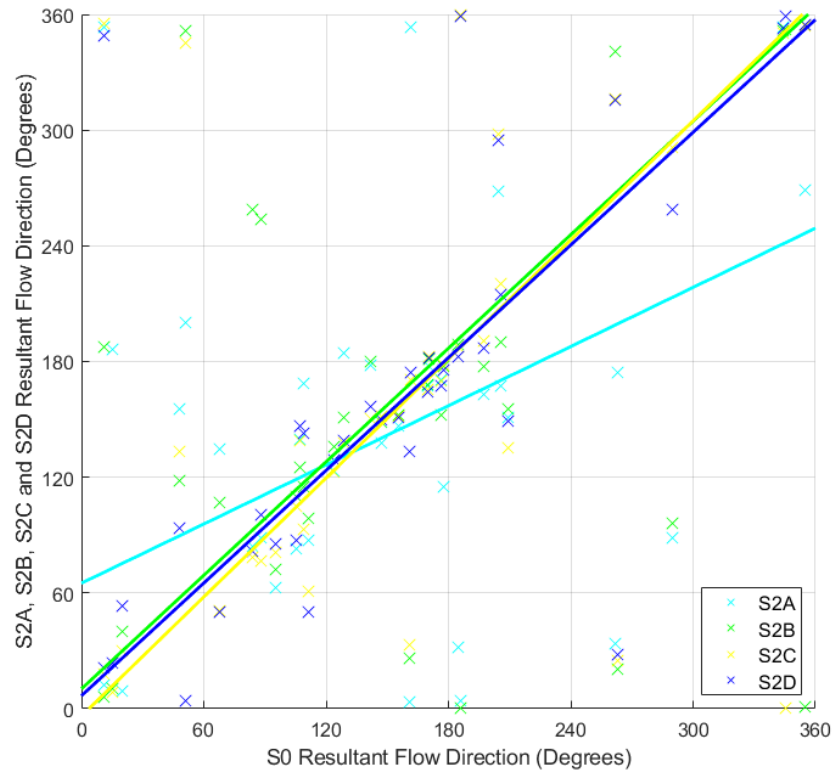


Figure 4.70 Comparison C - Regression analysis of residual flow direction.

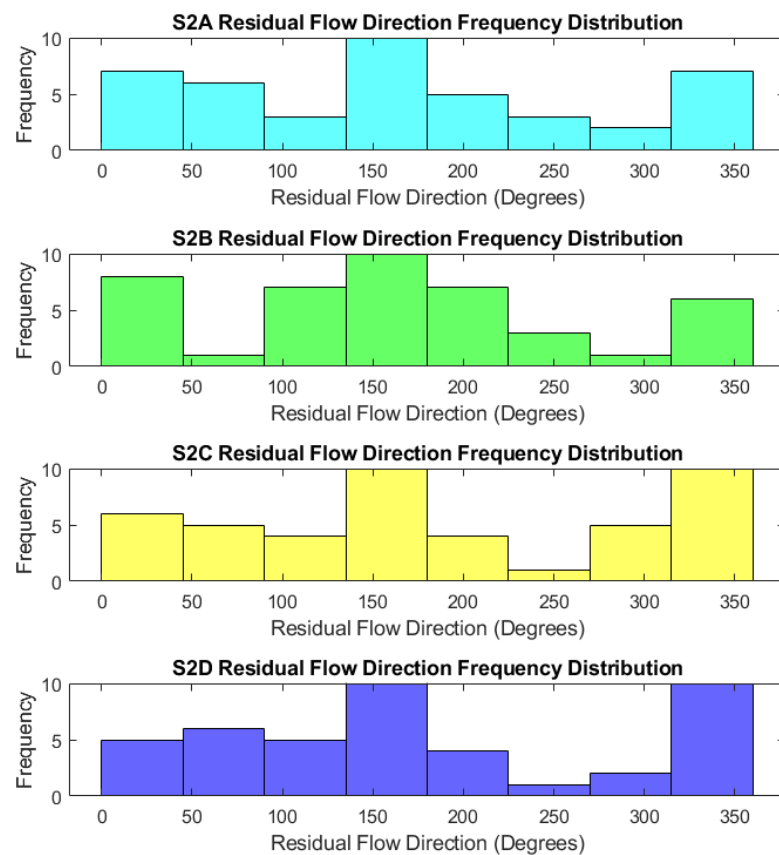


Figure 4.71 Comparison C – Distribution analysis of residual flow direction.

4. Test Case 1 – Impact of Varying Turbine Layout

4.3.4 Comparison G – Varying the position of two turbines in a rectangular TRS

Comparison G investigates the hydrodynamic impacts of varying the spacing of a pair of turbines in a rectangular TRS, comparing results from experiments R2A, R2B, R2C and R2D against pre-lagoon conditions in order to determine which configuration has the greatest effect. The layouts for the turbine spacing in each of these experiments is shown in Figure 4.72.

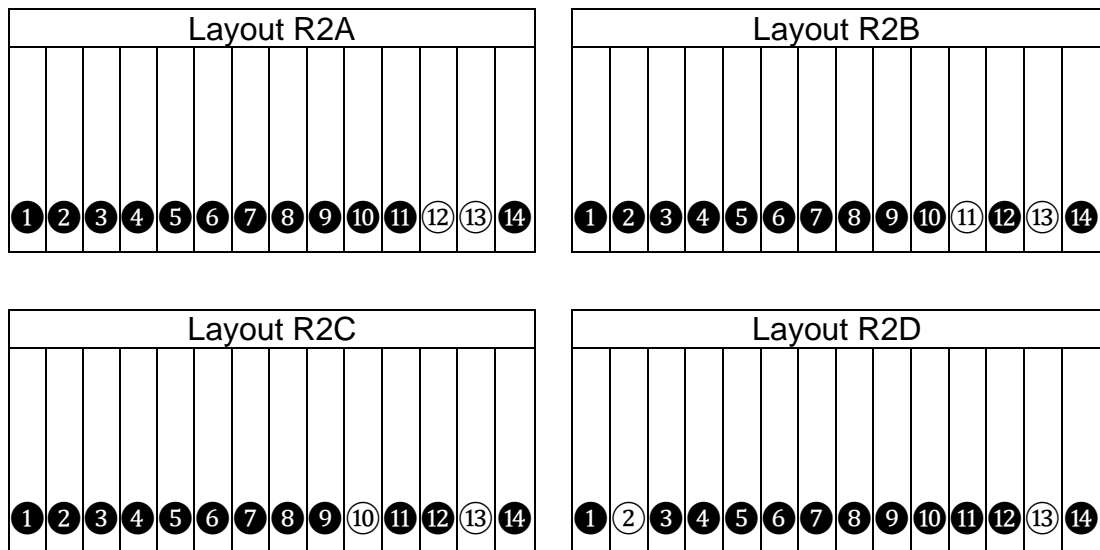


Figure 4.72 Experient layouts for Comparison G: R2A, R2B, R2C, R2D.

4.3.4.1 Velocity - Depth Averaged

Experiments R2A to R2D test different spacing of two turbines within a rectangular TRS to determine whether this TRS geometry is impacted to the same extent as a square TRS when turbines are spread out. The depth averaged results for all cases (presented in Figure 4.77) are extremely similar throughout the whole of the outer tank area agreeing with the findings of Cornett et al. (2013) who discussed the lack of impact caused by TRSs in the far field. The greatest variation across the whole tank can be found at (200,400) (Figure 4.73) where R2C has an extreme peak compared to the other experiments. This is most likely due to the location of the second turbine in R2C which is located closer to the centre of the TRS seawall, whereas the other experiments have turbines located near the side walls. Other than this location, at other points with extreme peaks, the experiments

4. Test Case 1 – Impact of Varying Turbine Layout

all closely match each other, e.g. (250,450) (Figure 4.74). It is only at point (225,475) (Figure 4.75) that there is a slight variation, and experiment R2B peaks above the rest. This is to be attributed to the slight spacing of the two turbines in this case where the second turbine is close to this location. It is interesting, however, to note the almost identical results at point (250,475) (Figure 4.76). That despite the wider spacing of cases R2C and R2D, the velocity at this location matches for all cases. The similarity in all these results suggest that the choice of turbine locations in the rectangular layout has not caused a significant difference to flow outside of the TRS.

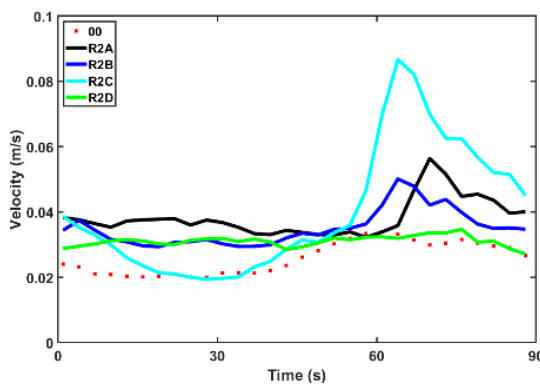


Figure 4.73 Closer detail of velocity at (200,400).

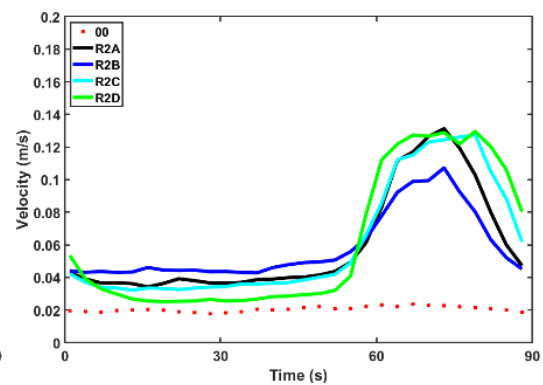


Figure 4.74 Closer detail of velocity at (250,450).

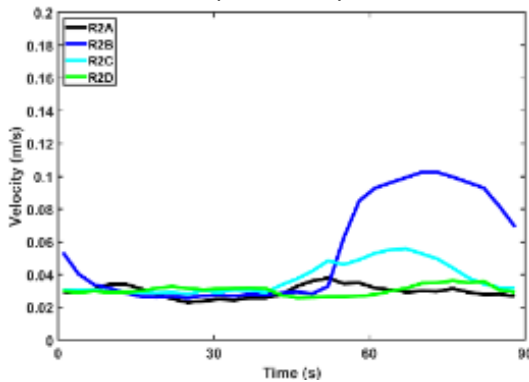


Figure 4.75 Closer detail of velocity at (225,475).

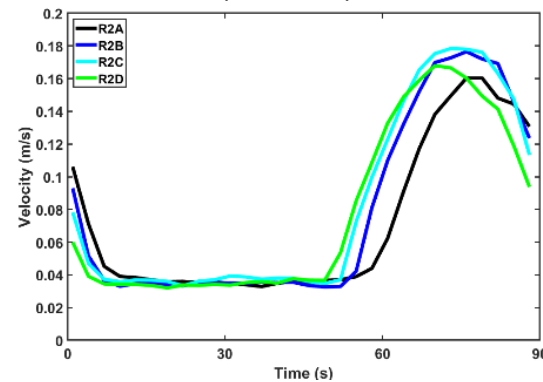


Figure 4.76 Closer detail of velocity at (250,475).

4. Test Case 1 – Impact of Varying Turbine Layout

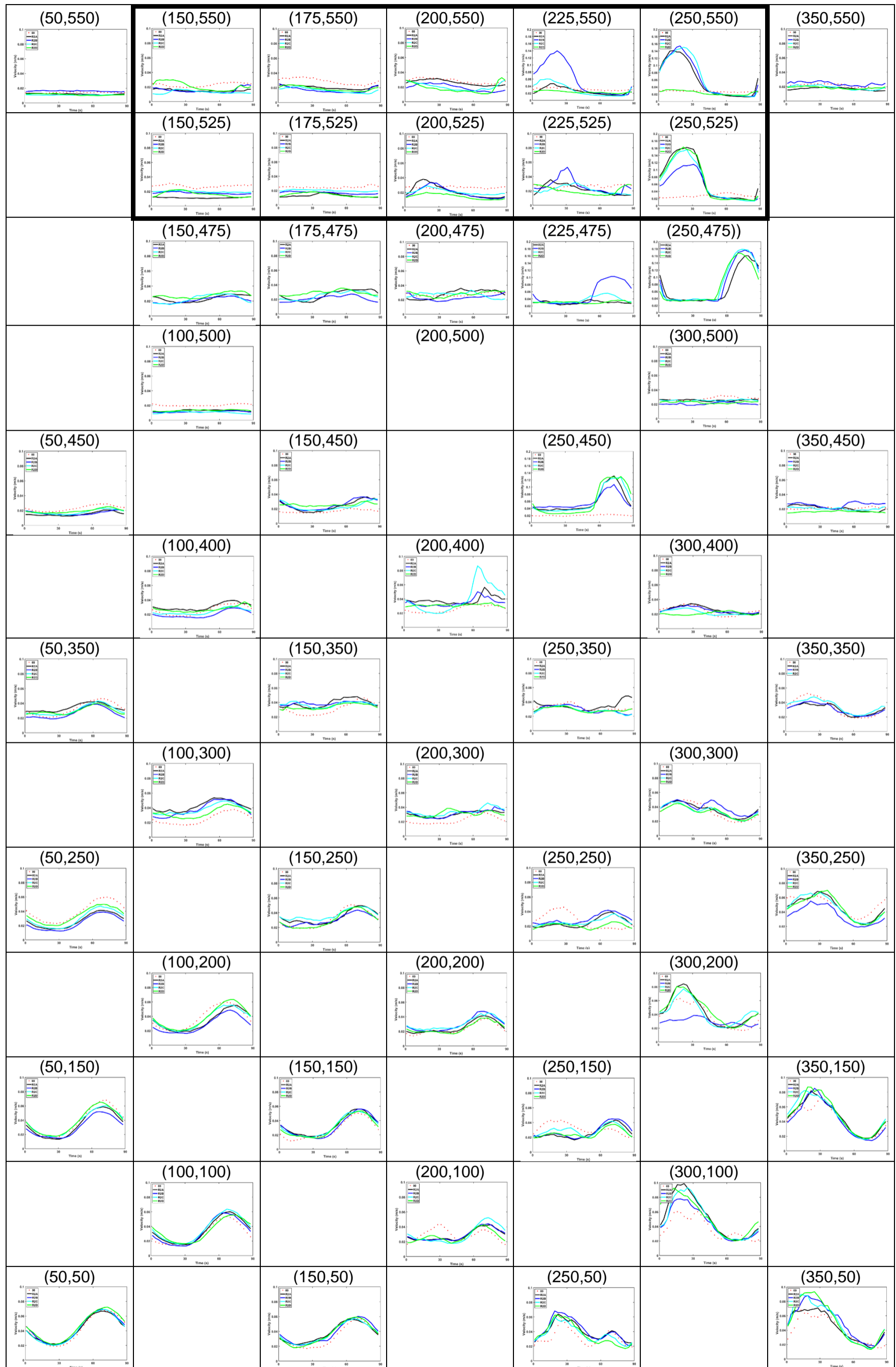


Figure 4.77 Map of depth averaged velocity plots for Comparison G: R2A, R2B, R2C, R2D.

4. Test Case 1 – Impact of Varying Turbine Layout

Inside the TRS flow is extremely slow, almost stagnant, in the left-hand side of the TRS. This is due to the turbines being predominantly located on the right-hand side of the seawall which restricts the currents from reaching the left-hand side. Flow is slightly peaked for R2D where there is a turbine on the left-hand side but is still very low. At the right-hand side of the TRS flow is much stronger for all cases, and there is a peak at point (250,525) (Figure 4.78) despite the wider spacing of R2C and D. This shows the influence that the asymmetric flow in the tank has had on results, causing water to rush through faster on this side. However, the single turbine on the right-hand side of the TRS has meant that the wake jet was not as far reaching in case R2D as the others and flow is much reduced at (250,550) (Figure 4.79). Other deviations can be seen at (225,550) (Figure 4.81) where it is R2B that experiences a peak compared to the other experiments which can be attributed to being closer to the location of the second turbine in this case. Elsewhere in the lagoon, flows are extremely similar which shows that the effects of the wake jets are not far reaching, and flow is slower than pre-lagoon conditions within 10 turbine diameters of the right-hand wall regardless of the turbine positioning in these cases.

Looking at the La Rance TRS, Rtimi et al. (2021), found that the barrage more than doubled the maximum flood velocity upstream and almost halved the maximum flood velocity downstream. This was found to be the case in these rectangular experiments, with flow more than tripled directly upstream of the turbines but reduced further away from them within the confines of the TRS walls. In their models of TRSs, Angeloudis et al. (2016a), found flow velocity through turbines of up to 10 m/s, which would influence local velocity fields, water quality, sediment transport and other ecological processes. In the present study, the greatest wake velocities reached 0.18 m/s. According to the scale of the experiments, these results correspond to a value of 1.8 m/s in a full scale TRS and so would not inhibit aquaculture or recreation inside the TRS but may cause issues for sediment transport and water quality. Outside the TRS, the largest value experienced was also 0.18 m/s for all cases at (250,475) which would not greatly disrupt the natural environment but may lead to increased scouring.

4. Test Case 1 – Impact of Varying Turbine Layout

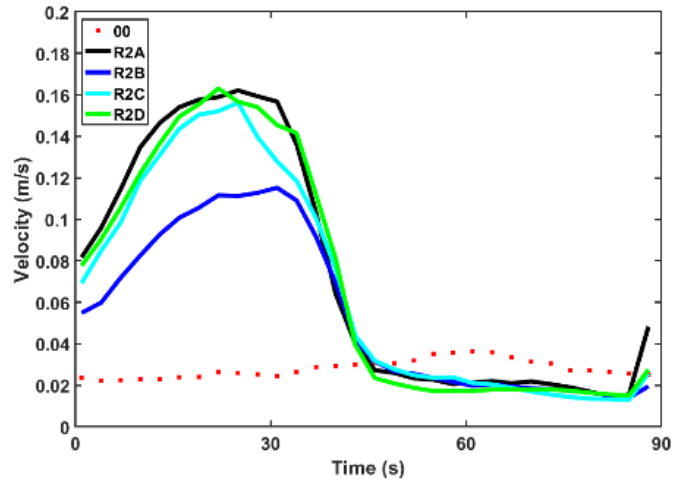


Figure 4.78 Closer detail of velocity at (250,525).

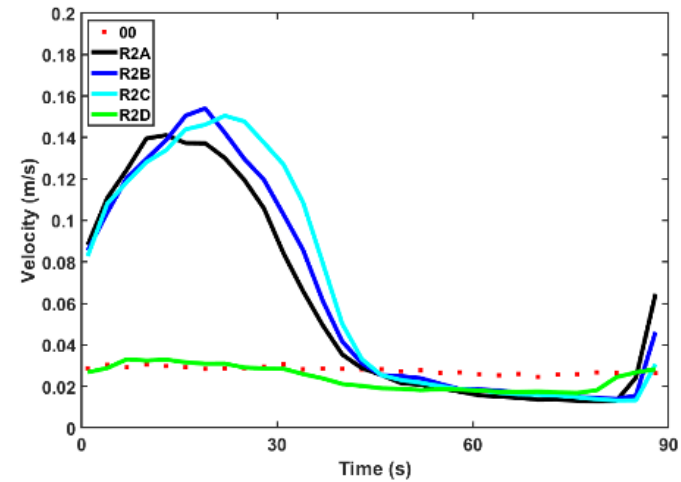


Figure 4.79 Closer detail of velocity at (250,550).

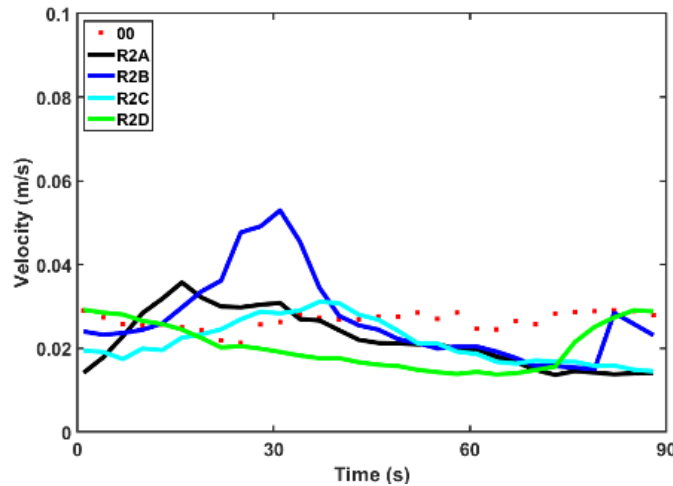


Figure 4.80 Closer detail of velocity at (225,525).

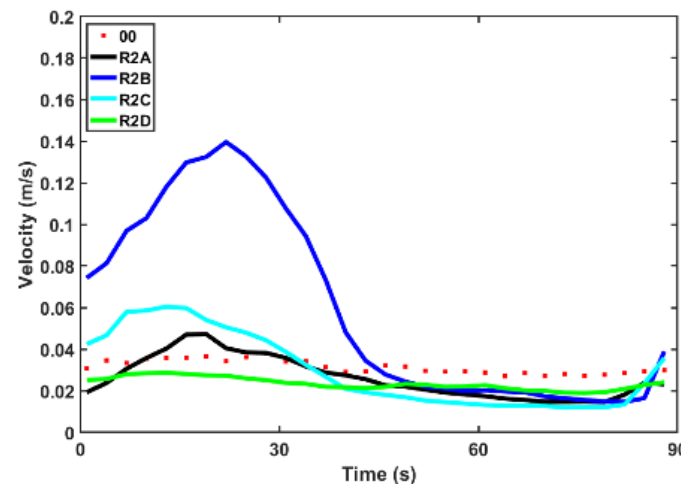


Figure 4.81 Closer detail of velocity at (225,550).

4. Test Case 1 – Impact of Varying Turbine Layout

4.3.4.2 Velocity – Analysed by tide and depth

Looking at the results from the ebb tide (Figure 4.82), as with previous comparisons, there is little variation between the depths, and all of the experiments show great similarities. A slight difference does appear in the area of strong flow outside of the TRS, in front of the turbine openings, which seems to grow as the space between the openings widens and so is largest for R2C but then shrinks again in R2D when the turbines are spaced furthest apart. Inside the TRS the pictures are quite similar for all cases with very little flow at this part of the tide as all flow ebbs out of the lagoon.

During low tide flow is weaker overall but more symmetrical throughout the tank as forces equal out during this time of slack water and there is little variation between depths as before (Figure 4.83). Inside the TRS some similarities can be seen in the flow patterns of S2A, S2B and S2C, in that the strongest flows occur on the right-hand side of the lagoon, behind the turbine openings, with weaker flows in the rest of the area. This shows how circulation is limited inside the TRS during low tide, which could cause a problem for trapping pollutants and needs to be considered when deciding upon turbine location. Water is better mixed in the lower half of the TRS in R2D where the water has two outlets, however it almost becomes stagnant near the surface.

The flood tide graphs (Figure 4.84) continue to show great similarity between depths and between experiments, which indicates that the spacing of the turbine openings does not make a difference in the outer tank at this point in the tide. During this tide, more than for the others, slower flows seem to swirl from the rear left of the tank along the left-hand wall towards the centre of the tank, especially in R2B and R2C. This suggests that during the flood tide, water is flowing faster on the right-hand side of the tank and through the turbine openings, whilst water is much slower on the left-hand side of the tank where it reflects off the seawall and recirculates. Inside the TRS, experiments R2A to R2C continue to display the strongest flow on the right-hand side, directly behind the turbine openings, but flow is still not strong enough to affect the left-hand side, even during the flood tide. This confirms that when the turbines are located close to one another the stronger flows

4. Test Case 1 – Impact of Varying Turbine Layout

are restricted to the area around the openings and this does not spread far throughout the TRS. Whereas, in the case of R2D, where the turbines are spread out furthest, water is able to flow in all areas of the tank, albeit very slowly. Both scenarios would cause issues for the flushing of nutrients and pollutants, with wider spread turbines leading to weak flows that are unable to mix waters sufficiently, and closely spaced turbines leading to stagnant areas where water does not circulate at all, as highlighted by Guo et al. (2021). This could be investigated further by adding floats or sediment inside the TRS to see where they are transported.

At high tide the velocity contour plots again reveal little difference between depths and the experiments have the most similar results of any phase of the tide (Figure 4.85). This suggests that once the water has reached its greatest depth there is less difference in the velocity profile than at other times of the tide regardless of turbine positioning. Once again, the flows within the TRS are extremely slow with little variation across the lagoon area above 100 mm elevation. R2C displays the greatest variation which is to be expected as the two turbines are positioned close enough together to cause a stronger current but far enough apart to impact a larger area of the TRS. Whereas the turbines in R2A and R2B are spaced so closely as to only affect a small area of the TRS. The turbines in R2D are spread so far apart that although they should be able to affect the whole area of the TRS, the force flowing through each is not strong enough to have a significant impact throughout the lagoon. This again emphasises the idea that close spacing leads to strong turbine wakes whose effects are concentrated in a small, localised area whilst wide spacing leads to weaker turbine wakes which can circulate into greater areas but with lesser impact.

4. Test Case 1 – Impact of Varying Turbine Layout

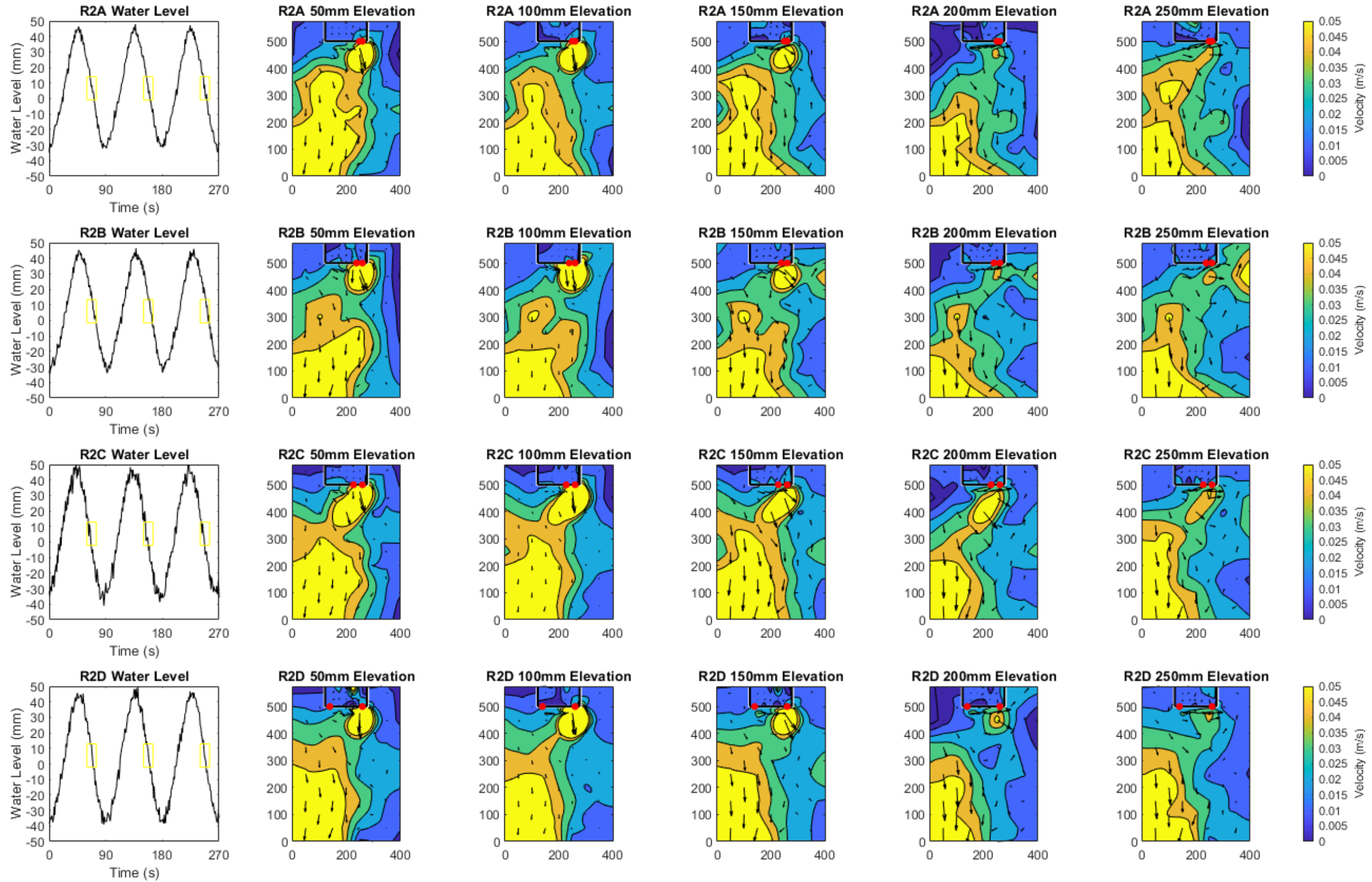


Figure 4.82 Comparison G - Velocity contour maps at elevations of 50, 100, 150, 200 and 250 mm above the bed during the ebb tide.

4. Test Case 1 – Impact of Varying Turbine Layout

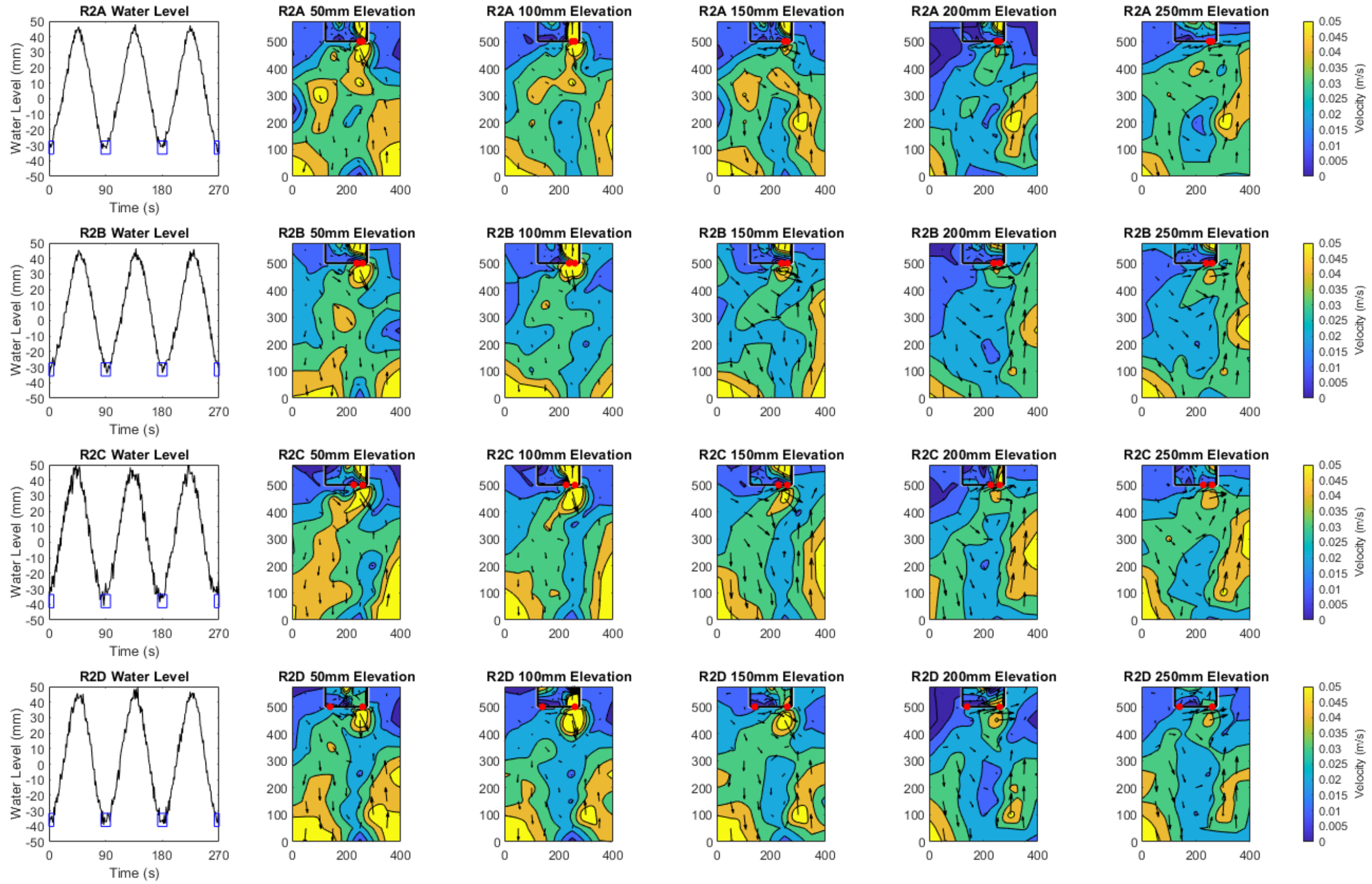


Figure 4.83 Comparison G - Velocity contour maps at elevations of 50, 100, 150, 200 and 250 mm above the bed during low tide.

4. Test Case 1 – Impact of Varying Turbine Layout

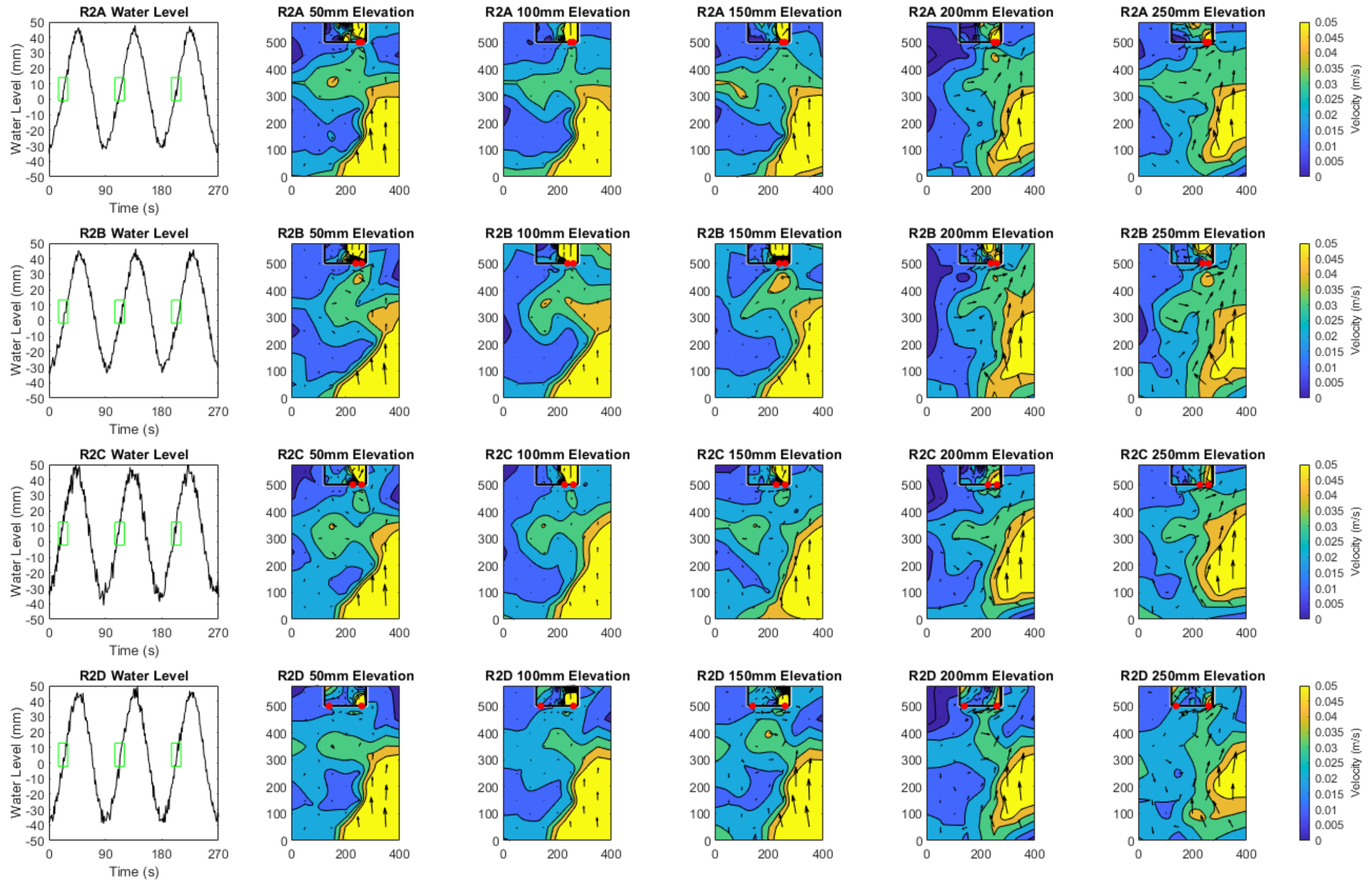


Figure 4.84 Comparison G - Velocity contour maps at elevations of 50, 100, 150, 200 and 250 mm above the bed during the flood tide.

4. Test Case 1 – Impact of Varying Turbine Layout

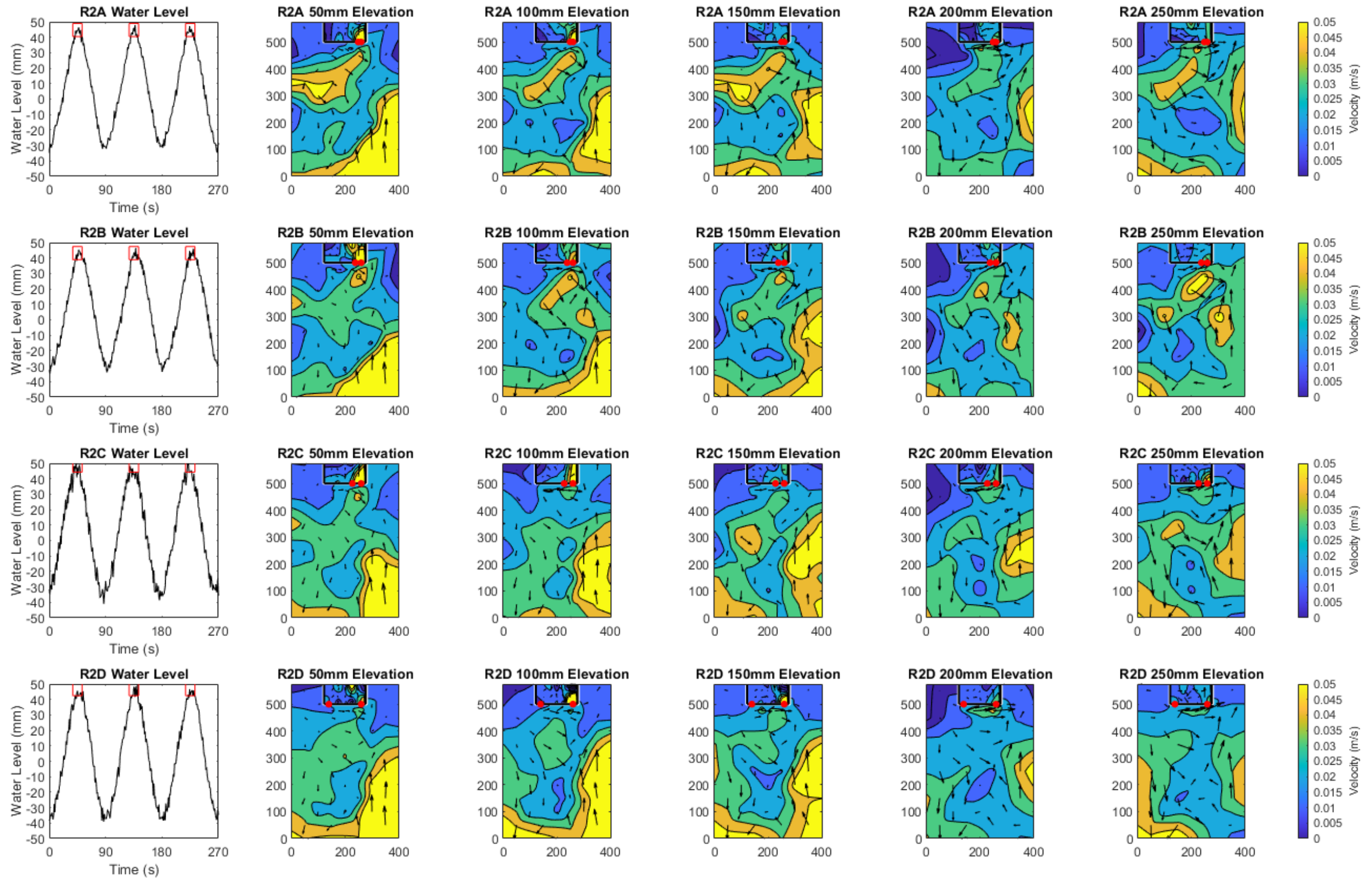


Figure 4.85 Comparison G - Velocity contour maps at elevations of 50, 100, 150, 200 and 250 mm above the bed during high tide.

4. Test Case 1 – Impact of Varying Turbine Layout

4.3.4.3 Velocity – Residual Velocity Magnitude and Direction

As with the square TRS experiments, the areas with the strongest positive flow are concentrated around the turbines on the right-hand side of the TRS seawall (see Figure 4.86), even in R2D where there is a turbine on the left-hand side too. This, in conjunction with the flow direction arrows, highlights how water is circulated in an anticlockwise manner. This is particularly clear from elevation 150 mm upwards, where the strongest flows extend around the right-hand wall of the TRS. (Section 8.2 discusses the issue of asymmetric flow and its impact in greater detail.) This was also highlighted in a very definite way when the tank was emptied to reveal mounds of sediment that had been circulated in whirlpools and deposited at the rear of the tidal basin next to the TRS (evidence provided in Figure 4.87 and Figure 4.88) demonstrating how strong the circulation currents are here. This can also be seen inside the TRS in R2A-C, where flow is strongest directly behind the turbine openings but weakens in the opposite side of the TRS. This will be due to the forcing of the water through the turbine openings which are circulated in a small area behind the orifices. Despite being modelled on such a small scale, these observations concur with the findings of Guo et al. (2021) who in modelling TRSs in the Severn Estuary reported that maximum velocity would be increased inside the TRS but decrease further away from turbine wakes. This pattern is less evident in R2D where flow enters the TRS at each side of the seawall and is able to circulate across a wider area, including the rear and centre of the TRS. However, flow nearest the surface is almost negligible in this experiment highlighting once again the weakness of the force through these two widely spaced openings which does not have a significant impact throughout the whole water column.

4. Test Case 1 – Impact of Varying Turbine Layout

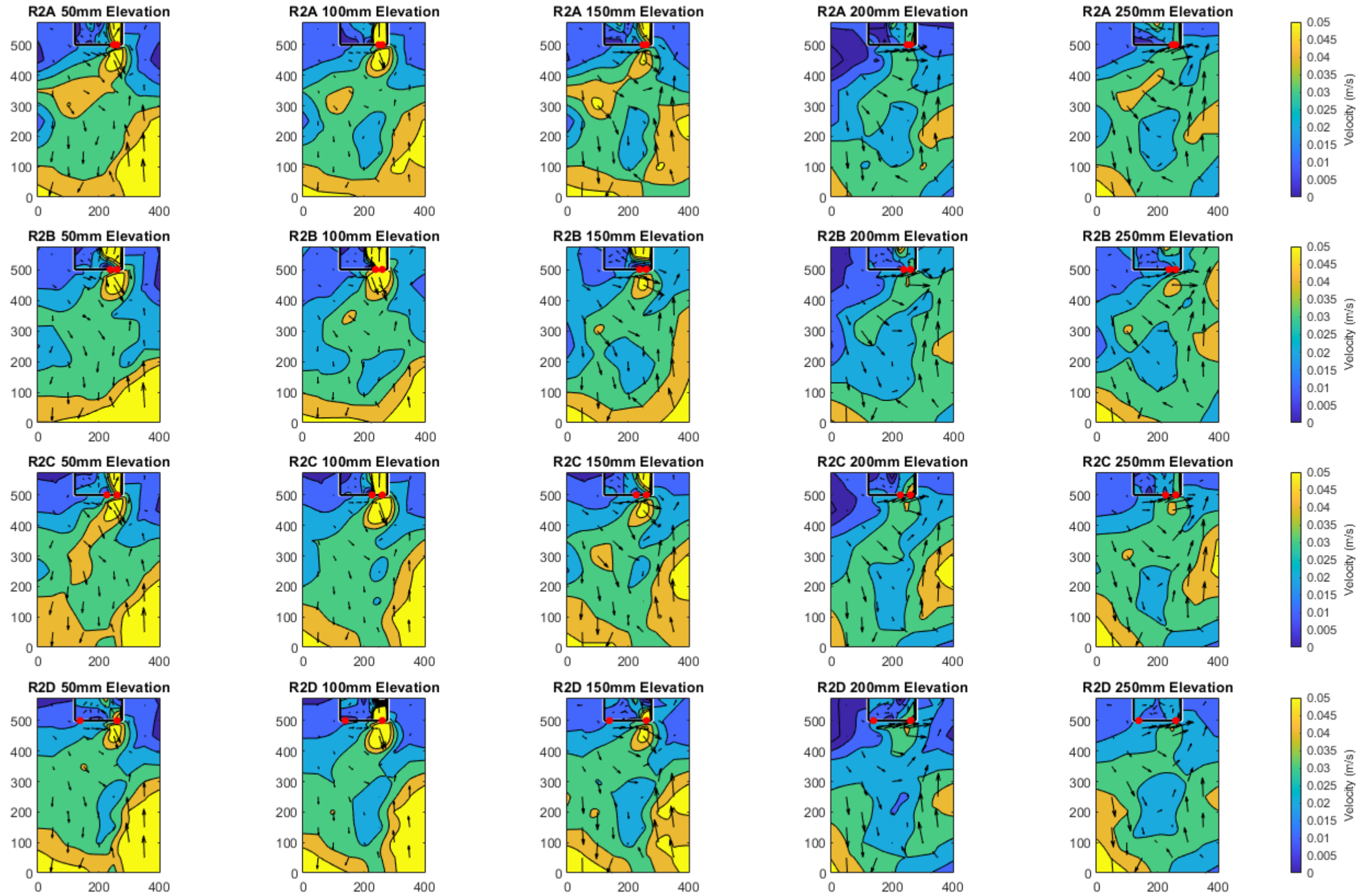


Figure 4.86 Comparison G – Contour maps of residual velocity magnitude and direction at elevations of 50, 100, 150, 200 and 200 mm from the bed.

4. Test Case 1 – Impact of Varying Turbine Layout



Figure 4.87 Whirlpool to left of TRS during tank filling.



Figure 4.88 Evidence of whirlpool left in dust once tank is emptied.

4. Test Case 1 - Impact of Varying Turbine Layout

4.3.4.4 Flow Visualisation

Flow visualisation for experiment R2A shows that although the left-hand plume is able to stay slightly distinct, the two plumes mix fairly early on and move with each other to flow towards the left-hand side of the tank (Figure 4.89). In this case, as with experiment S2A, it is the proximity of the turbine openings, to each other and to the right-hand side wall that dictate the circulation pattern and mixing of the wakes which are not able to stay parallel to each other for long after reaching the rear wall. The left-hand plume tends to follow the rear-wall whilst the right-hand plume sticks more closely to the front wall having reached there after being reflected off the rear-wall and following the right-hand wall around to the front of the lagoon. Both of these plumes continue to rotate and mix with each other as they spread to the left-hand side of the lagoon, but it took ninety seconds (one full tidal cycle) for either dye track to reach the front, left-hand corner. This shows that although the position of the turbine openings on the far right of the TRS seawall does allow mixing of the whole area, stagnation is a concern for the opposite end of the TRS as water is much slower to reach and recirculate in this area.

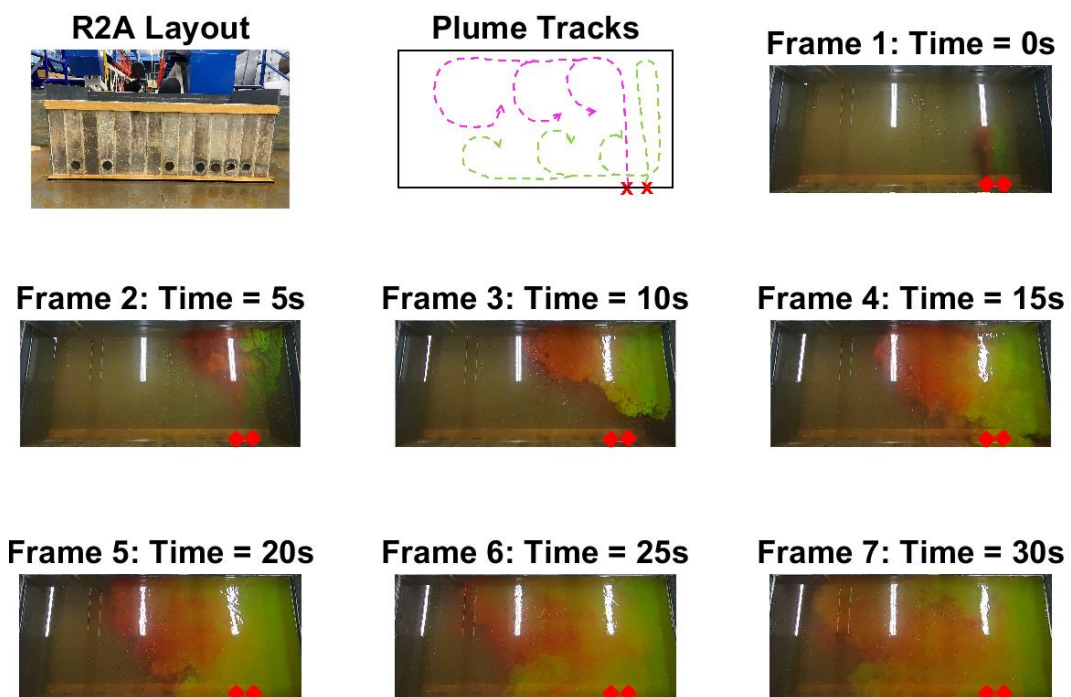


Figure 4.89 Flow visualisation for experiment R2A.

4. Test Case 1 - Impact of Varying Turbine Layout

Experiment R2B displays a very similar pattern to that of R2A, with the two wake jets reaching the rear wall before deflecting to the right and left (Figure 4.90). As with R2A, the left-hand plume (pink) follows the rear wall whilst the right-hand plume (green) sticks more closely to the front wall as they rotate and reach to the left-hand side of the TRS. The difference with this experiment being that the marginally wider turbine spacing has allowed the plumes to stay slightly more distinct and that the dye reaches the left-hand wall slightly quicker than in R2B, seventy seconds as opposed to ninety. This would be three-quarters of the tidal cycle, so the tide will have come all the way in and out and be starting to fill again before water in the lagoon is fully mixed. This shows that even just a slight increase in turbine spacing can encourage water to be replenished in the extremes of the lagoon area rather than tightly packed turbines which concentrate flow in one area for longer. However, there is still a tendency for stagnation in the front, left-hand corner and so spacing away from the side walls and closer to the centre of the TRS would be better for circulation and water quality overall.

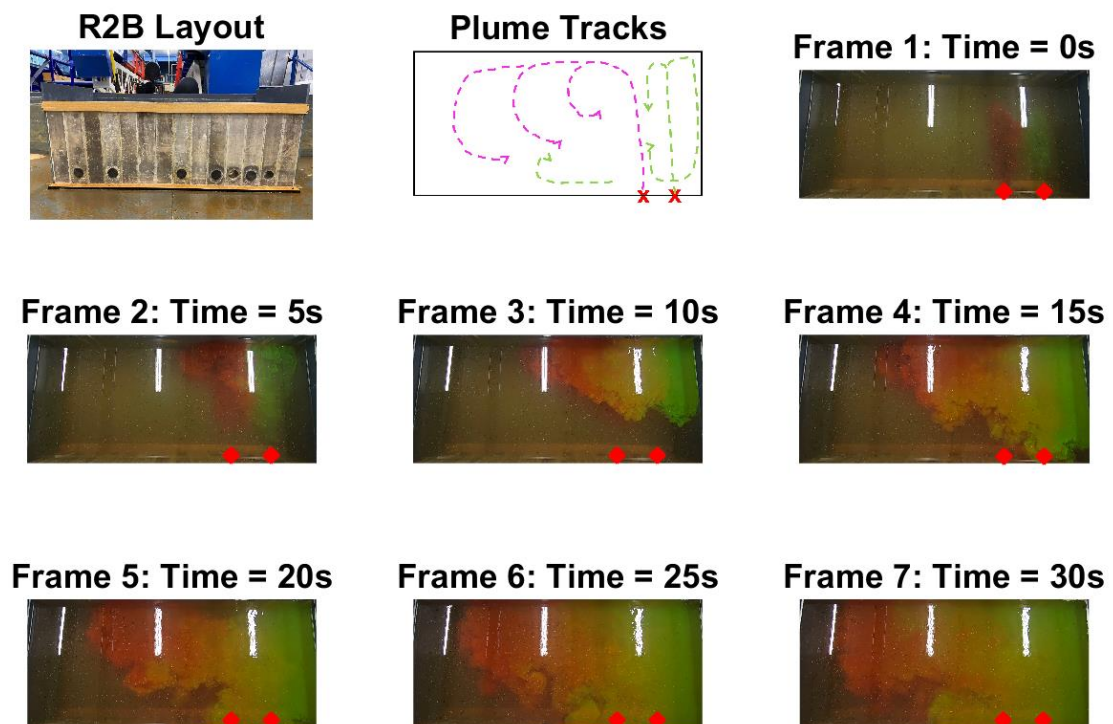


Figure 4.90 Flow visualisation for experiment R2B.

4. Test Case 1 - Impact of Varying Turbine Layout

As the spacing of the turbine openings increases again for experiment R2C, so the circulation patterns of the wakes changes again (Figure 4.91).

Although both plumes stay parallel to one another until reaching the rear wall as in the previous two cases, this time, the right-hand wake is able to travel left as well as right along the rear wall before being reflected to the front, creating a distinct green area on the right-hand side of the lagoon. As before the left-hand plume follows the rear wall to spread into the left-hand side of the lagoon but interestingly does not reach the whole way to the left-hand wall. This suggests that the slightly further spacing between the turbine openings in this case have meant that the individual wakes are not strong enough to permeate the whole lagoon area, whereas in the previous cases (R2A and R2B), the closer spacing has exaggerated the force of the wakes so that they are able to better fill the whole area. In this case, as in R2A, it took ninety seconds (one full tidal cycle) for the dye to reach the front, left-hand corner. This is interesting as we would expect that with a turbine placed closer to the left-hand wall the water would reach further into the left-hand side of the lagoon, however the wider spacing has meant that the wakes are not as strong. This presents a new challenge for TRS design, that there is an optimum position and spacing for turbine openings that needs to be carefully balanced to ensure water quality.

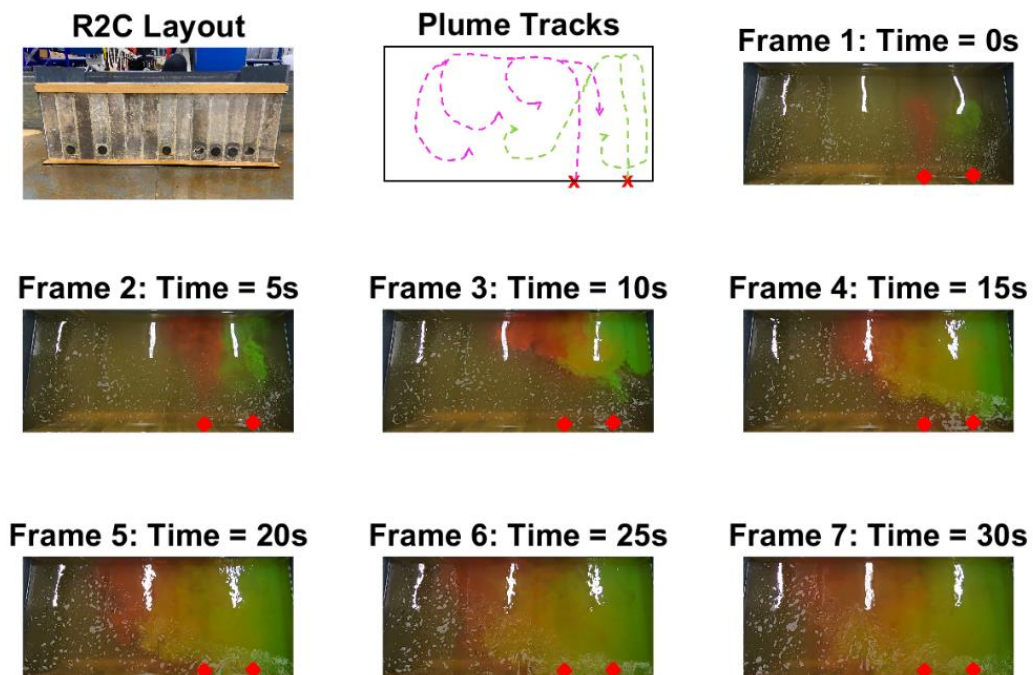


Figure 4.91 Flow visualisation for experiment R2C.

4. Test Case 1 - Impact of Varying Turbine Layout

Analysis of wake jets in experiment R2D (Figure 4.92) show very similar results to those of S2B (see Figure 4.65). In both cases the turbine openings have been placed at opposite ends of the seawall and maintain two distinct circulation currents, with wakes following the side walls before being reflected off the rear wall to travel along the centre line of the lagoon back to the front wall, with very little mixing between the two cells. Once again this demonstrates how wide, equal spacing between the turbine openings allows water to be fully renewed in the whole lagoon area but with less extreme flows caused by the combined effects of two wakes flowing together. This agrees with the findings of Angeloudis et al. (2016b) who, in studying TRS design, found that the distribution of turbines can affect recirculation zones and vortex size and confirms the findings of Nuernberg and Tao (2018) that wider spacing of turbines leads to clearer individual wakes. Unfortunately, it is not possible to visualise the 3D nature of these flows using this method, which would also help better understand the mixing and flushing of the TRS under each of these conditions and merits further study.

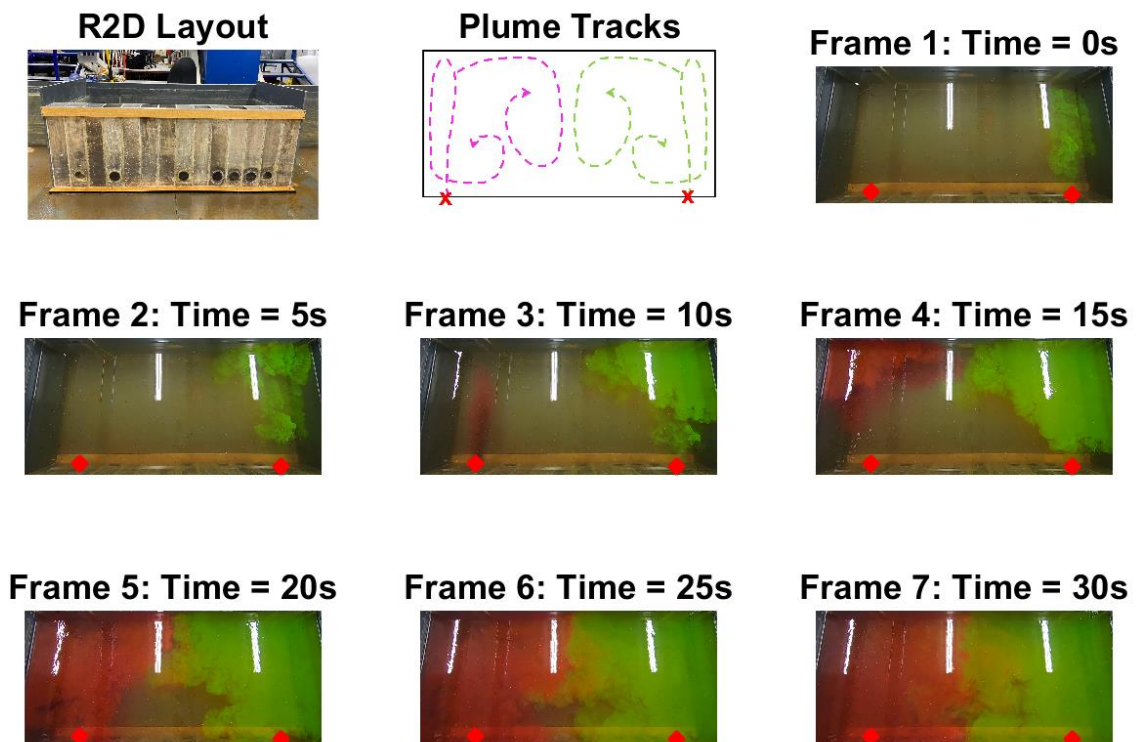


Figure 4.92 Flow visualisation for experiment R2D.

4. Test Case 1 - Impact of Varying Turbine Layout

4.3.4.5 Statistical Analysis

The residual velocity measurements for each location in these experiments were plotted against those of R0, a closed rectangular box, to determine the impact of each layout on baseline velocities. The scatter graph regression lines in Figure 4.93 illustrate how closely related the resultant velocities of these experiments were to each other, with stronger correlation between these cases and the baseline results than any previous experiments.

Analysing the histogram of these results (Figure 4.94) shows that there is little difference in velocity range between the cases and this is further proven by the statistical analysis of these results which shows that none of the experiments greatly altered the average flow magnitude, with very similar average values (Table 4.5). Experiments R2A, B and C reduced the baseline flow rate by less than 5% whilst the greatest alteration was caused by R2D which reduced the average flow velocity by 9%. Analysis of the residual flow direction show very little change between all cases (Figure 4.95 and Figure 4.96) and the baseline results and z-test results for all cases confirm that we can accept the null hypothesis that none of these layouts significantly alter the baseline velocity levels (Table 4.5).

Table 4.5 Comparison G - Statistical analysis of residual velocity magnitude of R2A, R2B, R2C and R2D compared to R0.

Comparison	\bar{x} (m/s)	SD	RMSE	r	z	Accept/ Reject h_0
R0	0.03399	0.01029				
R2A	0.03267	0.01377	0.00814	0.45225	0.50823	Accept
R2B	0.03225	0.01389	0.00947	0.35246	1.00939	Accept
R2C	0.03304	0.01433	0.00716	0.49489	0.35576	Accept
R2D	0.03100	0.01362	0.00898	0.53344	1.13505	Accept

4. Test Case 1 - Impact of Varying Turbine Layout

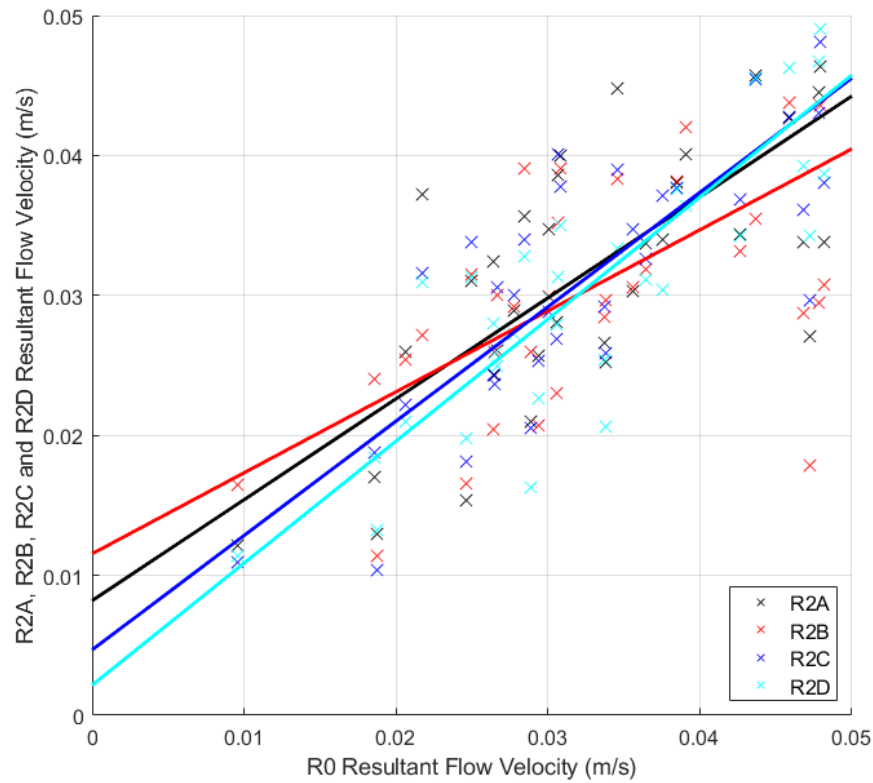


Figure 4.93 Comparison G - Regression analysis of residual flow velocity.

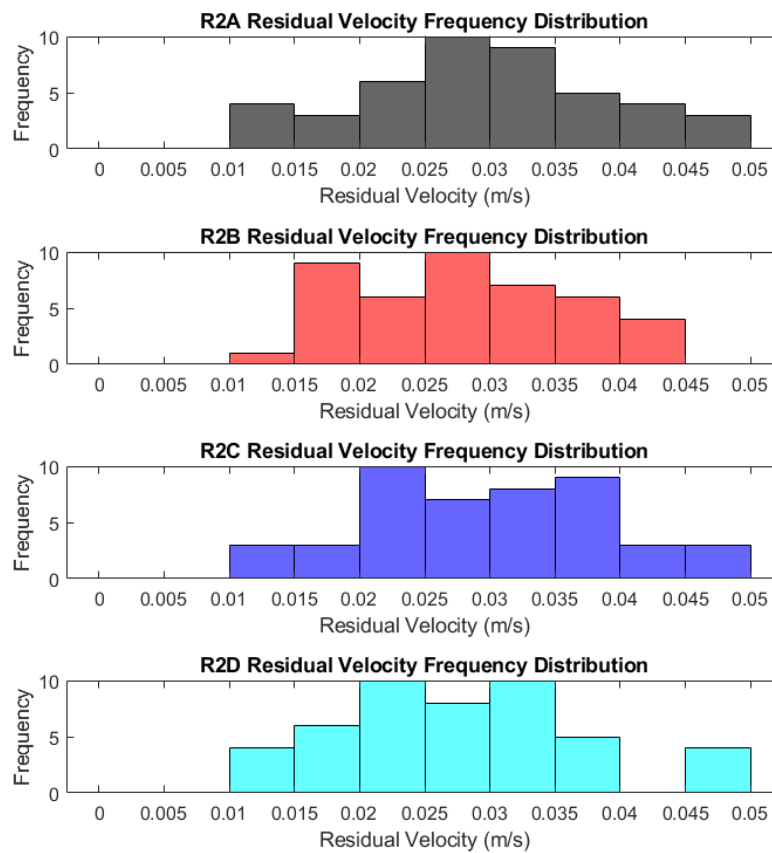


Figure 4.94 Comparison G – Distribution analysis of residual flow velocity.

4. Test Case 1 - Impact of Varying Turbine Layout

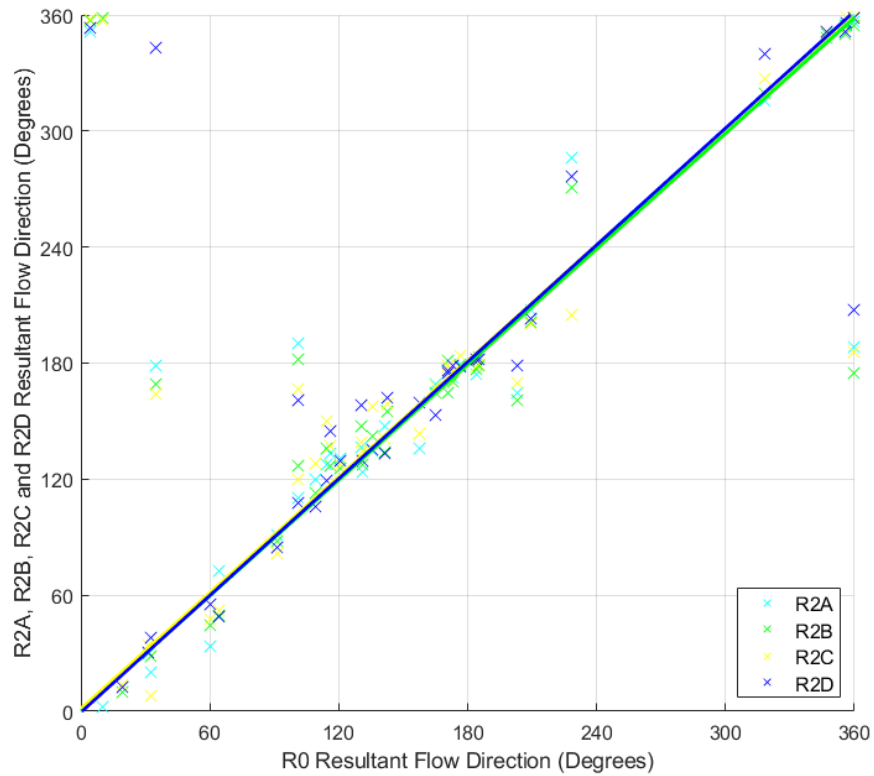


Figure 4.95 Comparison G - Regression analysis of residual flow direction.

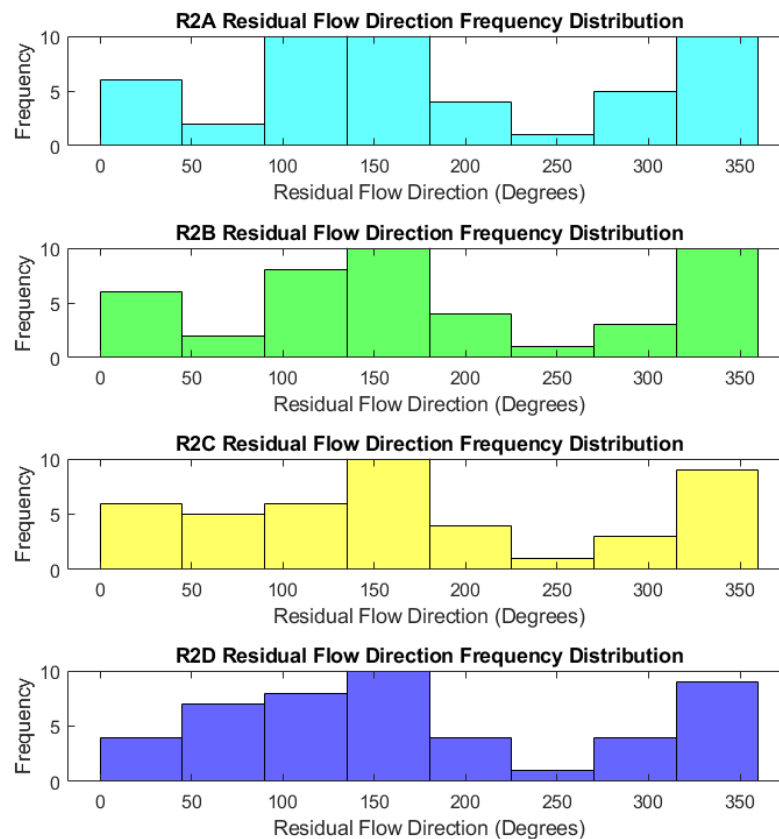


Figure 4.96 Comparison G – Distribution analysis of residual flow direction.

4.4 Summary

Chapter 4 deals with the comparison of turbine spacing in square and rectangular TRSs, examining the effects of the number of turbines and their positions in the seawall perpendicular to the direction of prominent flow.

Comparison A compared the difference in behaviour in a square TRS with zero, one and two turbines. Close analysis of velocities around the TRS showed that the presence of the structure itself did not cause significant changes to pre-lagoon conditions but that changes could be observed once openings in the seawall were made. Although the turbines were located in similar positions it was found that a single turbine caused less disruption to baseline conditions than two turbines and that statistically there was little difference between the closed box case (S0) and the single turbine case (S1A). The two-turbine case (S2A) revealed similar flow patterns to the single turbine case but with stronger flows and exaggerated currents due to the larger discharge area of two turbine openings.

Comparisons B and C examined the differences caused by altering the position of a single turbine or a pair of turbines, respectively. In moving the location of a single turbine, a central position was found to cause less alteration to baseline conditions both inside and outside of the TRS than an offset position, where interaction with seawalls affects flow circulation and the strength of currents. This was highlighted particularly in flow visualisation of S1A where vortices were restricted by proximity to the seawall. Therefore, turbines should be placed away from walls in order to avoid undue influence of obstructions on circulation currents. In the study of two turbines, it was proven that the closer the turbines were to each other the stronger the currents formed and the faster the velocity experienced inside in the TRS and further afield, up to a distance of 30 turbine diameters. Natural conditions were most closely maintained by wider turbine spacing which causes less disruption to flow but can lead to areas of stagnation inside the TRS due to such slow velocities.

These findings were confirmed by comparison G which looked at the effects of moving two turbines in a rectangular TRS. These experiments

4. Test Case 1 - Impact of Varying Turbine Layout

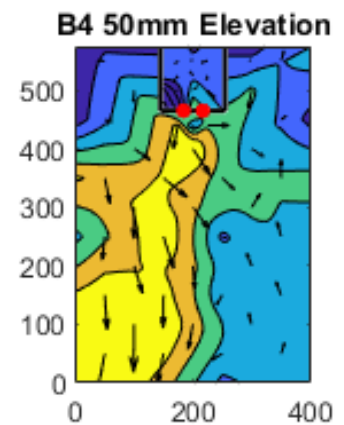
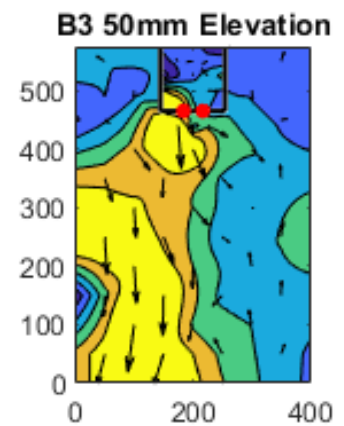
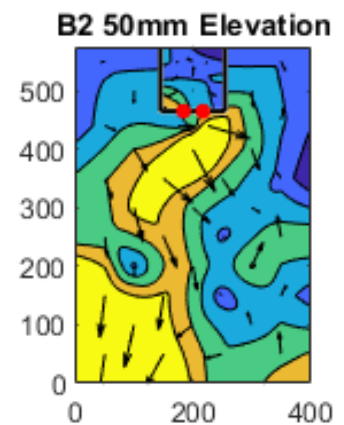
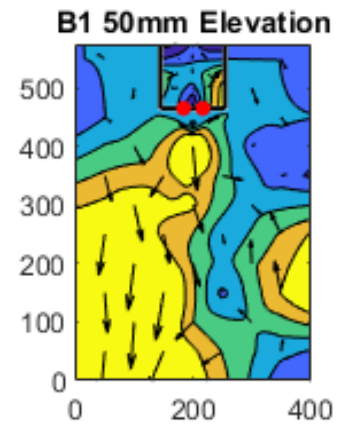
corroborated the conclusions of comparison C, that close turbine spacing leads to the greatest disruption and strongest flows, whilst wider spacing allows greater circulation around the TRS but slows flows overall. Slower velocities are preferable for the proposed secondary uses of tidal range lagoons, e.g., aquaculture and recreation, but may lead to issues of stagnation and prevent the flushing of contamination.

Overall single turbines were found to cause less disruption to natural flow conditions than two, but two turbines were found to allow better circulation and flushing which supports a healthier environment. Close turbine positioning leads to strong turbine wakes and exaggerated vortices, which are further affected by proximity to seawalls, so wider spacing is preferred for promoting balanced flows in the near and far field despite being the more expensive option.

Statistical analysis led to the conclusion that a square TRS with a single turbine and a rectangular TRS with two turbines does not significantly alter flow velocity and therefore we can accept the null hypothesis that pre-lagoon conditions are not significantly affected by these layouts. However, results for a square TRS with two turbines lead us to reject h_0 as they were found to cause a significant difference to baseline flow conditions. This has important implications for TRS design in that the position of multiple turbine openings in a compact TRS shape will have a significant impact on flow conditions both in and outside of the lagoon and therefore not only does the shape of the TRS need to be sympathetic to the local conditions but also the number and spacing of the turbines.

Chapter 5

Test Case 2 – Impact of Varying Bed Conditions



5 Test Case 2 – Impact of varying bed conditions

5.1 Introduction

Bed conditions will naturally vary depending on the existing conditions of TRS sites but can be altered artificially to improve conditions if issues are identified. However, it is often best to maintain natural conditions to reduce the disruption to the environment, as many species rely on specific sediment conditions for their feeding and breeding (Copping et al., 2014).

Anthropogenic changes to bed geometry, e.g., dredging for navigation or construction, can have significant impacts on circulation patterns and current distribution and need to be considered carefully before causing irreversible changes to the natural environment (Nguyen et al., 2018). Bed conditions will also have an impact on the hydrodynamic interactions of TRSs, potentially leading to scouring, erosion or sedimentation depending on bed material.

Test case 2 investigates the effects of different bed materials and slopes on flow conditions inside and outside a TRS, comparing the results to those of a smooth, flat bed as a control case. Turbine spacing and lagoon shape were both kept constant in this instance so that bed conditions are the only variable under consideration. Three cases were tested to investigate bed materials (Comparison D): fine sediment (10 mm gravel), coarse sediment (20 mm gravel) and artificial grass to represent sea grass. Whilst two slope angles, 5° and 10° were compared against the original flat bed (Comparison E). Table 5.1 sets out the parameters for each of these experiments.

Table 5.1 Test cases for bed materials in a square TRS.

Test Case	Geometry	Number of Turbines	Slope	Bed material
B1	Square	2	0°	Smooth plastic
B2	Square	2	0°	20 mm grass
B3	Square	2	0°	20 mm gravel
B4	Square	2	0°	10 mm gravel
B5	Square	2	10°	Smooth plastic
B6	Square	2	5°	Smooth plastic

5. Test Case 2 – Impact of Varying Bed Conditions

In the real world changes to bed conditions would not be confined only within the TRS and bed material or slope would also vary outside the TRS.

However, conditions in the lab mean that these alterations were only controllable inside the TRS which is what will be observed here.

Analysis of results from these experiments will help to answer the question: “to what extent do TRS bed conditions affect hydrodynamics?” and test the following hypotheses:

h_0 : There is no significant difference experienced in velocity by changing lagoon bed conditions.

h_1 : Changing lagoon bed conditions causes significant difference to velocity profiles.

5.2 Results

5.2.1 Comparison D – Varying bed materials

Comparison D investigates the effects of varying bed material in a square TRS, comparing results from experiments B1, B2, B3 and B4 against pre-lagoon conditions in order to determine the sensitivity of TRSs to different bed materials and their impact on flow characteristics.

Figure 5.1 presents images of the experiment layout and bed materials for each of these cases. Bed materials were chosen based on availability and also to test extremes to determine the impact of changes to the bed which could then be refined based on initial findings. For example, at the present scale, gravel with 20 mm particles represents a sediment size of 2 m, which would be boulders at a real-world scale. Whilst this size may seem extreme, it is still a realistic bed condition along the coast and will give an indication as to the effects of this type of bed on flow conditions inside the TRS. The artificial grass too would represent 2 m high seagrass in real life, a modest height for this type of plant and would therefore present a good idea of how flow is affected under these conditions. If results show a significant impact from these examples of bed materials further tests will be conducted using finer particle sizes to investigate the sensitivity of the model to different conditions.

5. Test Case 2 – Impact of Varying Bed Conditions

a) B1: Smooth PVC bed



b) B2: 20 mm artificial grass



c) B3: 20 mm gravel



d) B4: 10 mm gravel



Figure 5.1 Experient layout and bed materials for Comparison D: B1, B2, B3 and B4.

5. Test Case 2 – Impact of Varying Bed Conditions

5.2.1.1 Velocity - Depth Averaged

The depth averaged velocity plots of these experiments presented in Figure 5.2 demonstrate how similar flow velocity behaviour is despite changing bed conditions within the TRS. Transects from across the width of tank demonstrate how even when flow velocity is irregular and changes from the left-hand wall to the right, each of the different bed conditions still displays the same patterns of resultant velocity magnitude. E.g., along the line $x = 100$ cm, where all experiments start with a negatively skewed wave on the left-hand side of the tank, (100,100) (closer detail given in Figure 5.3), transition through the centre of the tank with two much smaller peaks at (200,100) (Figure 5.4) and end with a positively skewed wave on the right-hand side of the tank, (300,100) (Figure 5.5). This pattern is repeated across many transects in the tank, even at the inflow boundary, and each of the experiments also closely matches the results of the empty tank case, with the exception of measurements at point (200,400) (Figure 5.6), directly in front of the TRS. This has been a significant location in all experiments as water is reflected off the seawall, but most specifically in the case of Comparisons D and E, where the two turbine openings are positioned either side of this point (co-ordinates of turbine opening 1: (184,465), co-ordinates of turbine opening 2: (217,465)). However, at (200,400) all cases besides the empty tank measurements each exhibit the same pattern which gives us confidence that the results of each experiment are reliable and that the conditions in the tank are consistent as the results have been repeated under similar conditions.

Where there are subtle differences, it is B1 that tends to vary slightly from the other cases, either having slightly higher or lower results whilst the others cluster together e.g. (150,350) (Figure 5.7) and (350,350) (Figure 5.8). This is interesting as this smooth bed case is the one being used as a baseline in this comparison and reveals that although the other experiments behave differently from the baseline case, they all behave similarly to each other regardless of the new bed conditions.

5. Test Case 2 – Impact of Varying Bed Conditions

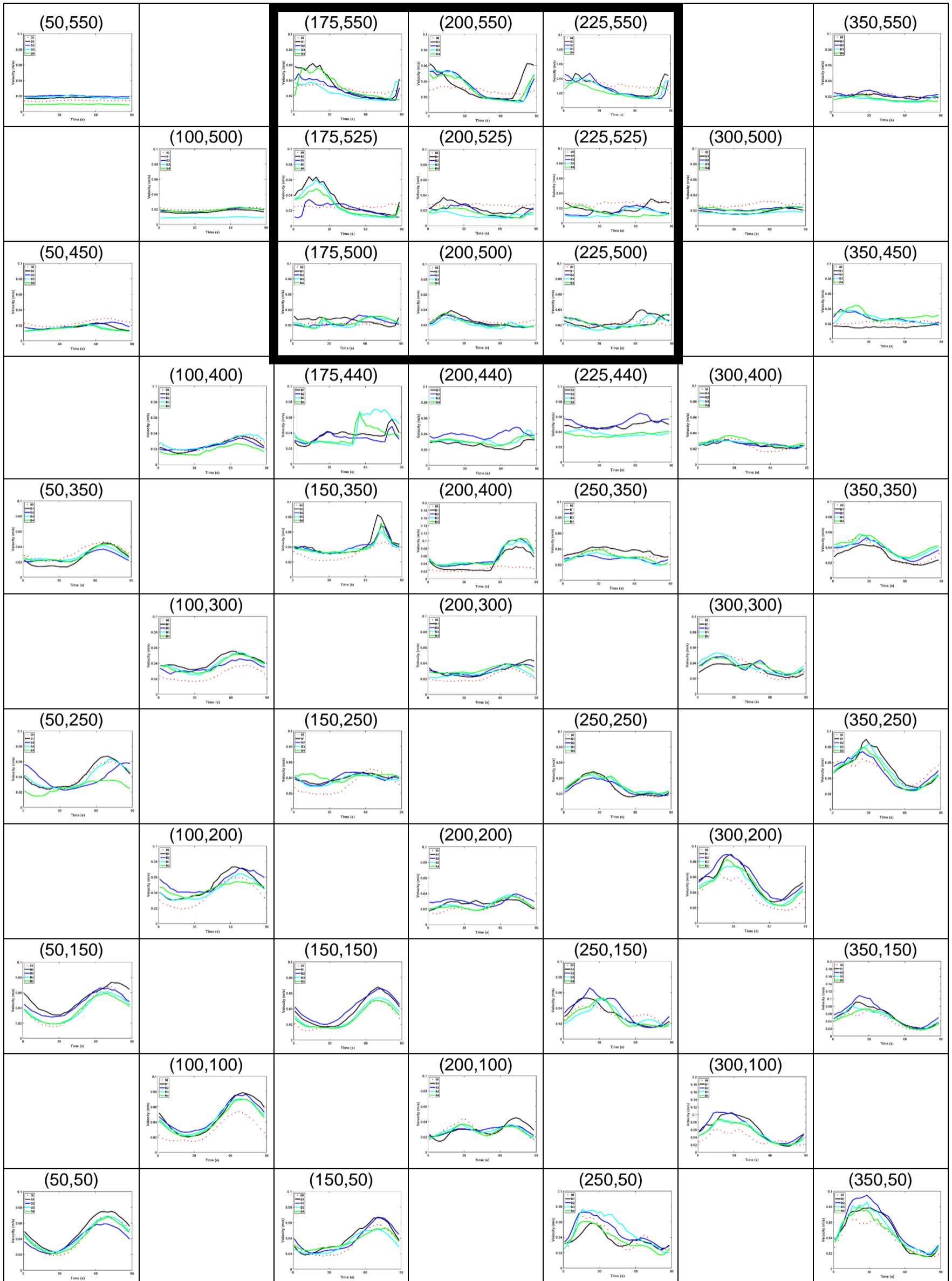


Figure 5.2 Map of depth averaged velocity plots for Comparison D: B1, B2, B3 and B4.

5. Test Case 2 – Impact of Varying Bed Conditions

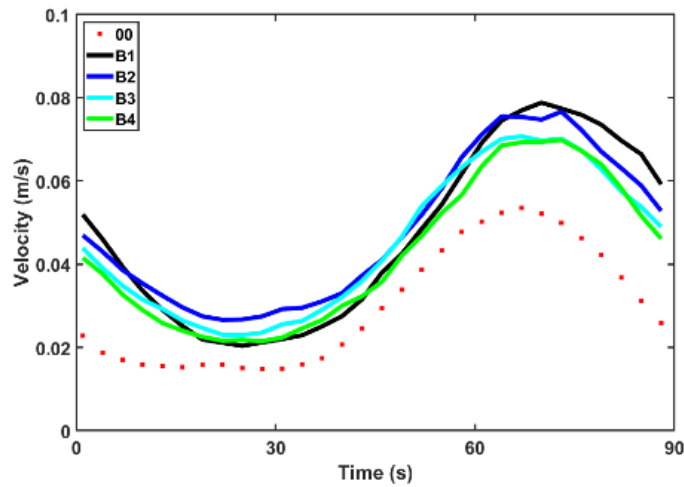


Figure 5.3 Closer detail of velocity at (100,100).

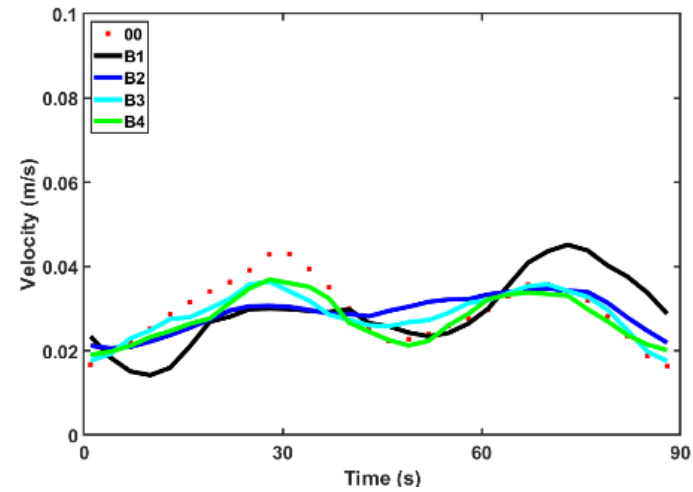


Figure 5.4 Closer detail of velocity at (200,100).

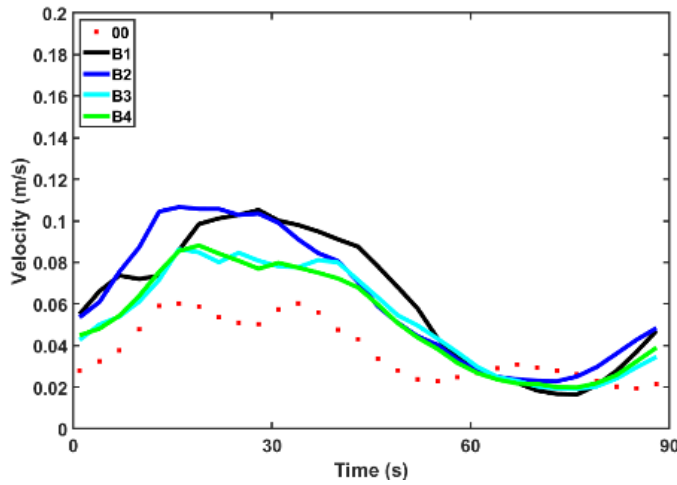


Figure 5.5 Closer detail of velocity at (300,100).

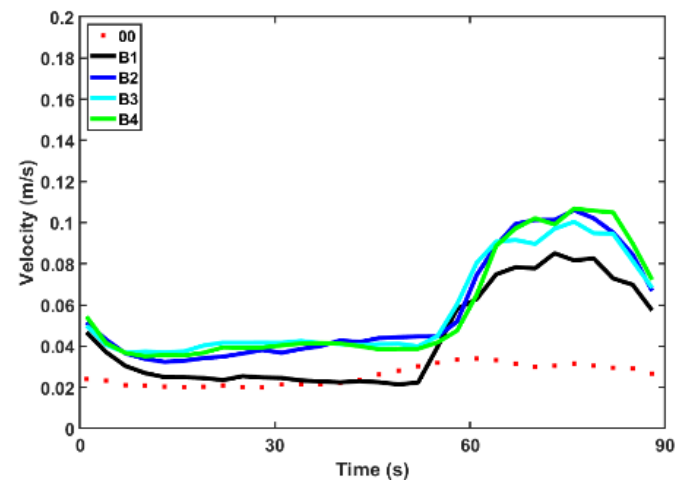


Figure 5.6 Closer detail of velocity at (200,400).

5. Test Case 2 – Impact of Varying Bed Conditions

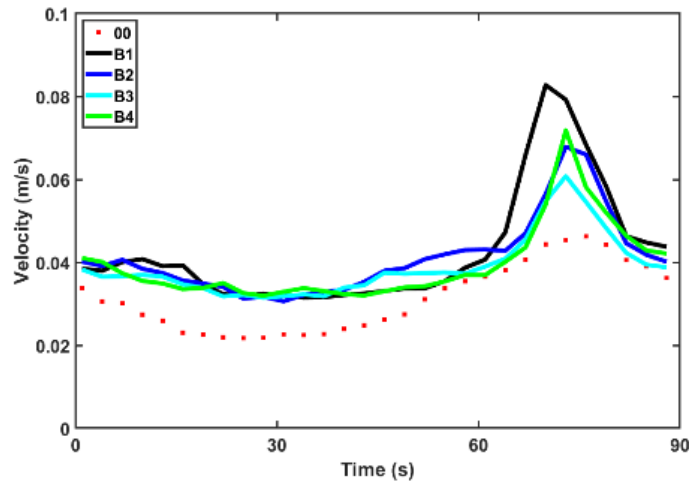


Figure 5.7 Closer detail of velocity at (150,350).

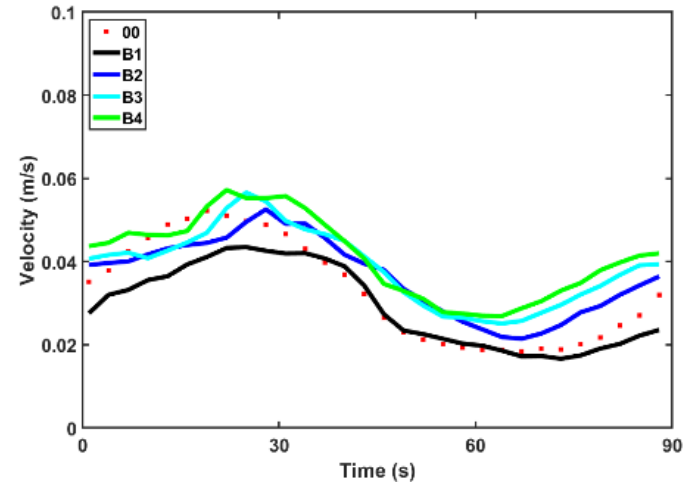


Figure 5.8 Closer detail of velocity at (350,350).

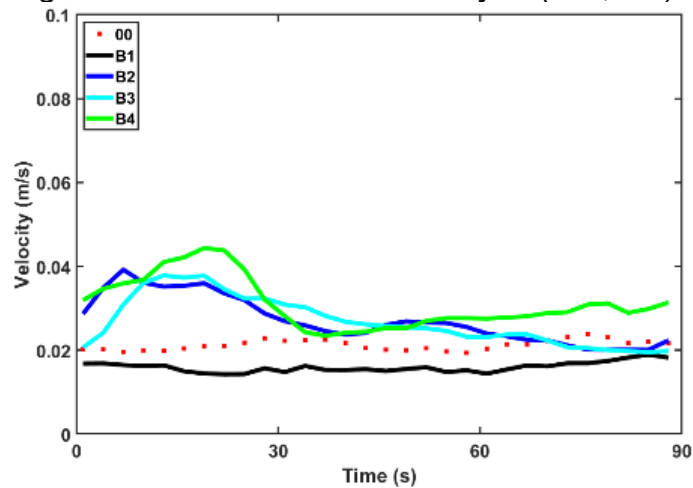


Figure 5.9 Closer detail of velocity at (350,450).

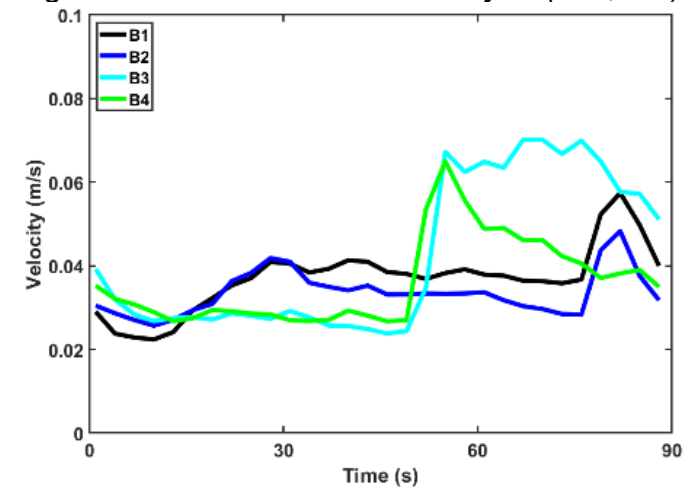


Figure 5.10 Closer detail of velocity at (175,440).

5. Test Case 2 – Impact of Varying Bed Conditions

The greatest differences between the cases can be found at (175,440) (Figure 5.10) and (350,450) (Figure 5.9). At (350,450) experiment B1 has very slow flow, slower even than the empty tank case, which shows that the presence of the square TRS reduces flow velocity in the area even with equally spaced turbines and a smooth bed. Each of the other three cases have similar flow velocity values but peak at completely different times: B2 at the start of the flood tide, B3 at the turn of high tide and B4 during the ebb tide. This is particularly unusual as we would expect bed materials to affect the degree to which water accelerates or decelerates but not the time at which it does so. This could be due to the different bed materials having a greater influence at different times of the tide.

Close to the left-hand turbine opening (175,440) (Figure 5.10), the results differ between cases. Although they each peak towards the end of the tidal cycle, B4 has a very abrupt peak at the same time as B3 but tails off much quicker, whilst B2 follows B1 more closely with a more modest peak. This suggests that the artificial grass behaves more in line with the smooth bed than the other materials which is not surprising since this material is much more flexible and should allow water to flow uninhibited but the coarser gravel has meant that water is not able to flow as quickly as over finer gravel where it maintains faster flows for longer. However, at (225,440), directly in front of the right-hand turbine, the results all follow a very similar pattern, so this does not explain why there is variation at the second opening. We must therefore deduce that the unusual results at this location are due to the effects of the bed materials in agreement with Jeffcoate et al. (2013) who observed that sediment transport and scour are highly susceptible to velocities through turbines, as they magnify bed shear stress.

Inside the TRS, the results are once again very similar to each other, consistently following the same peaks and troughs and only varying slightly in amplitude. The greatest difference is at (175,525) (Figure 5.11) where the results all follow the same steep starting peak, but B3 has a much lower and longer peak. This indicates that the long grass and coarse gravel both have an impact on flow further away from the turbine openings where they significantly reduce flow velocity. This concurs with the findings of Hajikandi

5. Test Case 2 – Impact of Varying Bed Conditions

et al. (2018) who, in studying flow and scour through orifices under multiple bed conditions, observed that the length and width of orifice wakes were reduced by larger sediment sizes due to flow-sediment interaction. There is also a difference between the results at (225,525) (Figure 5.12) where flow is much slower than the baseline measurements but with no discernible pattern between the cases. This is interesting as this location is the same distance away from the turbine openings as (175,525) (60 cm = 10 turbine diameters) and so we would expect to see the same effects, but flow is definitely faster on the left-hand side of the lagoon than the right, particularly in the rear left-hand corner at (175,550). This could be due to reflection off the rear wall of the lagoon deflecting to the left causing stronger cross currents and increasing the overall velocity in this location. These faster velocities on the left-hand side of the lagoon are consistent across all cases though and so are not a result of the bed material but rather the shape of the TRS and underlying flow conditions in the tank.

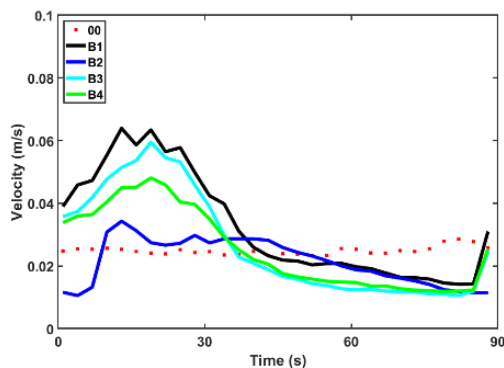


Figure 5.11 Closer detail of velocity at (175,525).

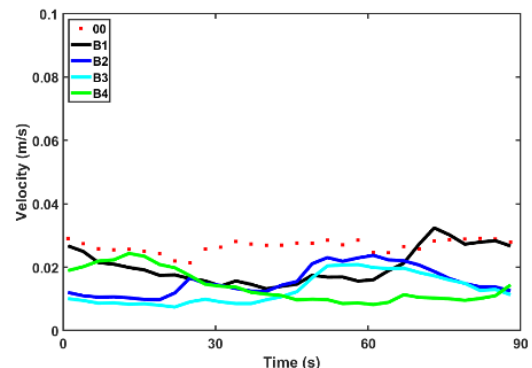


Figure 5.12 Closer detail of velocity at (225,525).

5. Test Case 2 – Impact of Varying Bed Conditions

5.2.1.2 Velocity – Analysed by tide and depth

The velocity contour plots during the ebb tide share many similarities between experiments and depths with some subtle differences (see Figure 5.13). As in previous cases, the strongest flows during the ebb tide are concentrated along the left-hand wall of the tank and in front of the TRS. However, the size and shape of these areas of strong flow varies slightly between the experiments which shows that the bed materials have made some difference since the turbine openings have not changed. In particular we can see that in B3 the area of strongest flow curves around the left-hand corner of the TRS wall whilst in B2 it curves around the right-hand corner, despite the turbines being in the same positions for both cases. This suggests that flow is stronger through the orifices in these scenarios, enough to radiate out of the openings and around the seawall. This finding is shared by Cornett et al. (2013) who noted that TRSs caused significant changes to the direction and strength of currents along the external side of the seawall. However, the strongest flows are all deflected to the left in each of these cases showing that effects in the far field do not vary greatly between these experiments.

Inside the TRS we would expect all cases to display a symmetrical pattern given the identical layout of the turbine openings, however, this is not to be seen. In B1, the baseline against which the other experiments are being compared, the strongest flow is located in the front right-hand corner, despite the turbines being evenly spaced. This could be due to the underlying asymmetry of the tank as previously discussed, but it is surprising that this is still having an effect within the TRS during the ebb tide. In cases B2 and B4 there is slightly stronger flow in the front left-hand corner which goes against the theory that the underlying tank asymmetric flow has an effect in these cases since it has the same turbine positioning as B1 and could therefore be due to resistance from the introduction of different bed materials but still does not explain why flow is asymmetrical. B3, shows the greatest symmetry inside the TRS, suggesting that any asymmetrical flow in the tank is evened out by the resistance introduced by the coarse gravel here.

5. Test Case 2 – Impact of Varying Bed Conditions

Figure 5.14 reveals extremely similar patterns throughout the tank at all depths and for all experiments meaning that the different bed materials have a negligible effect on conditions outside of the TRS during low tide. Inside the TRS a symmetrical flow pattern begins to emerge at this phase of the tide showing that during times of slack water the flow behaves more as we would expect, spreading equally through both turbines into the rest of the TRS. This pattern is less pronounced closer to the surface proving once more the three-dimensional nature of the turbine wakes which are not as strong further from the bed.

Plots for the flood tide show little variation between experiments once again (Figure 5.15), and the symmetrical pattern within the TRS is still evident at this phase of the tide. This implies that the forces acting near the turbine openings and in the rest of the tank are more equal during the flood tide than the ebb so that water is able to flow freely into the TRS rather than being constrained as it ebbs out.

At high tide the results are still extremely similar between the experiments, (Figure 5.16) highlighting that the effects of the different bed materials have limited effect outside of the TRS. The results inside the TRS differ slightly between the experiments which proves that the different bed materials do have an effect on flow, but at each point of the tide it is experiment B1 that stands out, showing that although the introduction of bed materials does alter conditions from the baseline they do not vary greatly between each other and therefore no single material can be deemed better or worse than any of the others for maintaining the natural environment.

5. Test Case 2 – Impact of Varying Bed Conditions

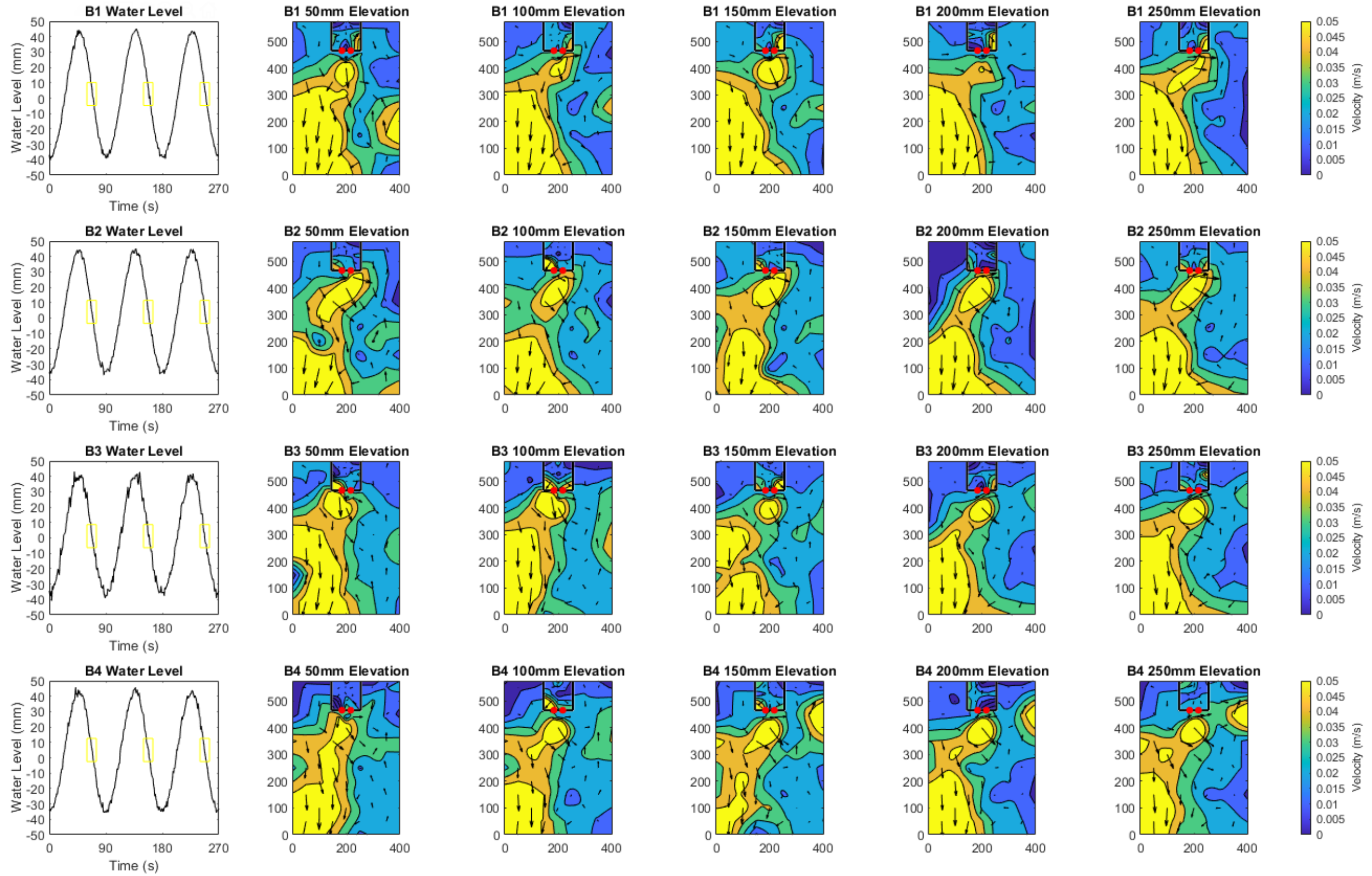


Figure 5.13 Comparison D - Velocity contour maps at elevations of 50, 100, 150, 200 and 250 mm above the bed during the ebb tide.

5. Test Case 2 – Impact of Varying Bed Conditions

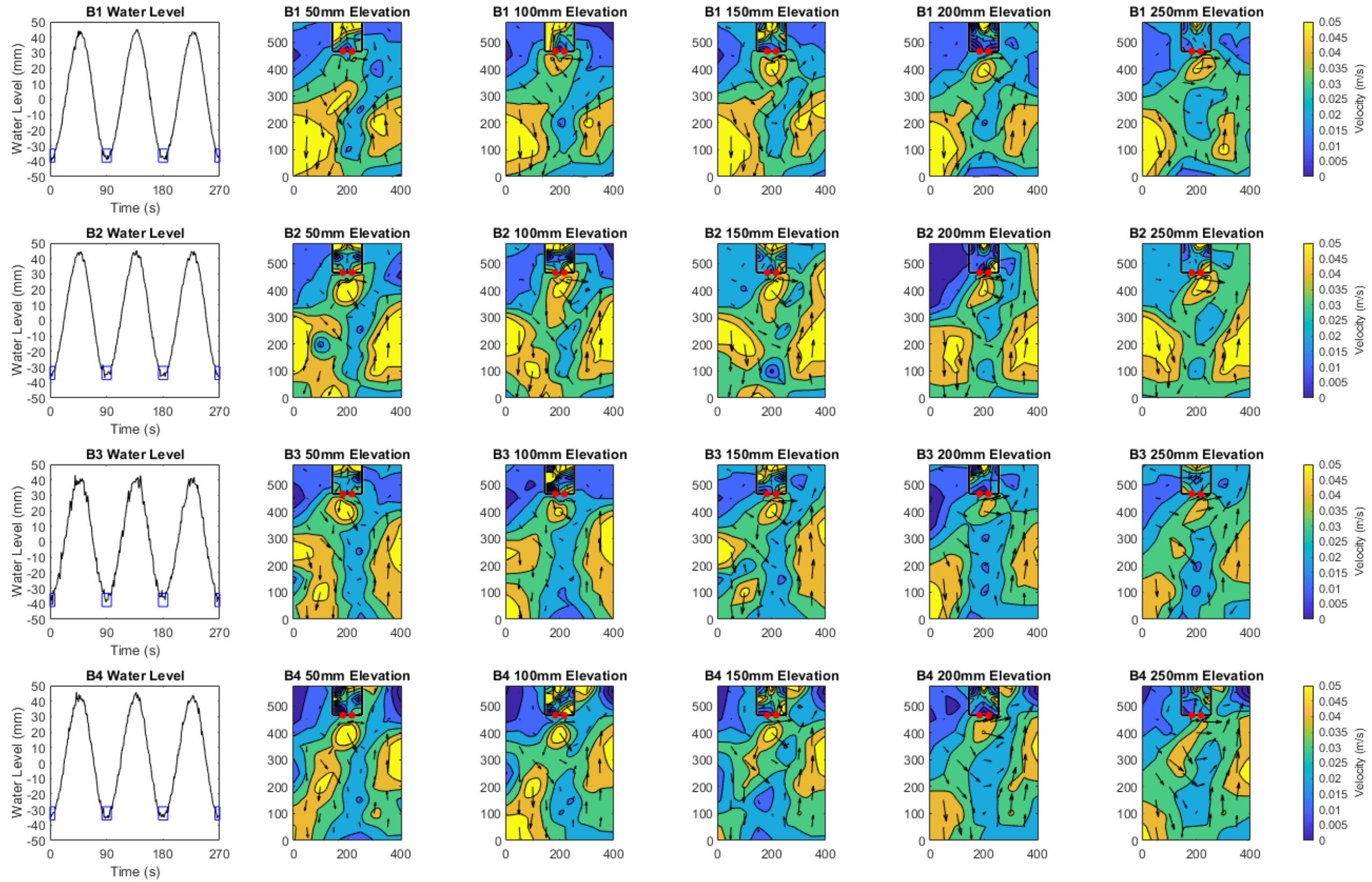


Figure 5.14 Comparison D - Velocity contour maps at elevations of 50, 100, 150, 200 and 250 mm above the bed during low tide.

5. Test Case 2 – Impact of Varying Bed Conditions

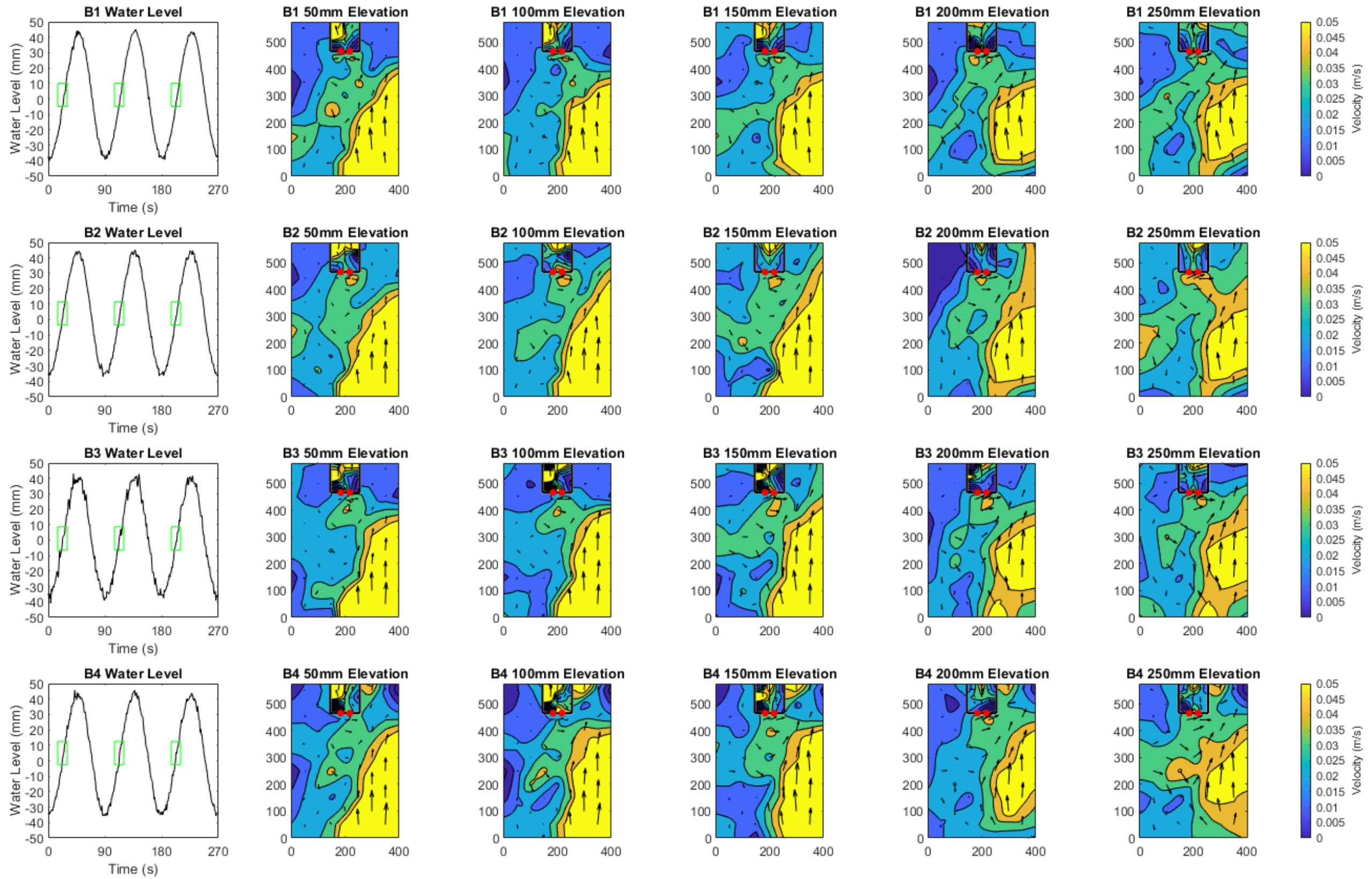


Figure 5.15 Comparison D - Velocity contour maps at elevations of 50, 100, 150, 200 and 250 mm above the bed during the flood tide.

5. Test Case 2 – Impact of Varying Bed Conditions

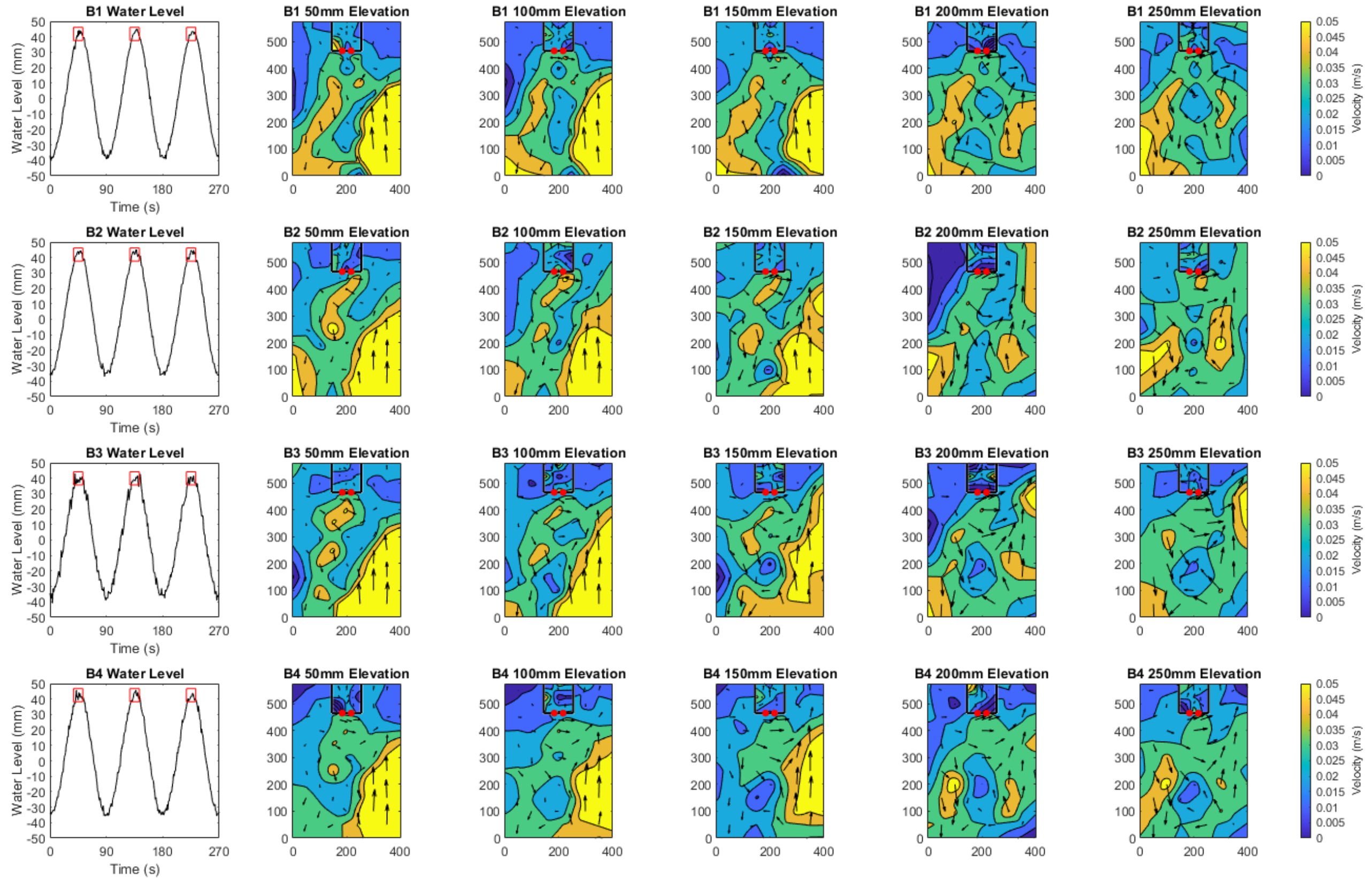


Figure 5.16 Comparison D - Velocity contour maps at elevations of 50, 100, 150, 200 and 250 mm above the bed during high tide.

5. Test Case 2 – Impact of Varying Bed Conditions

5.2.1.3 Velocity – Residual Velocity Magnitude and Direction

Graphs of the residual magnitude and direction of the velocity presented in Figure 5.17 show a more symmetrical pattern for the experiments, especially for B1 and for the other cases above an elevation of 150 mm. This suggests that although underlying flow in the tank causes circulation around the edge of the TRS, the force through the centralised turbines has a further reaching impact on the overall velocity magnitude. Inside the TRS however, flow is still irregular and asymmetrical especially near the bed, exposing the impact that the bed materials make by increasing friction and reducing flow.

5.2.1.4 Flow Visualisation

Unfortunately, it was not possible to capture images of the flow for B2, B3 and B4 as the fluorescent dye did not show up in high enough contrast against the artificial grass and gravel to be able to identify flow patterns clearly. Vortex circulation decay is greatly influenced by bottom friction (Wells and van Heijst, 2003) and therefore we would expect turbine wakes to dissipate more quickly in the coarse gravel case (B3) than the smooth bed case (B1). However, videos of the tank being filled at the start of the experiments show that for all of these layouts, the water entering the TRS through the two centralised turbines caused strong wakes that formed two counter-rotating cells of equal magnitude in each half of the TRS just as for B1, the baseline case. This indicates that the bed material did not cause a difference to the circulation in the tank although the strength of the flow may have been altered near the bed due to the different materials as exemplified by the contour maps.

5. Test Case 2 – Impact of Varying Bed Conditions

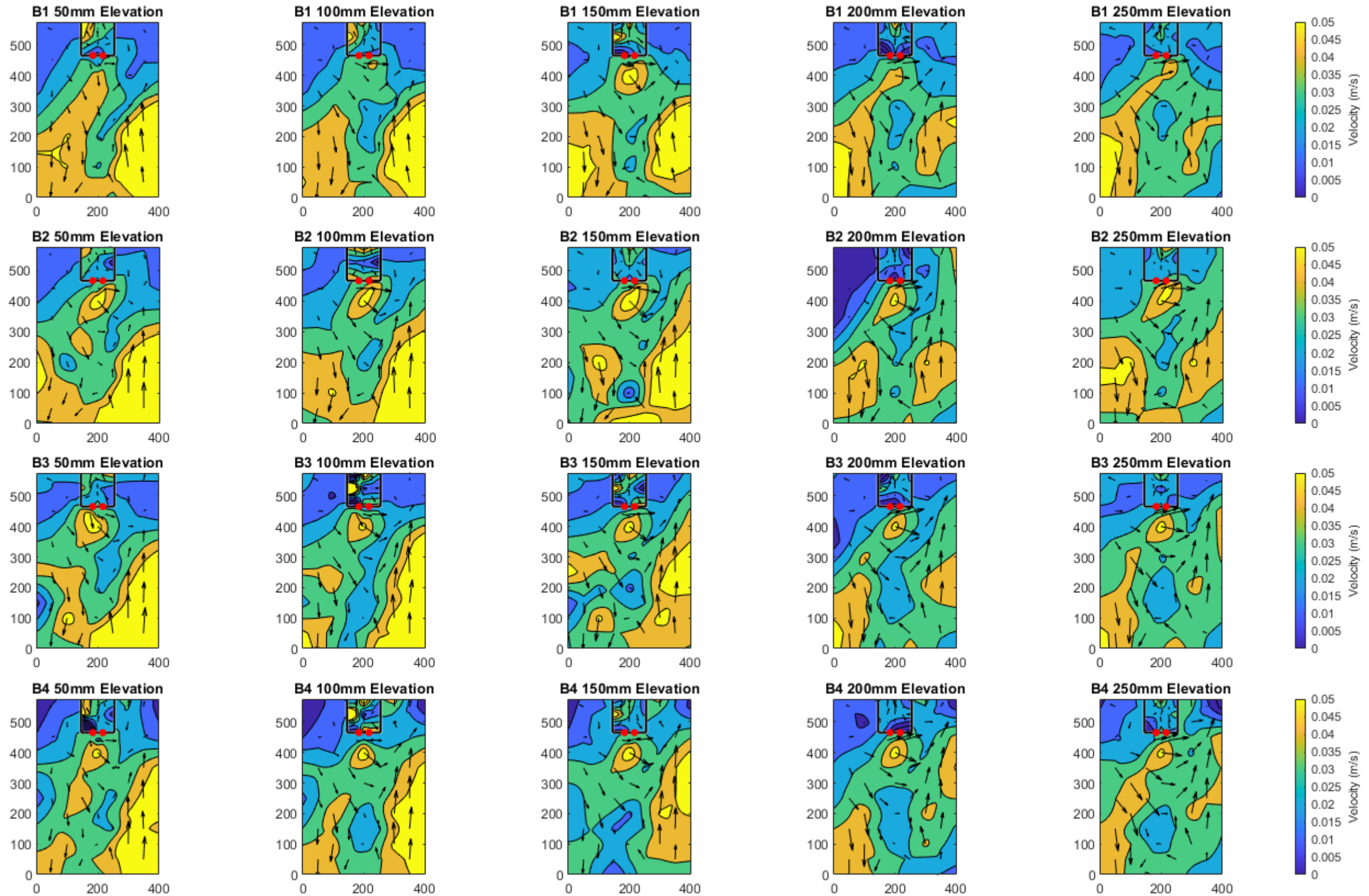


Figure 5.17 Comparison D – Contour maps of residual velocity magnitude and direction at elevations of 50, 100, 150, 200 and 250 mm from the bed.

5. Test Case 2 – Impact of Varying Bed Conditions

5.2.1.5 Statistical Analysis

Scatter plots comparing the residual velocity magnitude of B2-4 against B1 have the strongest correlation of all the comparisons so far, with a strong linear relationship between these experiments and the baseline results (see Figure 5.18). This is highlighted further by histograms of the frequency distribution of residual flow velocity with strong similarities seen between B1, B2 and B3 (Figure 5.19). This is also the case for the scatter plot and histogram of data for residual flow direction that shows near identical results for all cases (Figure 5.20 and Figure 5.21).

Statistical analysis of the residual flow magnitude results, presented in Table 5.2, also highlights how close conditions are for these experiments with less than 6% difference in average flow velocity between all cases and remarkably similar *r* values. In all cases, the *z*-test results lead to acceptance of the null hypothesis that bed material does not make a significant difference to natural velocity conditions.

Table 5.2 Comparison D - Statistical analysis of residual velocity magnitude of B2, B3 and B4 compared to B1.

Comparison	\bar{x} (m/s)	SD	RMSE	r	z	Accept/ reject h_0
B1	0.03506	0.01142				
B2	0.03517	0.01217	0.00579	0.88146	0.04624	Accept
B3	0.03285	0.01139	0.00656	0.85317	1.29599	Accept
B4	0.03245	0.01025	0.00648	0.85555	1.14001	Accept

5. Test Case 2 – Impact of Varying Bed Conditions

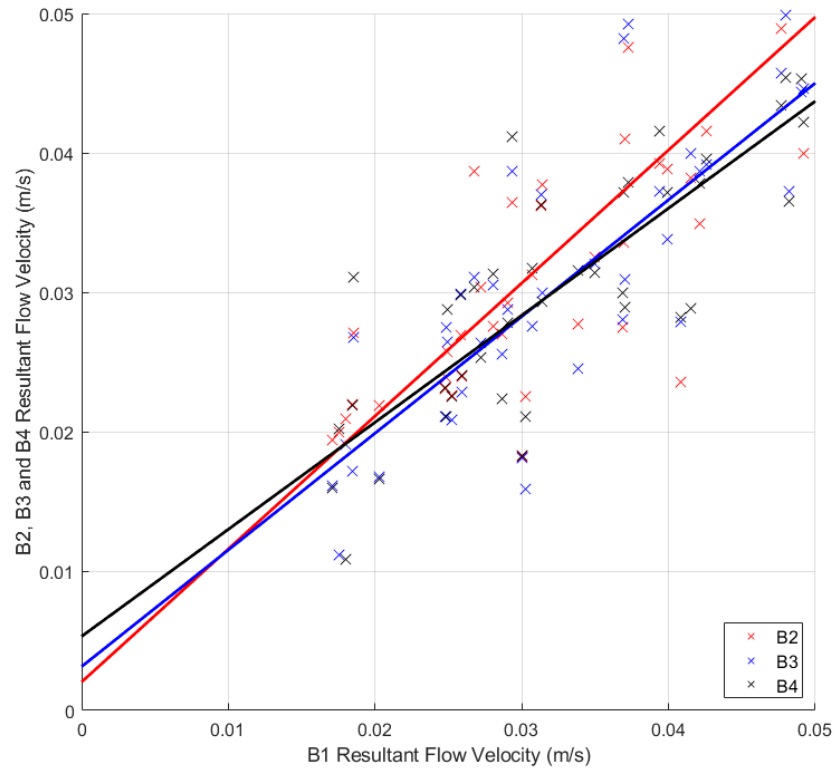


Figure 5.18 Comparison D - Regression analysis of residual flow velocity.

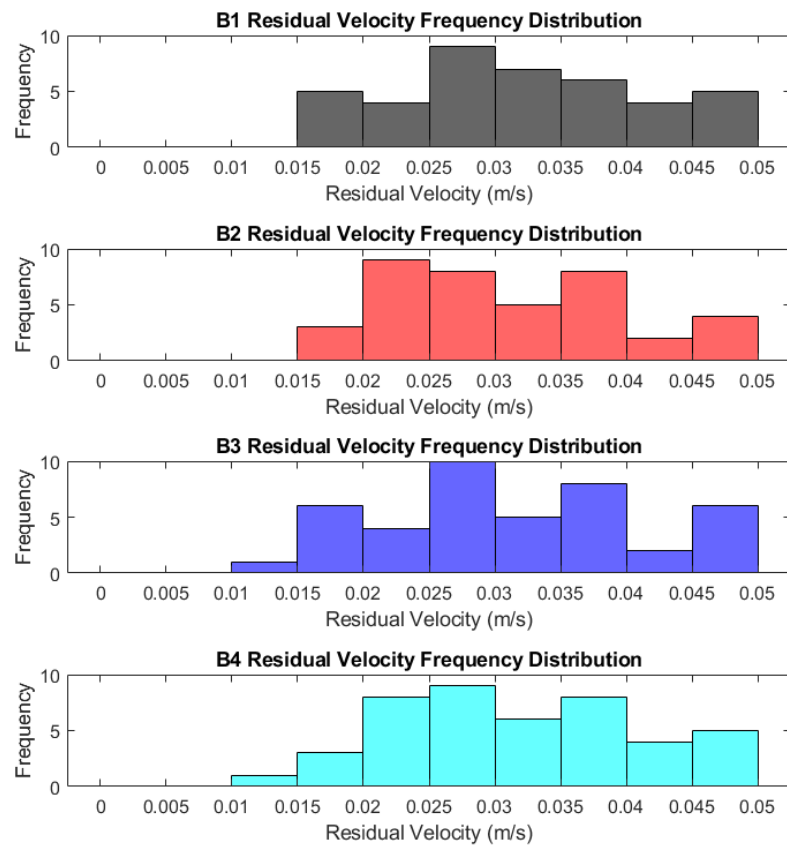


Figure 5.19 Comparison D – Distribution analysis of residual flow velocity.

5. Test Case 2 – Impact of Varying Bed Conditions

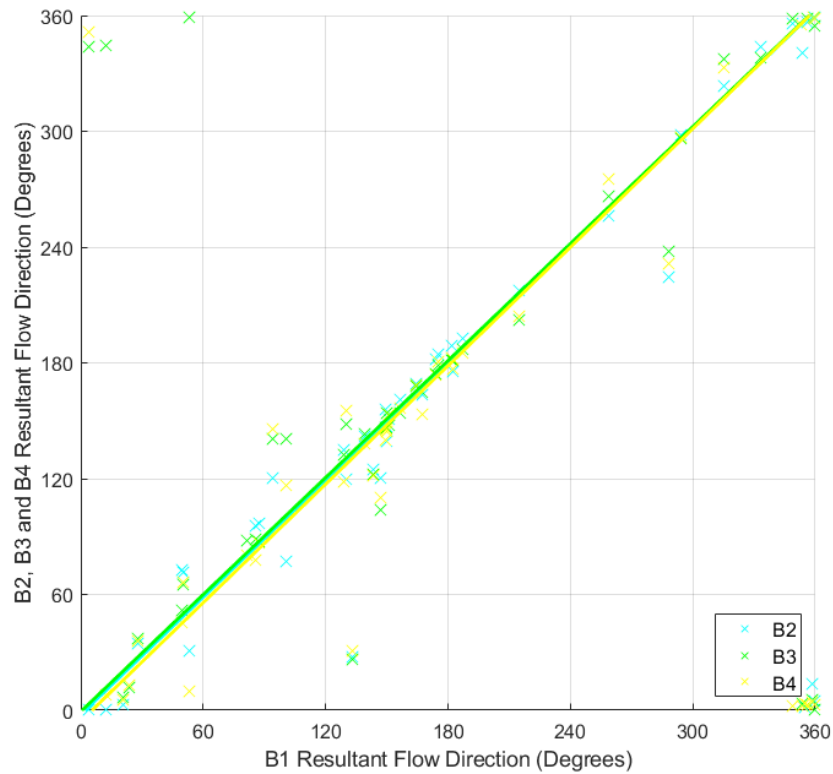


Figure 5.20 Comparison D - Regression analysis of residual flow direction.

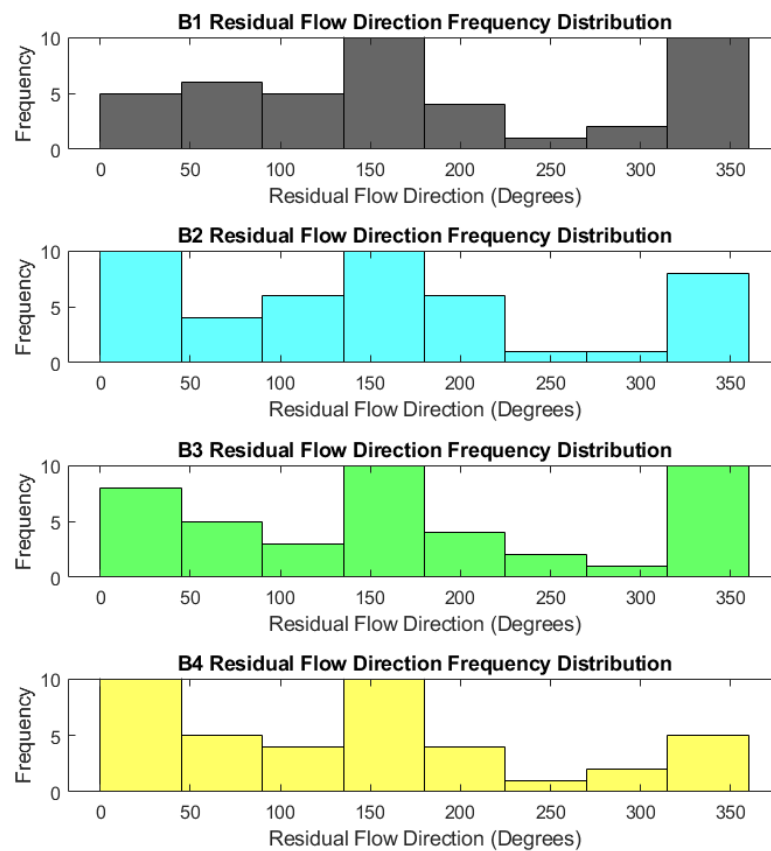


Figure 5.21 Comparison D – Distribution analysis of residual flow direction.

5. Test Case 2 – Impact of Varying Bed Conditions

5.2.2 Comparison E – Varying bed slopes

Comparison E investigates the effects of varying bed slope in a square TRS, comparing results from experiments B1, B5 and B6 against pre-lagoon conditions in order to determine the sensitivity of TRSs to different bed slopes and their impact on flow characteristics. Figure 5.22 shows the turbine layout used for all three of these experiments whilst Figure 5.23 illustrates the bed slopes in experiments B5 and B6.

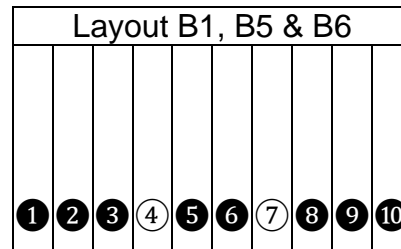


Figure 5.22 Experiment layout for Comparison E: B1, B5 and B6.

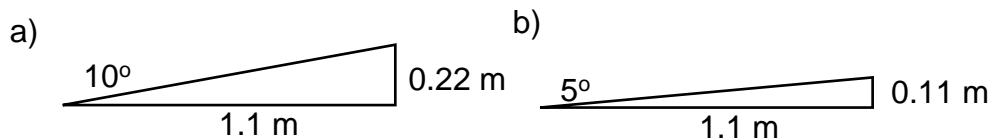


Figure 5.23 Bed configuration of experiments a) B5 and b) B6.

5.2.2.1 Velocity - Depth Averaged

As with the change of bed materials, the change of bed slope within the TRS does not appear to make a significant difference to flow conditions in the wider tank area with extremely similar results at almost all locations throughout the tank (see Figure 5.24). Whilst results from each of the experiments closely match each other they do consistently exceed those of the pre-lagoon measurements and, although they follow the same pattern as the baseline conditions, they frequently have higher flow velocities showing that the presence of the TRS and the introduction of a bed slope within the TRS has increased flow velocity overall. Even at locations where an unusual flow pattern emerges, each of the experiments still closely match each other, e.g. (150,350), (200,400) and (175,440) (closer detail given in Figure 5.25, Figure 5.26 and Figure 5.27). This shows that the spacing of the turbines has more of an influence than the bed conditions within the TRS as the same effects have been felt at these locations, close to the TRS seawall.

5. Test Case 2 – Impact of Varying Bed Conditions

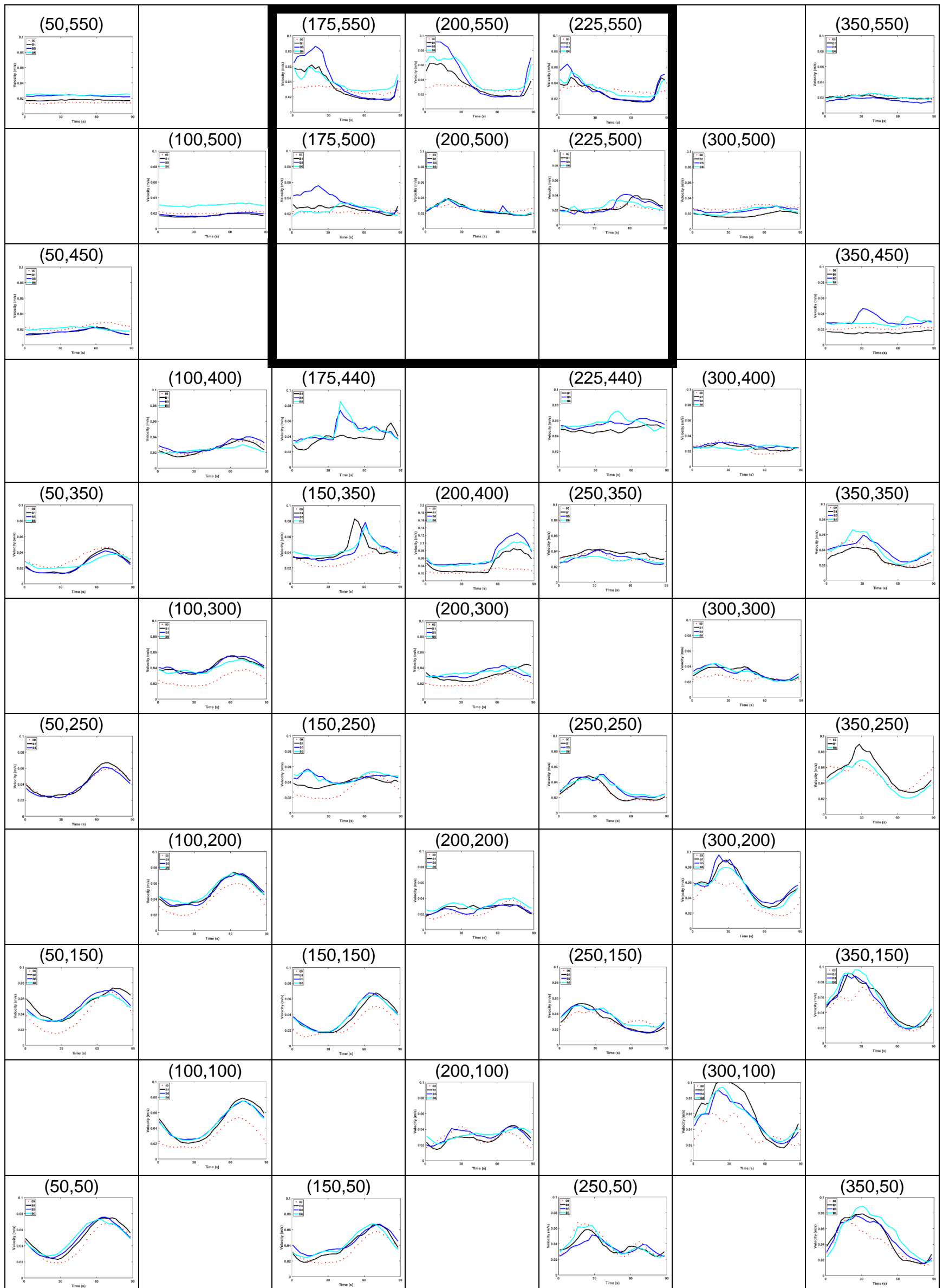


Figure 5.24 Map of depth averaged velocity plots for Comparison E: B1, B5 and B6.

5. Test Case 2 – Impact of Varying Bed Conditions

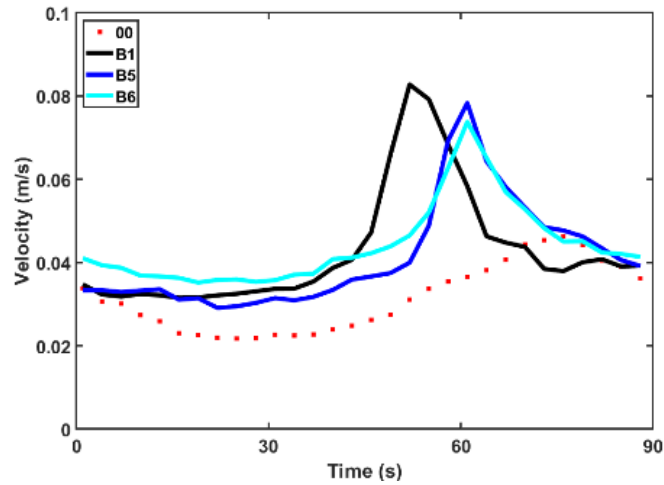


Figure 5.25 Closer detail of velocity at (150,350).

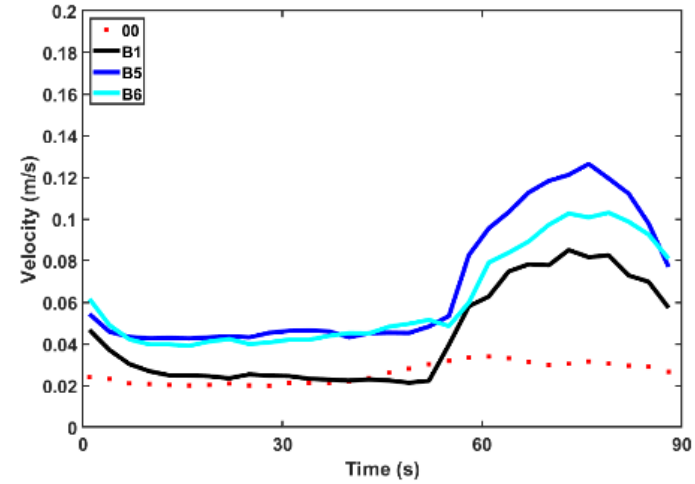


Figure 5.26 Closer detail of velocity at (200,400).

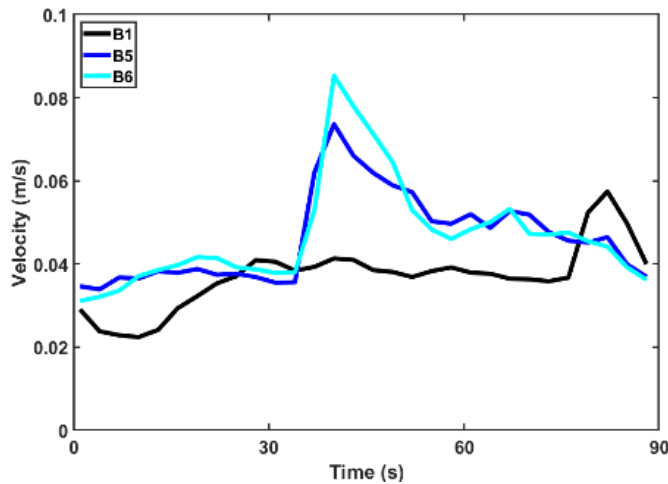


Figure 5.27 Closer detail of velocity at (175,440).

5. Test Case 2 – Impact of Varying Bed Conditions

Inside the TRS flow patterns remain extremely similar between the experiments, especially at (225,500) and (225,550), behind the right-hand turbine (closer detail provided in Figure 5.28 and Figure 5.29 respectively). However, the patterns vary slightly behind the left-hand turbine at (175,500) and (175,550) (Figure 5.32 and Figure 5.33). At these locations it is B5 that has the highest peaks whilst B6 more closely matches B1. This points to the fact that although B5 has a steeper slope the force of the water is able to reach the shallower waters at the rear of the tank to cause faster flows. Following this idea, B6 should have faster flows than B1 in these locations too as the water is shallower here than for the smooth bed but this is not the case. This could be due to reflection from the rear of the tank slowing water down in this scenario whereas the flow is fairly even throughout the tank for B1. Point (200,550) (Figure 5.31) owns the greatest variation between the experiments and although they all follow the same shape, B5 has the highest amplitude yet again, whilst B6 this time performs halfway between B1 and B5. This means that for both slopes the water is able to reach the back of the tank and flow faster in this shallower water, whereas velocity is more even across the whole TRS for B1. It is interesting then that there is not such a high peak at (225,550) which has the same water depth as locations (175,550) and (200,550) which both experience peaks. From looking at videos of water filling the TRS before measuring takes place, water from the right-hand cell encroaches and converges with the left-hand cell more often than the left-hand cell encroaches on the right, this could contribute to an increase in flow velocity and turbulence in the centre and the left-hand side of the TRS as demonstrated by the steeper peaks in these locations.

5. Test Case 2 – Impact of Varying Bed Conditions

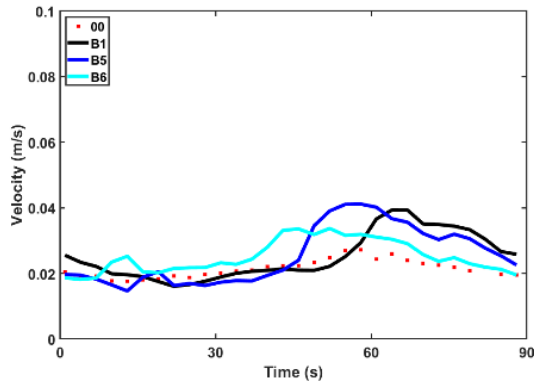


Figure 5.28 Closer detail of velocity at (225,500).

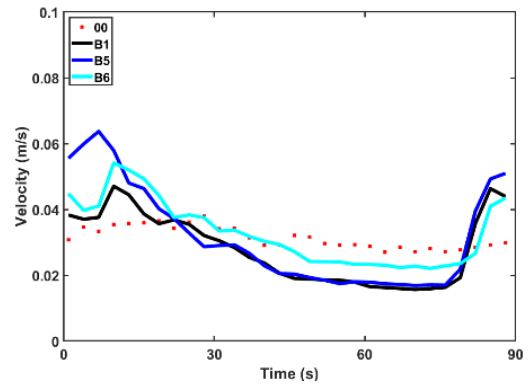


Figure 5.29 Closer detail of velocity at (225,550).

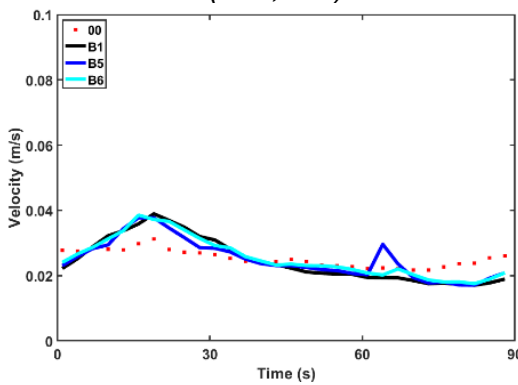


Figure 5.30 Closer detail of velocity at (200,500).

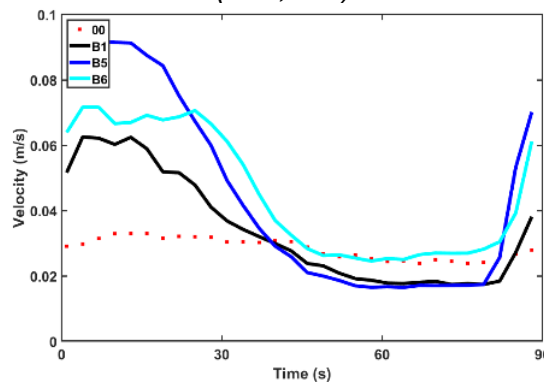


Figure 5.31 Closer detail of velocity at (200,550).

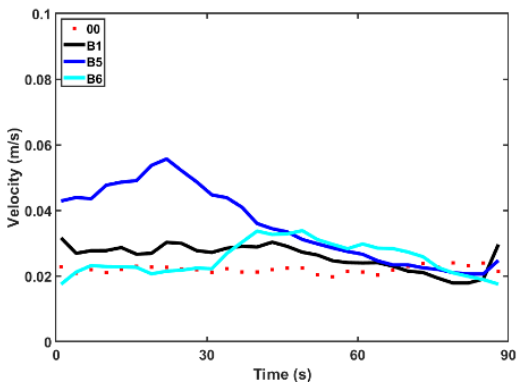


Figure 5.32 Closer detail of velocity at (175,500).

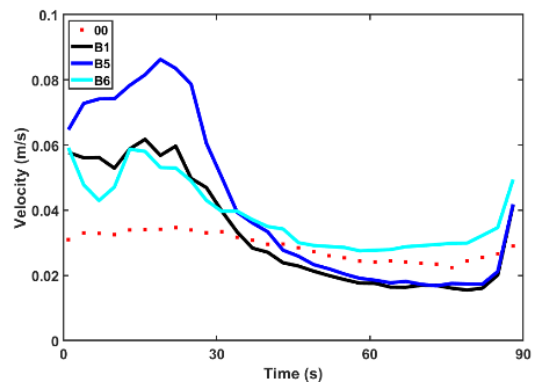


Figure 5.33 Closer detail of velocity at (175,550).

5. Test Case 2 – Impact of Varying Bed Conditions

5.2.2.2 Velocity – Analysed by tide and depth

The flow velocity patterns in the outer tank during the ebb tide look very similar for all scenarios at almost every depth (see Figure 5.34). This implies that the gradient of the bed does not have a significant impact on flows outside of the TRS. However, the velocity patterns do deviate widely inside the TRS. Experiment B6 has a clear symmetrical pattern close to the bed, which is also somewhat evident at the bottom layer of B1. However, this pattern weakens towards the surface suggesting that the flow through these equally spaced turbines is not particularly strong further away from the orifices. Flow within B5 follows a more linear pattern at the bed but again displays no particularly strong flow further up the water column during the tide. These differences prove that the bed slope has had an impact on flow velocity inside the TRS. During the ebb tide we would expect the force of the water leaving the TRS to be equal, with the strongest force being gravity as water flows from the top of the slope down towards the turbine openings. This idea is supported by Sang-Ho et al. (2016) who found that sloped beds increase discharge efficiency through sluices. This would support the image of a linear pattern, as in B5, or a symmetrical pattern, as displayed in B6, but does not explain the irregular pattern of B1.

During low tide there are still great similarities between the experiments at all depths (Figure 5.35). This could be due to the slack water allowing forces to equalise across the tank and further demonstrates the lack of impact of bed slope in the outer tank. Inside the TRS, flow is much more symmetrical in all of the experiments than during the ebb tide which shows that water to circulate is able to circulate evenly within the TRS in all cases. The most unusual velocity patterns can be seen at an elevation of 200 mm from the bed. This was noted as a critical depth in Comparison A, where the 3D component of the turbine wakes diminished and seems also to be the important here. In the case of the 10° slope, an elevation of 200 mm corresponds to the top of the inclined bed, whilst it is exactly double the height of the 5° slope. This would justify the irregular patterns at this level in experiments B5 and B6 where the water shallows and slows.

5. Test Case 2 – Impact of Varying Bed Conditions

The velocity patterns outside the TRS are once again very similar for all experiments at all depths during the flood tide (Figure 5.36), and there is greater symmetry of flow inside the TRS at certain depths. Inside the TRS, flow is most irregular closer to the bed in experiment B5. This would suggest that the steeper bed inhibits even circulation as water fights to reach the top of the slope. However, water is flowing more evenly through the turbine openings in B1 above an elevation of 150 mm, and at all elevations in B6. This indicates that the flood dominant tide is able to overcome irregularities caused by asymmetry in the tank to circulate in an even pattern higher up the water column.

At high tide, the flow velocity outside of the TRS remains similar for all experiments at all depths (Figure 5.37). Inside the TRS, flow is much slower, as expected during high tide, but there is still some symmetry evident in B5 and B6 which suggests that during slack water forces are more equal, as at low tide. 200 mm remains the critical depth, with extremely similar patterns displayed at this layer for every phase of the tide, showing how the sloped bed has a greater impact closer to the surface than the bed.

5. Test Case 2 – Impact of Varying Bed Conditions

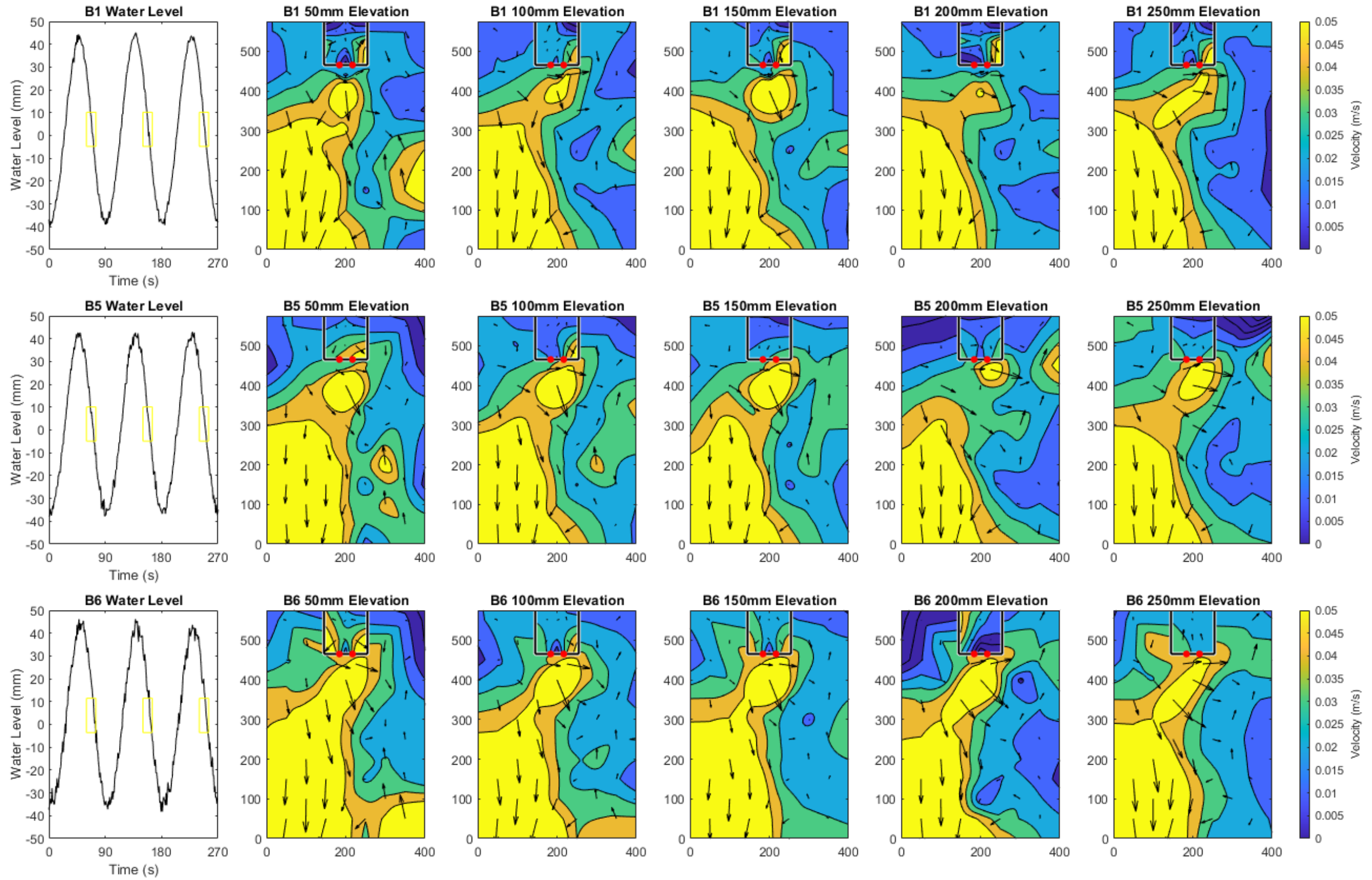


Figure 5.34 Comparison E – Velocity contour maps at elevations of 50, 100, 150, 200 and 250 mm above the bed during the ebb tide.

5. Test Case 2 – Impact of Varying Bed Conditions

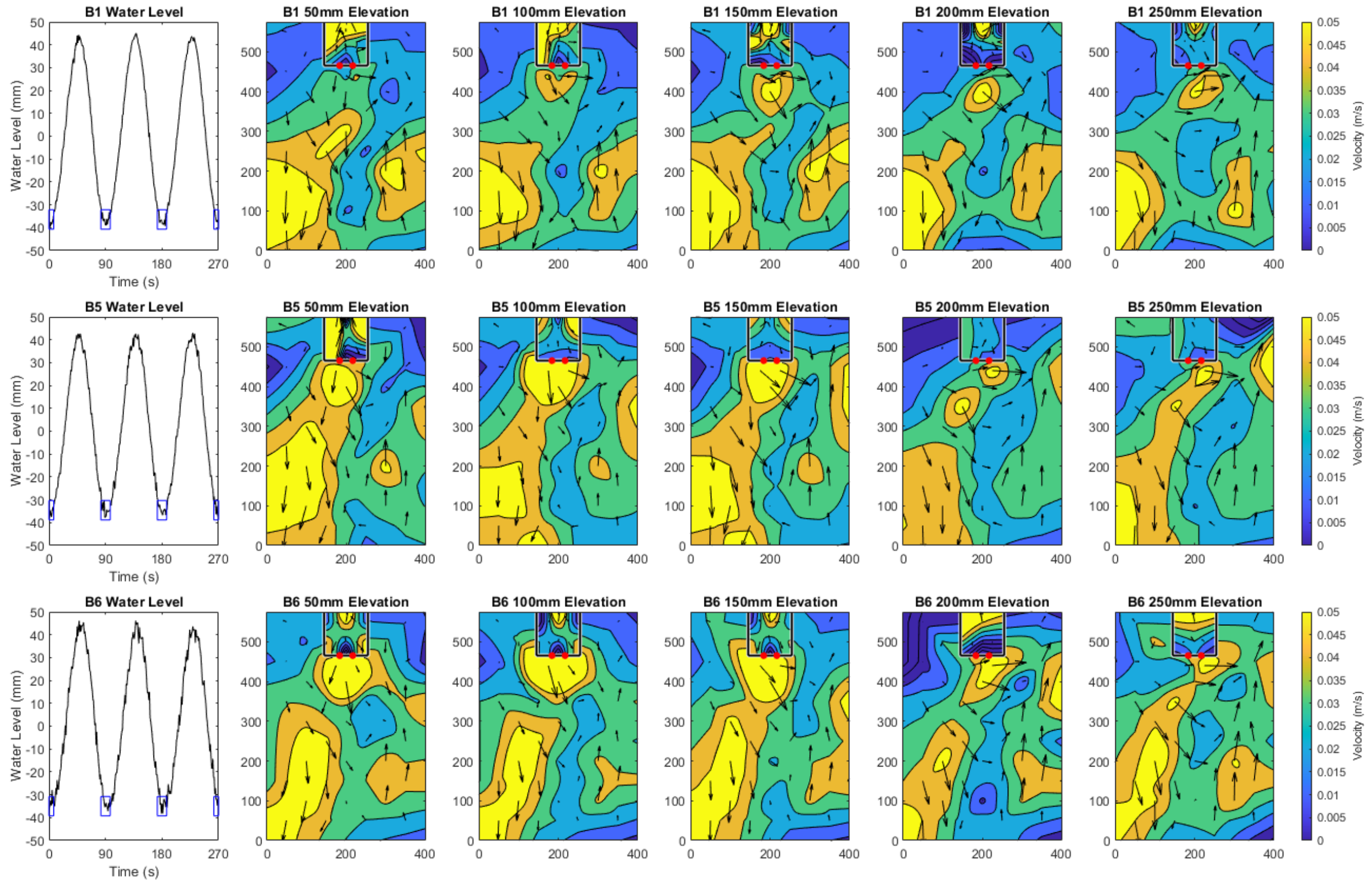


Figure 5.35 Comparison E – Velocity contour maps at elevations of 50, 100, 150, 200 and 250 mm above the bed during low tide.

5. Test Case 2 – Impact of Varying Bed Conditions

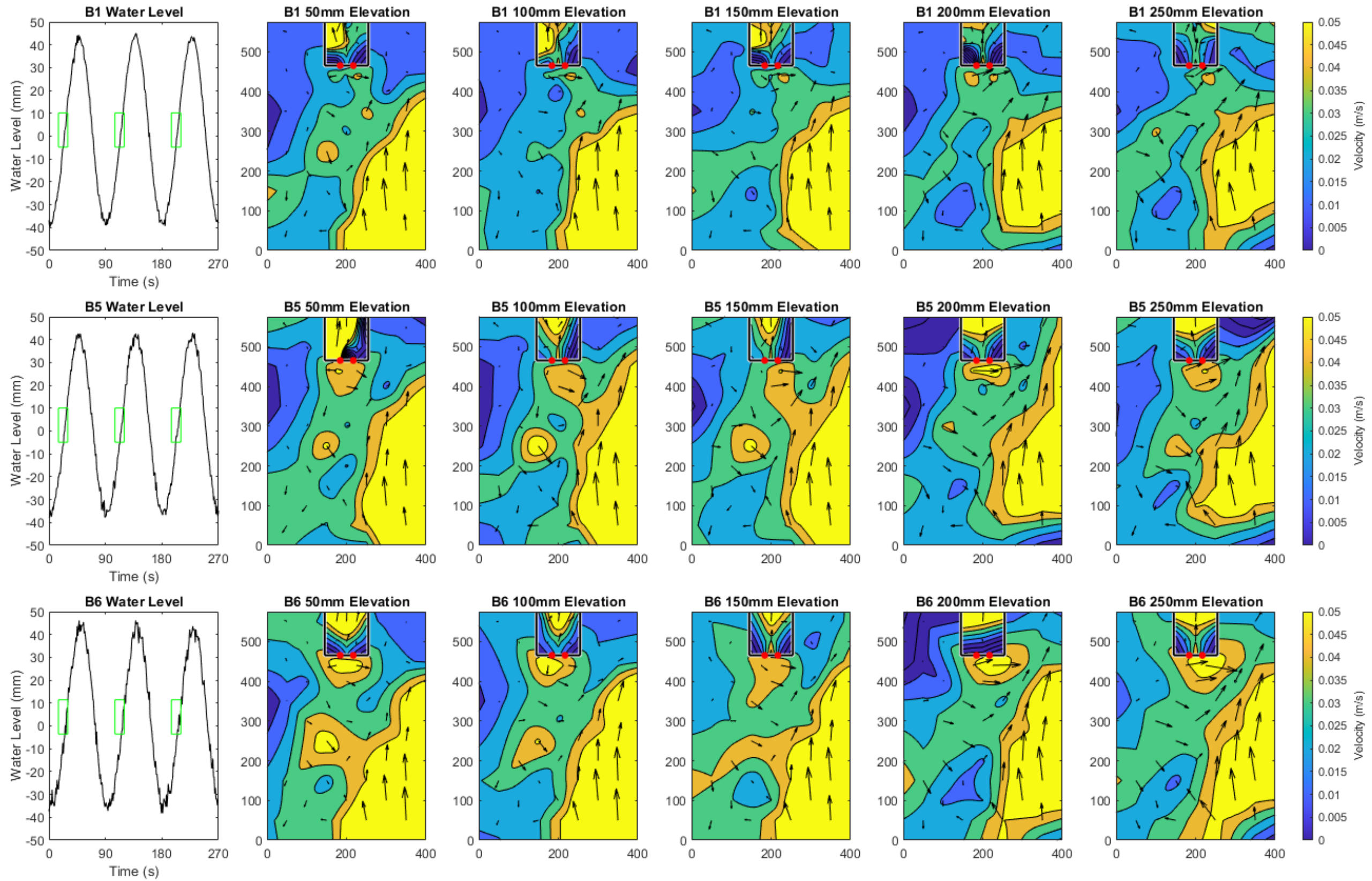


Figure 5.36 Comparison E – Velocity contour maps at elevations of 50, 100, 150, 200 and 250 mm above the bed during the flood tide.

5. Test Case 2 – Impact of Varying Bed Conditions

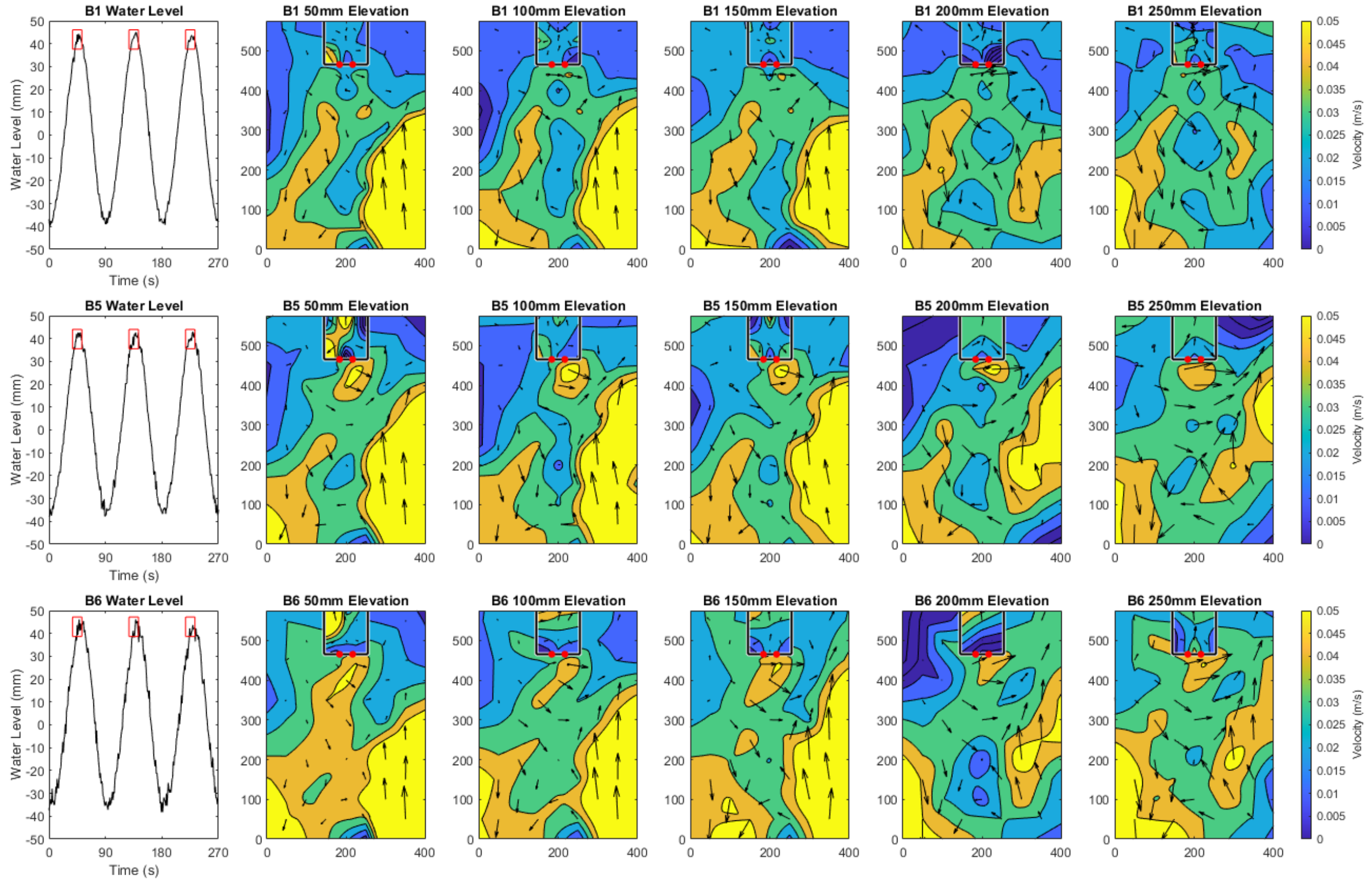


Figure 5.37 Comparison E – Velocity contour maps at elevations of 50, 100, 150, 200 and 250 mm above the bed during high tide.

5. Test Case 2 – Impact of Varying Bed Conditions

5.2.2.3 Velocity – Residual Velocity Magnitude and Direction

Contour plots of the residual velocity magnitude in the tank, presented in Figure 5.38, highlight the similarity of these three experiments (With areas of strong positive flow directly in front of the two turbine openings and near symmetrical flow throughout the tank. This shows that it is not just the equal spacing of the turbines that distributes flow velocity equally around the tank, but the presence of a slope also helps balance out forces, and that whilst the underlying current in the tank circulates anti-clockwise, the equal turbine spacing, and inclined slope have helped to balance out its effects. Inside the TRS B6 displays the greatest symmetry and even pattern of velocity, up to a depth of 200 mm, whilst B1 and B5 have more irregular patterns that change at every depth. This could be due to the steeper slope of B5 forcing water to roll back onto itself, thus disrupting any regular pattern, whilst for the flat bed it could be caused by deeper water prohibiting strong circulation cells from forming. In their study of TRS sluices, Sang-Ho et al. (2016) found that increased slope created better discharge performance than a flat bed and a 1:5 ratio slope was best. Although they concluded that the impact of varying bed slope was insignificant compared to altering the sluice width.

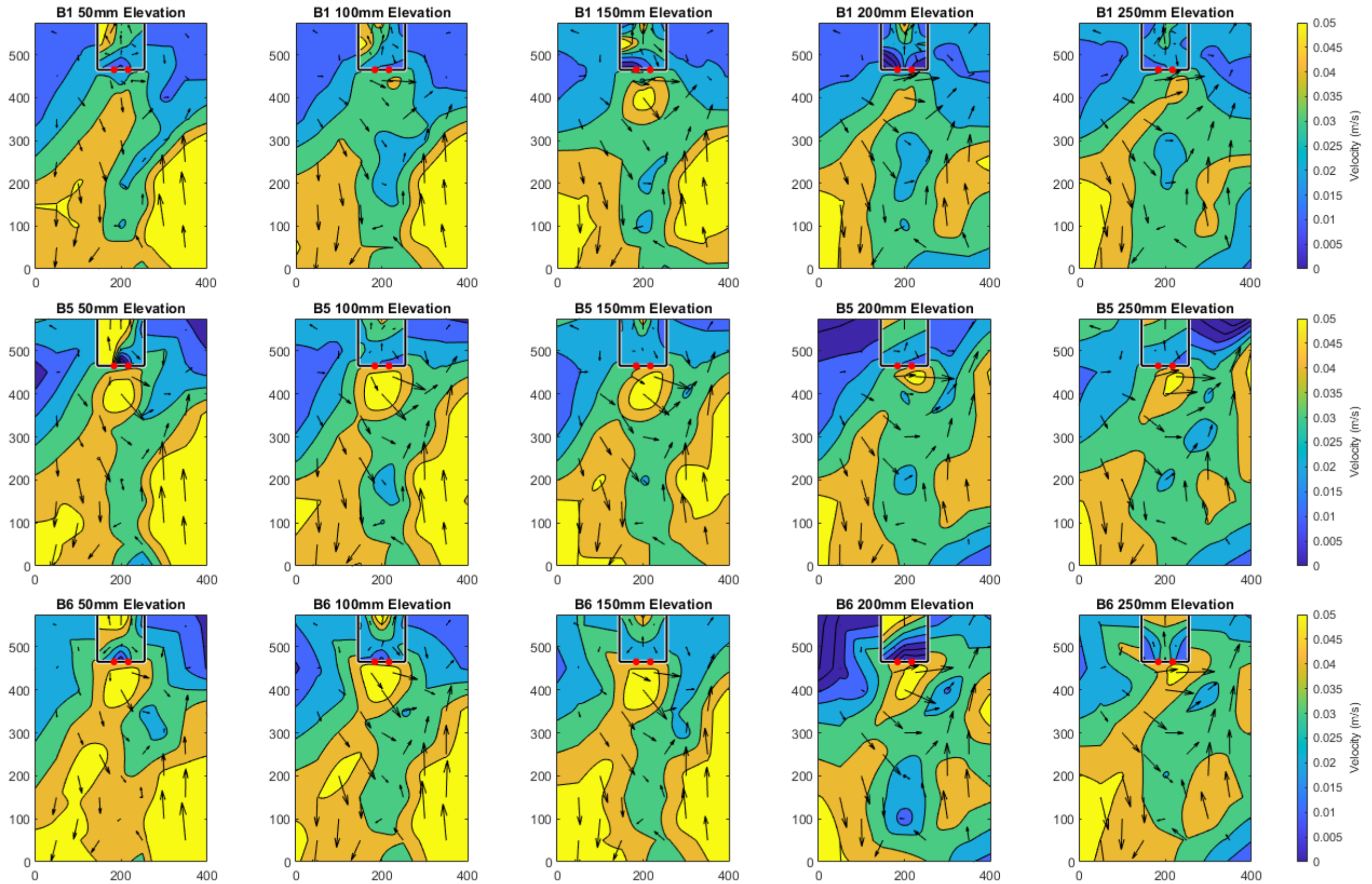


Figure 5.38 Comparison E – Contour maps of residual velocity magnitude and direction at elevations of 50, 100, 150, 200 and 200 mm from the bed.

5. Test Case 2 – Impact of Varying Bed Conditions

5.2.2.4 Flow Visualisation

To understand the effects of bathymetry on internal TRS flows, Vouriot et al. (2018) introduced a 1:50 slope from their inlet to the “coast”. (Although much shallower than the slopes investigated in the present study, this more closely represents the natural variation in bed geometry found around the Welsh coast. The present exaggerated slopes were tested to gain a distinct picture of the behaviour of TRS flows with steep beds.) They found that vortex dissipation was significantly influenced by sloping bathymetry due to bed shear stress, and so vortices last longer in deeper waters but dissipate more quickly with increased bed shear stress closer to the coast. Images of flow visualisation for experiments B5 and B6 are not clear enough to reproduce here but videos of dye circulating inside both TRSs reveal identical counter-rotating cells as in B1. Dipoles in B1 continue to rotate from the back to the front of the tank (see the plume tracks presented in Figure 5.39).

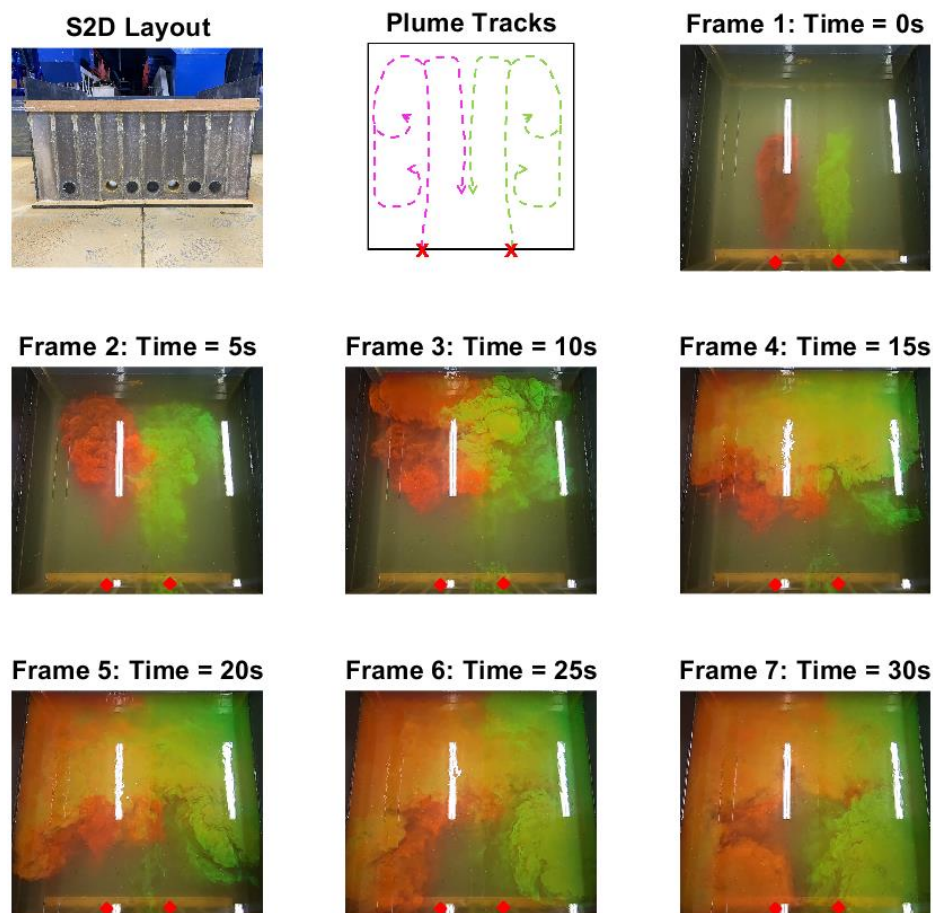


Figure 5.39 Flow visualisation for experiment B1.

5. Test Case 2 – Impact of Varying Bed Conditions

5.2.2.5 Statistical Analysis

In comparing the results of B5 and B6 against B1 as a baseline case, the similarities of both are evident for both residual flow magnitude (Figure 5.40) and direction (Figure 5.42). Histograms of these results also show how little the experiments vary from baseline conditions (Figure 5.41 and Figure 5.43), confirming that the bed slope introduced inside the TRS has not made a significant difference to overall flow in the tank. The 10° and 5° bed slopes have increased flow velocity slightly by 7% and 9% respectively, but in both cases the z-test results (see Table 5.3) lead us to accept the null hypothesis, that bed slope does not cause a significant difference to natural velocity conditions.

Table 5.3 Comparison E - Statistical analysis of residual velocity magnitude of B5 and B6 compared to B1.

Comparison	\bar{x} (m/s)	SD	RMSE	r	z	Accept /Reject h_0
B1	0.03506	0.01142				
B5	0.03776	0.01170	0.00597	0.86355	-0.17006	Accept
B6	0.03844	0.01093	0.00614	0.88430	-1.39673	Accept

5. Test Case 2 – Impact of Varying Bed Conditions

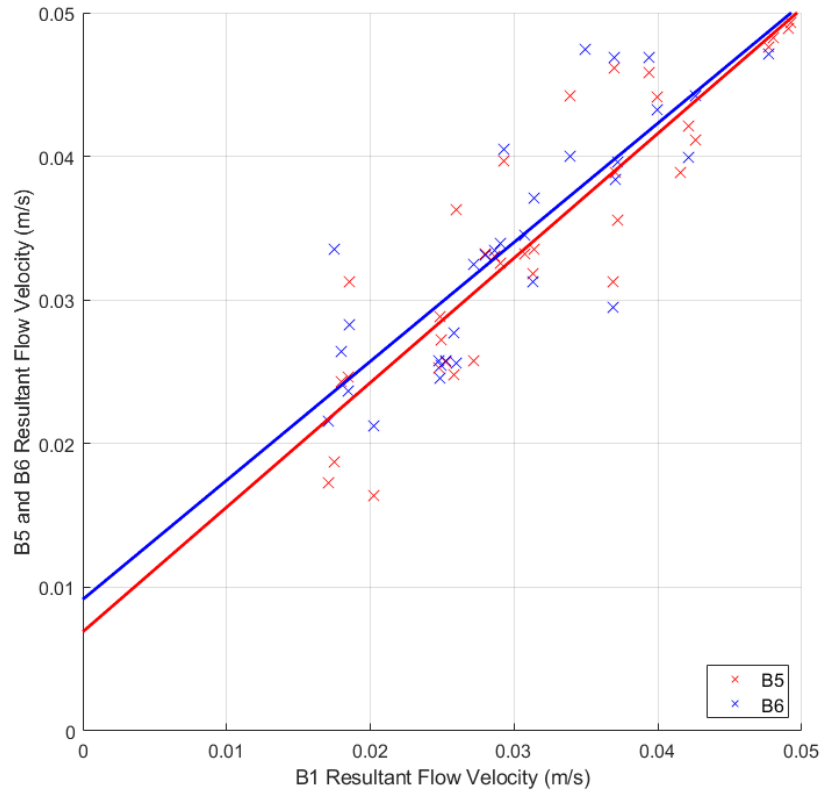


Figure 5.40 Comparison E - Regression analysis of residual flow velocity.

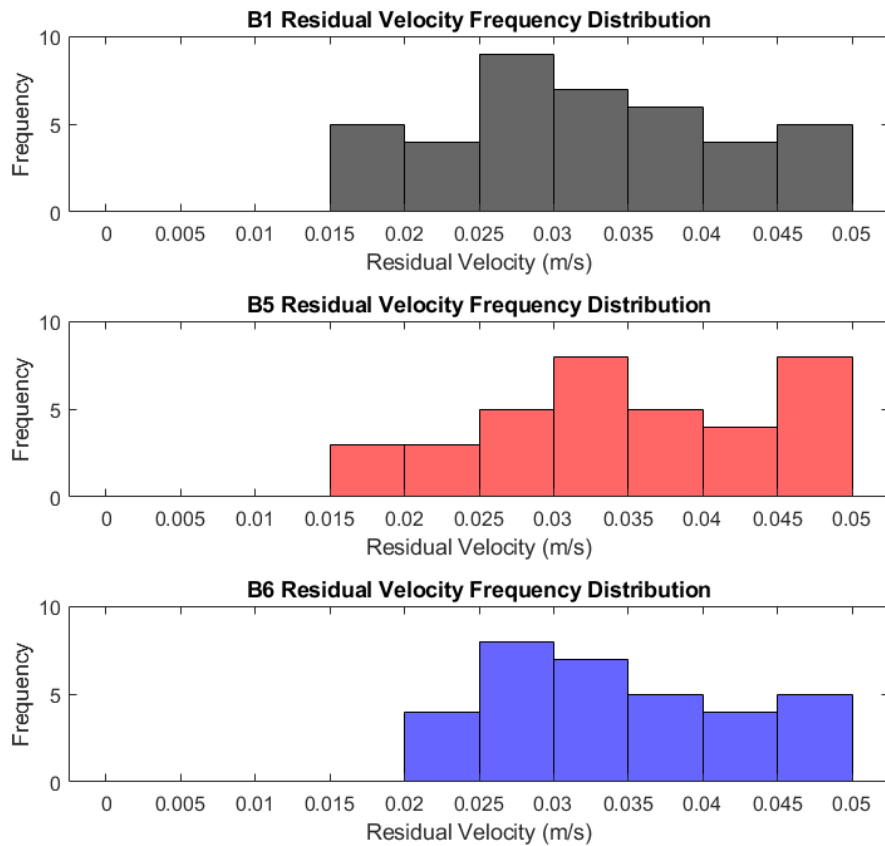


Figure 5.41 Comparison E – Distribution analysis of residual flow velocity.

5. Test Case 2 – Impact of Varying Bed Conditions

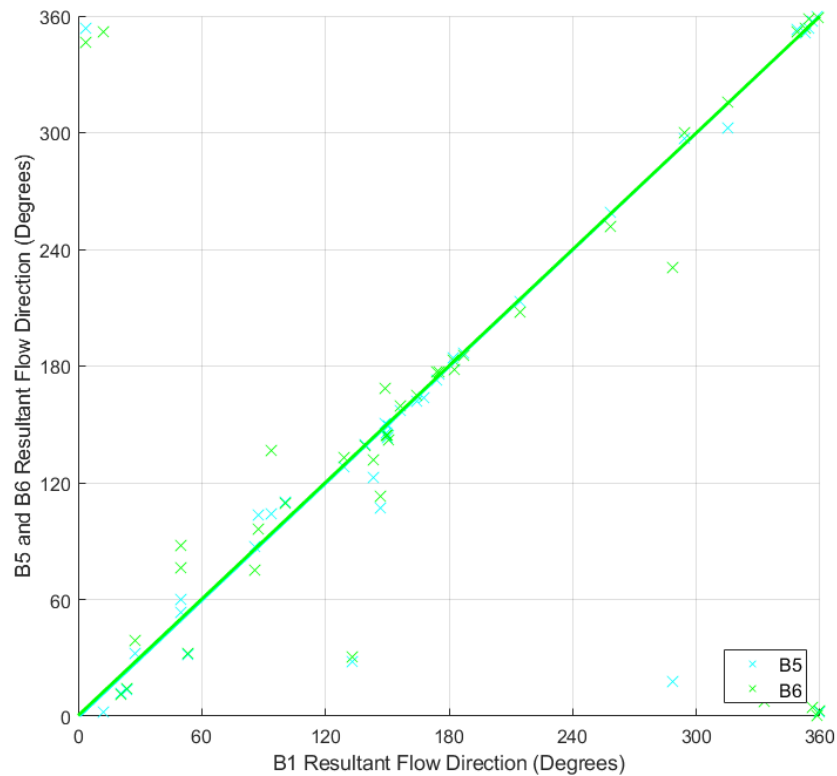


Figure 5.42 Comparison E - Regression analysis of residual flow direction.

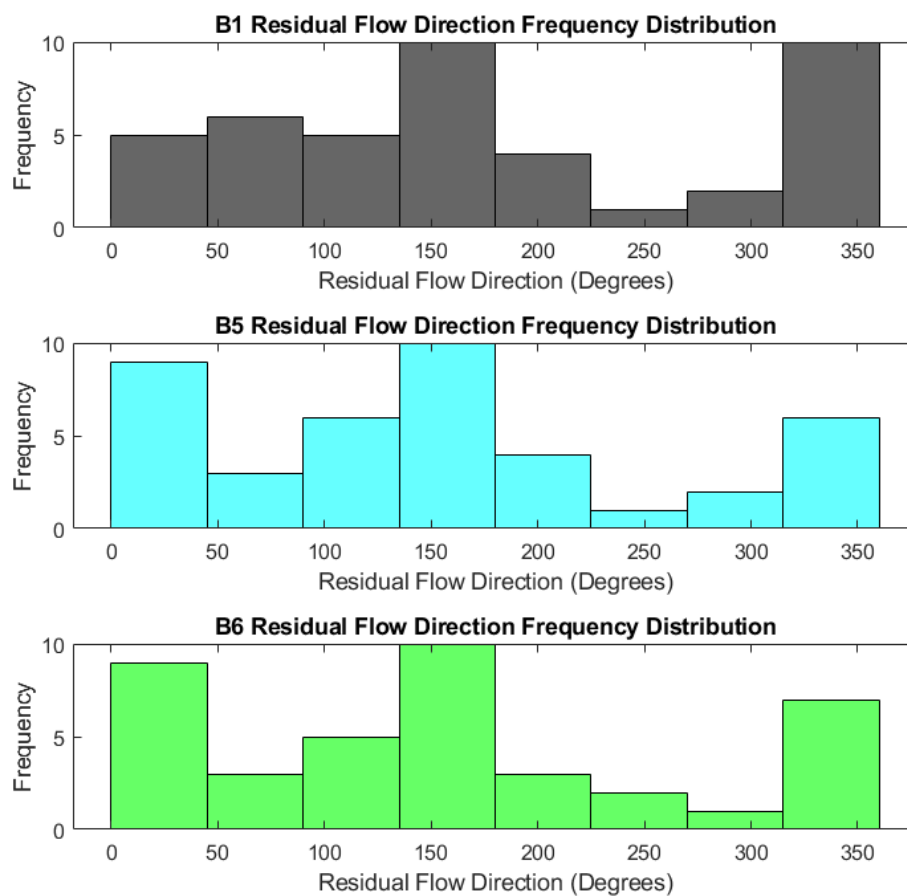


Figure 5.43 Comparison E – Distribution analysis of residual flow direction.

5.3 Summary

Chapter 5 is concerned with the effects of altering conditions within TRSs and how this impacts flow behaviour. Whilst the laboratory experiments have simplified parameters to test idealised conditions, bathymetry in the natural environment will vary in terms of slope and material.

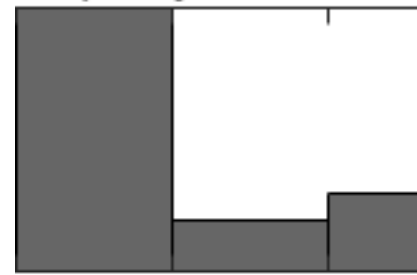
Comparison D tested three different bed materials: artificial grass, coarse gravel (20 mm) and fine gravel (10 mm), to model various seabed conditions. The spacing of two turbine openings remained constant throughout these experiments and very little deviation was found outside the TRS, showing that bed material did not cause significant alteration to far field flow. Inside the TRS flow velocities and circulation patterns were very similar for all of the cases but the greatest difference was observed on the ebb tide which suggests that bed material and its residual flow resistance has a greater effect on outflowing than inflowing water. This will have an impact on power output which is commonly generated on the ebb tide. Overall, the artificial grass caused the least disruption to baseline conditions due to its flexibility whilst both sizes of gravel caused slightly irregular flow patterns within the TRS. In terms of future TRS design this could lead to developers considering the dredging/removal of coarser material in areas with a naturally rough seabed or the planting of seagrass to support submarine habitats.

Comparison E altered the slope of the seabed to model the natural gradient of coastal sites. Experiment B1 maintained a flat bed in contrast to experiments B5 and B6 with angled slopes of 10° and 5° respectively. Changes to the internal slope of the TRS were found to have little effect on far field velocity. Inside the TRS, the steeper slope (B5) was found to increase flow velocity which is thought to be due to reflection from the rear wall of the tank where flows are increased in shallow water. Therefore, TRS design must consider the proximity of the shoreline and the seabed gradient of a site in order to prevent exaggerated reflection off the coast which can lead to erosion. Overall, the null hypothesis was accepted in all cases, that bed conditions did not significantly alter flow velocity in the experiments conducted here.

Chapter 6

Test Case 3 – Impact of Varying Geometry

Frequency Distribution



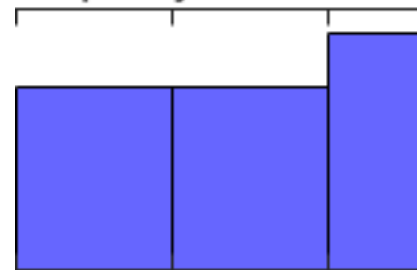
125
0.03 0.035
Velocity (m/s)

Frequency Distribution



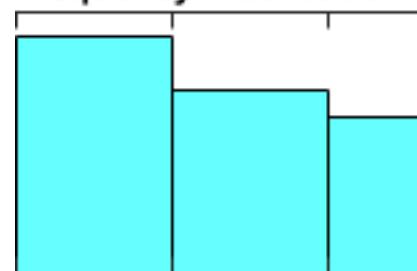
125
0.03 0.035
Velocity (m/s)

Frequency Distribution



125
0.03 0.035
Velocity (m/s)

Frequency Distribution



125
0.03 0.035
Velocity (m/s)

6 Test Case 3 – Impact of varying geometry

6.1 Introduction

Another consideration for the design of a TRS is its overall shape, proportion and seawall length. It has been shown that varying the length-to-width ratio of a harbour wall can affect hydrodynamics (Falconer, 1974) and it is to be expected that a TRS would have a similar impact. Therefore, it is important to investigate the effects of varying the TRS geometry on hydrodynamics.

These experiments were designed to compare similar conditions in a square and rectangular lagoon, maintaining a constant area but varying the length-to-width ratio of the seawall from 1:1 to 2:1. Different turbine layouts were then tested in each of the two shapes to be able to directly compare the flow regime under the given conditions (see Table 6.1). Bed material and bed slope were kept constant with smooth, flat beds examined in all experiments. Four scenarios were investigated for both the square and rectangular cases varying the number and layout of the turbines to try to match similar cases.

Table 6.1 Turbine layout for test configuration of square and rectangular case. Numbers 1 to 14 represent box section number.

Square TRS			Turbine Position													
Case	Shape	Turb.		1	2	3	4	5	6	7	8	9	10			
S0	Square	0														
S1A	Square	1										X				
S2A	Square	2									X	X				
S2B	Square	2		X								X				
Rectangular TRS			Turbine Position													
Case	Shape	Turb.	1	2	3	4	5	6	7	8	9	10	11	12	13	14
R0	Rectangle	0														
R1	Rectangle	1													X	
R2A	Rectangle	2												X	X	
R2D	Rectangle	2		X											X	

6. Test Case 3 – Impact of Varying Geometry

- Comparison F i: compares the closed lagoons for both geometries (S0 vs R0).
- Comparison F ii: looks at a single turbine in each lagoon close to the right-hand side wall (S1A vs R1).
- Comparison F iii: examines two turbines positioned next to each other (S2A vs R2A).
- Comparison F iv: compares two turbines placed at opposite ends of the seawall (S2B vs R2D).

Analysis of results from these experiments will help to answer the question: “to what extent does TRS geometry affect hydrodynamics?” and test the following hypotheses:

h_0 : There is no significant difference experienced in velocity by changing tidal lagoon geometry.

h_1 : Changing tidal lagoon geometry causes significant difference to velocity profiles.

6. Test Case 3 – Impact of Varying Geometry

6.2 Results

6.2.1 Comparison F i – Square vs Rectangular TRS with 0 turbines

Comparison F i compares results from experiments with a square (S0) and rectangular (R0) TRS, both without turbines (Figure 6.1), against pre-lagoon conditions to investigate the effects of TRS geometry on hydrodynamics.

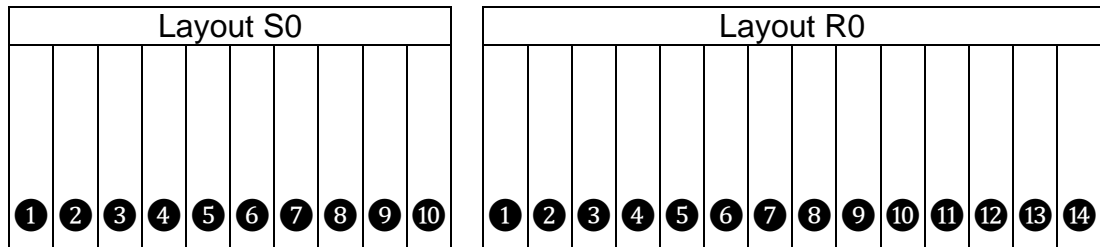


Figure 6.1 Experient layouts for Comparison F i: S0 and R0.

6.2.1.1 Velocity - Depth Averaged

The depth averaged velocity graphs of experiments S0 and R0 presented in Figure 6.5 reveal extremely interesting patterns. Although both cases demonstrate velocity waves with highly similar shapes and amplitude throughout the tank, it is the range of these values that deviate more widely with R0 displaying consistently higher flow velocities than S0. Whilst both experiments closely follow the pattern of the pre-lagoon conditions at most locations, results for R0 can exceed those of S0 by between 0.005 and 0.04 m/s, a variation of up to 50% of the flow velocity. Results are much closer to the rear of the tank and around the TRS seawalls showing how the presence of an obstruction affects flow to the same extent regardless of the shape and size of the structure. The greatest variation occurs at points (100,400) and (200,400) (closer detail given in Figure 6.2 and Figure 6.3 respectively), where results from R0 more closely follow those of the pre-lagoon case whilst S0 has increased flow velocity. This is to be expected due to the proximity to the front of the seawall in the square case where water has been reflected off the solid wall and increased flow along this transect. There is also a great difference in flow pattern at (350,250) (Figure 6.4). At this point R0 continues to follow the pre-lagoon results whilst S0 shows significantly reduced flow velocity. This is unusual since at this distance from the TRS we would not expect to see such a difference nor in such an offset location and therefore may be due to an anomaly.

6. Test Case 3 – Impact of Varying Geometry

When comparing the S0 and R0 results against pre-lagoon conditions it can be seen that the results of both experiments closely match the baseline measurements throughout the tank. This shows that the presence of a TRS (without any openings) does not cause a significant impact to the natural conditions regardless of the shape, a conclusion shared by Ma and Adcock (2020) who, in modelling TRSs in the Severn Estuary, found that a tidal lagoon did not cause significant changes to the large-scale hydrodynamics of the region.

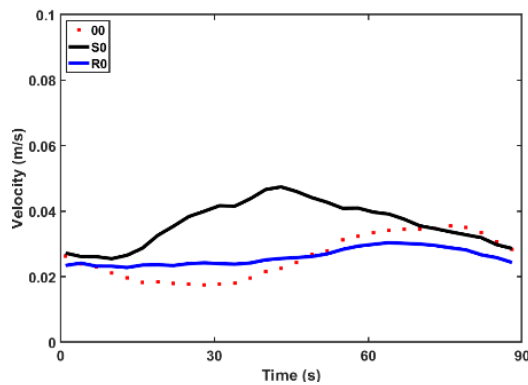


Figure 6.2 Closer detail of flow velocity at (100,400).

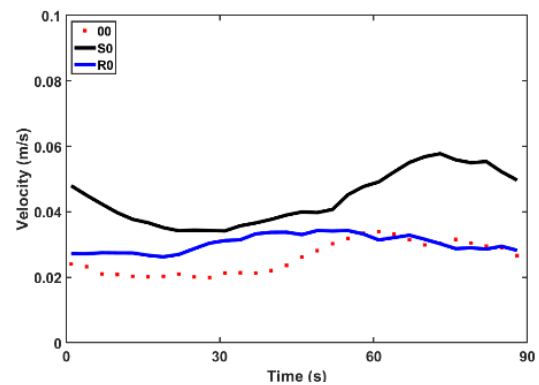


Figure 6.3 Closer detail of flow velocity at (200,400).

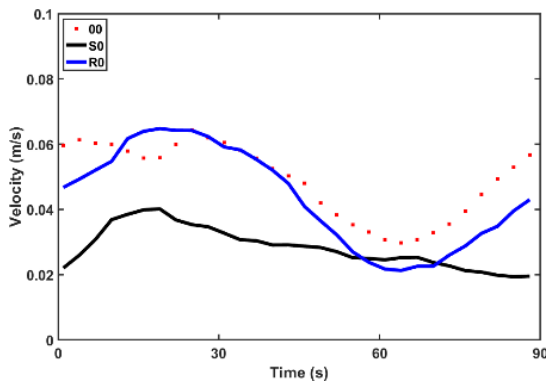


Figure 6.4 Closer detail of flow velocity at (350,250).

6. Test Case 3 – Impact of Varying Geometry

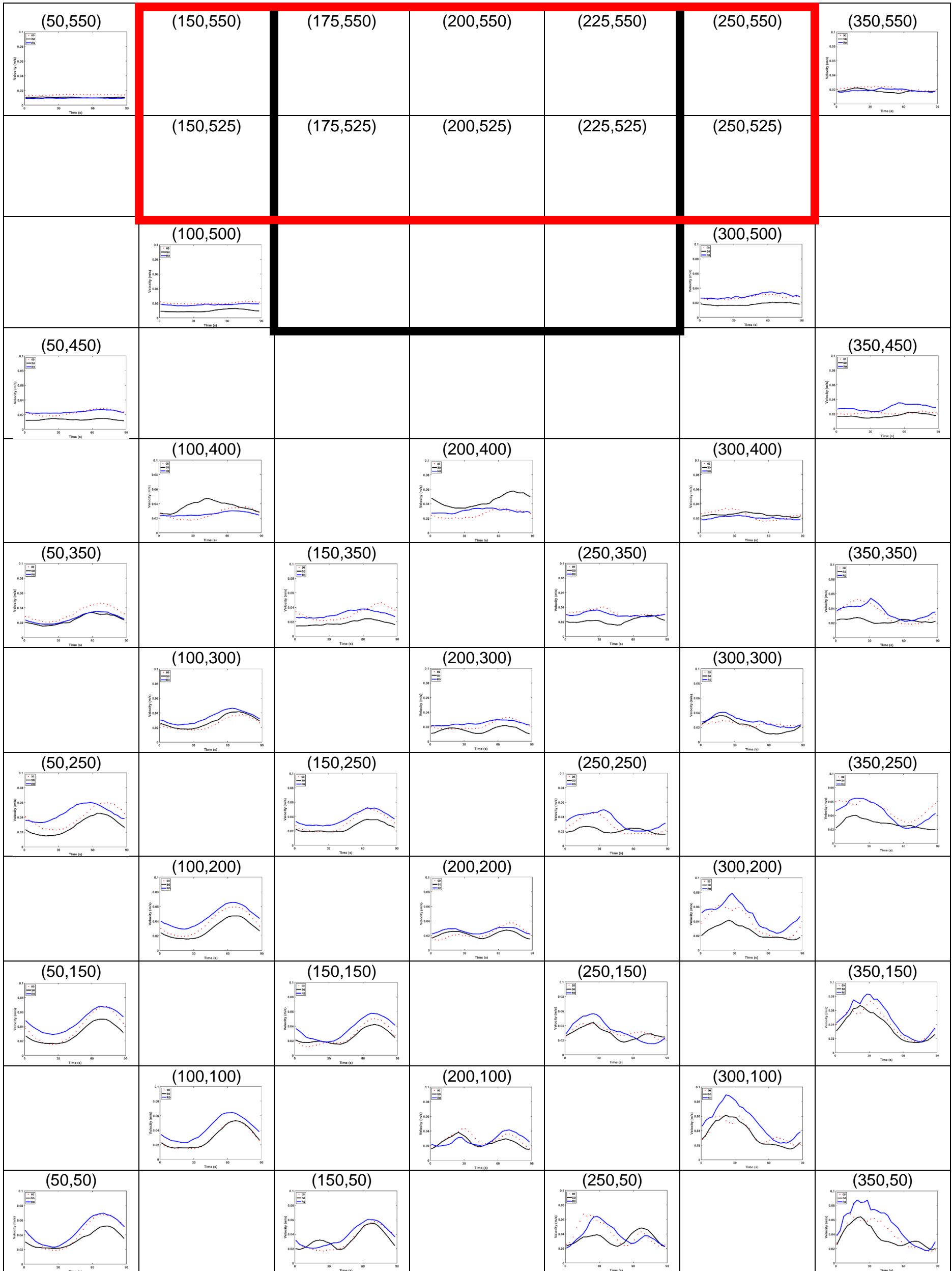


Figure 6.5 Map of depth averaged velocity plots for Comparison F i: S0 and R0.

6. Test Case 3 – Impact of Varying Geometry

6.2.1.2 Velocity – Analysed by tide and depth

Contour plots show very little variation between the depths for the closed TRS cases during the ebb tide and flow patterns are very similar between both S0 and R0 (see Figure 6.6). However, where there is an island of the strongest flow directly in front of the square TRS, there is a more irregular pattern for the rectangular TRS, with stronger flow starting further away from the seawall to the right-hand side of the TRS and migrating to the left. This could be due to the underlying asymmetric flow in the tank leading to stronger flows on the right-hand side in general, but also to the shape of the TRS which forces strong velocities into the rear-right hand corner. However, the similarity between the velocity at each depth suggests that without any turbines flow varies much less throughout the water column and that three-dimensional flow is only instigated by the addition of submerged hydraulic structures.

At low tide there is still little variation between the velocity pattern at each depth which is to be expected as no disruptions have been added to the water column and the seawall causes similar effects at each depth (Figure 6.7). Between the experiments, variation appears once again in the areas of strong velocity which is to be attributed to the narrower square TRS taking up less of the channel width allowing circulation to reach both rear corners of the basin. Whilst the wider rectangular TRS reflects more of the flow off the seawall and into the front half of the basin.

Although there is little variation between the depths of each case during high tide, this tidal phase reveals the greatest variation between S0 and R0 (Figure 6.9). Velocity is slow in S0 which is to be expected during times of slack water, however, water has almost come to a standstill in the centre of the tank. This could be due to forces not being very strong at this point in the tide, but it is not the case in R0, where strong flow is still evident in the front of the tank. It could therefore be due to greater reflection and recirculation occurring in the case of the rectangular TRS. Whereas flow can more easily reach the rear corners of the tank in the case of the square TRS causing energy to be spread over a wider area, thus slowing velocity overall.

6. Test Case 3 – Impact of Varying Geometry

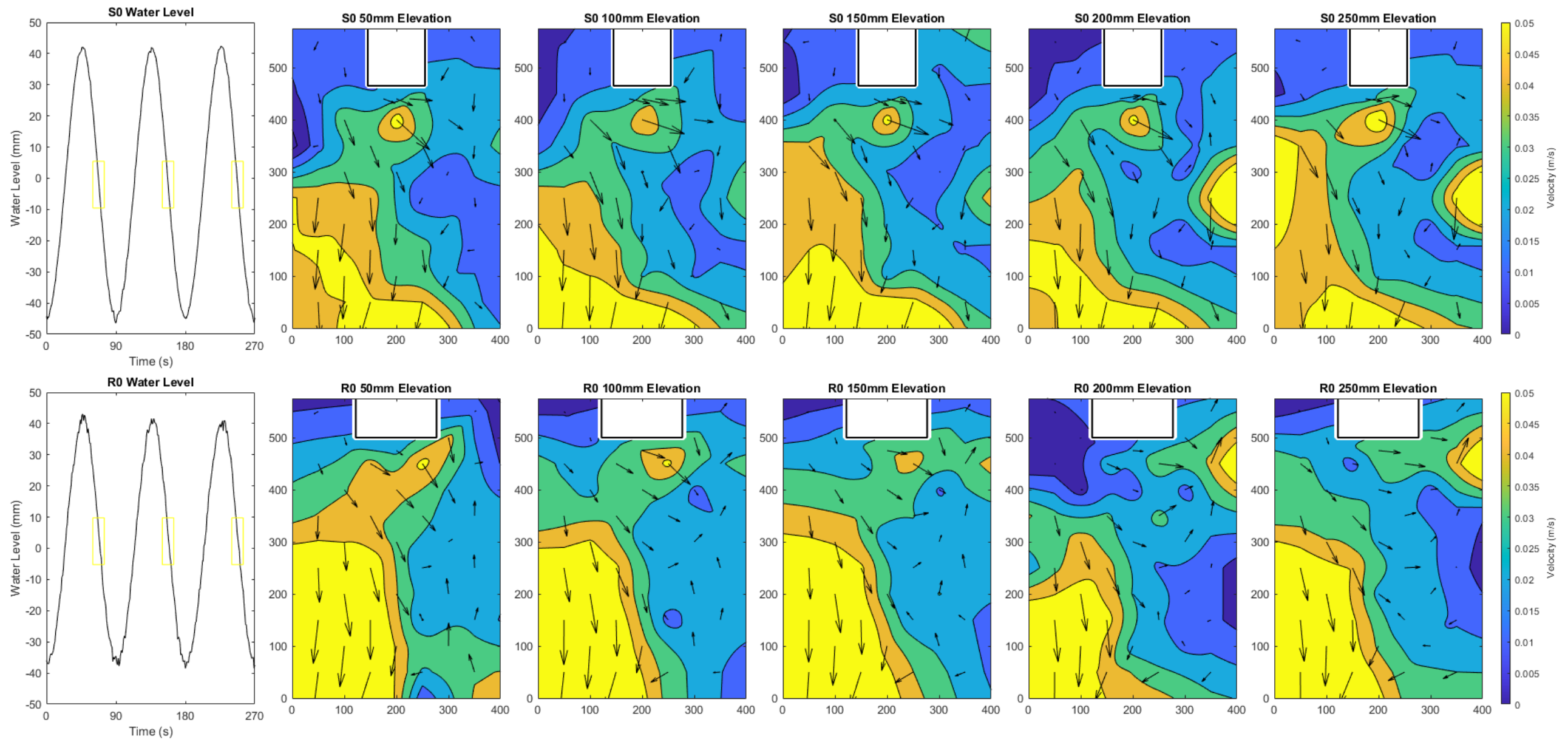


Figure 6.6 Comparison F i - Velocity contour maps at elevations of 50, 100, 150, 200 and 250 mm above the bed during the ebb tide.

6. Test Case 3 – Impact of Varying Geometry

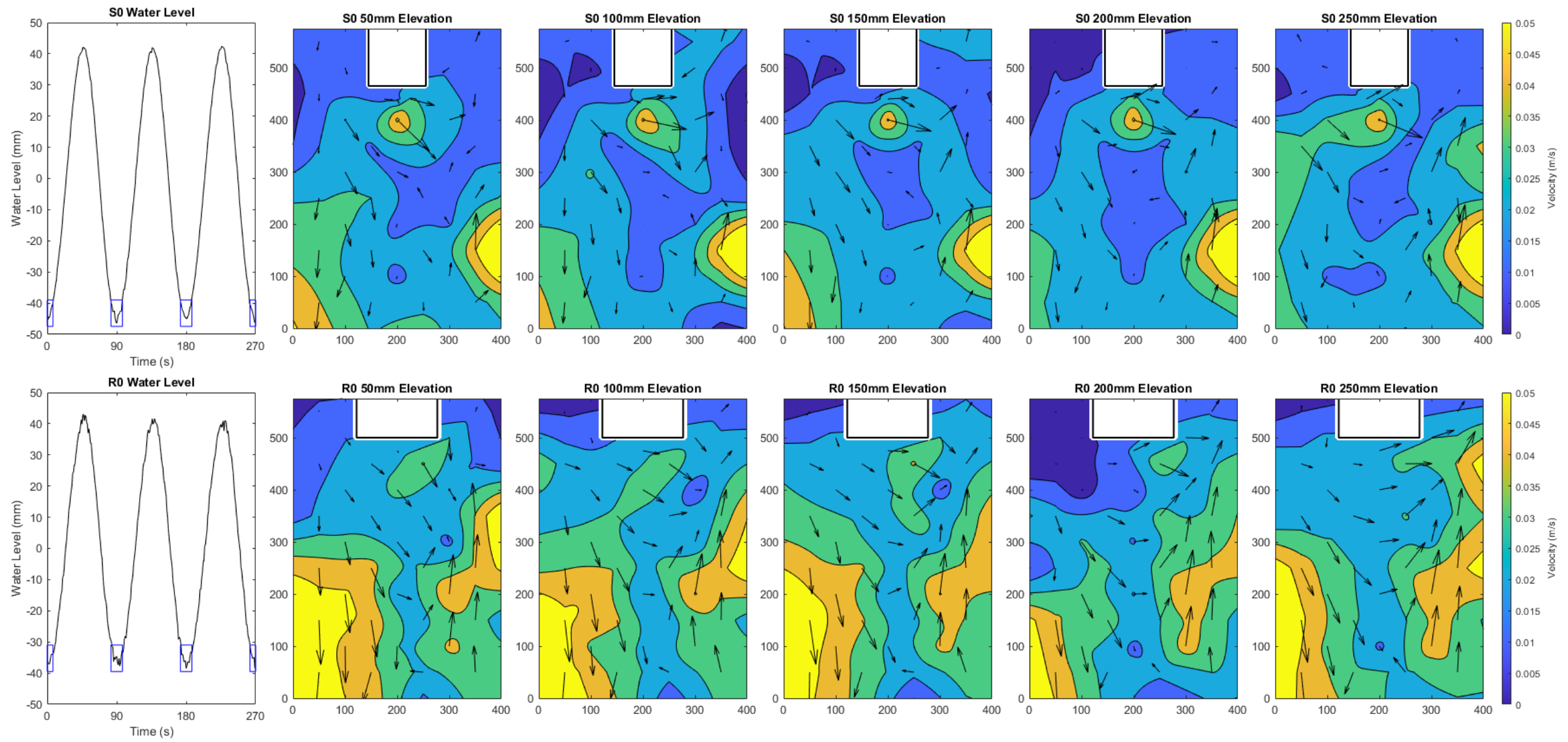


Figure 6.7 Comparison F i - Velocity contour maps at elevations of 50, 100, 150, 200 and 250 mm above the bed during low tide.

6. Test Case 3 – Impact of Varying Geometry

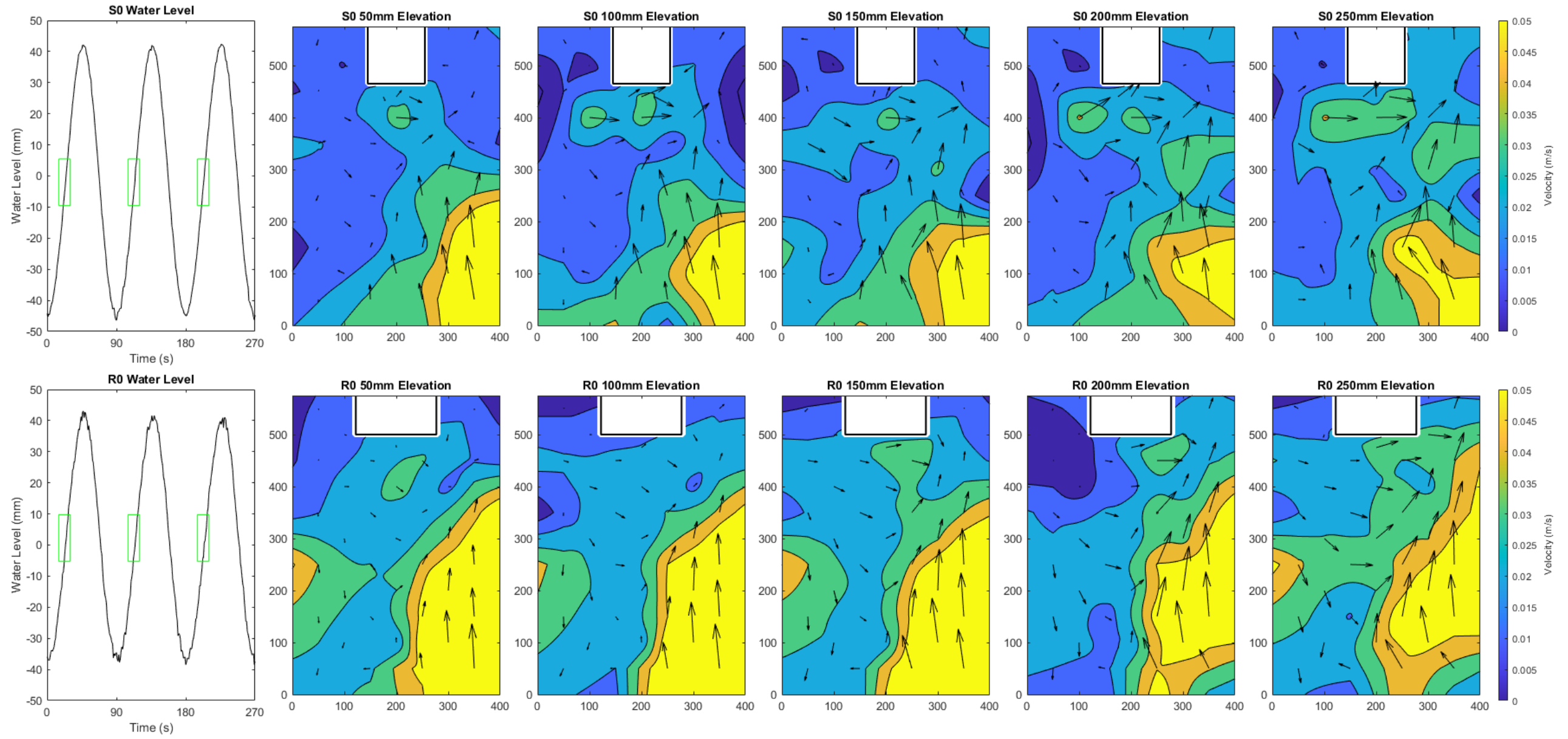


Figure 6.8 Comparison F i - Velocity contour maps at elevations of 50, 100, 150, 200 and 250 mm above the bed during the flood tide.

6. Test Case 3 – Impact of Varying Geometry

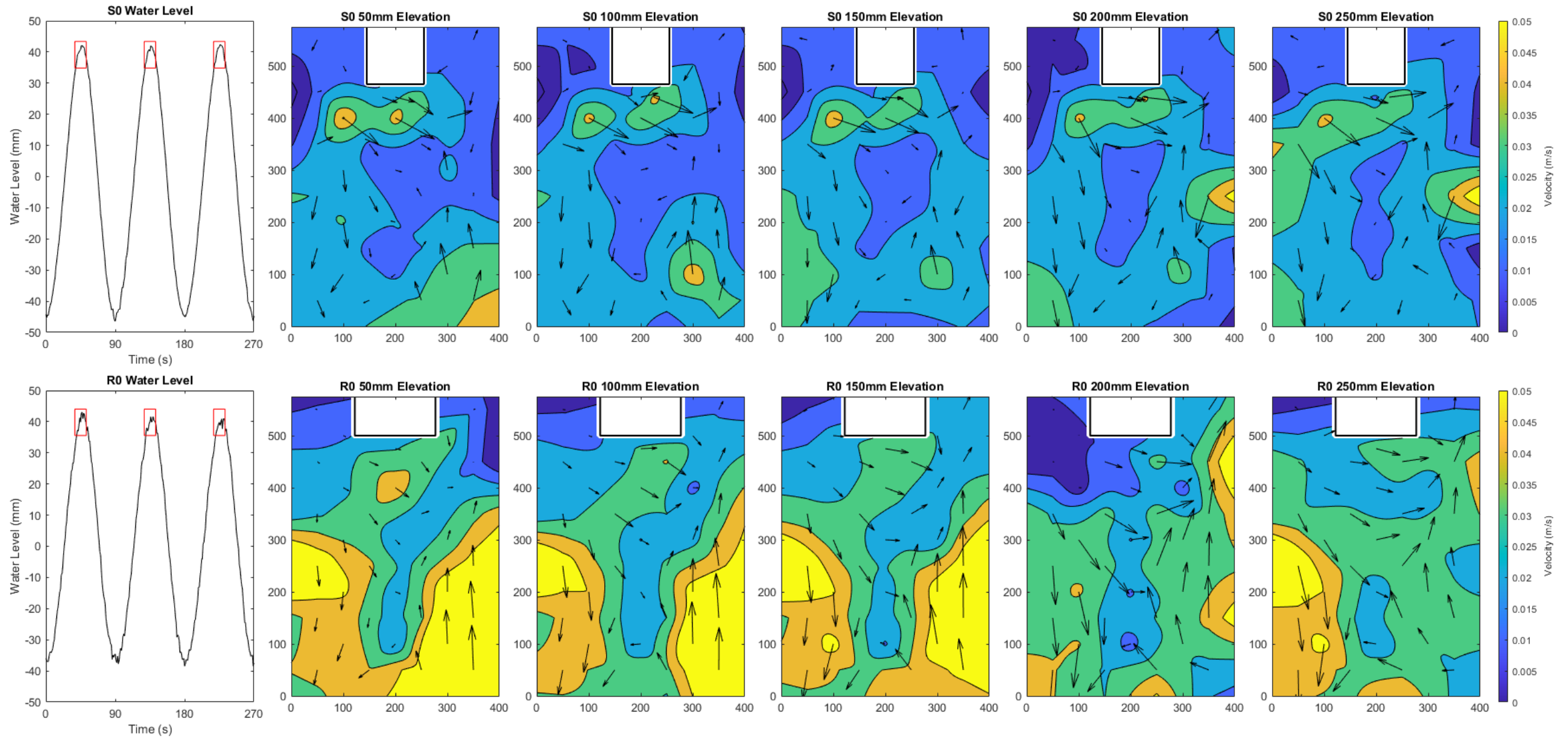


Figure 6.9 Comparison *F i* - Velocity contour maps at elevations of 50, 100, 150, 200 and 250 mm above the bed during high tide.

6. Test Case 3 – Impact of Varying Geometry

6.2.1.3 Velocity – Residual Velocity Magnitude and Direction

Contour plots of the residual magnitude and direction of velocity in the tank for these experiments, presented in Figure 6.10, illustrate how without turbine openings flow is deflected around the TRS walls and funnelled into the rear right-hand corner of the tank regardless of the shape of the structure. In the case of the square TRS there is an island of positive flow directly in front of the TRS which is missing from the rectangular case. This demonstrates how the water is most strongly reflected off the square TRS front wall and circulates more freely around it. Overall, there is a large difference between the square and rectangular TRSs in that flow is much stronger in the rectangular case. This highlights that the presence of the longer seawall causes greater disruption to flow overall whilst the narrower square TRS, despite intruding further into the tank allows greater circulation in the wider area, resulting in weaker currents and slower velocities overall.

6.2.1.4 Flow Visualisation

There is no flow visualisation for the S0 and R0 cases as there is no flow within the TRSs for these sealed box cases. Both TRSs were filled with water manually to ensure equal pressure across the TRS seawall and minimise the chance of leaks, and visual checks, alongside ADV measurements, confirmed there was no water entering or leaving the sealed TRSs.

6. Test Case 3 – Impact of Varying Geometry

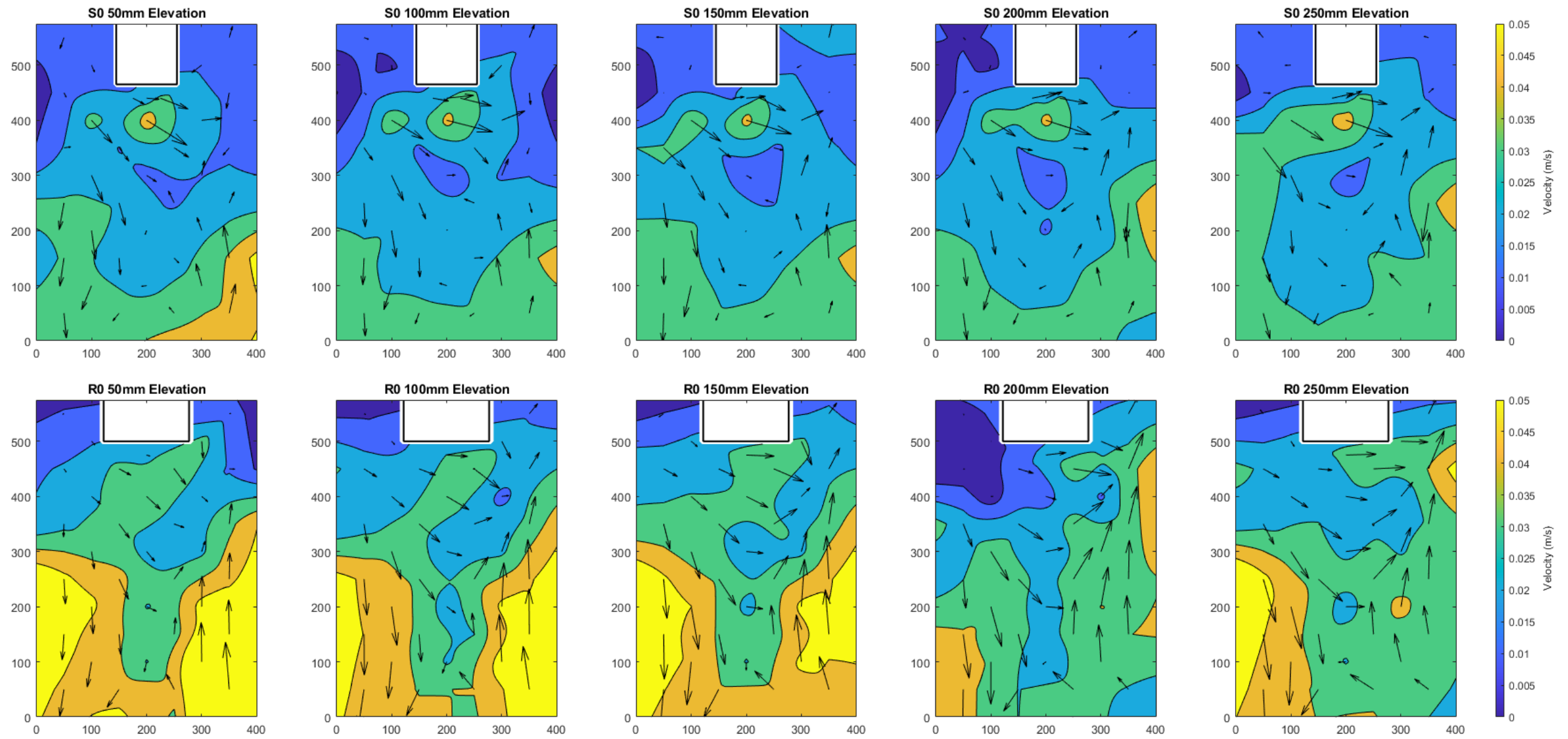


Figure 6.10 Comparison F i – Contour maps of residual velocity magnitude and direction at elevations of 50, 100, 150, 200 and 200 mm from the bed.

6. Test Case 3 – Impact of Varying Geometry

6.2.1.5 Statistical Analysis

The results of residual velocity magnitude for S0 and R0 were plotted against each other to compare the performance of each of these closed box cases (Figure 6.11). Although the results are somewhat scattered, the line of best fit reveals fairly strong positive correlation between the two experiments. This indicates a relationship between the values despite the change in TRS geometry. Histograms of the residual magnitude velocity show that S0 has a normal distribution but that R0 is more closely related to the pre-lagoon state (Figure 6.12). The velocities of S0 are reduced overall compared to the baseline conditions which concur with the findings of Ahmadian et al (2010) who found that full scale TRSs would reduce velocity in the estuary overall. However, R0 displays a wider range of values than the baseline conditions. This shows that although the presence of the rectangular TRS still changes the natural flow conditions in the tank it balances out to a range of both slower and faster velocities rather than just increasing or decreasing the flow throughout the tank. This suggests that a range of activities may be possible around the TRS due to the presence of slower flows whilst increased flows help maintain a healthy environment through flushing. Analysis of the results for residual flow direction show a very close relationship between S0 and R0 which shows that the different shaped TRSs have not caused a significant change to flow patterns in the tank. Z-test results presented in Table 6.2 suggest that there is a significant statistical difference between the experiments and to reject the null-hypothesis, however, the consistency of other results points to there being a relationship here. This statistical difference highlighted by the z-test is most likely due to the increased range in flow velocities in R0, and although the shape of the TRS does cause a difference to baseline conditions, these alterations are related.

Table 6.2 Comparison F – Statistical analysis of residual velocity magnitude.

Comparison	RMSE	r	z	Accept/ reject h_0
F i – S0 vs R0	0.011636	0.652601	3.90842	Reject
F ii – S1A vs R1	0.012304	0.202128	2.80260	Reject
F iii – S2A vs R2A	0.017949	0.130778	0.20919	Accept
F iv – S2B vs R2D	0.008248	0.443341	0.10675	Accept

6. Test Case 3 – Impact of Varying Geometry

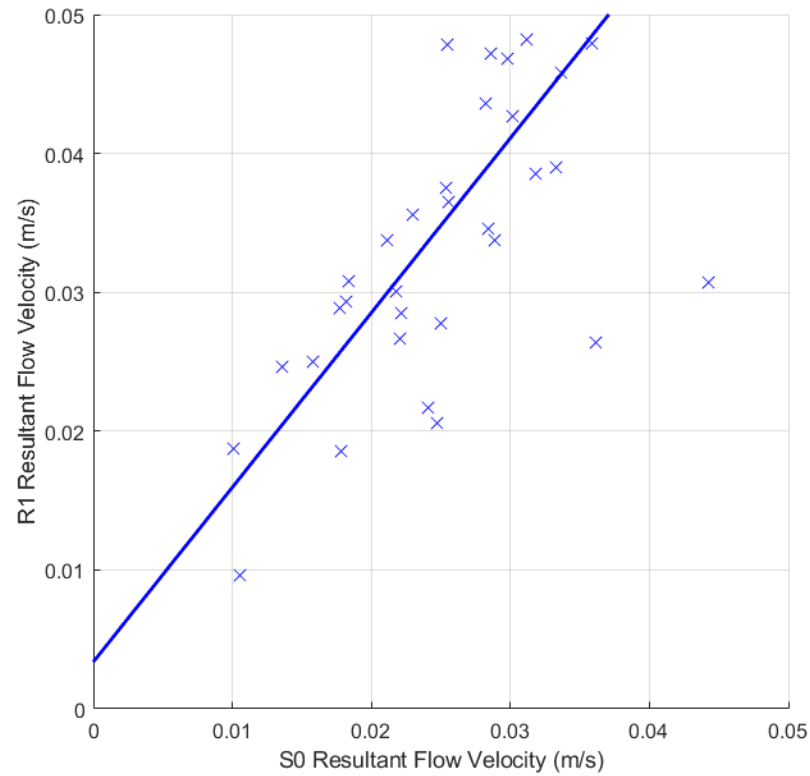


Figure 6.11 Comparison *F i* - Regression analysis of residual flow velocity.

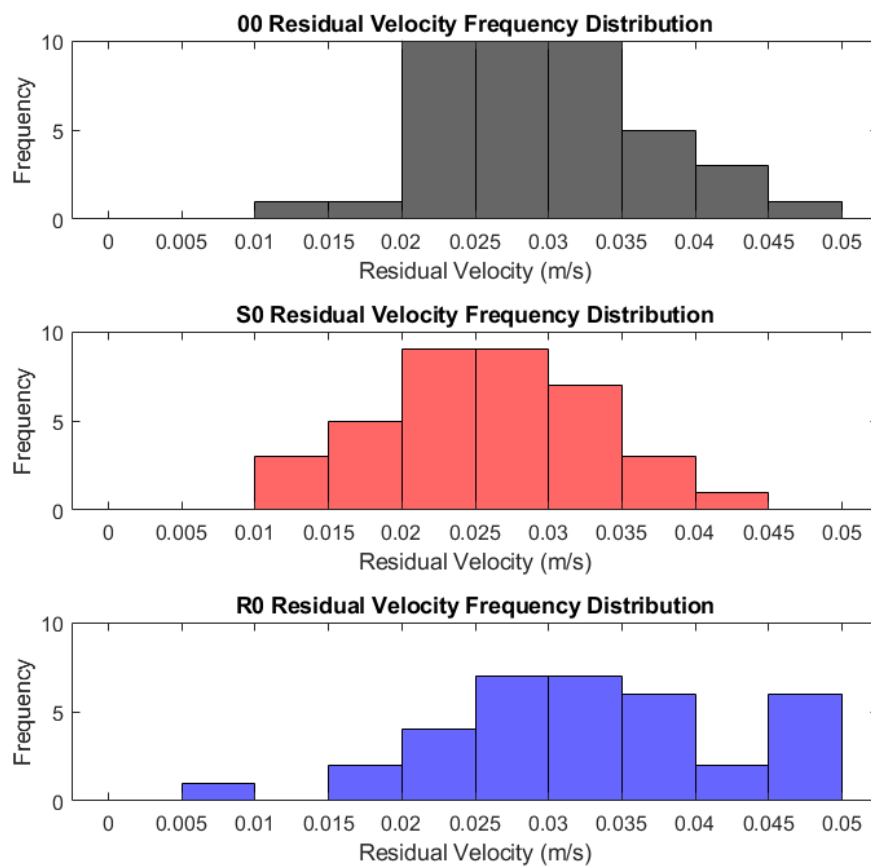


Figure 6.12 Comparison *F i* – Distribution analysis of residual flow velocity.

6. Test Case 3 – Impact of Varying Geometry

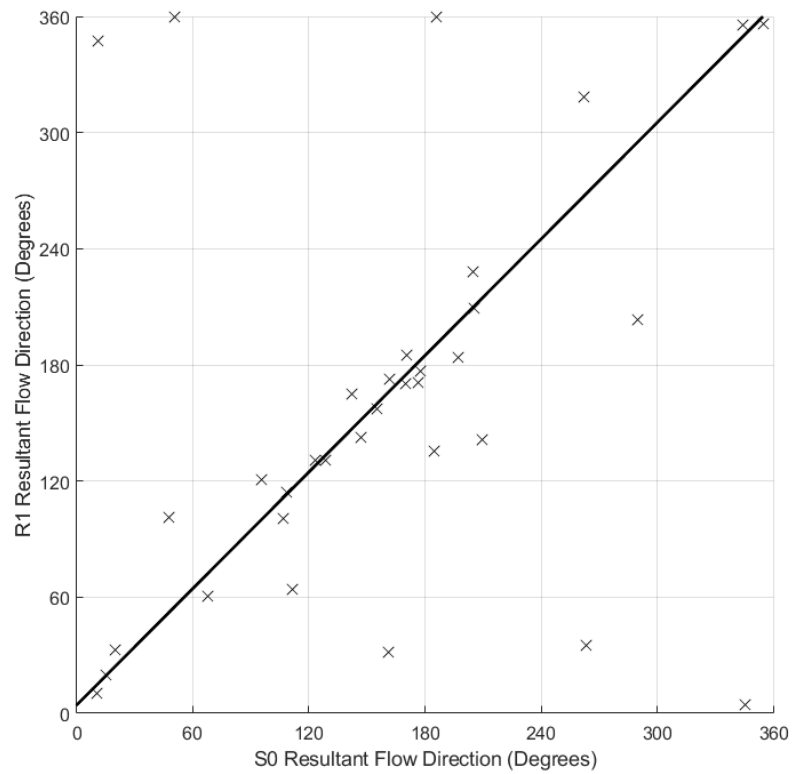


Figure 6.13 Comparison *F i* - Regression analysis of residual flow direction.

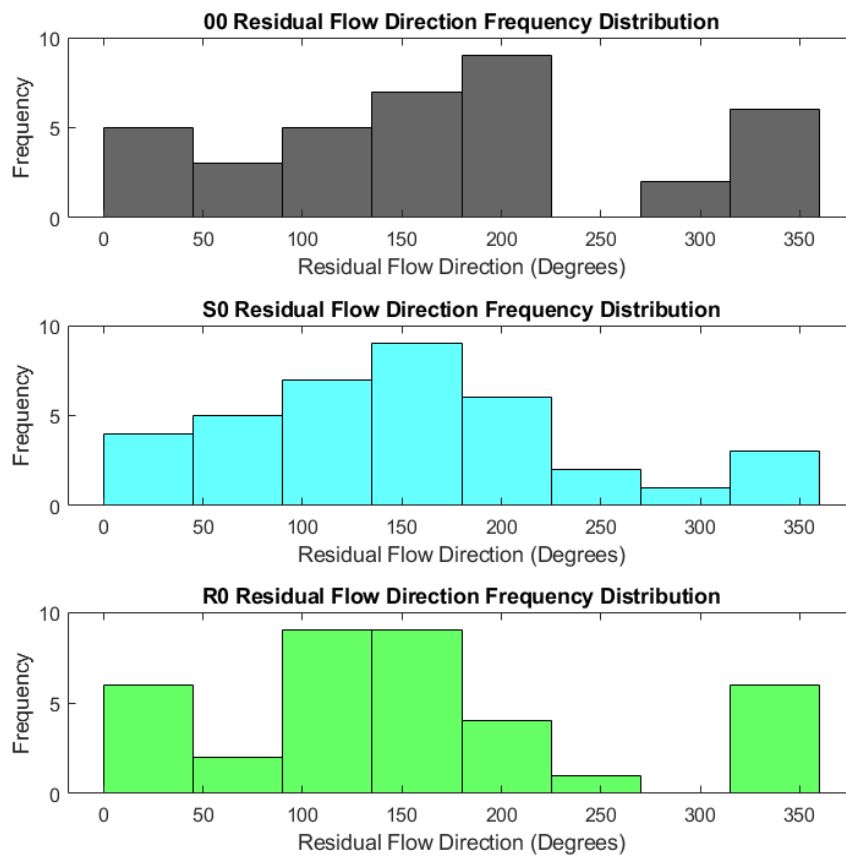


Figure 6.14 Comparison *F i* – Distribution analysis of residual flow direction.

6. Test Case 3 – Impact of Varying Geometry

6.2.2 Comparison F ii – Square vs Rectangular TRS with 1 turbine

Comparison F ii compares results from experiments with a square (S1A) and rectangular (R1) TRS, both with a single turbine positioned close to the TRS wall against pre-lagoon conditions to investigate the hydrodynamic impact of turbine position in different TRS geometries. Figure 6.15 shows the layout of these experiments.

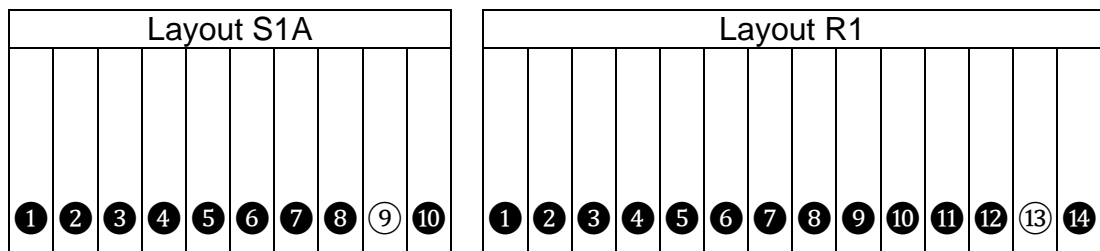


Figure 6.15 Experiment layouts for Comparison F ii: S1A and R1.

6.2.2.1 Velocity - Depth Averaged

Figure 6.16 presents a map of velocity-time plots comparing these results against pre-lagoon measurements. Along the inflow boundary, the graphs of depth averaged velocity appear very similar between S1A and R1 suggesting that conditions at the inflow boundary are consistent between the two experiments. However, further into the tank differences start to appear and although results for both cases follow the same shape and pattern at most locations experiment R1 consistently has higher flow velocities than S1A, as was previously observed in Comparison Fi. This difference is slightly less however, between 0.005 and 0.02 m/s, up to 25% of flow velocity. The greatest variation occurs at (200,300), where this time experiment S1A has the highest velocity, peaking at almost double that of experiment R1. This could be due to deflection of flow from the turbine in the square TRS reaching further into the centre of the tank than the rectangular TRS where the turbine opening is located closer to the right-hand wall, however this increased flow velocity is not noticed at (200,400), closer to the seawall and is therefore unaccountable.

6. Test Case 3 – Impact of Varying Geometry

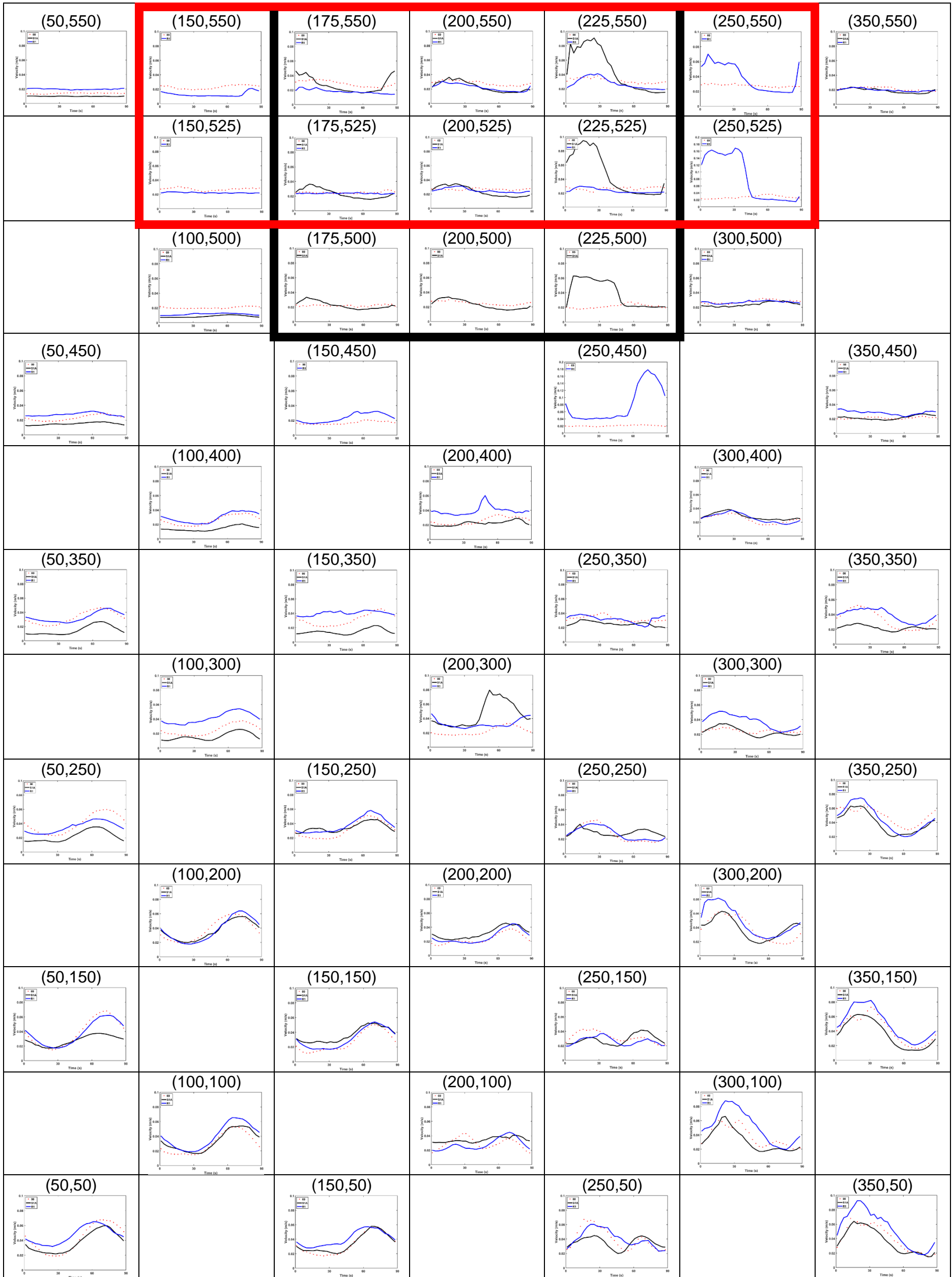


Figure 6.16 Map of depth averaged velocity plots for Comparison F ii: S1A and R1.

6. Test Case 3 – Impact of Varying Geometry

Inside the TRS, results are very similar in shape and amplitude in the centre of the lagoon (200,550) and (200,525) (Figure 6.17 and Figure 6.18). This shows that despite the different TRS shape, when turbine openings are placed in corresponding locations, they have a similar effect on flow in the centre of the TRS area. However, experiment S1A shows higher velocities at other locations. This is to be expected since although both TRSs have the same area, water travelling through the turbine opening in S1A has much less far to travel before it is reflected off each wall, meaning that it still has an effect on the left-hand side of the lagoon, unlike R1 which only appears to impact the right-hand side of the lagoon. On the right-hand side, close to the turbine openings, the amplitude of the wake velocities is in a similar range for both shapes of TRS (~0.1 m/s). However, this flow rate dissipates much more quickly for the rectangular TRS than the square due to the long thin shape meaning that the water has further to reach and so the flow is almost negligible by the time it reaches the left-hand side.

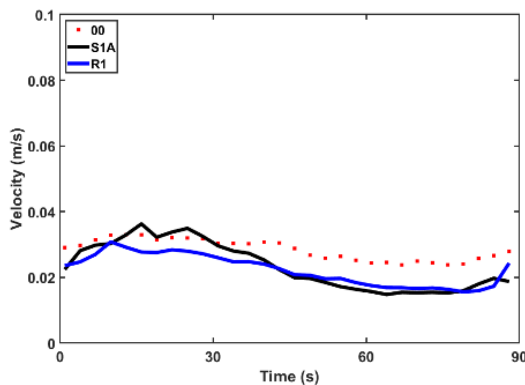


Figure 6.17 Closer detail of velocity at (200,550).

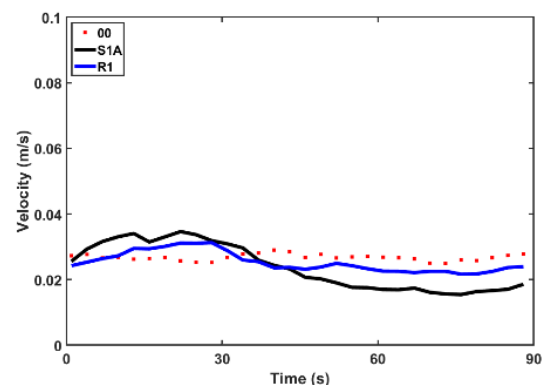


Figure 6.18 Closer detail of velocity at (200,525).

6. Test Case 3 – Impact of Varying Geometry

6.2.2.2 Velocity – Analysed by tide and depth

Analysis of the contour maps once turbine openings have been introduced shows some variation between the depths for each experiment as the area of strong flow decreases with depth in the case of the ebb tide (Figure 6.19).

This shows how turbines create complex three-dimensional flows that affect the entirety of the water column, in accordance with the findings of Jeffcoate et al. (2013). However, the patterns between S1A and R1 are very similar, with large areas of strong positive flow directly in front of the TRS seawalls, and in large areas to the left and front of the tank. This suggests that the ebbing flow of the outgoing tide affects both trials equally regardless of the shape of the TRS. Inside the TRS, there is very little flow in S1A, with the fastest flow occurring in the right-hand corner of the bottom layers as water escapes through the turbine opening. This is also the case in the R1 but with even slower flows in the rear and left-hand side of the TRS where circulation struggles to reach, as observed in Comparison Fi.

During low tide, there is still a great deal of similarity between the depths for each experiment in the outer tank (Figure 6.20) which is to be expected during times of slack water where currents are least strong but differences begin to appear between the experiments with stronger flows observed in the rectangular case. Inside the TRS there is more flow than during the ebb tide which is perhaps due to the reduced forces enabling water to circulate more freely. The velocity is particularly increased along the right-hand side of the rectangular TRS where water appears to be flowing into the TRS but still does not circulate throughout the whole of the impounded area. The 3D behaviour of the turbine wakes is even more evident during this part of the tide, as flow patterns are different at every depth.

There is slightly more variation between the depths during the flood tide as the area of strongest positive flow grows with depth (Figure 6.21) and there is greater variation between the two experiments too. This shows that the stronger forces of the incoming tide have a greater effect on the different shapes of the TRSs. Inside the TRS, the incoming tide has permeated more than half of the square TRS area, but 200 mm once again proves to be a critical depth where the effects of 3D flow are less felt. Flow is also increased

6. Test Case 3 – Impact of Varying Geometry

inside the TRS of R1 with stronger flow reaching further than during previous tidal phases but only filling around a third of the impounded area with the left-hand side remaining fairly stagnant overall. This compounds the idea that the incoming tide is not strong enough to reach the left-hand side of the long, thin rectangular TRS but is strong enough to reach the entirety of the square case. This indicates that TRS geometry has a greater effect on flow than TRS area does.

The results of S1A and R1 at high tide (Figure 6.22) show areas of strong flow decreasing with depths and although the flow velocity patterns inside the TRSs are similar in shape to those observed during the flood tide they vary in strength as is to be expected at the turn of the tide. Flow is still faster in the outer tank for the rectangular case overall. This is thought to be due to greater reflection off the longer front seawall, increasing flow velocity in the front of the tank but restricting flow around the TRS due to the increased blockage of the channel, with less room between the TRS seawalls and the edge of the tank. In full scale studies of TRSs it was found that the Bristol Channel was more susceptible to change due to blockage effects in this narrow channel compared to other more open areas, e.g., North Wales coast (Mackie et al., 2021).

6. Test Case 3 – Impact of Varying Geometry

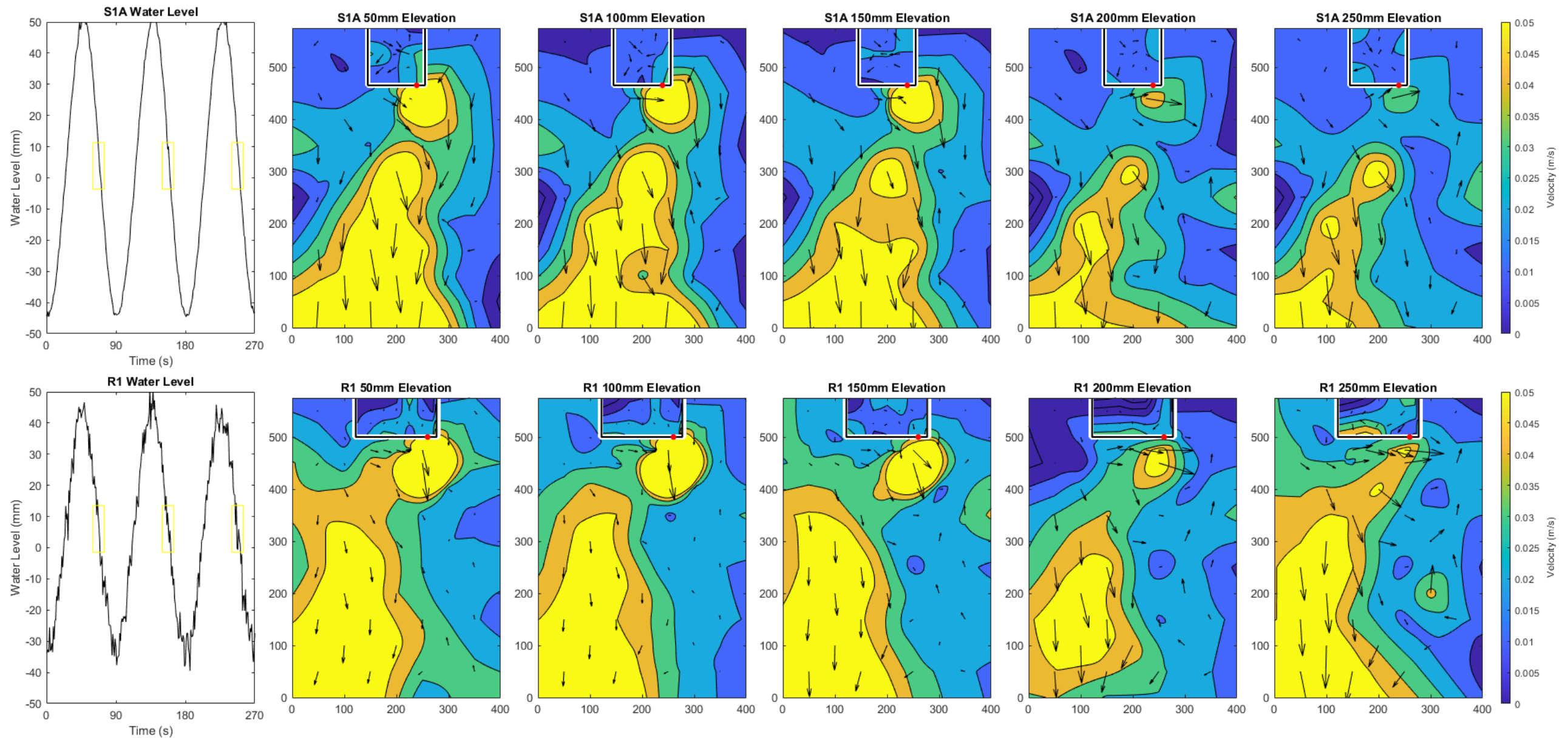


Figure 6.19 Comparison F ii – Velocity contour maps at elevations of 50, 100, 150, 200 and 250 mm above the bed during the ebb tide.

6. Test Case 3 – Impact of Varying Geometry

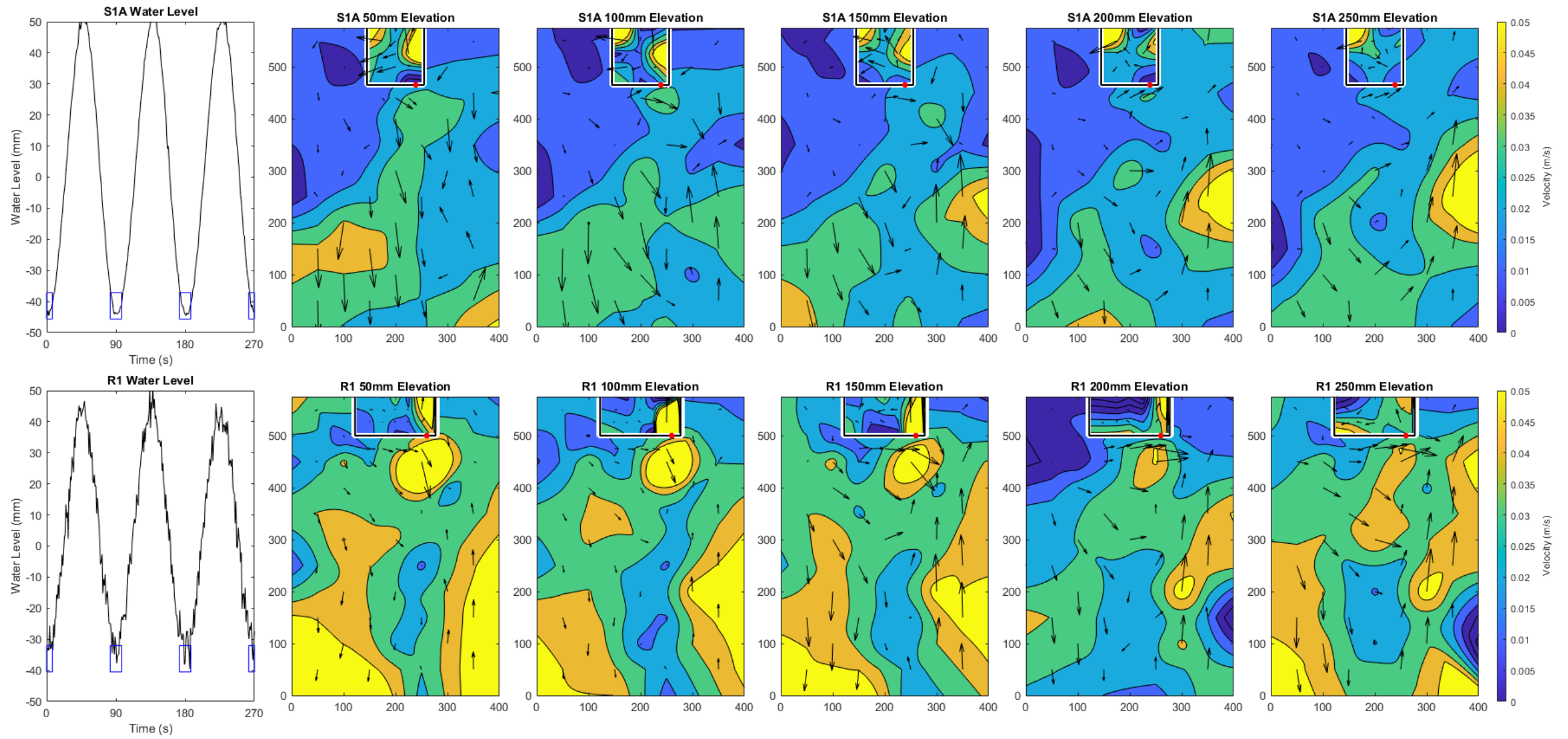


Figure 6.20 Comparison F ii – Velocity contour maps at elevations of 50, 100, 150, 200 and 250 mm above the bed during low tide.

6. Test Case 3 – Impact of Varying Geometry

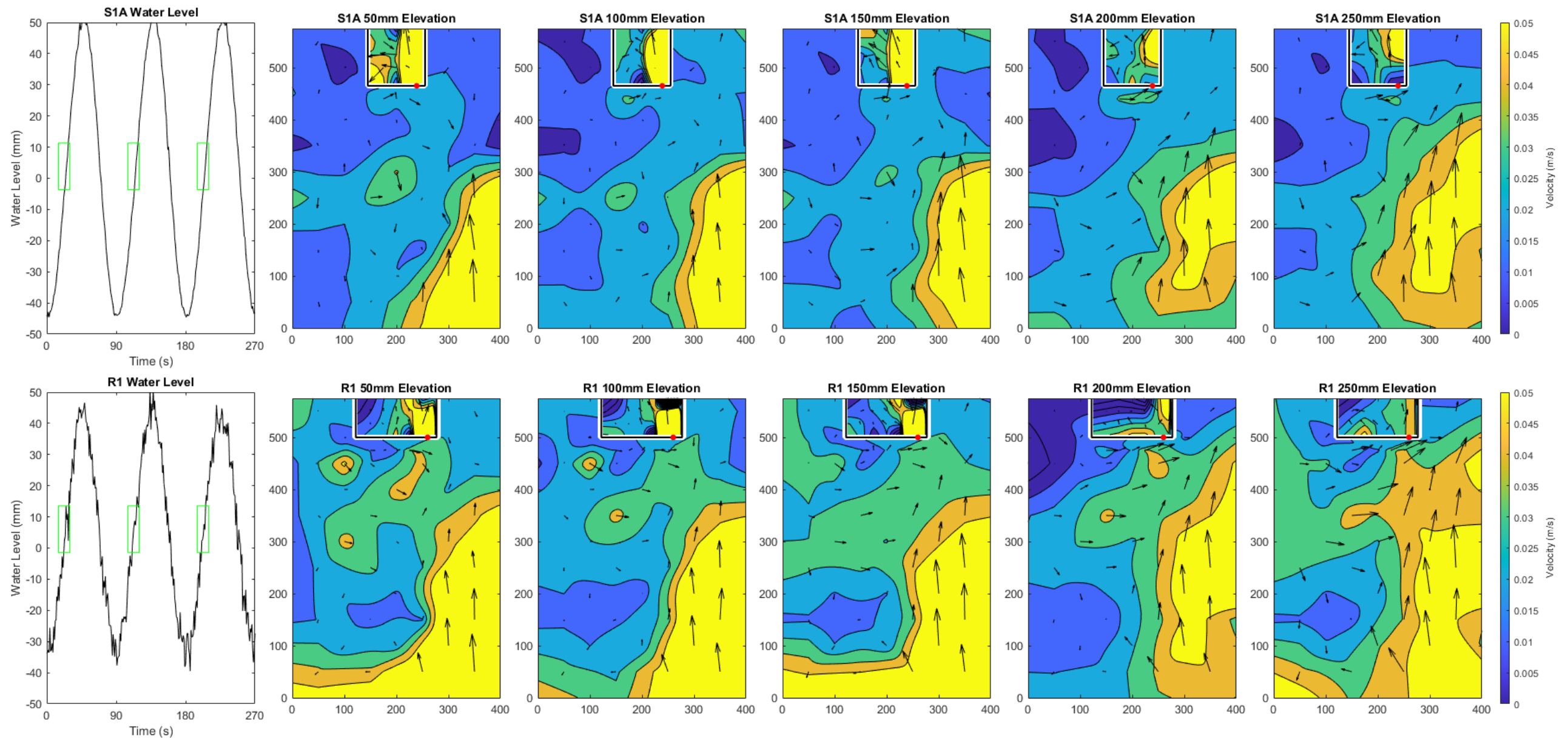


Figure 6.21 Comparison F ii – Velocity contour maps at elevations of 50, 100, 150, 200 and 250 mm above the bed during the flood tide.

6. Test Case 3 – Impact of Varying Geometry

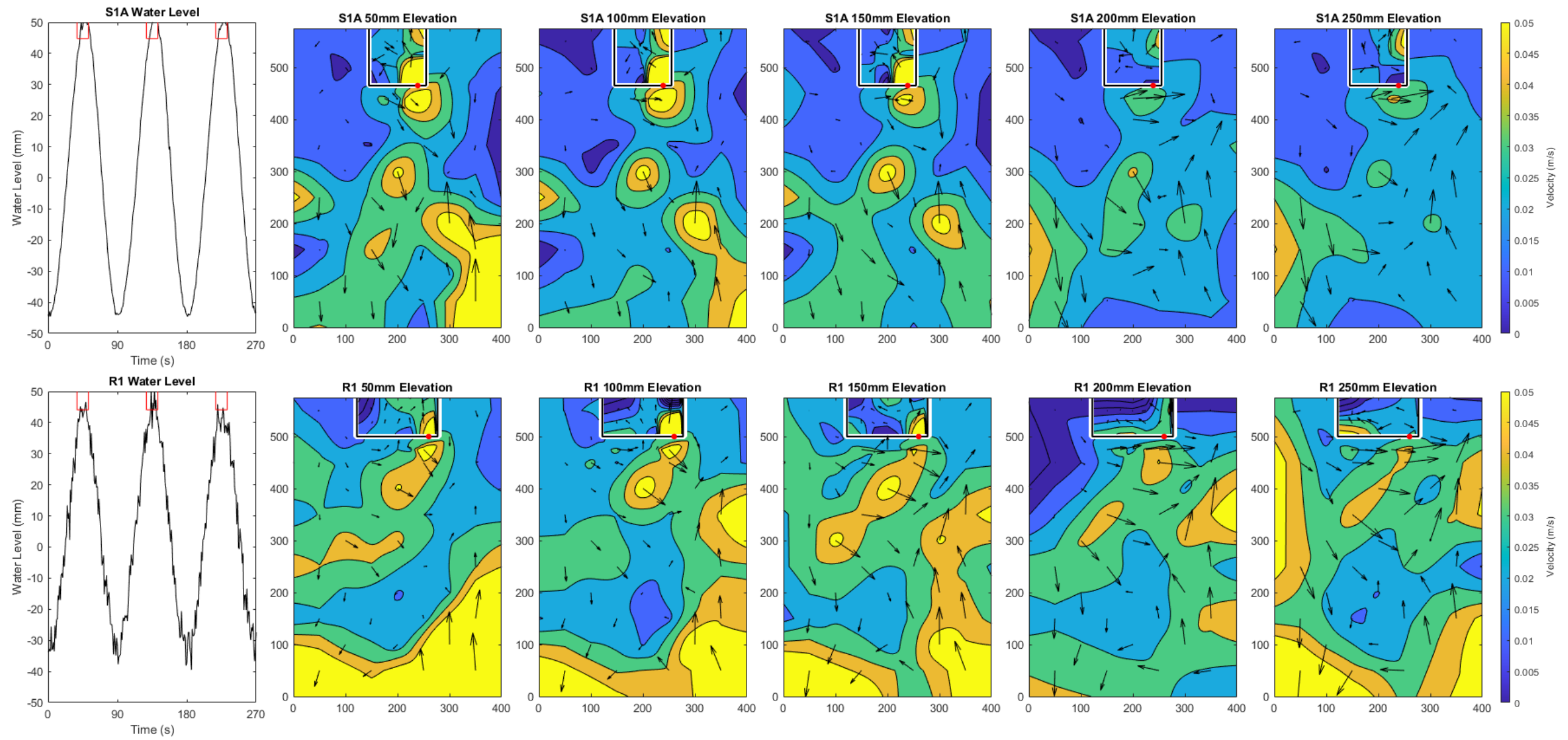


Figure 6.22 Comparison F ii – Velocity contour maps at elevations of 50, 100, 150, 200 and 250 mm above the bed during high tide.

6. Test Case 3 – Impact of Varying Geometry

6.2.2.3 Velocity – Residual Velocity and Direction

The contour plots of residual velocity shown in Figure 6.23 reveal some similarities between S1A and R1 in that there are islands of strong positive flow directly in front of the turbines for both cases. These seem to then deflect around the edges of the TRS walls to the right. Flow is still strongest along the front half of the tank in case R1 as thought to be attributed to stronger reflection off the wider TRS wall reaching further into the tank rather than being circulated around the corners of the TRS as in S1A. Inside the square TRS there is a linear pattern where the velocity is strongest behind the turbine which then decreases with distance from the opening. In the rectangular case there is more of a radial flow pattern, starting from behind the turbine and spreading to the far left of the TRS, but flow is much slower and weaker in the left half of the TRS. This further demonstrates how the force of water through the orifice is not strong enough to reach the far side of the elongated TRS.

6. Test Case 3 – Impact of Varying Geometry

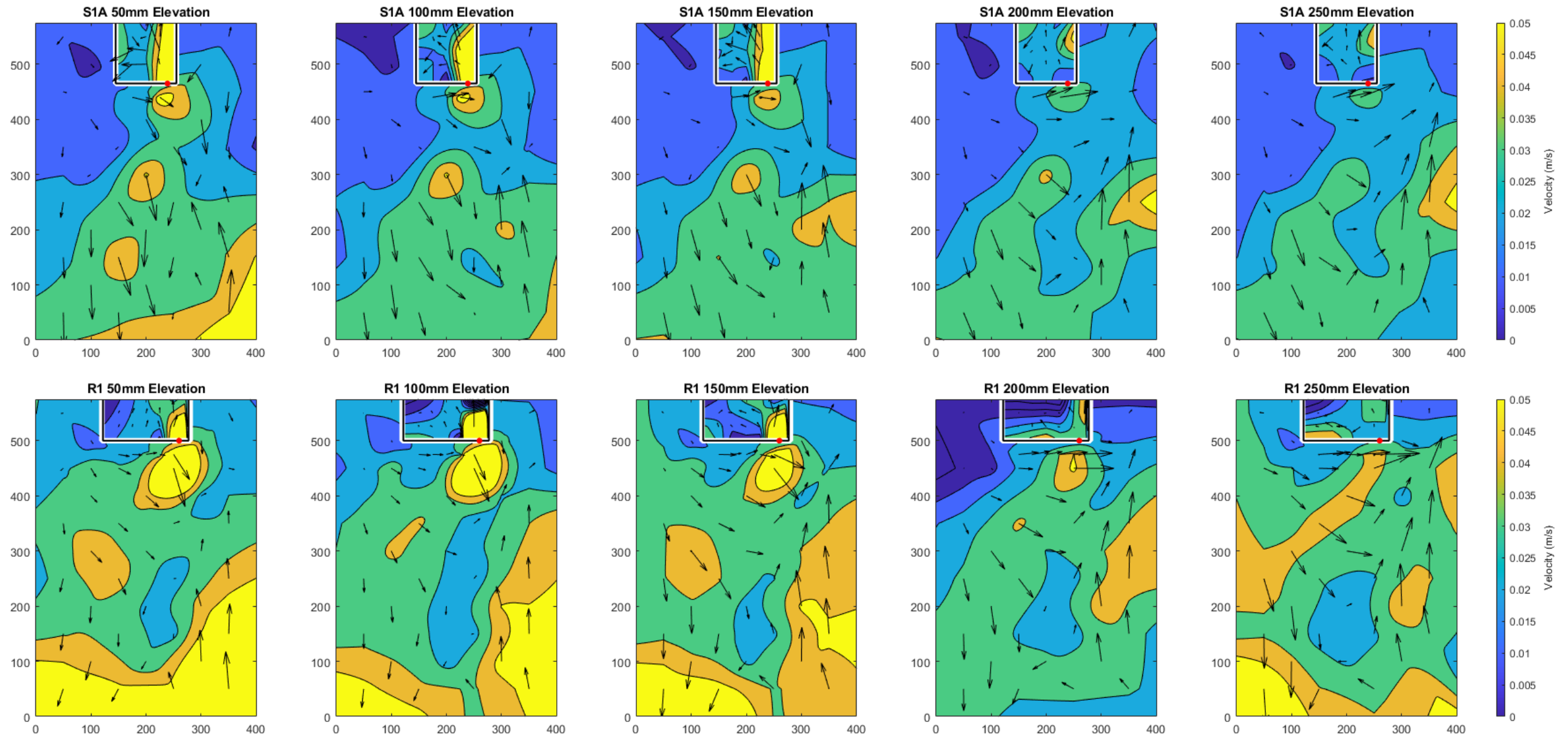


Figure 6.23 Comparison F ii – Contour maps of residual velocity magnitude and direction at elevations of 50, 100, 150, 200 and 200 mm from the bed.

6. Test Case 3 – Impact of Varying Geometry

6.2.2.4 Flow Visualisation

Flow visualisation of these two scenarios display clear similarities and differences (Figure 6.24 and Figure 6.25). Both experiments have two clear plumes with the left-hand track dominating, but whereas the plumes in the square TRS both rotate anti-clockwise to spread to the left-hand side of the lagoon, the plumes in the rectangular TRS split into rear and front cells. In both cases, the cells continue to circulate and migrate until the whole area is fully mixed, but it takes much longer for the dye in the rectangular lagoon to permeate the whole area (ninety seconds in R1 compared to thirty seconds in S1A). Overall, this is a clear demonstration of how the square TRS is much better mixed than the rectangular TRS which is better for maintaining a healthy environment by constantly replenishing fresh water and limiting the chance of stagnation.

In their study of flow through inlets in idealised tidal lagoons, Vouriot et al. (2018) concluded that lagoon shape had a large influence on the fate of internal vortices. They found that dipoles dissipated more quickly (within a single tide) in longer, thinner lagoons and endured longest in lagoons closer to a square shape. This was deemed to be due to a combination of the proximity of the side walls in the long, thin lagoon, and the distance from the rear, “coastal” boundary in the other cases. In the present study, the proximity of boundary walls has been shown to dictate the shape and trajectory of the dipoles formed through the turbine openings and it is the square case that results in the more defined and longer-lived circulation pattern than the rectangular in agreement with the observations of Vouriot et al. (2018).

6. Test Case 3 – Impact of Varying Geometry

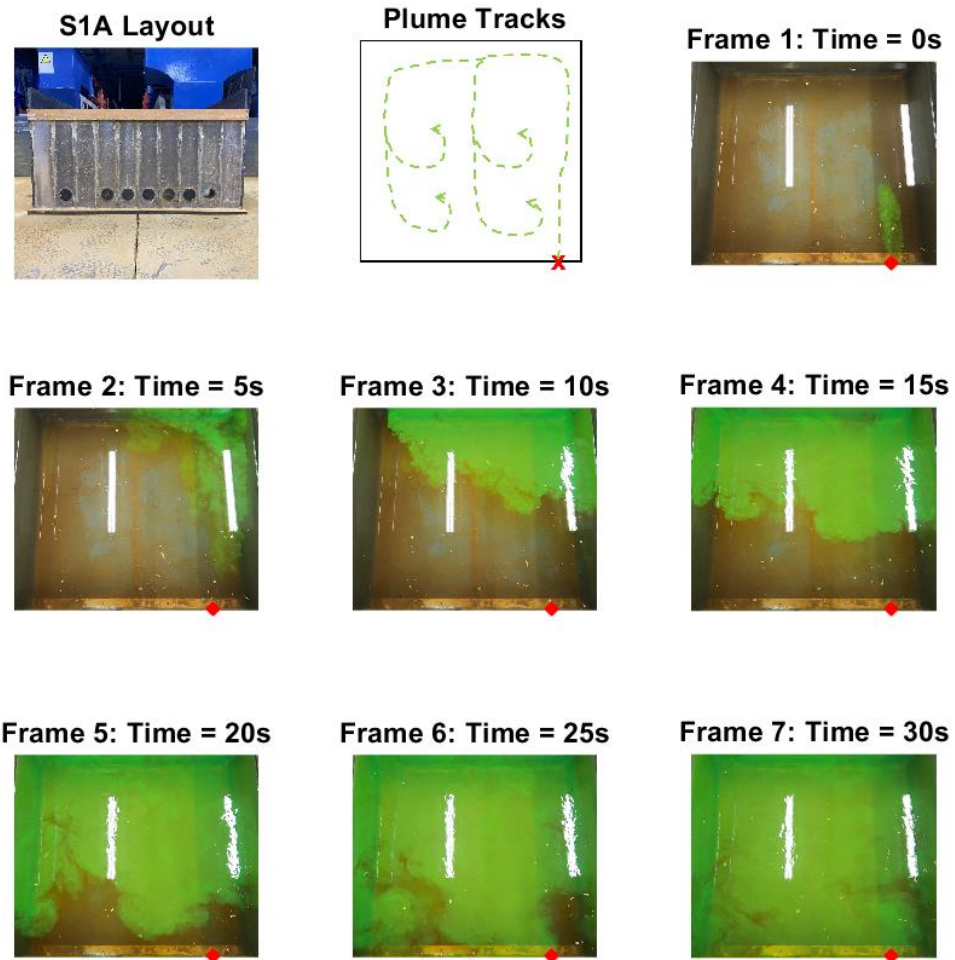


Figure 6.24 Flow visualisation for experiment S1A.

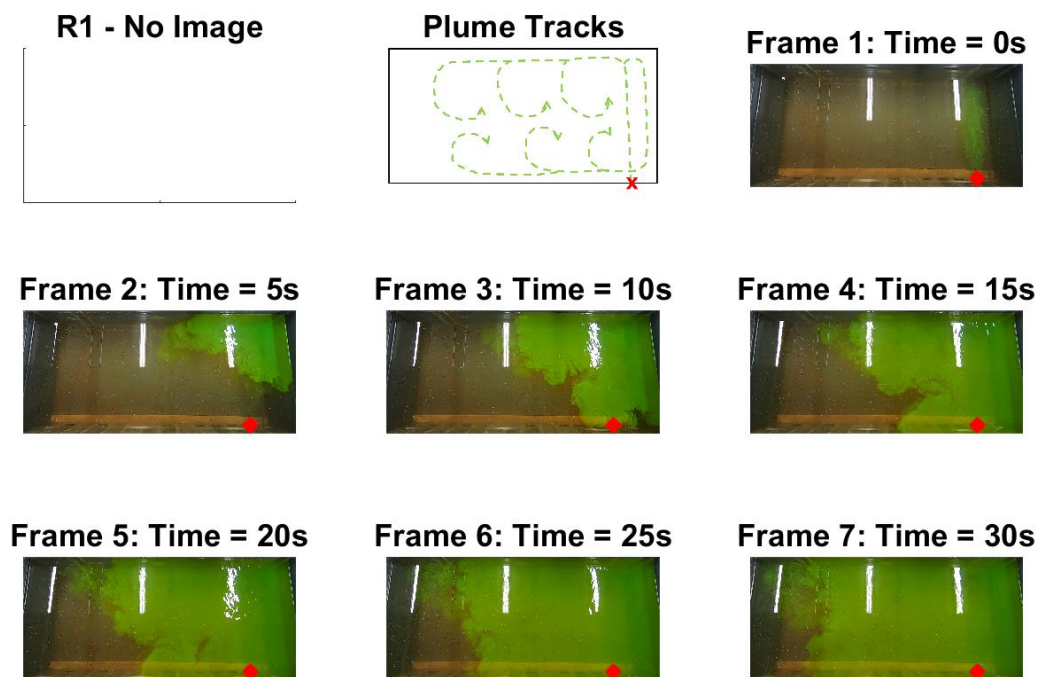


Figure 6.25 Flow visualisation for experiment R1.

6. Test Case 3 – Impact of Varying Geometry

6.2.2.5 Statistical Analysis

Regression analysis comparing the residual velocity of these two experiments in Figure 6.26 shows very little correlation. The results are highly scattered between the experiments and despite the histograms of frequency distribution showing some similarity between S1A and R1 (Figure 6.27). These similarities in velocity range do not correspond to the same locations showing how the configurations behave differently to one another.

Regression analysis of flow direction, however, is very similar (Figure 6.28) and the histogram of frequency distribution for flow direction shows how S1A and R1 behave more closely to each other than the baseline case (Figure 6.29). This shows that although these experiments have altered the natural flow pattern, they do behave fairly similarly to each other in terms of flow direction.

Despite the strong similarities between the two experiments statistical analysis of the residual velocity magnitude for these two cases shows a significant difference overall and the z-test result causes us to reject the null hypothesis (see Table 6.2 for z-test values). This means that when a single turbine is added, the shape of the TRS leads to a significant difference to flow velocities and needs to be carefully considered when designing TRSs.

6. Test Case 3 – Impact of Varying Geometry

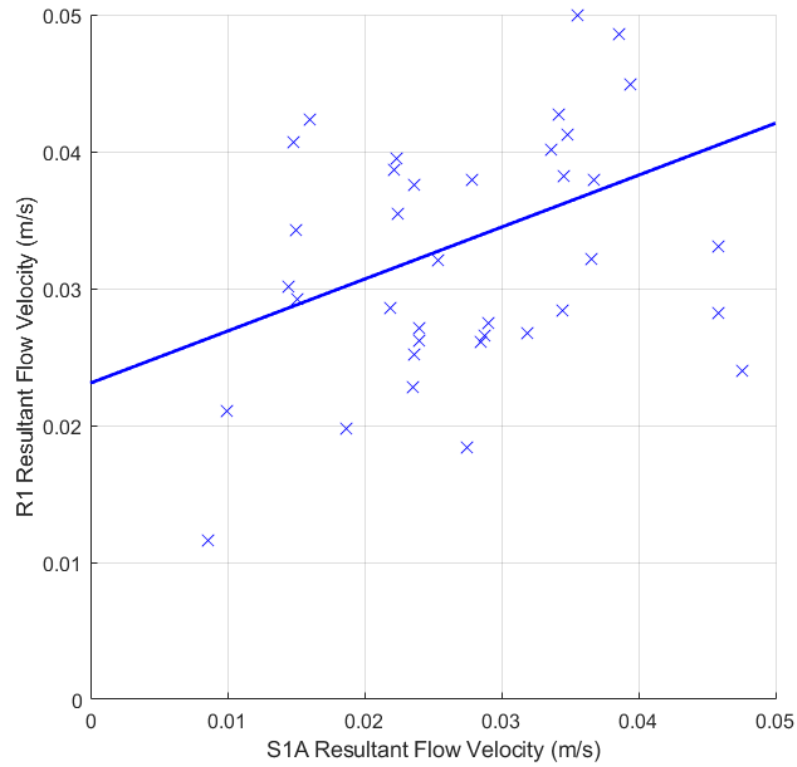


Figure 6.26 Comparison F ii - Regression analysis of residual flow velocity.

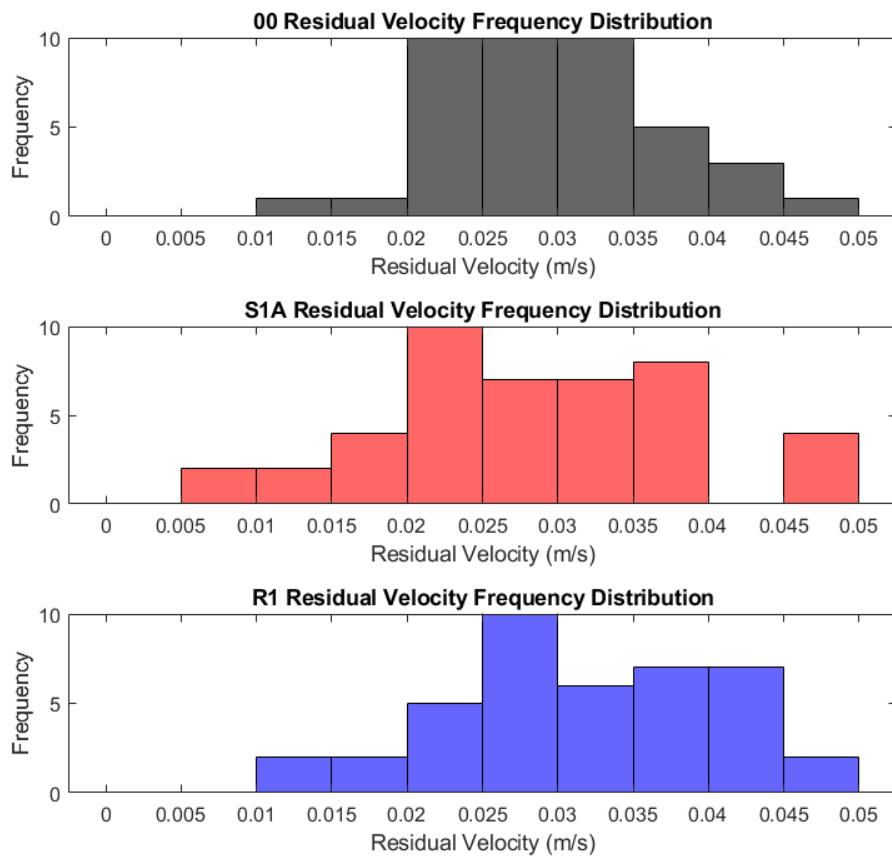


Figure 6.27 Comparison F ii – Distribution analysis of residual flow velocity.

6. Test Case 3 – Impact of Varying Geometry

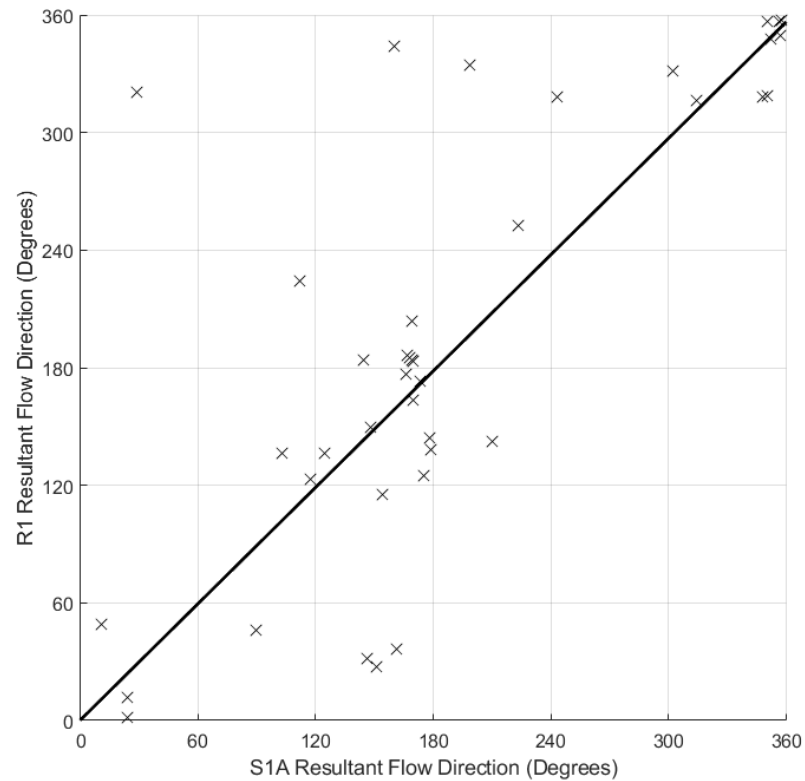


Figure 6.28 Comparison F ii - Regression analysis of residual flow direction.

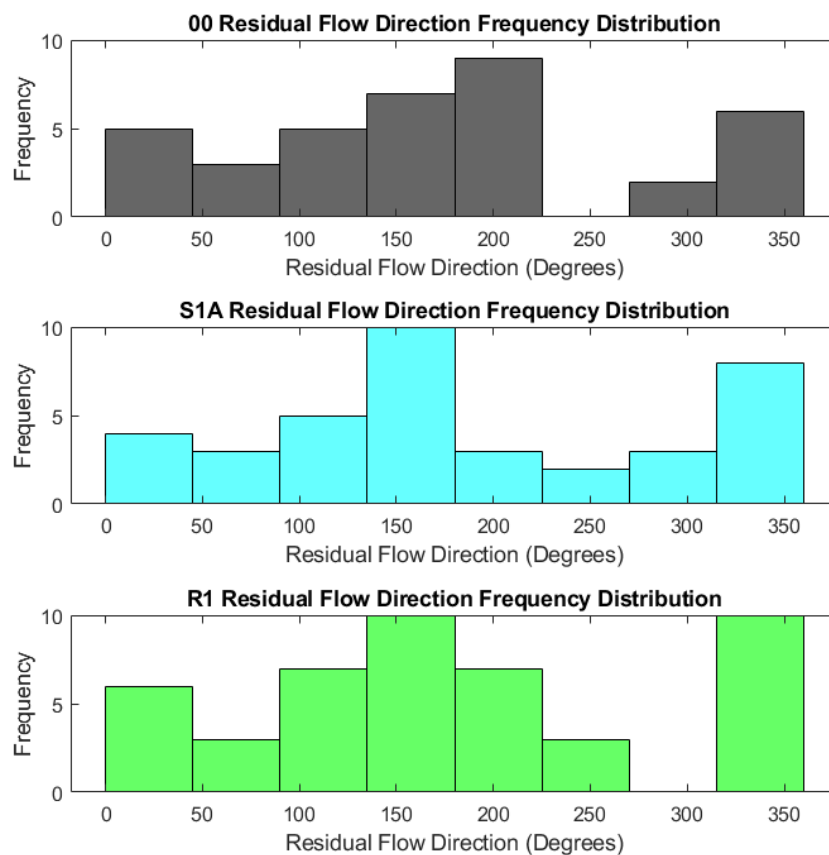


Figure 6.29 Comparison F ii – Distribution analysis of residual flow direction.

6. Test Case 3 – Impact of Varying Geometry

6.2.3 Comparison F iii – Square vs Rectangular TRS with 2 turbines side by side

Comparison F iii compares results from experiments with a square (S2A) and rectangular (R2A) TRS, both with a pair of turbines positioned close to the right hand TRS wall against pre-lagoon conditions to investigate the effects of turbine spacing and position on hydrodynamics. Figure 6.30 shows the layouts of these two experiments.

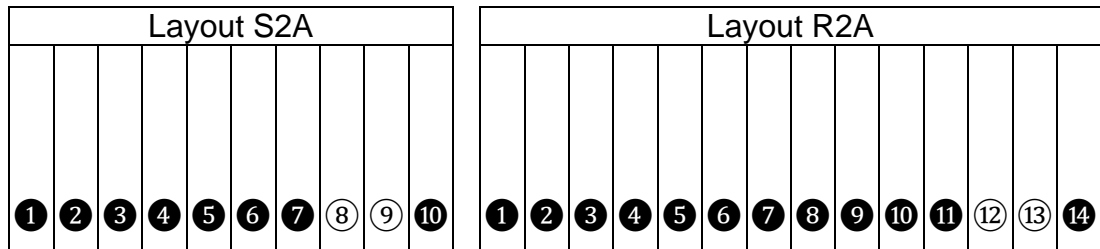


Figure 6.30 Experiment layouts for Comparison F iii: S2A and R2A.

6.2.3.1 Velocity – Depth Averaged

The depth averaged velocity results of this comparison, presented in Figure 6.33, are very similar to those of Comparison F ii (see Figure 6.16), where S1A and R1 were compared, each with a single turbine. In this case the experiments contain two turbines in corresponding locations and the flow patterns seems to be exaggerated as may be expected. The results for S2A and R2A are very similar throughout the tank, sharing the same velocity patterns, but it is the range of values that vary. Although the gap between the velocities has narrowed for this experiment compared to Comparison F ii, where there is a difference between the velocity range it tends to be experiment R2A that is faster than S2A as before. This could be due to reflection off the longer seawall of the rectangular TRS seawall causing faster flows in the outer tank compared to the square TRS where water is able to circulate more freely around the sides of the TRS.

Points where flow velocities for S2A exceed R2A are (200,100) and (200,300) along the centre line of the tank (closer detail provided by Figure 6.31 and Figure 6.32). S2A experiences peaks at both of these points whilst R2A more closely follows the pre-lagoon conditions. This is most likely due to reflections off the corners of the square TRS which protrude further into the centre of the tank than those of the rectangular TRS.

6. Test Case 3 – Impact of Varying Geometry

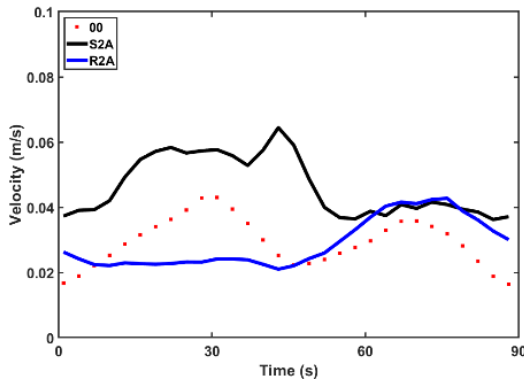


Figure 6.31 Closer detail of velocity at (200,100).

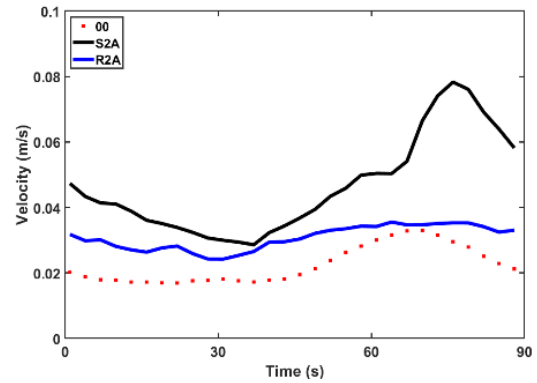


Figure 6.32 Closer detail of velocity at (200,300).

Inside the TRS, where measurements are available for comparison, a similar pattern again emerges to that of Comparison F ii, with peaked results of the same range for both experiments directly behind the turbine openings on the right-hand side, decreasing towards the centre of the lagoon. Flow velocities tail off towards the left-hand side of the lagoon in R2A as they get further from the turbine openings but experience a second peak in S2A due to reflection off the left-hand wall. This presents difference problems for both shapes of TRS. Velocity is strongest near turbine openings due to wake effects for both shapes but in a square TRS these do not fully dissipate across the lagoon area and high velocities can also be experienced at opposite seawalls due to reflection. These strong currents throughout the area could prohibit recreation or be harmful to marine life. In a rectangular TRS, wake jets do dissipate but currents are not strong enough to reach the whole of the lagoon area which makes for a safer swimming environment in terms of flow velocity but could cause problems with water quality. Both of these issues would have to be considered carefully when designing TRSs.

These similarities with Comparison F ii confirm flow behaviour when turbines are located near the edge of a TRS seawall, close to perpendicular side walls, and strengthens the argument that two turbines located close to one another exaggerate the effects of a single turbine, as found in Comparison A.

6. Test Case 3 – Impact of Varying Geometry

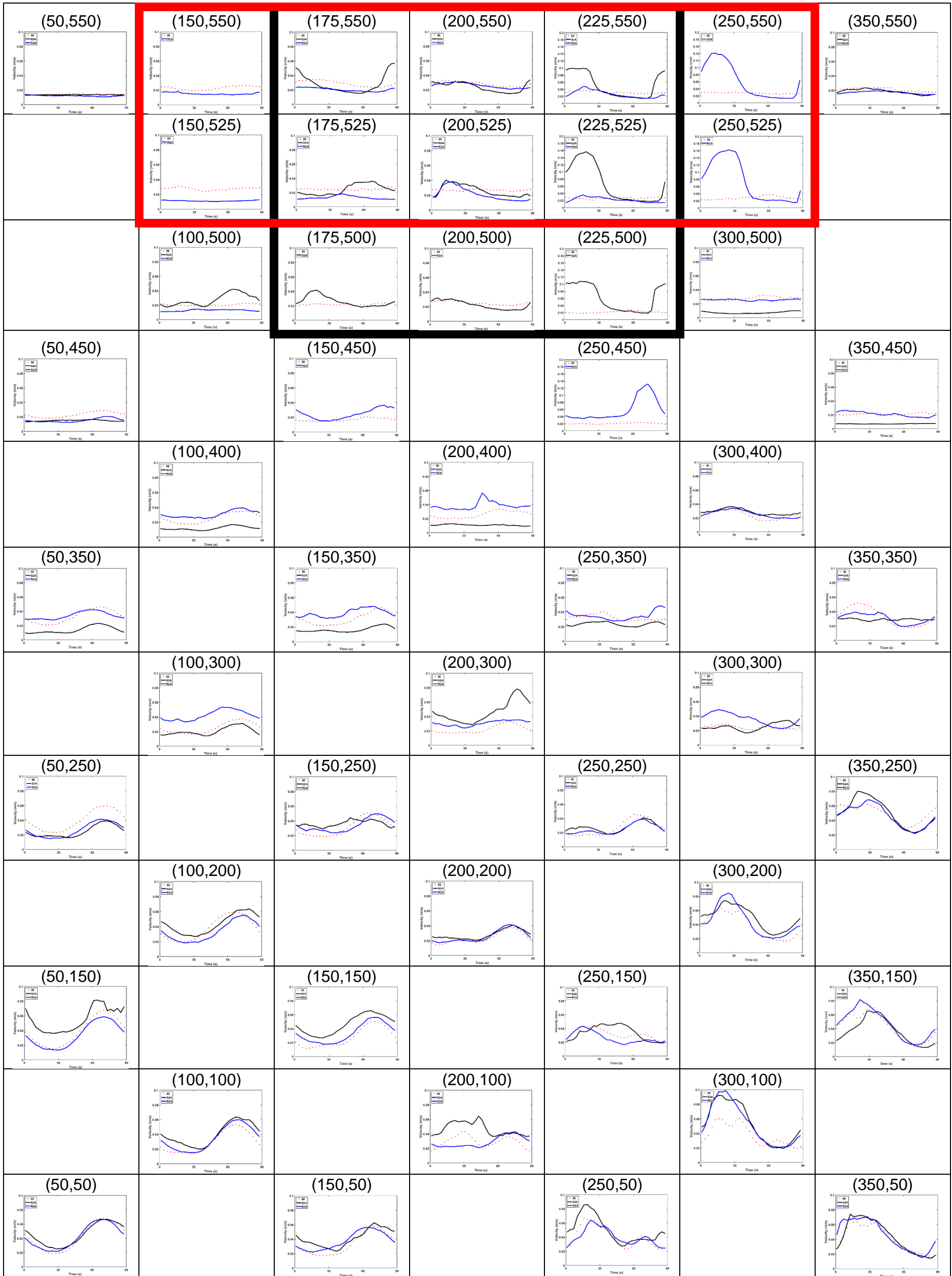


Figure 6.33 Map of depth averaged velocity plots for Comparison F iii: S2A and R2A.

6. Test Case 3 – Impact of Varying Geometry

6.2.3.2 Velocity – Analysed by tide and depth

The ebb contour plots display very little variation between depths and both experiments have similar patterns to each other (see Figure 6.34). This points to the ebb tide having similar effects on the outer tank area irrespective of TRS shape, as previously observed in Comparison F ii. Flows are very slow inside the TRS, with patterns matching those of S1A and R1 (Figure 6.19), although, flows are stronger in R2A than previously seen. This concurs with the findings of Comparison A, that when two turbines are positioned side by side, they create wakes that behave in a similar way to those of a single turbine in a corresponding location but are more concentrated and therefore produce stronger currents.

Figure 6.35 shows little variation between depths in the wider tank at low tide which indicates that three-dimensional flow does not affect the outer tank during this tidal phase. Within the TRS, flow is much stronger than during the ebb tide with strong flows filling over half of the inside of the square TRS which is most likely due to recirculation of residual flow. Velocity is also increased in R2A and reaches further than the single turbine allowed in R1.

During the flood phase of the tide (Figure 6.36) there continues to be little change between the depths for each scenario. As in Comparison C, these plots clearly show how the strongest flows migrate from the left-hand side of the tank during the ebb tide to the right-hand side for the flood tide, demonstrating how this behaviour has remained constant throughout all of the experiments. Inside the TRS there is more movement in the square case than during the other tides which demonstrates how the flood tide causes greater circulation within the TRS. The strongest flows are still found directly behind the turbine openings, with flow being reflected to the left. This is similar in the rectangular case too, where the strongest flows are directed to the rear right-hand corner and circulated around to the left, reaching slightly more of the TRS area than before. This demonstrates the strength of the incoming tide as it is forced through two closely spaced orifices.

At high tide there is little variation between the depths of each experiment (Figure 6.37). This suggests that at this phase of the tide, where there is no

6. Test Case 3 – Impact of Varying Geometry

dominant flow, water is able to flow freely around the tank and is less influenced by flow through the turbine openings. Velocity within the TRS in S2A is much reduced showing how flow inside the TRS is affected by the different phases of the tide. However, the flow pattern within R2A is similar to that of other tides which suggests that flow within the rectangular TRS is influenced more by the number of turbines and their position than by tidal phase and is therefore able to regulate flow continuously once a current is established.

6. Test Case 3 – Impact of Varying Geometry

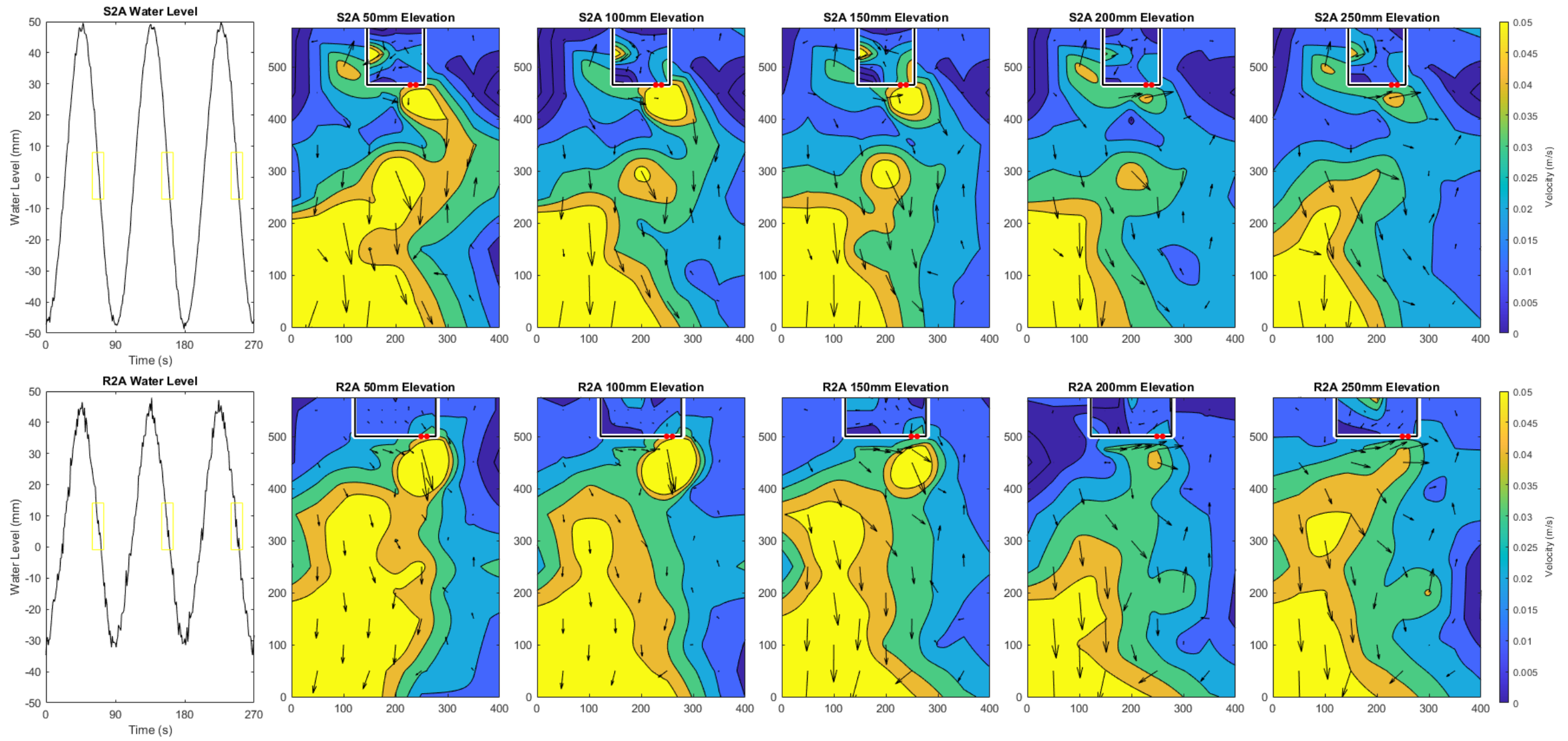


Figure 6.34 Comparison F iii - Velocity contour maps at elevations of 50, 100, 150, 200 and 250 mm above the bed during the ebb tide.

6. Test Case 3 – Impact of Varying Geometry

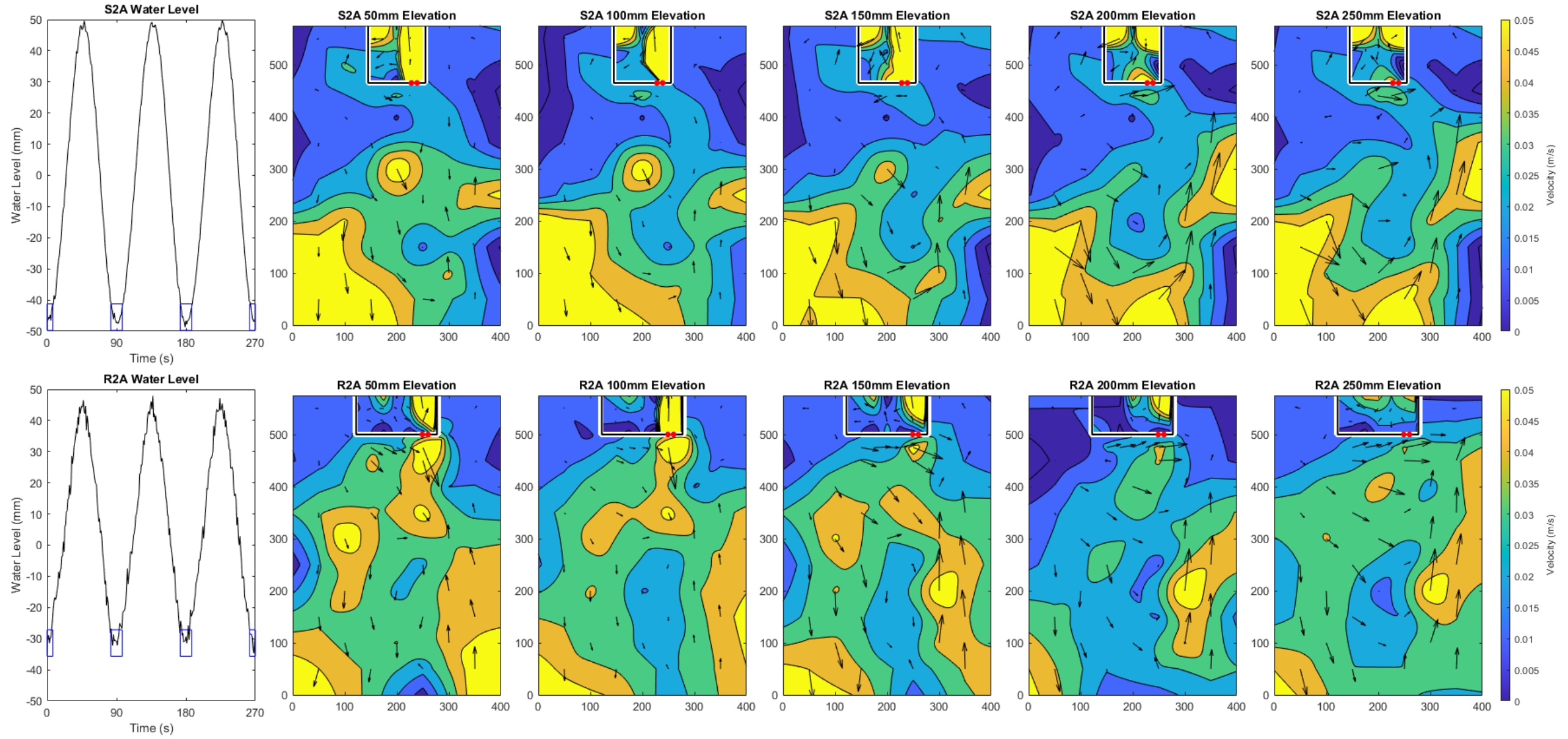


Figure 6.35 Comparison F iii - Velocity contour maps at elevations of 50, 100, 150, 200 and 250 mm above the bed during low tide.

6. Test Case 3 – Impact of Varying Geometry

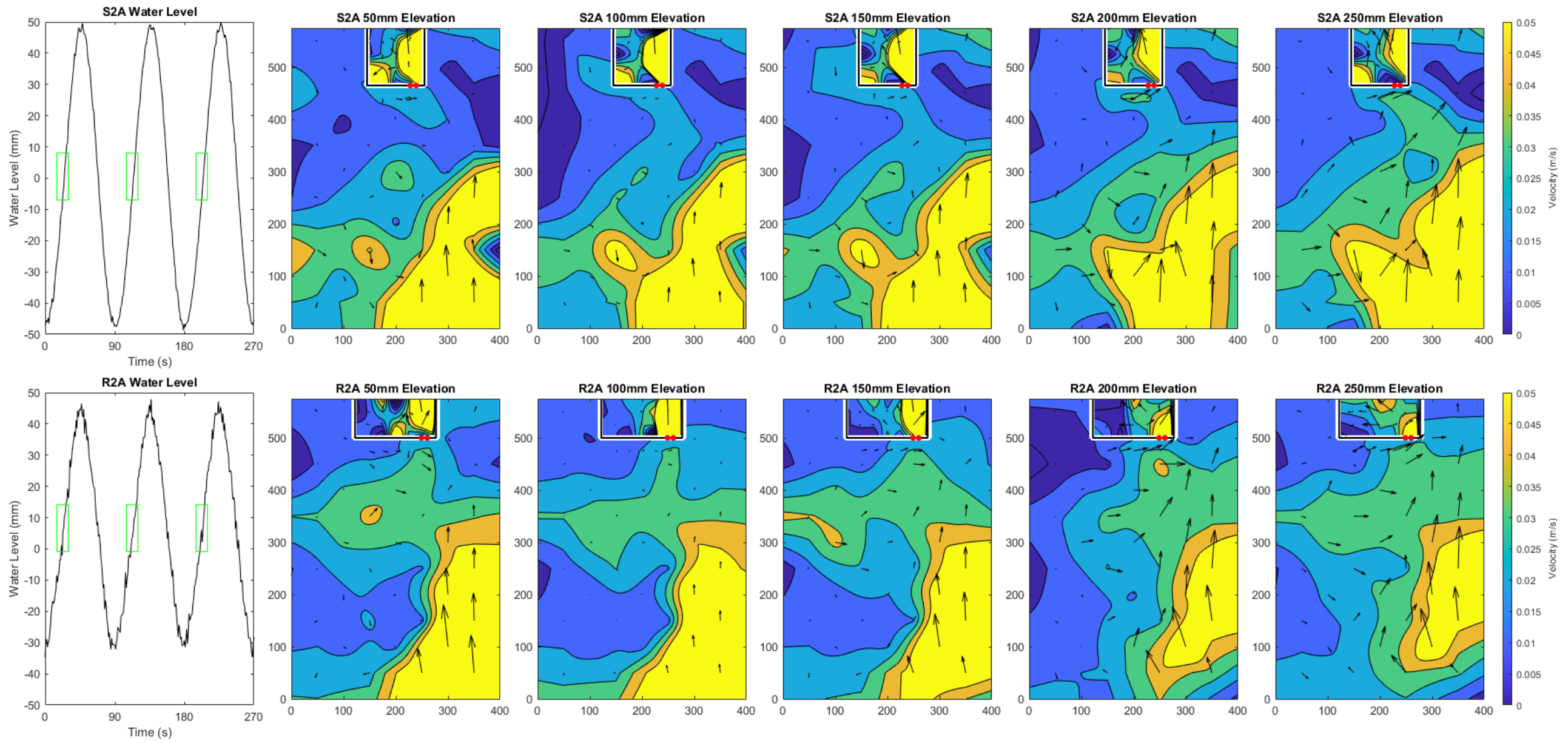


Figure 6.36 Comparison F iii - Velocity contour maps at elevations of 50, 100, 150, 200 and 250 mm above the bed during the flood tide.

6. Test Case 3 – Impact of Varying Geometry

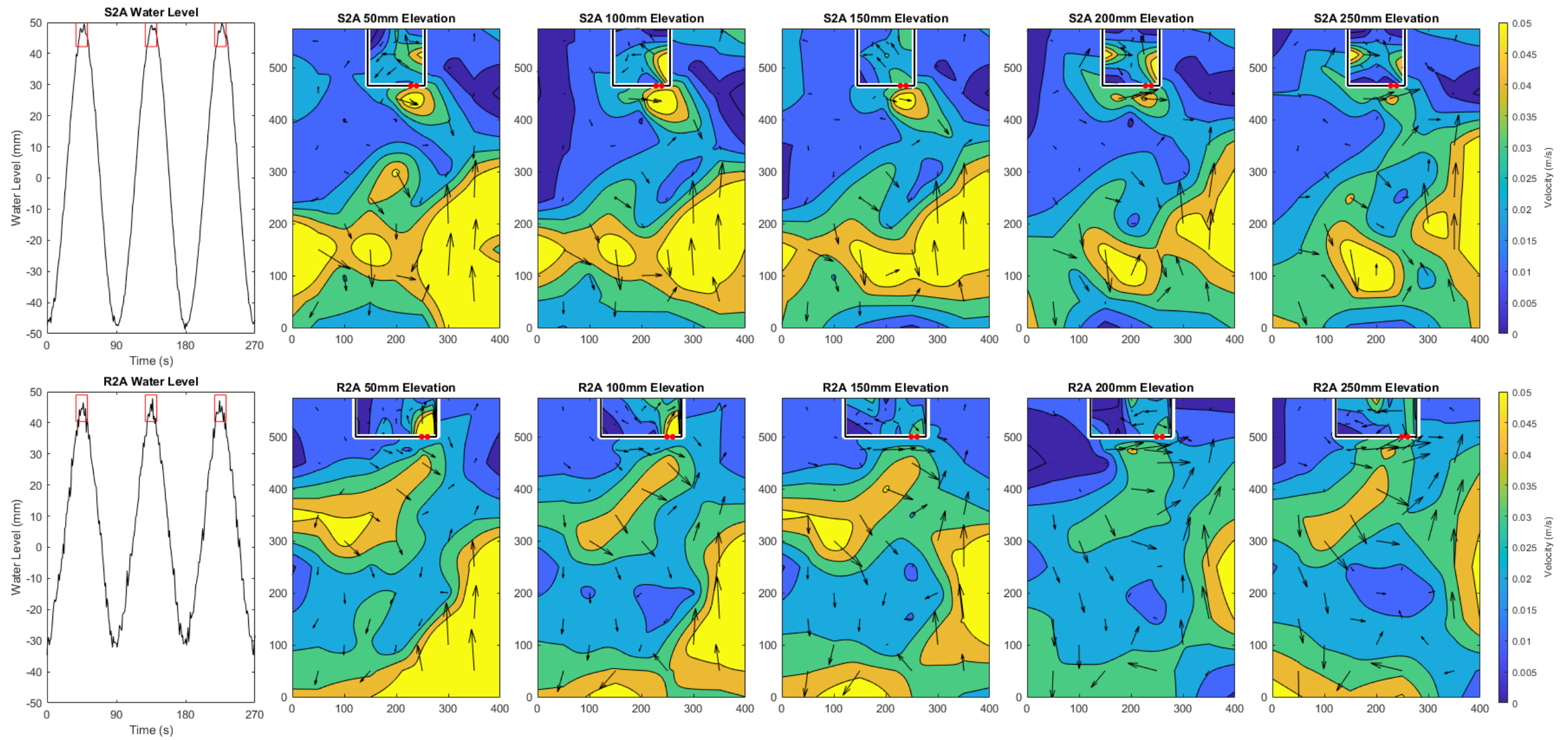


Figure 6.37 Comparison F iii - Velocity contour maps at elevations of 50, 100, 150, 200 and 250 mm above the bed during high tide.

6. Test Case 3 – Impact of Varying Geometry

6.2.3.3 Velocity – Residual Velocity Magnitude and Direction

The residual magnitude and direction of the velocity, plotted in Figure 6.38 as contours and arrows respectively, displays some symmetry in the square case Figure 6.38. This is unusual as we would expect the offset turbines to lead to stronger flows on one side of the tank or at least to deflect the flow to cause asymmetry in the outer tank. This is the case however inside the square TRS where the strongest flow is found directly behind the turbine openings along the right-hand wall and then ripples across to the left-hand wall. Whereas we would expect that two turbines together would cause greater disruption to the wider area, in the rectangular case there is less variation in flow across the tank which implies that flow through the turbines has little influence on the wider tank area. Inside the rectangular TRS however there is much greater variation with strong fast flows reaching along the right-hand and front wall of the TRS to reach further into the impounded area than before. This emphasises the findings of Comparison A that two turbines together enable greater circulation than a single turbine in the same location so that water is not left stagnant in the far reaches of the TRS as was the case in R1.

6. Test Case 3 – Impact of Varying Geometry

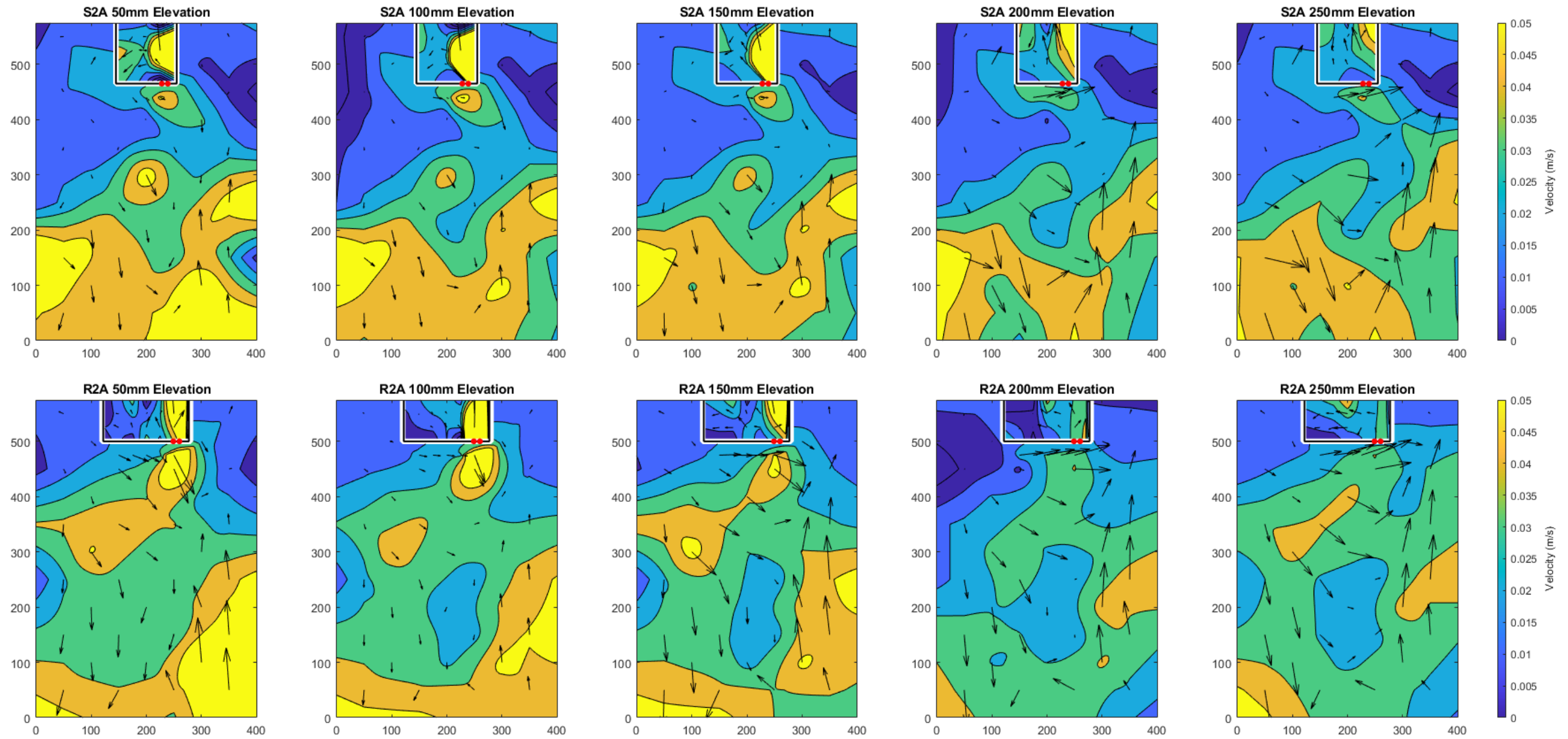


Figure 6.38 Comparison F iii – Contour maps of residual velocity magnitude and direction at elevations of 50, 100, 150, 200 and 200 mm from the bed.

6. Test Case 3 – Impact of Varying Geometry

6.2.3.4 Flow Visualisation

Flow visualisation of these two experiments, S2A vs R2A (Figure 6.39 and Figure 6.40 respectively), show extremely similar patterns to those observed in the previous comparison, S1A vs R1 (see Figure 6.24 and Figure 6.25). Flow visualisation in the square TRS shows two circulating cells, split right and left, whereas the two cells in the rectangular TRS are split front and back, as seen in the Comparison F ii. The circulating cells in both cases mix quite early on (within 30 seconds, a third of a tidal cycle), but mixing is much stronger in the square case. As with the single turbine cases these experiments show how when turbine openings are positioned at one end of the TRS seawall, a square shape is better for ensuring full mixing of the lagoon since the proximity of the side walls allows water to be reflected to fill the whole area, whilst the longer, thinner shape of the rectangular lagoon means that mixing takes longer and there can be areas where water is not replenished regularly enough to maintain an healthy environment. This follows the idea of Wells and van Heijst (2003) that if vortices are longer lived, they change the mixing properties of the tidal flow as circulation in the vortex forms a barrier to transport.

6. Test Case 3 – Impact of Varying Geometry

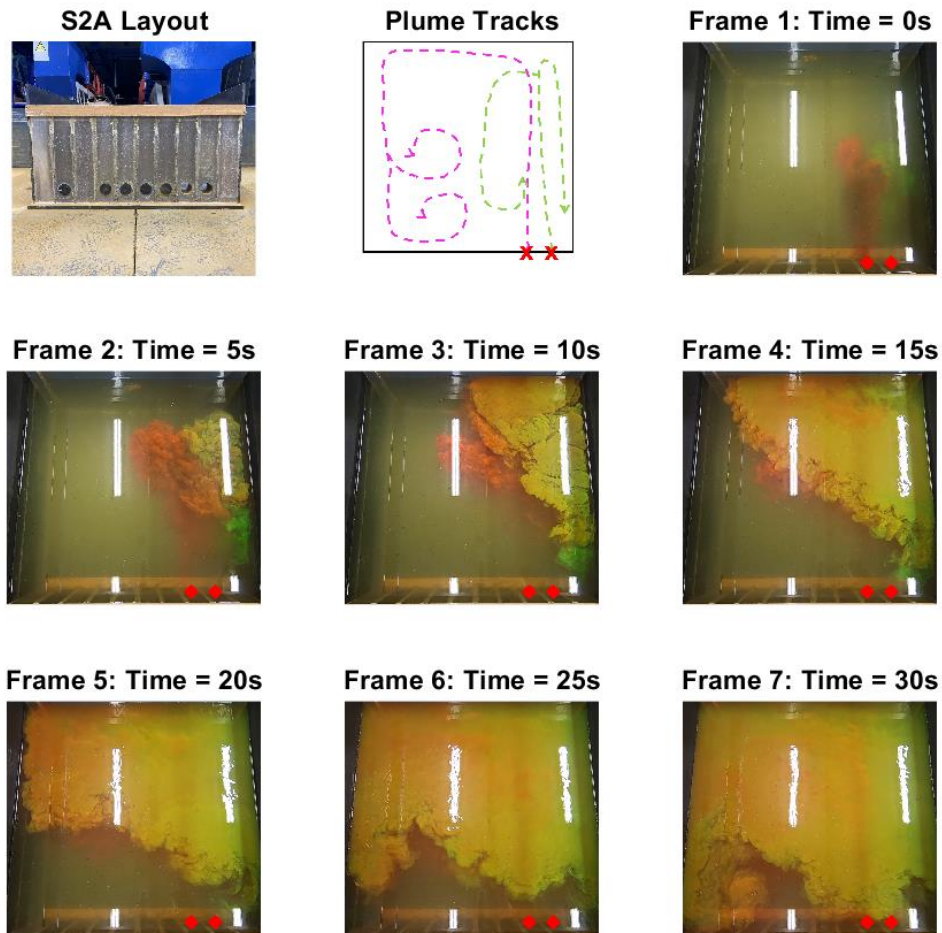


Figure 6.39 Flow visualisation for experiment S2A.

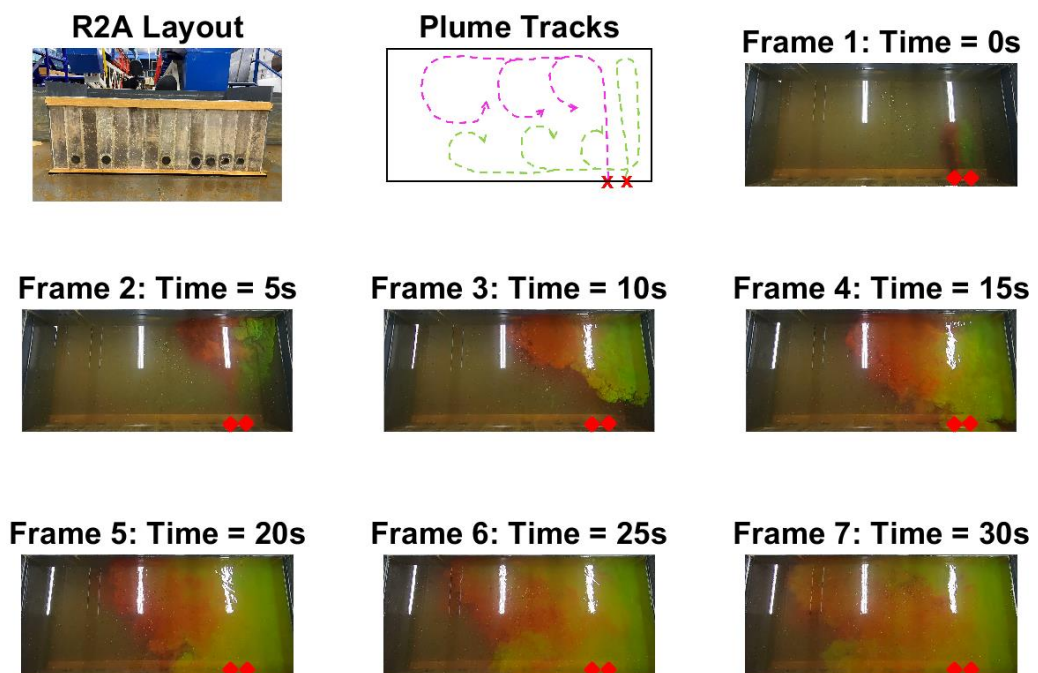


Figure 6.40 Flow visualisation for experiment R2A.

6. Test Case 3 – Impact of Varying Geometry

6.2.3.5 Statistical Analysis

When directly comparing the results of residual flow velocity for experiments S2A and R2A in Figure 6.41 there is no correlation evident between the two. This shows that even though the two turbines in each case have the same spacing, the shape of the TRS has caused a significant difference to flow conditions and the two shapes do not lead to corresponding flow velocities in the tank. This is confirmed by the histogram of frequency distribution for residual flow magnitude (Figure 6.42) which shows a very different range of values for each case.

In terms of flow direction however, there is some correlation between the experiments (Figure 6.43 and Figure 6.44) which suggests that although the different shape of TRS alters flow speed it does not make such a difference to flow direction.

Results of Pearson's correlation coefficient show the weakest correlation of any of the results (see Table 6.2 for r and z values) and although the z -test result suggests that we should accept the null hypothesis here, other evidence suggests that there is a significant difference between the cases and that when two turbines are placed side by side, they lead to very different results depending on the shape of the TRS. This is due to the wider rectangular TRS prohibiting flow in certain parts of the tank, both inside and outside of the lagoon.

6. Test Case 3 – Impact of Varying Geometry

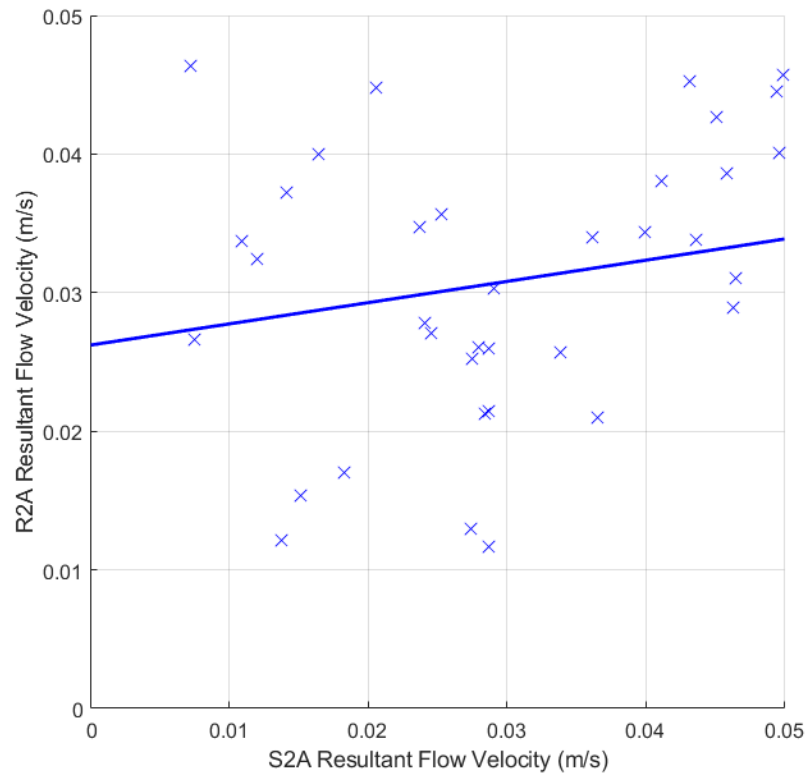


Figure 6.41 Comparison F iii - Regression analysis of residual flow velocity.

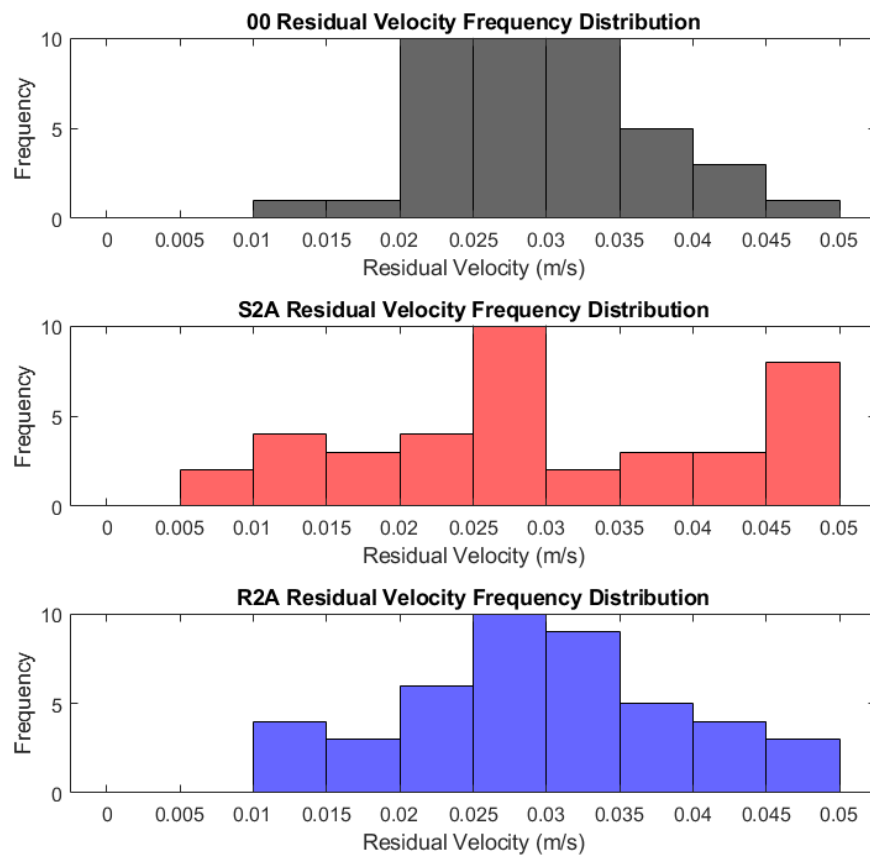


Figure 6.42 Comparison F iii – Distribution analysis of residual flow velocity.

6. Test Case 3 – Impact of Varying Geometry

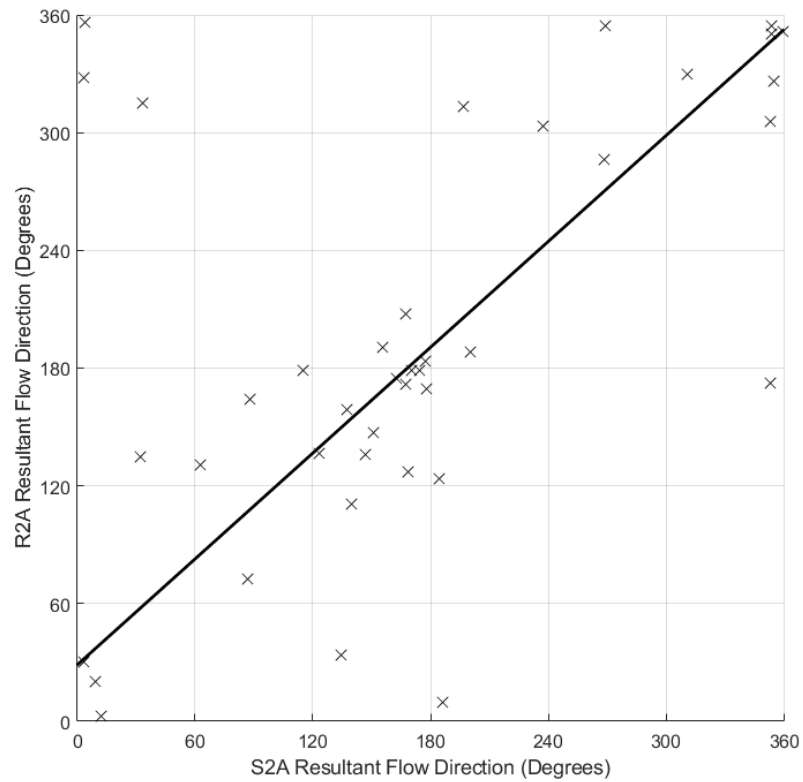


Figure 6.43 Comparison F iii - Regression analysis of residual flow direction.

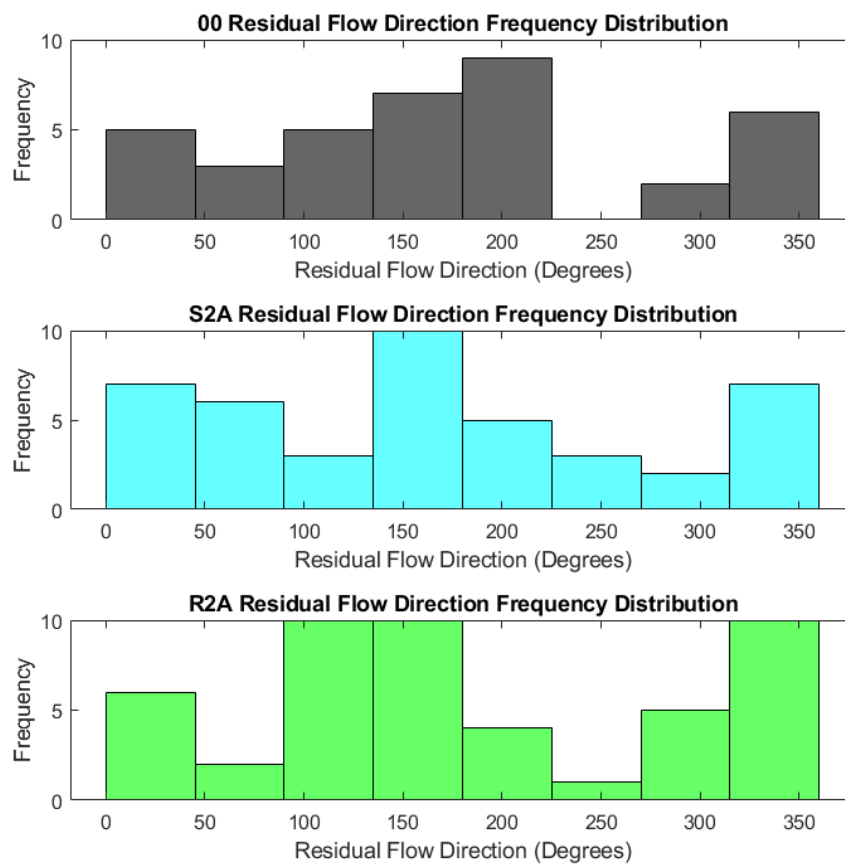


Figure 6.44 Comparison F iii – Distribution analysis of residual flow direction.

6. Test Case 3 – Impact of Varying Geometry

6.2.4 Comparison F iv – Square vs Rectangular TRS with 2 turbines at opposite ends of seawall

Comparison F iv compares results from experiments with a square (S2B) and rectangular (R2D) TRS, both with a pair of turbines positioned at opposite ends of the TRS wall, against pre-lagoon conditions to investigate the effects of turbine spacing and position on hydrodynamics. The layout of these experiments is illustrated in Figure 6.45.

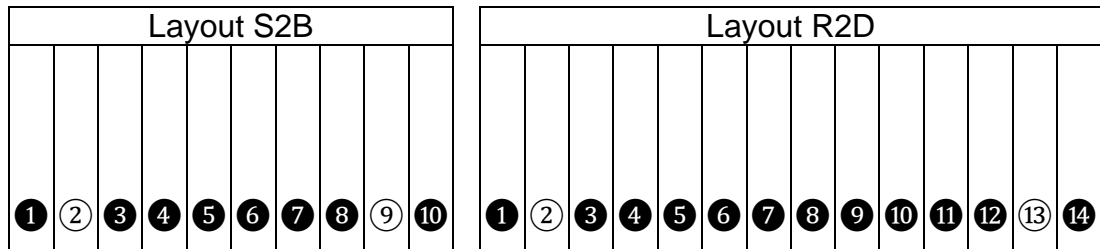


Figure 6.45 Experiment layouts for Comparison F iv: S2B and R2D.

6.2.4.1 Velocity - Depth Averaged

In these experiments, the turbines are placed at opposite ends of the TRS seawall, so although not entirely aligned with each other they should affect the inner and outer areas of the tank in similar ways. This can be seen in the similarity in flow patterns and velocity range throughout the tank, with the two scenarios closely matching each other in the majority of locations as seen in Figure 6.47. The greatest difference occurs at (150,350) (closer detail given by Figure 6.46) where S2B experiences a sudden peak. This is unusual since we would not expect a peak at this offset position in the tank, nor this far from the TRS and as it is not accompanied by any other peaked data along this transect could be due to an anomaly,

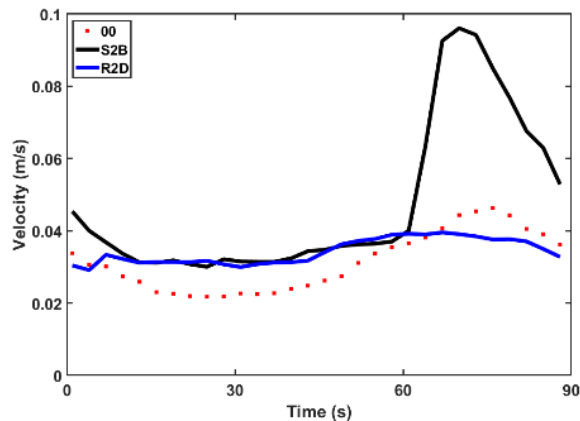


Figure 6.46 Closer detail of flow velocity at (150,350).

6. Test Case 3 – Impact of Varying Geometry

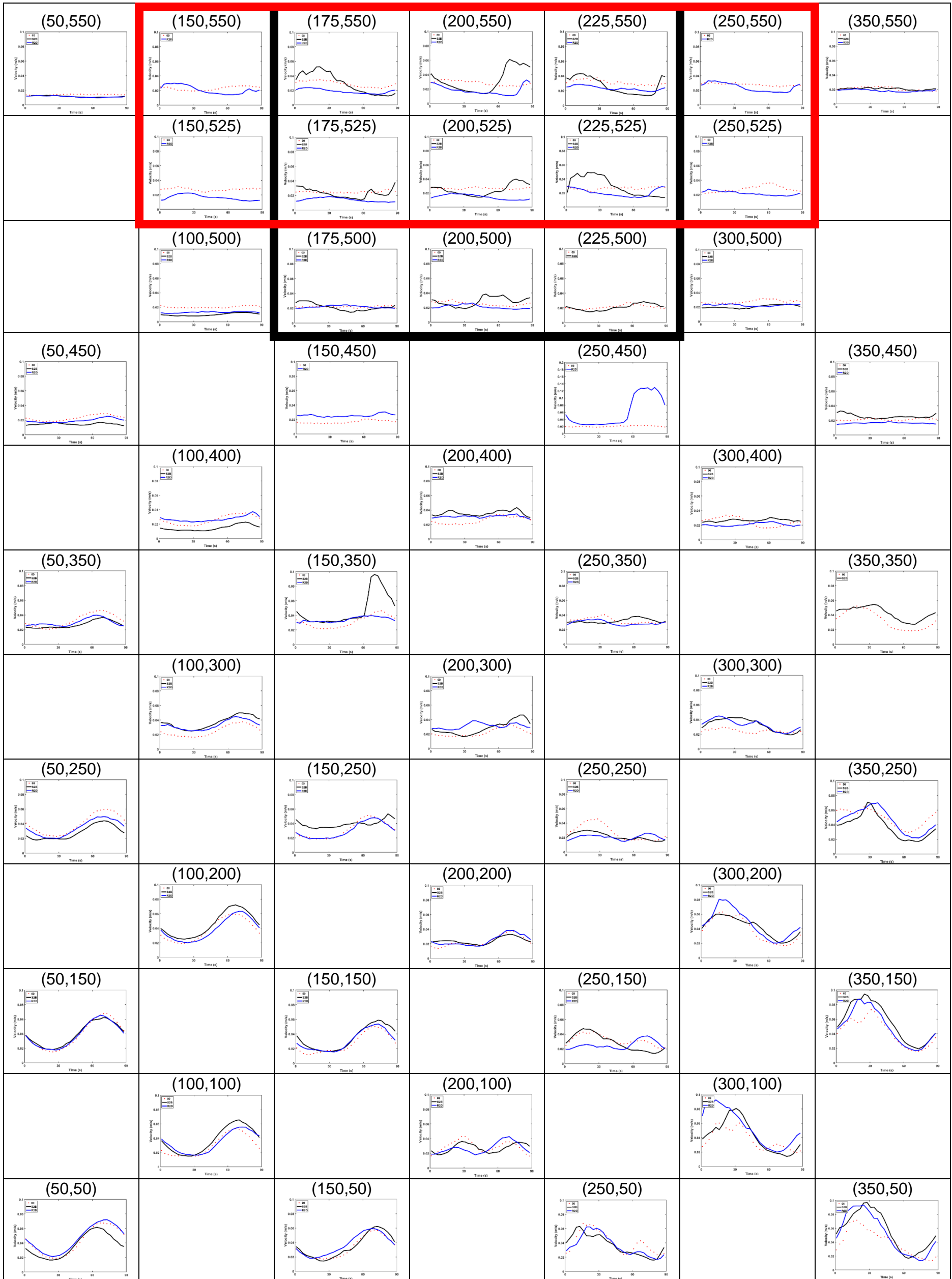


Figure 6.47 Map of depth averaged velocity plots for Comparison F iv: S2B and R2D.

6. Test Case 3 – Impact of Varying Geometry

Directly in front of the seawall there is peak in results for experiment R2D at (250,450) which is to be expected since it is close to the seawall and the right-hand turbine, however there is no data from this location for S2B with which to compare to see if this phenomenon happens in both experiments.

Inside the TRS, where points are available for comparison, it can be seen that flow through the turbine openings behaves in similar ways for both shapes of TRS but to different extents. For example, flow velocities peak along the side walls for both experiments, since this is where the turbines are positioned, e.g. (150,550) and (250,550) for the rectangular TRS and (175,550) and (225,550) for the square TRS (Figure 6.48 to Figure 6.51), but the peak is much greater in the square case than the rectangle. Also, along the centre line of the TRS for both cases, flow has reduced, as we would expect further away from the turbines, but is still much faster in the S2B than R2D, (200,550) (Figure 6.52). This is due to the proximity of the sidewalls in the square TRS, with wakes being reflected off both side walls before converging in the centre to maintain higher flow velocities than in the rectangular TRS. In R2D, the longer, thinner shape of the rectangular TRS means that although flows are increased at the edges of the lagoon, they are not strong enough to have an impact on the centre of the lagoon and in fact velocities within the rectangular TRS are all below the baseline conditions. This shows how the wider spacing of the rectangular TRS are able to slow flows overall which would enable other activities to take place in this area but may lead to problems with water quality if water is not circulated and flushed effectively.

6. Test Case 3 – Impact of Varying Geometry

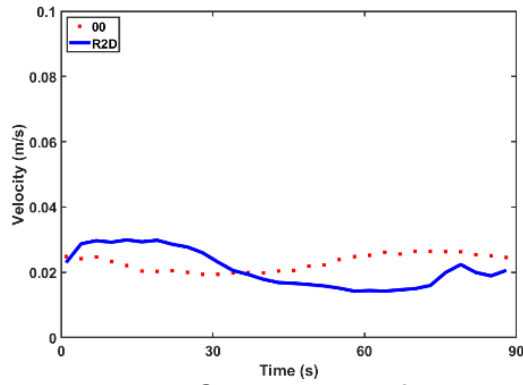


Figure 6.48 Closer detail of velocity at (150,550).

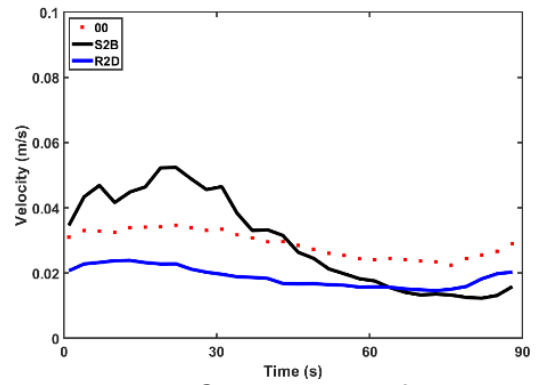


Figure 6.49 Closer detail of velocity at (175,550).

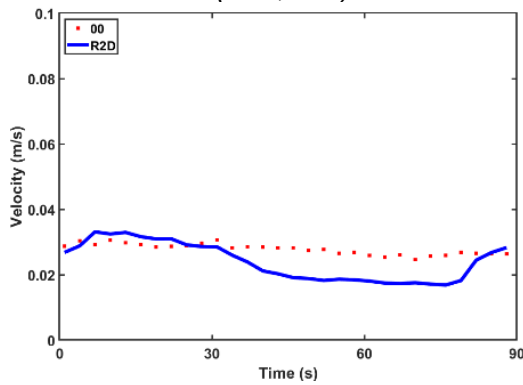


Figure 6.50 Closer detail of velocity at (250,550).

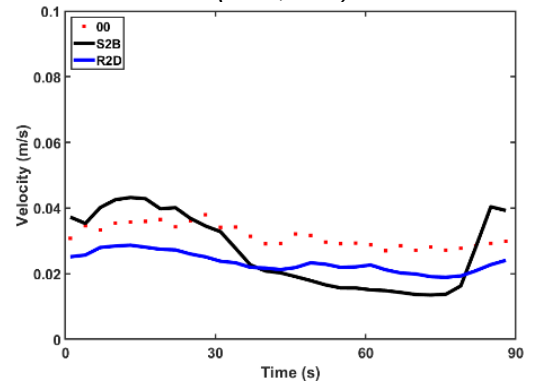


Figure 6.51 Closer detail of velocity at (225,550).

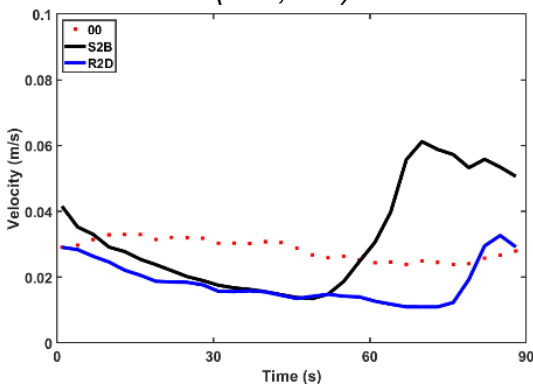


Figure 6.52 Closer detail of velocity at (200,550).

6. Test Case 3 – Impact of Varying Geometry

6.2.4.2 Velocity – Analysed by tide and depth

As with previous analysis, the velocity contour plots show little variation between each depth of the experiments compared here in Figure 6.53. This suggests that the spacing of the turbines has little effect on flow velocity throughout the water column outside of the TRS and that underlying flow conditions dictate flow behaviour to a greater extent than the presence or design of a TRS. Between the experiments the same patterns exist as before, with the strongest flows in front of the TRS and to the left of the basin. Strong symmetry can be seen inside the TRS in S2B, demonstrating how water ebbs evenly through the equally spaced turbines. Inside the TRS in R2D, there is some symmetry near the bed, but velocity is very low in the upper depths which suggests that during the ebb tide, flow is concentrated near the bed as water leaves the TRS and that there is less movement nearer the surface.

At low tide, flow patterns in the outer tank remain similar at all depths (Figure 6.54). Inside the square TRS symmetry is still present in the upper layers of S2B but is less defined near the bed showing how during this time of slack water the residual current is able to reach the upper layers, but that flow is more complex near the turbine openings themselves. Inside the TRS for case R2D, flow is irregular and changes at all depths but always with the strongest flows directly behind the right-hand turbine. This points to the three-dimensional element of the turbine wakes being stronger in the case of the square TRS than the rectangle since its impacts are felt at more depths and is most likely due to the proximity of the side walls in the compact square case causing a greater effect on the shape and direction of the current. This agrees with previous analysis that the elongated shape of the rectangular TRS means there is less interaction with the seawall preventing currents from circulating in the whole space despite having the same area as the square TRS.

The flood tide graphs (Figure 6.56Figure 6.55) maintain similarity between depths and show no great deviation from previous experiments. Inside the TRS, symmetry is once again present in S2B and there is more flow in S2D than before, with some symmetry near the surface. This means that the

6. Test Case 3 – Impact of Varying Geometry

three-dimensional component of the turbine wakes has been able to circulate throughout the whole water column during the flood tide.

High tide reveals similar patterns in the outer tank as before (Figure 6.56) but some changes have taken place inside the TRS. In S2B, symmetry is still evident up to an elevation of 150 mm demonstrating even forces closer to the bed. Inside R2D, flow is stronger near the bed but there is still very little circulation in the upper layers. In this case the residual flow from the flood tide is perhaps able to permeate the lowest depths but not reach further up the water column. Overall, there has been little flow within the rectangular TRS during any tide, confirming that this shape prohibits circulation.

6. Test Case 3 – Impact of Varying Geometry

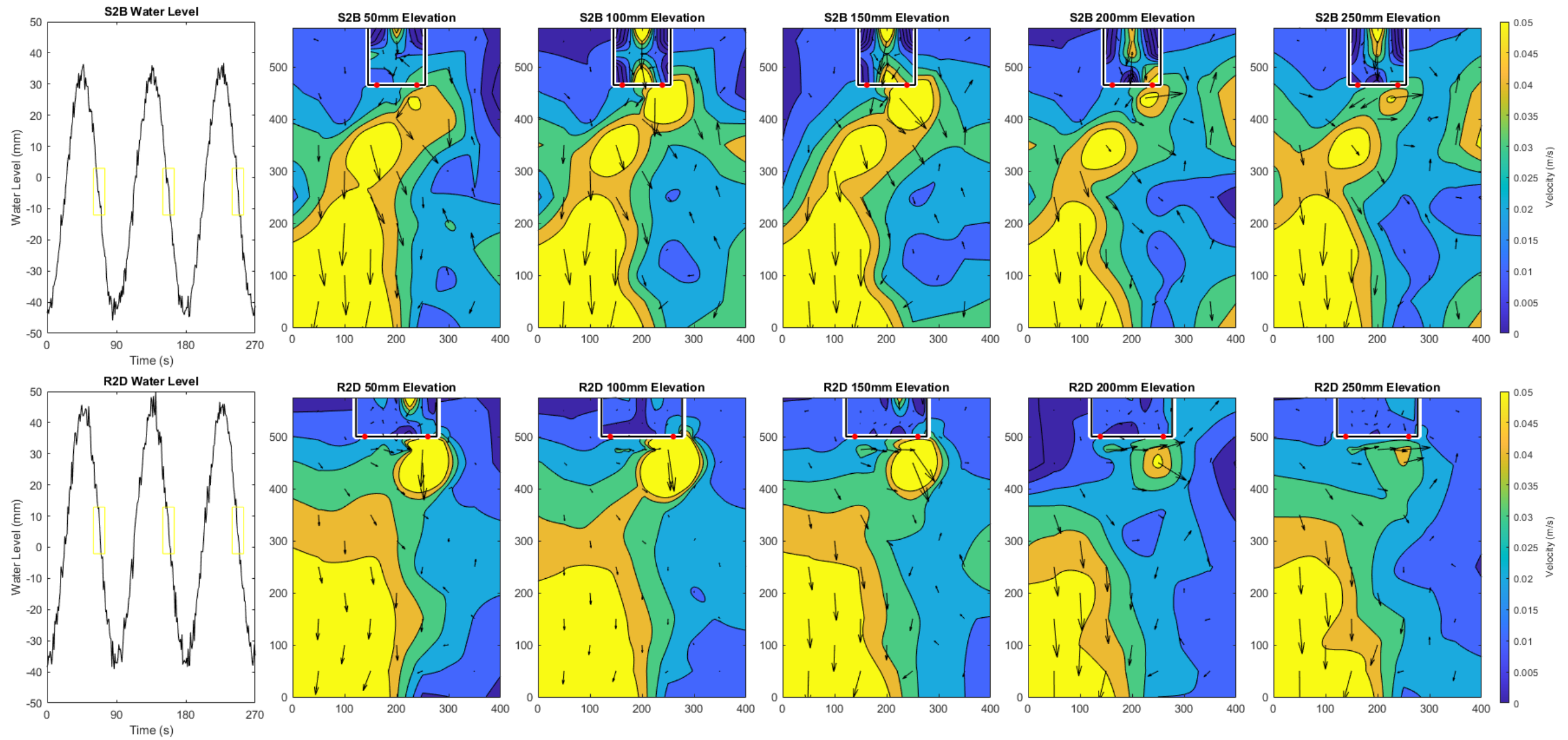


Figure 6.53 Comparison F iv - Velocity contour maps at elevations of 50, 100, 150, 200 and 250 mm above the bed during the ebb tide.

6. Test Case 3 – Impact of Varying Geometry

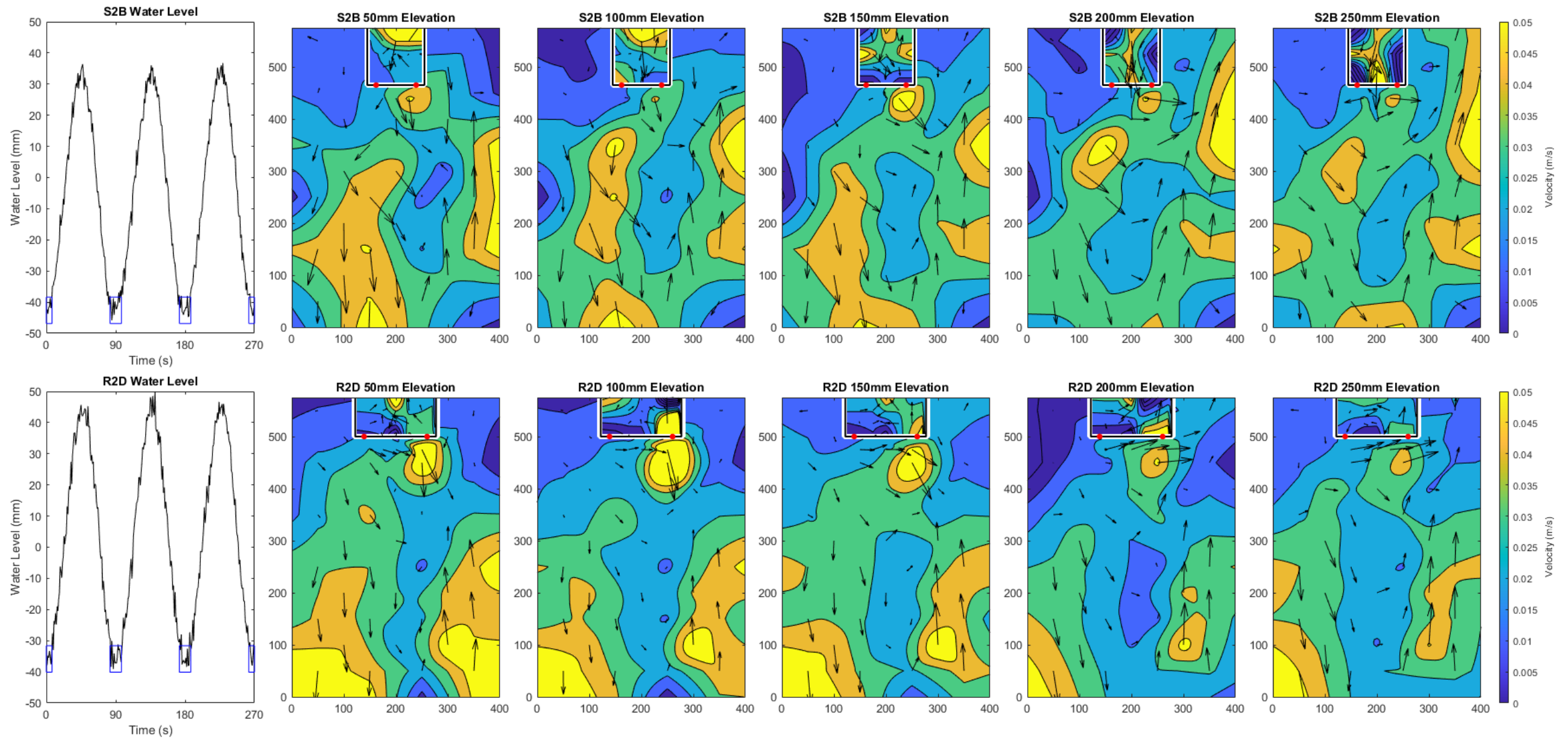


Figure 6.54 Comparison F iv - Velocity contour maps at elevations of 50, 100, 150, 200 and 250 mm above the bed during low tide.

6. Test Case 3 – Impact of Varying Geometry

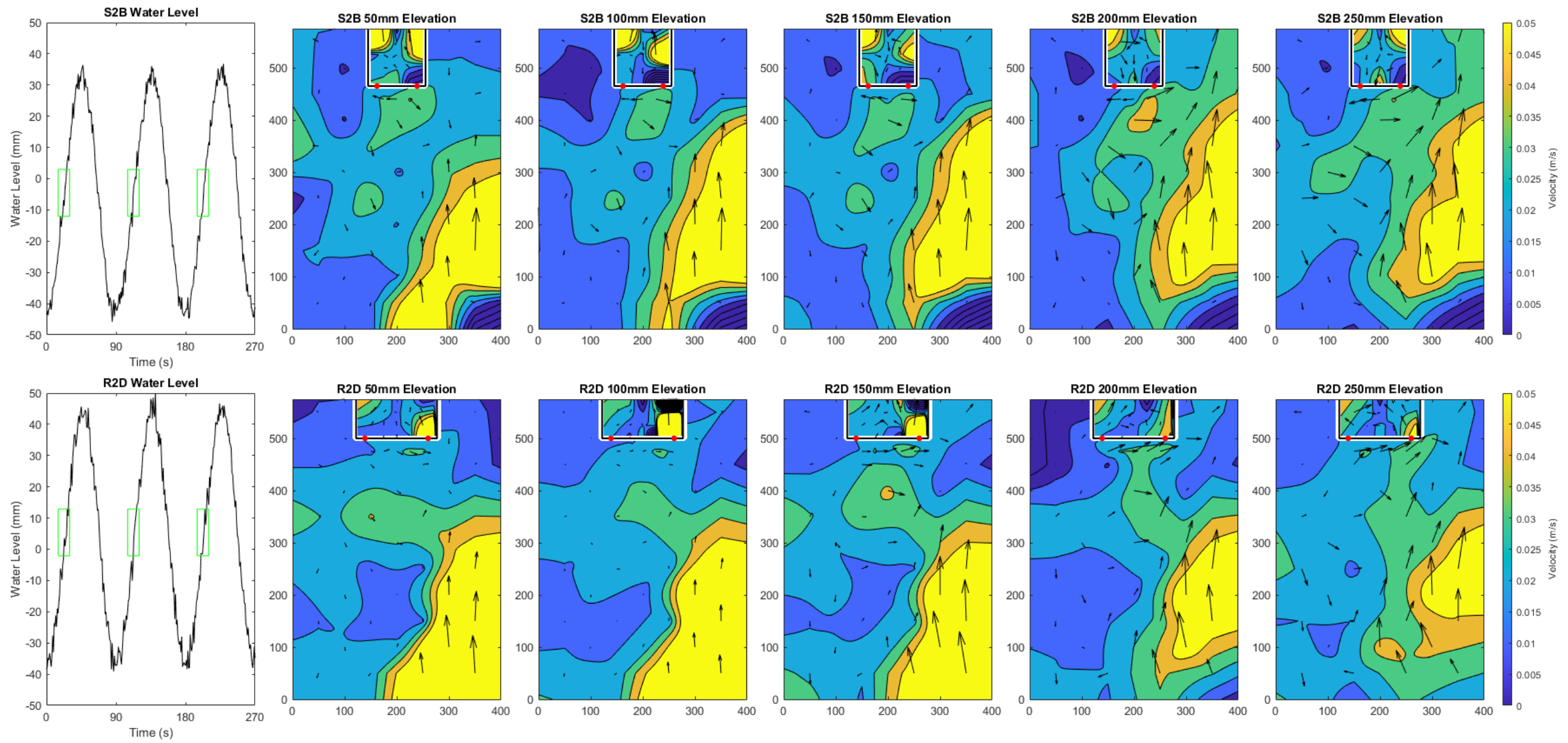


Figure 6.55 Comparison F iv - Velocity contour maps at elevations of 50, 100, 150, 200 and 250 mm above the bed during the flood tide.

6. Test Case 3 – Impact of Varying Geometry

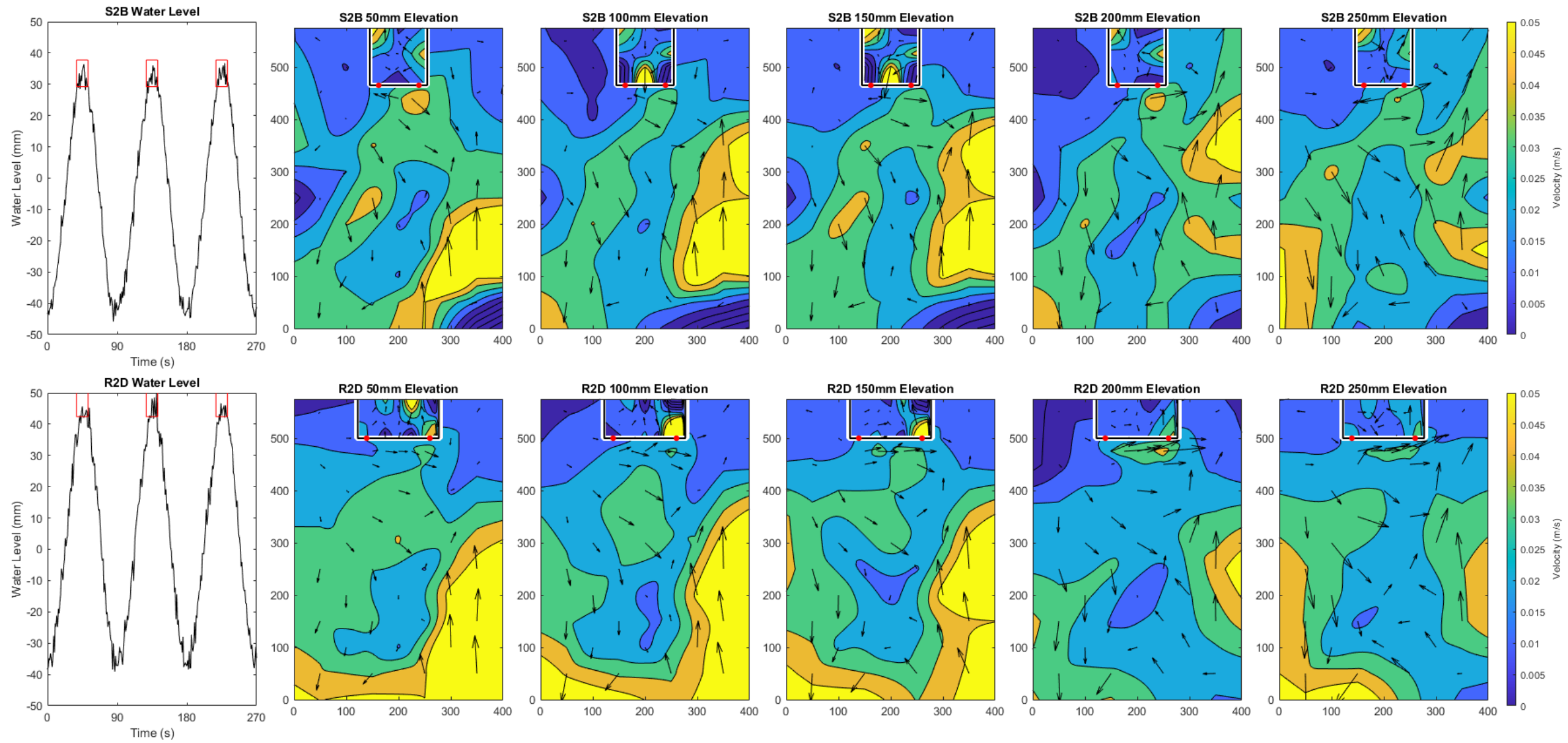


Figure 6.56 Comparison F iv - Velocity contour maps at elevations of 50, 100, 150, 200 and 250 mm above the bed during high tide.

6. Test Case 3 – Impact of Varying Geometry

6.2.4.3 Velocity – Residual Velocity Magnitude and Direction

Contour plots of the residual velocity magnitude and direction presented in Figure 6.57 show asymmetrical flow in both cases but with stronger forces around the outer tank in the square case than the rectangle. Inside the square TRS, there is some symmetry apparent as shown in the contour plots for each tide. Inside the rectangular case the strongest flows radiate from behind the right-hand turbine opening but flow is very weak around the left-hand turbine. The size of the directional arrows, denoting flow magnitude, show some circulation within the square TRS whilst circulation is very weak inside the rectangular TRS which confirms that the water is less able to flow around this longer, thinner shape.

6. Test Case 3 – Impact of Varying Geometry

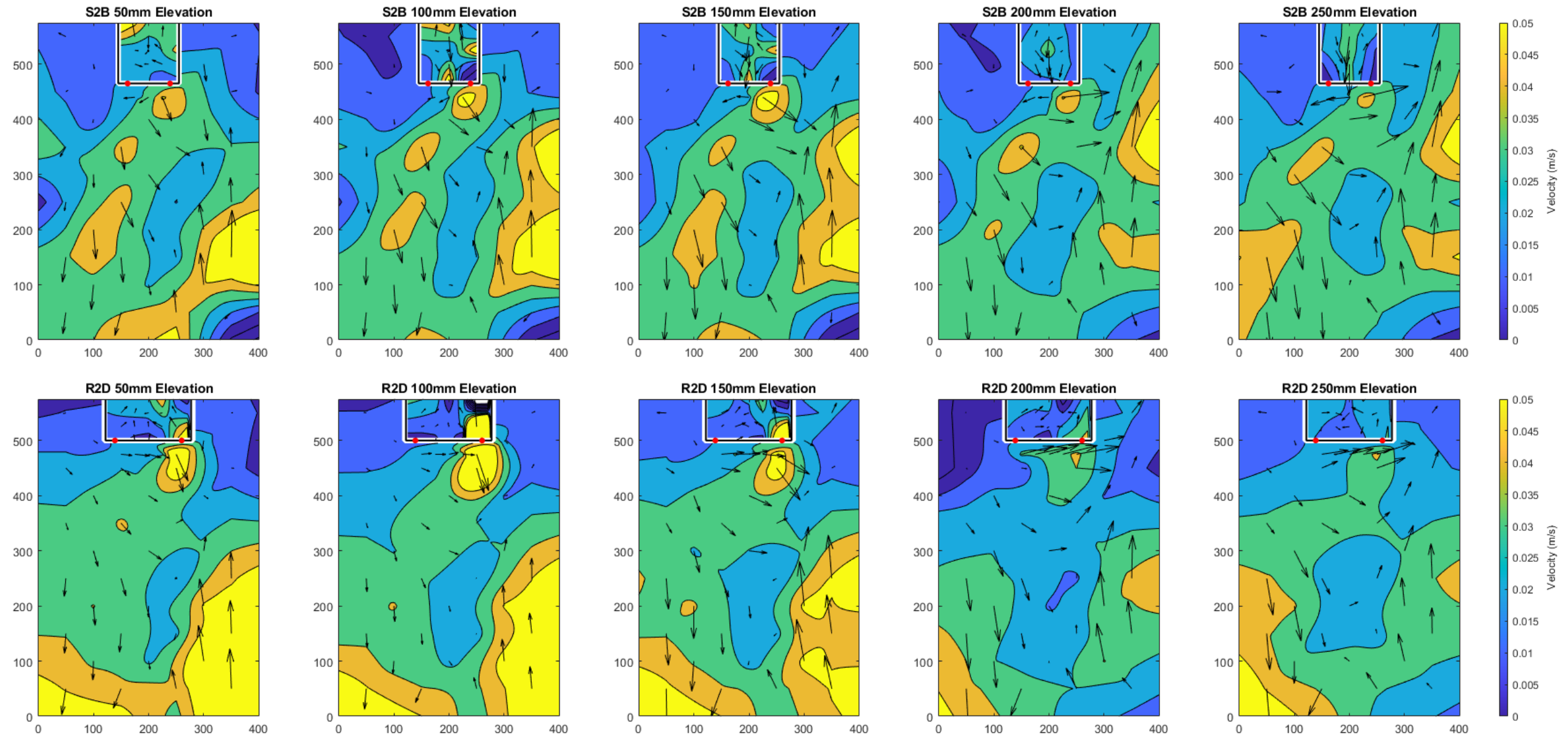


Figure 6.57 Comparison F iv – Contour maps of residual velocity magnitude and direction at elevations of 50, 100, 150, 200 and 200 mm from the bed.

6. Test Case 3 – Impact of Varying Geometry

6.2.4.4 Flow Visualisation

The results of flow visualisation between experiments S2B and R2D are very similar (see Figure 6.58 and Figure 6.59). In both cases the wake jets follow the side walls closest to the turbine opening before being reflected off the rear wall to return to the front wall along the centre line of the TRS, with two distinct circulation cells and slight mixing along the interaction boundary in the centre of the lagoon. These two distinct circulation currents, evident in both cases, prove that turbine spacing and proximity to side walls has more influence on flow patterns than the shape of the TRS since near identical patterns are observed in both the square and rectangular TRSs. This is most evident in the present comparison case as the wide spacing of the turbine openings allows the two separate dye plumes to be observed more clearly but has also been demonstrated in the previous comparisons, F ii and F iii, where circulation patterns were extremely similar between the square and rectangular cases where turbines were positioned in comparable locations.

6. Test Case 3 – Impact of Varying Geometry

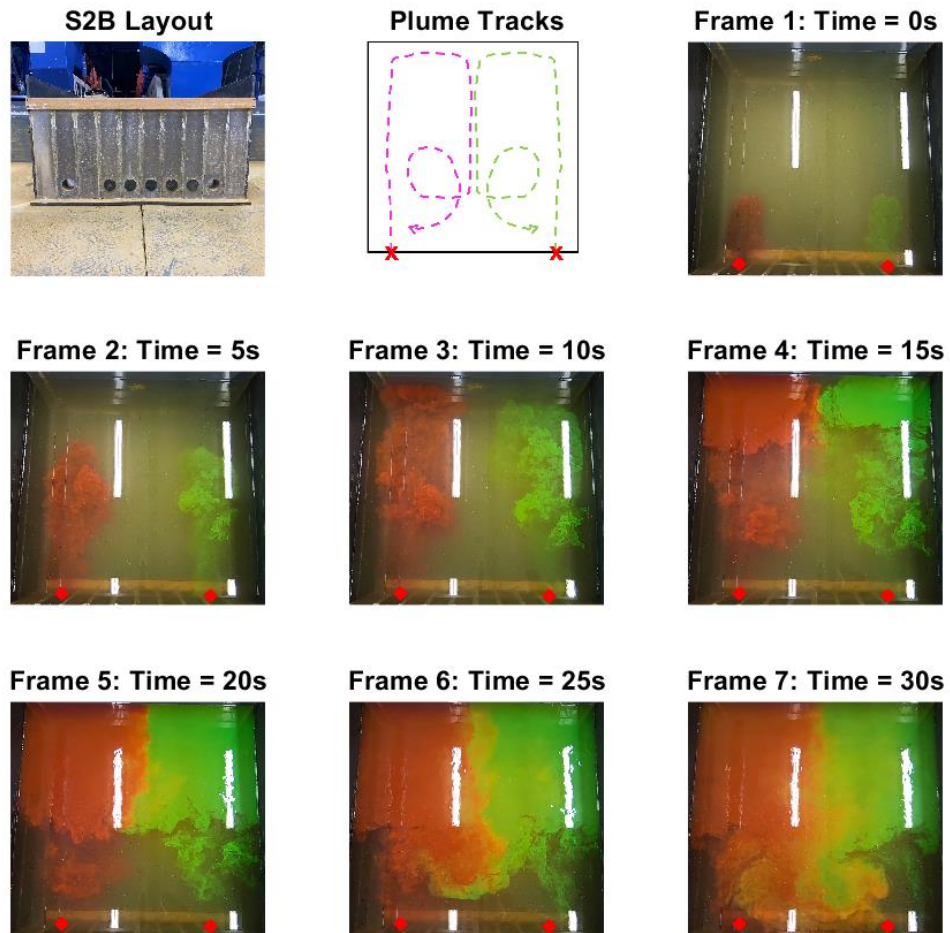


Figure 6.58 Flow visualisation for experiment S2B.

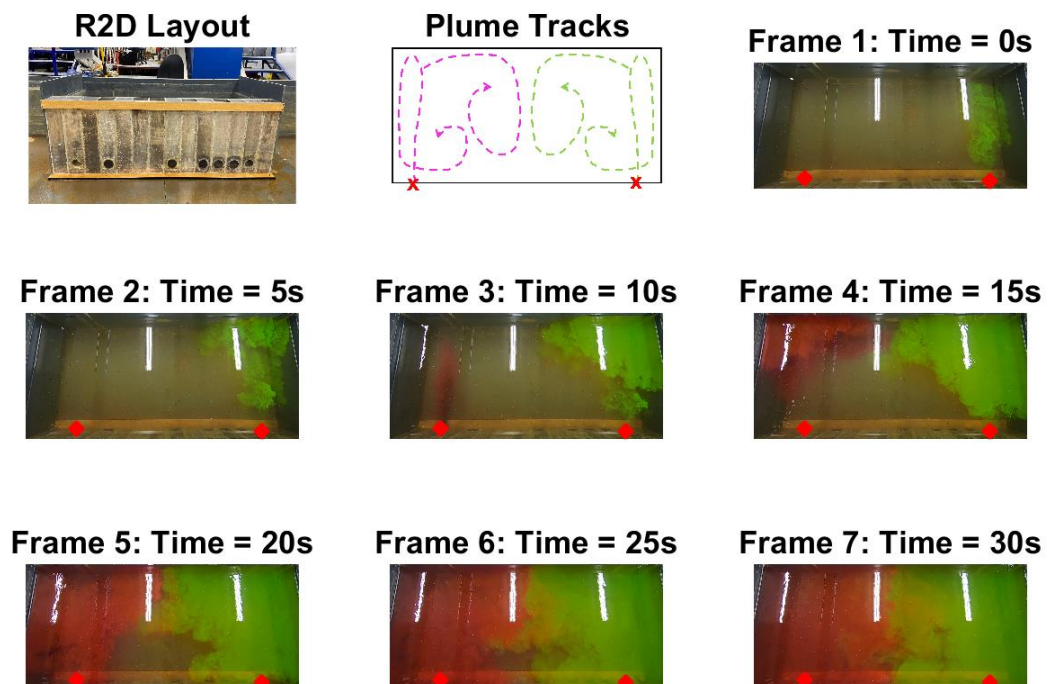


Figure 6.59 Flow visualisation for experiment R2D.

6.2.4.5 Statistical Analysis

Regression analysis of the results for S2B and R2D plotted in (Figure 6.60) show strong positive correlation. This suggests that when two turbines are positioned at opposite ends of the seawall there is less difference between the results for a square and rectangular TRS than when the turbines are placed close together. This is further shown in the results of residual flow direction in Figure 6.62 which displays a strong relationship between the results for both experiments.

It is therefore possible to trust the z-test result here (see Table 6.2 for z-test values) which leads us to accept the null hypothesis that there is not a statistically significant difference between the results of these experiments. Overall, this paints a positive picture for wider spaced turbines which allow circulation throughout the whole of the lagoon area and supports the findings of Angeloudis et al (2016b) who advocate wider turbine spacing for reducing strong currents and adverse hydro-ecological consequences.

6. Test Case 3 – Impact of Varying Geometry

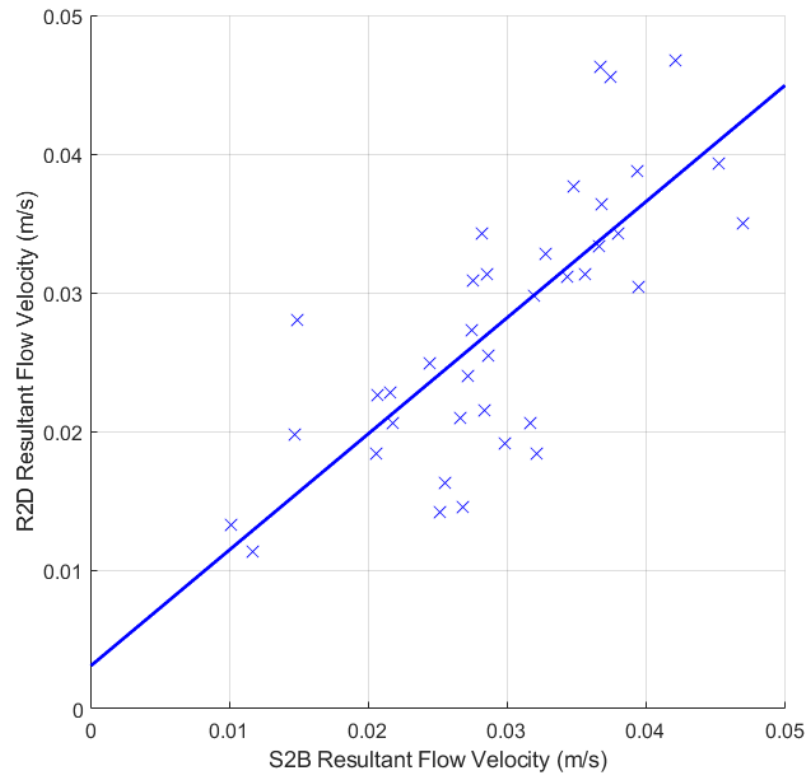


Figure 6.60 Comparison F iv - Regression analysis of residual flow velocity.

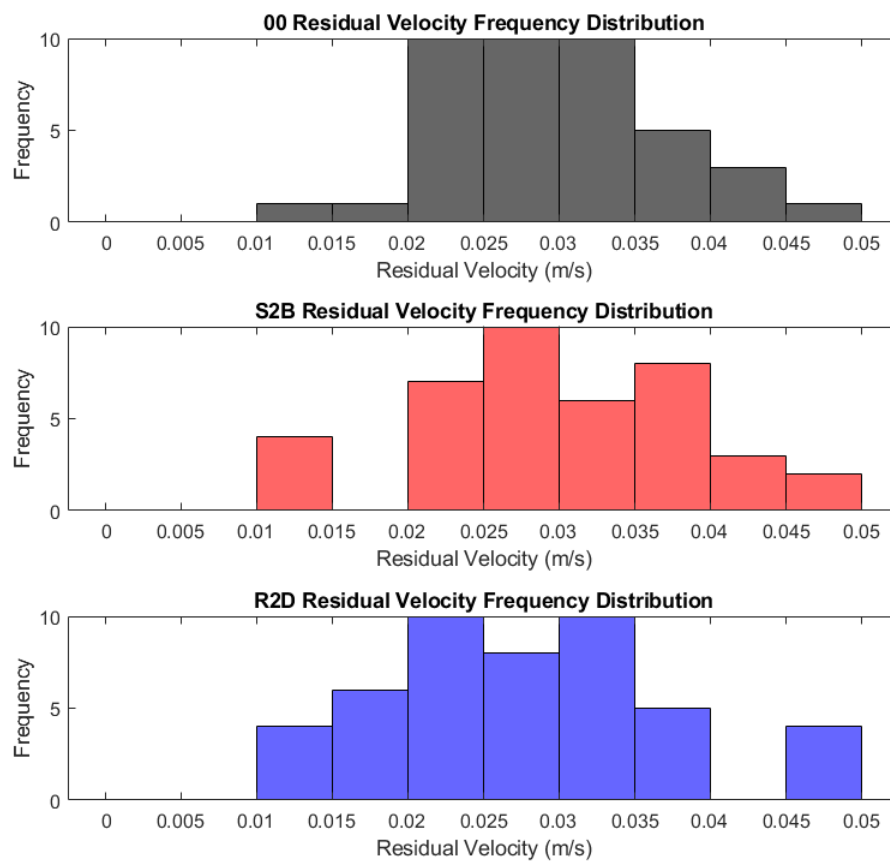


Figure 6.61 Comparison F iv – Distribution analysis of residual flow velocity.

6. Test Case 3 – Impact of Varying Geometry

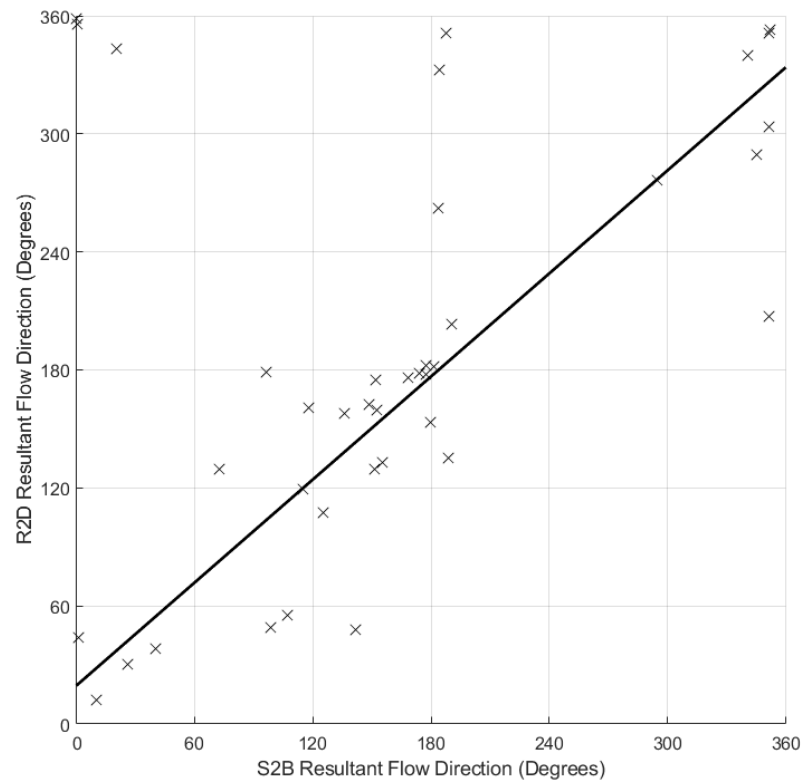


Figure 6.62 Comparison F iv - Regression analysis of residual flow direction.

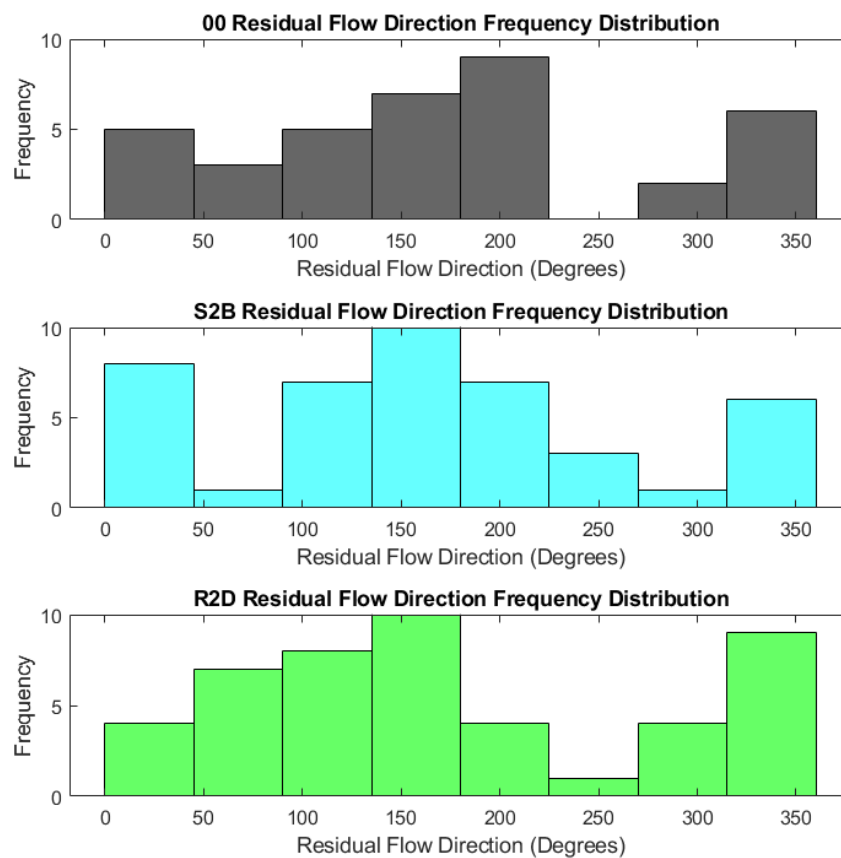


Figure 6.63 Comparison F iv – Distribution analysis of residual flow direction.

6. Test Case 3 – Impact of Varying Geometry

6.2.5 Comparison O – All cases compared to pre-lagoon levels

Having compared each of the experiments against each other it is also worth comparing the results of each scenario against the pre-lagoon state to see which of the configurations had the greatest impact in changing baseline conditions. This has been achieved by plotting linear models of the residual velocity from each experiment against those measured in the empty basin and by mapping the similarities and differences of values across the domain.

6.2.5.1 Regression Analysis

In order to determine which TRS design causes the least disruption to the original environmental conditions, residual velocity magnitude for each experiment has been plotted against the measurements from the pre-lagoon case. These results have been plotted to include a linear regression line of best fit as well as margins to indicate the 95% confidence level of this line (two standard deviations of the mean results) and are discussed in Table 6.3. (See Annex 2 for graphs.)

Table 6.3 Discussion of regression analysis between experiments and pre-lagoon conditions (Graphs in Annex 2).

Case	Comments
S0	The results of S0 are less scattered than other cases which indicates that when there are no turbines the velocity within the tank is less variable. Only a third of the data falls within the 95% confidence interval of the line of best fit which suggests that the S0 results are not closely related to pre-lagoon conditions overall and that the introduction of a TRS significantly impacts upon the natural environment.
S1A	The results of S1A are extremely scattered and the line of best fit does not represent a strong relationship between this scenario and pre-lagoon conditions. This suggests that the addition of single turbine to the square TRS has significantly altered conditions within the tank, causing great variation in the residual velocity and would likely cause great disruption to the natural environment.
S1B	The results of S1B display a similar pattern to those of S0, that although the results are scattered, a third of the observed values

6. Test Case 3 – Impact of Varying Geometry

	<p>fall within the 95% confidence interval. This shows that although the addition of this single turbine significantly alters the natural conditions, the position of this turbine, closer to the centre of the TRS seawall, causes less disruption than the S1A case where the turbine was positioned close to the edge of the seawall. This confirms that the positioning of turbines is an important aspect to consider when designing TRSs.</p>
S2A	<p>The results of S2A are the most scattered yet and extremely weak correlation which suggests little relation to the natural conditions overall. This formation was found to have the greatest effect on baseline conditions, as discussed earlier.</p>
S2B	<p>S2B reveals the closest correlation so far, and although only a third of the data falls within the 95% confidence interval, the data is much less scattered than the previous experiments and the gradient of the line of best fit much closer to one. This suggests that this experiment, with the greatest spacing between the turbines, causes the least disruption to natural conditions so far. An almost equal number of points fall above and below the line of best fit meaning that velocity is no more increased than decreased across the whole tank.</p>
S2C	<p>The results of S2C show an extremely similar picture to that of S2B, which is interesting because the turbines are much more closely spaced than in S2B. However, S2C again displays a relatively strong linear relationship with an equal number of locations with faster and slower flows than baseline conditions.</p>
S2D (B1)	<p>S2D has the strongest correlation and the least scattered results of all of the square TRSs. Two thirds of the data lie within or on the 95% confidence interval meaning that the relationship between these results and those of the baseline case are much stronger than any of the other square TRS experiments. This means we can be confident that the central positioning and equal spacing of the turbines, away from the edges of the TRS seawall is best for maintaining natural conditions. Of those results that do not fit within</p>

6. Test Case 3 – Impact of Varying Geometry

	<p>the 95% confidence interval the results are consistently lower than the baseline conditions meaning that the velocity will be reduced overall. This is consistent with the findings of Falconer et al. (2009) who found that a Severn Barrage would reduce maximum current speed in the estuary and argue that whilst this would lead to clearer waters with reduced turbidity it would cause changes in biodiversity.</p>
B2	<p>The results of B2 are fairly well clustered and although more than half of the results lie outside of the 95% confidence interval, they still appear to follow the overall trend which shows good agreement with pre-lagoon results. This means that despite changing conditions inside the TRS, conditions in the tank are relatively unchanged overall and that the centralised spacing of the turbines, first tested in B1, enables normal conditions to continue.</p>
B3	<p>Results from this experiment align very strongly with those of the pre-lagoon case with strong correlation displayed in the regression plot. This agrees with the previous findings of B1 and B2 which had the same turbine spacing. This suggests that bed material has limited impact on flow conditions inside and outside of the TRS in this case and that baseline conditions would be maintained under this configuration.</p>
B4	<p>These results are slightly more scattered with less strong correlation than B2 and B3, despite having the same turbine spacing. This suggests that the bed material has slightly altered flow, but the overall trend maintains a positive relationship with the pre-lagoon case. Where results are not aligned velocity is reduced which is preferable to increasing velocity as it promotes safety for recreational activities in the area.</p>
B5	<p>Regression analysis of the results of B5 shows strong positive correlation but widely scattered results. This means that although the flow velocities of B5 agree somewhat with those of the pre-lagoon case it has caused some change and appears to decrease the velocity overall. This is slightly surprising as we would expect the increased slope to increase discharge through the turbine</p>

6. Test Case 3 – Impact of Varying Geometry

	<p>openings and thus increase flow velocity outside of the TRS, however this does not appear to be the case. This could be due to the equal spacing of the turbines balancing out the force of the water leaving the TRS and restricting flow into the rest of the tank.</p>
B6	<p>These results reveal strong positive correlation once again with 50% of the data falling within the 95% confidence interval. This strong relationship suggests that bed slope does not have a significant impact on the natural conditions. This agrees with the findings of Sang-Ho et al. (2016) who demonstrated that that bed slope had an insignificant impact on flow compared to other factors such as altering sluice area.</p>
R0	<p>Interestingly, the regression analysis graph of R0 shows very similar results to that of S2D. This is surprising as R0 has no openings which we would expect to lead to a change in velocity conditions. However, as with S2D, two thirds of results lie within or on the 95% confidence interval and the majority of results outside of this threshold are slower than baseline conditions. This means that the rectangular case does not significantly alter the original conditions of the domain but where it does cause changes, the velocity is reduced in agreement with other studies of a barrage within the Severn Estuary (Ahmadian et al., 2010; Xia et al., 2010b; Zhou et al., 2014).</p>
R1	<p>R1 results show weaker correlation than R0 but stronger correlation than S1A, its square TRS counterpart. This suggests that a single turbine in this long, thin TRS has less of an impact on baseline conditions than a square TRS with a single turbine. Almost half of the data falls below the 95% confidence interval which shows that this configuration slows flows in the tank overall as observed from previous analysis.</p>
R2A	<p>As with the R0 case, R2A has more results below the 95% confidence level than above it, meaning that this configuration slows flows overall. However, the results are more scattered than the R0 case suggesting that once turbines are added to the TRS</p>

6. Test Case 3 – Impact of Varying Geometry

	<p>the relationship with the baseline conditions is weaker and velocity becomes more varied overall. This is particularly expected for this case as throughout results analysis, layouts with closer turbine spacing have been shown to cause most disruption to the natural environment. This experiment is therefore comparable to S2A, discussed further in Section 6.2.4.</p>
R2B	<p>Although the results of R2B look similar to those of R2A, correlation is much weaker, and the results more widely scattered overall. This suggests that we can have no more confidence in these results than those of S0, S1B or S2B. Overall, this case, with two turbines placed close to the near right-hand wall has still caused great disruption to the natural environment despite having a slight space between them.</p>
R2C	<p>The majority of results in this case lie below the 95% confidence boundary which suggests that the relationship between the results of this experiment and pre-lagoon conditions is not significant. Despite having a positive gradient, the results are scattered, and more results lie below the line of best fit than above, suggesting that this wider spacing of the turbines does nothing to help restore natural conditions and continues to slow flow but not in a predictable way.</p>
R2D	<p>Results from the R2D experiment are closely clustered when compared against pre-lagoon conditions. This suggests a very strong relationship between the results of this experiment and the natural environment. As with S2B, R2D has the largest spacing between the two turbines and strengthens the idea that wider spacing is best for maintaining natural conditions.</p>

Regression analysis plots for residual velocity direction show strong correlation with baseline measurements for all experiments with the exception of S1B which has negative correlation. This shows that although the configurations have caused a variety of changes to residual flow velocity they have not greatly altered flow direction in the tank overall.

6. Test Case 3 – Impact of Varying Geometry

6.2.5.2 Mapping similarities and differences

Another method for visualising the variation of each experiment with pre-lagoon conditions is to identify and plot the locations with the greatest similarity and difference from pre-lagoon velocity measurements. Annex 3 presents maps of points with the greatest similarity (less than 10% difference with pre-lagoon velocity), greatest difference (more than 50% difference) and so called “neutral” points (those between 10 and 50% difference that are statistically neither significantly similar nor different). By visualising the tank in this way, it reveals common points of similarity, difference or neutrality in order to spot trends across the whole area, discussed in Table 6.4.

Table 6.4 Discussion of regression analysis between experiments and pre-lagoon conditions (Graphs in Annex 3).

Case	Comments
S0	<p>Compared to pre-lagoon conditions, S0 only displays a significant difference in residual velocity at two points, directly in front of the TRS and to the left of it. This is perhaps not unexpected given the obstruction that has been introduced to the area and reflection off the TRS seawall will cause changes in velocity and turbulence.</p> <p>What is surprising is that there is only a significant difference to the left of the TRS and not also the right as we would expect reflection off the structure to be similar on both sides of the tank. However, as with previous analysis, this could be due to the asymmetric flow in the tank which is generally stronger and more positive along the right-hand wall and therefore has maintained its flow rate despite the addition of the TRS. Elsewhere in the tank there is little similarity around the central region, and this is again most likely due to changes caused by reflection off the TRS. This has not altered flow significantly though and the residual velocity here is neither statistically similar nor different from the pre-lagoon state. The front of the tank maintains the greatest similarity with the majority of points revealing statistically significant similarity up to 1 m from the inflow boundary. This means that the introduction of the closed box TRS has not had a significant impact at this distance.</p>

6. Test Case 3 – Impact of Varying Geometry

S1A	<p>S1A displays greater difference from the pre-lagoon case than the closed box of S0. The greatest difference can be found to the left of the structure, which was also discovered in the contour plots of residual magnitude that showed water deflecting from the turbine opening on the right to reach the left-hand wall. Interestingly there are some points of similarity in the very centre of the tank at (150,250) and (250,250). This could be due to reflection from the TRS wall balancing out any discharge deflected from the turbine opening leading to a resemblance to baseline conditions. As with S0 there is some similarity with the pre-lagoon case along the inflow boundary, however there are not as many similar points overall. This means that the addition of the turbine opening in the TRS causes greater change to the tank conditions overall than the introduction of the TRS alone. Inside the TRS, almost half of the points show significant similarity, and these are in the left-hand side of the tank, away from the turbine opening, whilst directly behind the turbine opening shows significant difference between baseline conditions. This aligns with what we would expect that in the presence of a turbine opening, wakes cause a dramatic change in velocity but that further away from the turbine opening velocities are not significantly impacted and can maintain natural conditions.</p>
S1B	<p>In scenario S1B, the turbine opening is placed closer to the centre line of the tank than in S1A. This has led to greater differences in residual velocity along the centre line of the tank but fewer differences overall and there are many more similar points on the right-hand side of the tank. This shows that it is not just the presence of a single turbine that causes changes to flow conditions but the positioning of the turbine too, as this more centralised position has led to fewer changes than when the opening was placed closer to the TRS and tank walls. This is also the case inside the TRS where there are now no significantly different points but still three points of significant similarity despite the presence of the turbine.</p>

6. Test Case 3 – Impact of Varying Geometry

S2A	<p>S2A leads to the greatest number of differences with pre-lagoon conditions so far. Unlike the previous experiments there is now very little similarity along the inflow boundary and greater differences are experienced across the whole of the tank area. This is unusual as previous studies reported that the effects of turbine wakes are not usually felt further than twenty turbine diameters away from the openings whereas here, they have extended as far as the inflow boundary, more than 60 turbine diameters away. This demonstrates the tremendous impact that placing two turbines side by side has had on conditions in the tank, creating the greatest difference across the whole area of the tank.</p>
S2B	<p>Although S2B also has two turbines it had a much less significant impact on conditions in the tank and in fact has the many points of similarity with pre-lagoon conditions. This shows that positioning the turbine openings at opposite ends of the TRS seawall rather than next to each other balances out the flow across the tank so that it more closely resembles the baseline conditions despite the presence of the TRS. However, it is interesting that there is little similarity along the inflow boundary where we would expect to see the least change as it is furthest away from the structure. This could be due to changes in conditions in the inflow control system which underwent some mechanical updates throughout the experiment period. Inside the TRS, positioning the turbines at opposite ends of the seawall has meant that flow has balanced out across the impounded area, and more than half of the locations are statistically similar to those of pre-lagoon conditions, a dramatic difference from the other square TRS cases.</p>
S2C	<p>S2C also has two turbines, this time positioned with one close to the centre line and the other close to the right-hand wall. This has led to greater changes along the centre line of the tank both inside and outside of the TRS impoundment. There are, however, a great number of similar points too. This suggests that whilst the new</p>

6. Test Case 3 – Impact of Varying Geometry

	turbine layout has deflected some flow, slight spacing has less of an overall impact on the tank than the close spacing of S2A.
S2D (B1)	The layout of S2D has symmetrical turbine spacing, as with S2B, but with the openings placed closer to the centre line and subsequently further from the walls. This has led to an almost symmetrical pattern of similar, different and neutral points in the tank compared to baseline conditions. This is encouraging as it means that although there is underlying asymmetrical flow in the tank, when a symmetrical turbine layout is introduced the effects on the overall flow pattern are still symmetrical. Interestingly the points displaying the greatest difference (other than directly between the turbines where we can expect the greatest turbulence) are near the front of the tank. This shows that although this layout caused little change to baseline conditions overall the disturbance caused by the turbine wakes has far reaching effects (greater than 50 turbine diameters). Inside the TRS, however, the changes are not symmetrical and although conditions directly between the turbines are similar to pre-lagoon conditions, to the left-hand side of the lagoon conditions have been significantly altered. This offsetting of the impacts of the turbines could be due to the combined wakes being diverted to the left-hand side by underlying asymmetric flow as observed in images of flow visualisation for this experiment.
B2	The pattern of similarity and difference outside of the TRS for this experiment are extremely similar to those of B1, demonstrating that although the bed conditions have changed within the TRS this has not had a significant difference outside the TRS and so turbine spacing is more influential than bed conditions in the far field. Inside the TRS however, conditions are much more similar to those pre-lagoon compared to B1 which shows that this change to the bed conditions has made a positive difference to flow velocities and enabled natural conditions to be maintained more closely.
B3	The change of bed conditions in B3 has changed the conditions inside the TRS so that the residual velocity is less statistically

6. Test Case 3 – Impact of Varying Geometry

	<p>similar to that of the pre-lagoon state. Outside of the TRS continues to display an extremely similar picture to that of B1 and B2, consolidating the idea that bed conditions do not have as much of an impact on far field flow conditions as turbine spacing.</p>
B4	<p>The conditions in B4 have led to a very similar pattern to that of B2 and is not too dissimilar from B1 either, in that it resembles the baseline conditions inside the TRS and in a somewhat symmetrical pattern outside it, with the greatest difference occurring directly between the two turbine openings. This conclusively proves that the bed conditions within the TRS do not have a significant impact on flow conditions outside of the TRS. Inside the TRS flow conditions have proved statistically similar to those of B2 showing that these two bed materials (20 mm artificial grass and 10 mm gravel) have had a similar effect on flow conditions overall and are better able to maintain natural flow conditions that either the 20 mm gravel or the flat plastic bed.</p>
B5	<p>This complete picture of the tank reveals a very similar pattern to that of B1, showing once again that conditions inside the TRS do not have a significant impact on flow patterns outside it and that the central spacing of the turbines does not cause great difference from pre-lagoon conditions. Inside the TRS, the sloped bed has altered conditions however, with half of the results significantly altered from baseline conditions. It is interesting to note that these points of difference are located to the left and rear of the lagoon, whilst points of similarity are located in the centre and to the right despite the turbines being equally spaced in the centre of the seawall. This could be attributed once again to asymmetric flow deflecting turbine wakes to the left and causing most disruption to flow conditions in this area despite having a symmetrical slope and evenly spaced turbines.</p>
B6	<p>It is perhaps surprising that this lower slope has a greater impact on the tank than the steeper slope of B5 and although it has a very similar underlying pattern to both B1 and B5, there are more neutral</p>

6. Test Case 3 – Impact of Varying Geometry

	<p>points and fewer similar points with the pre-lagoon case. This suggests that although not a big change there is some difference caused to the outer TRS by this slightly elevated bed. Inside the TRS too there is less change to pre-lagoon conditions with only one point of statistically significant difference and this in the centre at the rear of the tank. This is more in line with what we might expect in this scenario with evenly spaced turbines but a sloped bed causing a change in flow near the rear of the tank.</p>
R0	<p>This experiment is the first of the rectangular cases and appears to cause little disruption to baseline conditions. Compared to the pre-lagoon state there are only two points that are significantly different and given their location, directly in front of the TRS, can be attributed to reflection off the solid seawall. There are many points of similarity around the TRS and neutral points in the centre of the tank. However, unlike the square case there is little similarity along the inflow boundary. This could be due to greater reflection off the longer, thinner walls of the TRS reaching further into the tank or to a change in the physical conditions at the inflow boundary which is more likely as there were mechanical updates to the system throughout the experiment period.</p>
R1	<p>The first of the turbine trials in the rectangular TRS, R1 is analogous with S1A in that the turbine is offset to the right, close to the side wall. In this instance we can see some changes to the centre of the tank which is to be attributed to wakes deflected from the offset turbine. Inside the TRS the point of greatest difference lies behind the turbine which is to be expected. Other points within the TRS remain neutral or similar to pre-lagoon conditions since the strength of flow through this single turbine has not been strong enough to cause a significant difference in the wider lagoon area. The area of the tank that remains least altered lies along the right-hand wall which agrees with earlier observed patterns where flow is maintained in the right-hand section of the tank before being deflected to the left.</p>

6. Test Case 3 – Impact of Varying Geometry

R2A	<p>The next rectangular TRS case introduces a second turbine, tightly spaced so as to be side by side with the first turbine, close to the right-hand wall. This has resulted in a very similar pattern to that of R1 outside of the TRS, with similarity to pre-lagoon conditions most evident along the right-hand wall. However, there are fewer points of difference from the pre-lagoon conditions in this case showing that the second turbine openings have enabled more natural conditions to be maintained. This is surprising since earlier analysis had shown that two side by side turbines caused exaggerated flows. This is definitely still the case inside the TRS where results are significantly different from pre-lagoon conditions along the right-hand side of the lagoon, behind the turbine openings, and also in the front left-hand corner of the lagoon where water has not been able to circulate and so flows are reduced.</p>
R2B	<p>R2B displays little difference from the other rectangular cases and is especially similar to R0 in that it resembles pre-lagoon conditions along the right-hand wall and is neutral elsewhere. Also similar to the R0 case, the points of significant difference from the pre-lagoon state are fairly symmetrical. This could be due to the slightly wider turbine spacing balancing out flow around the tank more than when turbines are positioned closely together. Inside the TRS, flow is still significantly different behind the turbine openings but this spacing has led to more neutral areas in the left-hand side of the lagoon, meaning that the wider turbine positioning has caused less difference further away.</p>
R2C	<p>As the spacing is increased between the turbines for R2C, we would expect it to lead to a greater improvement to conditions, as with R2B, but instead it is more similar to that of R1. The area of greatest difference from the baseline case can be found in the centre of the tank. This could be due to flows deflected from both of the turbines as separate streams rather than a single wake and so having a greater influence further away as flows converge and try to stabilise. Inside the TRS the greatest difference is still found</p>

6. Test Case 3 – Impact of Varying Geometry

	along the right-hand wall, behind the turbine openings, but as with R2B, the rest of the lagoon area is fairly neutral as the increased spacing has led to more balanced flows throughout the lagoon area.
R2D	R2D has a large number of statistically similar points to pre-lagoon conditions, mostly found along the left-hand side of the tank, with the majority of remaining points being neutral. This shows that the wider spacing of this case has maintained natural conditions more closely than any of the other rectangular cases. Inside the TRS too there is only one point that is significantly different than the pre-lagoon state and this is directly behind the turbine opening on the right-hand side, but with neutral points throughout the rest of the lagoon.

6.3 Summary

In Chapter 6, the results of experiments with a square TRS were directly compared with equivalent layouts in a rectangular TRS. This was carried out in order to determine the effect that TRS geometry has on flow characteristics.

Comparison F i compared closed box cases to examine the effects of the shape of each TRS on conditions in the wider tank area before turbines were added. This revealed that both the square and rectangular TRSs caused disruption to the natural environment. The rectangular TRS (R0) had further reaching impacts than the square TRS (S0) as its longer shape restricted flow so that stronger, faster flows were funnelled to the right-hand side of the tank, whilst water was somewhat stagnant in the rear-left of the tank. This could cause issues of erosion and trapping contaminants if the shape of the TRS is not sympathetic to natural flow conditions and the shape of the coast. Different TRS geometries, e.g., semi-circles or trapezia, could be tested in future to minimise blockage effects and prevent areas of stagnation that can occur in the outer reaches of rectangular lagoons.

Comparison F ii looks at single turbine cases in both the square (S1A) and rectangular (R1) layouts. In these cases, it was found that the rectangular TRS caused less disruption to baseline conditions than the square TRS but still restricted flows as before. The square TRS therefore promotes better circulation in the outer tank and more consistent flow within, whereas the rectangular TRS increases flow outside the structure but decreases velocities inside it.

The next comparison, F iii, examined the flow characteristics in the tank when each TRS contained two turbines positioned side by side. The same patterns were observed as before in that the rectangular TRS (R2A) restricts flow in the outer tank whilst the square TRS (S2A) enables freer circulation in all areas of the tank, leading to a greater variation in results. Inside the TRS, water flows throughout the whole area of the square TRS but is not able to reach all areas of the rectangular TRS leading to areas of stagnation. This could be counteracted in a real TRS if a site incorporates a river or if flow

6. Test Case 3 – Impact of Varying Geometry

were managed with underwater pumps. Both of which would increase circulation in all areas of the impoundment but increase the cost of the project. Otherwise, these areas of low flow could be beneficial for aquaculture or recreation if water quality is managed.

In the final comparison, F iv, both TRSs were compared with two turbines at opposite ends of the seawall. This wider spacing of turbines led to the greatest similarity between results for the two shapes of TRS than any other configuration leading to the conclusion that wider turbine spacing is better for maintaining a healthy environment and that turbine spacing is the dominant variable over TRS shape.

Another way of analysing the effects of each scenario was to carry out regression analysis, plotting the residual velocity magnitude results of each experiment against pre-lagoon levels to quantify the discrepancies with baseline conditions. This revealed that the rectangular shape caused less disruptions to baseline conditions overall than the square, and that although bed material did not significantly alter conditions in the wider tank area, turbine spacing did make a difference. Centralised positioning with a slight space (S2D) was found to be the best overall. This confirms that turbine positioning is an important aspect in the consideration of TRS design. It also agrees with the conclusions of TST studies that reported that close spacing (less than two turbine diameters) leads to wakes merging to form strong vortices (Stallard et al., 2013). Spacing of at least three diameters is recommended in TST arrays for separating wakes (Nash and Phoenix, 2017), improving power output (Ahmadian and Falconer, 2012) and ease of maintenance (European Commission, 1996).

Maps of areas of statistically similar and different residual velocity (Annex 3), repeatedly showed the most difference from baseline conditions at points (200,400) where water is reflected off the front of the TRS seawall, and (100,500) where flow is often trapped and recirculated.

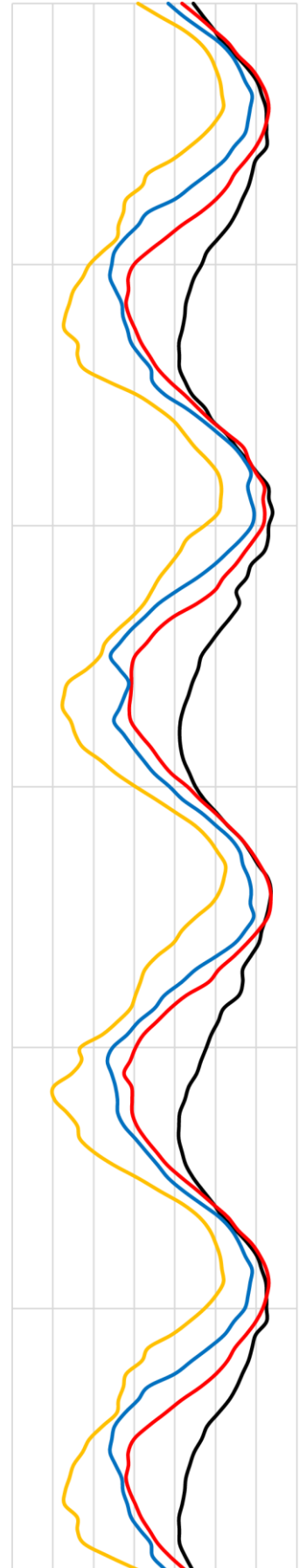
In answering the initial hypothesis, that TRS geometry does not significantly alter velocity, this was found to be true for square and rectangular TRSs with two turbines at opposite ends of the seawall, where the shape of the TRS did

6. Test Case 3 – Impact of Varying Geometry

not lead to a difference in velocity conditions in the tank. However, in the case of the closed boxes (S0 and R0) and single turbine experiments (S1A and R1), TRS geometry was found to cause a significant change in velocity leading us to reject the null hypothesis. Careful consideration of TRS shape is therefore needed in future project designs.

Chapter 7

Numerical Model



7 Numerical Model

7.1 Introduction

The ambitious schedule originally designed for the physical experiments had to be curtailed, for reasons previously discussed, and a series of numerical experiments were proposed in order to complement and extend the laboratory results. These would use the results of the physical experiment to calibrate and validate the computational model to explore more complex scenarios. This chapter describes the software and method used to further investigate hydraulic structures in idealised TRSs, detailing the difficulties of calibration due to the irregular flows in the laboratory system. Traditional tuning parameters such as Manning's n are investigated alongside variations in boundary conditions but ultimately could not match the irregular flow conditions of the tidal basin in the laboratory.

Key Words and Terms in Chapter 7

Delft3D: an open-source software package used for hydrodynamic modelling.

Navier Stokes/Shallow Water Equations: A series of partial differential equations used to describe flow.

Calibration: To adjust the performance of a numerical model to accurately recreate the results of a specific experiment or set of experiments.

Validation: To confirm the accuracy of the predictions of a calibrated model.

Manning's n : A coefficient for representing the roughness or friction acting on flow.

7.2 Methodology

This study used Delft3D to model the hydrodynamic impacts of TRSs. Delft3D is an open-source code developed by Deltares Systems (Deltares, 2022) comprising modules for modelling coastal, river and estuarine processes in two or three dimensions. It is a finite difference model that can solve 3D or depth averaged Navier Stokes equations including momentum and continuity equations (Lesser et al., 2004; Suárez-López et al., 2019). Hydrostatic pressure is assumed; however, no vertical momentum equation is incorporated so vertical velocity is determined from flow continuity (Parsapour-Moghaddam and Rennie, 2018). Open-source software has the benefit of allowing people to run simulations even on less powerful computers (Nuernberg and Tao, 2018) backed up by a wealth of community support available online. Delft3D was chosen for its capability to model hydraulic structures and is widely used by other members of the HRC at Cardiff University for investigating TRSs. It is also quick to set up and run and more user friendly than other available software. Other studies that demonstrate the advantages and functionality of Delft3D-FLOW include:

- Lesser et al. (2004) who developed a 3D morphological model to analyse sediment transport which they applied to harbours and offshore breakwaters.
- Tralli et al. (2015) who investigated TST turbine placement and performance to increase energy yields.
- Dai et al. (2017) who used Delft3D to analyse hydrodynamic processes with and without a dynamic tidal power system.
- Čož et al, (2019) who demonstrated a new method for improving the accuracy of modelling jets through TRS hydraulic structures.

The advantages and disadvantages of other types of numerical model and available software are discussed in further detail in Annex 4.

7.3 Model Design

Initial tests follow the same design as the laboratory experiments, comparing the effects of altering turbine spacing in idealised tidal lagoons. The computational model used the same scale as the laboratory tests (as outlined in Section 3.3.1) and calibration was attempted using results from the physical experiments to ensure accurate and reliable performance. The model deploys a regular grid with 5 cm resolution and a 0.03 second time step (chosen from sensitivity analysis so as to enable results to converge across the given grid size). Figure 7.1 shows the domain and regular grid in Delft3D with inflow boundary and TRSs highlighted.

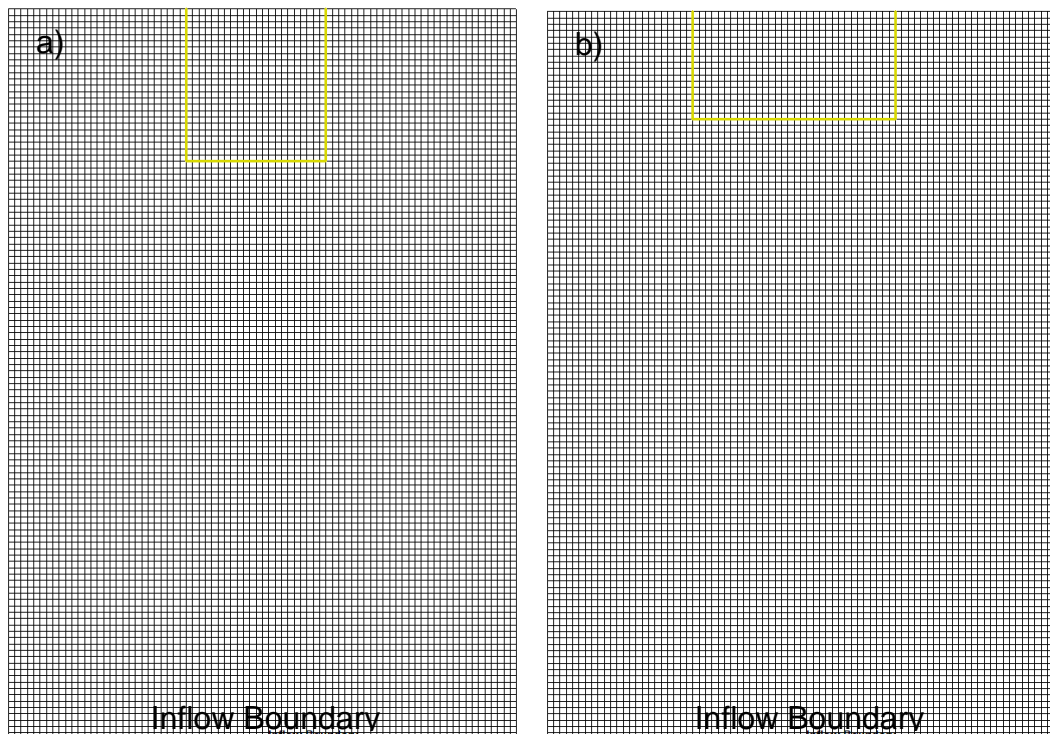


Figure 7.1 Model domain of idealised a) square and b) rectangular TRSs.

7.3.1 Assumptions

Charlier (2003) notes that simplification is necessary in all hydrodynamic models whether for bathymetry, coastal geometry or tidal conditions, etc., and it is important to acknowledge these limitations. The present study maintains a smooth bed with free slip conditions at the side boundaries, as demonstrated by Tralli et al. (2015) in modelling turbine placement. An idealised geometry with constant area (favoured by Mackie et al., 2021) will enable the focus on turbine spacing as a variable.

Other assumptions made for this simplified model are that the tide can be represented by a linear, sinusoidal wave (Falconer, 1974), that water flows through the turbines at a constant rate (Prandle, 1984) and that the effects of power generation are negligible for velocity rates.

7.4 Calibration

Numerical models are calibrated by comparing calculated results with those observed in physical experiments and improving statistical metrics, e.g., the Root Mean Square Error (RMSE), by tuning various parameters of the computational code to ensure accurate and reliable performance (Vouriot et al., 2018). Common tuning parameters include bed roughness (Gallego et al., 2017; Gao and Adcock, 2017; Mohammadian et al., 2019) and eddy viscosity (Parsapour-Moghaddam and Rennie, 2018; Saichenthur et al., 2022) but changes can also be made to open and closed boundary conditions (Harrison et al., 2010).

The numerical model presented here was calibrated using depth averaged velocity and water level measurements taken from the laboratory. Other TRS studies have also made use of physical model data for depth averaged velocity magnitude and direction (Čož et al., 2019; Rtimi et al., 2021) and tidal phase and amplitude (Mackie et al., 2020; Todeschini et al., 2022) to calibrate their numerical models. As well as conducting laboratory scale experiments, calibration data for TRS models can also be acquired from online repositories, field surveys and tidal gauge stations (Čož et al., 2019; Guo et al., 2021; Ross et al., 2021; Rtimi et al., 2021).

7.4.1 Boundary Conditions

Five inflow boundaries were considered during the calibration process with the sensitivity of the model tested for each of the following inflow conditions:

- 1) Idealised water level
- 2) Single velocity boundary
- 3) Single discharge boundary
- 4) Velocity boundary in four sections
- 5) Discharge boundary in four sections

7. Numerical Model

7.4.1.1 Idealised Water Level Inflow Boundary

The idealised water level (illustrated in Figure 7.2) is based on the equation:

$$h = 4 \cos 4x + 40 \quad \text{Equation 7.1}$$

Where h is the water level in centimetres and x is the time in seconds, as used to programme the mechanical weir gate in the laboratory. This is based on the 8 m tidal range of the Severn Estuary with a 90 second tidal period as used in the laboratory experiments. Measurements taken across the tank inflow boundary showed that water level did not vary and so this idealised water level time series accurately represents the inflow conditions.

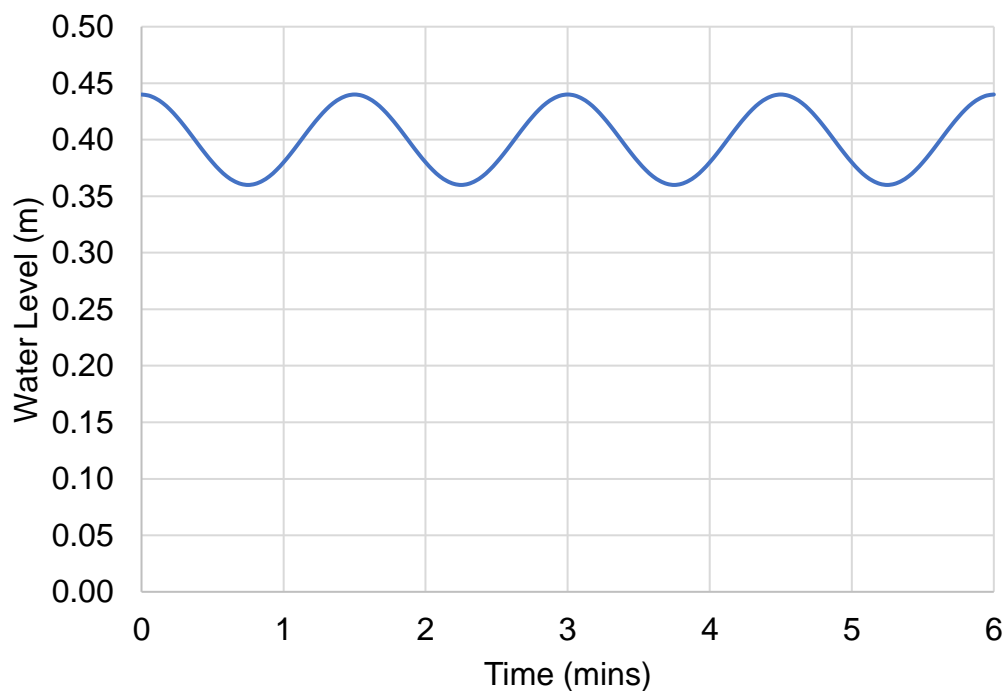


Figure 7.2 Water level inflow boundary conditions for Delft3D model.

7. Numerical Model

7.4.1.2 Single Velocity Inflow Boundary

The velocity inflow boundary was taken from ADV measurements from the laboratory for experiment S0 as representative of conditions in the tank (results were also repeated when using data from experiments S2B and R1). The inflow boundary files enable a different input value at each end of the boundary and so data for end A was taken from the corresponding point in the tank of (50,50) whilst data for end B was taken from the opposite side of the tank at (350,50). Values along the length of the inflow boundary are calculated by Delft3D through the interpolation of these end values. Using real values from the physical experiment should enable the model to make predictions that accurately reflect the unusual flow behaviour in the tank. Figure 7.3 highlights the significant difference in velocity at each end of the inflow boundary, showing the variation in flow across the tank.

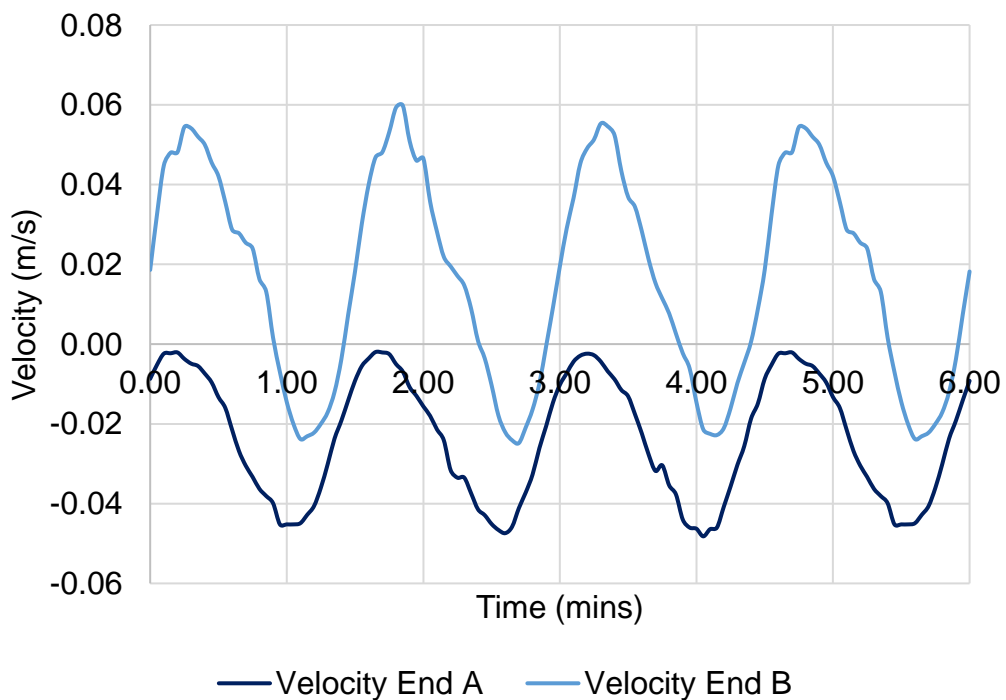


Figure 7.3 Velocity inflow boundary conditions for Delft3D model.

7. Numerical Model

7.4.1.3 Single Discharge Inflow Boundary

The discharge inflow boundary is calculated by Equation 7.2,

$$Q = \frac{vhw}{n} \quad \text{Equation 7.2}$$

Where:

Q = discharge per cell (m³/s)

v = depth averaged velocity (m/s)

h = idealised water level (m)

w = cell width (m)

n = number of cells

As with the velocity inflow boundary, Figure 7.4 emphasises the large variation in values between each end of the discharge inflow boundary. This is thought to be caused by asymmetrical flow in the tank leading to faster flows on the right (discharge end B) and negative flows on the left (discharge end A), as discussed in Section 8.2.1.

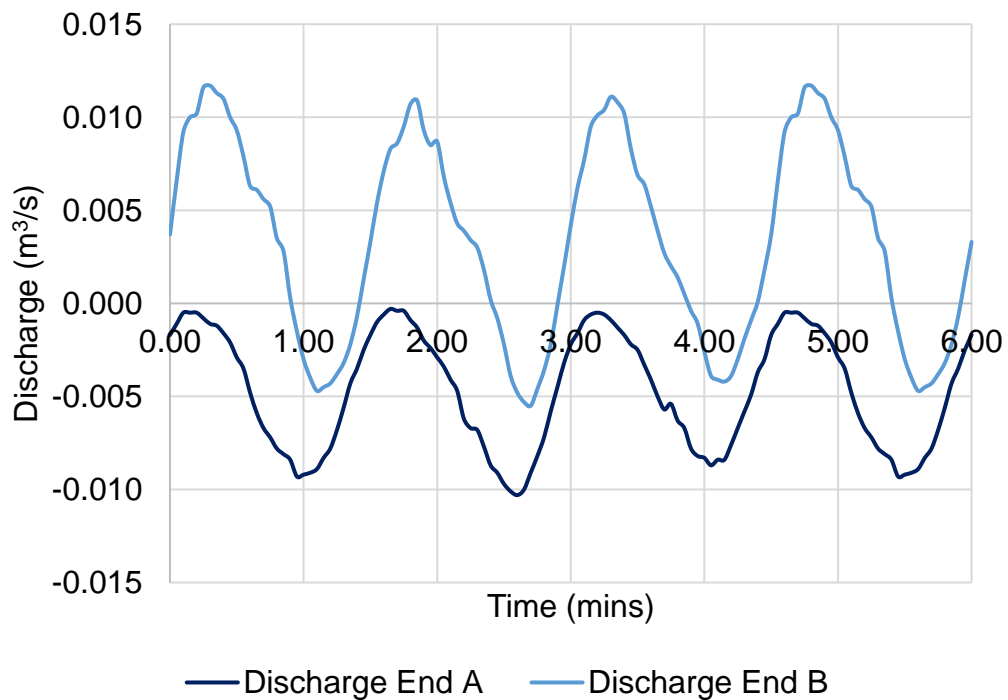


Figure 7.4 Discharge inflow boundary conditions for Delft3D model.

7. Numerical Model

Figure 7.5 compares the results of the numerical model when run with these three different inflow boundaries. (All calibration analysis is presented comparing S0 data, however, results were repeated when considering data from S2B and R0 too.) From this map we can see that the velocity and discharge inflow boundaries result in the most accurate predictions along the $x = 50$ cm cross section which is to be expected given that these boundaries were programmed using these very velocity measurements from the laboratory. They are also reliable along the centre line of the tank, however, they are much less accurate along the left and right-hand walls. As discussed in the analysis of the laboratory results this is due to underlying and uncontrollable asymmetric flow in the tank which results in faster flows along the right-hand wall and slower on the left, hence why the values at the ends of the inflow boundary were so different. This is also why the model tends to overpredict velocities on the left-hand side of the tank and underpredict on the right.

Predictions from the velocity and discharge inflow boundaries remain very close to each other throughout the tank (see Figure 7.5) and continually outperform the results of the water level inflow boundary which often overpredicts flow velocity, especially along the front section and left-hand wall of the tank. However, results from the water level inflow boundary model show closer correlation towards the rear of the tank, as demonstrated by the improvement in RMSE (shown in Figure 7.6 and Figure 7.7). Although the velocity and discharge inflow boundary models lead to more accurate results for velocity, they show some unusual results for water level, as presented in Figure 7.8 to Figure 7.10, with water appearing to drain out of the tank over time.

7. Numerical Model



Figure 7.5 Experiment S0 depth averaged velocity results for different inflow boundaries in Delft3D, black: ADVP measurements, red: water level inflow boundary, blue: velocity inflow boundary, yellow: discharge inflow boundary results.

7. Numerical Model



Figure 7.6 Regression analysis of experiment S0 depth averaged velocity results for different inflow boundaries in Delft3D, red: water level inflow boundary, blue: velocity inflow boundary, yellow: discharge inflow boundary results.

7. Numerical Model

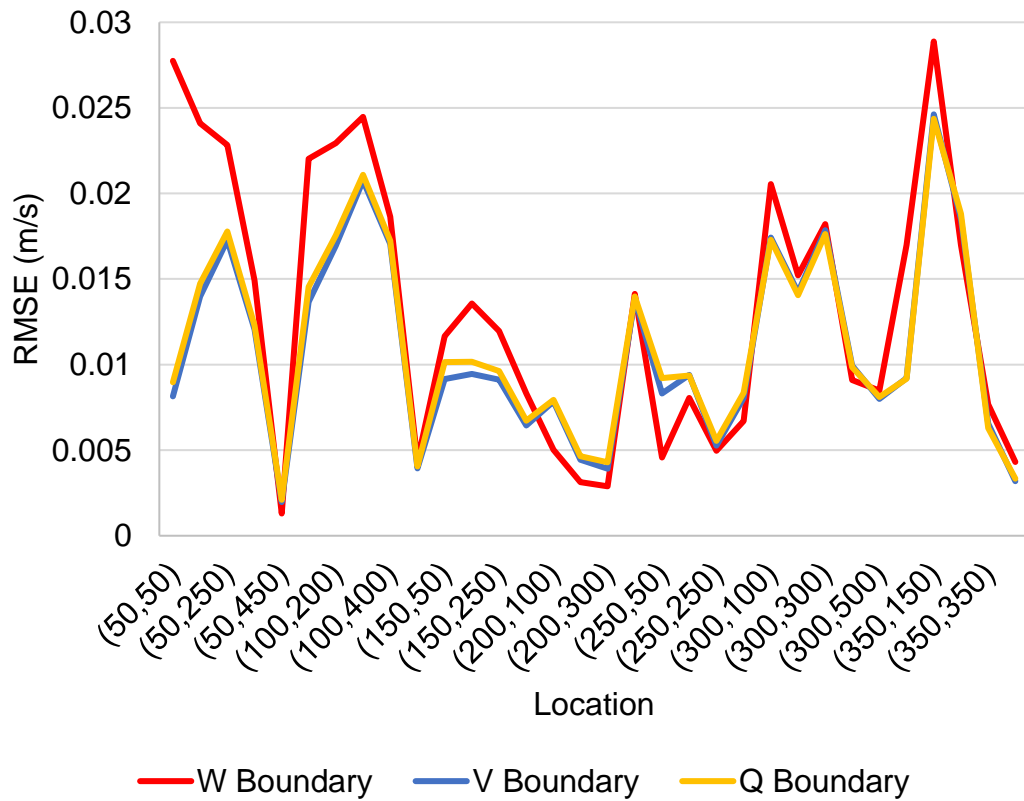


Figure 7.7 Root mean square error of Delft3D models calibrated with water, velocity and discharge inflow boundaries.

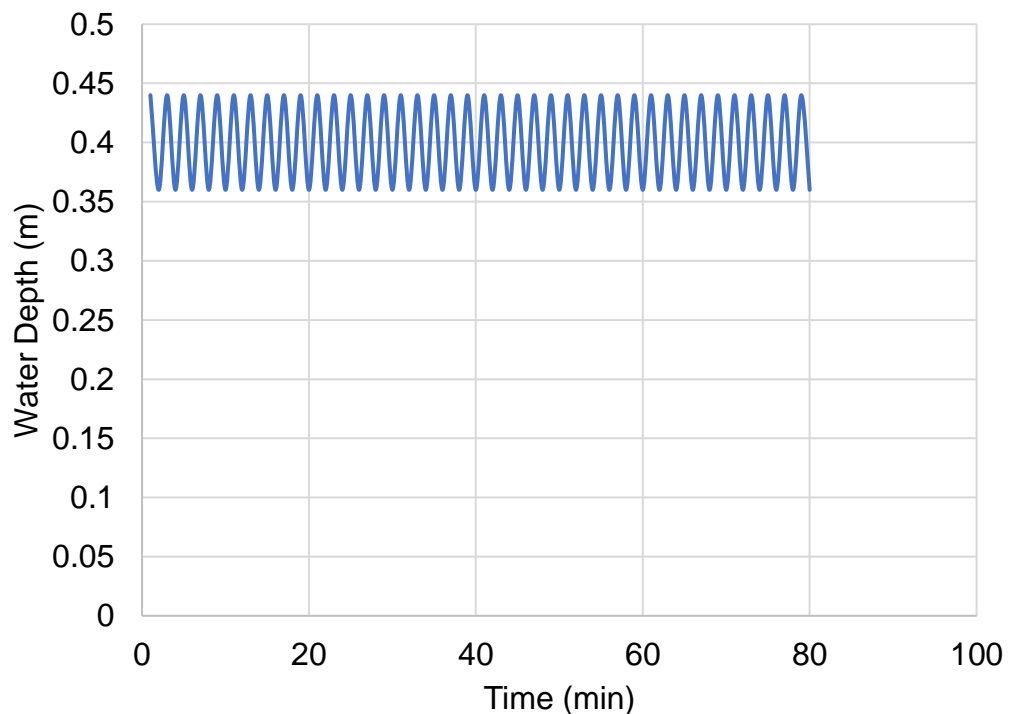


Figure 7.8 Water level results from water level inflow boundary model at (15,15).

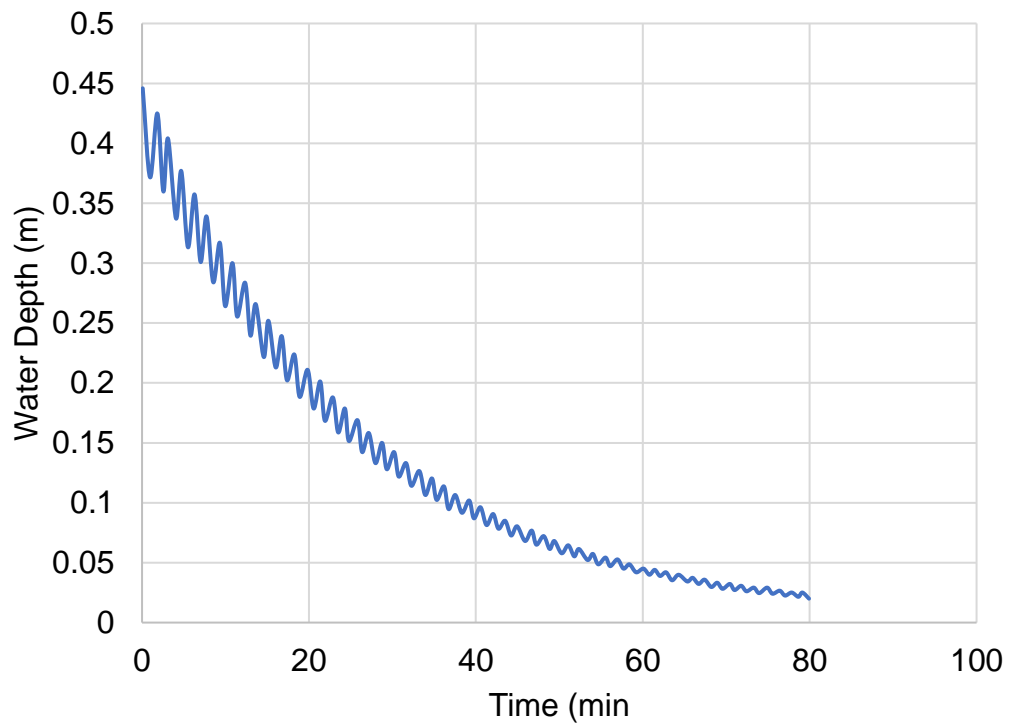


Figure 7.9 Water level results from velocity inflow boundary model at (15,15).

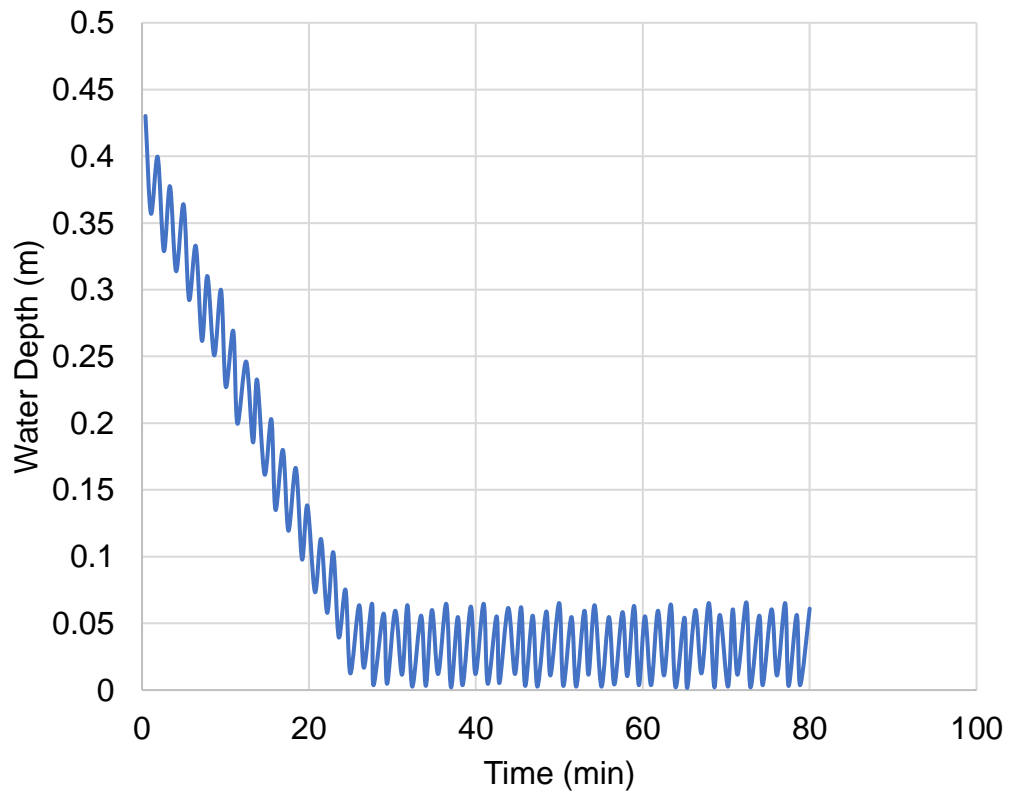


Figure 7.10 Water level results from discharge inflow boundary model at (15,15).

7. Numerical Model

7.4.1.4 Velocity and Discharge Inflow Boundaries in four sections

The strong lateral flow component within the tank is extremely difficult for the numerical model to compute, as such models are designed to calculate flows perpendicular to the inflow boundary and not parallel or at an angle to it as has been observed from the contour plots of residual flow magnitude and direction in the tidal basin in laboratory.

Given the extreme difference in flows at each side of the tank it could be useful to split the inflow boundary into sections rather than treating it as a single entity. This approach was adopted by Nguyen et al. (2018) who, after observing asymmetry in their study area, split their channel into three regions (left, right and middle channel) to look at circulation patterns more closely. To this end the present study split the inflow boundary into four equal sections to be populated with data taken close to the physical inflow boundary (sample points (50,50), (150,50), (250,50) and (350,50)) and interpolated between points, to see if this enables more accurate predictions across the whole tank area. Figure 7.11a shows the single section inflow boundary for the first comparison, which interpolated values only between ends A and B, whilst Figure 7.11b shows the inflow boundary split into four sections with data interpolated between values at the end of each of the four sections to include more of the variation between velocity data measured along the inflow boundary of the tank. Figure 7.12 and Figure 7.13 show the velocity and discharge data measured at each end of the section to be used to populate these inflow boundaries,

7. Numerical Model

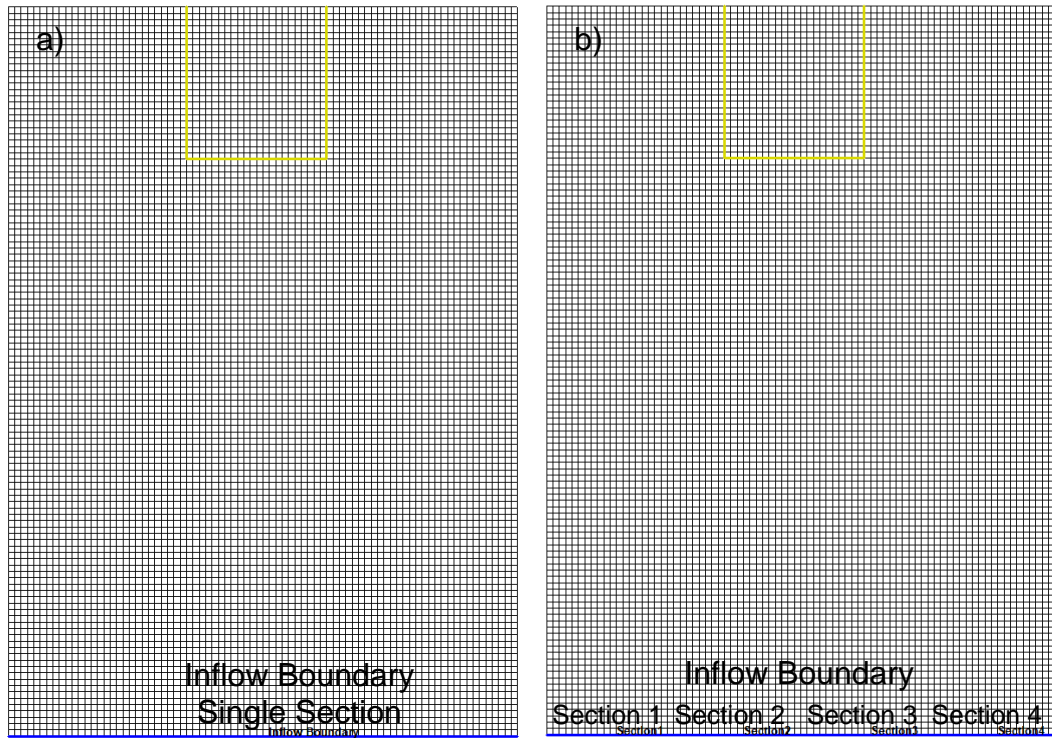


Figure 7.11 a) Single inflow boundary and b) inflow boundary in four sections in Delft3D model.

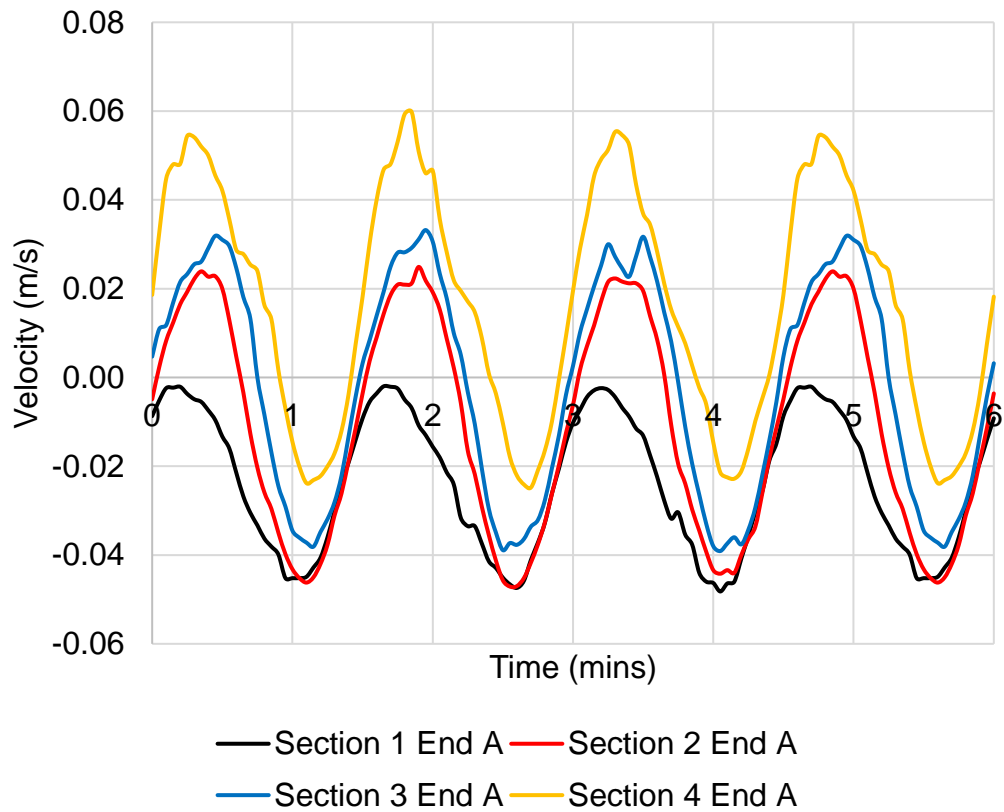


Figure 7.12 Velocity values for Delft3D inflow boundary in four sections.

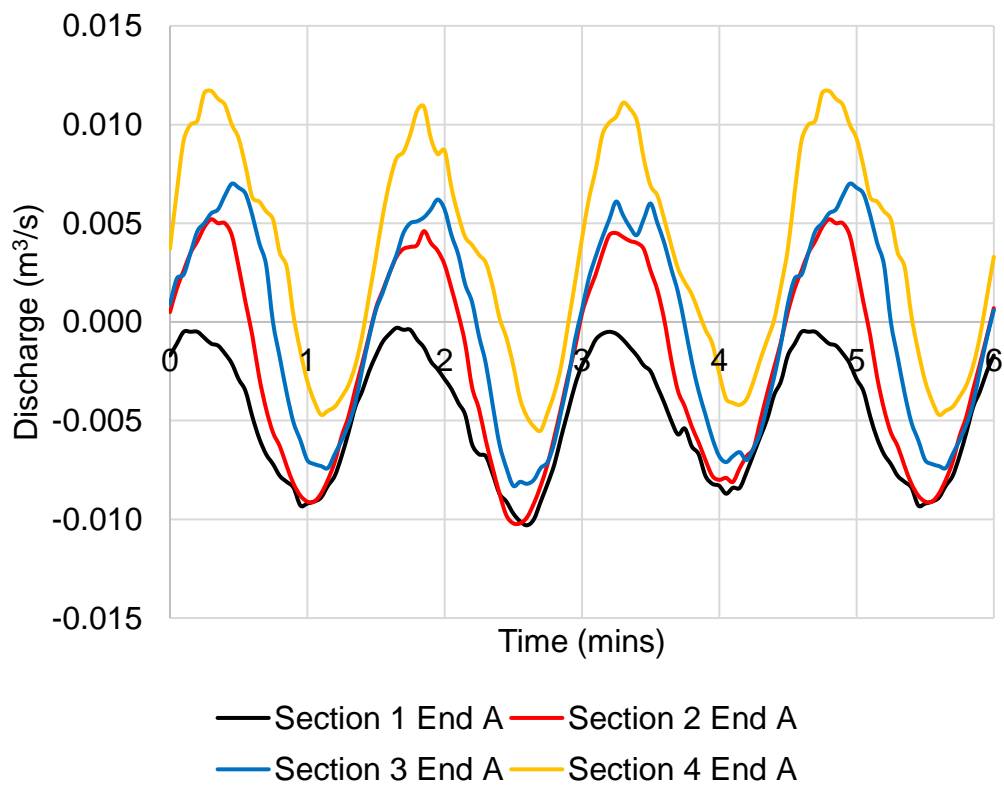


Figure 7.13 Discharge values for Delft3D inflow boundary in four sections.

7. Numerical Model

This led to some irregular results and did not improve velocity predictions (Figure 7.14), neither were the water level problems solved (Figure 7.15)

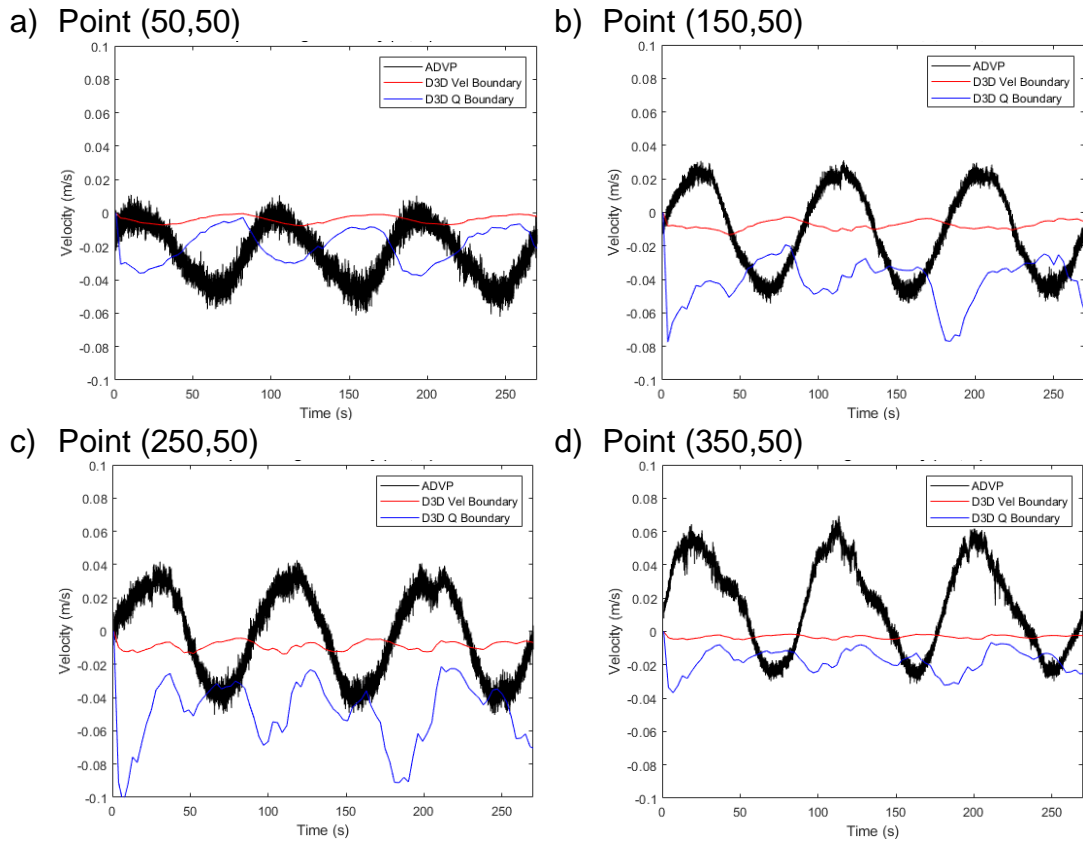


Figure 7.14 Depth averaged velocity results from Delft3D model with discharge and velocity boundaries split into four sections.

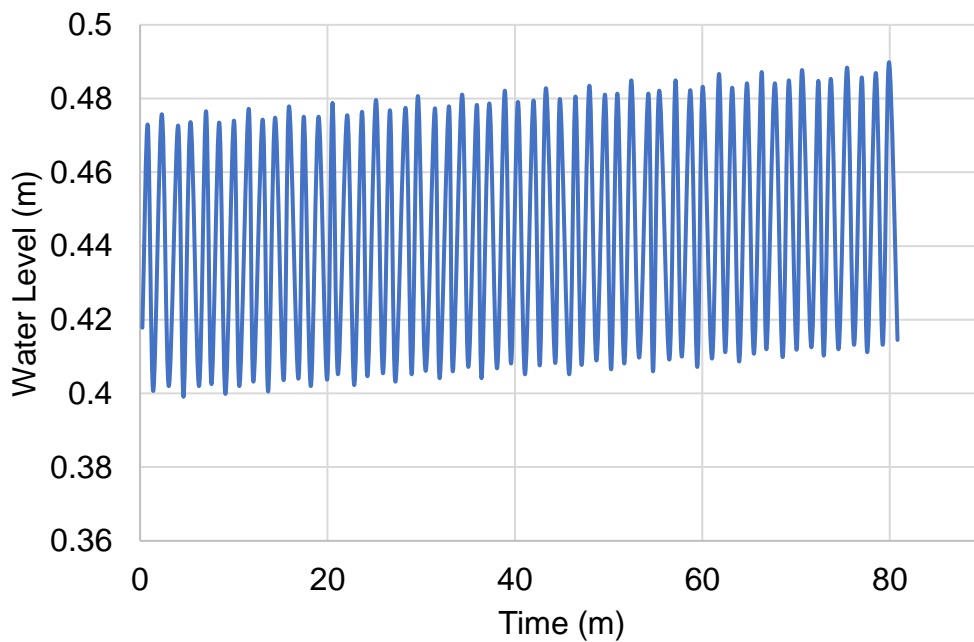


Figure 7.15 Water level results from Delft3D model with discharge inflow boundary split into four sections at (50,50).

7. Numerical Model

7.4.2 Bed Roughness

Attempts to calibrate the numerical model by adapting the inflow boundary have highlighted the difficulty that the tank's asymmetrical flow has made to predictions. Without this underlying peculiarity the numerical model performs well in certain places, e.g., along the centre line of the tank where lateral flows are less strong. However, to try to improve performance to resemble real world conditions more closely several other calibration parameters were investigated. During these additional tests the water level inflow boundary was used as it was found to calculate accurate results for water level despite being less accurate than the velocity and discharge inflow boundaries for predicting velocity.

Bed roughness is the most common tuning parameter with Manning's n values in the order of 0.02 (Vouriot et al., 2018) to 0.03 (Čož et al., 2019) used to accurately calibrate numerical models of marine renewable energy with varying topography. However, results of adapting this parameter can vary widely depending on other key parameters in the study area such as water depth and so tuning Manning's n can have a negligible effect on model performance in studies which are more sensitive to other factors e.g., topography.

Whilst realistic values of Manning's n for a smooth surface should range from 0.01 to 0.03, values outside this range can be considered for calibration purposes. To investigate the present model's sensitivity to bed roughness, values of 0.01, 0.02, 0.03, and 0.1 were tested uniformly across the tank to observe the effects. However, changes within this range made no observable difference to model results. Therefore, an impossible value of $n = 1$ was tested to see if this led to any changes and to investigate how the model was treating this variable. Figure 7.16 presents the results of this trial and shows that even the extreme value of $n = 1$ does not cause significant alteration to the model predictions. (N.B. Data for $n = 0.01$ (red line) does not appear to be shown on the graph as it is directly overlapped by data for $n = 0.1$ (blue line).) Overall, the model was found to be insensitive to bed roughness and other options were explored to try to improve model performance.

7. Numerical Model

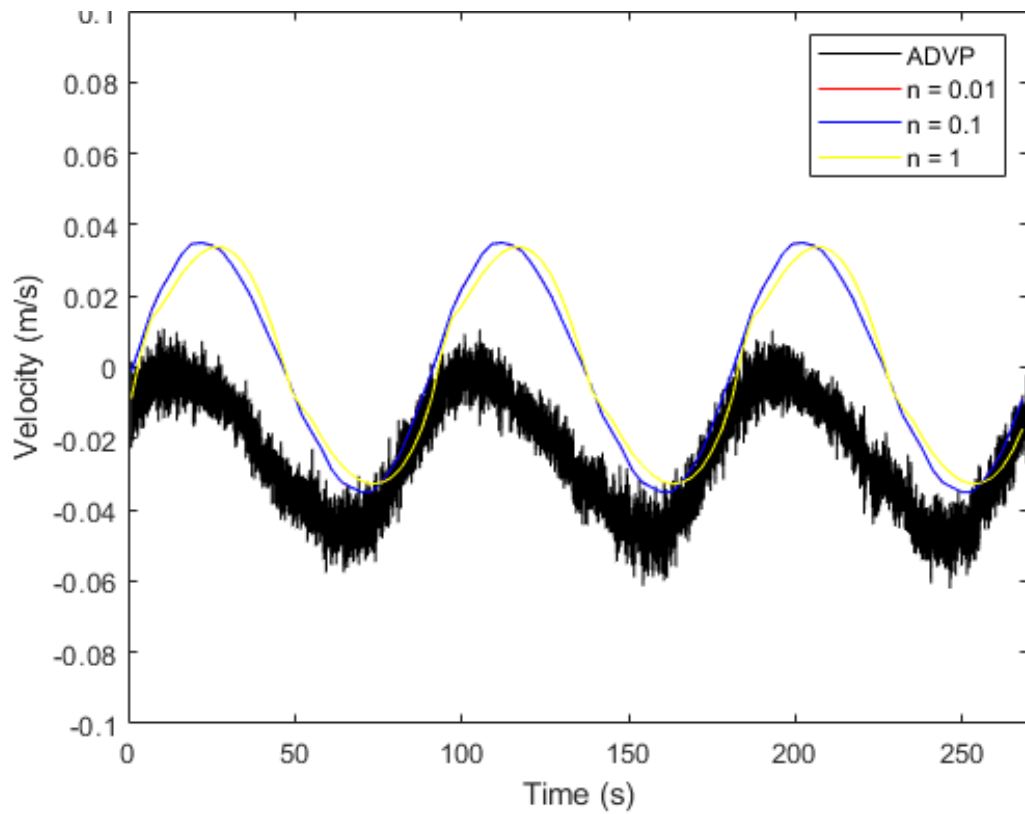


Figure 7.16 Depth averaged velocity results varying Manning's n .

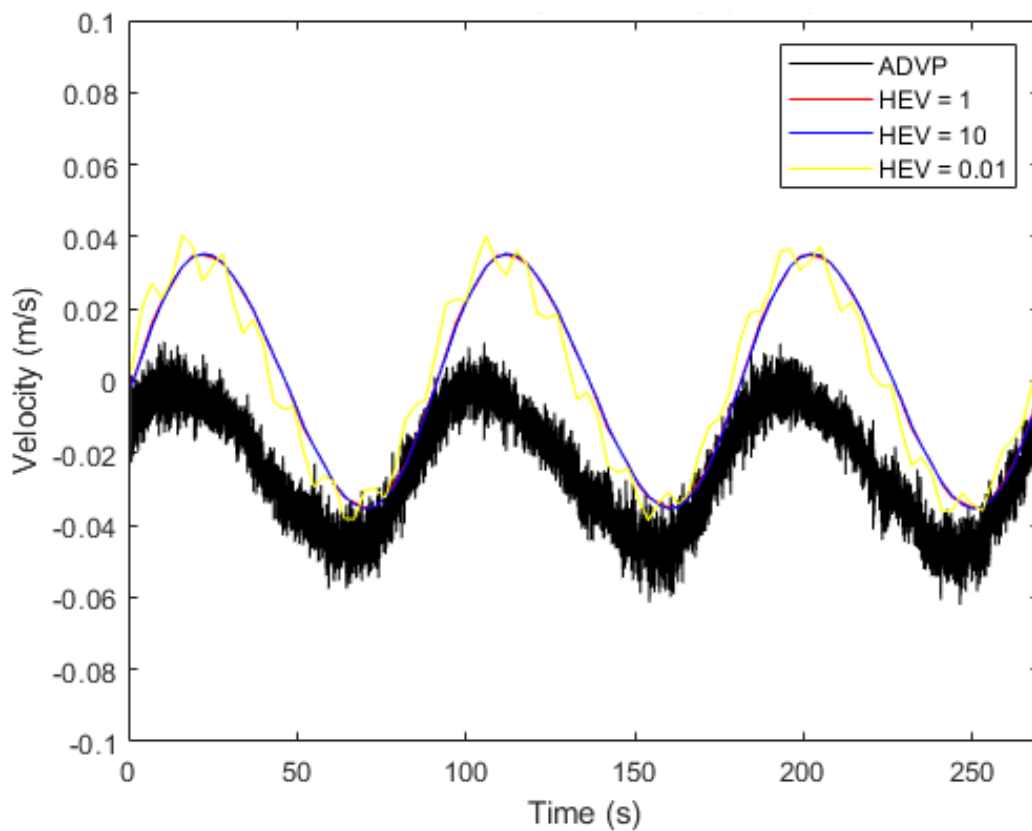


Figure 7.17 Depth averaged velocity results varying horizontal eddy viscosity.

7. Numerical Model

7.4.3 Horizontal Eddy Viscosity

In cases where bed roughness has little influence on results, horizontal eddy viscosity (HEV) has often been found to be the answer for calibration (Maulik and San, 2016; Parsapour-Moghaddam and Rennie, 2018; Saichenthur et al., 2022). Delft3D uses a default HEV value of $1 \text{ m}^2/\text{s}$, but it can be specified by the user as a uniform value or as a map file covering the whole domain. For a model of the scale used in the present study, the Delft3D user manual recommends an HEV value of between 1 and $10 \text{ m}^2/\text{s}$ (Deltares, 2018). These values were duly tried but with no discernible difference evident in the results as presented by Figure 7.17. (N.B. Data for HEV = 1 (red line) does not appear to be shown on the graph as it is overlapped by the data for $n = 10$ (blue line).)

Parsapour-Moghaddam et al. (2018) determined a value of $0.05 \text{ m}^2/\text{s}$ for their real world 2D river model and $0.1 \text{ m}^2/\text{s}$ for their 3D case. They demonstrated how lower background eddy viscosity led to significant differences in modelled depth averaged velocities and shear stresses. Following their example, a value of $0.01 \text{ m}^2/\text{s}$ was also tried here to test the sensitivity of the present model. This did produce some different results but only inasmuch as it destabilised the velocity, and it still did not alter the velocity range which is what needs to change to match the physical experiment data.

7. Numerical Model

7.4.4 Other Calibration Considerations

Other parameters that it is possible to adapt are the wall roughness, with slip conditions defined as free, partial or none. This controls the amount of friction at the closed boundaries of the domain and default settings for the program are for a free slip surface. Changing this parameter could lead to a reduction in the velocity range at each wall, which seems positive for adapting the extreme differences observed at each side of the tank. However, the scale of the present experiment is so small that it is not possible to run with partial or no slip conditions as it violates the Courant number at every time step by increasing eddy viscosity to such an extent that Delft3D cannot resolve the flow.

Another aspect to consider could be to model conditions in three dimensions rather than just two. Velocity measurements were taken in the laboratory at millimetre intervals from depths of 10 mm to 300 mm from the bed, making it possible to compare results at any depth of a 3D profile. Conventional calibration methods usually only tune models in two dimensions and rarely take three-dimensional flow fields into account. To counteract this Parsapour-Moghaddam et al. (2018) used fully spatially distributed ADV data to calibrate a 3D hydrodynamic model of a meandering river. They developed an algorithm in Matlab to match the location of each ADV measurement to the corresponding grid point in a 3D grid in Delft3D and reduced the mean absolute error between the observed and predicted velocity measurements using horizontal eddy viscosity and Manning's n as calibration terms. Once tuned, their model was validated using a subset of 3D velocity data taken from the river using an ADV. T-test analysis showed that the 3D model was highly sensitive to changes in background horizontal eddy viscosity which they deemed to be due to the 3D model needing higher dissipation to match observed individual point velocities than depth averaged ones. Overall, they found that 3D validation produced the best model performance and that compared to other studies they enhanced the potential for estimating river processes including channel morpho-dynamics, 3D flows and contaminant mixing.

7. Numerical Model

Three-dimensional modelling would also allow for the addition of secondary flow to be considered in the numerical model which is not available in the 2D depth averaged setup.

Three-dimensional experiments for scenarios S0, S2B and R0 were investigated to test the 3D capabilities of Delft3D and examine the effects on predictions for the current research. Figure 7.18 shows an example of the velocity results from these preliminary 3D trials which produced identical results at each depth of the six equal layers, even near the hydraulic structures. This agrees with the velocity contour plots of each tide, discussed in Chapters 4, 5 and 6, which showed very little variation between depths. Direct comparison of results from both the 2D and 3D trials also reveal identical values once the initial turbulence of the 2D trial evens out, an example of which is presented in Figure 7.19. This indicates that there is no benefit from modelling the present case in three dimensions, which is computationally more costly and time consuming than 2D trials.

In the case of all numerical models, it is possible to over-tune performance to match a specific set of results so that it is not flexible enough to make accurate predictions for other scenarios. Whilst graphs of RMSE (Figure 7.6) show close correlation in some areas of the tank it still does not perform well enough around the TRS seawalls, the crucial area for analysis in this study. Therefore, more work is needed to temper the performance of this model.

7. Numerical Model

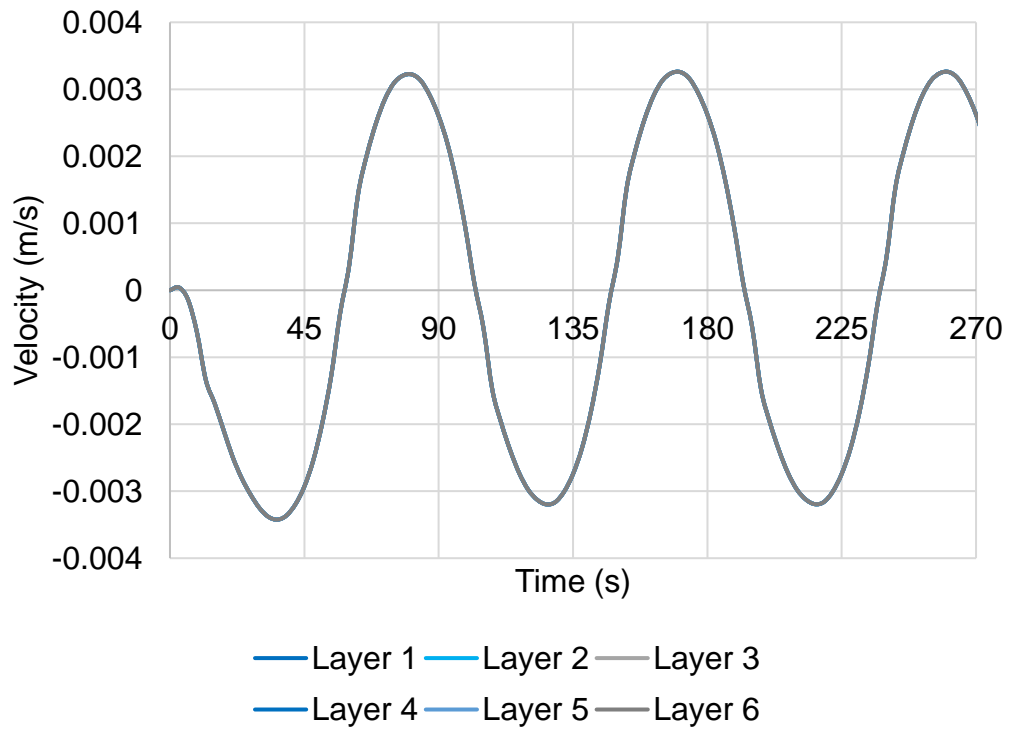


Figure 7.18 S2B 3D trial, velocity time series for different layers at (50,50).

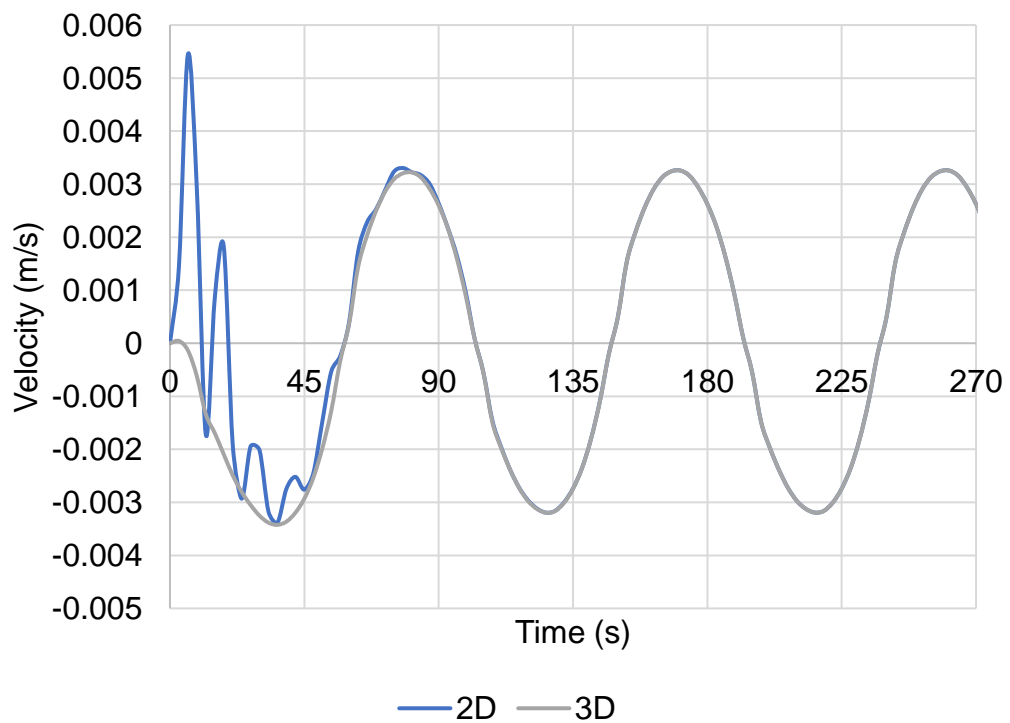


Figure 7.19 S2B velocity time series of 2D vs 3D trials at (50,50) (2D results not visible after 80 seconds as they align with 3D results).

7.5 Validation

Separate data is also required to validate the model, which checks that the numerical model continues to predict accurately for other cases beyond the tuning of calibration data. It is recommended that separate data should be reserved from physical experiments for this purpose (Gallego et al., 2017; Mohammadian et al., 2019; Vouriot et al., 2018). Maganga et al. (2010) advocate the development of an experimental database of flow characterisation and currents to be able to hold in reserve for validating future models.

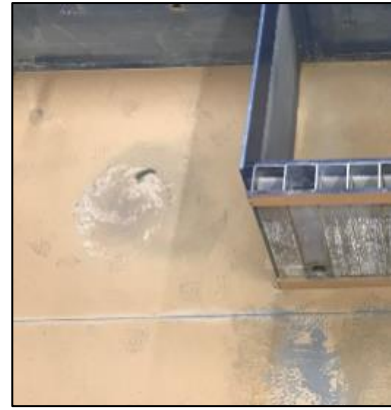
Once the model has been calibrated to an appropriate degree of accuracy and its performance has been validated, water level and velocity data can be extracted from the model to analyse different TRSs.

7.6 Summary

Analysis of various tuning parameters has shown how difficult it can be to calibrate a small-scale numerical model based on laboratory observations. Real life conditions often behave in complex ways that cannot always be matched by simplified computational calculations. Complex cross flows from the tank were unable to be modelled accurately by the numerical model which is designed to work with perpendicular flow at the inflow boundary and neither, Manning's n nor horizontal eddy viscosity, both common tuning parameters (Saichenthur et al., 2022), were able to adapt predictions to more closely match data observed in the laboratory. Inflow boundary conditions were also tested to adapt the model but were unable to compensate for the variation in flow velocity experienced at opposite sides of the inflow boundary making it impossible for the model to match predicted results with the observed laboratory data. Further investigation could test other modelling software to see if results are repeatable when governed by different equations, or if any other calibration parameters are available for investigation. Annex 5 presents the proposed schedule for test cases once the numerical model has been fully calibrated and validated.

Chapter 8

Discussion



8 Discussion

8.1 Introduction

This section focuses on the practicalities and limitations of the physical and numerical experiments already touched on in previous chapters. Details are given for solutions attempted to solve the problem of underlying asymmetric flow as well as the challenges this posed for the calibration of a numerical model.

8.2 Physical Limitations and Practicalities

The ambitious number of planned physical experiments had to be reduced for a number of reasons, some of which have already been touched upon. Major repairs delayed the initial start of the experiments for more than a year whilst university closures during the pandemic meant that the test schedule was streamlined from six TRS designs to two simplified geometries. However, three full test cases were still completed, comparing TRS geometry, turbine spacing and bed conditions.

8.2.1 Facilities

The scale of the physical TRS model was limited by the dimensions of the test facilities but the scale of the tide was also limited by the mechanical restrictions of the weir gate. Preliminary tests showed that tidal periods greater than 120 seconds resulted in such low flows that the velocity was too slow to measure, whilst a tidal period less than 45 seconds meant that the weir gate shifted too fast to be able to maintain the required tidal range. A tidal period of 90 seconds was found to be most accurate for measuring with the ADVP, therefore, the tidal period dictated much of the other scaling of the project. This study used a simplified sinusoidal wave to represent the tide in the laboratory, which is appropriate for experiments of this scale, but future studies could make use of a real-time control tidal generation system as developed by Rampazzo et al, (2019) who created an algorithm to control a weir gate with more live tidal data to more accurately model real conditions.

As well as the dimensions of the basin, other physical limitations include the age and capacity of the pumping equipment. The testing schedule was originally delayed by 12 months due to renovation of the pump and even

8. Discussion

once restored the pump was limited to a capacity of 47% to prevent overheating. This led to cavitation in the pipes and is thought to be one of the causes of asymmetric flow in the tank. The sampling grid was also limited by the rigging equipment and cable lengths which made gathering data in certain regions of the tank extremely difficult. The test schedule had to be designed so as to accommodate these considerations. Table 8.1 discusses other challenges faced in the laboratory and their effects on results.

Evidence of asymmetric flow in the tidal basin can be observed in water circulation patterns, sediment scour tracks and in all velocity results, proving that flow was stronger and faster on the right-hand side of the tank than the left (see evidence in Figure 8.1). This ongoing problem has had a large effect on experimental results especially when attempting to calibrate the numerical model (see Chapter 7 for full details). To address this issue, numerous potential solutions were tried with varying success. Table 8.2 discusses the various solutions attempted to rectify the problem of asymmetric flow, whilst Figure 8.2 illustrates the mechanisms of the holding basin that were adapted.

8. Discussion

Table 8.1 Laboratory challenges, tested solutions and their impacts.

Issue	Date	Impact and Solution
Asymmetric flow in tank	First observed 11/12/20	Evidence of asymmetric flow in the tidal basin can be observed by visible eddies, sediment scour tracks and velocity measurements, proving that flow is stronger and faster on the right-hand side of the tank than the left. This ongoing problem has a large effect on experimental results, especially when attempting to calibrate the numerical model, and is discussed in further detail below alongside trialed solutions.
ADVP buffering issues	First observed 25/11/20	The ADVP is extremely sensitive to velocity range settings and at points where the velocity range varied greatly the ADVP would shut down. This led to loss of time and data and requires careful selection of velocity range settings to avoid repetition of this problem.
Weir gate creep throughout the day	First observed 25/11/20	The water level in the tank fluctuated throughout the day and could vary by ± 0.005 m between experiments. To counteract this, the water level was measured manually between experiments and the weir gate adjusted accordingly to maintain the correct water level. This added more time to every experiment. Rampazzo et al. (2019) found that tide generation systems are not always consistent and may vary between experiments and so recommended calibration between each experiment and careful monitoring of the water level measurements to note any discrepancies.

8. Discussion

Weir gate computer crash	12/3/21	The weir gate often behaved jerkily at the start of each day. It was ruled out that this was due to any of the physical mechanisms of the weir gate and found to be the fault of aging computer equipment. The weir gate control computer eventually crashed completely, and more time was lost whilst it was rebuilt, however problems were reduced thereafter.
Broken pipe brackets	8/12/20 4/6/21 24/6/21	Cavitation in the inflow pipe meant that it shook quite violently and often became loose from the brackets which held it to the ceiling. Whilst the failure of one bracket was not catastrophic it did put more strain on the remaining brackets. When three brackets broke at once, experiments had to be stopped immediately to save the whole pipe from coming down. This took a week to fix, during which time no experiments could take place. This recurring problem can only be solved through regular maintenance as no sustainable solution to the cavitation in the inflow pipe has yet been found.
Reduced sensitivity of water level probes	2/2/21	The original water level probes lost sensitivity over time and eventually were only effective over a very small depth range. Pressure cells were introduced in order to take more accurate water level measurements and also meant that data could be taken at different locations since the pressure cells were not limited to a fixed position as the water level probes were.
Low ADVP SNR, seeding material circulation	22/3/21	ADVPs require suspended particles for their signal to reflect from to take accurate velocity readings. When water is too clear the signal to

8. Discussion

		<p>noise ratio (SNR) becomes low and readings are less accurate (Moeini et al., 2020). Seeding material can be added to the water to counteract this but due to size of the tidal basin and low velocities, it was difficult to keep the material in suspension and SNR often fell below the recommended level. Continual stirring and the addition of natural dust from the laboratory environment helped to maintain SNR at an appropriate level.</p>
Pressure cell rod sheered from base	11/6/21	<p>Whilst moving a pressure cell one day, the rod housing the communication wires sheered from the pressure cell base and stopped transmitting. This could easily be solved by epoxy glue but required a day to dry meaning that water level data could only be taken at half of the locations during that day.</p>
Pump overheated & stopped	5/7/21 20/7/21	<p>The pump stopped working on two occasions:</p> <ol style="list-style-type: none"> 1) When the pump rate was changed from 47% to 49% in an attempt to solve asymmetric flow in the tank. 2) Overheating from ambient temperature over 30°C. <p>The propensity to overheat is a longstanding problem with this pump which is why the pump rate is kept at the level it is and fans have been bought which need installing to prevent overheating again in future.</p>

8. Discussion

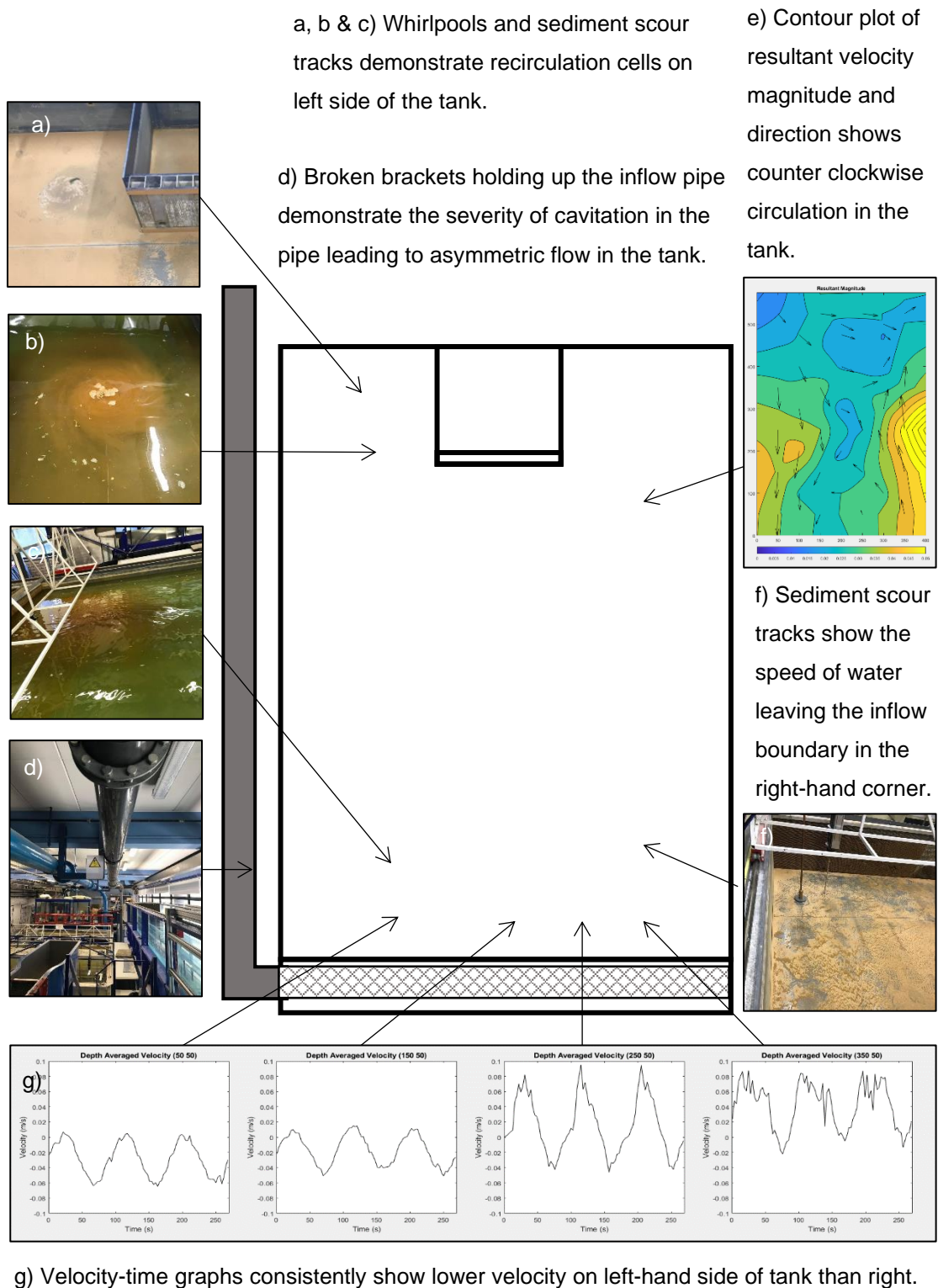


Figure 8.1 Evidence of asymmetric flow in tidal basin.

8. Discussion

Table 8.2 Evaluation of solutions to challenge of asymmetric flow.

Tested Solution	Date	Impact
a) Baffle screen repositioned to align with weir gate	22/1/21	A baffle screen sits between the weir gate and the inflow boundary to equalise the force of the water as it flows into the tidal basin. This screen had shifted over time and was realigned to return it to its original position, perpendicular to the flow. This ensured that all water was flowing in equal volume but had no impact on flow in the tank overall.
b) Inflow pipe recorked	12/2/21	The inflow pipe is surrounded by a mesh to distribute the incoming flow more equally across the inflow boundary and corks and sponges are added at various points to enhance this effect. Over time, many of the corks had been forced out and needed replacing. It was hoped that replacing more corks on the right-hand side of the pipe would reduce flow rates on this side of the basin, thus reducing the asymmetry, however results revealed that it actually made the problem worse and velocity on the right-hand side of the basin was even higher than before.
c) Additional honeycomb flow straighteners added behind weir gate	8/3/21	A wall of 50mm thick honeycomb flow straighteners lies at the inflow boundary to create laminar flow as the water enters the tidal basin. These had become damaged in the mid-section, and it was wondered if replacing or reinforcing this area could help balance flow across the inflow boundary as was demonstrated by Maganga et al. (2010). Additional sections of flow straightening

8. Discussion

		<p>material were thus placed at the right-hand side and towards the middle of the inflow boundary, but these small sections were not found to make a difference to the overall flow in the tank and so were removed.</p>
<p>d) Updated weir gate control computer hard and software</p>	<p>12/3/21</p>	<p>The weir gate controls the discharge rate of water flowing into the tidal basin and can be programmed to produce a sinusoidal wave to imitate tidal flow. Conditions should be uniform across its length but the age of the electrical and mechanical components of the weir gate system is such that it does not always behave ideally. The weir gate control computer underwent a complete rebuild which improved the performance of the weir gate and made flow smoother and more uniform but did not equalize flow velocity across the basin.</p>
<p>e) New pump flow rate</p>	<p>5/7/21</p>	<p>Water flow in the basin system is controlled by a pump initially set to a rate of 47%. In an attempt to settle the asymmetry in the tank this rate was increased to 49%. This slight increase dramatically reduced vibrations in the pipe, however it was not possible to find whether it made a difference to flow in the tank as the pump overheated within an hour of trialing this new setting which made it impossible to maintain.</p>

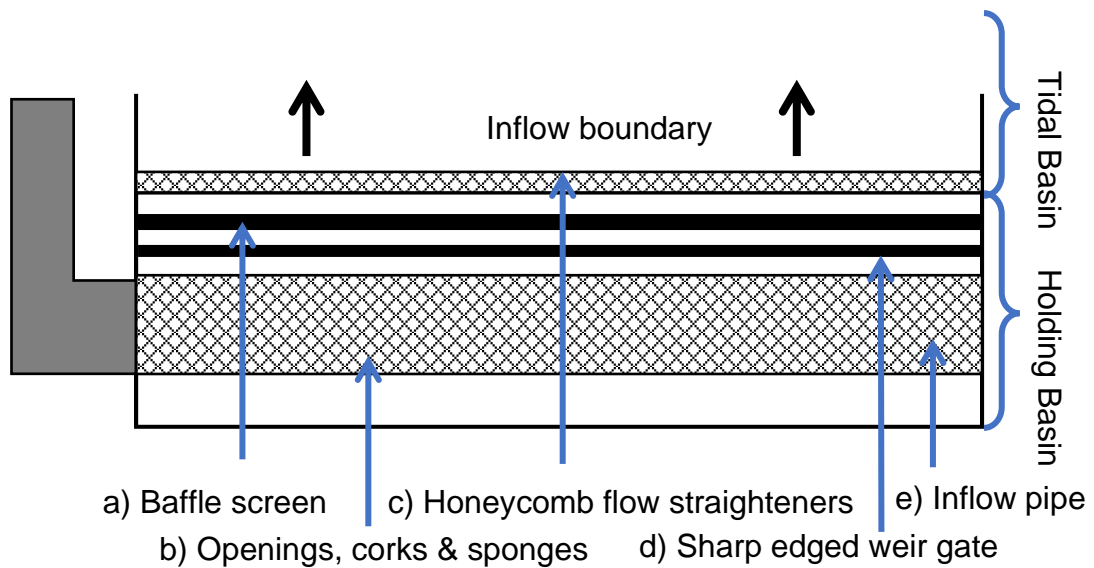


Figure 8.2 Holding basin components adapted to address asymmetric flow.

Overall, the asymmetry of flow in the tank is most likely due to uneven force across the length of the inflow pipe due to the Venturi effect caused by a 90° junction in the pipe at the edge of the holding basin. The water pressure is therefore much lower on the left-hand side of the tank (closest to the pipe junction) and returns to full force at the right-hand side. Despite attempts to equalise this force across the length of the pipe with additional dampening materials, none are sufficient to overcome this underlying problem of unequal pressure. The most effective attempt to solve the issue was found in adjusting the pump flow rate, which reduced the amount of air in the pipe, causing smoother flow throughout the system and also solving the problem of vibrations in the pipe which shook the whole lab. Whilst this solution was found to be the most successful at answering the problem it was not possible to maintain the new rate as it caused the pump to overheat. In order to increase the pump rate in future and reduce the problem of asymmetric flow more permanently fans need to be installed in the pump control housing to prevent it from overheating and enabling it to operate at an increased rate.

Previous experiments in the tidal basin had only used a portion of the whole basin area at very shallow depths and with low flow rates thus the issue of asymmetry had not been identified. Using a restricted area of the tank could help future experiments as would better characterisation of the nature of the

8. Discussion

asymmetry to understand its effect on results. Although this issue made calibrating the numerical model more difficult it does provide an insight into real life flow conditions which are rarely uniform or linear.

8.2.2 Equipment and Operation

Other factors that could have affected the accuracy of results are mechanical vibrations from different pieces of equipment as well as user error. Stepper motor vibrations whilst moving the ADVP between depths could cause interference with the transmission and reception of the ADVP signals creating artificial turbulence in the velocity readings. To compensate for this, the first and last six seconds of each reading were removed to avoid any data gathered whilst the stepper motor was working. Data was also gathered over a series of four tides whilst only three were reported on in order to gain the cleanest data set by being able to trim any anomalous results at the start and end of each time series.

Whilst the ADVP system was automated as far as possible, the initial start of the program required a user to simultaneously press record for both the ADVP and water level measurements. This synchronisation is important for being able to analyse velocities at the correct part of the tide but as the systems were operated using different computers there was always a slight delay between start times. This could be overcome by synchronising the time series by eye when analysing the results. Other potential errors from the use of the ADVP and how they were overcome are discussed in Table 8.3.

8. Discussion

Table 8.3 Potential issues with ADVs and how they were overcome.

Potential Issue	Solution
Inaccurate results from inappropriate velocity range settings	Make sure velocity range is set so that the maximum observed speed is in the middle of the range. Too large and bias is increased, too small and data wrapping will occur.
Interference from close boundaries	Ensure that ADV is kept at least 5 cm away from all boundaries and obstacles to ensure that signal is only reflected off particles.
Low SNR	Water must have sufficient suspended particles for signal to reflect from otherwise data readings will be inaccurate. Ensure particle suspension is maintained through regular stirring.
Low correlation	Low correlation occurs when there is interference between pulses this is minimised by keeping velocity range to an appropriate level and keeping ADVs away from obstructions.
Noisy data	Adjusting settings and positioning of the probes is the best way to solve the issue before taking readings. Another method for reducing noisy data is to use adaptive ping intervals to smooth flow.
Weak spots	Weak spots can occur in different locations at different settings, areas for concern for velocity range settings of 0.1-0.5 m/s are 0.1, 0.23 and 0.45 m and particular care should be taken to avoid obstructions in these zones.
Acoustic streaming	Acoustic streaming can occur in flows below 8cm/s which leads to secondary flows being generated as pulses are transmitted. These flows can be detected using probe checks before starting to take readings and can be solved by reducing the power level which reduces transducer induced flow.

8. Discussion

Setting the velocity range was the most difficult parameter when using the ADVP as the velocity varied greatly, especially around turbine openings and TRS seawall. Inappropriate choice of velocity range could lead to noisy or wrapped data or even in the ADVP stopping recording altogether. This could be managed by careful choice of velocity range and filtering data where anomalies occurred.

The accuracy of the flow visualisation was dictated by the clarity of the water within the TRS and the contrast between the fluorescent dye and the bed. This method for analysing flow patterns in the TRS proved positive as a simple and cost-effective for initial observations but only clearly showed flow variation in the horizontal axis. Future experiments could also investigate vertical variations by using a submerged camera to observe tracer dye movement throughout the water column.

8.2.3 Software and Calibration Challenges

When the physical experiments faced interruption, numerical modelling was proposed to extend the modelling capacity. However, difficulties of asymmetrical flow that plagued the physical experiments also impeded the calibration of the numerical counterpart as discussed in Chapter 7. Annex 5 presents proposals for a new series of experiments to be tested in future once the numerical model has been accurately calibrated and validated.

8.3 Summary

The very nature of laboratory experiments is to control the number of variables for testing in order to simplify real life cases for comparison and to make predictions. However, the reality of controlling every aspect of an experiment is hard to put into practice. The size of the laboratory facilities was small enough to limit the scale of the physical model but large enough to present secondary issues with flow in the tidal basin. These issues led to results that were interesting in themselves but made calibrating a numerical model extremely difficult. Despite these difficulties the results of the present study could still be applied to harbours and coastal reservoirs and lessons learned from these experiments can inform future studies to continue to improve the understanding of the hydrodynamic impacts of TRSs.

Chapter 9

Summary and Conclusions



9 Summary and Conclusions

9.1 Introduction

The current study set out to answer the following key questions:

1. To what extent does the presence of hydraulic structures alter the hydrodynamic environment?
2. How are baseline conditions affected by changes to hydrodynamics in the presence of hydraulic structures?
3. What difference, if any, does the spacing of turbines and sluices in tidal range schemes make to hydrodynamics?

This section looks at how well the research has answered these questions, summarising key findings, their accuracy, adroitness and further application.

9.2 Summary

This research used physical experiments to model the hydrodynamic impact of different aspects of TRS design. A TRS with simplified geometry was constructed in the hydro-environmental research centre at Cardiff University with horizontal scale of 1:5000 and vertical scale of 1:100 to investigate the effects of varying TRS turbine spacing, geometry and bed conditions. Flow velocity and water level were measured as indicators of change caused by the variation in TRS design and analysed using maps of velocity vs time series and contoured resultant and residual flow magnitude as well as statistical tests of the similarity between observed data and baseline conditions, including z-tests and Pearson's correlation coefficient.

Results from laboratory experiments were grouped into eight categories in order to compare the effects of changing specific variables:

- Comparison A – square TRSs with varying number of turbines.
- Comparison B – square TRSs varying the position of a single turbine.
- Comparison C – square TRSs varying the position of two turbines.
- Comparison D – square TRSs with two turbines, varying bed material.
- Comparison E – square TRSs with two turbines, varying bed slope.
- Comparison F – comparison of square and rectangular TRSs.

9. Summary and Conclusions

- Comparison G – rectangular TRSs varying the position of two turbines.
- Comparison O – all cases compared with pre-lagoon conditions.

These comparisons revealed that certain design characteristics have a greater impact on the natural environment than others and that turbine placement in particular has a greater effect than bed material or bed slope on resultant velocity magnitude and direction.

9.3 Discussion

9.3.1 Impact of varying turbine layout

The area of the turbine openings has been proven to impact flow conditions (Dai et al., 2017) and power output (Angeloudis et al., 2016a) and therefore varying the number of turbines should lead to differences in hydrodynamics. Comparison A presented the case of a square TRS with zero, one and two turbines to reveal that a single turbine causes less disruption to baseline conditions than two turbines in a similar location. Despite being located in the same part of the TRS, two turbines placed together led to stronger flows and exaggerated vortices than a single turbine in the same position, as the combined wake of two closely spaced turbines multiplied the effects of the single opening. This was confirmed by the results of the rectangular TRSs where two turbines also caused greater disruption than one. Where two turbines are present, the spacing of the openings can make a difference to flow conditions and comparisons B and C proved that turbine spacing has a greater impact than the number of turbines overall.

In comparing the position of a single turbine, central positioning, away from the walls and obstructions, caused less disruption to baseline conditions by allowing free circulation both in and outside of the TRS. Whereas turbines placed closer to the seawall lead to stronger wakes and recirculation currents inside the TRS and deflected flow in the wider tank. Based on these results we would therefore recommend that turbines should be placed away from walls in order to avoid undue influence of obstructions on circulation currents.

When analysing the positioning of pairs of turbines, it was found that wider spacing has less impact on hydrodynamics, a result that was repeated in

9. Summary and Conclusions

both the square and rectangular cases, and central turbine placement was once again confirmed to be most beneficial for maintaining natural conditions. Closer turbine positioning was shown to produce stronger currents and higher velocities inside the TRS and further afield, up to a distance of 30 turbine diameters due to the strength of the combined wakes, whilst wider spacing promotes greater circulation within the TRS but slows flow overall. Slower velocities would enable other activities to take place inside the TRS, e.g., fishing and recreation, but may lead to issues with water quality, which would have to be carefully considered in the development and management of any TRS.

Overall, single turbines were found to cause less disruption to natural flow conditions than two, but two turbines were found to allow better circulation and flushing which supports a healthier environment. Close turbine positioning leads to strong turbine wakes and exaggerated vortices, which are further affected by proximity to seawalls, so wider spacing is preferred for promoting balanced flows in the near and far field despite being the more expensive option. This was found to be the case in both square and rectangular TRSs leading us to conclude from these experiments that turbine spacing has a greater impact on hydrodynamics than TRS geometry itself does.

9.3.2 Impact of varying bed conditions

When investigating bed conditions, bed material was found to have very little influence on flow conditions overall but artificial grass caused slightly least disruption to baseline conditions due to its flexibility with gravel of both sediment sizes leading to more irregular flow patterns. Sloped bed conditions were found to have little impact on flow directly outside the TRS but could increase velocities inside the TRS by up to 80% which would mean coastal geomorphology would greatly influence TRS location and design. Very little deviation from baseline conditions was found when varying bed material or bed slope (comparisons D and E) overall and the statistically strong relationship between results from experiments B2-6 paint a reliable picture of the conclusion reached here that the bed conditions do not significantly impact upon flow conditions.

9. Summary and Conclusions

9.3.3 Impact of varying TRS geometry

Both TRS shapes were found to cause disruption to hydrodynamics, but their impact varied in extent and location. Both geometries reduced flow velocity overall, but the rectangular TRS had further reaching impacts as its wider shape resulted in greater channel blockage which restricted circulation at the rear of the tank. This highlights the importance of site-specific design, ensuring that TRS geometry is sympathetic to the natural shape of the coast in order to prevent problems such as erosion, flooding or stagnation. Other shapes such as semi-circles and trapezia could also be tested in future to investigate if shapes with wider angles help promote circulation and reduce the issue of stagnant corners.

In the single turbine cases (S1A and R1), the rectangular TRS was found to cause less disruption to baseline conditions than the square TRS but still confined flows along the tank boundaries. This is also evident in the cases with two side-by-side turbines (S2A and R2A) where the square TRS enables better circulation around the whole of the outer tank whilst the rectangular TRS restricts flow in certain areas. This is also true inside the TRS, where water is able to circulate throughout the whole of the square TRS but is limited within the rectangular TRS, leading to areas of stagnation which can hamper water quality. In real life this would have to be managed by expensive engineering solutions. One such solution could be to space the turbines further apart, as in comparison F iv, where the two turbines were placed at opposite ends of the seawall. This resulted in improved circulation in both TRSs but still with slower flows in the rectangular case. Despite these issues inside the TRS, the rectangular shape was again shown to be better able to maintain natural conditions overall.

Overall, comparisons varying TRS geometry with one or no turbine openings (comparisons F i and ii) showed a significant difference between results, proving that TRS shape does have an impact on hydrodynamics. However, this difference was less prominent once both TRSs had two turbines (comparisons F iii and iv) proving that turbine positioning was the dominant variable over TRS geometry as identified in Comparisons A and G. Comparison F iv also revealed that the three-dimensional element of wakes

9. Summary and Conclusions

from the turbine openings was more strongly felt in the square TRS than the rectangular case. This was deemed to be due once again to the proximity of the side walls in the square TRS which had a greater influence on flow patterns in all dimensions than the rectangular TRS where the perpendicular seawalls were further away from the turbine openings and therefore had less of an impact on circulation.

Throughout the experiments, results were compared back to the baseline (pre-lagoon) conditions to determine which designs caused the least disruption to natural conditions, in order to be considered truly sustainable. Regression analysis (Annex 2) proved that wider spacing was the best for maintaining natural conditions, with the central spacing of S2D proving best in the square TRS and wider spacing in R2B and R2D performing best in the rectangular TRS. The scenarios with the least correlation between their results and those of the baseline case were S1A and S2A, both square TRSs but with a single vs two turbines offset to the right of the TRS seawall. This analysis confirms that the rectangular shape causes least disruption to baseline conditions and that although bed conditions do not significantly alter performance, turbine spacing is a defining factor in the effects of TRS on the natural environment.

Underlying asymmetry caused by uneven distribution of pressure along the inflow boundary was a concern throughout these experiments and although it is not ideal for analysing the effects of the turbines it has proven to be consistent throughout all experiments and therefore the effects of the turbines can confidently be separated from those of underlying tank conditions.

9.4 Applications

Flow velocity in the experiments presented here are very low, with all conclusions based on these conditions. Further investigation at larger scales would enable the findings of these experiments to be applied in other situations. Although the present study has looked specifically at conditions in TRSs, the findings of these experiments could also be applied to other natural and manmade marine structures, e.g., flood defences (Elliott et al.,

2019) and coastal reservoirs (Vouriot et al., 2018). This study has demonstrated how structural design, including bed materials, bed slope, shape and the positioning of hydraulic structures can affect flow conditions in the surrounding area, causing changes to velocity magnitude and direction in both the near and far field. These findings can be applied to harbours and marinas, which are also coastally attached and may need to consider bed conditions and the proportions of their seawalls in order to minimise effects on hydrodynamics.

Coastal reservoirs are of increasing interest for providing fresh water to islands and coastal conurbations. These structures use sluice gates to manage water levels inside the reservoir and can learn from the results presented here on the spacing of openings in a seawall in order to minimise disruption to the natural environment. Observations of flushing in the TRSs can also be applied to in natural lagoons with restricted openings, e.g., Fleet Lagoon in Dorset, where artificial openings may need to be introduced in order to improve water quality.

9.5 Overall Conclusion

Tidal range energy is a promising prospect in the UK, given its predictability, proliferation and proximity to demand. It has been proposed as a sustainable alternative to fossil fuels for providing baseload energy and could accelerate the marine renewable industry in the UK whilst helping to meet decarbonisation targets. Previous prohibitors to its implementation boil down to environmental and financial costs of such an undertaking and whilst this research has not addressed any financial aspects it has gone some way to answering concerns around the environmental impact of TRSs.

In answering the original study questions, it has been shown that:

1. Hydraulic structures alter the hydrodynamic environment by restricting currents to specific areas around the edge of seawalls and near the coast. Rectangular shaped TRSs are better able to maintain natural conditions than square TRSs and wider spaced turbines promote circulation over a larger area compared to closely spaced turbines which lead to exaggerated wakes and strong vortices.

9. Summary and Conclusions

2. All hydraulic structures cause changes to hydrodynamics, increasing the range of velocities across the wider area but particularly in the vicinity of the TRS, and especially around turbine openings. Where velocity is changed in the wider tank area it is most often reduced.
3. Closely spaced turbines lead to strong wakes which increase circulation inside the TRS and deflect flow in the wider outside area. Wider spacing leads to reduced flow velocity and greater circulation throughout the tank as a whole. Centrally positioned turbines, away from seawalls and other obstructions, most closely match natural conditions.

Proposed TRS schemes from around the UK incorporate secondary functions, such as opportunities for aquaculture and recreation. The findings of the present study show that a rectangular shaped TRS with widely spaced turbines would enable these activities to take place by reducing velocities inside the structure but that measures would need to be taken to manage water quality. Closely spaced turbines would result in exaggerated wake effects with high velocities and strong vortices prohibiting activities in the area.

Many numerical studies have already been undertaken in order to investigate aspects of TRS design, operation and impact. This research adds to this body of knowledge through physical experiments, supporting the design process for tidal range structures in the hope that it will help TRE to become a reality in the UK.

9.6 Recommendations for Future Study

Further to the findings of the present research, future studies could consider:

- Repetition of physical experiments. Serious consideration of the conditions in the tidal basin to solve the problem of asymmetric flow would enable experiments to be conducted to show the extent to which results were affected by system behaviour and which conditions were due to TRS design. Repeating the experiments at a different scale, i.e., with higher velocities would also help promote the application of these findings to other settings.

- Increasing the number of turbines. This would help to find at what point the area of openings in the seawall returns flow conditions to the most natural levels as greater turbine and sluice areas have been shown to have less impact on regional velocity (Dai et al., 2017).
- Other length-to-width seawall ratios. Only two TRS geometries were able to be tested at the present time. The shape of the TRS was found to have a significant impact on flow velocity inside the impoundment but also on circulation patterns in the outer region, both of which will have impacts on water quality and the ability of other groups to use the area. It would therefore be worth investigating if any other TRS shapes, e.g., semi-circles or trapezia, or proportions are better for balancing hydrodynamic conditions.
- Different representations of turbines and sluices. The present experiments used open orifices to represent turbine draft tubes, but further study could implement scaled turbines or actuator discs to improve the representation of flow resistance to more accurately model real-life conditions. Accurate representation of hydraulic structures is often cited as a challenge to physical and numerical models of TRSs (Adcock et al., 2015).
- Three-dimensional flow visualisation. The use of tracer dye and video imagery is a simple and cost-effective method for flow visualisation in two-dimensions, however it does not allow for understanding of the three-dimensional nature of flow through a turbine. Future experiments could use PIV to analyse flow in the vertical as well as horizontal dimensions to try to quantify wake characteristics as described by Jeffcoate et al. (2017).
- Applications for other coastal structures. The present results regarding TRS geometry and the area of the openings in the structure can also be applied to other marine structures, e.g., harbours and coastal reservoirs. The model could be modified to represent these structures more accurately and further investigate the impacts of design on the hydrodynamics.

Chapter 10

References

- Draycott, S., Steynor, J.,
Experimental assessment
over a tidal cycle.
*Journal of Marine Energy
Conversion*, 5(2), 173-187. doi:
10.1016/j.jmeco.2018.05.001
- DTOceanPlus. (2018). M
Elliott, K., Smith, H. C. M
(2019). A systems approach
environmental impact
assessment. *Journal of Marine
Energy Conversion*, 10(1),
doi:10.1016/j.jmeco.2019.01.001
- Energy and Climate Change
*Renewables in the
Mediterranean Region*
Etemadi, A., Emami, Y.,
Renewable Energy
Generation by the
Mediterranean Sea
doi:10.1016/j.egypr.2019.01.001
- European Commission. (1998).
*Study on the
feasibility of tidal marine current
energy conversion*
- Falconer, R. A. (1974). Tidal
current energy conversion
(MSc MSc Thesis
University of
Liverpool)
- Falconer, R. A., Angelou
K., Hydroenvironmental
Impact Assessment of
Projects in Coastal
Areas, ed., pp. 1552-157
1572
- Falconer, R. A., Guo, B.,
Renewable Energy
their potential for
tidal current energy
conversion. *Sustainable Water
Resources* (pp. 143-172).
- Falconer, R. A., and Kol
M., Morphological
Modelling
Sediment Research
- Fallon, D., Hartnett, M., C
configuration on the
tidal current energy
Renewable Energy
- Federov, M. P., Shillin, N
Projects. *Power T*
- Frau, J. P. (1993). Tidal
current energy conversion
industrial-scale ex
Conversion, 8(3),
173-187
- Funke, S. W., Farrell, P.
Renewable Energy
optimisation using
tidal current energy
673. doi:10.1016/j.
jre.2019.01.001
- Gallego, A., Side, J., Bas
Burrows, M. (2017).
Renewable energy
and tidal energy
resources
for quantifying acc
*Ocean & Coastal
Management*
doi:10.1016/j.oceco
man.2017.01.001
- Gao, C., and Adcock, T.
Renewable Energy
Channel. *Internati
onal Journal of
27(2), 177-183. doi:*

10 References

- Acadia Tidal Energy Institute. (2013). *Community and Business Toolkit for Tidal Energy Development*. Retrieved from <https://tidalenergy.acadiau.ca/community-business-toolkit.html>
- Acadia Tidal Energy Institute. (2016). *ecoEnergy Innovation Initiative Research and Development Component Public Report*. Retrieved from https://tidalenergy.acadiau.ca/tl_files/sites/atei/Content/EcoEII/Acadia%20ecoEII%20Final%20Public%20Report%20English.pdf
- Adcock, T. A. A., Draper, S., and Nishino, T. (2015). Tidal power generation – A review of hydrodynamic modelling. *Proceedings of the Institution of Mechanical Engineers, Part A: Journal of Power and Energy*, 229(7), 755-771. doi:10.1177/0957650915570349
- AECOM Canada Ltd. (2014). *Tidal Energy: Strategic Environmental Assessment Update for the Bay of Fundy*. Retrieved from <https://oera.ca/sites/default/files/2019-05/Tidal%20Energy-%20Strategic%20Environmental%20Assessment%20%28SEA%29%20Update%20for%20the%20Bay%20of%20Fundy.pdf>
- Aggidis, G. A., and Feather, O. (2012). Tidal range turbines and generation on the Solway Firth. *Renewable Energy*, 43, 9-17. doi:10.1016/j.renene.2011.11.045
- Aggidis, G. A., and Židonis, A. (2014). Hydro turbine prototype testing and generation of performance curves: Fully automated approach. *Renewable Energy*, 71, 433-441. doi:10.1016/j.renene.2014.05.043
- Ahmadian, R., Falconer, R., and Lin, B. (2010). Hydro-environmental modeling of proposed Severn barrage, UK. *Proceedings of the Institution of Civil Engineers - Energy*, 163(3), 107-117. doi:10.1680/ener.2010.163.3.107
- Ahmadian, R., and Falconer, R. A. (2012). Assessment of array shape of tidal stream turbines on hydro-environmental impacts and power output. *Renewable Energy*, 44, 318-327. doi:10.1016/j.renene.2012.01.106
- Ahmadian, R., Falconer, R. A., and Bockelmann-Evans, B. (2014). Comparison of hydro-environmental impacts for ebb-only and two-way generation for a Severn Barrage. *Computers & Geosciences*, 71, 11-19. doi:10.1016/j.cageo.2014.05.006
- Alifidini, I., Kismawardhani, R. A., Wirasatriya, A., Sugianto, D. N., Yaakob, O. B., and Widodo, A. B. (2018). *Identification of Tidal Energy Resources using Satellite Altimetry Data for Indonesian Seas*. Paper presented at the 4th International Symposium on Geoinformatics.
- American Society of Civil Engineers. (2000). *Hydraulic Modeling: Concepts and Practice*. Virginia, USA: American Society of Civil Engineers,.
- Andritz. (2018). HydroNews. *HydroNews*, 32(1).
- Angeloudis, A. (2019). Tidal range structure operation assessment and optimisation. *Dams and Reservoirs*, 29(2), 45-54. doi:10.1680/jdare.18.00042
- Angeloudis, A., Ahmadian, R., Falconer, R. A., and Bockelmann-Evans, B. (2016a). Numerical model simulations for optimisation of tidal lagoon

10. References

- schemes. *Applied Energy*, 165, 522-536.
doi:10.1016/j.apenergy.2015.12.079
- Angeloudis, A., and Falconer, R. A. (2017). Sensitivity of tidal lagoon and barrage hydrodynamic impacts and energy outputs to operational characteristics. *Renewable Energy*, 114, 337-351.
doi:10.1016/j.renene.2016.08.033
- Angeloudis, A., Falconer, R. A., Bray, S., and Ahmadian, R. (2016b). Representation and operation of tidal energy impoundments in a coastal hydrodynamic model. *Renewable Energy*, 99, 1103-1115.
doi:10.1016/j.renene.2016.08.004
- Angeloudis, A., Kramer, S. C., Avdis, A., and Piggott, M. D. (2018). Optimising tidal range power plant operation. *Applied Energy*, 212, 680-690. doi:10.1016/j.apenergy.2017.12.052
- Angeloudis, A., Kramer, S. C., Hawkins, N., and Piggott, M. D. (2020). On the potential of linked-basin tidal power plants: An operational and coastal modelling assessment. *Renewable Energy*, 155, 876-888.
doi:10.1016/j.renene.2020.03.167
- Angeloudis, A., Piggot, M. D., Cramer, S. C., Avdis, A., Coles, D., and Christou, M. (2017). *Comparison of 0-D, 1-D and 2-D model capabilities for tidal range energy resource assessments*. Paper presented at the EWTEC2017, Cork, Ireland.
- Bae, Y. H., Kim, K. O., and Choi, B. H. (2010). Lake Sihwa tidal power plant project. *Ocean Engineering*, 37(5-6), 454-463.
doi:10.1016/j.oceaneng.2010.01.015
- Baig, M. S., Uddin, Z., and Insaf, A. (2021). GIS-linked tidal range energy resource assessment. *Arabian Journal of Geosciences*, 14(6).
doi:10.1007/s12517-021-06811-2
- Baker, A. L., Craighead, R. M., Jarvis, E. J., Stenton, H. C., Angeloudis, A., Mackie, L., . . . Hill, J. (2020). Modelling the impact of tidal range energy on species communities. *Ocean & Coastal Management*, 193.
doi:10.1016/j.ocecoaman.2020.105221
- Bas, A., Jacob, C., Hay, J., Pioch, S., and Thorin, S. (2016). Improving marine biodiversity offsetting: A proposed methodology for better assessing losses and gains. *Journal of Environmental Management*, 175, 46-59. doi:10.1016/j.jenvman.2016.03.027
- BBC News. (2020). River Mersey tidal power plan granted £2.5m funding. *BBC News*.
- Bijankhan, M., Kouchakzadeh, S., and Belaud, G. (2017). Application of the submerged experimental velocity profiles for the sluice gate's stage-discharge relationship. *Flow Measurement and Instrumentation*, 54, 97-108. doi:10.1016/j.flowmeasinst.2016.11.009
- Bijlsma, A., van Roermund, M., van Duren, L. (2015). *Tools to optimise power production and environmental effects*. Retrieved from https://www.slideshare.net/Delft_Software_Days/dsd-int-2015-tools-to-optimise-power-production-and-environmental-effects-arnout-bijlsma-luca-van-duren
- Binnie, C. (2016). Tidal energy from the Severn estuary, UK. *Proceedings of the Institution of Civil Engineers - Energy*, 169(1), 3-17.
doi:10.1680/jener.14.00025

10. References

- Boehler, G. W., and Gill, A. B. (2010). Environmental and Ecological Effects of Ocean Renewable Energy Development. A Current Synthesis. *Oceanography*, 23(2), 68-81.
- Bonar, P. A. J., Adcock, T. A. A., Venugopal, V., and Borthwick, A. G. L. (2018). Performance of non-uniform tidal turbine arrays in uniform flow. *Journal of Ocean Engineering and Marine Energy*, 4(3), 231-241. doi:10.1007/s40722-018-0118-x
- Borthwick, A. G. L. (2016). Marine Renewable Energy Seascape. *Engineering*, 2(1), 69-78. doi:10.1016/j.Eng.2016.01.011
- Brammer, J., Falconer, R. A., Ellis, C., and Ahmadian, R. (2014). Physical and numerical modelling of the Severn Barrage. *Science China Technological Sciences*, 57(8), 1471-1481. doi:10.1007/s11431-014-5602-5
- Bryant, D. B., Whilden, K. A., Socolofsky, S. A., and Chang, K.-A. (2012). Formation of tidal starting-jet vortices through idealized barotropic inlets with finite length. *Environmental Fluid Mechanics*, 12(4), 301-319. doi:10.1007/s10652-012-9237-4
- Bulleri, F., and Chapman, M. G. (2010). The Introduction of Coastal Infrastructure as a Driver of Change in Marine Environments. *Journal of Applied Ecology*, 47(1), 26-35.
- Burrows, R., Walkington, I., Yates, N., Hedges, T. S., Li, M., Zhou, J., . . . Prandle, D. (2009a). *Tapping the Tidal Power Potential of the Eastern Irish Sea*. Retrieved from <https://core.ac.uk/download/pdf/80780476.pdf>
- Burrows, R., Walkington, I. A., Yates, N. C., Hedges, T. S., Li, M., Zhou, J. G., . . . Proctor, R. (2009b). Tidal Energy Potential in UK Waters. *Maritime Engineering*, 162(MA4), 10.
- Centre for Economics and Business Research. (2014). *The Economic Case for a Tidal Lagoon Industry in the UK*. Retrieved from https://www.tidallagoonpower.com/wp-content/uploads/2016/08/The-Economic-Case-for-a-Tidal-Lagoon-Industry-in-the-UK_final.pdf
- Charlier, R. (2007). Forty candles for the Rance River TPP tides provide renewable and sustainable power generation. *Renewable and Sustainable Energy Reviews*, 11(9), 2032-2057. doi:10.1016/j.rser.2006.03.015
- Charlier, R. H. (2003). Sustainable co-generation from the tides. *Renewable and Sustainable Energy Reviews*, 7(3), 187-213. doi:10.1016/s1364-0321(02)00011-4
- Clarke, J. A., Connor, G., Grant, A.D., Johnstone, C.M., (2006). Regulating the output characteristics of tidal current power stations to facilitate better base load matching over the lunar cycle. *Renewable Energy*, 31, 173-180. doi:10.1016/j.renene.2005.08.024
- Climate Change Committee. (2021a). *Progress in adapting to climate change. 2021 Report to Parliament*. Retrieved from <https://www.theccc.org.uk/publication/2021-progress-report-to-parliament/>
- Climate Change Committee. (2021b). *Progress in reducing emissions. 2021 Report to Parliament*.
- Copping, A., Battey, H., Brown-Saracino, J., Massaua, M., and Smith, C. (2014). An international assessment of the environmental effects of

10. References

- marine energy development. *Ocean & Coastal Management*, 99, 3-13. doi:10.1016/j.ocecoaman.2014.04.002
- Copping, A., Grear, M., Jepsen, R., Chartrand, C., and Gorton, A. (2017). Understanding the potential risk to marine mammals from collision with tidal turbines. *International Journal of Marine Energy*, 19, 110-123. doi:10.1016/j.ijome.2017.07.004
- Copping, A., Sather, N., Hanna, L., Whiting, J., Zydlewski, G., Staines, G., . . . Masden, E. (2016). *Annex IV State of the Science Report: Environmental Effects of Marine Renewable Energy Development Around the World*. Retrieved from <https://tethys.pnnl.gov/publications/state-of-the-science-2016>
- Cornett, A., Cousineau, J., and Nistor, I. (2013). Assessment of hydrodynamic impacts from tidal power lagoons in the Bay of Fundy. *International Journal of Marine Energy*, 1, 33-54. doi:10.1016/j.ijome.2013.05.006
- Čož, N., Ahmadian, R., and Falconer, R. A. (2019). Implementation of a Full Momentum Conservative Approach in Modelling Flow Through Tidal Structures. *Water*, 11(9). doi:10.3390/w11091917
- Dai, P., Zhang, J.-s., Zheng, J.-h., Hulsbergen, K., van Banning, G., Adema, J., and Tang, Z.-x. (2018). Numerical study of hydrodynamic mechanism of dynamic tidal power. *Water Science and Engineering*. doi:10.1016/j.wse.2018.09.004
- Dai, P., Zhang, J., and Zheng, J. (2017). Tidal current and tidal energy changes imposed by a dynamic tidal power system in the Taiwan Strait, China. *Journal of Ocean University of China*, 16(6), 953-964. doi:10.1007/s11802-017-3237-4
- Deltares. (2018). *Delft3D - Flow User Manual*. Delft, The Netherlands: Deltares.
- Deltares. (2022). Delft3D 4 - Open Source Community. Retrieved from <https://oss.deltares.nl/web/delft3d>
- Denny, E. (2009). The Economics of Tidal Power. *Energy Policy*, 37(5), 1914-1924. doi:10.1016/j.enpol.2009.01.009
- Department for Business Energy and Industrial Strategy. (2018). *TLP Tidal Lagoon Programme: Summary value for money assessment*.
- Department for Business Energy and Industrial Strategy. (2021). *Energy Trends: UK, July to September 2021*. Retrieved from <https://www.gov.uk/government/statistics/energy-trends-september-2021>
- Department for Business Energy and Industrial Strategy. (2022). *Climate Change Agreement: proposals for a future scheme*. Retrieved from <https://www.gov.uk/government/consultations/climate-change-agreements-ccas-proposals-for-a-future-scheme>
- Department for Trade and Industry. (2003). *Our energy future - creating a low carbon economy*. HMSO
- Department of Energy and Climate Change. (2011). *UK Renewable Energy Roadmap*.
- Draper, S., and Nishino, T. (2014). Centred and staggered arrangements of tidal turbines – ERRATUM. *Journal of Fluid Mechanics*, 743, 636. doi:10.1017/jfm.2014.53

10. References

- Draycott, S., Steynor, J., Nambiar, A., Sellar, B., and Venugopal, V. (2019). Experimental assessment of tidal turbine loading from irregular waves over a tidal cycle. *Journal of Ocean Engineering and Marine Energy*, 5(2), 173-187. doi:10.1007/s40722-019-00136-9
- DTOceanPlus. (2018). Marine Renewable Energy [Press release]
- Elliott, K., Smith, H. C. M., Moore, F., van der Weijde, A. H., and Lazakis, I. (2019). A systematic review of transferable solution options for the environmental impacts of tidal lagoons. *Marine Policy*, 99, 190-200. doi:10.1016/j.marpol.2018.10.021
- Energy and Climate Change Committee. (2012). *The Future of Marine Renewables in the UK*.
- Etemadi, A., Emami, Y., AsefAfshar, O., and Emdadi, A. (2011). Electricity Generation by the Tidal Barrages. *Energy Procedia*, 12, 928-935. doi:10.1016/j.egypro.2011.10.122
- European Commission. (1996). *Non-nuclear energy - Joule II: The exploitation of tidal marine currents*. Brussels: European Commission
- Falconer, R. A. (1974). *Tidal Circulation Effects in Rectangular Harbours*. (MSc MSc Thesis), Washington,
- Falconer, R. A., Angeloudis, A., and Ahmadian, R. (2017). Modelling Hydroenvironmental Impacts of Tidal Range Renewable Energy Projects in Coastal Waters. In *Handbook of Coastal Engineering* (2nd ed., pp. 1552-1574).
- Falconer, R. A., Guo, B., and Ahmadian, R. (2020). Coastal reservoirs and their potential for urban regeneration and renewable energy supply. In *Sustainable Water Resource Development Using Coastal Reservoirs* (pp. 143-172).
- Falconer, R. A., and Kolahdoozan, M. (2003). Three-Dimensional Geo-Morphological Modelling of Estuarine Waters. *International Journal of Sediment Research*, 18(1), 16.
- Fallon, D., Hartnett, M., Olbert, A., and Nash, S. (2014). The effects of array configuration on the hydro-environmental impacts of tidal turbines. *Renewable Energy*, 64, 10-25. doi:10.1016/j.renene.2013.10.035
- Federov, M. P., Shillin, M.B. (2010). Ecological Safety of Tidal-Power Projects. *Power Technology and Engineering*, 44(2), 5.
- Frau, J. P. (1993). Tidal Energy: Promising Projects. La Rance, a successful industrial-scale experiment. *IEEE Transactions on Energy Conversion*, 8(3), 7.
- Funke, S. W., Farrell, P. E., and Piggott, M. D. (2014). Tidal turbine array optimisation using the adjoint approach. *Renewable Energy*, 63, 658-673. doi:10.1016/j.renene.2013.09.031
- Gallego, A., Side, J., Baston, S., Waldman, S., Bell, M., James, M., . . . Burrows, M. (2017). Large scale three-dimensional modelling for wave and tidal energy resource and environmental impact: Methodologies for quantifying acceptable thresholds for sustainable exploitation. *Ocean & Coastal Management*, 147, 67-77. doi:10.1016/j.ocecoaman.2016.11.025
- Gao, C., and Adcock, T. (2017). On the Tidal Resonance of the Bristol Channel. *International Journal of Offshore and Polar Engineering*, 27(2), 177-183. doi:10.17736/ijope.2017.as19

10. References

- Garcia-Oliva, M., Hooper, T., Djordjević, S., and Belmont, M. (2017). Exploring the implications of tidal farms deployment for wetland-birds habitats in a highly protected estuary. *Marine Policy*, 81, 359-367. doi:10.1016/j.marpol.2017.04.011
- Gibson, A. J. F., Fulton, S. J., and Harpe, D. (2019). *Review of Existing Scientific Literature Pertaining to Fish Mortality and its Population - Level Impacts at the Annapolis Tidal Hydroelectric Generating Station, Annapolis Royal, Nova Scotia*. Retrieved from Canada: https://publications.gc.ca/collections/collection_2019/mpo-dfo/Fs97-6-3305-eng.pdf
- Gill, A. B. (2005). Offshore renewable energy: ecological implications of generating electricity in the coastal zone. *Journal of Applied Ecology*, 42(4), 605-615. doi:10.1111/j.1365-2664.2005.01060.x
- Guo, B., Ahmadian, R., and Falconer, R. A. (2021). Refined hydro-environmental modelling for tidal energy generation: West Somerset Lagoon case study. *Renewable Energy*, 179, 2104-2123. doi:10.1016/j.renene.2021.08.034
- H.R. Wallingford. (2015). *Wave Gauge System: User Manual*. Wallingford, U.K.: H.R. Wallingford.
- Hajikandi, H., Vosoughi, H., and Jamali, S. (2017). Comparing the Scour Upstream of Circular and Square Orifices. *International Journal of Civil Engineering*, 16(9), 1145-1156. doi:10.1007/s40999-017-0269-5
- Hamill, L. (2011). *Understanding Hydraulics*. (3rd ed.). Basingstoke, U.K.: Palgrave Macmillan.
- Harcourt, F., Angeloudis, A., and Piggott, M. D. (2019). Utilising the flexible generation potential of tidal range power plants to optimise economic value. *Applied Energy*, 237, 873-884. doi:10.1016/j.apenergy.2018.12.091
- Harries, D., McHenry, M., Jennings, P., and Thomas, C. (2006). Hydro, tidal and wave energy in Australia. *International Journal of Environmental Studies*, 63(6), 803-814. doi:10.1080/00207230601046943
- Harrison, M. E., Batten, W. M. J., Myers, L. E., and Bahaj, A. S. (2010). Comparison between CFD simulations and experiments for predicting the far wake of horizontal axis tidal turbines. *IET Renewable Power Generation*, 4(6), 613. doi:10.1049/iet-rpg.2009.0193
- Henderson, P. A., and Bird, D. J. (2010). Fish and macro-crustacean communities and their dynamics in the Severn Estuary. *Mar Pollut Bull*, 61(1-3), 100-114. doi:10.1016/j.marpolbul.2009.12.017
- Hendry, C. (2016). *The Role of Tidal Lagoons*. Retrieved from <https://hendryreview.files.wordpress.com/2016/08/hendry-review-final-report-english-version.pdf>
- Hinson, S. (2018). *Tidal Lagoons*. London: House of Commons Library
- HM Government. (2009). *The UK Low Carbon Transition Plan*.
- Hooper, T., and Austen, M. (2013). Tidal barrages in the UK: Ecological and social impacts, potential mitigation, and tools to support barrage planning. *Renewable and Sustainable Energy Reviews*, 23, 289-298. doi:10.1016/j.rser.2013.03.001
- Hough, D., and Delebarre, J. (2016). *Tidal Lagoons and UK Energy Strategy*. London: House of Commons Library

10. References

- Howard, D. C., Aggidis, G., Smith, V., Robinson, D., and Catterson, N. (2007). *Tidal Power from the Solway Firth; barriers, impacts and capacity*. Paper presented at the BHA Annual Conference Proceedings.
- Hunt, R. (2021). Boost for Fleetwood tidal power proposals as campaigners lobby ministers. *Blackpool Gazette*.
- Inger, R., Attrill, M. J., Bearhop, S., Broderick, A. C., Grecian, W. J., Hodgson, D. J., . . . Godley, B. J. (2009). Marine renewable energy: potential benefits to biodiversity? An urgent call for research. *Journal of Applied Ecology*, 46(6), 1145-1153. doi:10.1111/j
- International Renewable Energy Agency. (2014). *Tidal Energy. Technology Brief*. Retrieved from <https://www.irena.org/publications/2014/Jun/Tidal-Energy>
- Jacob, C., Pioch, S., and Thorin, S. (2016). The effectiveness of the mitigation hierarchy in environmental impact studies on marine ecosystems: A case study in France. *Environmental Impact Assessment Review*, 60, 83-98. doi:10.1016/j.eiar.2016.04.001
- Jeffcoate, P., Stansby, P., and Apsley, D. (2013). Flow Due to Multiple Jets Downstream of a Barrage: Experiments, 3D Computational Fluid Dynamics, and Depth-Averaged Modeling. *Journal of Hydraulic Engineering*, 139(7), 754-762. doi:10.1061/(asce)hy.1943-7900.0000729
- Jeffcoate, P., Stansby, P., and Apsley, D. (2017). Flow and Bed-Shear Magnification Downstream of a Barrage with Swirl Generated in Ducts by Stators and Rotors. *Journal of Hydraulic Engineering*, 143(2), 06016023. doi:10.1061/(asce)hy.1943-7900.0001228
- Kadiri, M., Ahmadian, R., Bockelmann-Evans, B., Rauen, W., and Falconer, R. (2012). A review of the potential water quality impacts of tidal renewable energy systems. *Renewable and Sustainable Energy Reviews*, 16(1), 329-341. doi:10.1016/j.rser.2011.07.160
- Kadiri, M., Zhang, H., Angeloudis, A., and Piggott, M. D. (2021). Evaluating the eutrophication risk of an artificial tidal lagoon. *Ocean & Coastal Management*, 203. doi:10.1016/j.ocecoaman.2020.105490
- Langston, W. J., Jonas, P. J., and Millward, G. E. (2010). The Severn Estuary and Bristol Channel: a 25 year critical review. *Mar Pollut Bull*, 61(1-3), 1-4. doi:10.1016/j.marpolbul.2009.12.009
- Lesser, G. R., Roelvink, J. A., van Kester, J. A. T. M., and Stelling, G. S. (2004). Development and validation of a three-dimensional morphological model. *Coastal Engineering*, 51(8-9), 883-915. doi:10.1016/j.coastaleng.2004.07.014
- Lewis, M., McNaughton, J., Márquez-Dominguez, C., Todeschini, G., Togneri, M., Masters, I., . . . Robins, P. (2019). Power variability of tidal-stream energy and implications for electricity supply. *Energy*, 183, 1061-1074. doi:10.1016/j.energy.2019.06.181
- Lian, Q., and Liu, Z. (2015). Turbulence and mixing in a freshwater-influenced tidal bay: Observations and numerical modeling. *Science China Earth Sciences*, 58(11), 2049-2058. doi:10.1007/s11430-015-5093-7
- Ma, Q., and Adcock, T. A. A. (2020). Modification of tidal resonance in the Severn Estuary by a barrage and lagoon. *Journal of Ocean*

10. References

- Engineering and Marine Energy*, 6(2), 171-181. doi:10.1007/s40722-020-00166-8
- Ma, Q., Moreira, T. M., and Adcock, T. A. A. (2019). The impact of a tidal barrage on coastal flooding due to storm surge in the Severn Estuary. *Journal of Ocean Engineering and Marine Energy*, 5(3), 217-226. doi:10.1007/s40722-019-00143-w
- Mackay, D. (2009). *Sustainable Energy - without the hot air*. UIT Cambridge Ltd.
- Mackie, L., Coles, D., Piggott, M., and Angeloudis, A. (2020). The Potential for Tidal Range Energy Systems to Provide Continuous Power: A UK Case Study. *Journal of Marine Science and Engineering*, 8(10). doi:10.3390/jmse8100780
- Mackie, L., Harcourt, F., Angeloudis, A., and Piggot, M. (2019). *Income optimisation of a fleet of tidal lagoons*. Paper presented at the 13th EWTEC 2019, Naples, Italy.
- Mackie, L., Kramer, S. C., Piggott, M. D., and Angeloudis, A. (2021). Assessing impacts of tidal power lagoons of a consistent design. *Ocean Engineering*, 240. doi:10.1016/j.oceaneng.2021.109879
- Mackinnon, K., Smith, H. C. M., Moore, F., van der Weijde, A. H., and Lazakis, I. (2018). Environmental interactions of tidal lagoons: A comparison of industry perspectives. *Renewable Energy*, 119, 309-319. doi:10.1016/j.renene.2017.11.066
- Maganga, F., Germain, G., King, J., Pinon, G., and Rivoalen, E. (2010). Experimental characterisation of flow effects on marine current turbine behaviour and on its wake properties. *IET Renewable Power Generation*, 4(6), 498-510. doi:10.1049/iet-rpg.2009.0205
- Mardani, N., Suara, K., Fairweather, H., Brown, R., McCallum, A., and Sidle, R. C. (2020). Improving the Accuracy of Hydrodynamic Model Predictions Using Lagrangian Calibration. *Water*, 12(2). doi:10.3390/w12020575
- Marine Energy Group. (2012). *Marine Energy Action Plan*. Retrieved from Maulik, R., and San, O. (2016). Dynamic modeling of the horizontal eddy viscosity coefficient for quasigeostrophic ocean circulation problems. *Journal of Ocean Engineering and Science*, 1(4), 300-324. doi:10.1016/j.joes.2016.08.002
- McLelland, S. J., and Nicholas, A. P. (2000). A New Method for Evaluating Errors in High Frequency ADV Measurements. *Hydrological Processes*, 14, 351-366.
- Mejia-Olivares, C. J., Haigh, I. D., Angeloudis, A., Lewis, M. J., and Neill, S. P. (2020). Tidal range energy resource assessment of the Gulf of California, Mexico. *Renewable Energy*, 155, 469-483. doi:10.1016/j.renene.2020.03.086
- Melikoglu, M. (2018). Current status and future of ocean energy sources: A global review. *Ocean Engineering*, 148, 563-573. doi:10.1016/j.oceaneng.2017.11.045
- Michelet, N., Guillou, N., Chapalain, G., Thiébot, J., Guillou, S., Goward Brown, A. J., and Neill, S. P. (2020). Three-dimensional modelling of turbine wake interactions at a tidal stream energy site. *Applied Ocean Research*, 95. doi:10.1016/j.apor.2019.102009

10. References

- Moeini, M., Khorsandi, B., and Mydlarski, L. (2020). Effect of Acoustic Doppler Velocimetry Sampling Frequency on Statistical Measurements of Turbulent Axisymmetric Jets. *Journal of Hydraulic Engineering*, 146(7). doi:10.1061/(asce)hy.1943-7900.0001767
- Mohammadian, A., Morse, B., and Robert, J.-L. (2019). Assessment of tidal stream energy resources in a hypertidal estuary with highly irregular bathymetry using 3D numerical modelling. *Journal of Ocean Engineering and Marine Energy*. doi:10.1007/s40722-019-00138-7
- Moreira, T. M., de Faria, J. G., Vaz-de-Melo, P. O. S., Chaimowicz, L., and Medeiros-Ribeiro, G. (2022). Prediction-free, real-time flexible control of tidal lagoons through Proximal Policy Optimisation: A case study for the Swansea Lagoon. *Ocean Engineering*, 247. doi:10.1016/j.oceaneng.2022.110657
- Müller, S., Muhawenimana, V., Wilson, C. A. M. E., and Ouro, P. (2021). Experimental investigation of the wake characteristics behind twin vertical axis turbines. *Energy Conversion and Management*, 247. doi:10.1016/j.enconman.2021.114768
- Mycek, P., Gaurier, B. t., Germain, G., Pinon, G., and Rivoalen, E. (2013). Numerical and experimental study of the interaction between two marine current turbines. *International Journal of Marine Energy*, 1, 70-83. doi:10.1016/j.ijome.2013.05.007
- Myers, L. E., Keogh, B., and Bahaj, A. S. (2011). Experimental investigation of inter-array wake properties in early tidal turbine arrays. *Oceans*, 2011.
- Nash, S., and Phoenix, A. (2017). A review of the current understanding of the hydro-environmental impacts of energy removal by tidal turbines. *Renewable and Sustainable Energy Reviews*, 80, 648-662. doi:10.1016/j.rser.2017.05.289
- Natural Energy Wyre. (2016). Investor Accelerates Wyre Project. Retrieved from <http://www.naturalenergywyre.org/>
- Neary, V. S., Gunawan, B., Hill, C., and Chamorro, L. P. (2013). Near and far field flow disturbances induced by model hydrokinetic turbine: ADV and ADP comparison. *Renewable Energy*, 60, 1-6. doi:10.1016/j.renene.2013.03.030
- Neill, S. P., Angeloudis, A., Robins, P. E., Walkington, I., Ward, S. L., Masters, I., . . . Falconer, R. (2018). Tidal range energy resource and optimization – Past perspectives and future challenges. *Renewable Energy*, 127, 763-778. doi:10.1016/j.renene.2018.05.007
- Neill, S. P., Haas, K. A., Thiébot, J., and Yang, Z. (2021). A review of tidal energy—Resource, feedbacks, and environmental interactions. *Journal of Renewable and Sustainable Energy*, 13(6). doi:10.1063/5.0069452
- Nguyen, N.-T., Nakajo, S., Mukunoki, T., and Tsujimoto, G. (2018). Estuarine Circulation Patterns in a Complex Geometry Estuary: Dinh An Estuary, Mekong River. *Environmental Processes*, 5(3), 503-517. doi:10.1007/s40710-018-0308-5
- Nishino, T., and Willden, R. H. J. (2012). The efficiency of an array of tidal turbines partially blocking a wide channel. *Journal of Fluid Mechanics*, 708, 596-606. doi:10.1017/jfm.2012.349

10. References

- Nortek. (2018). *The Comprehensive Manual for Velocimeters*. Norway: Nortek.
- Northern Tidal Power Gateway. (2019). Business Forum outlines next steps for tidal power gateway and highway. Retrieved from <https://northerntidalpowergateways.co.uk/category/news/>
- Nuernberg, M., and Tao, L. (2018). Three dimensional tidal turbine array simulations using OpenFOAM with dynamic mesh. *Ocean Engineering*, 147, 629-646. doi:10.1016/j.oceaneng.2017.10.053
- O'Rourke, F., Boyle, F., and Reynolds, A. (2010). Tidal energy update 2009. *Applied Energy*, 87(2), 398-409. doi:10.1016/j.apenergy.2009.08.014
- Omega Engineering. (2019). How Does A Pressure Transducers Work. Retrieved from <https://www.omega.com/en-us/resources/pressure-transducers-how-it-works#:~:text=A%20pressure%20transducer%20measures%20pressure,the%20force%20acting%20on%20them>.
- Pappas, K., Angeloudis, A., Mackie, L., and Zilakos, I. (2022). *Selecting representative tide conditions for tidal range and energy assessments*. Paper presented at the Trends in Renewable Energies Offshore.
- Parliamentary Office of Science and Technology. (2020). *Marine Renewables*. Retrieved from <https://post.parliament.uk/research-briefings/post-pn-0625/>
- Parsapour-Moghaddam, P., and Rennie, C. D. (2018). Calibration of a 3D Hydrodynamic Meandering River Model Using Fully Spatially Distributed 3D ADCP Velocity Data. *Journal of Hydraulic Engineering*, 144(4). doi:10.1061/(asce)hy.1943-7900.0001424
- Pennock, S., Coles, D., Angeloudis, A., Bhattacharya, S., and Jeffrey, H. (2022). Temporal complementarity of marine renewables with wind and solar generation: Implications for GB system benefits. *Applied Energy*, 319. doi:10.1016/j.apenergy.2022.119276
- Petley, S., and Aggidis, G. (2016). Swansea Bay tidal lagoon annual energy estimation. *Ocean Engineering*, 111, 348-357. doi:10.1016/j.oceaneng.2015.11.022
- Petley, S., Starr, D., Parish, L., Underwood, Z., and Aggidis, G. A. (2019). Opportunities for tidal range projects beyond energy generation: Using Mersey barrage as a case study. *Frontiers of Architectural Research*. doi:10.1016/j.foar.2019.08.002
- Prandle, D. (1984). Simple theory for designing tidal power schemes. *Advanced Water Resources*, 7, 7.
- Qian, Y., and Jin, J. (2018). *Recommending the most ecological sustainable option for the generation of tidal power in the Severn Estuary*. Paper presented at the International Conference on Civil and Hydraulic Engineering.
- Ramos, V., Giannini, G., Calheiros-Cabral, T., Rosa-Santos, P., and Taveira-Pinto, F. (2021). Legal framework of marine renewable energy: A review for the Atlantic region of Europe. *Renewable and Sustainable Energy Reviews*, 137. doi:10.1016/j.rser.2020.110608
- Rampazzo, M., Tognin, D., Pagan, M., Carniello, L., and Beghi, A. (2019). Modelling, simulation and real-time control of a laboratory tide generation system. *Control Engineering Practice*, 83, 165-175. doi:10.1016/j.conengprac.2018.10.016

10. References

- Renewable UK. (2016). *Ocean Energy Race: The UK's inside track*. Retrieved from <https://www.renewableuk.com/news/332280/Ocean-Energy-Race---The-UKs-Inside-Track.htm>
- Retiere, C. (1994). Tidal power and the aquatic environment of La Rance. *Biological Journal of the Linnean Society*, 51(1), 11.
- Roberts, A., Thomas, B., Sewell, P., Khan, Z., Balmain, S., and Gillman, J. (2016). Current tidal power technologies and their suitability for applications in coastal and marine areas. *Journal of Ocean Engineering and Marine Energy*, 2(2), 227-245. doi:10.1007/s40722-016-0044-8
- Roche, R. C., Walker-Springett, K., Robins, P. E., Jones, J., Veneruso, G., Whitton, T. A., . . . King, J. W. (2016). Research priorities for assessing potential impacts of emerging marine renewable energy technologies: Insights from developments in Wales (UK). *Renewable Energy*, 99, 1327-1341. doi:10.1016/j.renene.2016.08.035
- Rodrigues, N., Pintassilgo, P., Calhau, F., González-Gorbeña, E., and Pacheco, A. (2021). Cost-benefit analysis of tidal energy production in a coastal lagoon: The case of Ria Formosa – Portugal. *Energy*, 229. doi:10.1016/j.energy.2021.120812
- Ross, L., Sottolichio, A., Huybrechts, N., and Brunet, P. (2021). Tidal turbines in the estuarine environment: From identifying optimal location to environmental impact. *Renewable Energy*, 169, 700-713. doi:10.1016/j.renene.2021.01.039
- Rtimi, R., Sottolichio, A., and Tassi, P. (2021). Hydrodynamics of a hyper-tidal estuary influenced by the world's second largest tidal power station (Rance estuary, France). *Estuarine, Coastal and Shelf Science*, 250. doi:10.1016/j.ecss.2020.107143
- Saichenthur, N., Murali, K., and Sundar, V. (2022). Influence of horizontal eddy viscosity and bottom friction coefficients on morpho-dynamic evaluations. *Journal of Hydro-environment Research*, 40(1), 13.
- Sandbach, S. D., Nicholas, A. P., Ashworth, P. J., Best, J. L., Keevil, C. E., Parsons, D. R., . . . Simpson, C. J. (2018). Hydrodynamic modelling of tidal-fluvial flows in a large river estuary. *Estuarine, Coastal and Shelf Science*, 212, 176-188. doi:10.1016/j.ecss.2018.06.023
- Sang-Ho, O., Kwang, S. L., and Weon-Mu, J. (2016). Three-dimensional experiment and numerical simulation of the discharge performance of sluice passageway for tidal power plant. *Renewable Energy*, 92, 462-473. doi:10.1016/j.renene.2016.02.023
- Schmitt, P., and Lieber, L. (2021). *Assessment of a Tidal Lagoon Test-Bed using Aerial Drone Photogrammetry*. Paper presented at the EWTEC.
- Schramm, M. P., Bevelhimer, M. S., and DeRolph, C. R. (2016). A synthesis of environmental and recreational mitigation requirements at hydropower projects in the United States. *Environmental Science & Policy*, 61, 87-96. doi:10.1016/j.envsci.2016.03.019
- Sentchev, A., Thiébaud, M., and Guillou, S. (2020). Turbulence characterization at tidal-stream energy site in Alderney Race. In *Developments in Renewable Energies Offshore* (pp. 616-623).
- Shadman, M., Silva, C., Faller, D., Wu, Z., de Freitas Assad, L., Landau, L., . . . Estefen, S. (2019). Ocean Renewable Energy Potential,

10. References

- Technology, and Deployments: A Case Study of Brazil. *Energies*, 12(19). doi:10.3390/en12193658
- Shields, M. A., Dillon, L. J., Woolf, D. K., and Ford, A. T. (2009). Strategic priorities for assessing ecological impacts of marine renewable energy devices in the Pentland Firth (Scotland, UK). *Marine Policy*, 33(4), 635-642. doi:10.1016/j.marpol.2008.12.013
- Shields, M. A., Woolf, D. K., Grist, E. P. M., Kerr, S. A., Jackson, A. C., Harris, R. E., . . . Side, J. (2011). Marine renewable energy: The ecological implications of altering the hydrodynamics of the marine environment. *Ocean & Coastal Management*, 54(1), 2-9. doi:10.1016/j.ocecoaman.2010.10.036
- SIMEC Atlantis Energy. (2017). Wyre Tidal Project. Retrieved from <https://simecatlantis.com/2017/06/19/2477/>
- Simmons, S. M., McLelland, S. J., Parsons, D. R., Jordan, L.-B., Murphy, B. J., and Murdoch, L. (2018). An investigation of the wake recovery of two model horizontal-axis tidal stream turbines measured in a laboratory flume with Particle Image Velocimetry. *Journal of Hydro-environment Research*, 19, 179-188. doi:10.1016/j.jher.2017.03.003
- Soudan, B. (2019). Community-scale baseload generation from marine energy. *Energy*, 189. doi:10.1016/j.energy.2019.116134
- Stallard, T., Collings, R., Feng, T., and Whelan, J. (2013). Interactions between tidal turbine wakes: experimental study of a group of three-bladed rotors. *Philos Trans A Math Phys Eng Sci*, 371(1985), 20120159. doi:10.1098/rsta.2012.0159
- Stansby, P. K. (2006). Limitations of Depth Average Modelling for Shallow Waters. *Journal of Hydraulic Engineering*, 132(7), 4. doi:10.1061/ASCE10733-9429(2006)132:7(737)
- Suárez-López, M. J., Espina-Valdés, R., Fernández Pacheco, V. M., Navarro Manso, A., Blanco-Marigorta, E., and Álvarez-Álvarez, E. (2019). A Review of Software Tools to Study the Energetic Potential of Tidal Currents. *Energies*, 12(9). doi:10.3390/en12091673
- Sucsy, P. V., Pearce, B.R., Panchang, V.G., (1993). Comparison of Two- and Three-Dimensional Model Simulation of the Effect of a Tidal Barrier on the Gulf of Maine Tides. *American Meteorological Society*, 23, 1231-1249.
- Tang, H., Nichols, C. R., Wright, L. D., and Resio, D. (2021). Modeling Multiscale and Multiphysics Coastal Ocean Processes: A Discussion on Necessity, Status, and Advances. *Journal of Marine Science and Engineering*, 9(8). doi:10.3390/jmse9080847
- Thiébot, J., Guillou, N., Guillou, S., Good, A., and Lewis, M. (2020). Wake field study of tidal turbines under realistic flow conditions. *Renewable Energy*, 151, 1196-1208. doi:10.1016/j.renene.2019.11.129
- Tidal Lagoon Swansea Bay. (2014a). *Environmental Statement: Non-Technical Summary. The Proposed Tidal Lagoon Swansea Bay Order*. Retrieved from http://www.tidallagoonpower.com/wp-content/uploads/2018/01/6.1_Environmental-Statement-Non-Tech-Summary.pdf
- Tidal Lagoon Swansea Bay. (2014b). *The Proposed Tidal Lagoon Swansea Bay (Generating Station) Order*. Retrieved from

10. References

- http://www.tidallagoonpower.com/wp-content/uploads/2018/01/6.1_Environmental-Statement-Non-Tech-Summary.pdf
- Tidal Lagoon Swansea Bay. (2020). Tidal Lagoon Swansea Bay Project Update. In.
- Tidal Lagoon Swansea Bay. (2022). *Harnessing the power of our tides*. Retrieved from <http://www.tidallagoonpower.com/>
- Todeschini, G. (2017). Review of Tidal Lagoon Technology and Opportunities for Integration within the UK Energy System. *Inventions*, 2(3). doi:10.3390/inventions2030014
- Todeschini, G., Coles, D., Lewis, M., Popov, I., Angeloudis, A., Fairley, I., . . . Masters, I. (2022). Medium-term variability of the UK's combined tidal energy resource for a net-zero carbon grid. *Energy*, 238. doi:10.1016/j.energy.2021.121990
- Tognin, D., Rampazzo, M., Pagan, M., Carniello, L., and Beghi, A. (2018). Modelling and Simulation of an Artificial Tide Generation System. *IFAC Papers Online*, 51(5), 13-18.
- Torres, C., Borman, D., Sleigh, A., and Neeve, D. (2018). *Investigating Scale Effects of a Hydraulic Physical Model with 3D CFD*. Paper presented at the Smart Dams and Reservoirs.
- Tralli, A., Bihlsma, A.C., te Velde, W., de Haas, P. (2015). CFD Study on Free-Surface Influence on Tidal Turbines in Hydraulic Structures. *Proceedings of the ASME 2015 34th International Conference on Ocean, Offshore and Arctic Engineering*.
- Uihlein, A., and Magagna, D. (2016). Wave and tidal current energy – A review of the current state of research beyond technology. *Renewable and Sustainable Energy Reviews*, 58, 1070-1081. doi:10.1016/j.rser.2015.12.284
- Vennell, R. (2010). Tuning turbines in a tidal channel. *Journal of Fluid Mechanics*, 663, 253-267. doi:10.1017/s0022112010003502
- Verbeek, M. C., Labeur, R. J., and Uijtewaal, W. S. J. (2021). The performance of a weir-mounted tidal turbine: An experimental investigation. *Renewable Energy*, 168, 64-75. doi:10.1016/j.renene.2020.12.013
- Vogel, C. R., Houlsby, G. T., and Willden, R. H. J. (2016). Effect of free surface deformation on the extractable power of a finite width turbine array. *Renewable Energy*, 88, 317-324. doi:10.1016/j.renene.2015.11.050
- Vouriot, C. V. M., Angeloudis, A., Kramer, S. C., and Piggott, M. D. (2018). Fate of large-scale vortices in idealized tidal lagoons. *Environmental Fluid Mechanics*. doi:10.1007/s10652-018-9626-4
- Waldman, S., Weir, S., O'Hara Murray, R. B., Woolf, D. K., and Kerr, S. (2019). Future policy implications of tidal energy array interactions. *Marine Policy*, 108. doi:10.1016/j.marpol.2019.103611
- Wang, Z. J., and Wang, Z. W. (2019). A review on tidal power utilization and operation optimization. *IOP Conference Series: Earth and Environmental Science*, 240. doi:10.1088/1755-1315/240/5/052015
- Waters, S., and Aggidis, G. (2016a). Tidal range technologies and state of the art in review. *Renewable and Sustainable Energy Reviews*, 59, 514-529. doi:10.1016/j.rser.2015.12.347

10. References

- Waters, S., and Aggidis, G. (2016b). A World First: Swansea Bay Tidal lagoon in review. *Renewable and Sustainable Energy Reviews*, 56, 916-921. doi:10.1016/j.rser.2015.12.011
- Waters, S., and Aggidis, G. A. (2015). Over 2000 years in review: Revival of the Archimedes Screw from Pump to Turbine. *Renewable and Sustainable Energy Reviews*, 51, 497-505. doi:10.1016/j.rser.2015.06.028
- Wells, M. G., and van Heijst, G.-J. F. (2003). A model of tidal flushing of an estuary by dipole formation. *Dynamics of Atmospheres and Oceans*, 37(3), 223-244. doi:10.1016/j.dynatmoce.2003.08.002
- Willis, M., Masters, I., Thomas, S., Gallie, R., Loman, J., Cook, A., . . . Mason-Jones, A. (2010). Tidal turbine deployment in the Bristol Channel: a case study. *Proceedings of the Institution of Civil Engineers - Energy*, 163(3), 93-105. doi:10.1680/ener.2010.163.3.93
- Withers, P. (2021). Nova Scotia Power to pull plug on tidal station, seeks \$25M from ratepayers. *CBC News*.
- Wolf, J., Walkington, I.A., Holt, J., Burrows, R. (2009). *Environmental impacts of tidal power schemes*. Paper presented at the Proceedings of ICE Maritime Engineering.
- Wu, Y., Xu, C., Ke, Y., Chen, K., and Xu, H. (2017). Multi-criteria decision-making on assessment of proposed tidal barrage schemes in terms of environmental impacts. *Mar Pollut Bull*, 125(1-2), 271-281. doi:10.1016/j.marpolbul.2017.08.030
- Xia, J., Falconer, R. A., and Lin, B. (2010a). Hydrodynamic impact of a tidal barrage in the Severn Estuary, UK. *Renewable Energy*, 35(7), 1455-1468. doi:10.1016/j.renene.2009.12.009
- Xia, J., Falconer, R. A., and Lin, B. (2010b). Impact of different operating modes for a Severn Barrage on the tidal power and flood inundation in the Severn Estuary, UK. *Applied Energy*, 87(7), 2374-2391. doi:10.1016/j.apenergy.2009.11.024
- Xia, J., Falconer, R. A., Lin, B., and Tan, G. (2011). Estimation of future coastal flood risk in the Severn Estuary due to a barrage. *Journal of Flood Risk Management*, 4(3), 247-259. doi:10.1111/j.1753-318X.2011.01106.x
- Xue, J., Ahmadian, R., and Falconer, R. (2019). Optimising the Operation of Tidal Range Schemes. *Energies*, 12(15). doi:10.3390/en12152870
- Xue, J., Ahmadian, R., and Jones, O. (2020). Genetic Algorithm in Tidal Range Schemes' Optimisation. *Energy*, 200. doi:10.1016/j.energy.2020.117496
- Xue, J., Ahmadian, R., Jones, O., and Falconer, R. A. (2021). Design of tidal range energy generation schemes using a Genetic Algorithm model. *Applied Energy*, 286. doi:10.1016/j.apenergy.2021.116506
- Yates, N., Walkington, I., Burrows, R., and Wolf, J. (2013). Appraising the extractable tidal energy resource of the UK's western coastal waters. *Philos Trans A Math Phys Eng Sci*, 371(1985), 20120181. doi:10.1098/rsta.2012.0181
- Zainol, M. Z., Zainol, I., and Ismail, N. (2017). A Review on the Status of Tidal Energy Technology Worldwide. *Science International (Lahore)*, 29(3), 10.

10. References

- Zanforlin, S. (2018). Advantages of vertical axis tidal turbines set in close proximity: A comparative CFD investigation in the English Channel. *Ocean Engineering*, 156, 358-372.
doi:10.1016/j.oceaneng.2018.03.035
- Zhang, L. X., Tang, S. J., Hao, Y., and Pang, M. Y. (2018). Integrated energy and economic evaluation of a case tidal power plant in China. *Journal of Cleaner Production*, 182, 38-45.
doi:10.1016/j.jclepro.2018.02.011
- Zhao, Y., Li, J., and Wu, B. (2018). An exploitation plan of tidal power in the Severn Estuary. *MATEC Web of Conferences*, 246.
doi:10.1051/mateconf/201824602012
- Zhou, J., Falconer, R. A., and Lin, B. (2014). Refinements to the EFDC model for predicting the hydro-environmental impacts of a barrage across the Severn Estuary. *Renewable Energy*, 62, 490-505.
doi:10.1016/j.renene.2013.08.012

Annex 1

Studies of TST Spacing



Annex 1: Studies of TST Spacing

Ross et al. (2021) carried out a case study of the Gironde estuary in France to determine the effects of TSTs in order to create a method for optimising TST placement based on available energy, site practicalities and environmental impacts. They found that TSTs reduced currents by up to 10% and decreased suspended sediment concentration by up to 15 mg/L, both of which meant increased deposition and changing bed conditions. They found that to reduce these impacts it was best to place turbines mid water column or closer to the surface rather than the bed. However, unlike other reports, this study does not look deeper into the spacing of TSTs which has been proven to increase efficiency and decrease environmental impacts in other ways, choosing instead to use a regular grid of 50 m spacing between turbines and changing only the depth and channel location of the whole array.

In their research into tidal stream turbine spacing, Draper and Nishino (2014) found that staggered configurations performed more efficiently and with a higher power output than centred layouts but that turbines aligned side-by-side in a single row performed better still (Draper and Nishino, 2014). These findings concur with those of Zanforlin (2018) who found that side-by-side configurations performed 2.5 times better than triangular formats due to the wake contraction of side-by-side schemes which increased efficiency but did not occur when the turbines were laid out as a triangle (Zanforlin, 2018). This bodes well for TRSs where turbines are restricted to side-by-side configuration in straight sea walls. Table A1.0.1 presents a timeline of studies carried out into TST spacing as well as the findings of these studies which could have implications for TRSs.

Table A1.0.1 Timeline and outcomes of studies on TST spacing.

Source	Study and Conclusions
(European Commission, 1996)	Recommend lateral spacing of at least one turbine diameter but larger spacing of 2 or 3 diameters is better as it helps with safety and uninterrupted operation and allows easy access for maintenance.
(Harrison et al., 2010)	In studying wind farms, they report that wind turbines must be at least 7D apart because of turbulence effects.
(Myers et al., 2011)	Found that spacing greater than 2.5 turbine diameters increases bypass velocity and available kinetic energy whilst spacing less than 2.5D slows bypass velocity to below free stream levels due to wake merging. This has impacts on the environment, especially flora, fauna, sediment and water quality.
(Ahmadian and Falconer, 2012)	Studied TST array layout in Severn Estuary and found that layout has a significant impact on power output but lesser impact on hydro-environmental factors.
(Nishino and Willden, 2012)	Recommend optimal spacing of: $0.4 < \frac{l}{d} < 4$ Where: L = turbine spacing and D = turbine diameter. This balances the cross-sectional blockage effect with the choking effect to increase global power coefficient. Outside of these limits, the efficiency decreases due to local blockage.
(Stallard et al., 2013)	Commercial scale TST arrays are expected to have lateral spacing of between 1.5 to 5 turbine diameters but are limited by available space. Studied single rows of 2, 3 and 5 scaled TST turbines. Found that if spacing is greater than 3 turbine diameters, wakes behave like isolated turbines, but if spacing is less

Annex 1: Studies of TST Spacing

	than 2 diameters, wakes of adjacent turbines merge to form a single expanded wake.
(Fallon et al., 2014)	Tested lateral spacings of 0.5, 2 and 5 turbine diameters. They determined 5D to be the best spacing and 0.5D to be the worst as the magnitude and extent of environmental impact reduces as the density and capacity of the TST array increased.
(Funke et al., 2014)	Investigated curved rows of TSTs with non-uniform spacing. They found this pattern enhanced energy recovery from natural flows.
(Vogel et al., 2016)	Tested lateral turbine spacings of 1.5 to 9.5 turbine diameters. They found better power extraction when turbines were closely packed to allow flow to divert freely around turbines so thrust velocity is low.
(Nash and Phoenix, 2017)	Recommend lateral spacing of at least 3 turbine diameters and a minimum distance of 10D longitudinal between turbines in a regular grid. They found 20D to be the optimal longitudinal distance to avoid wake merging and reduction in power availability.
(Bonar et al., 2018)	Recommend equal spacing to manage resistance between devices.
(Nuernberg and Tao, 2018)	<p>Tested combinations of lateral spacing (1.5, 2 and 3D) and longitudinal spacing (3 & 5D). They found that:</p> <ul style="list-style-type: none"> • Transverse spacing determines whether adjacent wakes combine within array sections. • Close spacing leads to slow, stagnant wake recovery within an array section and large areas of high velocity deficit, but less pronounced wakes. • Increased spacing shows clear individual wakes and increases wake recovery.

Annex 1: Studies of TST Spacing

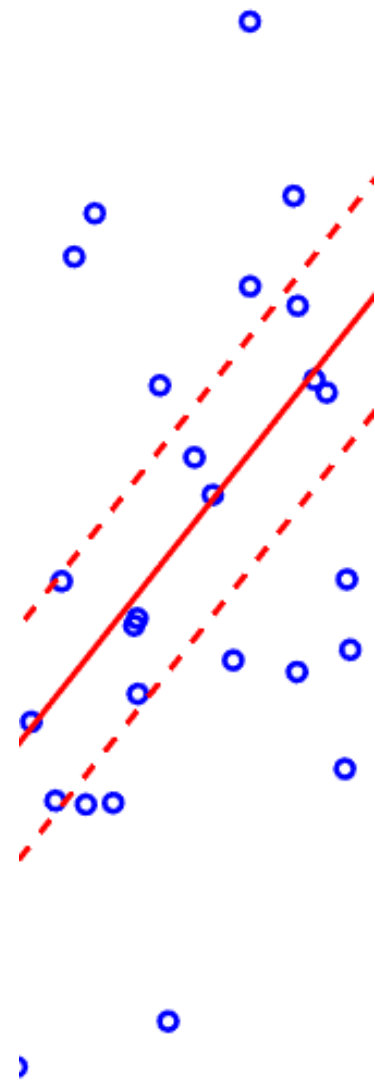
(Michelet et al., 2020)	<p>Following recommendations from previous studies they investigated a staggered configuration with lateral spacing of 5D and longitudinal spacing of 10D. These parameters were purported to resolve velocity and turbulence intensity along device wakes, but they actually found that adapting array layout minimised wake interactions and optimised energy conversion, so lateral spacing should be reduced to 3D.</p>
(Thiébot et al., 2020)	<p>Rather than using idealised bathymetry and inflow conditions, they looked at more realistic conditions in Alderney Race. They tested isolated, aligned and staggered turbine layouts with different spacing to see the effect of arrangement and density on energy production.</p> <p>Found that staggered layout produced 16% more energy than aligned layout and that a minimal lateral spacing of 5D is needed to avoid wake overlapping. In aligned layouts, lateral spacing had little influence on energy production so they can be packed closer together.</p>
(Müller et al., 2021)	<p>Their results showed that wake dynamics were influenced more by turbine rotational direction than lateral spacing and that the greatest lateral wake expansion and reduced velocities happened when turbines rotated in same direction. They recommend twin turbine arrays to have at least 2D spacing between turbines to allow kinetic energy in wake to fully recover 5D downstream.</p>
(Ross et al., 2021)	<p>The aim of this study was to produce a method for choosing optimal location for turbine depth placement rather than spacing. They looked at 10 years of average river discharge data to calculate energy intensity at the water surface, mid depth and near the</p>

Annex 1: Studies of TST Spacing

	bed. They found it best to place turbines mid water column or closer to the surface rather than the bed.
(Verbeek et al., 2021)	Investigated the spacing of TSTs installed between barriers, e.g., storm surge barrier or bridge pillars. They found that the turbine power coefficient could be increased by optimising channel blockage and distance between the turbine and the structure it was attached to. This also influenced wakes, which extended up to 10D downstream where streamwise flow velocities are lower and turbulence intensities are higher than the corresponding ambient flow. Found that overall wake configuration is affected by relative weir area, blockage and turbine position relative to weir.

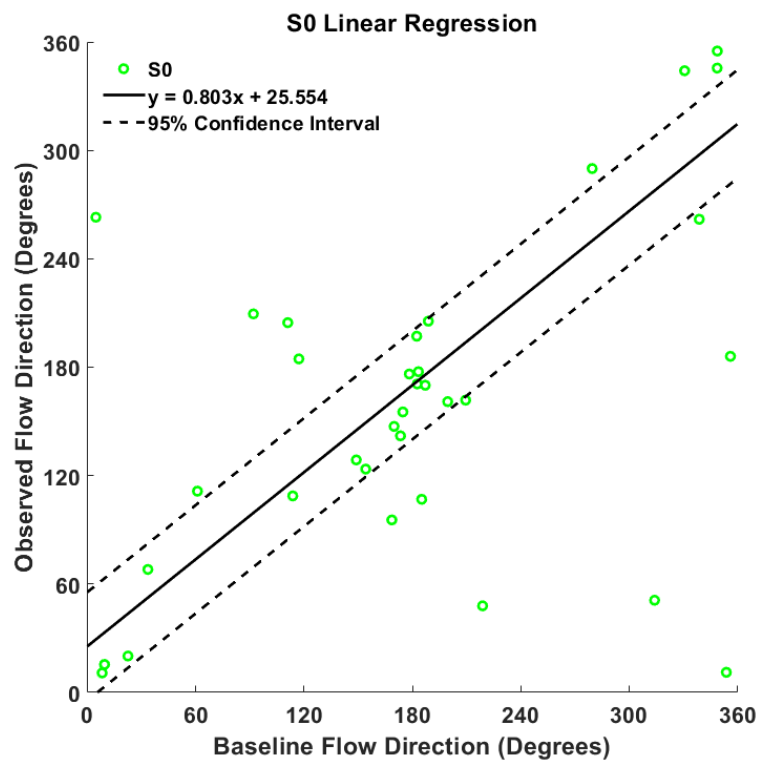
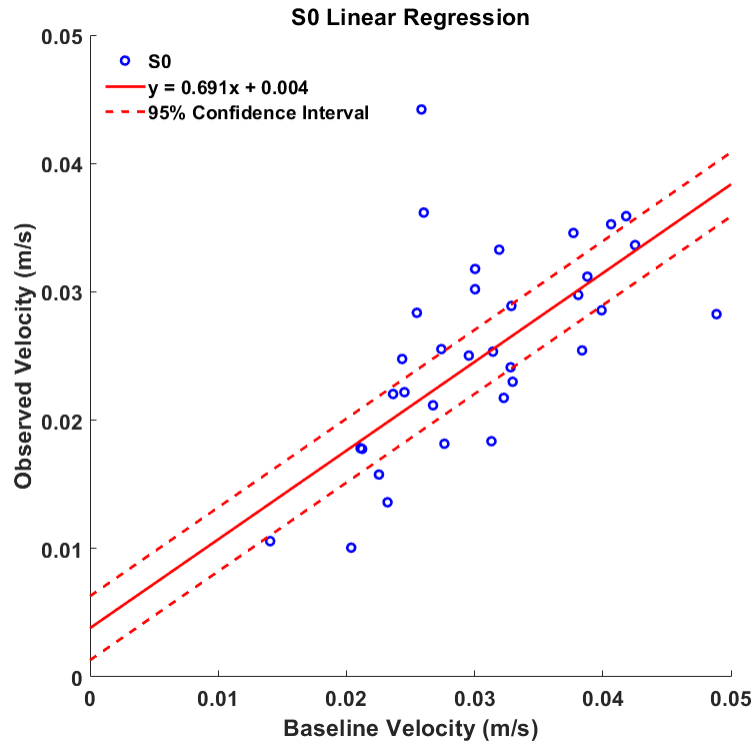
These studies have some contrasting specific results but also some consistent generic themes. Dense spacing is needed to optimise channel blockage to increase energy generation efficiency, however if turbines are spaced too closely their wakes merge which has a larger environmental impact and also makes them harder to maintain. A minimum spacing of 2.5 turbine diameters is recommended with an ideal of 5 diameters, space allowing. Staggered and curved grids bear further investigation for maximising power output.

Annex 2
Regression Analysis of
Experiment Results
Compared to
Pre-lagoon Conditions

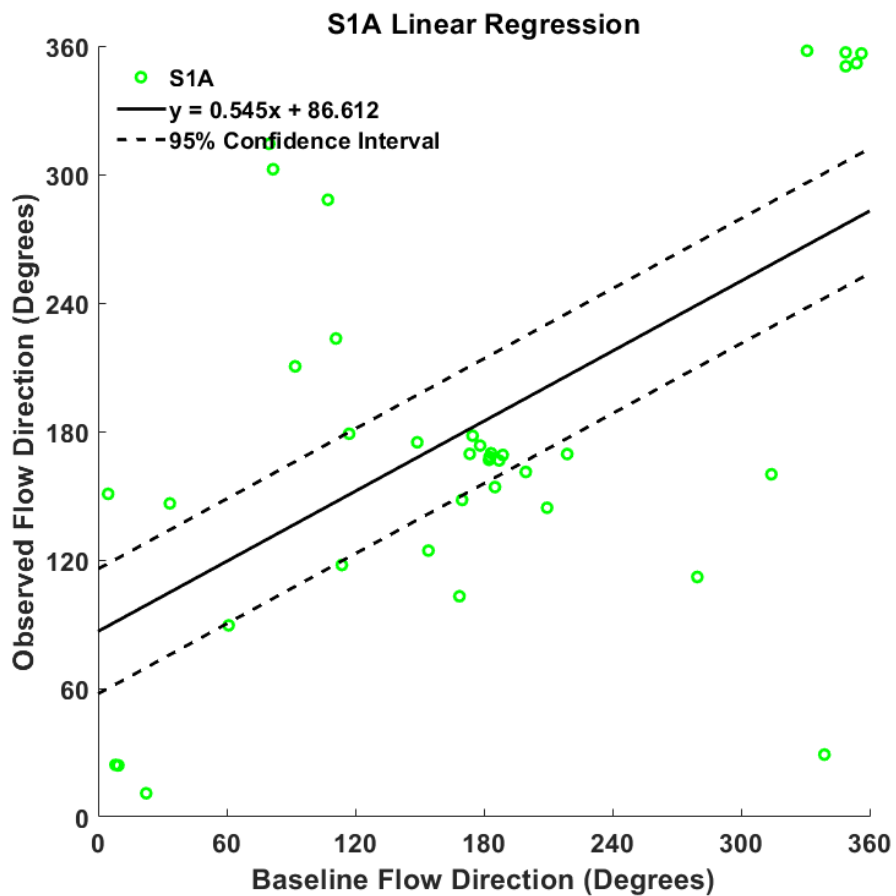
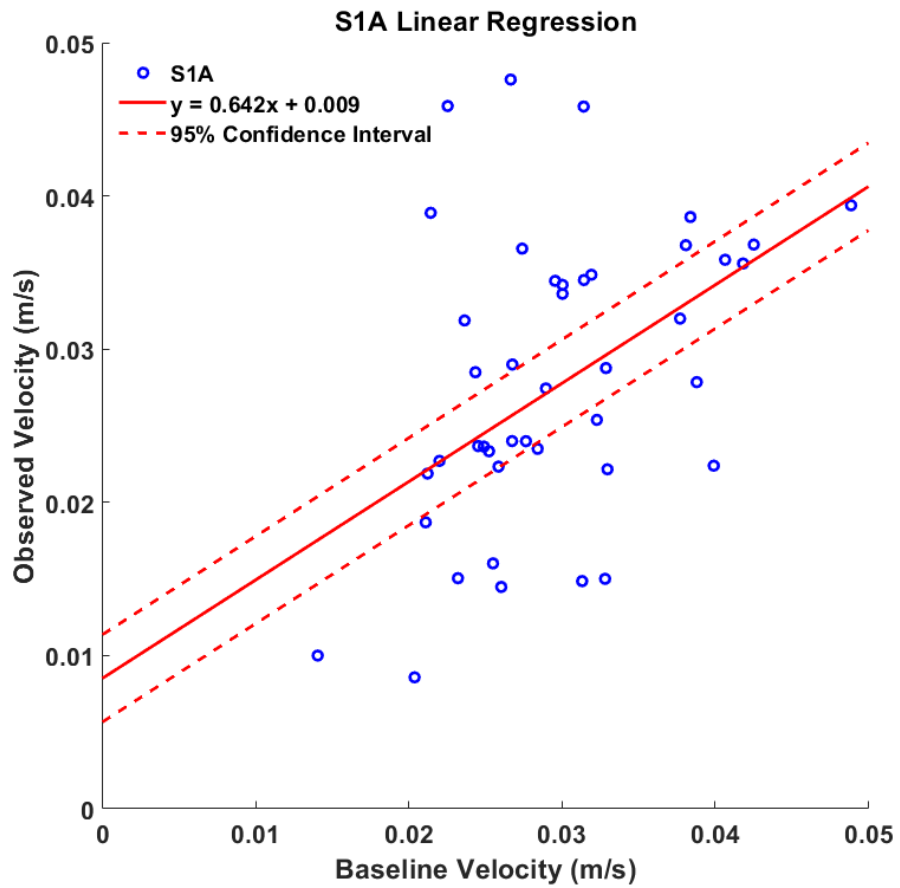


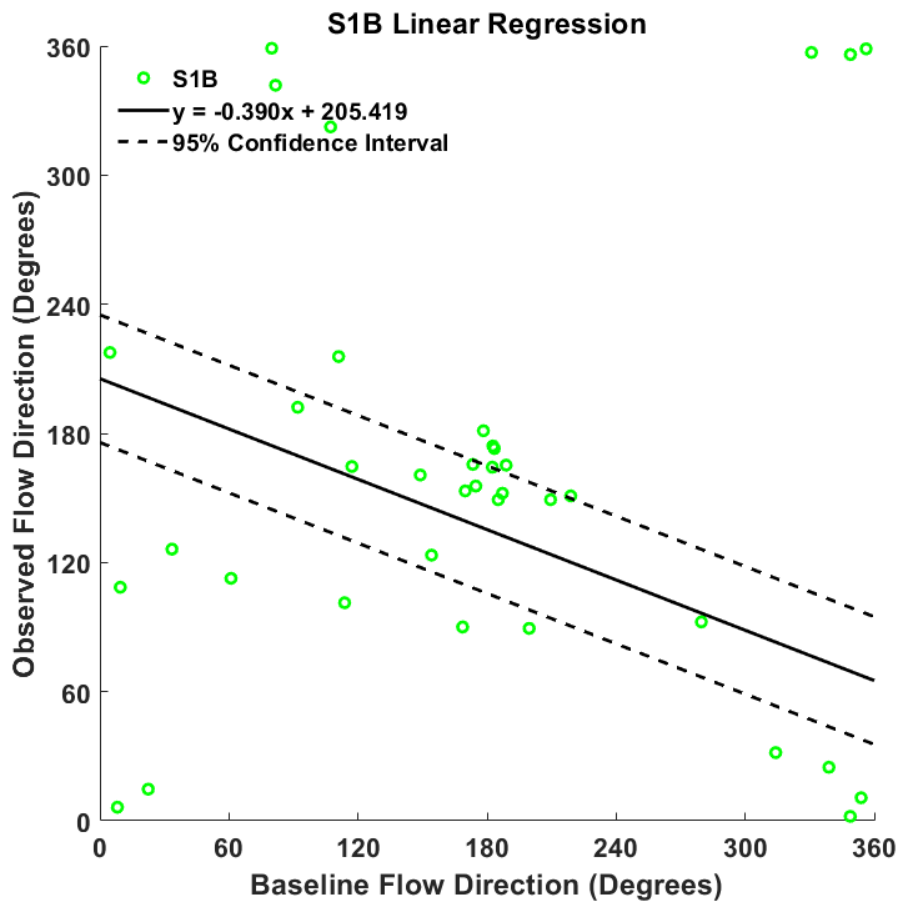
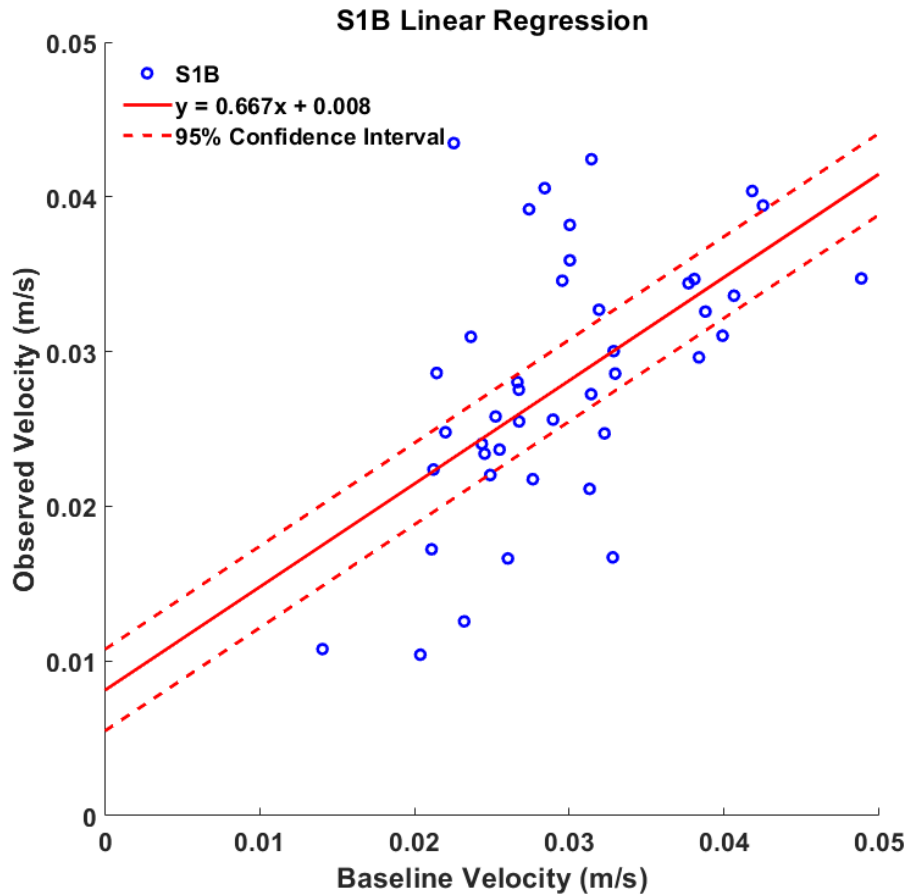
0.03
Velocity (m/s)

Annex 2: Regression analysis of experiment results for flow velocity magnitude and direction compared to pre-lagoon tank conditions.

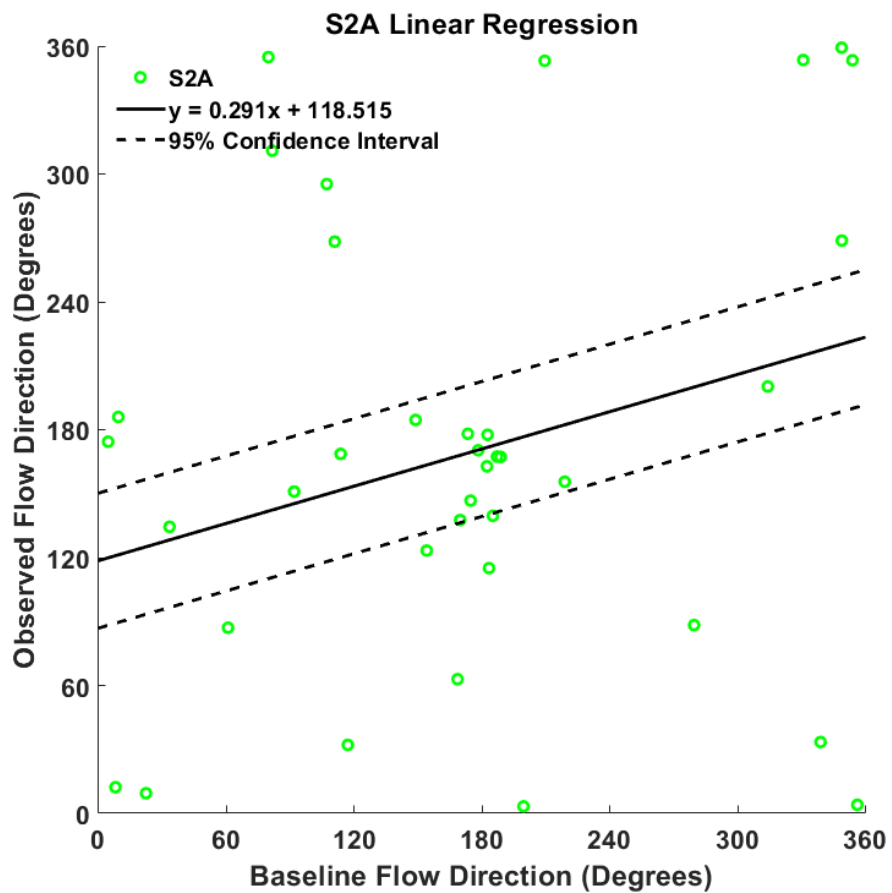
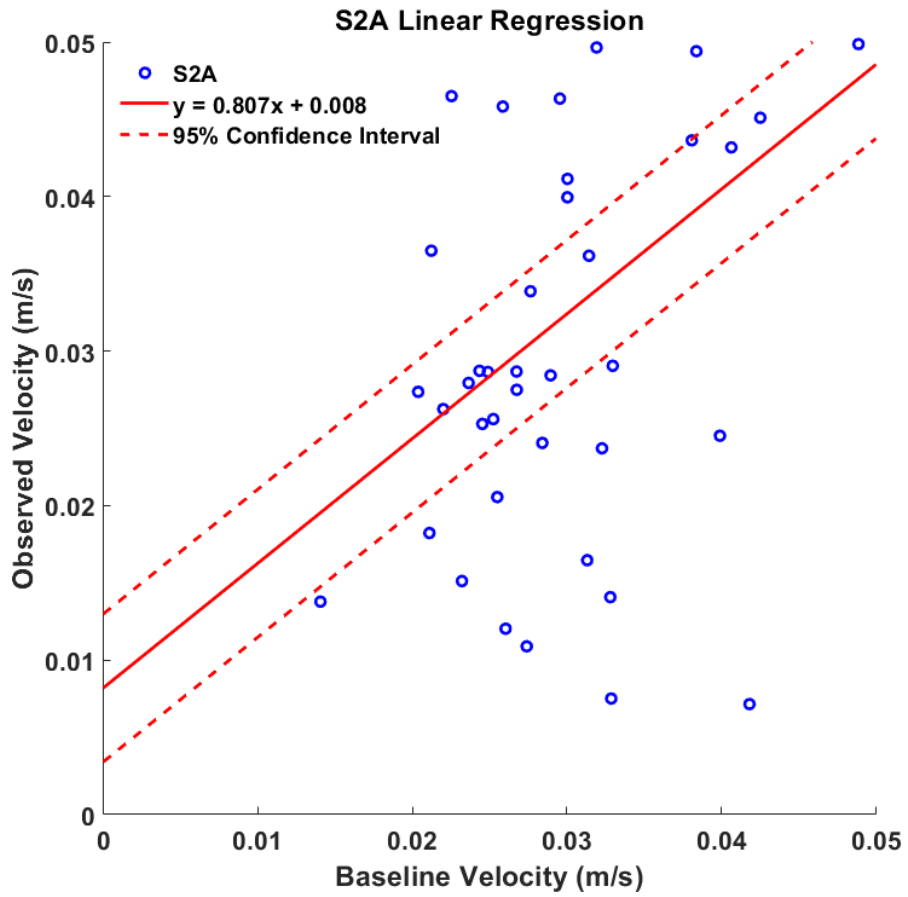


Annex 2: Regression Analysis of Experiment Results Compared to Pre-lagoon Conditions.

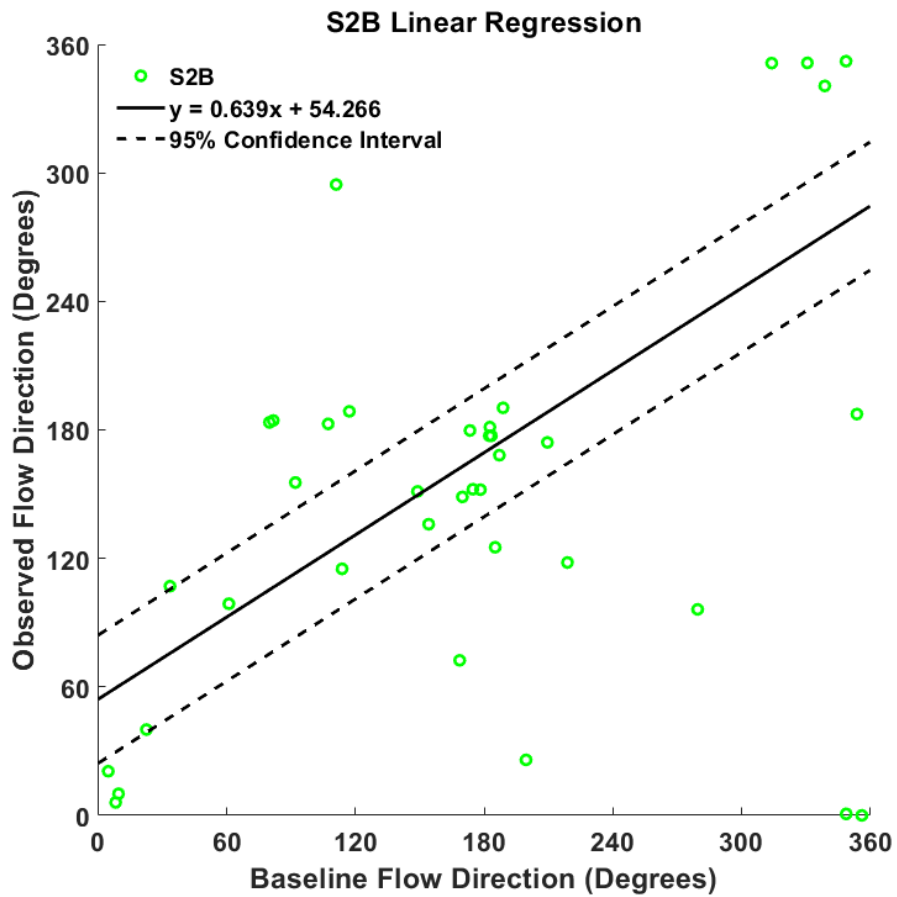
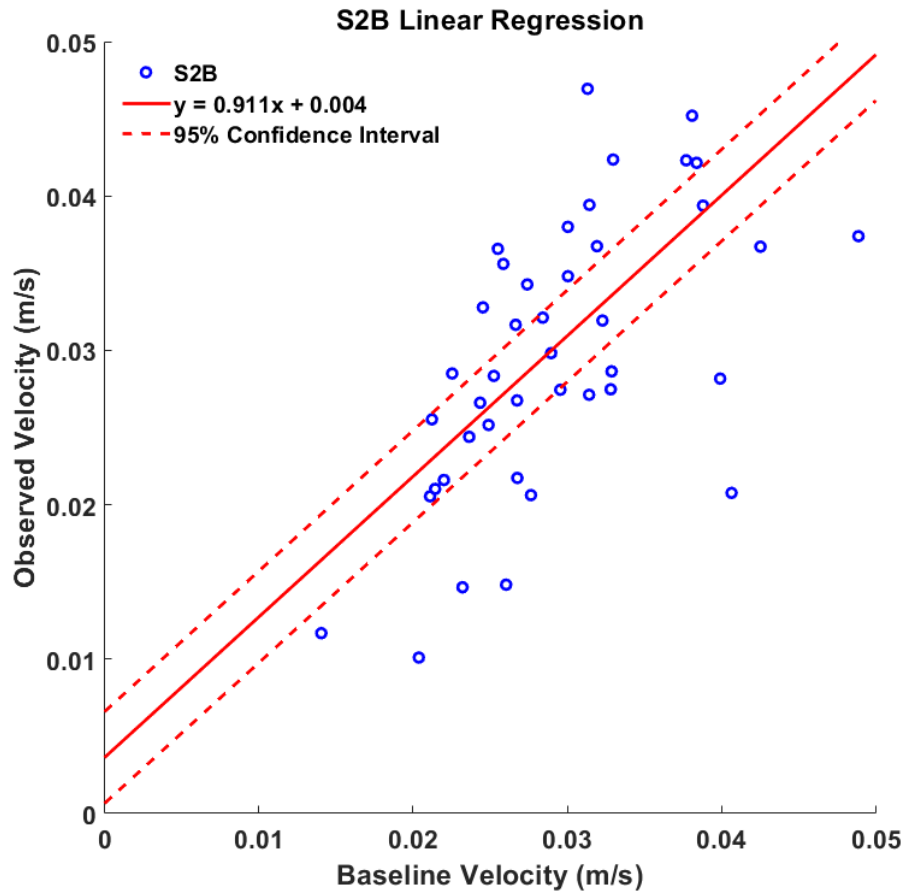




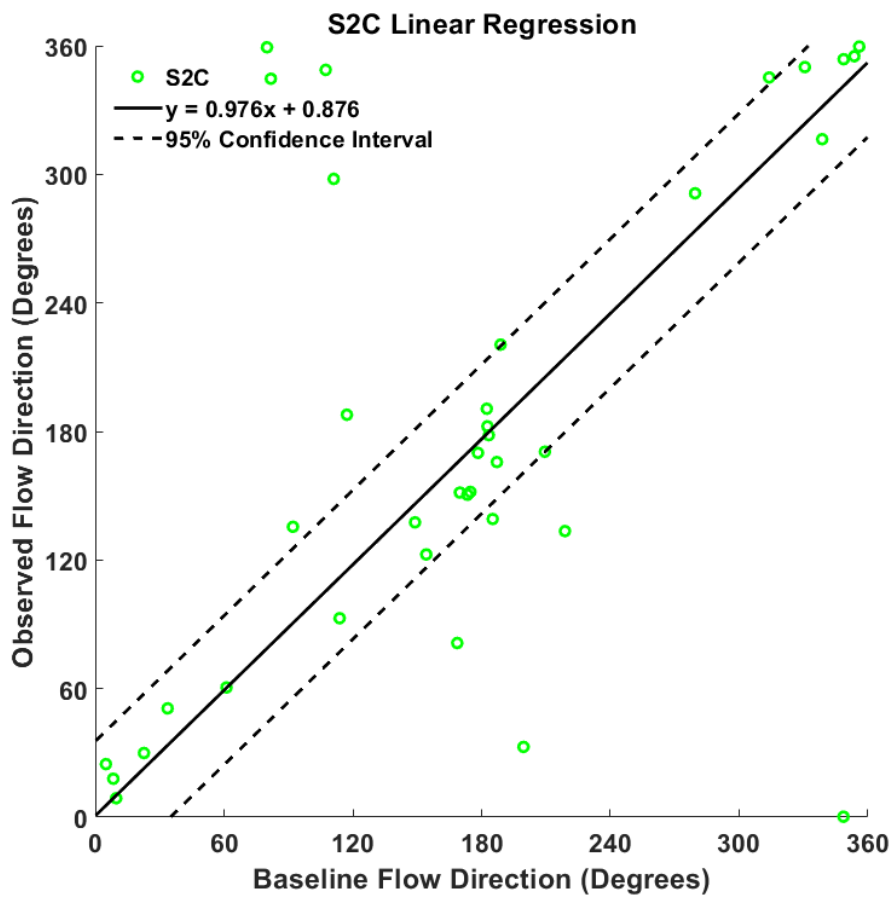
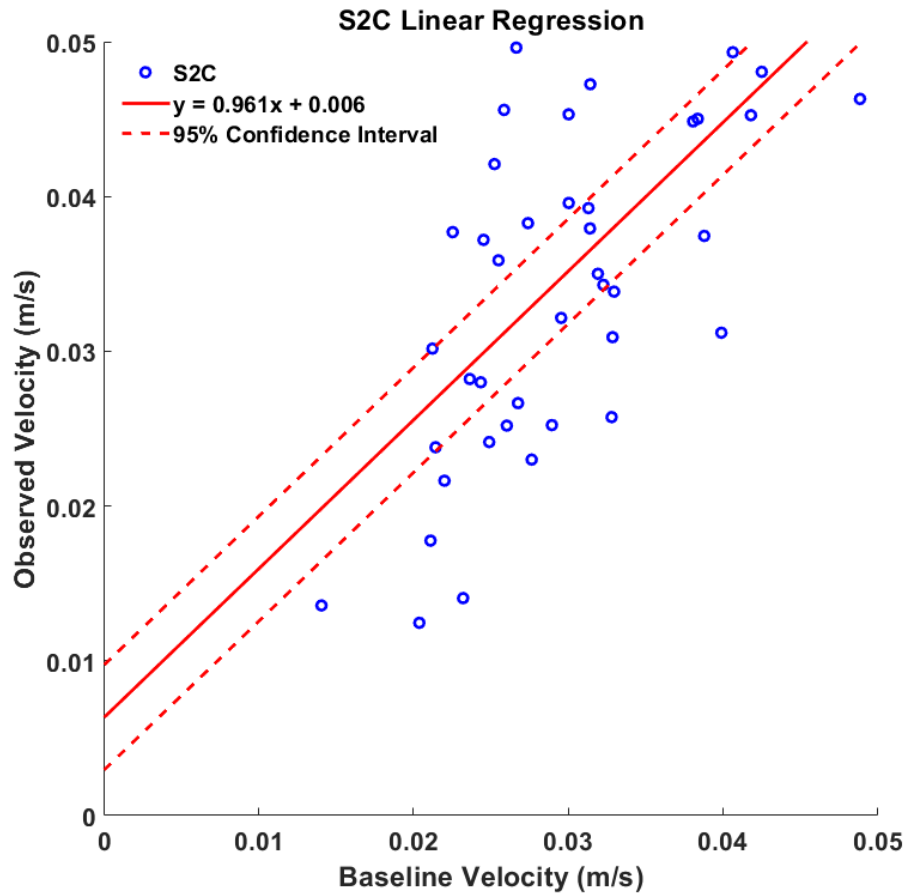
Annex 2: Regression Analysis of Experiment Results Compared to Pre-lagoon Conditions.



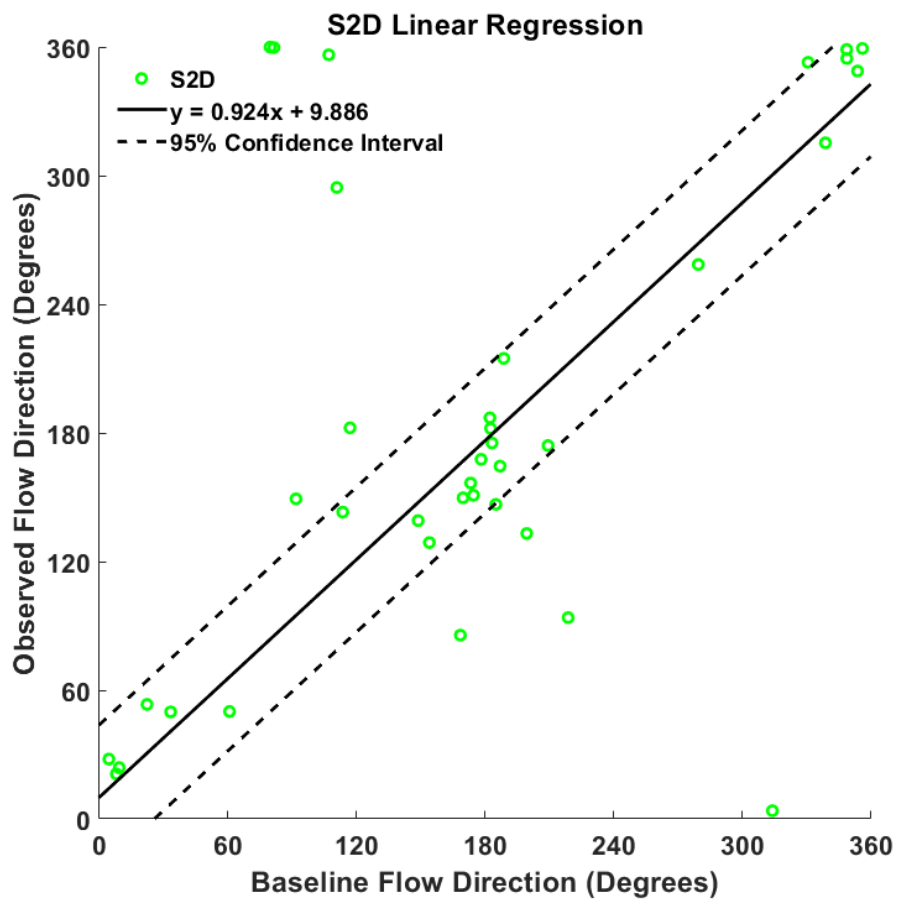
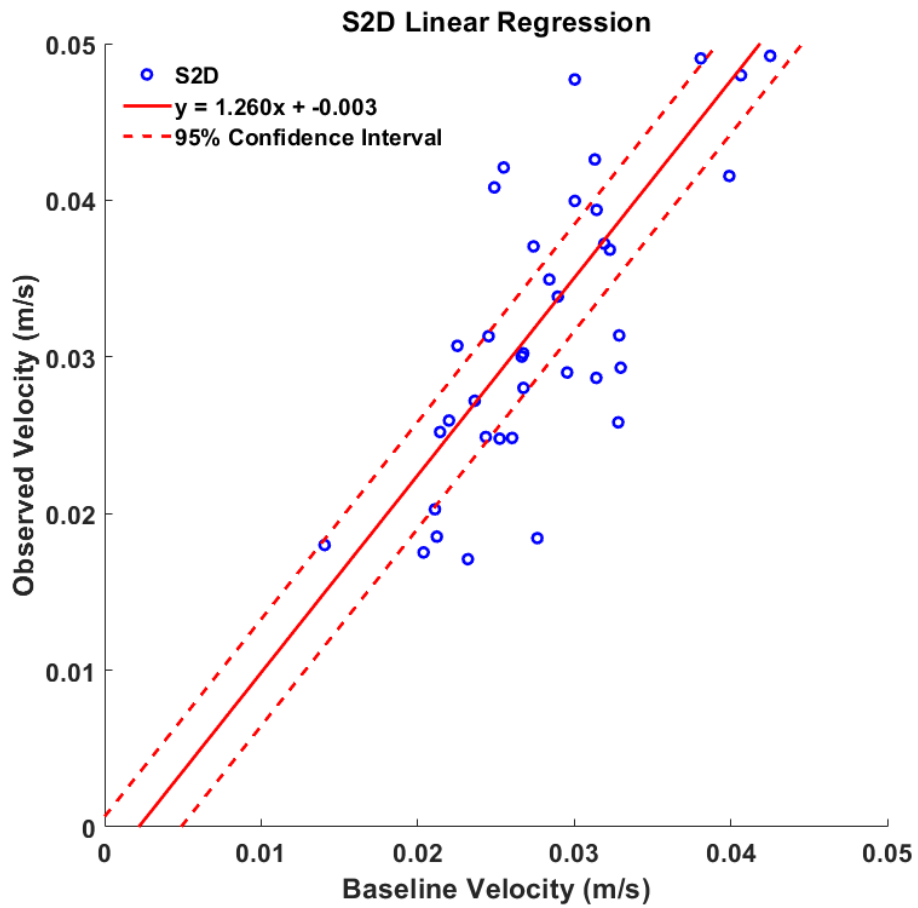
Annex 2: Regression Analysis of Experiment Results Compared to Pre-lagoon Conditions.



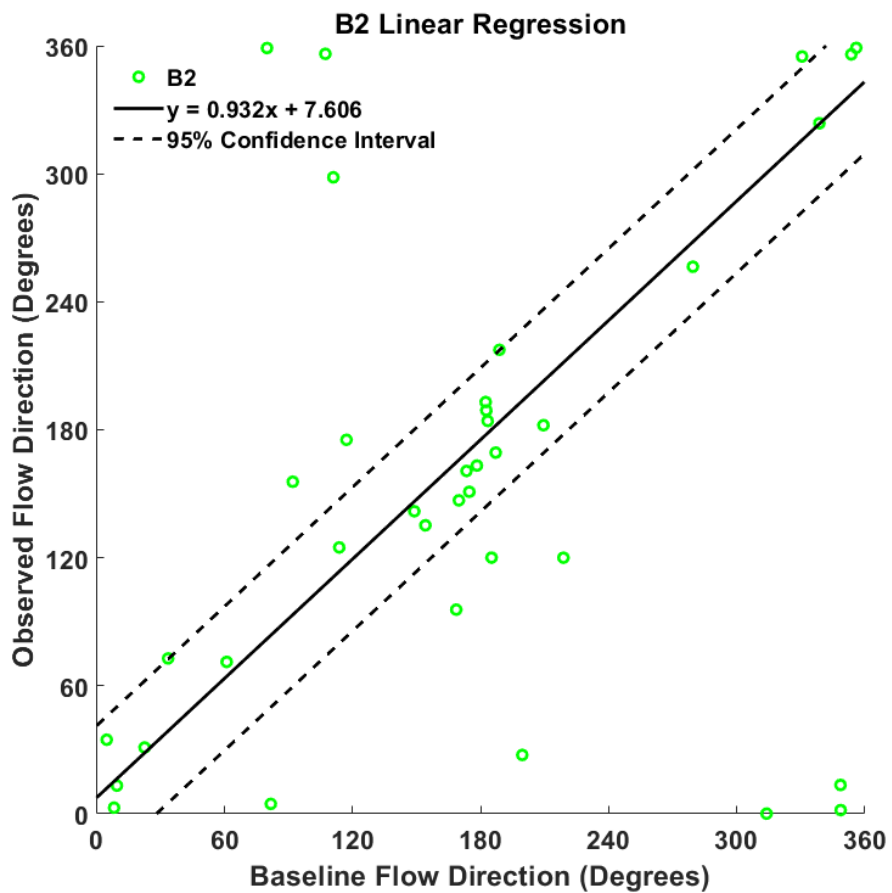
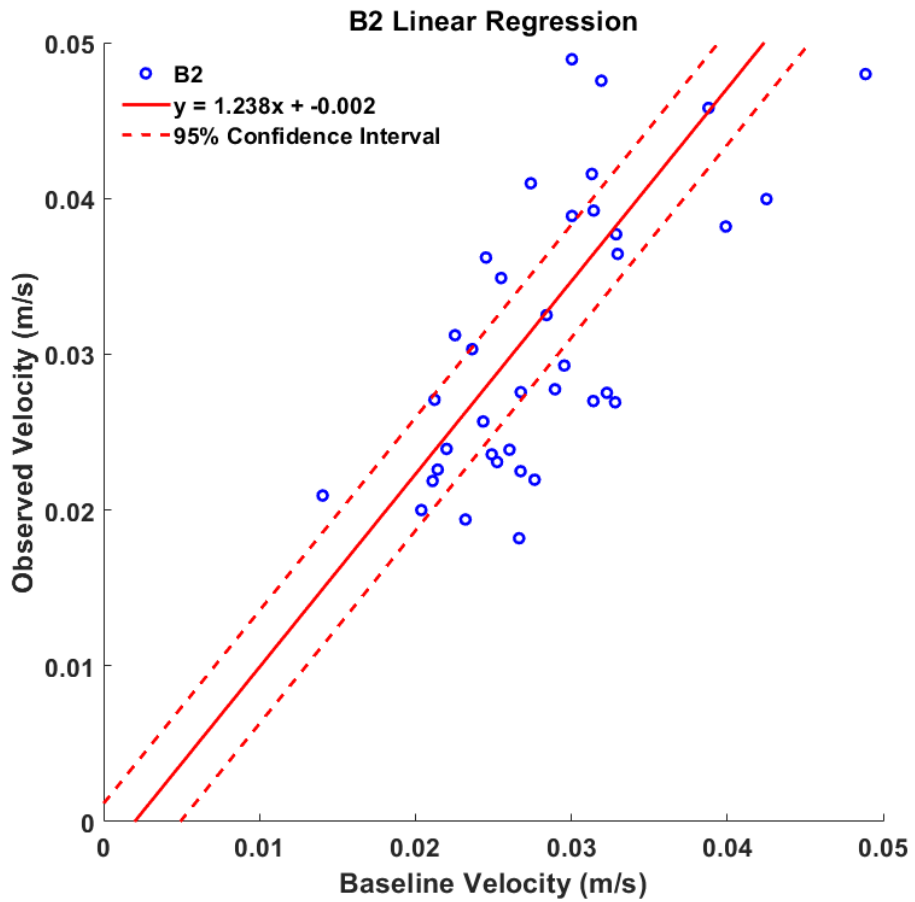
Annex 2: Regression Analysis of Experiment Results Compared to Pre-lagoon Conditions.



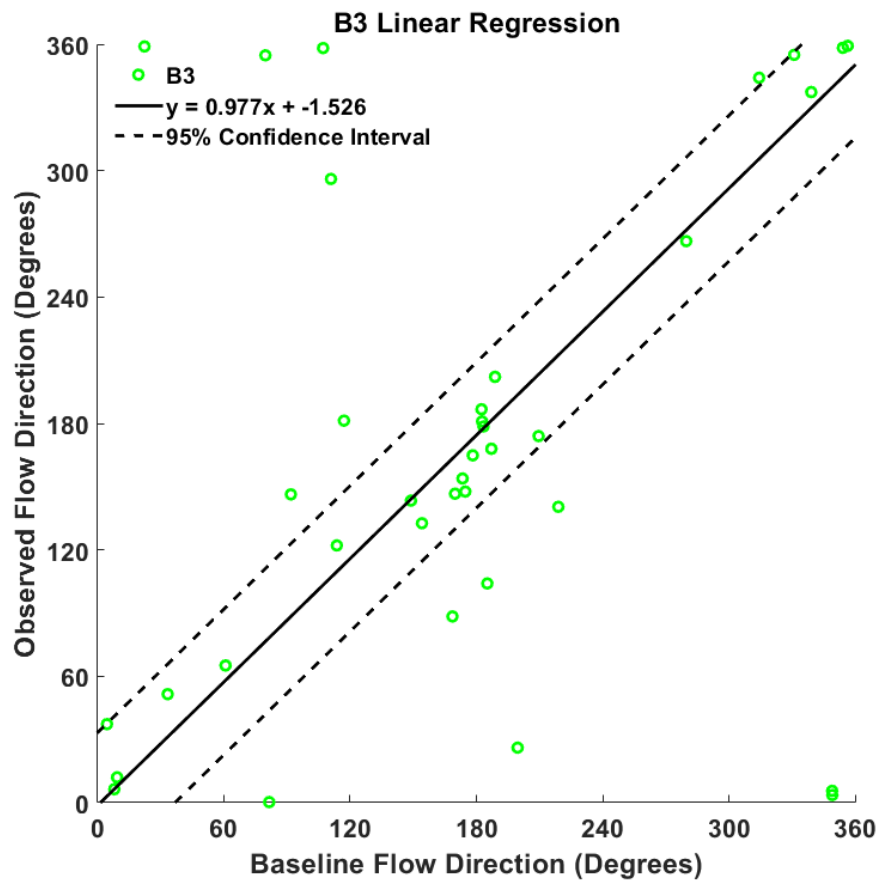
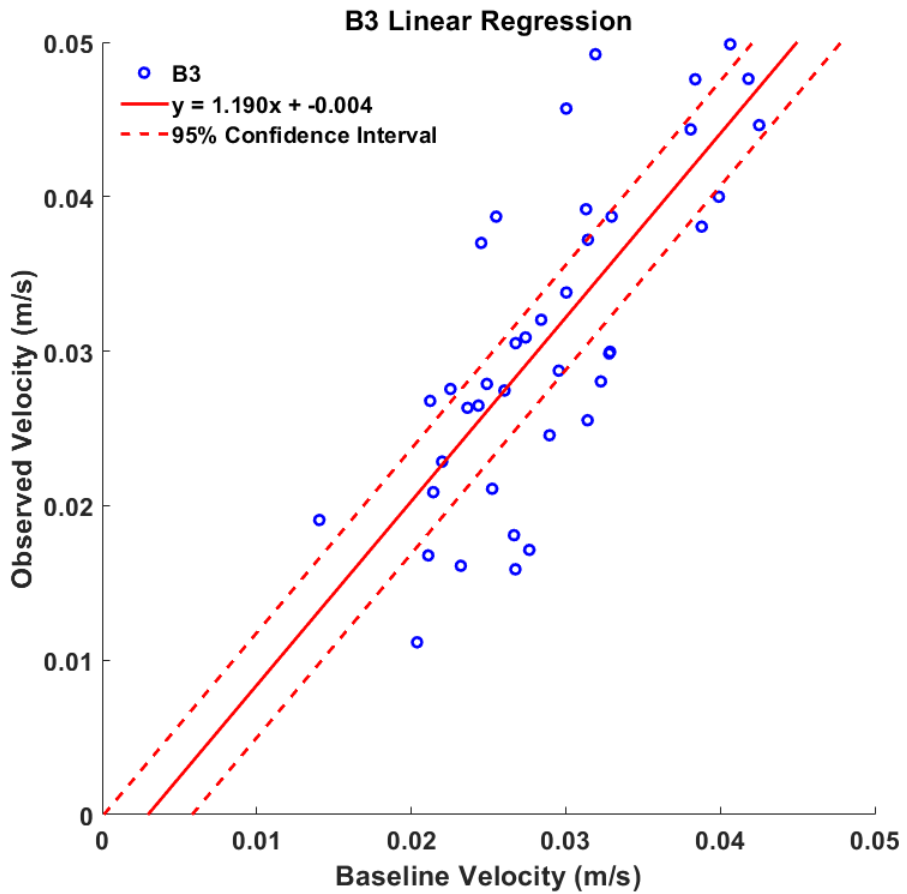
Annex 2: Regression Analysis of Experiment Results Compared to Pre-lagoon Conditions.



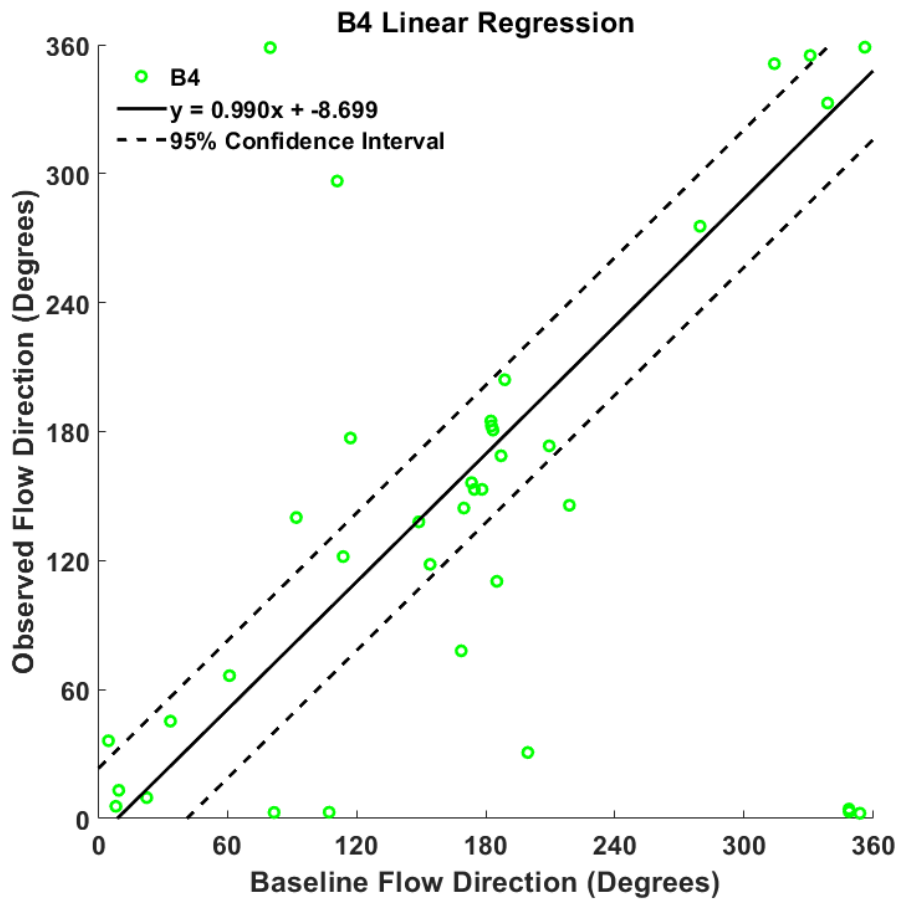
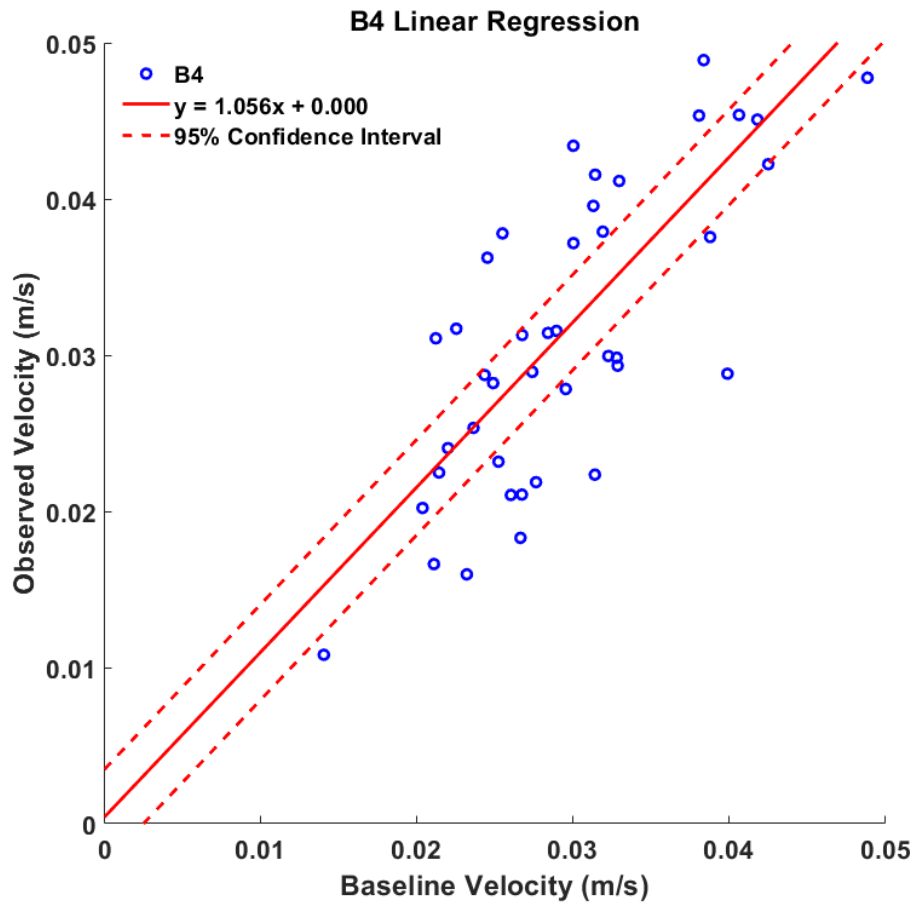
Annex 2: Regression Analysis of Experiment Results Compared to Pre-lagoon Conditions.



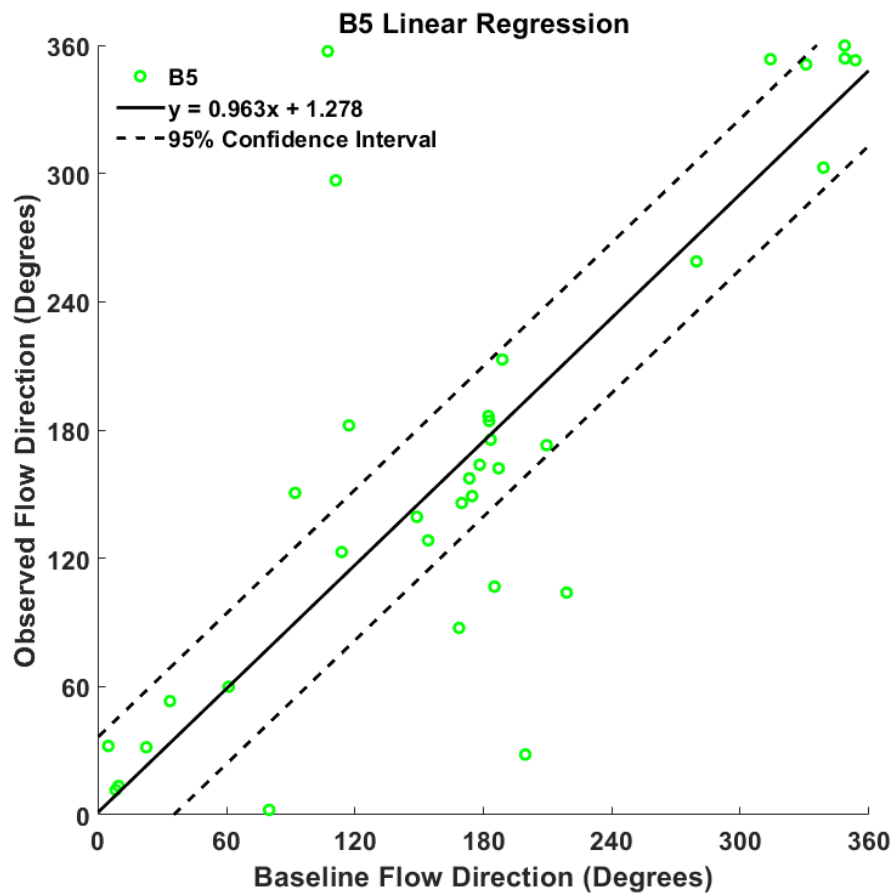
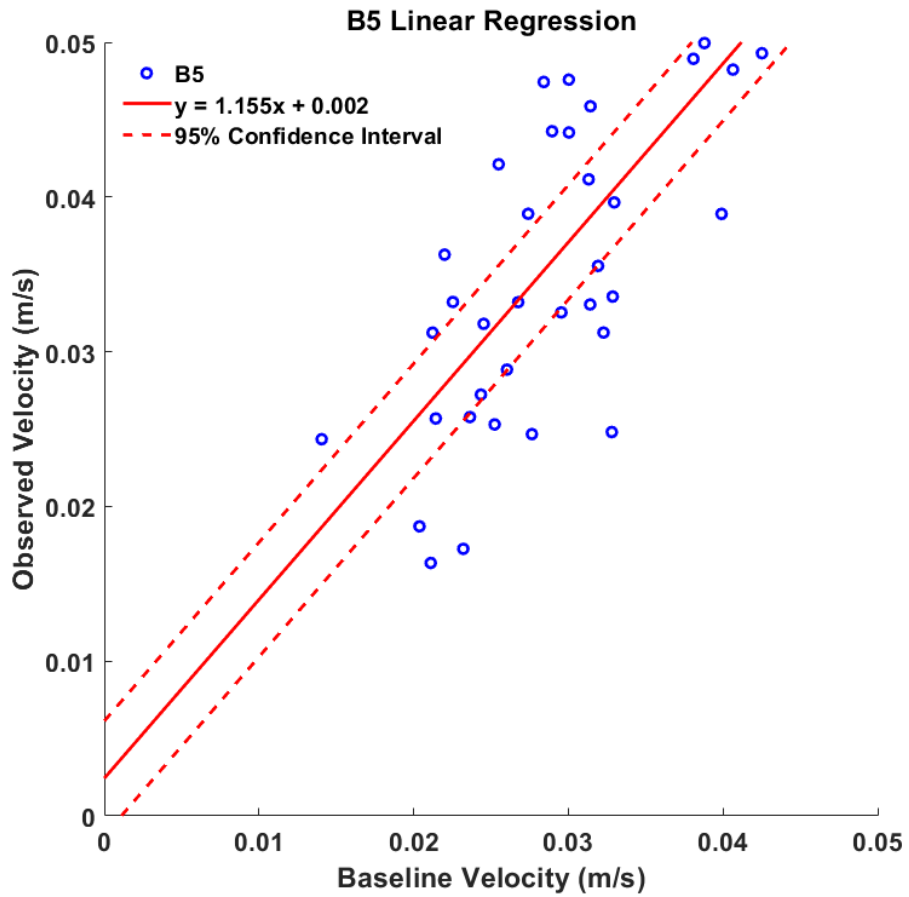
Annex 2: Regression Analysis of Experiment Results Compared to Pre-lagoon Conditions.



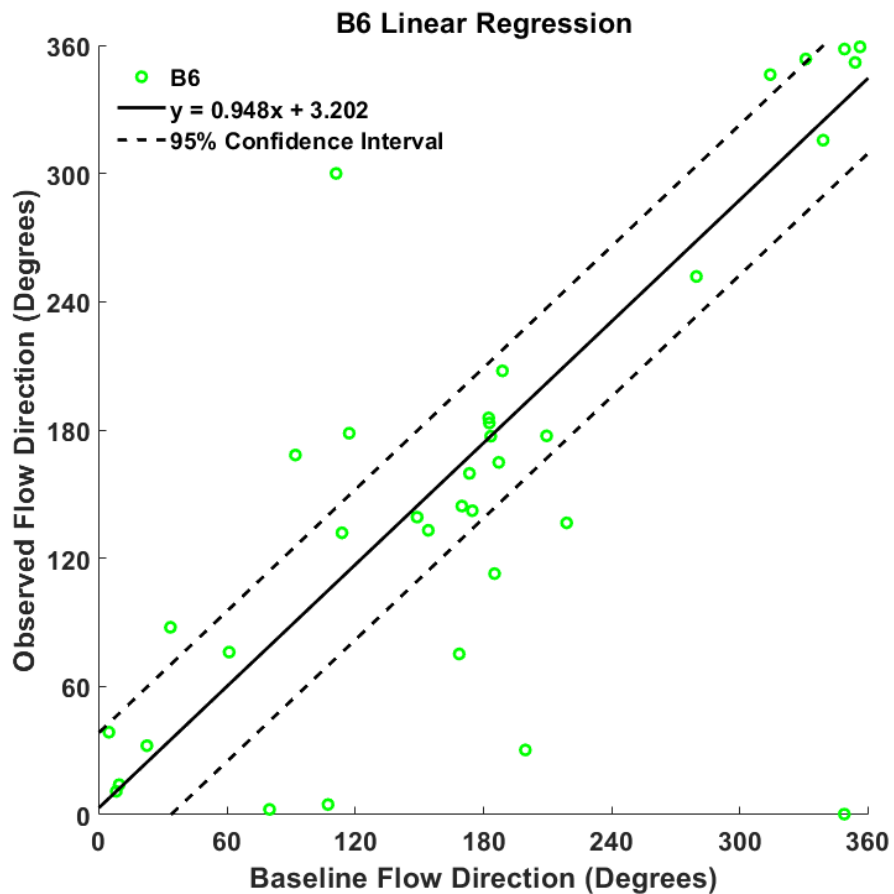
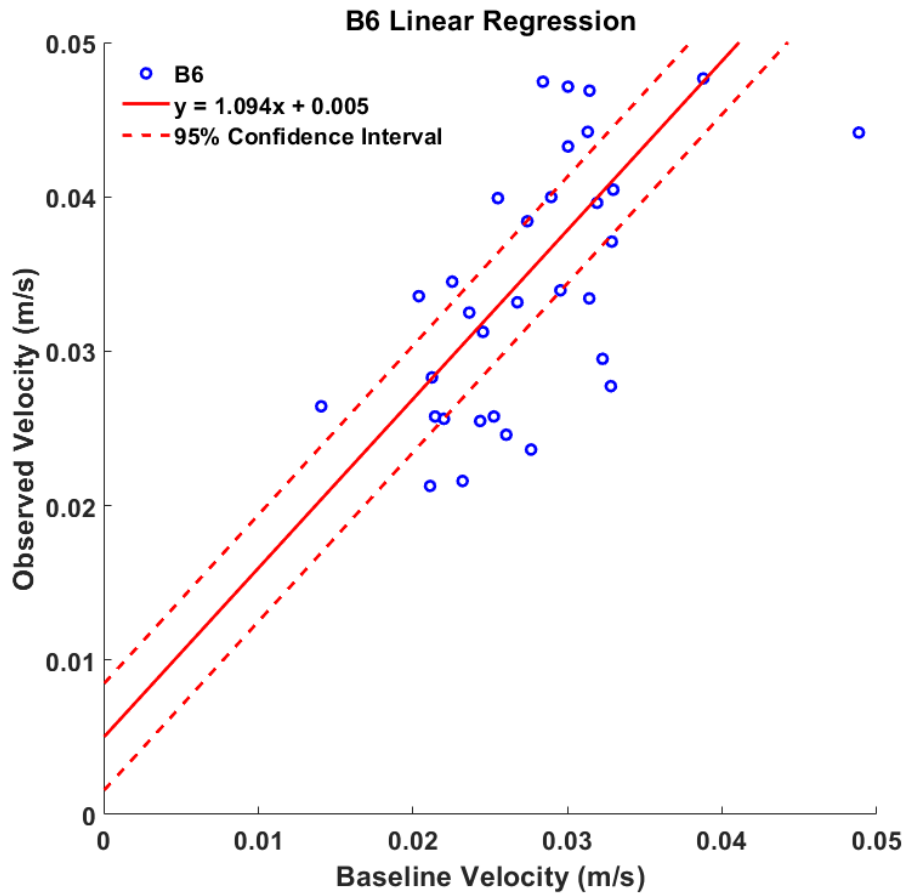
Annex 2: Regression Analysis of Experiment Results Compared to Pre-lagoon Conditions.



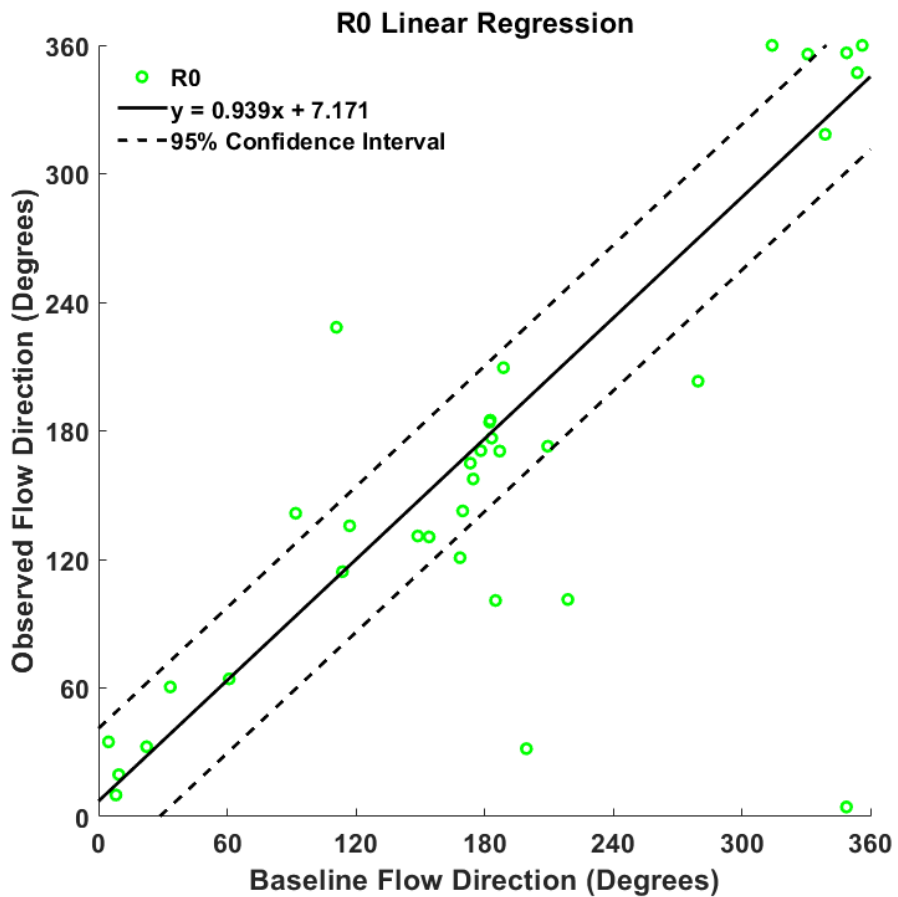
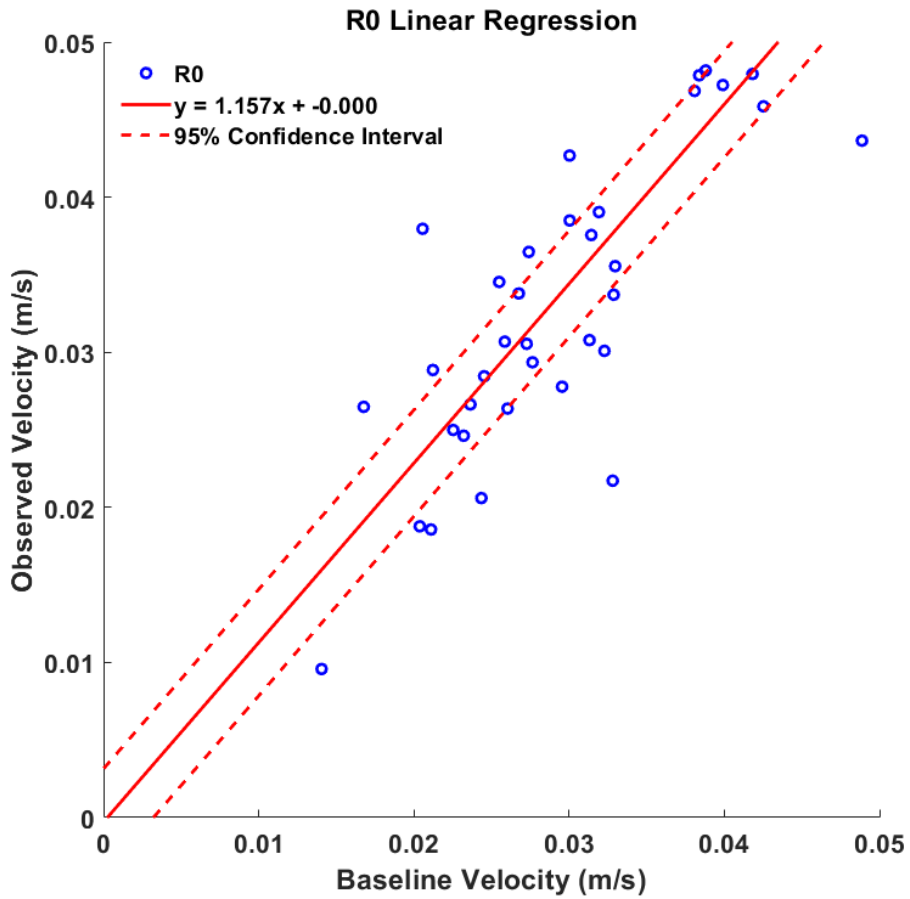
Annex 2: Regression Analysis of Experiment Results Compared to Pre-lagoon Conditions.



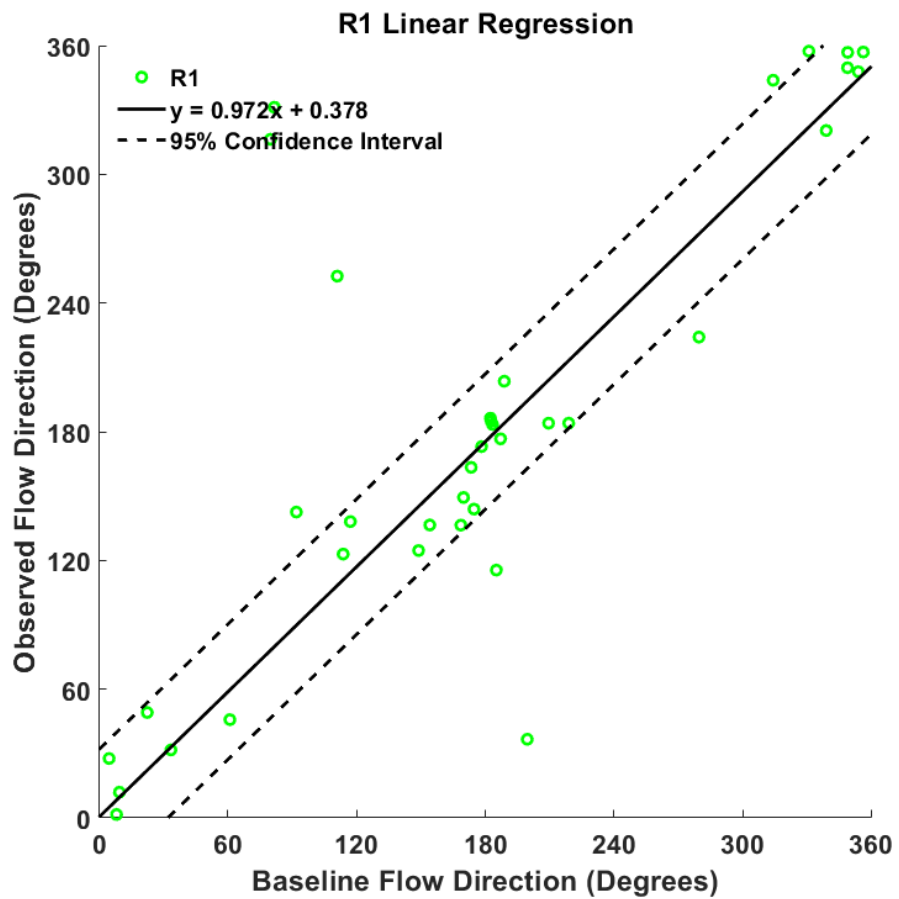
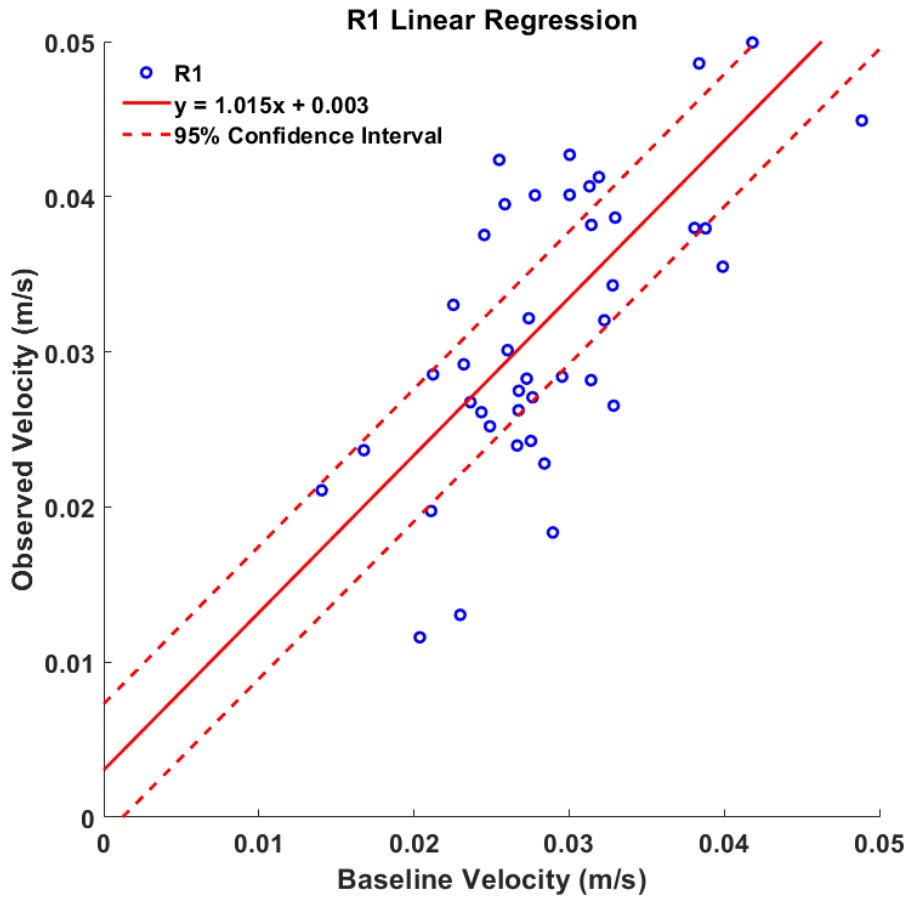
Annex 2: Regression Analysis of Experiment Results Compared to Pre-lagoon Conditions.



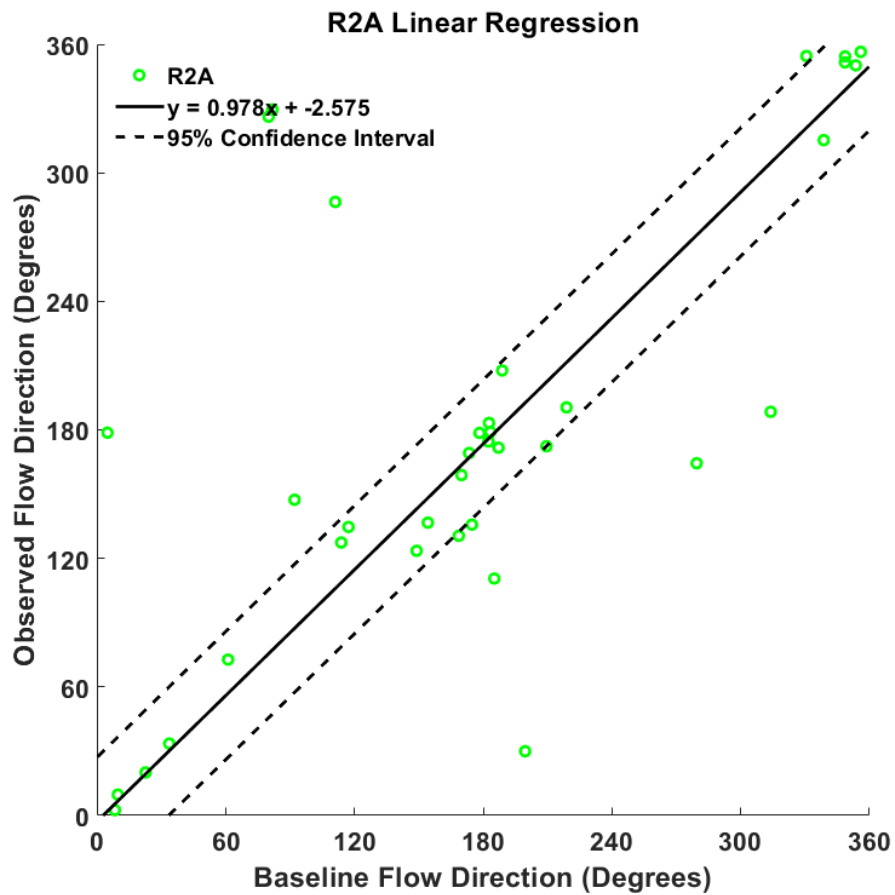
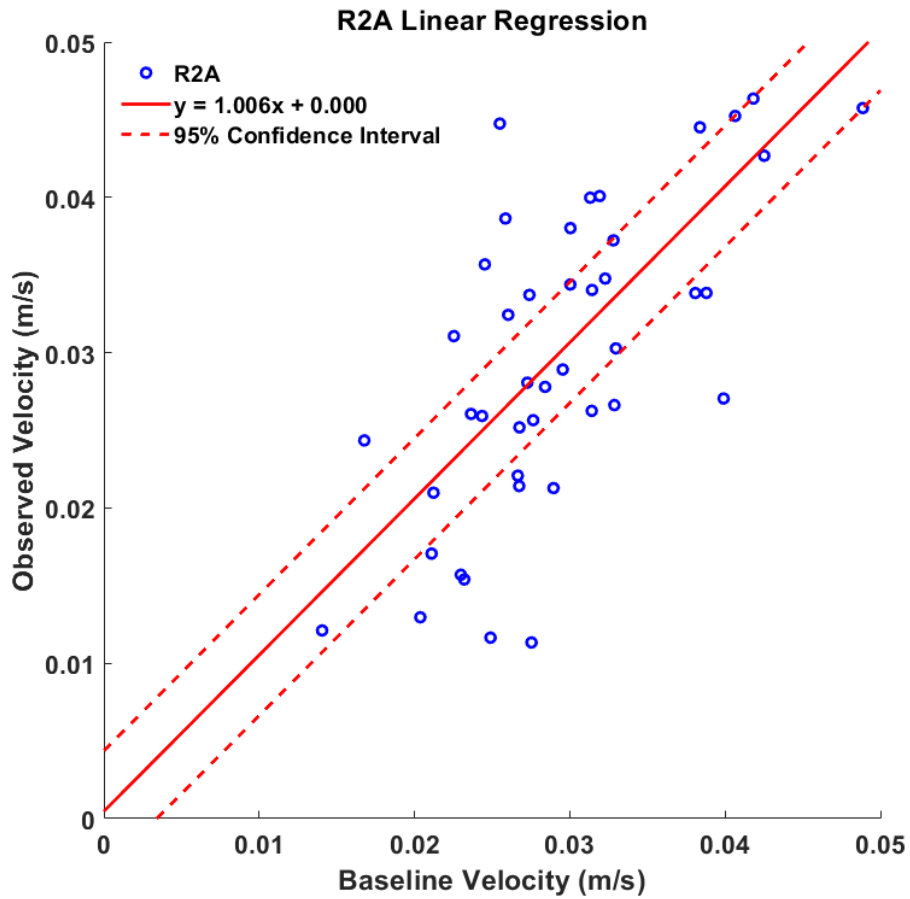
Annex 2: Regression Analysis of Experiment Results Compared to Pre-lagoon Conditions.



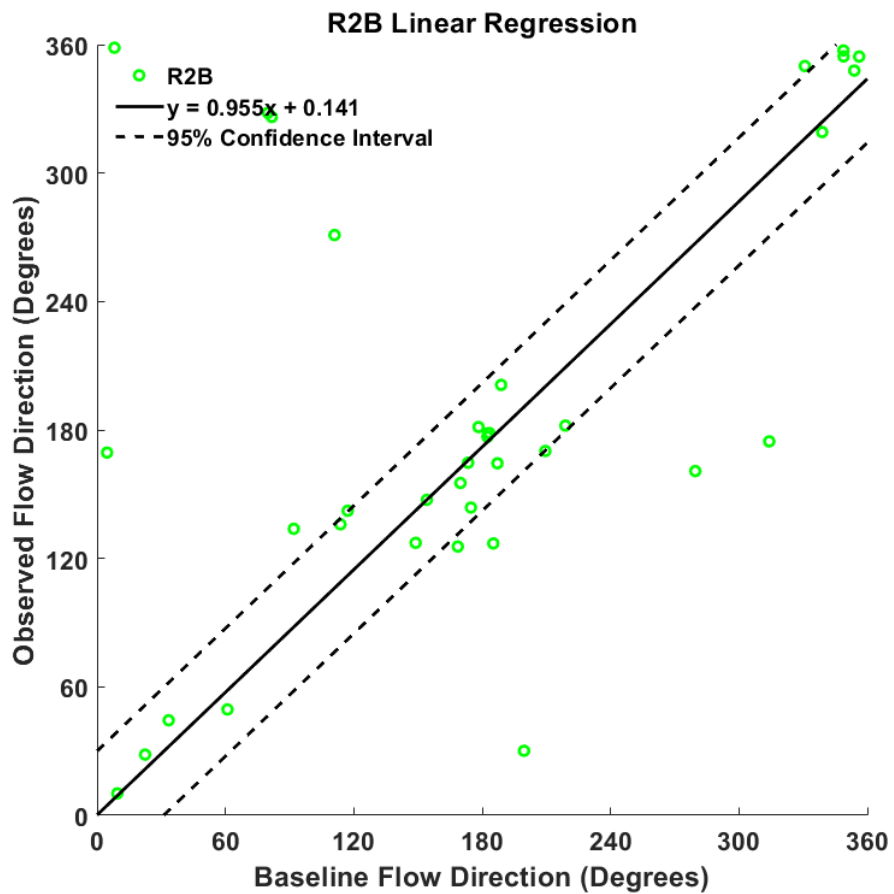
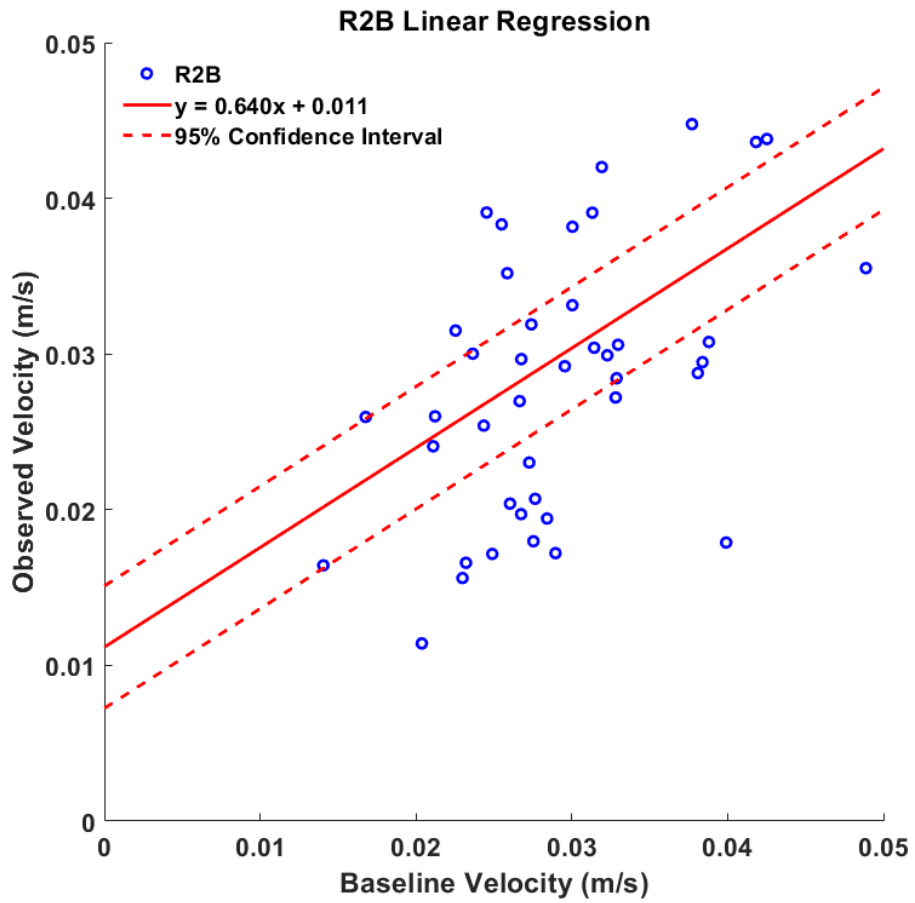
Annex 2: Regression Analysis of Experiment Results Compared to Pre-lagoon Conditions.



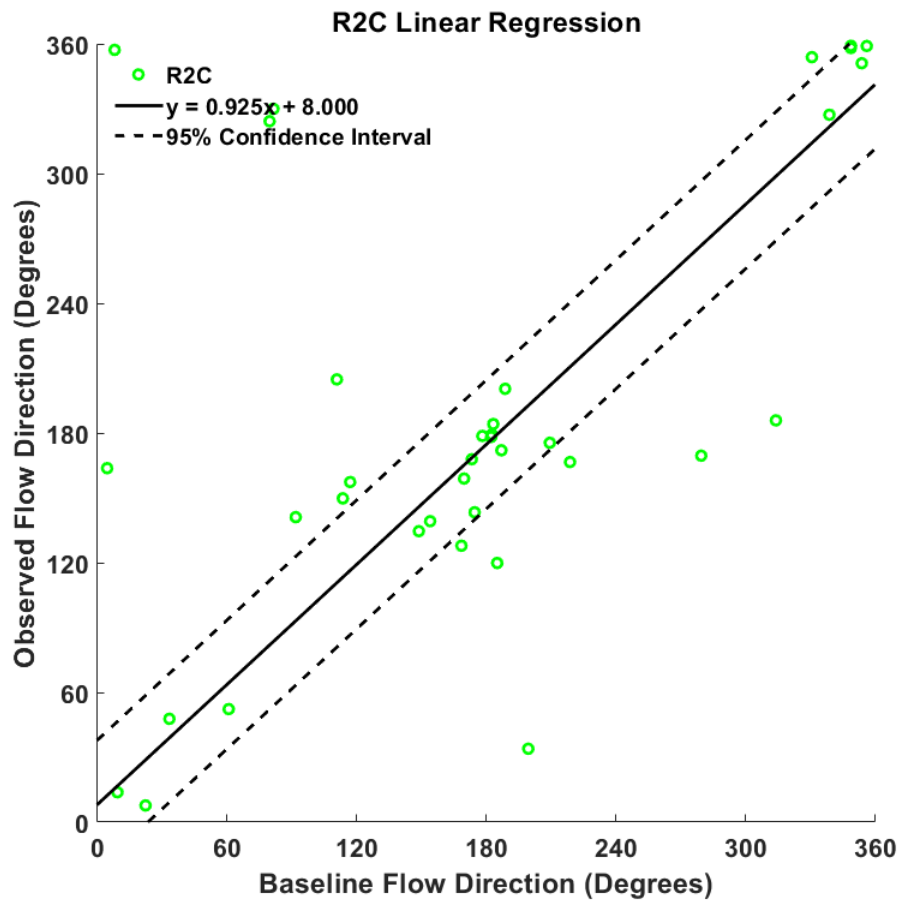
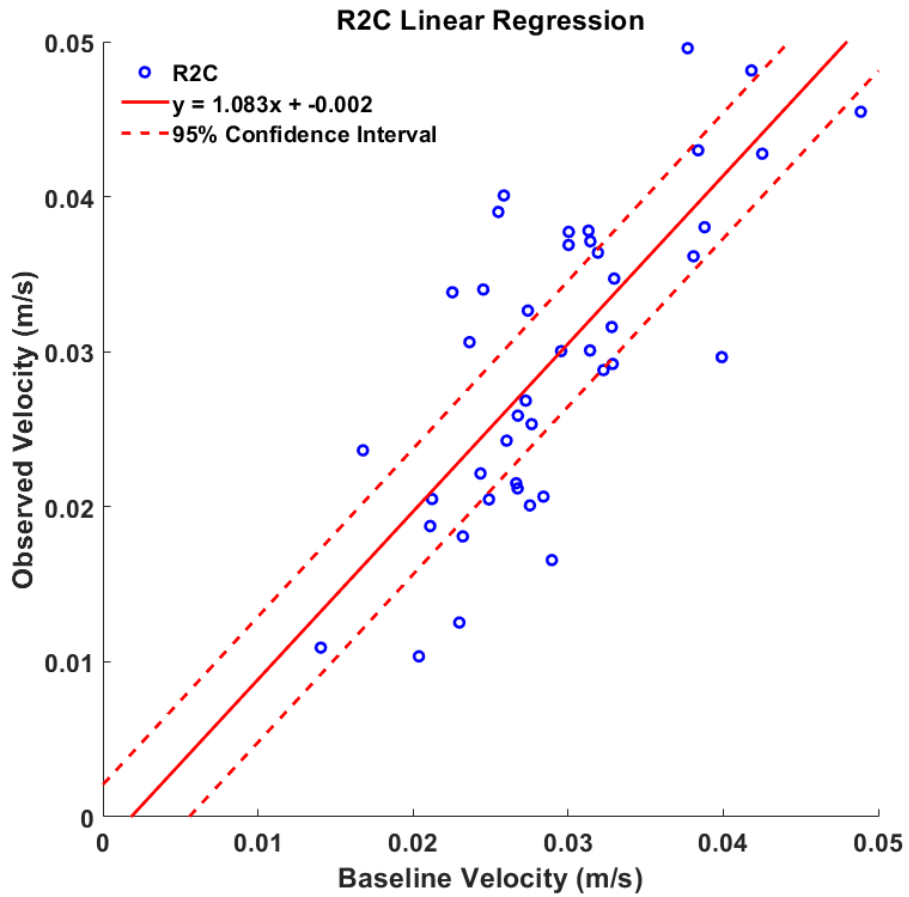
Annex 2: Regression Analysis of Experiment Results Compared to Pre-lagoon Conditions.



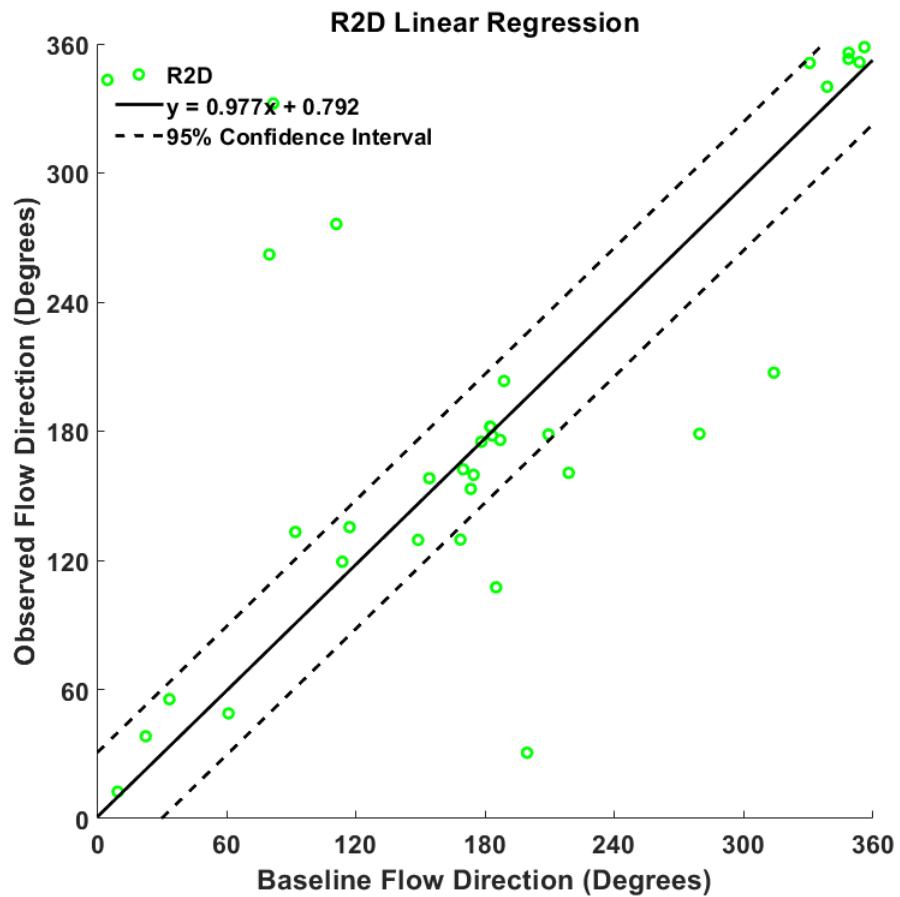
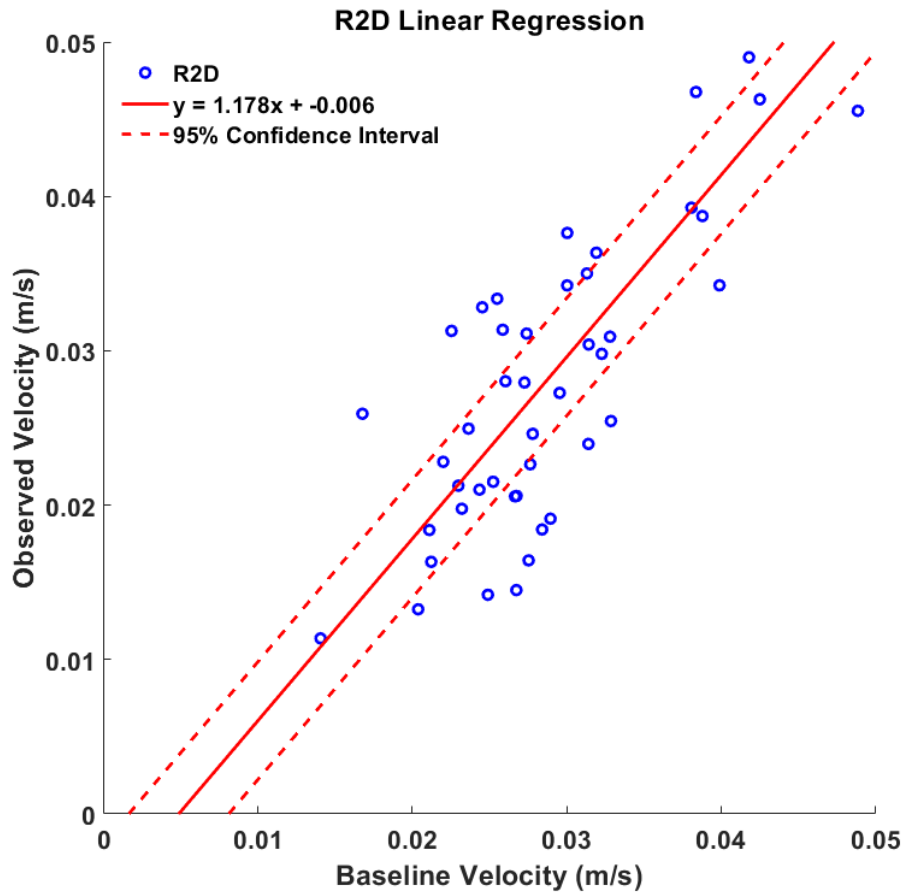
Annex 2: Regression Analysis of Experiment Results Compared to Pre-lagoon Conditions.



Annex 2: Regression Analysis of Experiment Results Compared to Pre-lagoon Conditions.

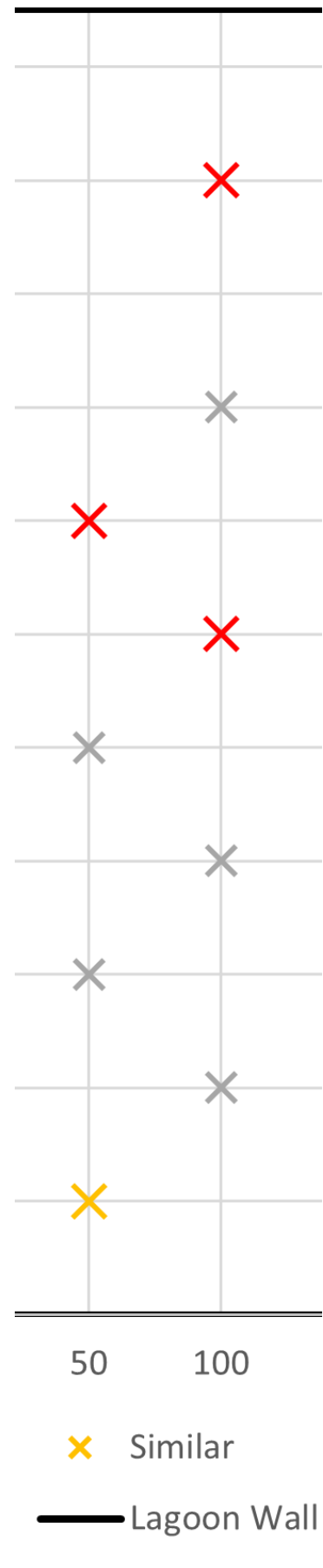


Annex 2: Regression Analysis of Experiment Results Compared to Pre-lagoon Conditions.

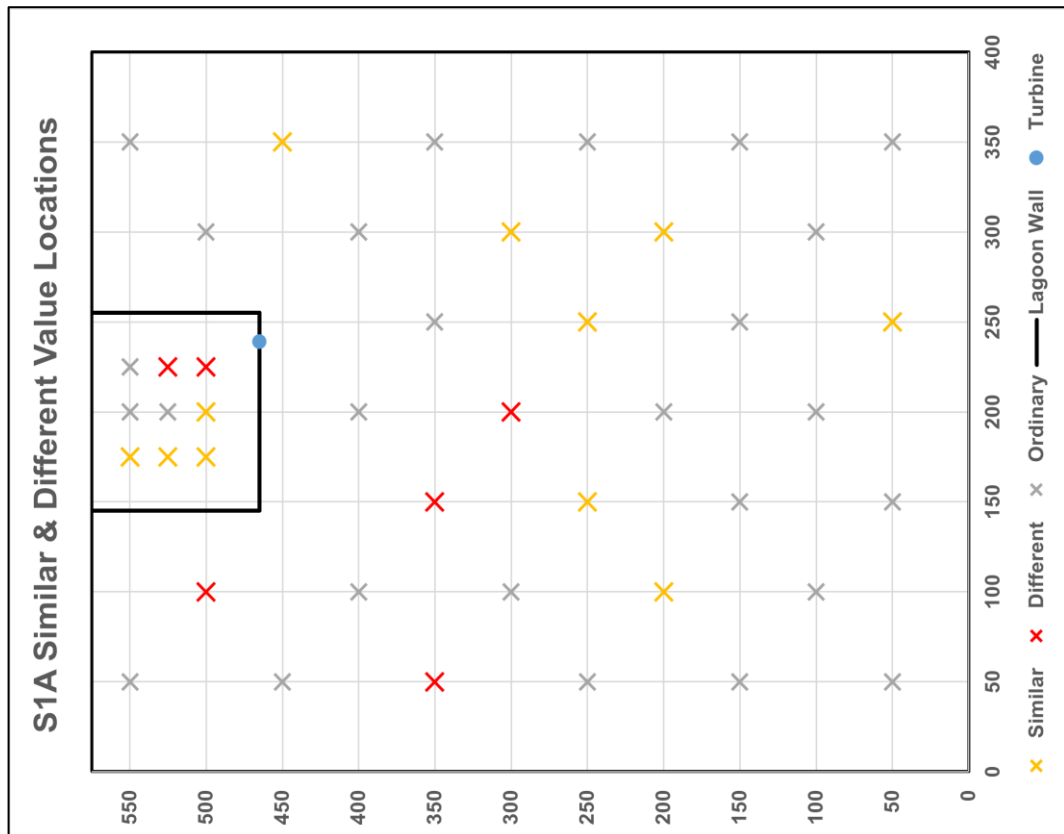
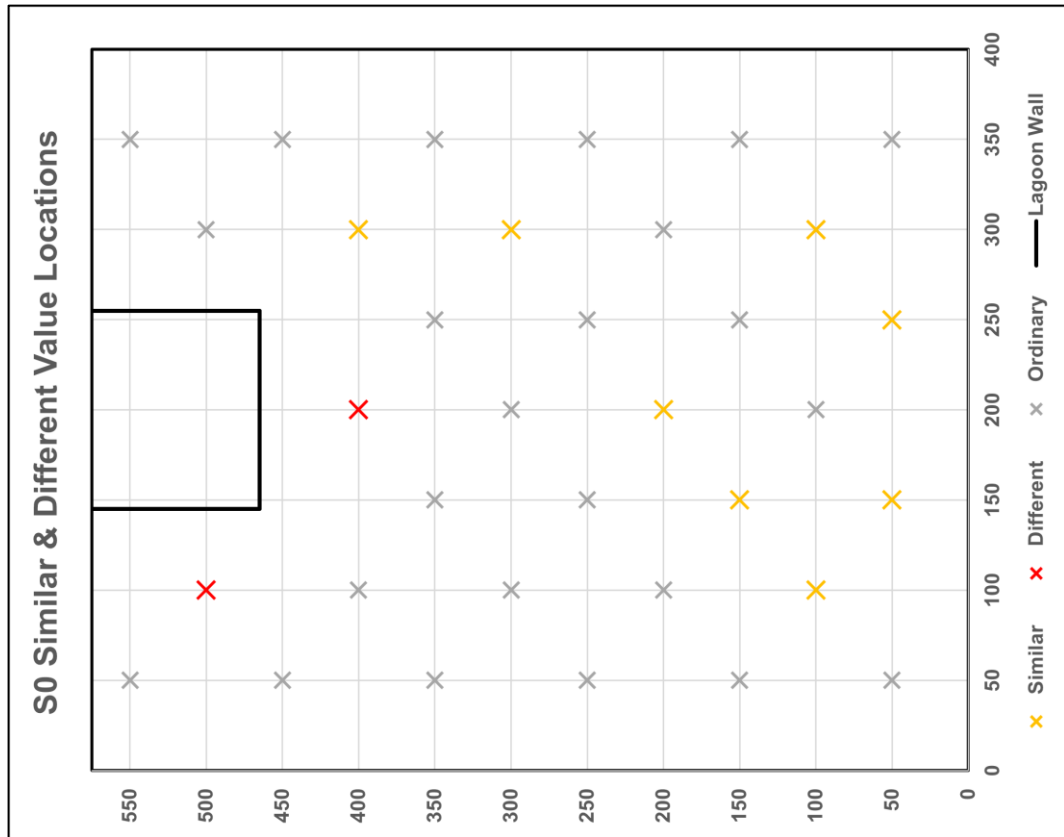


Annex 3

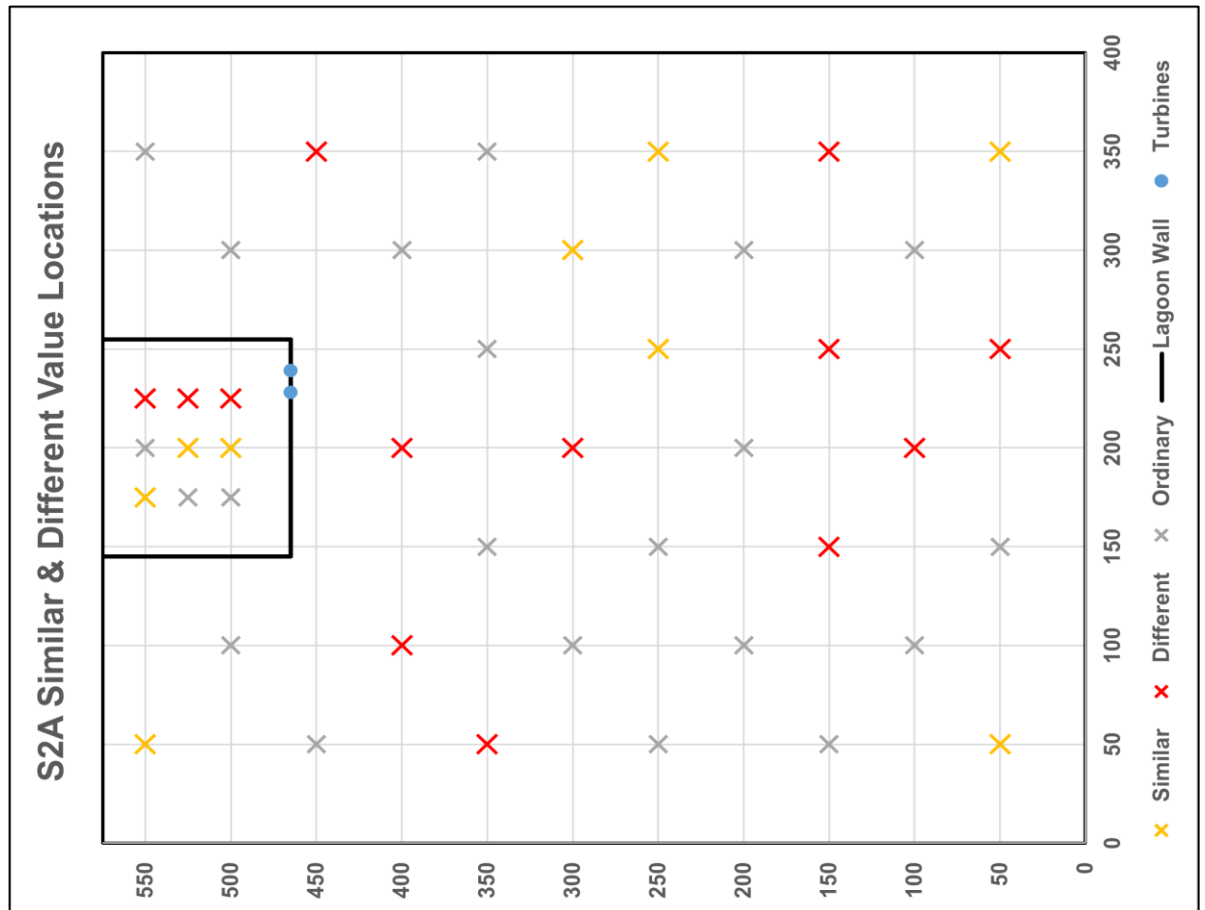
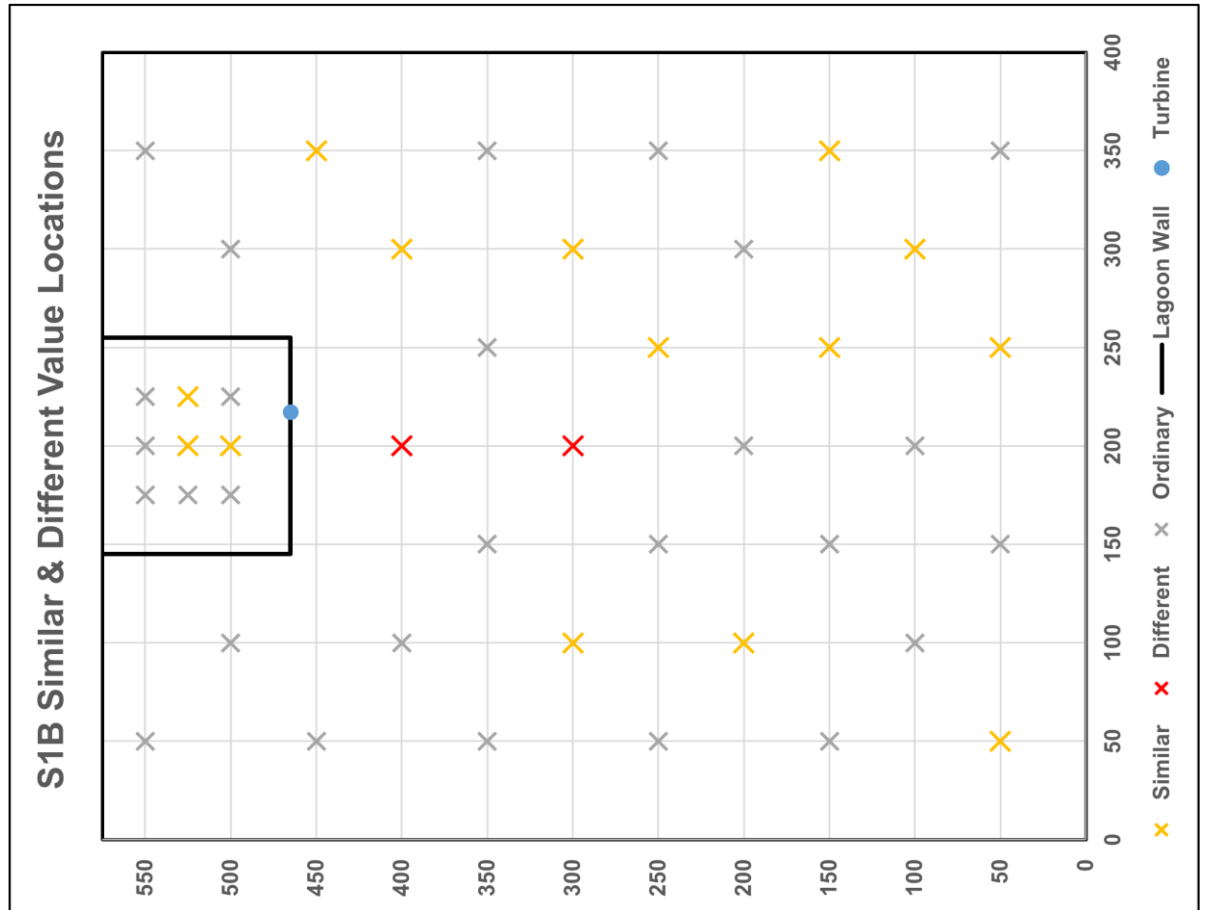
Comparison of Points of Statistically Similar and Different Residual Velocity



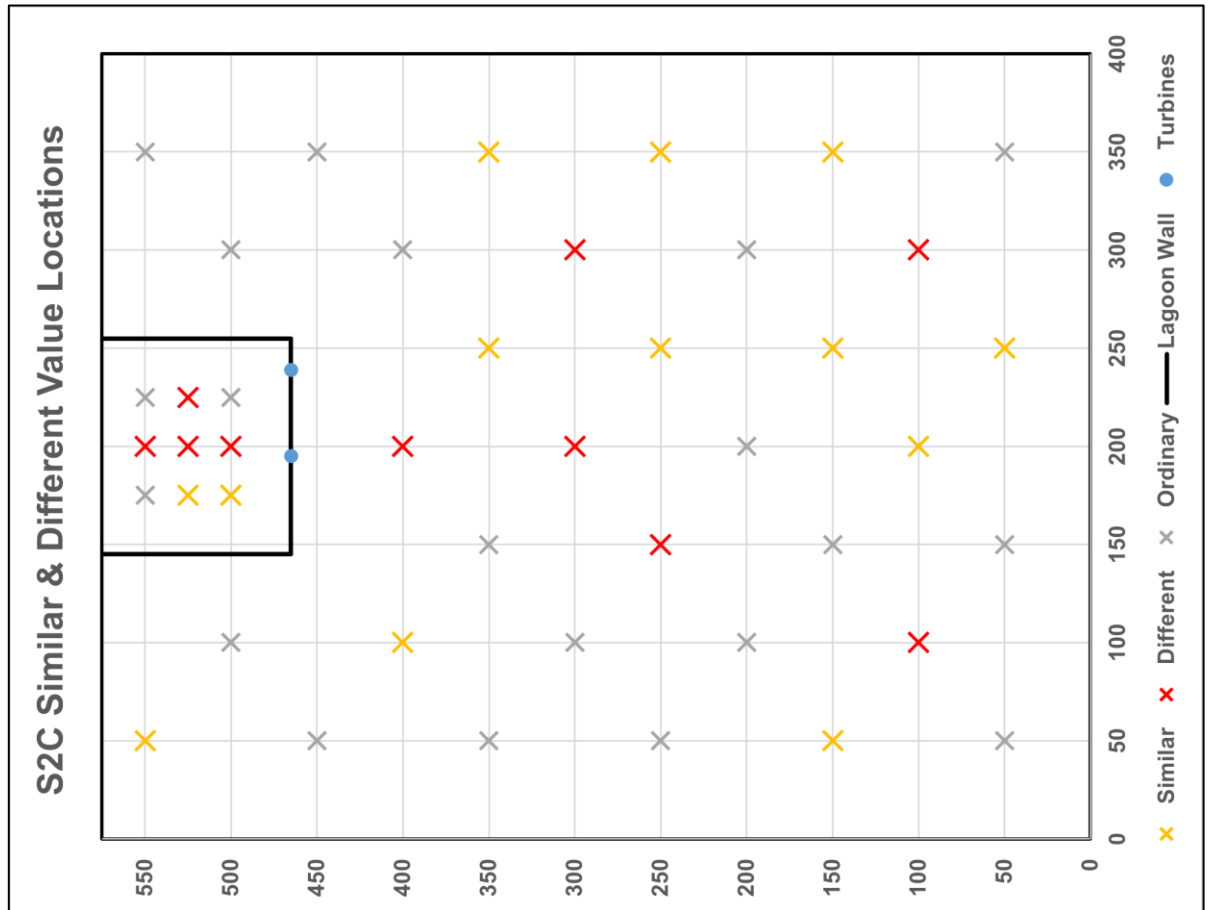
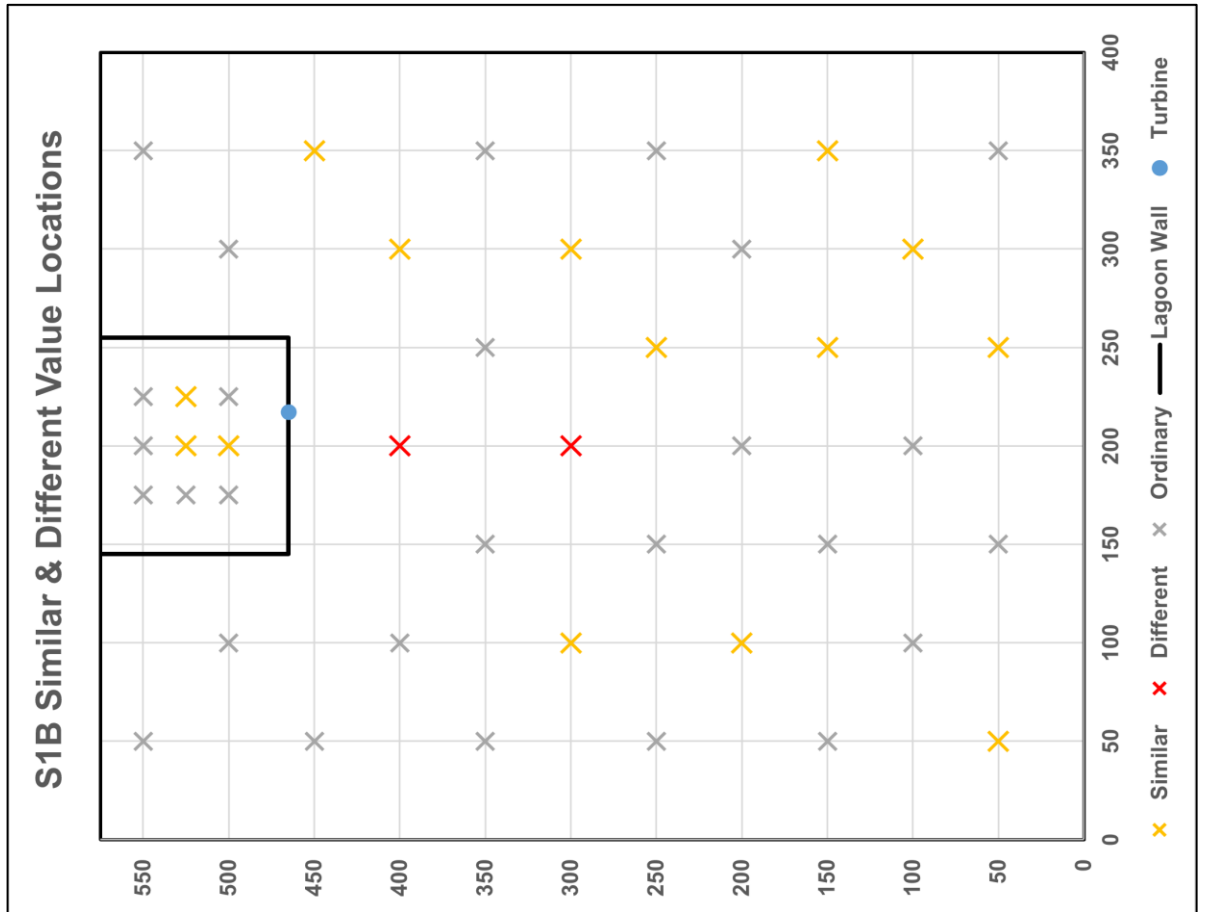
Annex 3: Comparison of points of statistically similar and different resultant velocity



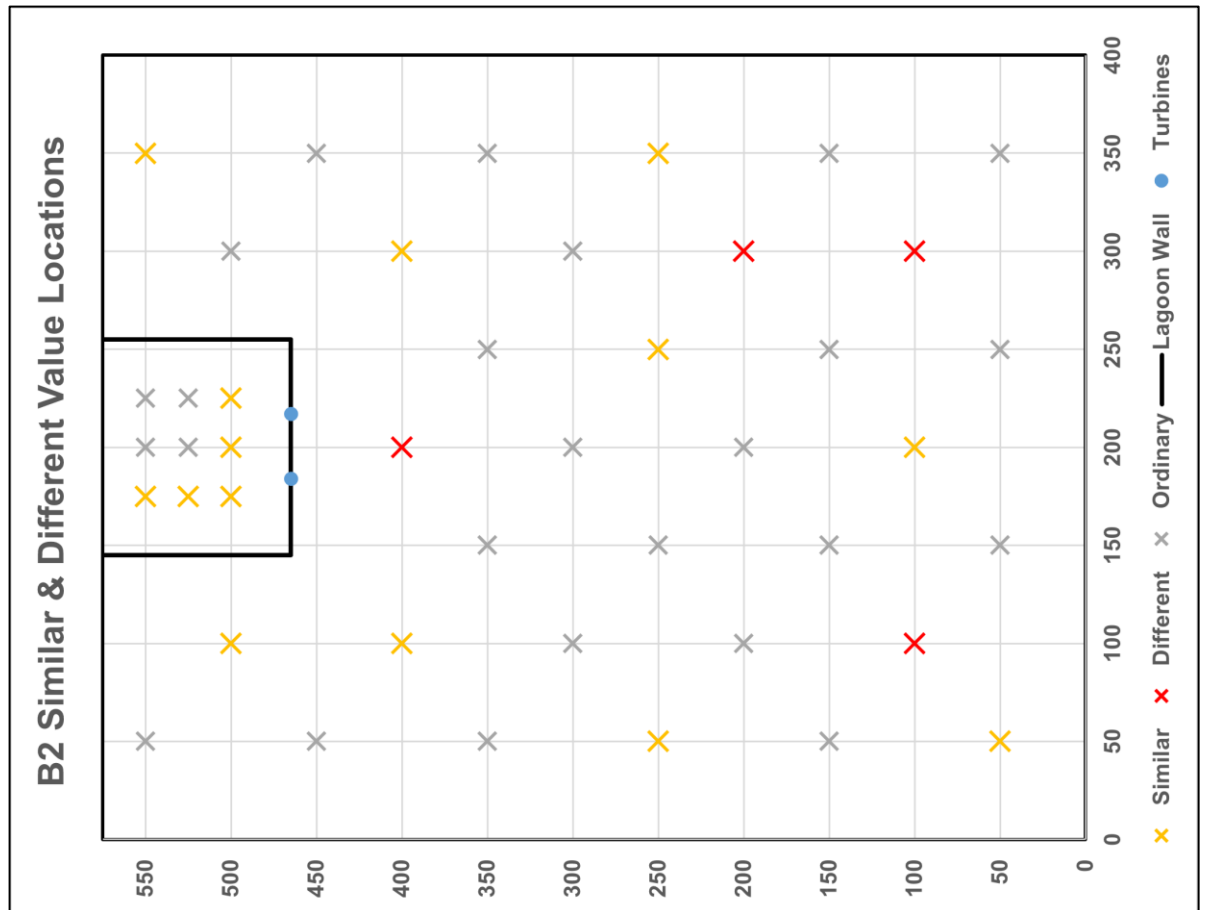
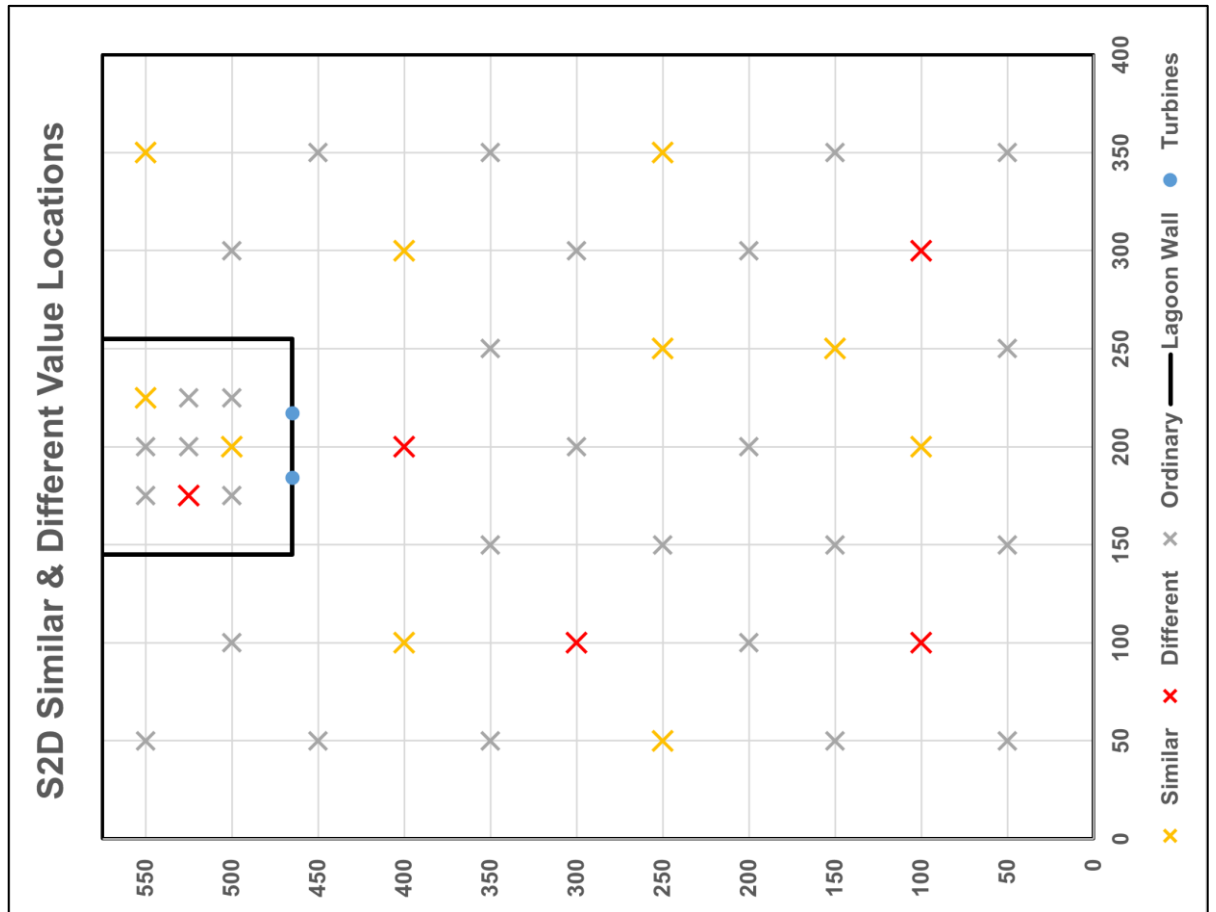
Annex 3: Comparison of Points of Statistically Similar and Different Resultant Velocity



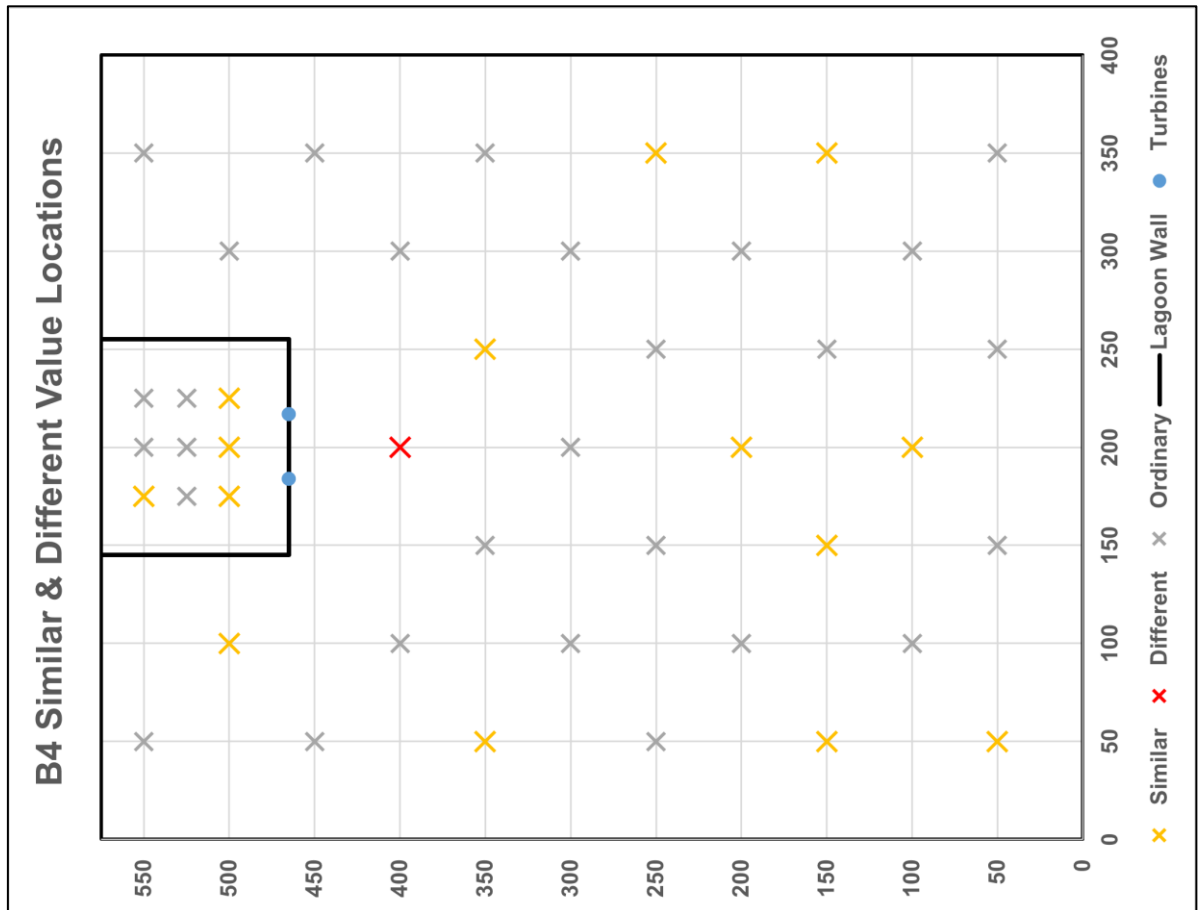
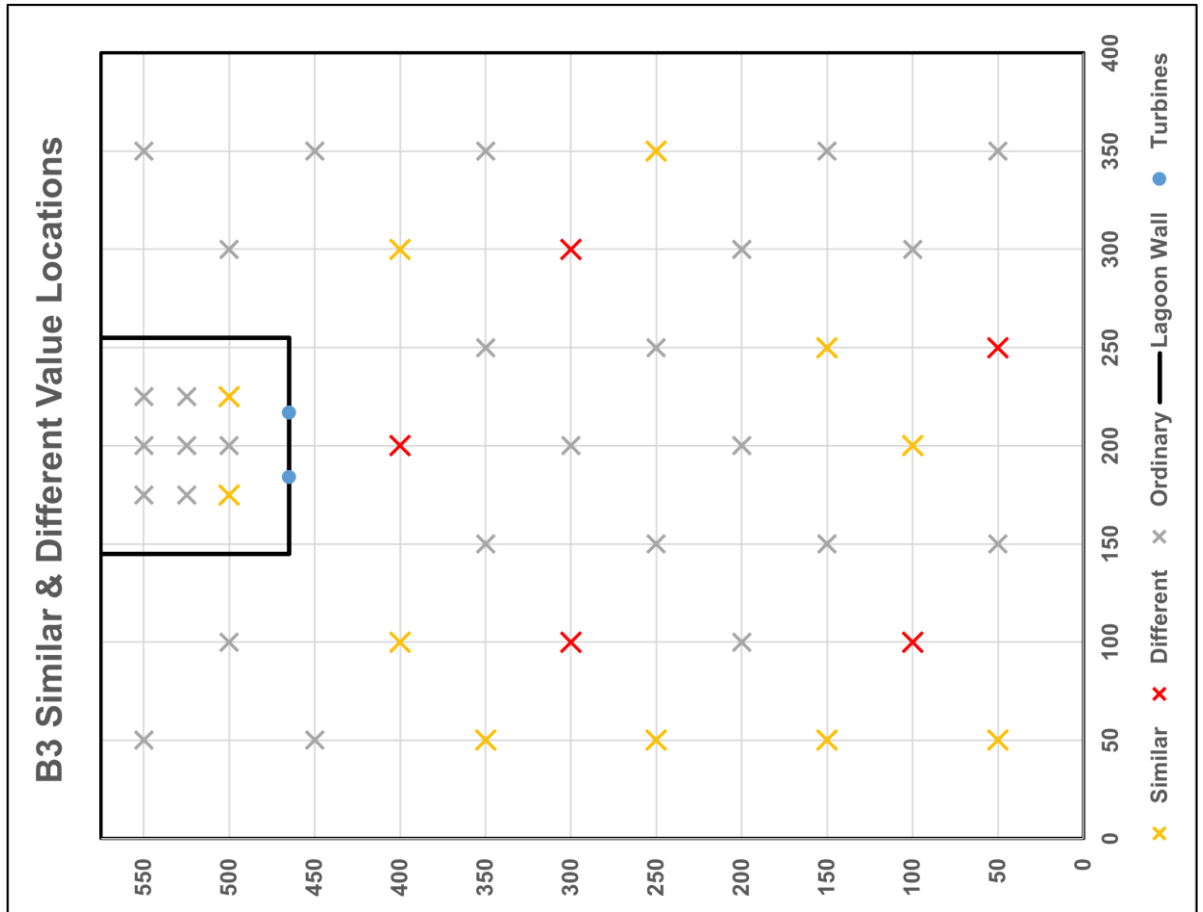
Annex 3: Comparison of Points of Statistically Similar and Different Resultant Velocity



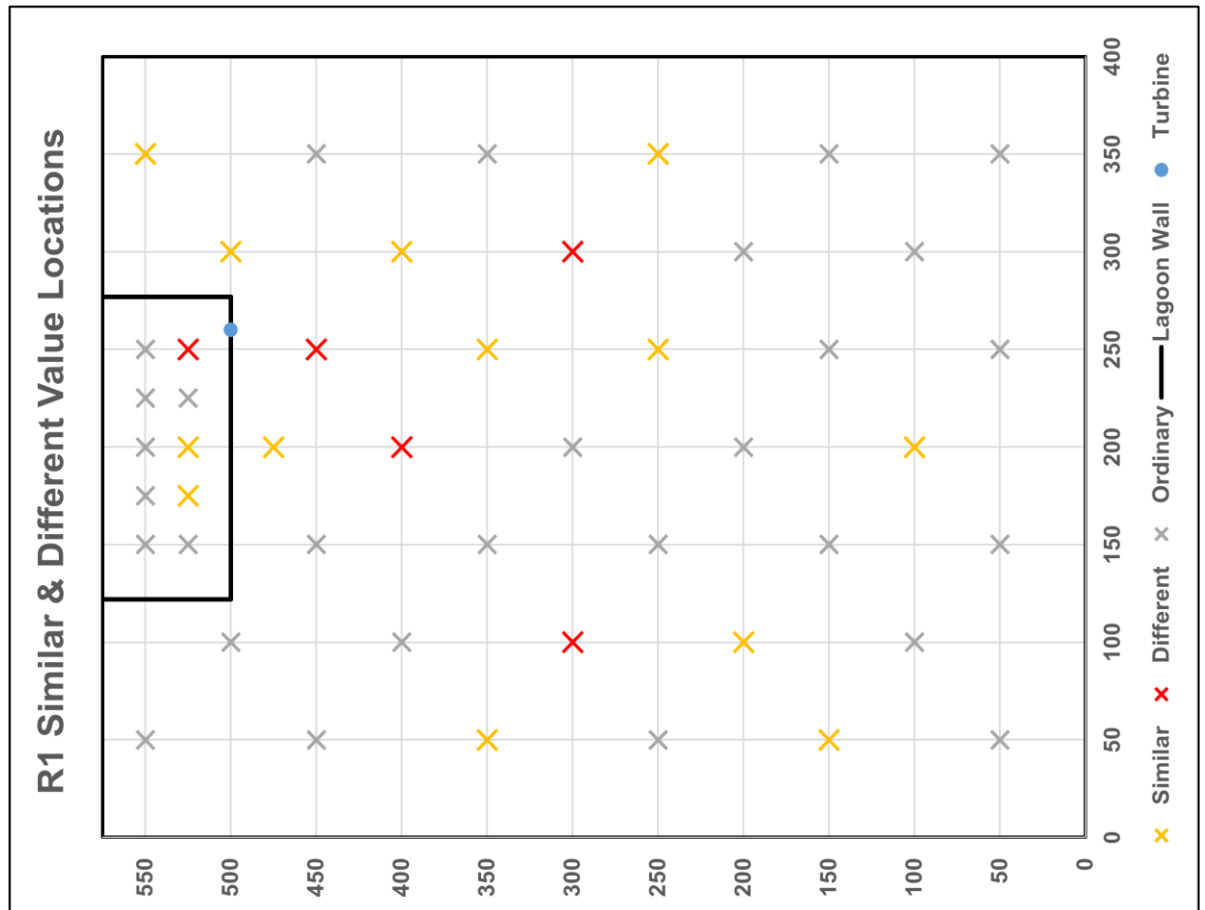
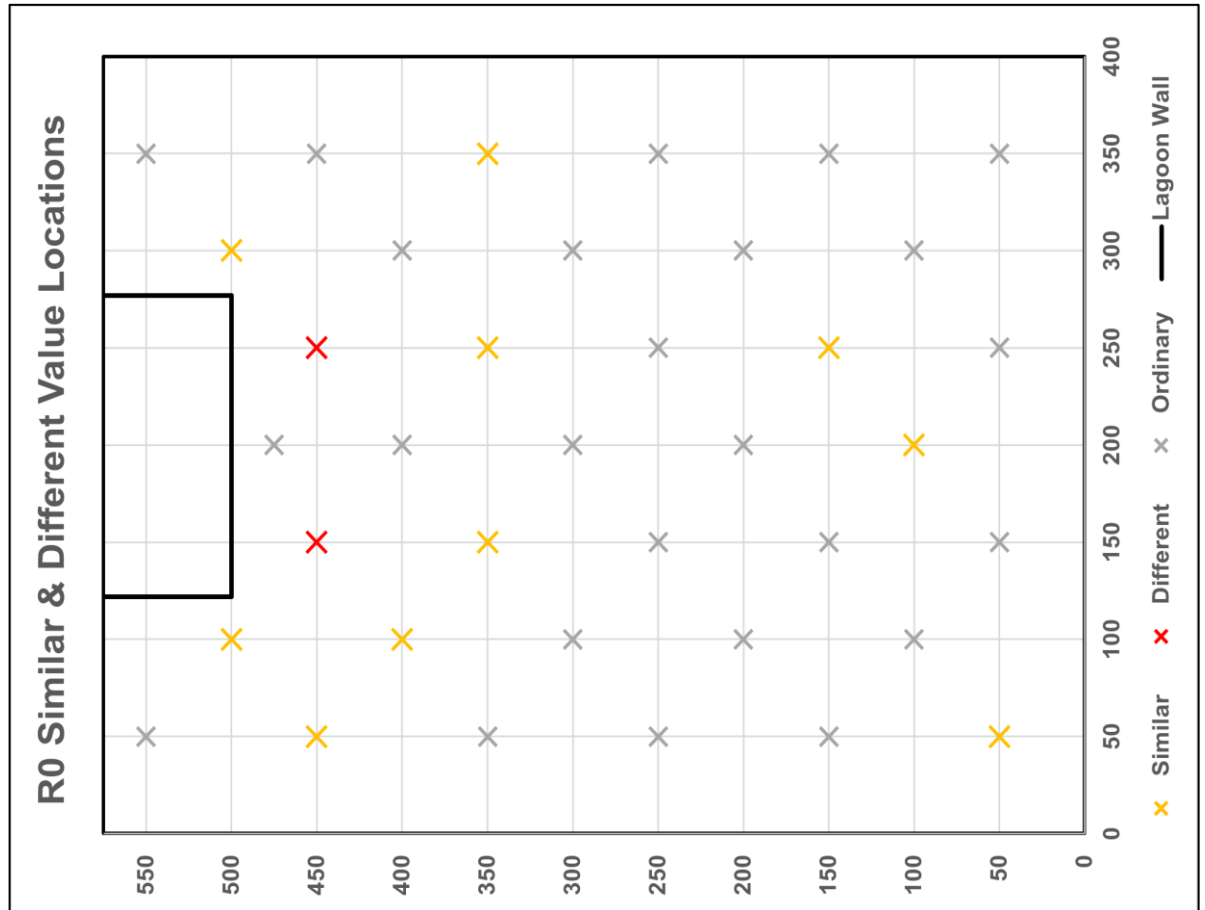
Annex 3: Comparison of Points of Statistically Similar and Different Resultant Velocity



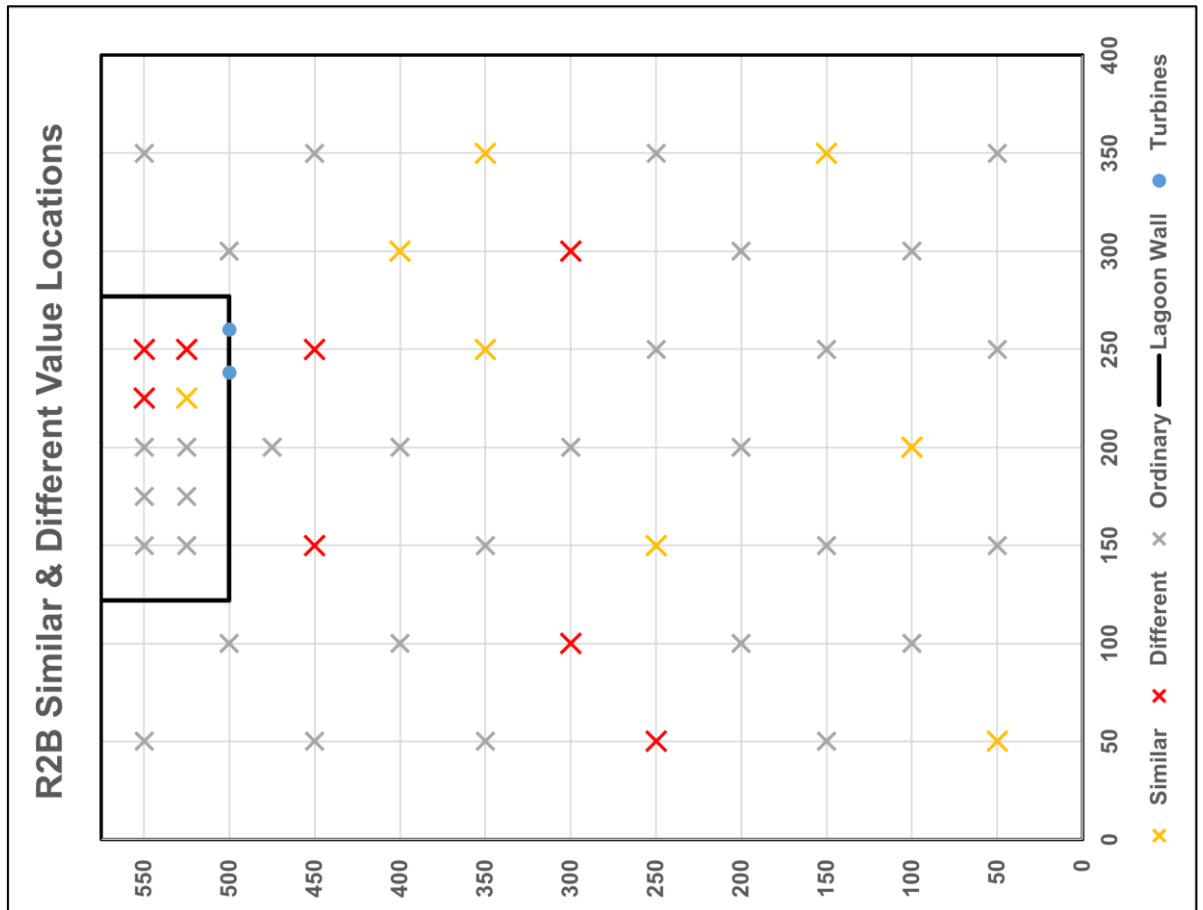
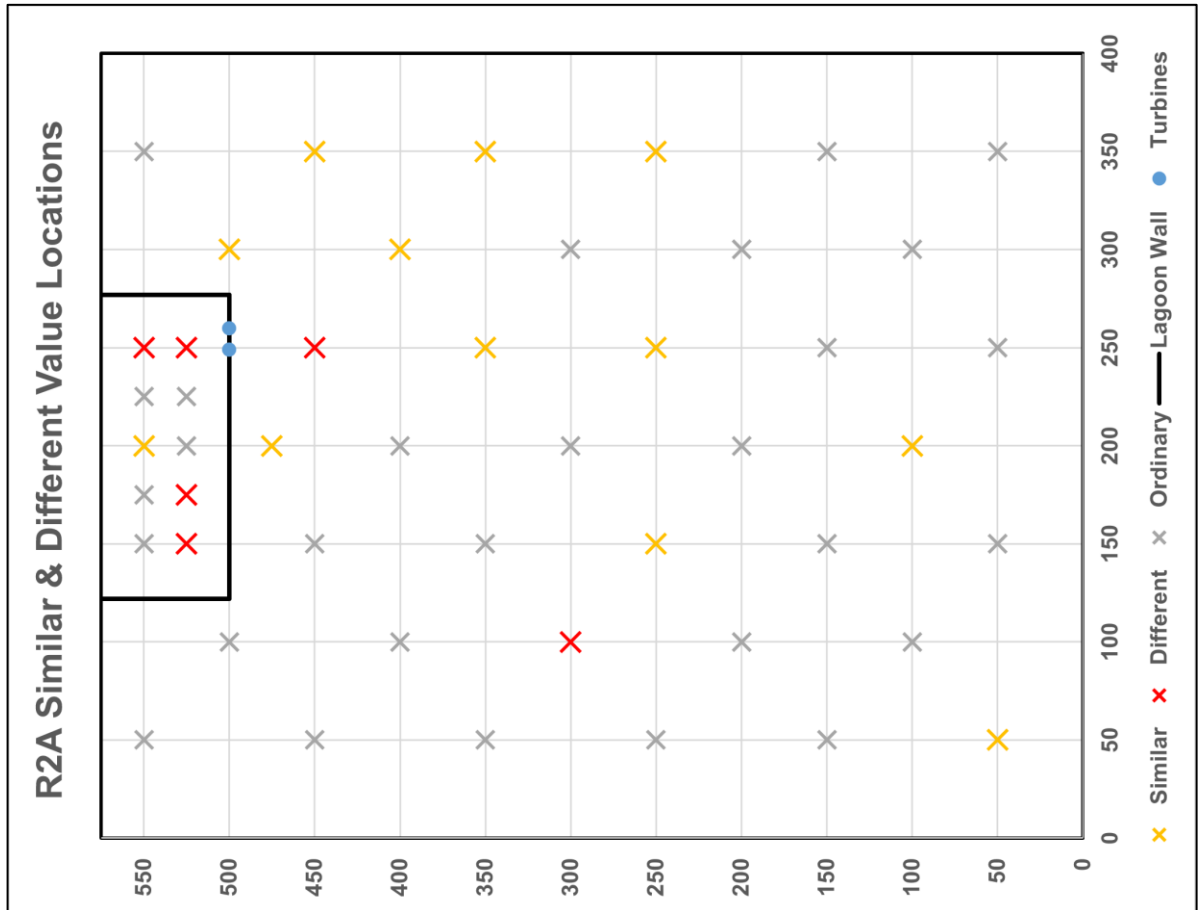
Annex 3: Comparison of Points of Statistically Similar and Different Resultant Velocity



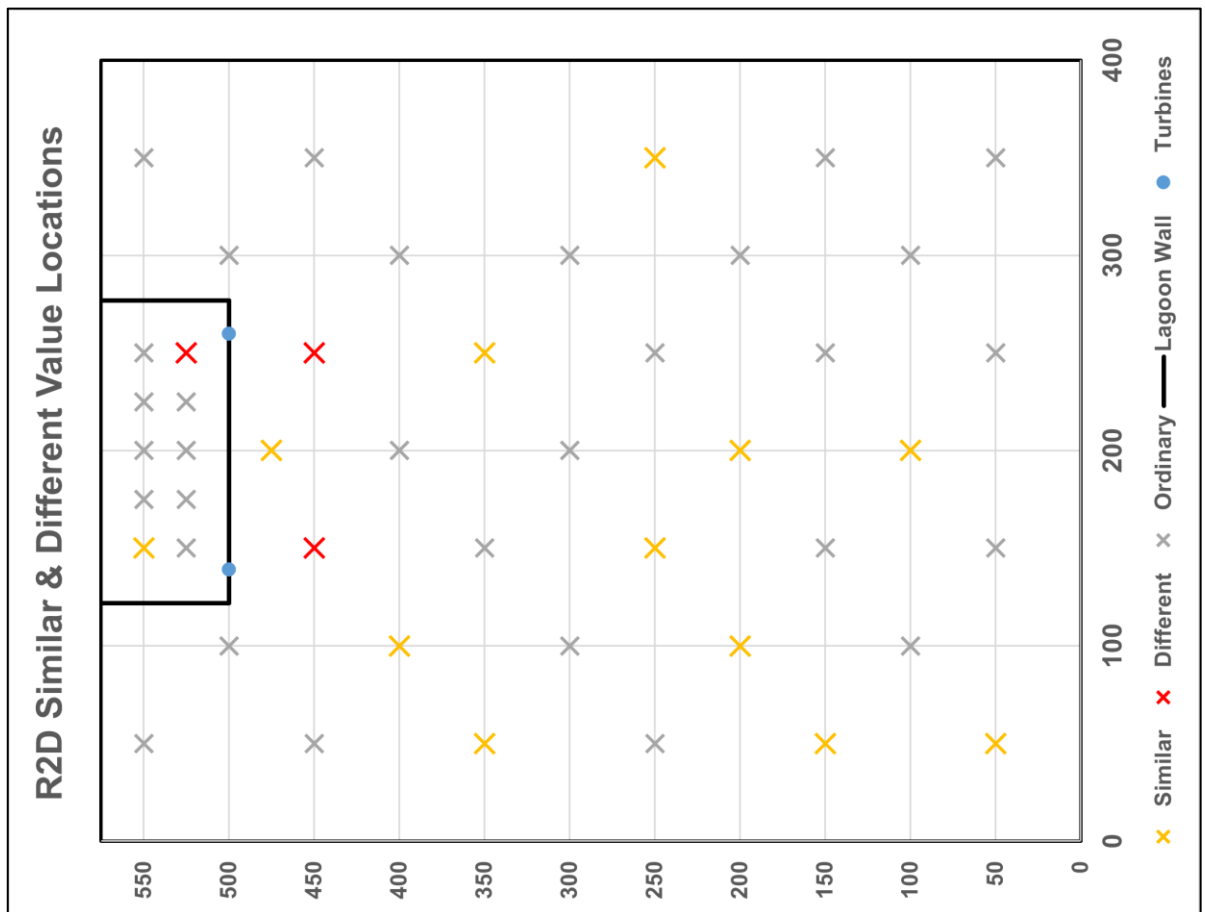
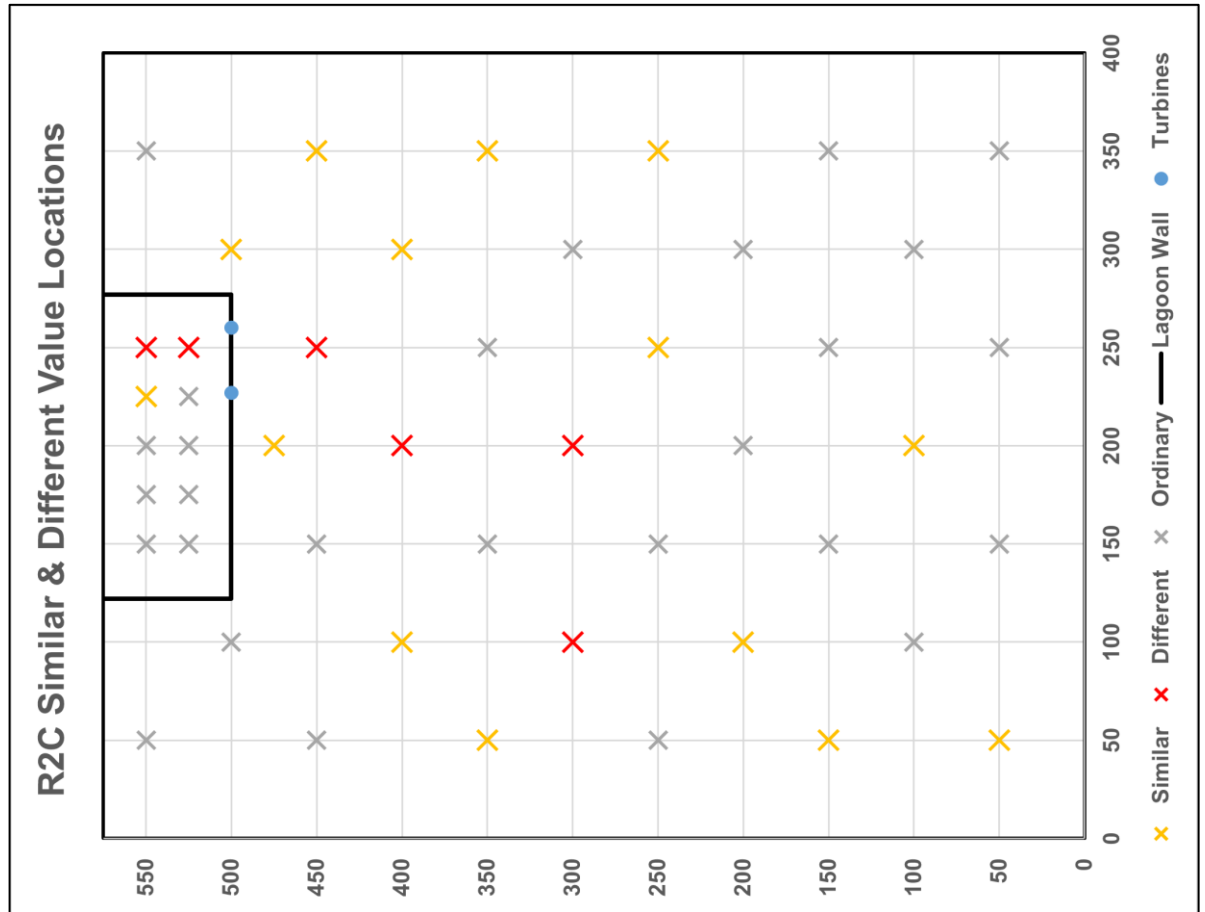
Annex 3: Comparison of Points of Statistically Similar and Different Resultant Velocity



Annex 3: Comparison of Points of Statistically Similar and Different Resultant Velocity

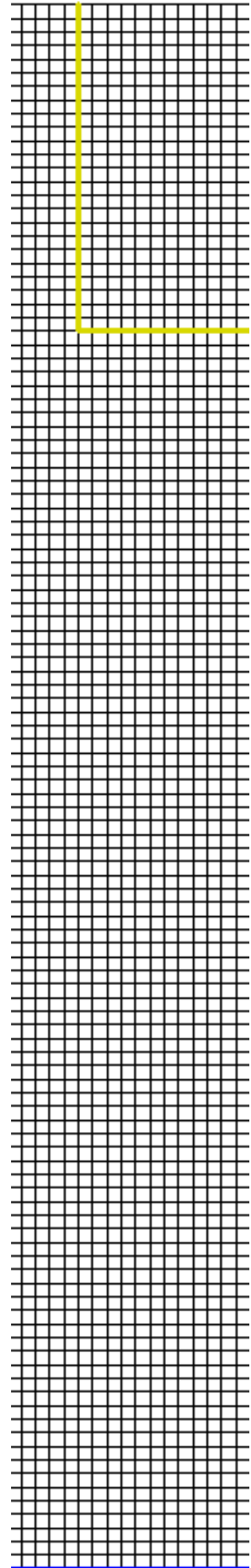


Annex 3: Comparison of Points of Statistically Similar and Different Resultant Velocity



Annex 4

Advantages & Disadvantages of Dimensional Numerical Models



Annex 4: Advantages and disadvantages of dimensional numerical models

	Modelling Software	Example of TRS Studies	Advantages	Disadvantages
0D	<ul style="list-style-type: none"> MS Excel Matlab 	<ul style="list-style-type: none"> Burrows et al, (2009) Modelling energy extraction in NW. UK. Yates et al, (2013) Modelling extractable resource NW. UK. Petley and Aggidis (2016) Annual energy estimation of Swansea Bay tidal lagoon. Xue et al, (2021) Optimising TRS operation. 	<ul style="list-style-type: none"> Useful for initial testing of water level, discharge, energy output and operation mode (Neill et al., 2018; Xue et al., 2021). Computational simplicity & efficiency, can be extended if needed (Harcourt et al., 2019; Xue et al., 2021). 	<ul style="list-style-type: none"> Assumes negligible impact in multiple directions and so overestimates power output (Angeloudis and Falconer, 2017).
1D	<ul style="list-style-type: none"> HECRAS 1D ISIS 1D MASCARE T 1D SOBEK 1D MIKE 11 	<ul style="list-style-type: none"> Ahmadian et al, (2010) Hydro environmental modelling of proposed Severn barrage UK. Angeloudis et al, (2017) TRS resource estimates. 	<ul style="list-style-type: none"> Can help look at flow variations along length of estuary (Adcock et al., 2015). More accurate than 0D and can closely match 2D in certain cases (Angeloudis et al., 2017). Useful for first stage estimates of energy potential (Suárez-López et al., 2019). Useful for qualitative assessment of the scale of impacts (Neill et al., 2018). 	<ul style="list-style-type: none"> Valid only where tidal flow is one dimensional (Suárez-López et al., 2019). Poor representation of tidal range and amplitude (Neill et al., 2018).

Annex 4: Advantages and Disadvantages of Dimensional Numerical Models

2D	<ul style="list-style-type: none"> • HECRAS 2D • IBER • MIKE 21 • TELEMAC 2D • SOBEK 2D • TUFLOW • ISIS 2D • ADCIRC 2D • Thetis • DIVAST • ANSYS CFX 	<ul style="list-style-type: none"> • Angeloudis et al, (2016) Environmental impacts of tidal lagoons. • Angeloudis & Falconer (2017) Hydrodynamic impacts of TRS operation. • Vouriot et al, (2018) Vortex behaviour in idealised tidal lagoons. • Angeloudis et al, (2018) Optimising TRS plant operation. • Mackie et al, (2021b) Impact of tidal power lagoons with consistent design. 	<ul style="list-style-type: none"> • More complex detail than 0D or 1D (Adcock et al., 2015). • Useful for tidal flows in shallow water conditions (Stansby, 2006; Suárez-López et al., 2019). • Helps understanding of environmental impacts (Angeloudis et al., 2017). • Similar results to 3D modelling for surface elevations, tidal amplitude and average velocities (Sandbach et al., 2018; Sucsy, 1993). • Cheaper than 3D modelling (Neill et al., 2018). 	<ul style="list-style-type: none"> • Can miss complex 3D flows (Čož et al., 2019; Jeffcoate et al., 2013). • Depth averaging is less accurate for modelling near field flows (Jeffcoate et al., 2017). • Assumes that behaviour will be mostly 2D (Adcock et al., 2015). • Overlooks some sediment transport and mixing processes (Stansby, 2006).
3D	<ul style="list-style-type: none"> • Delft 3D • ROMS • FVCOM • MITgcm • MIKE 3 FM • TELEMAC 3D 	<ul style="list-style-type: none"> • Cornett et al, (2013) Hydrodynamic impacts from tidal power lagoons. • Jeffcoate et al, (2017) Flow and bed shear stress downstream of barrage. • Falconer and Kolahdoozan (2003) Geo-morphological change in estuaries. • Jeffcoate et al. (2013) Modelling flow through a barrage. • Michelet et al. (2020) Modelling TST turbine wakes. 	<ul style="list-style-type: none"> • Improved detail and more accurate than 2D (Falconer and Kolahdoozan, 2003). • Can identify alterations at all depths and in all directions (Suárez-López et al., 2019). • Can look at hydrodynamic structures near turbines (Angeloudis et al., 2017). • 3D model more sensitive to roughness than 2D (Sandbach et al., 2018). 	<ul style="list-style-type: none"> • Computationally expensive (Čož et al., 2019). • 3D model in D3D found to over-predict, more sensitive to tidal amplitude than 2D model (Sandbach et al., 2018).

Annex 5
Numerical Model
Design Schedule

Physical Test Code
00
S0
S1A
S1B
S2A
S2B
S2C
S2D/ B1
B2
B3
B4
B5
B6
R0
R1
R2A
R2B
R2C
R2D

Annex 5: Numerical Model Design Schedule

Numerical modelling was proposed as an extension of the physical experiments to test more complex cases in a time effective manner. The following test schedule outlines proposals for future tests once the numerical model has been accurately calibrated and validated.

A5.1 Test Cases and Configurations

Once the numerical model has been calibrated it can then be extended to consider other cases. These could include:

- Further testing of different turbine spacings.
- Investigation of different lagoon geometries and length to width ratios.
- Modelling of more realistic TRSs based on current proposals.

A5.1.1 Further testing of different turbine spacings

Laboratory experiments were carried out to test the impact of varying the location and spacing of turbines and the observed results can be used to calibrate a numerical model in order to test further configurations. The physical models showed that placing two turbines close together near a wall had a far-reaching impact on velocity magnitude and direction both within and outside of the TRS. Numerical modelling could investigate more turbine spacings and positions in order to identify the optimum configuration for reducing the effect on the hydro-environment. Table A5.0.1 presents a possible test schedule for future numerical modelling of turbine spacing with laboratory test cases available for calibration highlighted in yellow.

Table A5.0.1 Test schedule for turbine spacing in idealised square lagoon.

Turbine position/ Test Case	a	b	c	d	e	f	g	h	i	j
1								x	x	
2							x		x	
3						x			x	
4					x				x	
5				x					x	
6			x						x	
7		x							x	
8	x								x	
9					x	x				

Annex 5: Numerical Model Design Schedule

10				x			x			
11			x					x		
12		x							x	
13	x									x

The decision to model only one or two turbines within the laboratory was made based upon the area of the turbine openings. Existing proposals for TRSs in the UK (laid out in Table 3.1) include designs ranging from an installed capacity of 320 MW (Swansea) to 6480 MW (Bridgewater) which would include between 16 and 320 turbines. At the current scale, two turbines represent an installed capacity of approximately 1440 MW, the size of the scheme proposed at Newport. Further investigations could examine the spacing of three or more turbines to see what effect this has on flow conditions.

A5.1.2 Investigation of different lagoon geometries

As with previous studies by Vouriot et al, (2018) and Falconer (1974) it is also worth investigating the geometry of TRSs to determine the effects of seawalls of different lengths and proportions as this aspect has been found to have an impact on flushing and recirculation. In the laboratory it was possible to compare the results of a square TRS with a rectangle of length-to-width ratio, 1:2. Time and the physical constraints of the tank limited the testing of other configurations which could now be modelled numerically. Possible layouts for further investigation are presented in Table A5.0.2 with laboratory test cases available for calibration highlighted in yellow.

Table A5.0.2 Dimensions for varying lagoon length-to-width ratio with constant area.

Scheme	Turbine units	Length	Width	Length to width ratio
Square	10	1.10	1.10	1:1
Rectangle 1	14	1.55	0.75	1:2
Rectangle 2	11	1.21	1.00	4:5
Rectangle 3	13	1.43	0.85	5:8
Rectangle 4	7	0.77	1.55	2:1

Plans for TRSs in the UK also vary in shape from pentagonal to semi-circular and future tests could also look at varying the shape of the TRS from a straight sided square or rectangle to more complex geometry. This would be

difficult to achieve given the physical constraints of the laboratory but become possible with a computational model.

A5.1.3 Modelling more realistic TRSs

The original physical experiment design intended to test the impacts of several schemes proposed by the Hendry Review (2016) (see Table 3.1), these plans were curtailed due to the pandemic but could now be modelled numerically. Table A5.0.3 presents the original proposed schemes with the laboratory test cases available for calibration highlighted in yellow.

Table A5.0.3 Scaled dimensions of proposed TRSs.

Scheme	Turbines	Area (km ²)	Approx. Area (km ²)	Sq.	Rec. 1		Rec. 2		Rec. 3	
				L (m)	L (m)	W (m)	L (m)	W (m)	L (m)	W (m)
Stepping Stones	1	18.0	20	0.9	1.2	0.6	1.0	0.8	0.7	1.1
The Wash	1	50.0	50	1.4	2.0	1.0	1.6	1.4	1.1	1.8
Barrow	2	56.8	50	1.4	2.0	1.0	1.6	1.4	1.1	1.8
Cardiff	4	71.8	70	1.7	1.2	2.4	1.9	1.5	1.4	2.0
Liverpool	2	67.1	70	1.7	1.2	2.4	1.9	1.5	1.4	2.0
Minehead	4	90.0	90	1.9	1.3	2.6	2.1	1.7	1.5	2.4
Sheerness	2	100	90	1.9	1.3	2.6	2.1	1.7	1.5	2.4

A5.2 Domain and Boundary Conditions

As previously noted, the model domain was created to match the laboratory conditions, measuring 4 m by 5.75 m with closed boundaries on three sides, free slip conditions at the sides and base, and a smooth, flat bed. The simplified TRS lies along the closed boundary at the rear of the tank, corresponding to the coast, whilst the inflow boundary is at the opposite end of the tank representing the incoming tide flowing from the sea (presented originally in Figure 7.1). Whilst most coastal flows are unbounded, the side walls in this case could be analogous to the shoreline of an estuary.

D3D enables inflow boundaries to be programmed using time series data of water level, velocity or discharge, inputting a single value at the start and end points of the boundary section which are then interpolated to generate the values in between. Boundary conditions can be used as a calibration parameter, as discussed in greater detail in Section 7.5.1.